

CONTRACTOR REPORT

SAND82-8180
UC-62d
Unlimited Release

THIS REPORT IS FOR YOUR RETENTION
DO NOT RETURN TO THE LIBRARY

**Molten Salt Solar Receiver
Subsystem Research Experiment
Phase 1 — Final Report
Volume I — Executive Summary and
Volume II — Technical**

**Foster Wheeler Solar Development Corporation
Livingston, New Jersey**

Prepared by Sandia National Laboratories, Albuquerque, New Mexico 87185
and Livermore, California 94550 for the United States Department of Energy
under Contract DE-AC04-76DP00789.

Printed October 1984

Issued by Sandia National Laboratories, operated for the United States Department of Energy by Sandia Corporation.

NOTICE: This report was prepared as an account of work sponsored by an agency of the United States Government. Neither the United States Government nor any agency thereof, nor any of their employees, nor any of the contractors, subcontractors, or their employees, makes any warranty, express or implied, or assumes any legal liability or responsibility for the accuracy, completeness, or usefulness of any information, apparatus, product, or process disclosed, or represents that its use would not infringe privately owned rights. Reference herein to any specific commercial product, process, or service by trade name, trademark, manufacturer, or otherwise, does not necessarily constitute or imply its endorsement, recommendation, or favoring by the United States Government, any agency thereof or any of their contractors or subcontractors. The views and opinions expressed herein do not necessarily state or reflect those of the United States Government, any agency thereof or any of their contractors or subcontractors.

Printed in the United States of America
Available from
National Technical Information Service
5285 Port Royal Road
Springfield, VA 22161

NTIS price codes
Printed copy: A21
Microfiche copy: A01

SAND82-8180
Unlimited Release
Printed October 1984

PHASE 1--FINAL REPORT

MOLTEN SALT SOLAR RECEIVER
SUBSYSTEM RESEARCH EXPERIMENT

VOLUME 1
EXECUTIVE SUMMARY

AND

VOLUME 2
TECHNICAL

Prepared for
Sandia National Laboratories
Livermore, California

By
G. Carli
Project Manager

November 1982

Contract 84-2292C

FWSDC No. 9-71-9203



FOSTER WHEELER SOLAR DEVELOPMENT CORPORATION

12 Peach Tree Hill Road, Livingston, New Jersey 07039

Abstract

This report presents the results of the work done in Phase 1 of a Department of Energy (DOE)-funded project for developing a cost-effective molten salt Receiver Subsystem (RS) for a commercial-size Solar Central Receiver System (SCRS) and providing the commercial fabrication process development for molten salt receivers.

The report comprises three volumes. Volume 1, the Executive Summary, presents an overview of the study, including major results and conclusions along with a concise description of the RS. Volume 2 presents the discussions, evaluations, and results of work done during Tasks 1 through 7. Volume 3 contains Appendices A through T--detailed analyses and supporting information.

An executive summary of this report is available from TIC as SAND84-8176.

CONTENTS*

<u>Section</u>		<u>Page</u>
	<u>VOLUME 1--EXECUTIVE SUMMARY</u>	
	ACRONYMS	v
1	EXECUTIVE SUMMARY	1-1
	1.1 Introduction	1-1
	1.1.1 Background	1-1
	1.1.2 Project Objective	1-2
	1.1.3 Definition of the RS (Receiver Subsystem)	1-3
	1.1.4 Technical Approach	1-3
	1.1.5 Project Team	1-7
	1.2 Selection of the RS	1-8
	1.2.1 Trade-Off Studies	1-8
	1.2.2 Selected Configuration	1-10
	1.2.3 Materials Selection	1-13
	1.3 RS Design Analysis	1-16
	1.3.1 Design Point	1-16
	1.3.2 Thermal/Hydraulic Design Analysis	1-18
	1.3.3 Stress Analyses	1-22
	1.3.4 Mechanical Design Analysis	1-25
	1.3.5 Operation and Control Analysis	1-26
	1.4 RS Summary Description	1-28
	1.5 Panel Fabrication Development	1-36
	1.6 Weight and Cost Estimates	1-44
	1.7 Receiver Development	1-46

*Published in three separate volumes.

ILLUSTRATIONS

<u>Number</u>		<u>Page</u>
1.1	Schematic of RS	1-4
1.2	Absorber Isometric and Circuitry	1-11
1.3	Temperature Profile of Absorber Hottest Tube	1-19
1.4	320-MW Molten Salt Solar Cavity Receiver	1-29
1.5	RS Flow Schematic	1-34
1.6	Overall View of Welding Set-Up Showing the Welding Head, Wire Reel, Controls, Cross-Beam Carriage, and Pneumatically Actuated Toggle Clamps	1-37
1.7	Cross Section of Welded Panel Tubes	1-38
1.8	Welding of Third Development Panel	1-41
1.9	Support Lug Attachment Methods	1-41
1.10	Third Development Panel Showing Support Lugs at Each End	1-43
1.11	Schematic of the SRE Test Cavity	1-48

TABLES

<u>Number</u>		<u>Page</u>
1.1	Team Responsibilities	1-7
1.2	RS Design Data Summary	1-17
1.3	RS Performance	1-21
1.4	Thermal/Hydraulic Performance Data Summary	1-23
1.5	Configuration Data Summary	1-30
1.6	Receiver Weight	1-44
1.7	Construction Cost Estimate	1-45

CONTENTS

<u>Section</u>		<u>Page</u>
	<u>VOLUME 2--TECHNICAL</u>	
	ACRONYMS	xx
2	INTRODUCTION	2-1
	2.1 Background	2-2
	2.2 Program Goals and Project Objectives	2-4
	2.3 Definition of the RS	2-5
	2.4 Technical Approach	2-8
	2.5 Project Team	2-15
3	RS REQUIREMENTS SPECIFICATION	3-1
	3.1 Review of SNLL Specification	3-1
	3.2 System Level Definition	3-1
	3.2.1 RS Scope	3-2
	3.2.2 Applicable Codes and Standards	3-3
	3.2.3 Technical Requirements	3-3
	3.2.4 Interface Requirements	3-9
	3.2.5 Environmental Requirements	3-9
	3.3 Summary of RS Requirements	3-11
4	SELECTION OF THE RS	4-1
	4.1 Selection of Receiver Concept	4-1
	4.1.1 Comparison of PCR With Alternative Concepts	4-3
	4.1.2 Rationale for the Selection of the PCR Concept	4-8
	4.2 Refinements/Improvements Selection Approach	4-9
	4.2.1 Review of Key Issues	4-9
	4.2.2 Identification of Design Options	4-14
	4.2.3 Development of a Selection Process	4-17
	4.2.4 Definition of Selection Criteria	4-18

CONTENTS (Cont)

<u>Section</u>	<u>Page</u>
4.3 Trade-Off Studies	4-22
4.3.1 Absorber Surface Arrangement	4-26
4.3.2 Materials Selection	4-28
4.3.3 Tube Size Selection	4-35
4.3.4 Allowable Flux Levels	4-36
4.3.5 Serpentine Flow vs. All Up Flow	4-37
4.3.6 Panel Geometry and Flow Routes	4-38
4.3.7 Aperture Door Configuration	4-38
4.3.8 Feed Pump Arrangement	4-39
4.3.9 Approach to Overnight Conditioning	4-40
4.3.10 Approach to Receiver Protection for Fault Conditions	4-44
4.3.11 Single Tube Heat Flux Analysis	4-50
4.3.12 Aperture Size Optimization	4-51
4.4 Selected Configuration Summary	4-59
5 RS DESIGN ANALYSIS	5-1
5.1 Design Analysis Plan	5-2
5.2 Thermal/Hydraulic Design Analysis	5-4
5.2.1 Steady-State T/H Analysis	5-8
5.2.2 Transient Analysis	5-36
5.2.3 Overnight Conditioning	5-45
5.2.4 Performance	5-49
5.3 Stress Analyses	5-58
5.3.1 Design Standards and Criteria	5-58
5.3.2 Joining and Attachment Methods	5-62
5.3.3 Effect of Incident Heat Flux Angle on Absorber Panels	5-72
5.3.4 Creep-Fatigue Evaluation of Absorber Panels	5-75
5.3.5 In-Plane Temperature Gradient	5-85
5.3.6 Transient Analysis	5-86
5.3.7 Shear Stress Analysis of Absorber Panel	5-89

CONTENTS (Cont)

<u>Section</u>	<u>Page</u>
5.4 Mechanical Design Analysis	5-97
5.4.1 Absorber Panels	5-97
5.4.2 Interconnecting Piping and Surge Tanks	5-113
5.4.3 Receiver Aperture Door	5-116
5.4.4 Receiver Support Structure	5-128
5.4.5 Cavity Floor and Ceiling	5-136
5.4.6 Receiver Tower Design	5-140
5.4.7 Riser/Downcomer Piping	5-141
5.5 Operation Analysis	5-146
5.5.1 Operating Modes	5-146
5.5.2 Mode Transitions	5-148
5.5.3 Major Operations	5-150
5.5.4 Emergency Operations	5-151
5.5.5 Operating Timelines	5-153
5.6 Control Analysis	5-155
5.6.1 RS Control System	5-155
5.6.2 Overall Model	5-165
5.6.3 System Response	5-172
6 PANEL FABRICATION DEVELOPMENT	6-1
6.1 Background	6-1
6.2 Fabrication Process Development Plan	6-1
6.3 Panel Welding Development	6-3
6.3.1 Welding Process	6-4
6.3.2 Welding Head and Power Supply	6-4
6.3.3 Welding Head Travel and Tracking	6-4
6.3.4 Welding Fixture	6-7
6.3.5 Trial Welding	6-8
6.4 Development Panel Fabrication	6-13
6.4.1 Development Panel 1	6-13
6.4.2 Development Panel 2	6-17
6.4.3 Development Panel 3	6-19

CONTENTS (Cont)

<u>Section</u>		<u>Page</u>
	6.5 Support Lug Attachment	6-30
	6.6 Evaluation and Tests	6-34
	6.6.1 Weld Evaluation	6-34
	6.6.2 Panel Weld Strength Tests	6-36
	6.6.3 Panel Lug Strength Test	6-40
	6.7 Repair Welding	6-46
	6.8 Preparation of Development Panel 3 for Shipment	6-48
	6.9 Discussion and Conclusion	6-51
7	RS DESCRIPTION AND COST ESTIMATE	7-1
	7.1 RS Description	7-1
	7.1.1 Receiver Unit	7-1
	7.1.2 Receiver Tower and Foundation	7-30
	7.1.3 Energy Transport Loop	7-35
	7.1.4 Auxiliary Equipment	7-37
	7.1.5 RS Interfaces	7-42
	7.2 Cost Estimate	7-44
8	RECEIVER DEVELOPMENT	8-1
	8.1 Verification Status	8-2
	8.1.1 Design Issues	8-2
	8.1.2 Operating Issues	8-6
	8.1.3 Performance Issues	8-6
	8.1.4 Technological Issues	8-7
	8.2 Verification Options	8-9
	8.3 Summary of Test Requirements and Test Capabilities	8-10
	8.3.1 Simulation Requirements	8-10
	8.3.2 Test Limitations	8-11
	8.3.3 Test Capabilities	8-12

CONTENTS (Cont)

<u>Section</u>	<u>Page</u>
8.4 Test Program Options and Risk Reductions	8-16
8.5 Proposed Test Program	8-19
8.5.1 CRTF Cavity Test Program	8-21
8.5.2 CRTF Panel Test Program	8-29
8.5.3 Irradiated Panel Test Program	8-31
8.5.4 Aperture Door Test Program	8-31
9 REFERENCES	9-1

ILLUSTRATIONS

<u>Number</u>		<u>Page</u>
2.1	Definition of RS	2-6
2.2	Work Flow Diagram	2-9
2.3	Work Flow Diagram/Critical Path Chart	2-13
2.4	Project Schedule	2-14
2.5	Project Organization Chart	2-16
3.1	Collector Field Performance Design Point	3-5
4.1	Proposal Baseline Configuration	4-2
4.2	Effect of Optical Interface Requirements on Receiver Design	4-12
4.3	Candidate Absorber Configurations	4-15
4.4	Concept Selection Process	4-17
4.5	Flow Chart of Parametric Analyses	4-24
4.6	Allowable Heat Flux on Absorber Panel Tubes	4-36
4.7	Aperture Plane Peak Heat Flux Decay	4-47
4.8	Modifications to V12 Geometry	4-52
4.9	Revised Panel Circuitry	4-53
4.10	Typical Aperture Sizing Process	4-54
4.11	Optimum Aperture/Panel Length	4-55
4.12	Cavity Arrangement	4-57
4.13	Cavity Isometric	4-60
4.14	RS/CS Interface Drawing	4-61
4.15	RS Flow Schematic	4-63

ILLUSTRATIONS (Cont)

<u>Number</u>		<u>Page</u>
5.1	Flow Chart--Design Analysis Process	5-3
5.2	Developed View of Absorber Panels	5-5
5.3	Receiver Absorbed Power vs. Time of Day	5-9
5.4	Absorbed Power per Panel at Design Point	5-10
5.5	Panel Flow Diagram Showing Salt Outlet Temperature	5-12
5.6	Salt Inlet/Outlet Temperature Profile	5-13
5.7	Peak Heat Flux	5-15
5.8	Temperature Profile of Hottest Tube in Pass 1	5-15
5.9	Temperature Profile of Hottest Tube in Pass 2	5-16
5.10	Temperature Profile of Hottest Tube in Pass 3	5-16
5.11	Temperature Profile of Hottest Tube in Pass 4	5-17
5.12	Temperature Profile of Hottest Tube in Pass 5	5-17
5.13	Pass 5 Temperature Summary	5-21
5.14	Effect of Fouling Factor on Tubewall Temperatures	5-26
5.15	Reynolds Number vs. Percent Mass Flow	5-27
5.16	Convective Coefficient vs. Percent Mass Flow	5-28
5.17	Salt Flow Regimes	5-28
5.18	Morning Start-Up Transient	5-38
5.19	Noon Start-Up Transient	5-40
5.20	Hot Shutdown Transient	5-41
5.21	Emergency Shutdown Transient	5-43

ILLUSTRATIONS (Cont)

<u>Number</u>		<u>Page</u>
5.22	Cloud Cover Transient	5-44
5.23	Radiant Heater Configuration	5-47
5.24	Location of Cavity Radiant Heaters	5-47
5.25	Molten Salt Receiver Efficiency	5-50
5.26	Receiver Design Point Losses	5-54
5.27	RS Output Power for Design Point Day	5-54
5.28	Comparison of Elastic and Inelastic Analyses on 25.4 mm (1 in.) O.D. Incoloy 800 Tube	5-61
5.29	Finite Element Model	5-63
5.30	Tube-to-Tube Joint Configurations	5-66
5.31	Buckstay Lug Reactions per Tube	5-70
5.32	Absorber Panel Deflections	5-71
5.33	Finite-Element Model of Full Tube	5-73
5.34	Definition of Incident Angle	5-74
5.35	Temperature Distribution and Equivalent Stresses in the Tube	5-76
5.36	Tubewall Temperature Profile	5-77
5.37	Revised Finite-Element Model of Full Tube With Spacer Strips	5-79
5.38	Temperature Contours and Effective Stresses--Pass 2	5-81
5.39	Temperature Contours and Effective Stresses--Pass 3	5-82
5.40	Temperature Contours and Effective Stresses--Pass 4	5-83

ILLUSTRATIONS (Cont)

<u>Number</u>		<u>Page</u>
5.41	Creep-Fatigue Damage Envelope	5-84
5.42	Temperature Differential--Morning Start-Up, Pass 2	5-88
5.43	Tubewall Temperatures--Morning Start-Up, Pass 2	5-88
5.44	Emergency Shutdown--Temperature Differentials, Pass 2	5-90
5.45	Emergency Shutdown--Metal Temperatures, Pass 2	5-90
5.46	Finite-Element Model of the Panel	5-92
5.47	Temperature Contours in Absorber Panels	5-93
5.48	Stress Contours in Wing Panel	5-95
5.49	Side Elevation of Absorber Panel Showing Configuration and Governing Dimensions	5-99
5.50	Preliminary Jumper-Tube Configurations	5-100
5.51	Selected Jumper-Tube Configuration	5-100
5.52	Candidate Header Arrangements	5-102
5.53	Selected Tube-To-Header Attachment Configuration	5-103
5.54	Front View of Absorber Panel Subassembly	5-105
5.55	Side View of Absorber Panel Subassembly	5-106
5.56	Panel Support Eye Lug	5-108
5.57	Buckstay Lug	5-110
5.58	Link Support Arrangement	5-111
5.59	Movement at Bottom End of Panel 10 as a Result of Thermal Expansion	5-111
5.60	Arrangement of Insulation Between Absorber Panels	5-112

ILLUSTRATIONS (Cont)

<u>Number</u>		<u>Page</u>
5.61	Absorber Inlet Piping Arrangement	5-114
5.62	Absorber Outlet Piping Arrangement	5-115
5.63	Side Elevation of Receiver	5-117
5.64	Front Elevation of Aperture Door	5-121
5.65	Cross Section of Aperture Door	5-122
5.66	Top Door Seals	5-124
5.67	Seals Between Door Sections	5-124
5.68	Side Seal of Aperture Door	5-125
5.69	Side View of Door Trolley	5-126
5.70	Plan View of Door Edge and Trolley	5-127
5.71	Front Elevation of Receiver Structure	5-129
5.72	Side Elevation of Receiver Structure	5-130
5.73	Plan View of Top Platform	5-131
5.74	Deflection Analysis of Receiver Structure	5-137
5.75	Plan View of Cavity Floor/Roof	5-138
5.76	Seal Between Cavity Floor and Absorber Panels	5-138
5.77	Attachment of Cavity Roof and Floor to Structure	5-139
5.78	General Arrangement of Steel Tower	5-142
5.79	General Arrangement of Concrete Tower	5-143
5.80	Operating Modes and Transitions	5-147
5.81	Operating Schematic	5-149

ILLUSTRATIONS (Cont)

<u>Number</u>		<u>Page</u>
5.82	Process Control Elements	5-156
5.83	Salt Temperature Control	5-161
5.84	Surge Tank (Accumulator) Pressure Control	5-162
5.85	Surge Tank (Accumulator) Level Control	5-163
5.86	Receiver Model Panel Numbering	5-166
5.87	RS Model Diagram	5-167
5.88	Panel Model Configuration	5-169
5.89	Panel Salt Valve Control Block Diagram	5-170
5.90	Accumulator/Surge Tank Model	5-171
5.91	Accumulator/Surge Tank Control Block Diagram	5-173
5.92	Beckman PID as Used in Valve Controllers	5-174
6.1	Automatic Welding Torch for Butt-Welding Thin-Walled Tubes	6-2
6.2	Weld-Induced Panel Distortion	6-3
6.3	Metal Inert Gas (MIG) Welding Head	6-5
6.4	Esterline Angus Recorders Used To Record Current (Amps) and Voltage	6-5
6.5	Welding Head With Wire Reel and Controls Mounted on Cross-Beam Carriage	6-6
6.6	Pneumatically Actuated Toggle Clamps and Roller Guide	6-7
6.7	Scalloped Support Block Used During Fabrication of First and Second Development Panels	6-8
6.8	Cross Sections of Trial Welds for Joining Tubes	6-9

ILLUSTRATIONS (Cont)

<u>Number</u>		<u>Page</u>
6.9	Roller Guide With Lip Used To Position Welding Head and To Restrain Spacer Strip During Welding	6-11
6.10	Fixture Employed During Fabrication of First Development Panel	6-15
6.11	Fixture Employed During Fabrication of Second Development Panel	6-18
6.12	Procedure Used for Fabricating Third Development Panel	6-20
6.13	Welding of Four-Tube Subassemblies for Third Development Panel	6-21
6.14	Welding of Four-Tube Subassembly to In-Process Panel	6-22
6.15	Macroscopic Cross Section of Typical Tube-to-Tube Weld in Third Development Panel	6-23
6.16	Fixture Employed During Fabrication of Third Development Panel	6-25
6.17	In-Process Welding of Last Four-Tube Subassembly	6-25
6.18	Last Stage of Third Development Panel Fabrication	6-26
6.19	Typical Front and Back Close-Up of Third Development Panel Before Welding Last Spacer Strip	6-27
6.20	Comparison of End Views of First and Third Development Panels	6-28
6.21	Candidate Methods for Attaching Support Lugs to Panel Tubes	6-31
6.22	Prototypical Panel Support Lug Integrally Welded With Panel Tubes	6-31
6.23	Close-Up of Prototypical Lugs Welded to Spacer Strip	6-33

ILLUSTRATIONS (Cont)

<u>Number</u>		<u>Page</u>
6.24	Macroscopic Cross Sections of Panel Weld Cut From First Development Panel	6-35
6.25	Top and Side Views of One of Two Longitudinal Bend Test Specimens	6-37
6.26	Top and Side Views of One of Two Transverse Bend Test Specimens	6-37
6.27	Front and Back Views of Transverse Tensile Test Specimen Before Test	6-38
6.28	Transverse Tensile Test Specimen During Testing	6-39
6.29	Front and Edge Views of Transverse Tensile Test Specimen After Test	6-41
6.30	Panel Support Lug Test Panel Before Test	6-42
6.31	Baldwin Universal Tensile Test Machine Used for Tensile Tests	6-43
6.32	Close-Up of Test Rig Used To Tensile Load Prototypical Panel Support Lugs	6-44
6.33	Failed Prototypical Support Lug	6-45
6.34	Close-Up of Failed Support Lug	6-45
6.35	Weld Repair	6-47
6.36	End View of Third Development Panel Showing Support Lugs	6-48
6.37	Finished Third Development Panel With Lugs	6-49
6.38	Third Development Panel Ready for Shipment to SNLL	6-50
7.1	General Arrangement	7-3
7.2	Circuitry Arrangement	7-7

ILLUSTRATIONS (Cont)

<u>Number</u>		<u>Page</u>
7.3	Piping and Instrumentation Diagram	7-9
7.4	Typical Panel and Support	7-13
7.5	Roof and Floor Details	7-17
7.6	Support Structure Plan Views	7-21
7.7	Support Structure Elevation Views	7-23
7.8	Door Arrangement	7-27
7.9	Tower Details	7-31
7.10	Tower Plot Plan	7-33
7.11	Fabrication Schedule for Receiver	7-45
7.12	Master Project Construction Schedule	7-46
8.1	Test Cavity Arrangement	8-23
8.2	SRE Test Cavity Circuitry Schematic	8-25
8.3	Developed View of SRE Test Cavity Absorber Area	8-26
8.4	Required Modifications to MSEE P&ID for Cavity Test at CRTF	8-27
8.5	CRTF Cavity Test Preliminary P&ID	8-28

TABLES

<u>Number</u>		<u>Page</u>
2.1	Team Responsibilities	2-17
2.2	Team Member Functions	2-18
3.1	RS Specifications Summary	3-12
4.1	Cost/Performance Comparison Between PCR and Cylindrical External Receiver at Barstow Location--MDC Second-Generation Heliostats	4-4
4.2	Key Parameter Comparison Between PCR and QCR Concepts	4-5
4.3	Cost/Performance Comparison Between PCR and QCR Concepts at Barstow Location--MDC Second-Generation Heliostats	4-7
4.4	Key Issues for RS	4-10
4.5	Concept Selection Criteria	4-19
4.6	Trade-Off Studies Selection Data	4-23
4.7	Comparison of Tilted and Vertical Orientations	4-27
4.8	Material Selection	4-34
4.9	Minimum Wall Thicknesses	4-35
4.10	Overnight Conditioning Evaluation	4-42
4.11	Comparison of Thermal Conditioning Methods	4-45
4.12	Loss of Receiver Flow	4-48
4.13	High/Low Temperature of Receiver Fluid	4-49
4.14	Selected Configuration Data Summary	4-62
5.1	Typical Heat Flux Map	5-6
5.2	Absorbed Power per Pass	5-10

TABLES (Cont)

<u>Number</u>		<u>Page</u>
5.3	T/H Characteristics--Design Point Conditions	5-14
5.4	Average Tubewall and Surface Temperatures	5-18
5.5	Panel Thermal Expansion	5-19
5.6	Maximum Values per Pass	5-20
5.7	Effect of Uncertainties on Peak Tubewall (O.D.) Temperatures	5-24
5.8	Effect of Fouling on Calculated Tubewall Temperatures	5-26
5.9	Average T/H Values at Rated Flow	5-29
5.10	Effect of Flow Distribution--Pass 1	5-31
5.11	Frictional Pressure Drop Through Receiver at Design Point	5-34
5.12	Frictional Pressure Drop Through Receiver vs. Time on Design Day	5-34
5.13	Insulation	5-35
5.14	Heat Losses During Overnight Shutdown	5-46
5.15	Overnight Duty for Cavity Radiant Heaters	5-48
5.16	RS Performance Train	5-51
5.17	Part-Load Performance--Molten Salt Receiver	5-55
5.18	RS Auxiliary Power Requirement	5-57
5.19	Boundary Conditions for Half Tube Model	5-64
5.20	Input Conditions for Tube Joint Analyses	5-67

TABLES (Cont)

<u>Number</u>		<u>Page</u>
5.21	Temperatures and Stresses in the Panel Tube	5-68
5.22	Boundary Conditions for Full Tube Model	5-74
5.23	Comparison of Normal vs. Non-Normal Incident Heat Flux	5-77
5.24	Maximum Tubewall Temperatures and Thermal Gradients	5-78
5.25	Creep-Fatigue Analysis	5-80
5.26	Receiver Pipe Sizes	5-113
5.27	IST/OST Tank Specifications	5-118
5.28	Aperture Door Design Considerations	5-118
5.29	Load and Reaction Summary	5-132
5.30	Riser/Downcomer Piping Characteristics	5-144
5.31	RS Control Variables and Setpoints	5-158
5.32	RS Equipment With On-Off Control	5-159
5.33	Types of Control	5-160
5.34	Control Instruments	5-164
6.1	Trial Welds	6-10
6.2	Panel Fabrication	6-14
7.1	RS Data Summary	7-2
7.2	Receiver Weight	7-41
7.3	320-MWt Molten Salt Receiver Subsystem Construction Cost Estimate	7-47
7.4	Direct Field Cost Breakdown	7-48
8.1	Commercial and SRE Comparison Summary	8-30

ACRONYMS

ACR	Advanced Central Receiver
ACR-SRE	Advanced Central Receiver Molten Salt Subsystem Research Experiment
AISC	American Institute of Steel Construction
ANSI	American National Standards Institute
ANSYS	Finite element program for static structural, heat-transfer, thermal, thermal stress, dynamic, seismic, and inelastic analyses. Contains many element types, such as beam, plane stress, axisymmetric solid, axisymmetric shell, general shell, and three-dimensional solid.
APS	Arizona Public Service
ASME	American Society of Mechanical Engineers
CONCEN	MDC code for detailed analysis of receiver flux profiles. Predicts flux profiles for a field layout consisting of individual heliostat locations. Also provides detailed performance analysis (diurnal and annual).
CRTF	Central Receiver Test Facility
CS	Collector Subsystem
CST	Cold Storage Tank
DAP	Design Analysis Plan
DELSOL	SNLL computer code for quantifying the performance, determining field layouts, and optimizing cost/performance of large central solar receiver systems.
DFR	Design Flow Rate
DOE	Department of Energy
FPDP	Fabrication Process Development Plan
FWDC	Foster Wheeler Development Corporation
FWEC	Foster Wheeler Energy Corporation

ACRONYMS (Cont)

FWSDC	Foster Wheeler Solar Development Corporation
FWSPEC	Foster Wheeler Special Projects Engineering and Construction, Inc.
GTA	Gas Tungsten Arc
HAZ	Heat-Affected Zone
HST	Hot Storage Tank
IST	Inlet Surge Tank
MDC	McDonnell Douglas Corporation
MIG	Metal Inert Gas
MMC	Martin Marietta Corporation
MSEE	Molten Salt Electric Experiment
NASA	National Aeronautics and Space Administration
NRC	Nuclear Regulatory Commission
NONAX	FWDC-developed special-purpose program to solve for thick-walled cylinders made of homogeneous and isotropic material under non-axisymmetric loading (loading may consist of an arbitrary combination of internal and external tractions, axial load, axial bending, and an arbitrary temperature distribution). Determines thermoelastic, elastic-plastic, and creep solutions under varying load cycles and hold times.
OST	Outlet Surge Tank
PCR	Partial Cavity Receiver
P&ID	Piping and Instrumentation Diagram
QCR	Quad-Cavity Receiver
RFQ	Request for Quotation
RS	Receiver Subsystem

ACRONYMS (Cont)

RSS	Root Sum Square Method
SCRS	Solar Central Receiver System
SINDA	General software system designed primarily for the solution of thermal analog models presented in network format. Can be used as a general-purpose program with its array and constant capability along with library of user subroutines.
SNLL	Sandia National Laboratories, Livermore
SOLAR	FWSDC-developed program to perform the steady-state thermal/hydraulic analysis of molten salt-cooled solar receivers. Calculates tubewall and salt temperatures at each node location and absorbed power, salt bulk temperature change, and pressure drop for each zone. Calculates variations in flow (flow distribution) among panel tubes caused by variations in heat flux across panel.
SPP	Sierra Pacific Power Company
SRE	Subsystem Research Experiment
TEMA	Tubular Exchanger Manufacturers Association
T/H	Thermal/Hydraulic
TIG	Tungsten Inert Gas
TRASYS	Geometric modeling program that computes the black and gray body view factors and determines the solar and infrared radiation interchange between surfaces in cavity and partial cavity receivers.
UBC	Uniform Building Code
VDCRP	Voltage, Direct Current Reverse Polarity

Section 1

EXECUTIVE SUMMARY

1.1 INTRODUCTION

This report presents the results of the work done in Phase 1 of a Department of Energy (DOE)-funded project for developing a cost-effective molten salt Receiver Subsystem (RS) for a commercial-size Solar Central Receiver System (SCRS) and providing the commercial fabrication process development for molten salt receivers.

The report comprises three volumes. Volume 1, the Executive Summary, presents an overview of the study, including major results and conclusions along with a concise description of the RS. Volume 2 presents the discussions, evaluations, and results of work done during Tasks 1 through 7. Volume 3 contains Appendices A through T--detailed analyses and supporting information.

1.1.1 Background

Recent DOE studies have shown that, technically and economically, molten nitrate salt (60 wt% NaNO_3 /40 wt% KNO_3) is one of the leading candidates for a high-temperature, central receiver heat-transfer fluid. The advantages of molten salt include low cost, chemical stability, low corrosion rates, a low melting point, a high usable temperature at a low operating pressure, and high heat capacity for thermal storage. It has been used successfully in process heat applications for many years. However, at the temperature and duty cycle of an SCRS, it has a limited industrial application and data base.

Recognizing the attractiveness of molten nitrate salt, DOE has conducted an extensive program to identify uncertainties and concerns relating to its use and to develop the data base, technology, and hardware components that are essential for the development of a commercial molten salt SCRS.

DOE and Sandia National Laboratories, Livermore (SNLL) have been systematically developing this data base and the technology for SCRS applications. This study is an important element in these activities.

In several recent molten salt SCRS studies, the receiver was studied as a part of the entire plant. Consequently, even though a considerable body of information has been generated, important receiver design, fabrication, and operating issues require additional investigation.

1.1.2 Project Objective

The overall project objective was to design a reliable and cost-effective molten salt RS. Specifically, the project was aimed at resolving all critical design, fabrication, operating, and performance uncertainties.

The work done under this contract (Phase 1) consists of the definition of the requirements specification, the preliminary design of a 320-MW* molten salt RS, and a fabrication development task to resolve any fabrication uncertainties, performed in sufficient detail to achieve the objectives of developing a reliable, cost-effective molten salt RS for a commercial SCRS.

*Thermal unless otherwise specified.

1.1.3 Definition of the RS

The RS, shown schematically in Figure 1.1, provides a means of transferring the incident radiant flux energy from the heliostat field into the molten salt heat-transfer fluid. The RS consists of an elevated receiver to intercept the radiant flux, the tower structure to support the receiver, and the riser and downcomer piping. The RS also includes the pumps, valves, and control system necessary to regulate fluid flow, temperature, and pressure and the required thermal conditioning necessary for its safe and efficient operation, start-up, shutdown, and standby.

The terminal points defining components within the scope of the RS are at the boundary of the tower structure where the riser and downcomer meet the cold and hot salt lines from the Thermal Storage Subsystem. These terminal points were selected so that the RS design is not dependent upon the physical layout of a specific job site.

1.1.4 Technical Approach

The project was divided into 10 tasks. After a review of SNLL's Preliminary RS Specification (Task 1), the RS Requirements Specification was developed (Task 2). Based on these Requirements, technical and economic parametric analyses were performed and a configuration was selected (Task 3). Detailed preliminary design of the RS was made and its performance was evaluated (Task 4). Fabrication and construction plans were prepared and capital costs were estimated (Task 5). Panel fabrication techniques were developed (Task 6), and a development plan for Phase 2 was prepared (Task 7). Following a redirection of

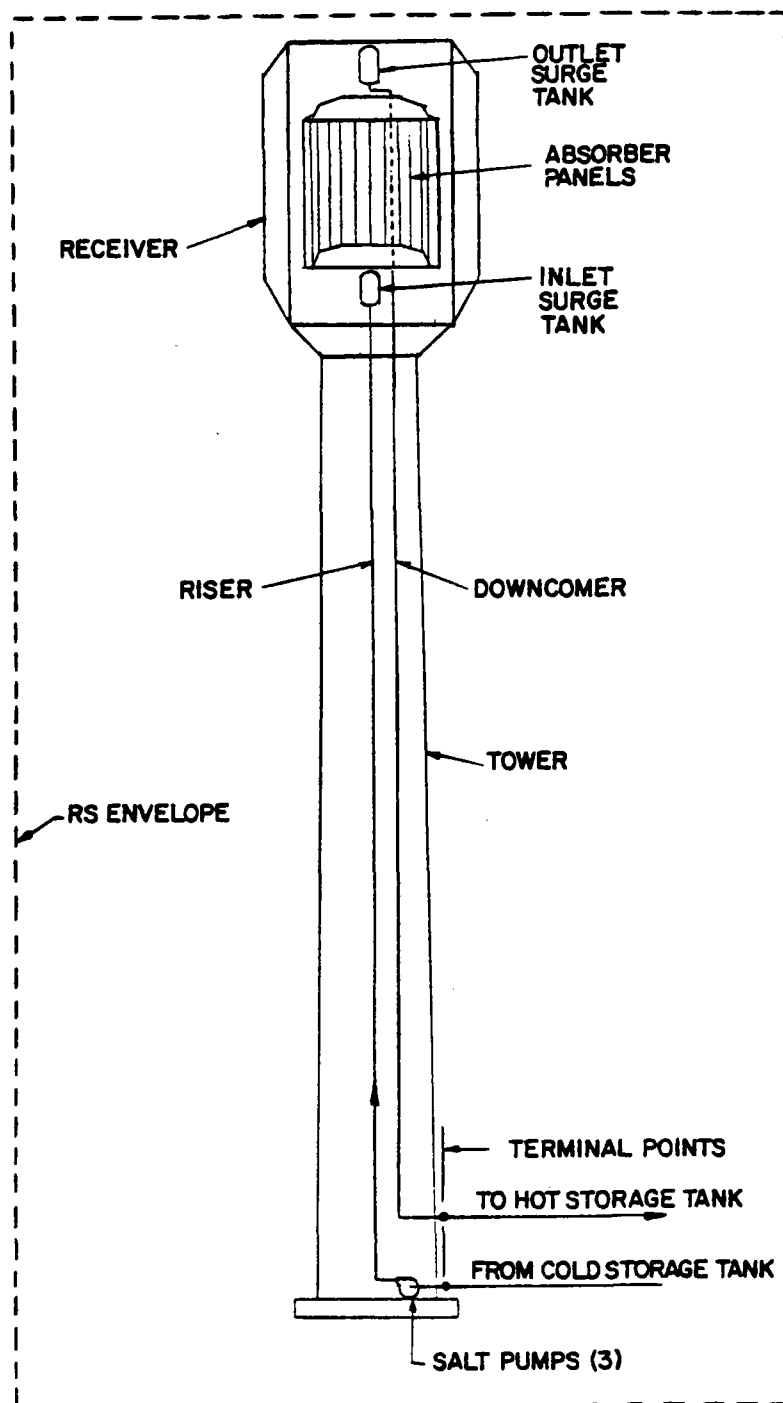


Figure 1.1 Schematic of RS

effort by SNLL, the Phase 2 proposal (Task 8) was deleted. Task 9 consisted of reports and meetings; Task 10, project management and administration. The contract period of performance was from September 1981 through November 1982. An outline of the contract Statement of Work follows.

Task 1--Review of RS Specification

- Review Molten Salt Subsystem Specification given by SNLL
- Submit changes to SNLL within 15 days after authorization to proceed
- Update specifications, if necessary, as work proceeds.

Task 2--Definition of RS Requirements

- Review literature on molten salt, molten salt receivers, and salt-based solar central receiver plants
- Develop system-level requirements specification for the RS.

Task 3--RS Concept Selection

- Define evaluation criteria
- Perform technical and economic parametric analyses of the potential design improvements to the baseline RS
- Select concept.

Task 4--RS Design and Analysis

- Prepare Design Analysis Plan
- Analyze receiver operation and define auxiliary equipment required
- Perform thermal/hydraulic (T/H), structural, mechanical, and control design and analysis, and efficiency analysis.

Task 5--RS Cost and Fabrication Plans

- Develop shop fabrication and field construction plans
- Estimate RS cost.

Task 6--Receiver Fabrication Process Development

- Prepare detailed Fabrication Process Development Plan
- Develop techniques for tube-to-tube and tube-to-header joining and methods for attaching panels or panel tubes to support structure
- Evaluate techniques with mechanical tests
- Perform stress analysis to evaluate the effect of stresses and strains arising from the joining and attaching methods.

Task 7--Subsystem Research Experiment and Development Plan

- Identify Subsystem Research Experiment (SRE) requirements
- Prepare SRE design, plan, and schedule.

Task 8--Phase 2 Plan and Proposal (deleted)

- Prepare detailed proposal for continuing effort into Phase 2.

Task 9--Reports and Data

- Prepare and submit reports and data as specified by SNLL
- Attend contract meetings.

Task 10--Program Management

- Coordinate and direct project effort
- Establish budgets and control costs
- Conduct independent technical and design reviews
- Monitor technical progress
- Interface with the SNLL Technical Contract Manager.

1.1.5 Project Team

To perform the Phase 1 design study, we assembled a team of organizations with valuable complementary backgrounds in systems and design integration; design, fabrication, construction, and testing of central receiver solar thermal power systems and components; and operation of utility generating plants. Foster Wheeler Solar Development Corporation (FWSDC), prime contractor for Phase 1, had overall responsibility for the project. The team consisted of our affiliated companies--Foster Wheeler Energy Corporation (FWEC) and Foster Wheeler Special Projects Engineering and Construction, Inc. (FWSPEC); McDonnell Douglas Corporation (MDC); Arizona Public Service Company (APS); Sierra Pacific Power Company (SPP); and Olin Corporation. Table 1.1 shows the team members and their primary areas of responsibility.

Table 1.1 Team Responsibilities

<u>Organization</u>	<u>Responsibility</u>
FWSDC	Overall project management and coordination, receiver design and analysis, fabrication process development, SRE conceptual design
FWEC	Fabrication plan and cost estimates, receiver mechanical design
FWSPEC	Design of receiver tower and piping system, specification of salt pump and auxiliary equipment, construction plan and cost estimates
MDC	Development of system-level requirements and specifications, selection of preferred receiver configuration, definition of incident fluxes, performance estimates, control system, SRE plan
APS, SPP	Provide utility engineering review
Olin	Molten salt technology advisor.

1.2 SELECTION OF THE RS

1.2.1 Trade-Off Studies

Absorber configuration trade-off studies included parametric analyses of:

- Absorber surface arrangement, including tilted vs. vertical orientation
- Absorber materials
- Tube dimensions
- Allowable flux levels
- T/H stability
- Panel geometry, arrangement, and flow routing

Other trade-offs that were made in parallel include:

- Aperture door configuration and size
- Overnight conditioning
- Feed pump arrangement
- Receiver protection

The output of these analyses was used to complete the definition of the RS equipment, cost, and performance and to provide data for the final configuration selection. For those configurations that were most attractive, we estimated receiver losses, rescaled the collector field and tower configurations, and calculated annual energy delivered to thermal storage.

We defined the auxiliary equipment required for overnight conditioning, start-up, shutdown, and emergency operation. In these analyses we investigated options for keeping the panels hot overnight as opposed to draining them overnight and preheating them before early morning start-up. The requirements for overnight heating were assessed and the trade-offs between electrical trace and

radiant heating of the panels and the circulation of heated salt were investigated. We compared the fill and drain of the downcomer with overnight hold. In all of these cases, we addressed both equipment costs and parasitic power requirements. Surge tanks and selected pumping or pressurizing schemes were sized to provide emergency coolant flow in the event of a power or receiver feed-pump failure. We also identified options for the aperture door.

Dominant factors in the initial screening of absorber configurations were minimum area consistent with peak heat flux, with heat flux levels near the outlet where high salt film (I.D.) temperatures occur, and with heat flux gradients across the panels. Tube characteristics were selected to satisfy a combination of high-temperature thermal structural (i.e., peak heat flux) capabilities, ease of fabrication, and low cost. Flow routing was selected primarily because of the need for low heat flux in the high-temperature panels and to ensure a low pumping power requirement and good T/H stability over a wide load range. The selected absorber configuration ultimately embodied all these factors.

At SNLL's request, we investigated overnight drain and either preheat with the aperture door closed or preheat with heliostats (no door required) before fill and start-up. The analysis indicated that, by utilizing the heliostat field to preheat the panels, a start-up delay of 19 minutes and thus a loss of 1.3 percent of the annual collected energy would result, compared with a saving of 0.7 percent in auxiliary electricity if the receiver were not heated overnight. The major impact on annual energy will be caused by time lost from

either door problems in the heated case or fill problems in the unheated case. While door reliability/availability has not been assessed, the panel preheat analysis has shown that substantial differences in panel temperatures are likely for a partial cavity configuration and that a slow and careful heat-up will be required to preheat the panels in a safe manner. The complexity of this procedure is such that its application to commercial practice is questionable. In addition, some fraction of operating time beyond initial morning hours may be lost as a result of inability to fill. Final resolution of this trade-off study appears to depend on the reliability and cost of the aperture door. In this study we decided to use the door/no-drain/heated option and proceed with the effort to generate a detailed door design and cost estimate. These data, along with door reliability data from Phase 2, will be used to reevaluate this trade-off for future commercial receiver designs.

1.2.2 Selected Configuration

The cavity configuration was selected primarily to minimize thermal losses during operation and overnight or cloudy-day shutdown. It is a partial cavity absorber with 20 vertical up-flow panels (Figure 1.2). This arrangement combines high performance with low-cost fabrication and construction based on modular replaceable panels. There are 18 internal panels and two semi-external "wing" panels--one on each side of the aperture at an angle of 45 deg to the aperture plane. Because they are low-temperature panels, the wing panels reduce spillover without major increases in losses.

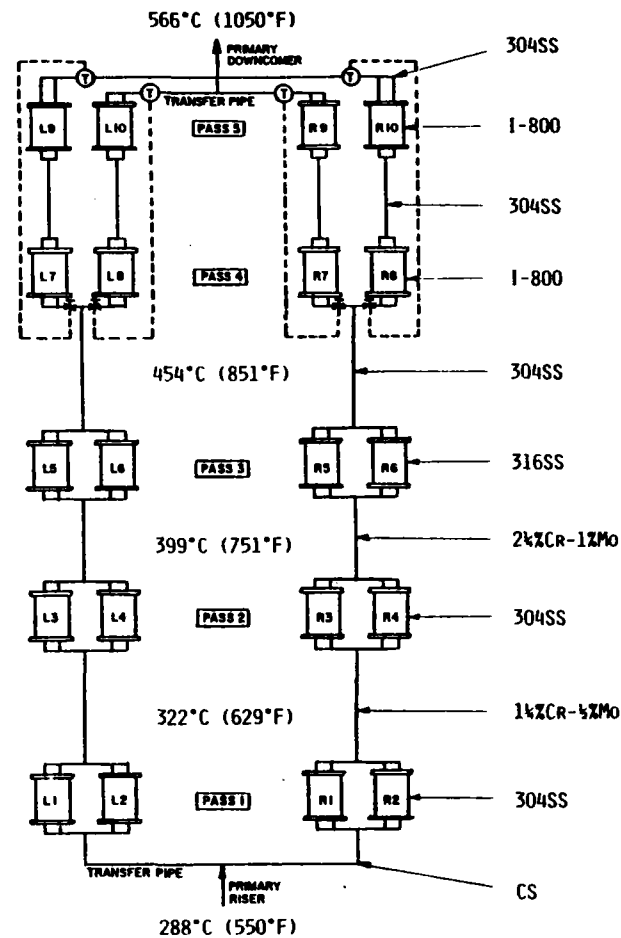
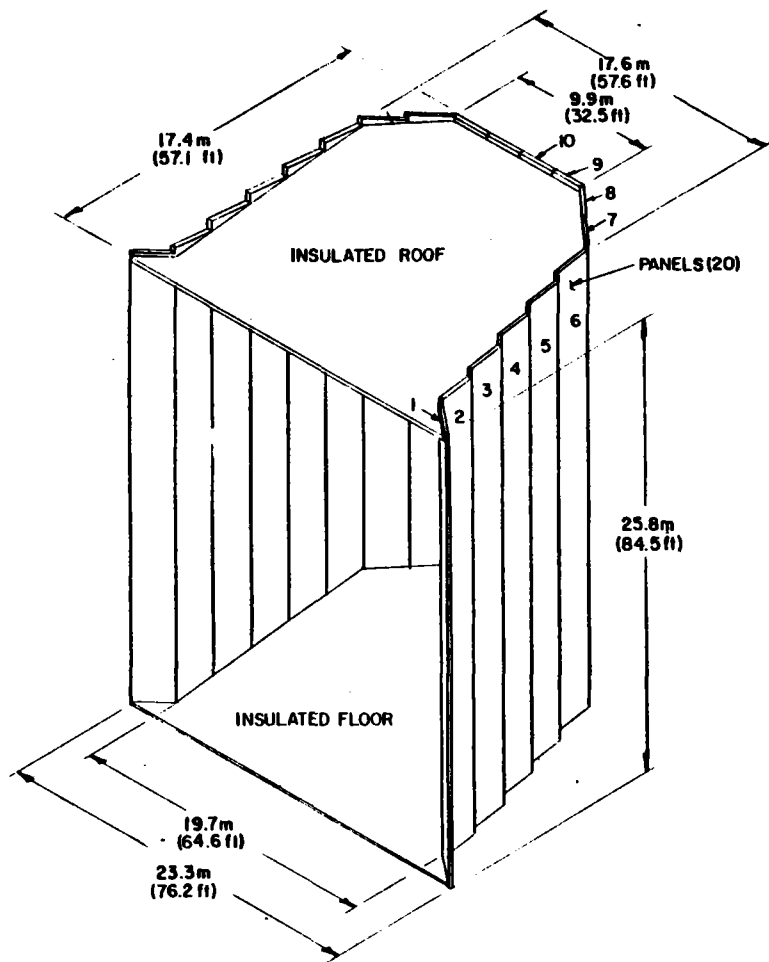


Figure 1.2 Absorber Isometric and Circuitry

The receiver feed pump arrangement--three half-capacity pumps (two operational and one spare)--was chosen on the basis of reliability and to minimize auxiliary power--especially at the low loads common during early morning and evening operation.

Primary requirements for the door include good sealing to minimize heat loss through air convection, rapid closing (by gravity) to protect the absorber in the event of loss of salt flow and the inability to defocus the heliostat field because of either power or control system failures, and ability to withstand incident flux in the closed position without permanent damage. We selected a fast-closing two-section door that could close either mechanically or by gravity.

The criteria most important in the evaluation of the overnight conditioning approach were cost, reliability, ease of installation, and maintenance. The selected approach utilizes an aperture door with double seals, radiant cavity heaters, trace heating of all salt piping, and thermal energy from the Outlet Surge Tank (OST). Radiant heaters were selected because of operating simplicity, low capital cost, and inherent redundancy in the modularity of the units. This approach was selected because it offers the greatest flexibility, provides for morning start-up without heliostat preheat of the panels, and provides for receiver protection in the event of a power failure, using the aperture door.

Receiver protection included considerations of redundancy, use of proven components, and cost. Features include 1 minute of emergency salt flow from the

pressurized Inlet Surge Tank (IST), rapid heliostat field defocus, diesel generator backup power, aperture door with sacrificial ablator on the outside, and three half-capacity pumps that will permit operation to continue if one pump fails.

The most serious failure is the loss of salt flow to the absorber panels under solar incident flux, which could result in tube failure, warping, or reduction in panel life. In this case, the heliostats must be defocused from the receiver while the emergency flow supply from the IST maintains some coolant flow. As long as the collector field can operate, such an approach is adequate; however, if the heliostats cannot be defocused because of either power or control system failures, the length of time required for the earth to rotate to reduce incident fluxes is too long to prevent damage to the absorber panels. Protection during this combination failure is provided by the quick-closing door with ablative face and emergency salt flow from the pressurized IST.

A concrete tower was selected because of its lower capital and maintenance costs.

1.2.3 Materials Selection

The material for the absorber panels and headers was selected after a review of high-temperature mechanical properties and a number of SNLL's corrosion testing programs. These tests determined the degrees of susceptibility of various alloys to general corrosion and stress corrosion in a molten salt environment.

Uncertainty regarding creep-fatigue data exists not only for molten salt receivers but for all types of solar receivers. Lack of appropriate data will create uncertainty in the life of the receiver components, especially the absorber panels. Extensive creep-fatigue tests with hold times of 1 to 6 minutes on tubes of various materials in a molten salt loop are recommended. However, while these tests would be very useful in the long term, data would not be generated in time to meet the schedule for this program. In our opinion, the best alternative would be to design the receiver so that panels or individual tubes can be replaced easily and to accept the fact that tube life in certain critical, high-temperature zones in the receiver might be less than the desired design life.

In view of these considerations and to meet the 30-year design life requirement, Incoloy 800 material was selected for the high-temperature absorber panels. The Incoloy 800 was selected over the austenitic stainless steels because it is much stronger at elevated temperatures and has good low-cycle fatigue strength and ductility. Type 316SS could have been used in the high-temperature panels, but our analysis indicated that it would not meet the 30-year design life. For the low- and medium-temperature panels, Types 304SS and 316SS alloys were selected.

For panel modularity, which would minimize the number of spares required by the utility, one option was to have all absorber panels made of Incoloy 800. The other option was to have identical panels made of different materials: Types 304SS and 316SS and Incoloy 800 for the low-, medium-, and high-temperature panels respectively. Because the "all-Incoloy 800"

option imposes a very high cost penalty, we selected the "multiple materials" option--panels identical in all respects but materials. Thus the utility can still have a minimum number of spares made of Incoloy 800 to use as a replacement for any receiver panel.

As shown in Figure 1.2 the panel tubes are Type 304SS for Passes 1 and 2, Type 316SS for Pass 3, and Incoloy 800 for Passes 4 and 5. The inlet transfer pipe, primary riser, and cold surge tank are carbon steel. The outlet transfer pipe, primary downcomer and hot surge tank are Type 304SS. Downcomers between passes are 1-1/4%Cr-1/2%Mo for Pass 1, 2-1/4%Cr-1%Mo for Pass 2, and Type 304SS for Passes 3 and 4.

1.3 RS DESIGN ANALYSIS

The conditions to which the molten salt RS is designed are defined in the RS Requirements Specification, which was prepared based on the requirements in the revised specification from Task 1, the data obtained in the literature review, and the experience of the team members. It was updated at the end of Task 3 and was compiled in final form at the end of Task 4. The document defines the following:

- RS scope
- Applicable codes and standards
- Technical requirements
- Interface requirements
- Environmental requirements.

The design conditions are summarized in Table 1.2.

1.3.1 Design Point

Since the best collector field performance occurs at or near noon on February 19 (day 50 in DELSOL numbering), we selected this time as the design point. Maximum performance on February 19 rather than winter solstice (best field cosine time) results from decreased shadowing and blocking losses, which more than compensate for the reduction in field cosine.

RS operation without defocus was limited to 1000 W/m^2 ($317 \text{ Btu/h}\cdot\text{ft}^2$). This limit results from analysis of 4 years of detailed direct normal insolation data for Barstow. These data show that, on the average, only 12.5 percent of the days have insolation above 1000 W/m^2 ($317 \text{ Btu/h}\cdot\text{ft}^2$), whereas over

Table 1.2 RS Design Data Summary

Reference site	Barstow, California
Configuration	Partial cavity. Replaceable modular panels (20). All up-flow panels. Gravity-closing aperture door.
Aperture midpoint elevation	216 \pm 1.0 m (709 \pm 3.3 ft)
Heat-transfer fluid	Molten nitrate salt
Service life	30 years
Availability and reliability	0.95, exclusive of insolation
Maximum transportation length	35 m (115 ft)
Design point	Noon, February 19 (Day 50)
Design point insolation	950 W/m ² (301 Btu/h \cdot ft ²)
Maximum insolation	1000 W/m ² (317 Btu/h \cdot ft ²)
Absorbed power	320 MW (1092 \times 10 ⁶ Btu/h)
Minimum absorbed power at rated conditions	80 MW (273 \times 10 ⁶ Btu/h)
Maximum incident flux	0.65 MW/m ² (0.206 \times 10 ⁶ Btu/h \cdot ft ²)
Salt flow rate	760 kg/s (6.018 \times 10 ⁶ lb/h)
Salt inlet/outlet temperature	288/566°C (550/1050°F)
Overnight salt temperature	288°C (550°F)

50 percent of the days have insolation above 950 W/m^2 ($301 \text{ Btu/h}\cdot\text{ft}^2$), and none have insolation greater than 1069 W/m^2 ($339 \text{ Btu/h}\cdot\text{ft}^2$).

Results of a preliminary trade-off between the energy gained by increasing receiver size to accept higher powers and additional annual energy and the energy lost from increases in receiver losses because of its larger size indicated that the trade-off is very close between 950 and 1000 W/m^2 (301 and $317 \text{ Btu/h}\cdot\text{ft}^2$). Because of the potential for operating errors and the reliability of measured insolation, 950 W/m^2 ($301 \text{ Btu/h}\cdot\text{ft}^2$) was chosen as the design point for a first-of-a-kind plant.

As a design margin, peak tubewall temperatures for stress analysis were also calculated at the maximum insolation conditions-- 1000 W/m^2 ($317 \text{ Btu/h}\cdot\text{ft}^2$).

1.3.2 Thermal/Hydraulic Design Analysis

The major T/H design analysis tasks were:

- Steady state
- Thermal conditioning
- Transient
- Performance

The T/H analysis was based on the revised molten salt properties received from SNLL during Task 3. At the design point heat flux, receiver power output is 320.04 MW ($1092.04 \times 10^6 \text{ Btu/h}$). Performance calculations show that the required receiver output to meet the RS rated power of 320 MW ($1091.88 \times 10^6 \text{ Btu/h}$) is 318.3 MW ($1086.08 \times 10^6 \text{ Btu/h}$); the difference is made up by 1.7 MW ($5.8 \times 10^6 \text{ Btu/h}$) of viscous dissipation in the downcomer and drag valve.

The maximum absorbed heat flux and peak front-to-back tube ΔT --0.614 MW/m² (195 x 10³ Btu/h·ft²) and 153°C (275°F) respectively--occur in the center tube of Panel 4, Pass 2. The peak tubewall (O.D.) and salt film (I.D.) temperatures--633°C (1171°F) and 601°C (1114°F) respectively--occur in the left tube of Panel 9, Pass 5 (Figure 1.3). At this location the absorbed peak heat flux is 0.381 MW/m² (121 x 10³ Btu/h·ft²). Thus the recommended maximum salt film (I.D.) temperature--593°C (1100°F)--is exceeded in Pass 5.

At the point of maximum salt film (I.D.) temperature, the salt bulk temperature is 554°C (1029°F), which results in a salt ΔT (I.D. temperature minus bulk temperature) of $\approx 47^\circ\text{C}$ ($\approx 84^\circ\text{F}$). To meet the recommended maximum, we will

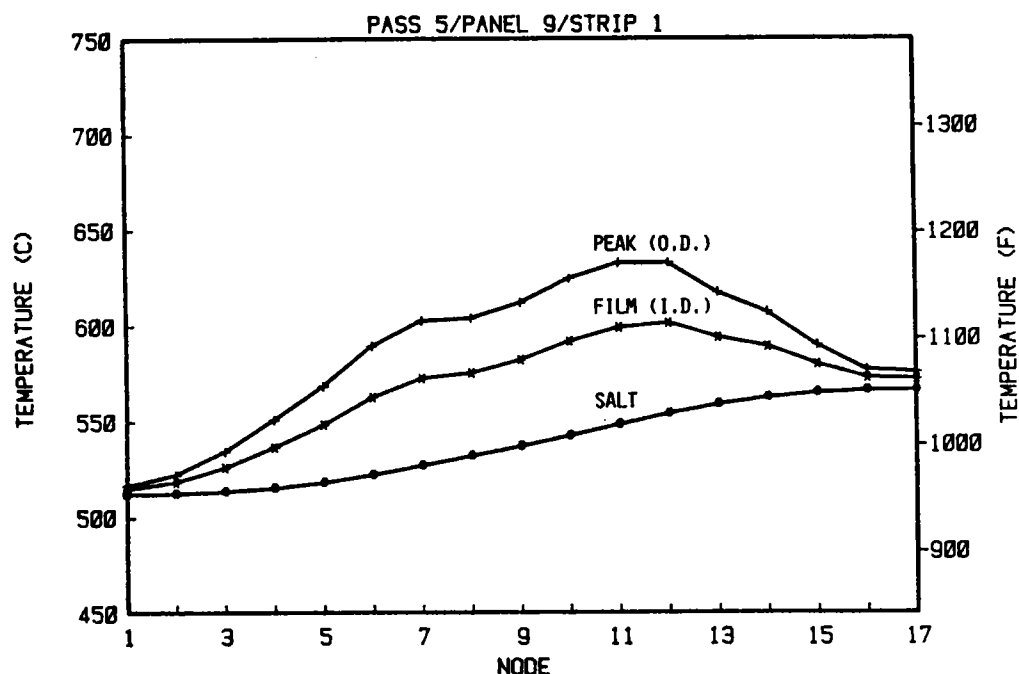


Figure 1.3 Temperature Profile of Absorber Hottest Tube

have to reduce the heat flux at this location by about 17 percent--a reduction that could be difficult to achieve within acceptable cost limits.

Experimental programs at Olin show that some alternatives exist that should solve the salt decomposition problem, such as physically adding nitrates or oxidizing the nitrites to nitrates to restore the original salt composition. These molten salt stabilizer research methods have been demonstrated by Olin under laboratory test conditions, but further testing is required under conditions at pilot plant scale.

The quantity of salt exposed to this temperature is only a small fraction of the total salt flow rate, and it is exposed for only a short period of time because of the velocity of salt through the tubing [about 3 m/s (10.1 ft/s) in the outlet panels] and the resultant turbulent mixing. As a solution, we recommend that the required salt outlet temperature be reduced by 14°C (25°F) to 552°C (1025°F) for the first commercial plant, unless methods to make the salt fully compatible with the higher temperature limit have been fully demonstrated by that time.

The sensitivity of salt flow and of salt outlet and tubewall temperatures to variations in heat flux across the panels was investigated at full- and part-load conditions at the design point. The results indicate that changes in salt flow rate and outlet temperatures for the worst variation in heat absorption (Pass 1) are not significant at or near full load. The coldest tube within that pass has approximately 1.8 percent less flow than the average tube. Consequently, salt flow through the panel tubes is very insensitive to heat flux

variations across the panel width, and each tube within a given panel has essentially the same salt flow rate. This is not the case for 10-percent flow, where the assumption of equal flow per tube is no longer valid. Because of this and the possibility of being in the transition region, we do not recommend operation with less than 25-percent full flow. From 0 to 25 percent is considered start-up.

The RS performance was calculated for both annual average operating conditions and design point conditions. The receiver was analyzed for spillover, reflection, reradiation, convection, and conduction losses; using the results of these analyses, the RS efficiency was calculated. Table 1.3 summarizes the design point and annual average losses/efficiency for the RS.

Table 1.3 RS Performance

	Design Point (MW)	Annual Average (10 ³ MWh)
Incident power at aperture plane	363.3	849
Spillover	-14.7	-34
Reflection	- 6.4	-14
Reradiation	-10.0	-32.1
Convection	-13.6	-42.9
Conduction	- 0.3	- 2.6
Viscous dissipation	+ 1.7	+ 4.0
RS output power at base of tower	320.0	727.4
RS overall efficiency	0.88	0.86

The RS heat loss rate during overnight shutdown with the electric radiant and trace heaters maintaining the salt at 287.8°C (550°F) was calculated as ≈ 560 kW (1.91×10^6 Btu/h) at the design point ambient temperature and wind speed.

Table 1.4 summarizes the T/H data.

1.3.3 Stress Analyses

Those sections of the receiver subjected to radiant heating (i.e., the absorber panels) are the most critical component from the thermal-stress and creep-fatigue points of view. Hence we analyzed the panels extensively to determine the severity of the thermal stresses and their impact on the structural integrity and creep-fatigue life of the receiver.

In the design of the pressure boundary, all requirements of the ASME Boiler and Pressure Vessel Code, Section VIII-Division 1 were satisfied. In addition, because of the highly cyclic nature of receiver operations, the fatigue criteria of Section VIII-Division 2 for temperatures in the sub-creep regime were satisfied. For elevated temperature design, we analyzed for creep-fatigue based on the linear damage addition approach of Code Case N-47. Strict adherence to Code Case N-47, however, is too conservative for solar applications and will result in severe economic penalties. Hence the approach in Code Case N-47 was used with some modifications. One modification that we have proposed for use with solar applications is the use of inelastic fatigue curves (Figure T-1420-1C of Code Case N-47) in conjunction with inelastic strains approximated from an elastic analysis.

Table 1.4 Thermal/Hydraulic Performance Data Summary

Heat-transfer fluid	Molten nitrate salt
Maximum absorbed power	336.8 MW (1149.3×10^6 Btu/h)
Nominal absorbed power	320.0 MW (1092.0×10^6 Btu/h)
Peak absorbed heat flux	0.614 MW/m^2 (195×10^3 Btu/h·ft ²)
Average absorbed heat flux	0.254 MW/m^2 (81×10^3 Btu/h·ft ²)
Design point RS efficiency	0.881
Annual average RS efficiency	0.859
Peak tubewall (O.D.) temperature	633°C (1171°F)
Peak salt film (I.D.) temperature	601°C (1114°F)
Peak front-to-back tube ΔT	153°C (275°F)
Salt flow rate	760 kg/s (6.018×10^6 lb/h)
Salt inlet/outlet temperature	288/566°C (550/1050°F)
Salt Reynolds number, minimum to maximum	34,800 to 114,700
Salt velocity, minimum to maximum	3.0 to 3.4 m/s (9.7 to 11.2 ft/s)
Salt film coefficient, minimum to maximum	5780 to 10,250 W/m ² ·°C (1020 to 1800 Btu/h·ft ² ·°F)
Receiver frictional Δp	1517 kPa (220 lb/in ²)
Feed pump inlet pressure	345 kPa (50 lb/in ² g)
Feed pump outlet pressure	6895 kPa (1000 lb/in ² g)
Inlet surge tank operating pressure	2410 kPa (350 lb/in ² g)
Outlet surge tank operating pressure	103 kPa (15 lb/in ² g)

We estimated the creep-rupture life using the rupture life curves of Code Case N-47. However, only the pressure stresses (as opposed to thermal plus pressure stresses as recommended in Code Case N-47) were used in evaluating the rupture life. We added the creep and fatigue damage fractions and limited this value to 1. This analysis showed the receiver life requirements were satisfied for diurnal and cloud cyclic operation.

With regard to material properties, both Types 304SS and 316SS are qualified materials under the Code, and their creep and fatigue properties are well documented. Although Incoloy 800 is an accepted Code material, the Code does not list its creep and fatigue data. However, the Code has rupture life and allowable cycles graphs for Incoloy 800H. Because the material properties are very similar for Incoloy 800 and 800H at the absorber panel design temperatures, the creep-fatigue data for 800H were used.

Transient temperature distribution and stress analyses were done for the receiver panels for several start-up and shutdown transient conditions. Essentially, five transients were evaluated:

- Morning hot start-up
- Noon hot start-up
- Hot shutdown
- Emergency shutdown
- Cloud-cover

Of the three locations chosen for creep-fatigue evaluation (Pass 2--Type 304SS, Pass 3--Type 316SS, and Pass 4--Incoloy 800), we selected Pass 2 and Pass 4 for transient analysis. We did not perform the analysis for Pass 3 because the

effect of transient stresses is primarily on fatigue, and Pass 2 fatigue conditions are more severe than those in Pass 3. [The fatigue properties of Type 304SS (Pass 2) and Type 316SS (Pass 3) are identical.]

At no time during the transient event do the tubewall temperatures and ΔT s--and thus the stresses--exceed the corresponding steady-state values.

1.3.4 Mechanical Design Analysis

The major mechanical design tasks were:

- Absorber panels
- Surge tanks and interconnecting piping
- Absorber door
- Receiver structure
- Tower and tower foundation
- Riser and downcomer piping

Component-level drawings were prepared in sufficient detail to allow preparation of RS fabrication and construction/erection plans and cost estimates.

The RS mechanical design was performed in accordance with the RS Requirement Specification. All pressure parts were designed in accordance with the ASME Boiler and Pressure Vessel Code. The structural analysis complies with all the requirements of the Uniform Building Code (UBC), the American Institute of Steel Construction (AISC), and all other applicable codes and standards.

The design salt flow rate was used to size the riser/downcomer pipes. It is a conservative assumption, since the average salt flow rate will be less than the design value. The primary riser was sized to minimize combined costs for both pumping and piping. The optimum riser size was determined as 0.41 m.

(16 in.) O.D. Since pumping costs are independent of downcomer size, the downcomer was sized to dissipate a large percentage of the gravity head at the design flow rate. A 0.30 m (12 in.) O.D. was selected; it will dissipate ~75 percent of the gravity head by friction. The remainder is dissipated by the drag valve and the field return piping to the Storage Subsystem.

Piping materials were selected based on results of the material selection work. The carbon steel riser carries cold salt at 288°C (550°F). The Type 304SS downcomer carries hot salt at 566°C (1050°F). Piping wall thickness was calculated in accordance with the American National Standards Institute (ANSI) B31.1 Power Piping Code. Insulation thickness was chosen from Foster Wheeler design manuals.

1.3.5 Operation and Control Analysis

Six major operating modes were identified--cold drained, hot drained, hot standby, derated operation, rated operation, and overnight standby--and the transitions between these modes were developed. These transitions are:

- Cold drained to hot drained
- Hot drained to hot standby
- Hot standby to derated operation
- Derated to rated operation
- Overnight standby to hot standby
- Rated operation to derated operation
- Derated operation to hot standby
- Hot standby to overnight standby
- Overnight standby to hot drained
- Hot drained to cold drained

The operating procedures for the RS were specified to aid in the design and selection of the RS control system.

The control system response was analyzed in three sequential stages. The controller was modeled using a state variable representation of an analog controller. During this stage only a 10-percent cloud variation was modeled using back tubewall temperatures for feed-forward information. Subsequent to this analysis, the controller models used in the simulation were updated to represent more accurately the type of controller proposed for the RS. The new controller model simulates a Beckman controller with simple derivative filtering. Using this updated controller model, we addressed both a 10- and a 50-percent cloud and considered both back tubewall temperatures and flux gages for feed-forward information. Because the results were preliminary, a final analysis of a 50-percent cloud was performed.

The results indicate that 50-percent step changes in power level will produce transient temperature variations of approximately $+10/-15^{\circ}\text{C}$ ($+18/-27^{\circ}\text{F}$) damping down to $\pm 3^{\circ}\text{C}$ ($\pm 5.4^{\circ}\text{F}$) in approximately 150 seconds. The flux gage data showed a slight advantage [$\approx 3^{\circ}\text{C}$ ($\approx 5.4^{\circ}\text{F}$) less undershoot in temperature]. Both systems appear promising based on the simulation results. Actual test data will be essential to validate the simulation models for the key physical processes and the simulation results.

1.4 RS SUMMARY DESCRIPTION

The receiver is located south of the heliostat field, atop a reinforced concrete tower. Figure 1.4 shows the front and back views of the receiver; configuration data are summarized in Table 1.5.

The right and left sides of the absorber are symmetrical, mirror images. The panels on each side form two independent parallel-flow circuits. Each circuit comprises 10 panels connected into five passes (Figure 1.2). Upward flow in the panels minimizes the possibility of T/H instability. Four control valves (two per side) maintain the desired outlet temperature by controlling both the amount and distribution of salt flow.

The absorber panels are fabricated in individual modules or subassemblies to facilitate handling during fabrication, shipment, and erection. Panel configuration is basically very similar to that of a typical, conventional utility boiler panel. The panels are made of 88 tubes continuously welded to adjacent tubes with spacer strips to form three solid subpanel sections 28, 32, and 28 tubes wide. Each subassembly--consisting of the panel tubes, inlet and outlet headers, buckstays, support struts, and strongbacks--is shop-built and shipped as a unit. Insulation and sheathing are added during erection. Including insulation, the gross weight of an entire subassembly is 10,900 kg (24,000 lb).

Key features of the absorber panel are:

- Modular shop assembly simplifies transportation, erection, and replacement.
- All panels are identical except for tube/header materials and insulation thickness.

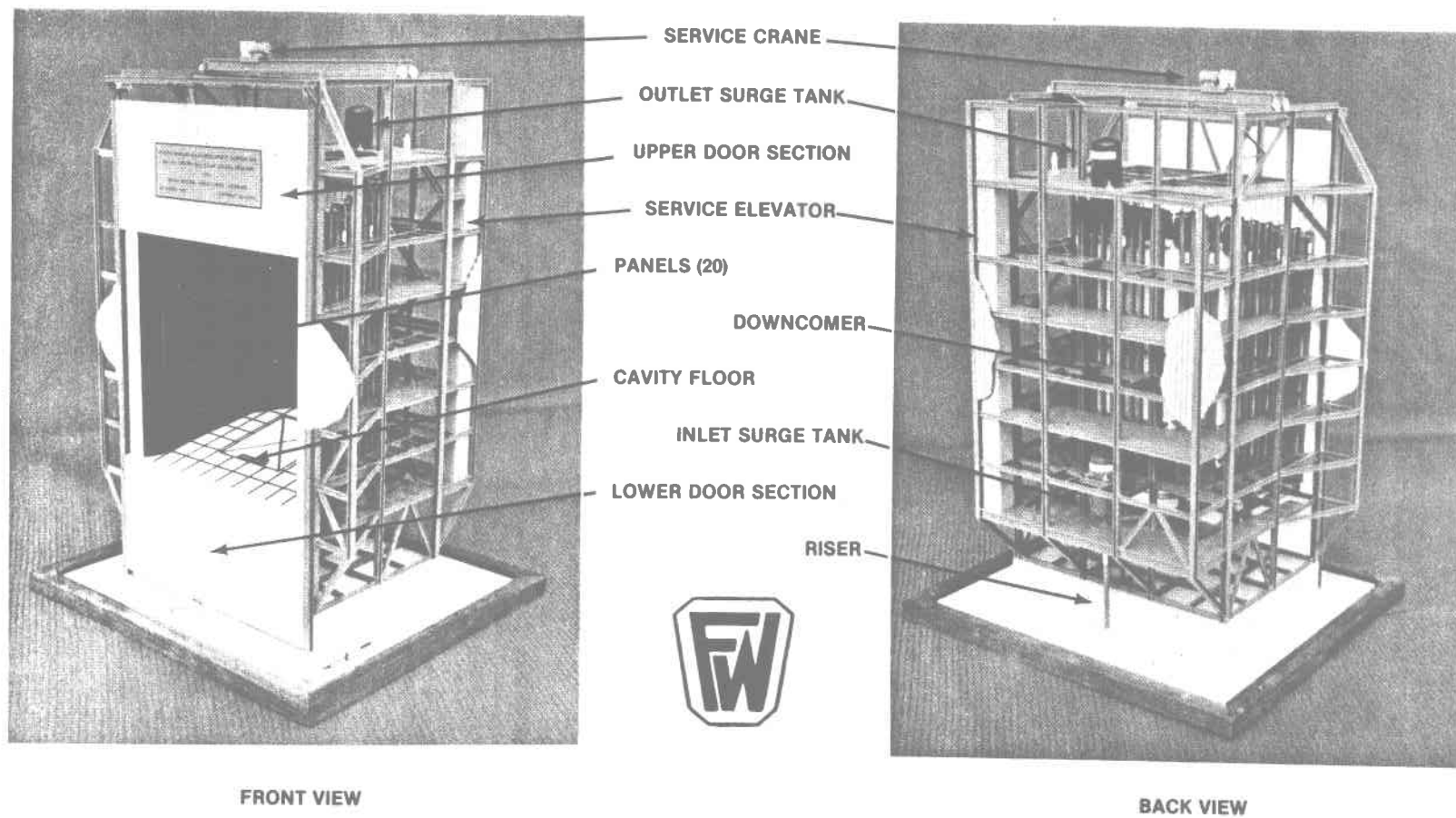


Figure 1.4 320-MW Molten Salt Solar Cavity Receiver

Table 1.5 Configuration Data Summary

Receiver

Overall [height x depth (N-S) x width (E-W)]	55.2 x 25.6 x 32.0 m (181 x 84 x 105 ft)
Cavity (width x height x depth)	19.8 x 25.8 x 17.4 m (65 x 84.5 x 57 ft)
Aperture (width x height)	19.8 x 25.8 m (65 x 84.5 ft)
Aperture area	510.2 m ² (5492 ft ²)
Total frontal area including wing panel	592.2 m ² (6375 ft ²)
Total exposed (active) area	1258 m ² (13,542 ft ²)
Total wet weight	1341 x 10 ³ kg (2950 x 10 ³ lb)

Absorber Panels

Construction type	Continuously welded tubes with a spacer strip between
Tube material	304SS/316SS/Incoloy 800
Number of panels	20
Number of tubes per panel	88
Overall length x width	28.4 x 2.44 m (93.4 x 8.01 ft)
Distance between header centerlines	27.5 m (90.25 ft)
Exposed (active) length	25.8 m (84.5 ft)
Exposed (active) surface	62.9 m ² (677.1 ft ²)
Tube O.D. x wall thickness	25.4 x 1.65 mm (1.0 x 0.065 in.)
Spacer strips, thickness x depth	2.381 x 11.1 mm (3/32 x 7/16 in.)
Design pressure	3463 kPa (350 lb/in ² g)
Panel weight (empty)	10,000 kg (24,000 lb)

- Swing links eliminate frictional restraint of expansion, but provide excellent strength.
- Vertical splits in panel reduce forces required to keep panel straight and in plane.
- Horizontal expansion is controlled by limit stops between buckstays and tube lugs.
- Jumper tubes permit differential thermal expansion.

The cavity floor and ceiling are uncooled surfaces consisting of Fiberfrax Duraboard weatherproof insulation anchored to carbon steel plate. The floor supports radiant heaters for absorber thermal conditioning to prevent salt from freezing during shutdown. The floor and ceiling are made of sections that can be lifted out by an overhead crane. Flexible seals between the floor and absorber panels minimize thermal losses from the cavity.

A skeletal structure supports the absorber and associated equipment. There are two major platform levels (one at the top and one at the bottom) and two intermediate levels. The height of the structure was determined by the travel of the upper door section. A bridge crane runway and machine room for the elevator are located at the top level of the structure (Figure 1.4).

Key features of the receiver structure are:

- Four major support columns that comprise part of the four major braced bents
- Bent arrangement that minimizes torsional loading on rear of structure
- No obstruction to lifting and positioning of panel modules
- A service crane to complete receiver installation when basic structure is erected.

One of the major advantages of our design is the ability to remove complete panel modules for maintenance. The 15-ton overhead crane can travel across the receiver, remove sections of the roof and floor, pick up any panel/strongback module, and lower it through the center of the receiver and tower to the ground. The overhead crane can also be used during construction, as soon as the structure is erected. During receiver operation the crane will be stored in the rear of the structure, away from the hot air coming from the cavity aperture.

The aperture door is a two-section guillotine-type with a hollow core for heat dissipation within the door structure to prevent it from warping. It minimizes thermal losses when the receiver is not in operation and protects the receiver in the event of feed pump or power failure. Each section of the door spans the receiver aperture horizontally. When the door is opened and closed by a cable drum-type hoist mechanism, the sections move up and down parallel to the receiver aperture on vertical tracks. The lower section counterbalances the upper section, minimizing the power required for opening and closing it. The two sections are similar in construction, but the upper section is larger and heavier to permit closing by gravity in the event of a power failure. The aperture side of the door is faced with a layer of Fiberfrax blanket insulation. The front side is protected by a layer of ablative material to protect the door (and the absorber) during an emergency until the motion of the earth moves the incident solar flux away from the receiver or the heliostats are otherwise defocused.

Key features of the door are:

- Fabricated truss plus corrugated sheet surface give light and rigid door.
- Maximum free area through door structure assists convective cooling of door.

- Four-point spherical bearing attachment to trolleys eliminates binding as a result of distortion.
- Double seal minimizes convection losses when receiver is "bottled up."
- Short and direct load path exists from door rails to structural steel.
- Operation is simple and reliable compared with multiple-section or "up and over" doors.

The receiver tower is a slip-formed, reinforced-concrete structure rising 193.7 m (635.5 ft) above ground level. The tower contains an internal elevator, lightning protection equipment, aircraft warning lights, and receiver auxiliary machinery. The primary salt riser and downcomer are supported along the inside of the tower shell with expansion loops at appropriate intervals.

The energy transport loop consists of the primary riser, the primary downcomer, IST, OST, the receiver feed pumps, valves, and associated instrumentation. All energy transport loop equipment is fully drainable, heat traced, and insulated.

Figure 1.5 illustrates the overall flow schematic. Cold salt at 288°C (550°F) is pumped from the Cold Storage Tank (CST) through the field supply piping and tower riser to the receiver. At the inlet to the receiver, the salt flow is divided in two, one stream for each half of the absorber. Each proceeds through 10 panels in both series and parallel paths, heating in the process to 566°C (1050°F). The hot salt then flows by gravity through the tower downcomer, drag control valve, and field return piping to the Hot Storage Tank (HST). Downcomers are provided after each pass through a panel or set of panels so that all panels have upward flow. Separate control valves

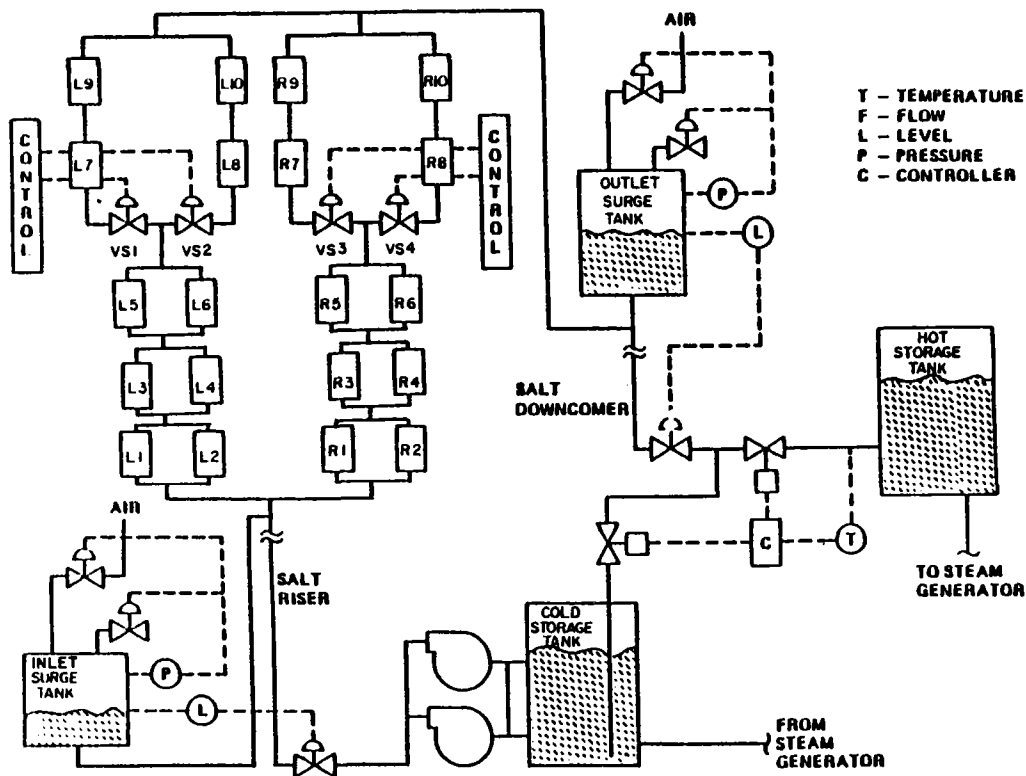


Figure 1.5 RS Flow Schematic

downstream of Pass 3 control the outlet temperatures of Passes 4 and 5 by distributing the flow in proportion to the absorbed power. In addition to outlet temperature data, flow control uses feed-forward information on input power changes (either flux gage data or temperature data) to anticipate rapid flow changes required during partly cloudy conditions.

Figure 1.5 also illustrates the relationship of the surge tanks to the receiver circuitry. The IST and OST atop the tower buffer the faster acting control valves from the slower responding salt pump and drag control valves. Level sensors on these tanks control the feed pump recirculation valve and the

drag valve at the bottom of the downcomer. Tank levels are set at one-half to provide a control margin and a ready supply of salt. The pressurized IST provides an emergency salt flow to protect the receiver in case of feed pump or power failure. The OST connected to the primary downcomer is located above the highest absorber panel header for positive filling of the absorber panels and piping. Compressed air for the surge tanks is supplied by an air compressor and storage tank located at the base of the tower.

1.5 PANEL FABRICATION DEVELOPMENT

Welding development was undertaken to resolve fabrication issues and to develop basic methods for continuous longitudinal welding of thin-walled tubes to form flat panels and for attachment of support lugs to the panels.

A semiautomatic short-circuiting arc (dip transfer) metal inert gas (MIG) welding process was chosen for longitudinally welding tubes to form a panel. This process was chosen because of its ability to produce sound welds in thin sections with minimal tubewall penetration.

A MIG welding head (Figure 1.6) was designed and fabricated to feed a consumable bare electrode into the weld zone at a constant rate and supply a continuous blanket of inert gas to shield the weld zone from atmospheric contamination. As shown in the figure, the welding head was mounted on a horizontal cross-beam carriage. A drive mechanism moved the head along the carriage at a constant, predetermined rate.

For trial welding, we bolted a series of scalloped support blocks to a rigid, flat table. These blocks supported three tubes on the table at 0.15-m (6-in.) intervals. Pneumatically activated toggle clamps (also shown in the figure) held the tubes firmly on the support blocks and prevented them from moving during welding. The clamps were automatically activated to open at each clamp site as the welding head traversed the length of the tubes.

Several trial welds were made to determine the best tube-to-tube longitudinal weld configuration. They indicated the need for a spacer strip.

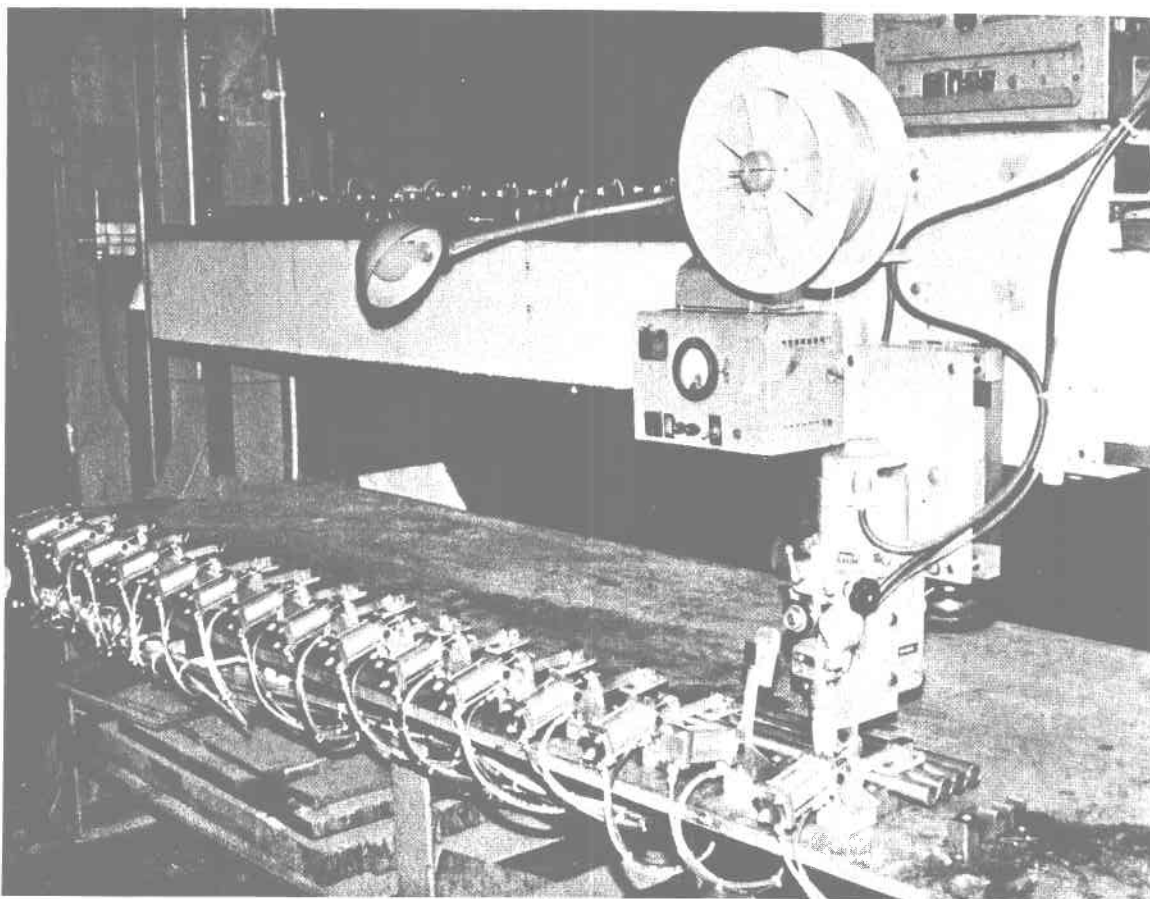


Figure 1.6 Overall View of Welding Set-Up Showing the Welding Head, Wire Reel, Controls, Cross-Beam Carriage, and Pneumatically Actuated Toggle Clamps

Several thicknesses of strip were considered and parametrically studied for thermal stresses. The results of the study indicated that a spacer strip 2.38 mm (3/32 in.) thick was best (Figure 1.7).

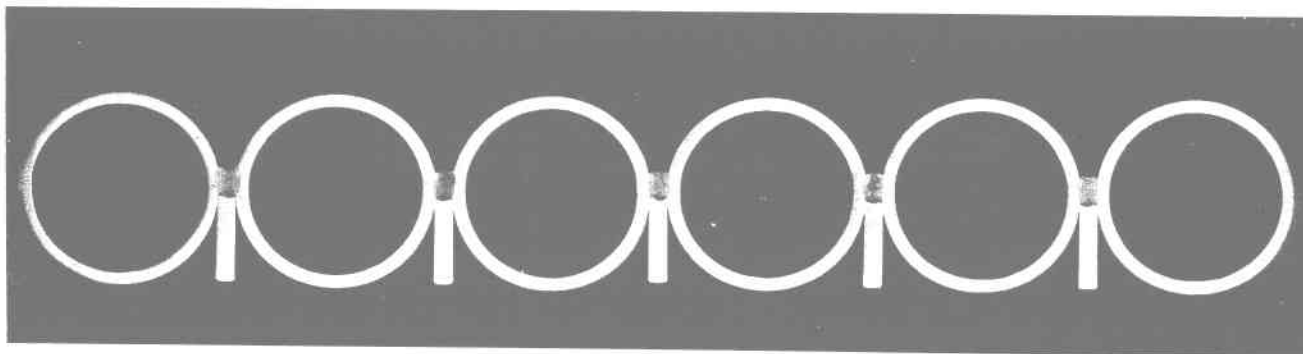


Figure 1.7 Cross Section of Welded Panel Tubes

Three 2.44-m (8-ft)-long development panels, 28 to 31 tubes wide, were fabricated using prototypical tubes. The first panel was fabricated from 25.4-mm (1-in.)-dia x 1.65-mm (0.065-in.)-wall thickness, Incoloy 800 seamless tubing and a 2.36-mm (0.093-in.) wide x 3.18-mm (1/8-in.) deep, rectangular, Incoloy 800 spacer strip. The fixture for welding the tubes was essentially the same as that used for trial welding. Scalloped support blocks with rectangular grooves for the spacer strip were spaced 0.15 m (6 in.) apart. Pneumatic clamps and end clamps restrained the tubes. Weights and 'C' clamps kept the in-process panel flat. Using welding parameters developed from trial welds, two-tube subassemblies were fabricated; these subassemblies were then joined to form a panel 30 tubes wide. A 31st tube was added separately.

Two major problems were encountered during this panel fabrication. First, the spacer strip often bowed in the vertical plane during welding, causing erratic welding behavior and also contributing to panel distortion. The second problem was differential expansion of adjacent tubes during welding, which contributed significantly to in-plane distortion in the form of "hour-glassing" (i.e., the panel was narrower at the midpoint than at the ends).

Aside from several fabrication changes, the second development panel was fabricated of the same materials and in the same manner as the first panel. The changes were intended to eliminate spacer strip bowing and to eliminate, or at least significantly reduce, the differential expansion of adjacent tubes. These fabrication modifications were partially successful; spacer strip bowing still occurred occasionally; panel distortion was decreased, but was still considered too great.

The third and last development panel was 28 tubes wide and was constructed of Type 304SS welded tubing of prototypical size and wall thickness and an 11.11-mm (7/16-in.)-deep x 2.34-mm (0.092-in.)-wide, rectangular, spacer strip, Type 304SS. We had to use Type 304SS in lieu of Incoloy 800 because of an unacceptable procurement delay for Incoloy 800 tubes and strip. Spacer strip depth was increased to retard bowing; the added mass reduced the differential expansion between the tube and the spacer strip and the added depth stiffened the strip in the vertical plane.

Distortion was eliminated by welding two-tube subassemblies, welding these into four-tube subassemblies, and then welding the four-tube subassemblies to

make up the 28-tube panel, thus maintaining symmetry in the process. In addition, the fixture for the third panel was modified and made more rigid to reduce panel distortion. No serious problems were experienced during the fabrication of the third panel (Figure 1.8). The strip bowing problem previously encountered was completely eliminated. Out-of-plane distortion was reduced considerably, and no measurable in-plane distortion was present.

We evaluated three methods for attaching support lugs to the panel (Figure 1.9). The first utilized integral welding of the lug and tubes--the lug legs replaced a section of the spacer strip. In the second, lug legs were butt-welded to the top of the spacer strips. In the third, the lug legs were placed inside and in contact with two adjacent spacer strips and were fillet welded to them. The third method was selected because it is easier to position and to weld.

Weld quality, tubewall penetration, and overall weld geometry were continuously monitored during trial welding and development panel fabrication by both destructive and nondestructive tests and examinations.

Strength tests were conducted at ambient temperature on specimens removed from the first development panel. The tests were designed to subject the specimens to loading and bending conditions exceeding those anticipated during normal panel operation. No cracks occurred in the welds or tubes. These tests showed that the tube-to-tube longitudinal welds were at least as strong as the tubes themselves.

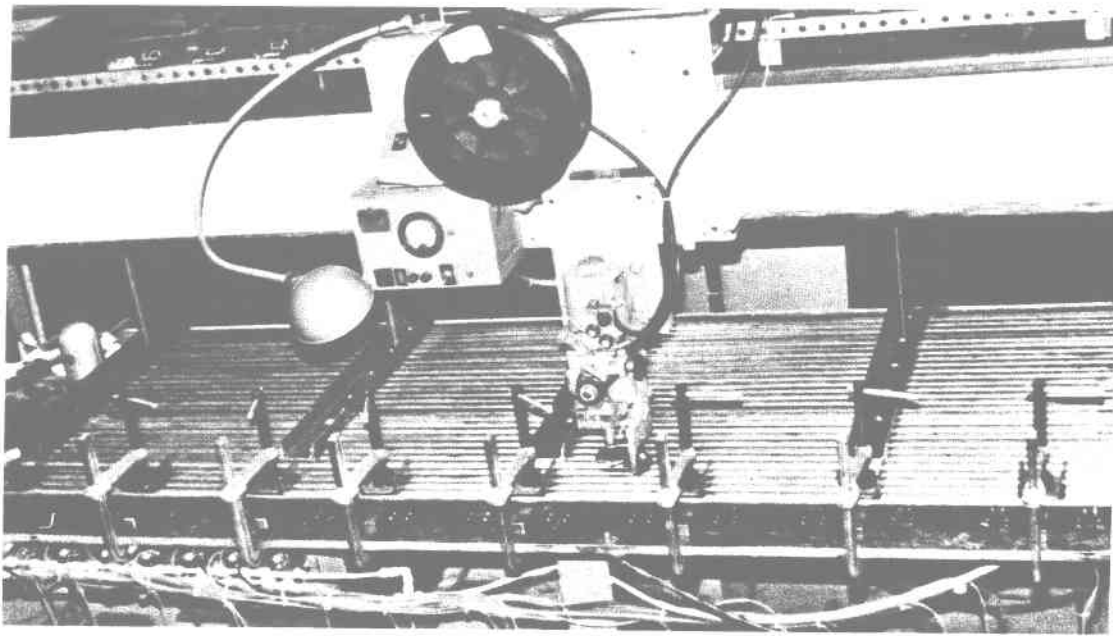


Figure 1.8 Welding of Third Development Panel

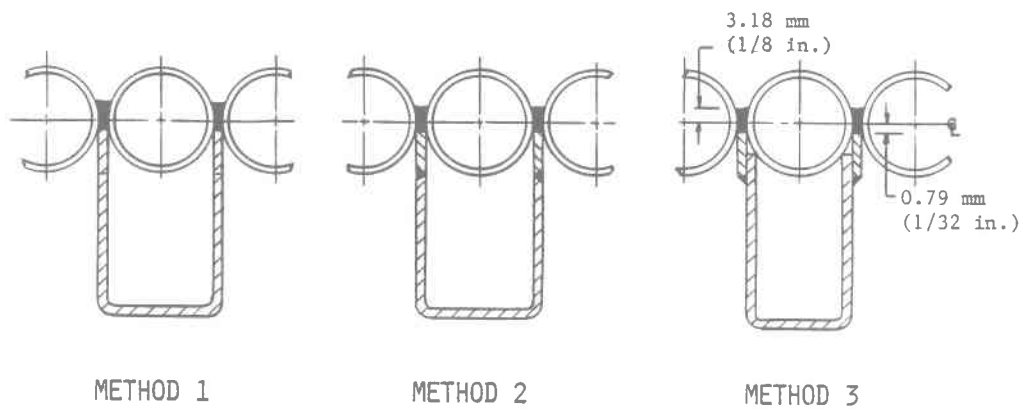


Figure 1.9 Support Lug Attachment Methods

Two prototypical panel lugs were subjected to a tensile strength test to show that the lug design would prevent tube distortion under maximum design load conditions and to determine the maximum load-carrying capacity of lugs and attachment welds. They successfully withstood loading to ≈ 32 times their design load.

Weld repairs were performed on 30.5-mm (1-ft)-long two-tube welded specimens prepared from Type 304SS tubes and spacer strip and Inconel 82 electrode. Repair welds were made using the same cross-sectional geometry, parameters, and fixtures employed to fabricate Panel 3, except that the original roller guide was replaced with a roller guide without a protruding lip. However, rewelding at these settings tended to distort the tubewalls, causing them to bow inward. Repair welds were made with a slightly colder setting (lower voltage) than used originally to minimize distortion.

Weld repairs should not be difficult provided the cavity created when the weld is removed is fairly precise dimensionally and the cavity is thoroughly cleaned. Weld repairs should be performed while the in-process panel is still in the welding fixture. A milling machine could be adapted to ride on the same cross-beam carriage as the welding head. The welding head used to make the original weld could also be used to make the repair weld with minimum modification.

Figure 1.10 shows the finished third development panel.

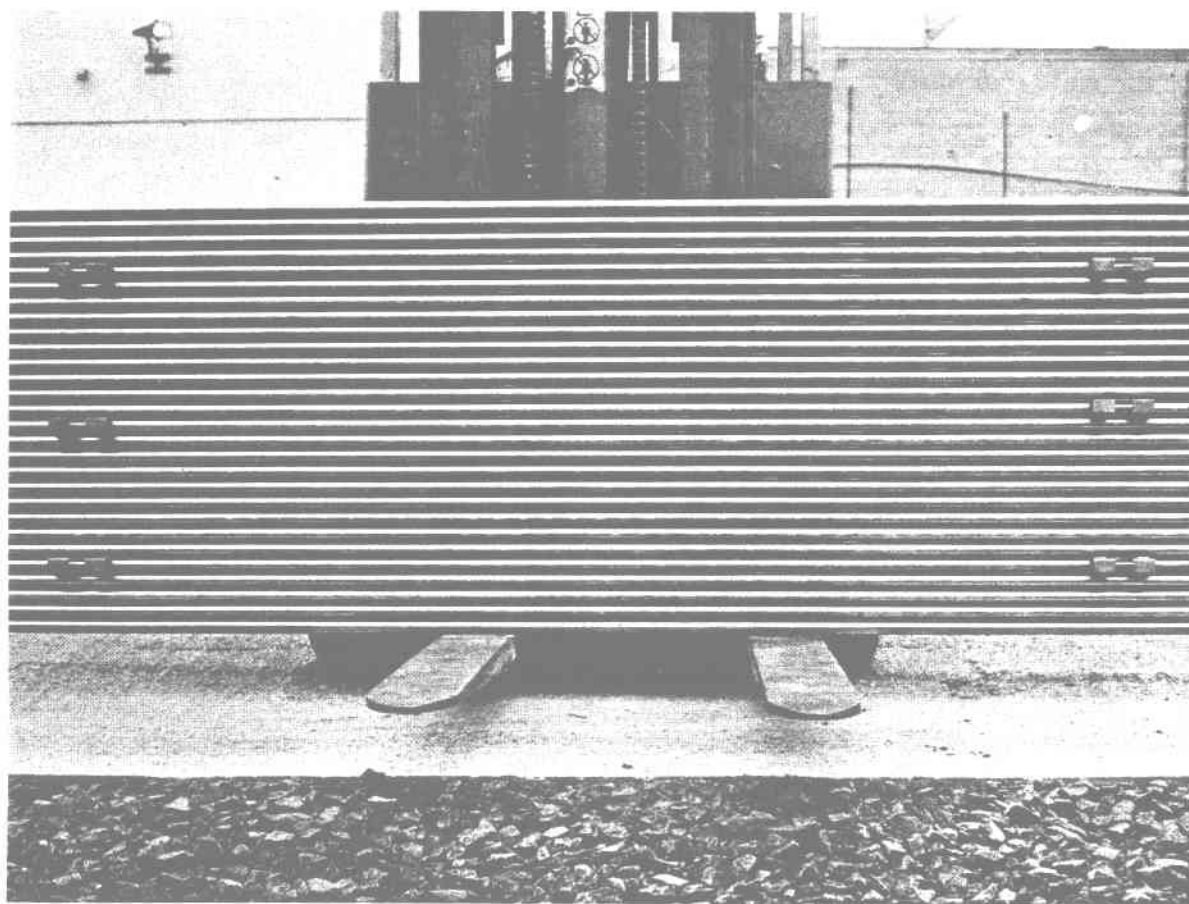


Figure 1.10 Third Development Panel Showing Support Lugs at Each End

1.6 WEIGHT AND COST ESTIMATES

The receiver weight breakdown--including salt and all components located above the tower--is shown in Table 1.6. Table 1.7 gives construction cost estimate in 1982 dollars for the complete RS including the receiver, concrete tower, riser and downcomer piping, feed pumps, and ancillary equipment.

Table 1.6 Receiver Weight

	Weight	
	<u>10³ kg</u>	<u>(10³ lb)</u>
Absorber panel modules	109	240
Roof and floor	65	144
Casing and insulation	93	204
Aperture door	109	240
Piping	50	110
Salt and air storage tanks	57	126
Controls and miscellaneous equipment	25	56
Platforms and ladders	173	380
Structural steel	327	720
Overhead crane	50	110
Normal charge of salt	<u>282</u>	<u>620</u>
Total estimated receiver weight (wet)	1341	2950

FOSTER WHEELER SOLAR DEVELOPMENT CORPORATION

REF.: 84-2292C
DATE: November 1982

Table 1.7 Construction Cost Estimate (\$ 1982)

Excavation and civil	53,200
Tower and foundation	5,373,400
Structural steel	1,277,500
Machinery and equipment	10,743,700
Piping and valves	2,930,700
Electrical	308,100
Instruments	620,100
Painting and insulation	588,300
Direct field costs	<u>21,895,000</u>
Indirect field costs	437,700
Total field costs	<u>22,332,700</u>
Total office costs	<u>2,283,000</u>
Total field and office costs	24,615,700
Contingency	3,047,300
Fee 8%	<u>2,213,000</u>
Total construction cost	29,876,000

1.7 RECEIVER DEVELOPMENT

The major development issues for the molten salt receiver cover four broad areas:

- Design
- Performance
- Operation
- Molten salt and receiver technology

A considerable amount of development activity has been devoted to these issues and, based on these activities, a molten salt receiver can be designed, constructed, and operated. However, residual risks remain relating to absorber panel design, fabrication, and lifetime; receiver operation, availability, and maintenance; receiver performance and auxiliary power use; molten salt stability and corrosion; and creep-fatigue design requirements.

During Task 7 the verification status was reviewed, and verification options identified and correlated with the verification issues. Based on these reviews and a review of test capabilities and requirements, test programs for each of the major verification options and the risk reductions resulting from these programs were identified. Finally, a baseline test program with several options was proposed.

Candidate test program options include the following tests at Central Receiver Test Facility (CRTF) using the basic salt loop elements (with appropriate modifications) of the Molten Salt Electric Experiment (MSEE):

- Absorber Panel Test--of relatively short duration to verify the panel structural design and support system under realistic flux/temperature conditions.

- Cavity Test--would follow the panel test and be longer. It would investigate RS operability and utilization of available sunshine, overnight conditioning and door operation, outlet temperature control, receiver auxiliary power use, performance, and availability. Figure 1.11 gives the proposed SRE cavity configuration.
- Salt Loop Irradiated Panel Test--would be a small sub-loop of the MSEE and would have the capability for radiant heating of small test panel sections to investigate high bulk temperature/flux level phenomena in a tightly controlled environment.

In addition to these CRTF tests, a scale model section of the aperture door should be constructed and tested in an appropriate test facility. This test should include extensive thermal cycling of the door, seals, and trolley mechanism.

The cavity test was given first priority because it is the most comprehensive of the tests and it offers important information relating to operability and usability of insolation and receiver salt control experience--especially verification of physical modeling of salt flows. Additional data relating to aperture door and overnight conditioning, performance, and auxiliary power use will also be obtained; however, because of the limitations of instrumentation and scale, these data will provide verification of analysis methods more than verification of design.

The absorber panel test is second in priority because it will provide a meaningful scale test of the panel and its support structure and, by preheating the inlet salt, it is possible to operate the panel over the entire panel operating envelope. While past panel tests have provided only limited thermal/structural data because of limited test time and competing test objectives (e.g., control), this panel would be operated purely to simulate realistic

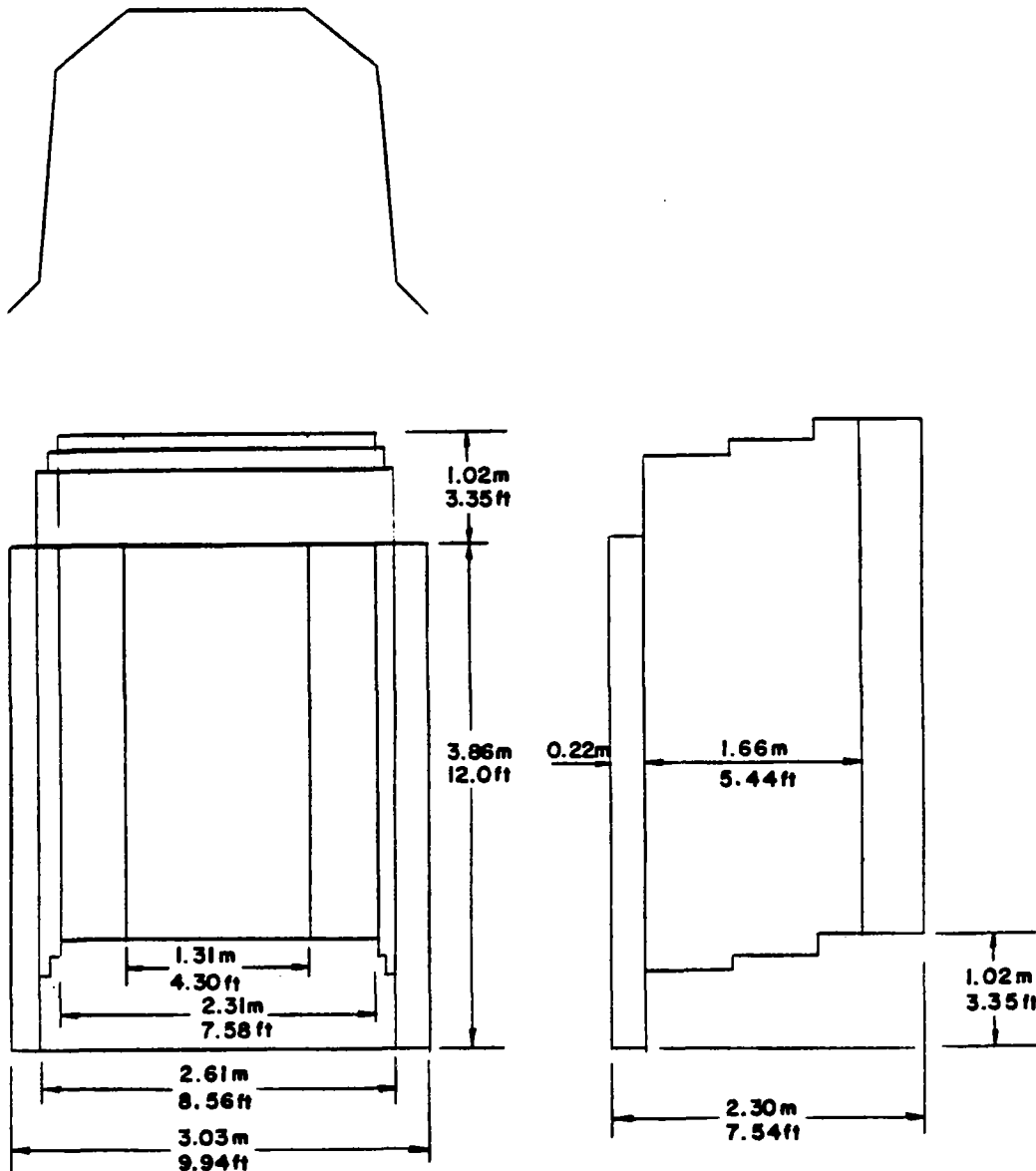


Figure 1.11 Schematic of the SRE Test Cavity

flux/temperature environments and cycles, which should maximize the useful thermal/structural design data obtained.

Supplementing the panel test is the salt loop panel section irradiation test. This test would use the mixed hot/cold tank salts bleed flows in panel test sections with radiant heaters. Both salt decomposition and panel corrosion would be monitored to provide better design criteria for receiver outlet pass flux limits.

Finally, included as an option is a subscale aperture door test. This test, which has not yet been designed, would supplement the cavity configuration door test in the same way that the panel test supplements the small-scale cavity panels. By combining the cavity test at small scale with the larger scale component tests (i.e., panel and door), both the overall integration and individual component problems can be investigated and corrected.

While these tests all offer useful information, detailed cost analyses of each are beyond the scope of this study. Of the tests considered, the most general and the one that will provide the best overall data is the cavity configuration test. The other tests, which are optional, can only be evaluated after better cost estimates are available.

Section 2

INTRODUCTION

This report presents the results of the work done in Phase 1 of a two-phase DOE-funded project for:

- Developing a cost-effective molten salt RS for a commercial-size SCRS
- Providing the commercial fabrication process development for molten salt receivers.

Recent DOE SCRS studies have shown that, technically and economically, molten nitrate salt is one of the leading candidates for use as a high-temperature, central receiver heat-transfer fluid.^{1-7*} The advantages of molten nitrate salt include low cost, chemical stability, low corrosion rates, a low melting point, a high usable temperature, and high heat capacity.^{8,9} The selected salt is a binary mixture of 60 wt% sodium nitrate (NaNO_3) and 40 wt% potassium nitrate (KNO_3) commonly known as "draw salt" because of its use in tempering, or drawing, heat-treated steels. Molten salt has been used successfully in process heat applications for many years--as a heat-transfer medium in phthalic anhydride and melamine chemical process plants and for heat treatment of steel and aluminum parts. However, at the temperature and duty cycle required by a central receiver power plant, it has a limited industrial application and data base. DOE and SNLL have been systematically developing this data base and the technology for SCRS applications. This study is an important element in these activities.

*Numbers designate references in Section 9.

2.1 BACKGROUND

Recognizing the attractiveness of molten nitrate salt, DOE has conducted an extensive program to identify uncertainties and concerns relating to its use and to develop the data base, technology, and hardware components that are essential for the development of commercial molten salt SCRS. Key areas of uncertainty include: salt properties, thermal stability, and corrosion of materials at temperatures above 482°C (900°F); the role of impurities in salt behavior (stability, corrosion, etc.); thermal performance, especially convection losses, of receiver configurations; design criteria for solar equipment, such as structural design criteria relating to receiver lifetime; and fabrication processes for thin-walled tube receiver panels.

The Advanced Central Receiver (ACR) program involved the design, construction, and testing of a second-generation receiver using fluids other than that used for the Barstow receiver (water/steam). A molten salt single-cavity receiver was tested at the Central Receiver Test Facility (CRTF) in Albuquerque as a part of the ACR program.¹⁰ This successful test of the first molten salt receiver SRE at CRTF provided answers to many design and operating questions and uncovered unanticipated problem areas in flux measurement, thermal efficiency, heat loss, absorber panel fabrication technique, and system control.

In addition SNLL has developed a comprehensive experimental program to examine what effects proposed SCRS operating conditions would have on the salt. The experiments include corrosion testing, investigation of environmental cracking of containment materials, and determination of physical properties and

decomposition mechanisms. Experimental programs are also going on at Oak Ridge National Laboratory; the State University of New York; EIC Laboratories, Inc.; and the Norwegian Institute of Technology.

In several recent molten salt SCRS studies, the receiver was studied as a part of the entire plant. Consequently, even though a considerable body of information has been generated, important receiver design, fabrication, and operating issues require additional investigation; for example:

- Part-load performance
- Load range limitations
- Controls and operational interfacing
- Conditions imposed by emergencies and operating upsets
- Procedures for start-up and shutdown
- Receiver configuration
- Development of fabrication techniques for the thin-walled tube receiver panels
- Auxiliary systems for heat tracing, preheating, filling, and draining
- Assessment of uncertainties in heat-transfer correlations, fouling factors, and salt properties and their effects on design
- Design for ease of maintenance
- Reliability and safety
- Evaluation and selection of the most cost-effective materials of construction, considering design life and the latest information on material properties and their compatibility with salt
- Creep-fatigue considerations of the pressure boundaries in a molten salt atmosphere.

2.2 PROGRAM GOALS AND PROJECT OBJECTIVES

The overall program goals are:

- To help in establishing a broad data base for an SCRS that uses molten nitrate salt as the receiver working fluid
- To aid potential commercial users in determining the value of a molten nitrate salt SCRS
- To encourage industrial suppliers to develop manufacturing capabilities and processes for molten nitrate salt components.

The objectives of this project are to:

- Design and demonstrate a reliable and cost-effective molten salt RS for solar thermal power plants
- Resolve all critical design, fabricating, operating, and performance uncertainties associated with a molten salt RS
- Minimize uncertainty in capital, operating, and maintenance costs.

The project is divided into two parts:

- Phase 1 - Subsystem Specification, Preliminary Design, and Fabrication Process Development
- Phase 2 - Detailed Design and SRE.

The work done under this contract (Phase 1) consists of the definition of the requirements specification, the preliminary design of a 320-MW molten salt RS, a detailed fabrication plan that addresses all critical fabrication issues, and laboratory-scale tests to resolve any fabrication uncertainties, performed in sufficient detail to achieve the objectives of developing a reliable, cost-effective molten salt RS for a commercial SCRS.

2.3 DEFINITION OF THE RS

The RS, shown schematically in Figure 2.1, provides a means of transferring the incident radiant flux energy from the Collector Subsystem (CS) into the molten salt working fluid. The RS consists of an elevated receiver to intercept the radiant flux from the CS, the tower structure to support the receiver, the riser pipe from the ground to the receiver, and the downcomer pipe from the receiver to the ground. The RS also includes the pumps, valves, and control system necessary to regulate fluid flow, temperature, and pressure and the required thermal conditioning necessary for its safe and efficient operation, start-up, shutdown, and standby.

The terminal points defining components within the scope of the RS are at the boundary of the tower structure where the riser and downcomer meet the cold and hot salt lines from the Thermal Storage Subsystem. These terminal points were selected so that the RS design is not dependent upon the physical layout of a specific job site. Consequently, interface piping between the RS and other plant components is not within the scope of the RS. The following items are included:

- Tower and its foundation
- Receiver structure
- Shop-fabricated modular absorber panels
- Aperture door and door-actuating mechanism
- IST and OST mounted with the receiver atop the tower
- Interconnecting piping and valves for panels and surge tanks
- Riser and downcomer piping

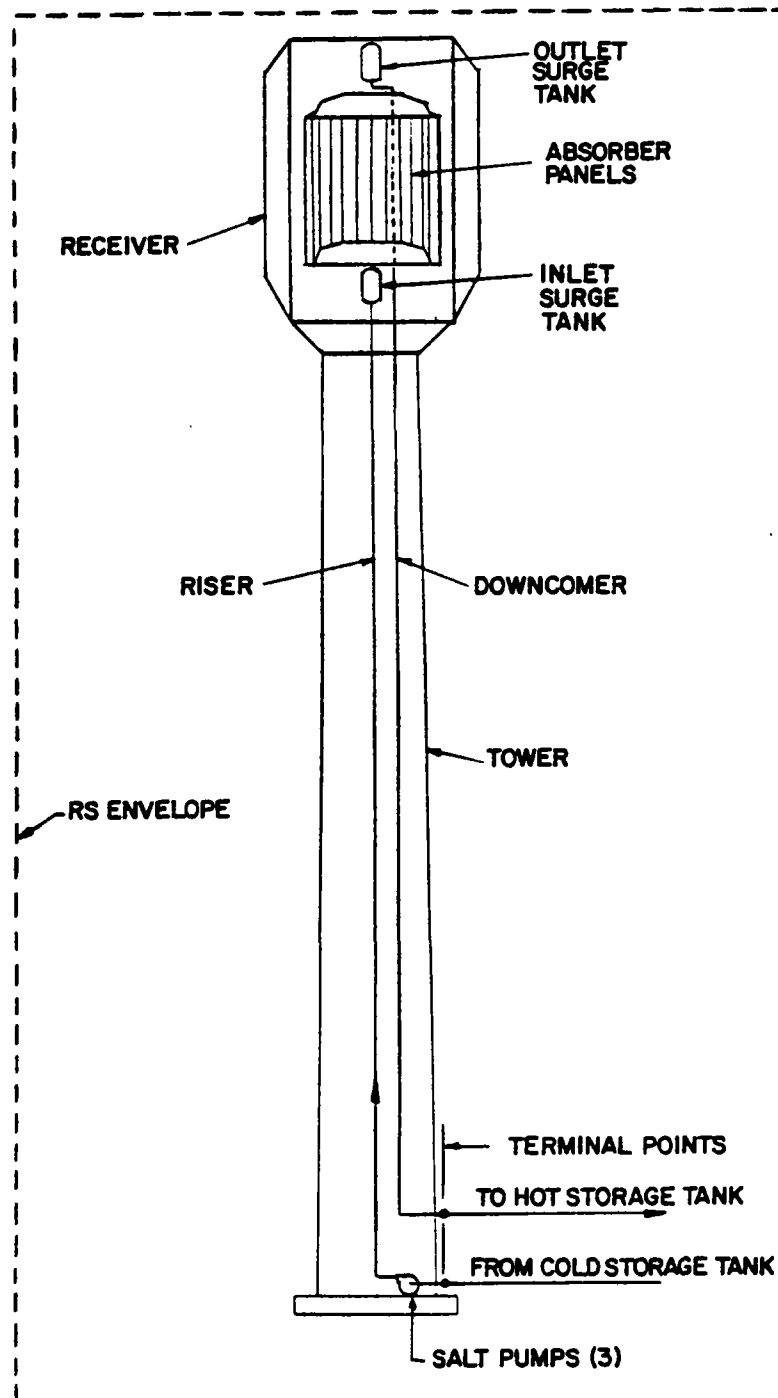


Figure 2.1 Definition of RS

FOSTER WHEELER SOLAR DEVELOPMENT CORPORATION

REF.: 84-2292C
DATE: November 1982

- Molten salt pumps
- Instrumentation and controls
- Thermal insulation and sheathing
- Drain system
- Trace and radiant heaters
- Ancillary equipment including:
 - Air compressors and dryers
 - Electrical power distribution (e.g., wiring, transformers, outlets)
 - Overhead crane
 - Service elevators

2.4 TECHNICAL APPROACH

To achieve the project objectives, the Phase 1 study was divided into 10 tasks. These tasks were performed according to the work flow diagram shown in Figure 2.2. After a review of SNLL's Preliminary RS Specification (Task 1), the RS Requirements Specification was developed (Task 2). Based on these requirements, technical and economic parametric analyses were performed and a configuration was selected (Task 3). Detailed preliminary design of the RS was made and the RS performance was evaluated (Task 4). Fabrication and construction plans were prepared and capital costs were estimated (Task 5). Tube-to-tube welding techniques were developed (Task 6), and a development plan for Phase 2 was prepared (Task 7). Following a redirection of effort by SNLL, the Phase 2 plan and proposal (Task 8) were deleted. Task 9 consisted of reports and meetings; Task 10 covered project management and administration. A summary of the contract Statement of Work follows.

Task 1--Review of RS Specification

- Review the molten salt RS Specification given in the Request For Quotation (RFQ) to ensure our understanding of the requirements and to evaluate its completeness and suitability for the design of the RS.
- Submit recommended changes with supporting rationale to SNLL within 15 days after the contract effort is begun. On the basis of these recommendations, SNLL will provide a revised specification to be employed in the conduct of the project.

Task 2--Definition of RS Requirements

- Review the existing literature on molten salt, molten salt receivers, and salt-based central receiver solar plants.
- Develop system level requirements specification.

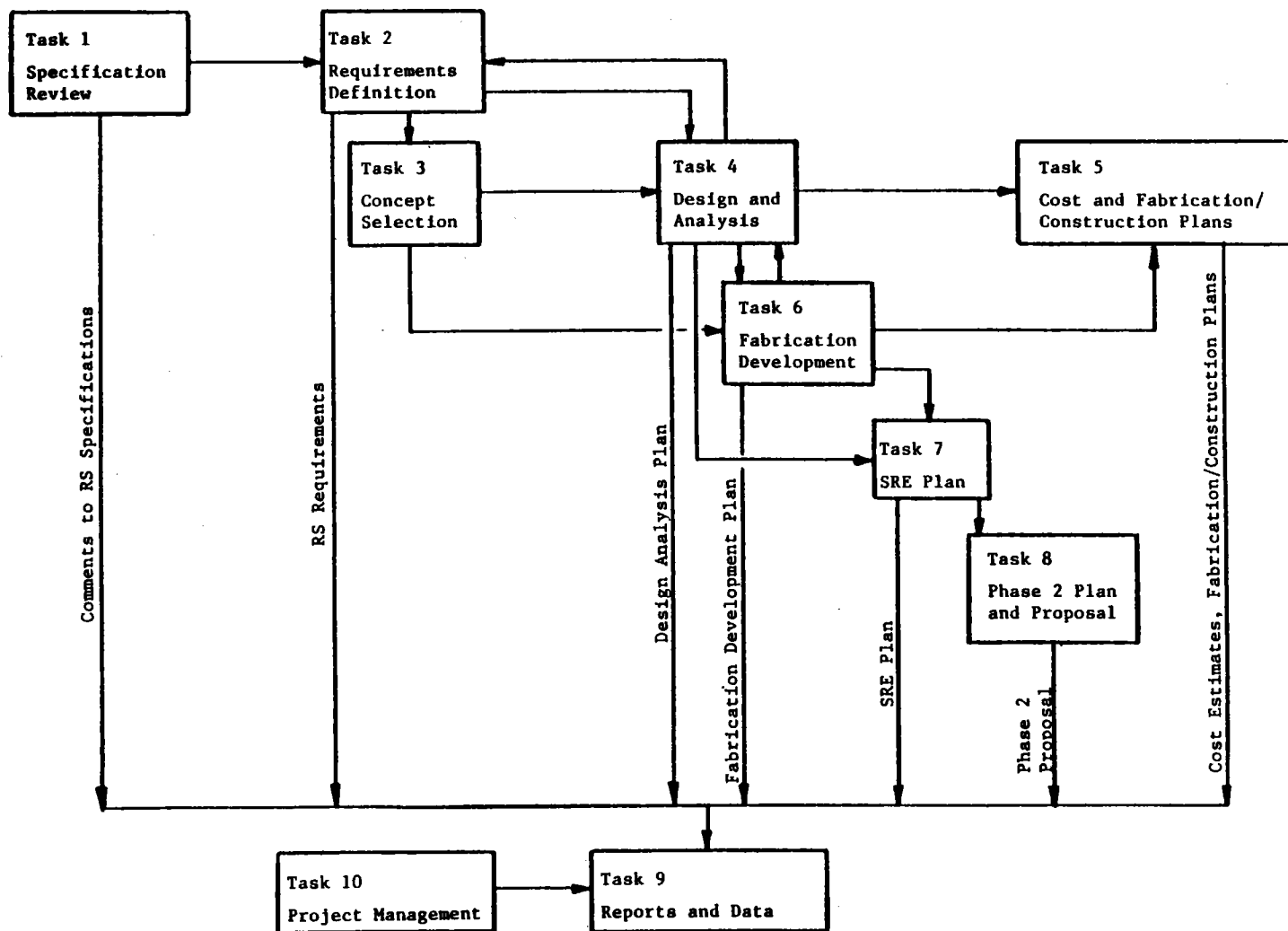


Figure 2.2 Work Flow Diagram

Task 3--RS Concept Selection

- Define the criteria for selection of the preferred RS concept, reviewing the selection criteria and parameters given in the RFQ and identifying additional criteria.
- Perform the technical and economic parametric analyses necessary to select and define the optimum receiver configuration consistent with the updated system level requirements from Task 2.
- Select the preferred RS concept based on the evaluation criteria and the parametric cost and performance data. This concept will be the basis for further activities in Tasks 4 through 8.

Task 4--RS Design and Analysis

- Develop an RS design as a basis for the cost and fabrication plan (Task 5) with the selected RS and its individual components designed and analyzed based on the requirements developed in Task 2.
- Prepare a system and component Design Analysis Plan for review and approval by SNLL before beginning the detailed analysis of the system and components. This plan identifies the various T/H and structural analyses to be performed and the man-hours associated with each and shows the sequence in which they are performed and their interrelationships.
- Identify the procedure for receiver start-up, shutdown, and response to emergency conditions. Define receiver operating procedure during intermittent cloudy periods and all auxiliary equipment required for these operations.
- Perform steady-state and transient T/H designs and analyses of the RS, size the RS components and evaluate their performance characteristics, and calculate the receiver efficiency. Predict part-load performance for differing load conditions. Calculate proper flow distributions, particularly as affected by flux gradients on the absorber surface, and estimate their effects on flow stability, tubewall temperature, and variations in tube-outlet temperature.
- Perform a stress analysis, including an elevated-temperature creep and fatigue evaluation. Determine the stresses and strains developed in the receiver and support structure under normal and abnormal operating conditions.
- Prepare a preliminary design of the receiver, riser/downcomer piping, structural supports, surge and drain tanks, tower, and tower foundations; select circulating pumps, valves, and controls. Prepare subsystem and component-level design requirements and specifications and layout drawings for the RS in sufficient detail to allow preparation of a fabrication plan and estimation of the RS fabrication, shipping, construction, operating, and maintenance costs.

- Perform control system analysis, analyzing the control requirements for both individual series flow paths and parallel flow paths fed from the same source. Determine the relative performance of flux and back-side tubewall temperature for flow control during cloud transients and define the major elements of the receiver control system and the interface between receiver control and overall plant control.

Task 5--RS Cost and Fabrication/Construction Plans

- Develop a step-by-step fabrication plan for the fabrication and assembly of the RS components, including all significant fabrication and inspection operations.
- Prepare shop fabrication schedules for the receiver and major subassemblies, such as headers and panels, as well as schedules for tool and mock-up design and fabrication.
- Prepare a field construction plan for the RS, showing all the major steps involved.
- Prepare a labor and materials cost estimate for the RS, covering detailed engineering, shop fabrication, shipping and handling, field construction, and preoperational testing.

Task 6--Receiver Fabrication Process Development

- Prepare a detailed Fabrication Process Development Plan for review and approval by SNLL before its implementation. The plan should address all critical fabrication issues related to tube-to-tube joining, tube-to-header joining, and methods for attaching panels or individual absorber tubes to the supporting structures.
- Develop the techniques for tube-to-tube joining and tube-to-header joining and determine methods for attaching panels or individual panel tubes to the support structure.
- Consider the effect of stresses and strains arising from joining and attaching methods in arriving at a receiver fabrication plan.

Task 7--Subsystem Research Experiment and Development Plan

- Identify the requirements for the SRE that will establish RS performance characteristics.
- Prepare an SRE preliminary design and an SRE plan and schedule.

Task 8--Phase 2 Plan and Proposal (deleted)

- Prepare a proposal for continuation of our effort into Phase 2 based on the SRE and Development Plan prepared in Task 7.
- Submit proposal to SNLL.

Task 9--Reports and Data

- Provide contract-required project reports data as specified in the RFQ.
- Support and attend meetings as specified in the RFQ.

Task 10--Program Management

Provide project and technical management including the:

- | | |
|----------------|--------------|
| • Planning | • Review |
| • Direction | • Scheduling |
| • Coordination | • Control |

required to satisfactorily complete all tasks.

Figure 2.3 is the project critical path chart. Figure 2.4 shows the overall project schedule divided into finite tasks. As part of this schedule critical project milestones are identified.

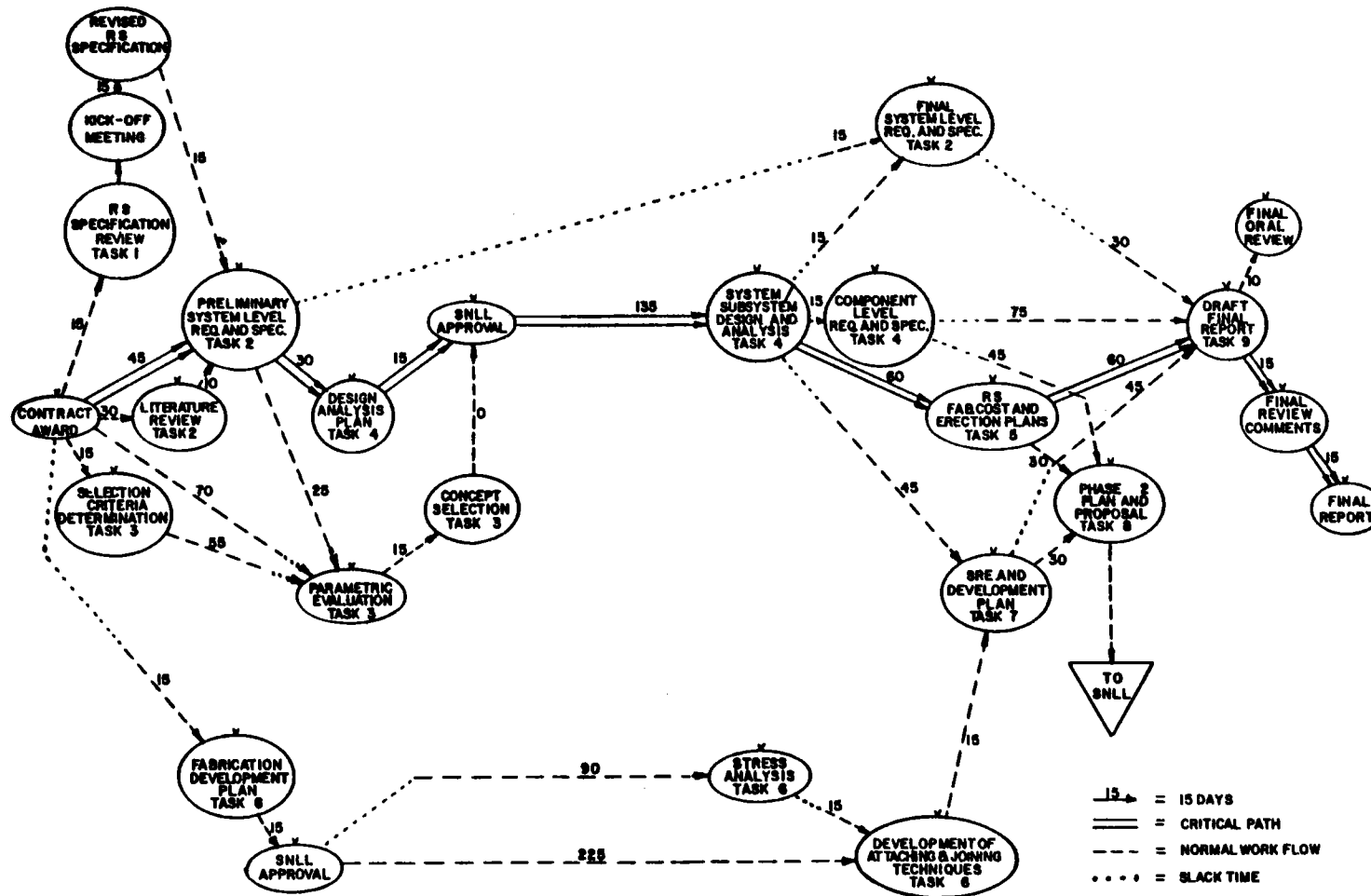


Figure 2.3 Work Flow Diagram/Critical Path Chart

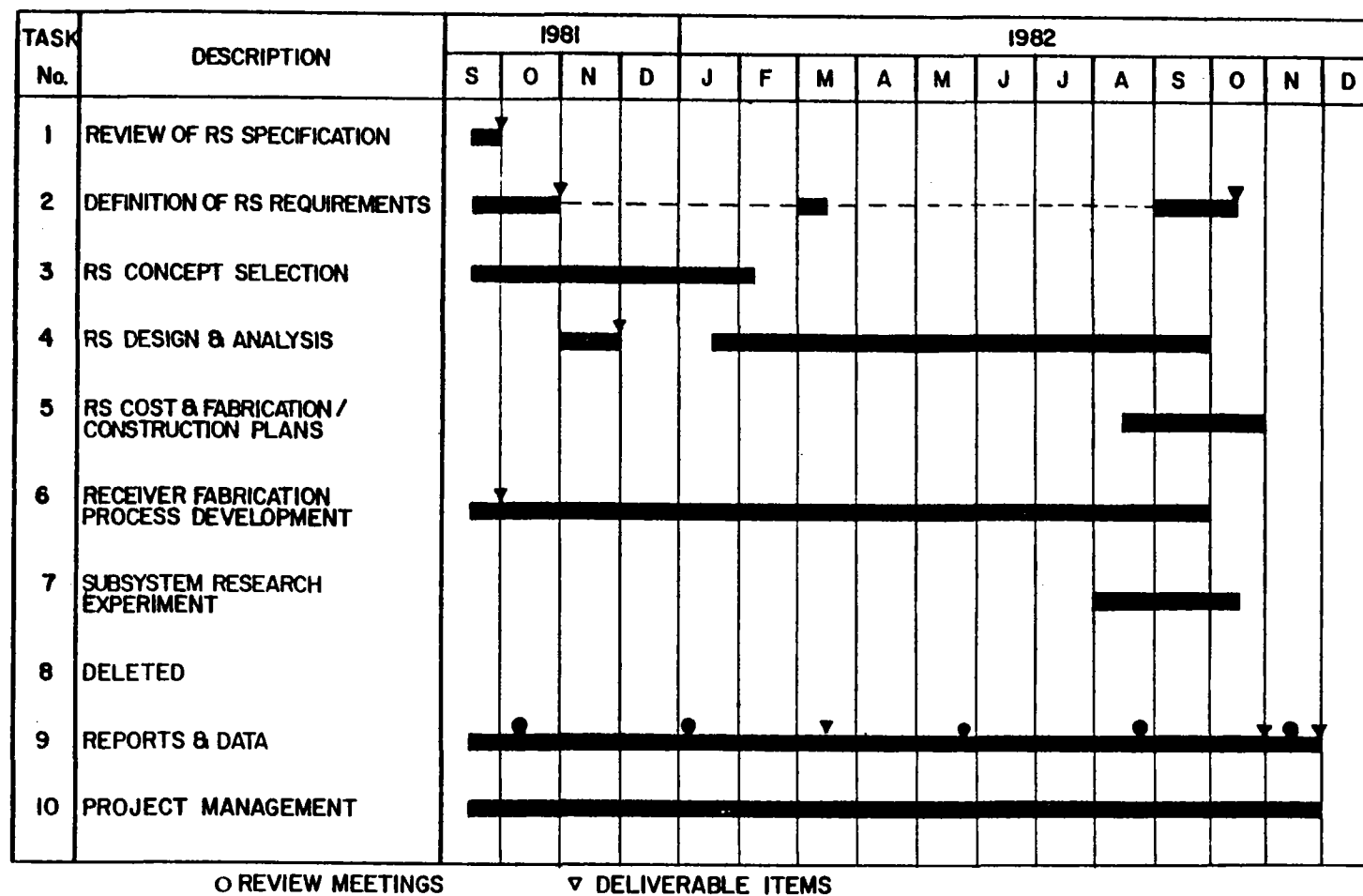


Figure 2.4 Project Schedule

2.5 PROJECT TEAM

To perform the Phase 1 design study, we assembled a team of organizations with valuable complementary backgrounds in systems and design integration; design fabrication, construction, and testing of central receiver solar thermal power systems and components; and operation of utility generating plants. Foster Wheeler Solar Development Corporation (FWSDC), as prime contractor for the Phase 1 preliminary design, had overall responsibility for the RS design.

FWSDC is a separate operating entity within Foster Wheeler Development Corporation (FWDC)--the research and development arm of the parent holding company, Foster Wheeler Corporation. FWDC fills virtually all of the research and development needs of Foster Wheeler's operating divisions and domestic affiliates, conducts research and development, and provides project management and administrative services for other companies and Government agencies.

The overall Project Organization is shown in Figure 2.5. The team consists of our affiliated companies--Foster Wheeler Energy Corporation (FWEC) and Foster Wheeler Special Projects Engineering and Construction, Inc. (FWSPEC); McDonnell Douglas Corporation (MDC); Arizona Public Service Company (APS); Sierra Pacific Power Company (SPP); and Olin Corporation. Tables 2.1 and 2.2 identify the team members, their primary areas of responsibility, and the functions of each organization.

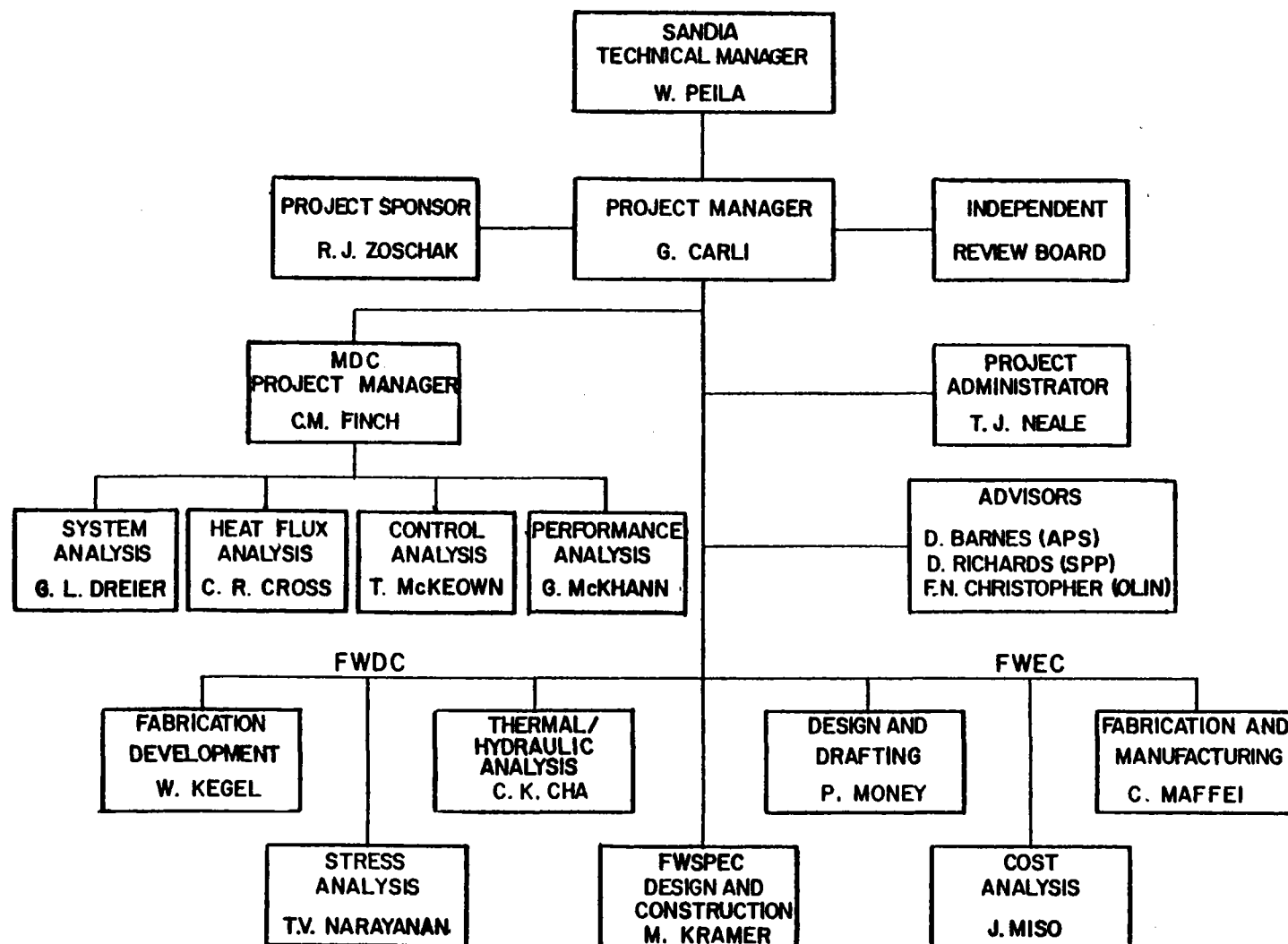


Figure 2.5 Project Organization Chart

Table 2.1 Team Responsibilities

Customer

Sandia National Laboratories Livermore (SNLL)

Prime Contractor

Foster Wheeler Solar Development Corporation (FWSDC)

- Overall Project Management and Coordination
- Receiver Design and Analysis
- Fabrication Process Development
- SRE Preliminary Design, Plan, and Schedule

Subcontractors

Foster Wheeler Energy Corporation (FWEC)

- Fabrication Plan
- Fabrication Cost Estimates
- Receiver Structural Design

Foster Wheeler Special Projects Engineering and Construction, Inc. (FWSPEC)

- Tower and Piping System Design
- Salt Pump and Auxiliary Equipment Selection
- Construction Plan
- Construction Cost Estimate

McDonnell Douglas Corporation (MDC)

- Development of System-Level Requirements Specification
- Preferred Configuration Selection
- Flux Mapping, Performance Estimates, Operation Analysis, and Control System Design
- SRE Test Planning

Advisors

Arizona Public Service Company (APS) and Sierra Pacific Power Company (SPP)

- Provide Utility Engineering Review

Olin Chemicals Group

- Provide Molten Salt Technology

Table 2.2 Team Member Functions

Task No.	Description	FWSDC	FWEC	FWSPEC	MDC	APS SPP OLIN
1	Review of RS Specification	P	S	S	S	R
2	Definition of RS Requirements				P	
	2.1 Literature Review	P			S	
	2.2 System Level Requirements Specification	S	S	S	P	R
3	RS Concept Selection				P	
	3.1 Definition of Evaluation Criteria	A/S			P	
	3.2 Parametric Analyses of RS Concept Improvements	S	S	S	P	
	3.3 Concept Selection	A			P	
4	RS Design and Analysis	P				
	4.1 Design Analysis Plan	P	S	S	S	
	4.2 Operation Analysis	S			P	
	4.3 Thermal/Hydraulic Design and Analysis	P			S	
	4.4 Structural Analysis	P	S			
	4.5 Subsystem Mechanical Design and Analysis	S	S	P	S	
	4.6 Control Analysis	S			P	
5	RS Cost and Fabrication/Construction Plans		P	P		
	5.1 Shop and Field Fabrication/Construction Plans	A/S	P	P	S	
	5.2 Cost Estimating for the RS	A/S	P	P	S	
6	Receiver Fabrication Process Development Plan	P				
	6.1 Fabrication Process Development Plan	P				
	6.2 Development of Joining and Attaching Techniques	P	S			
	6.3 Stress Analysis Consideration	P				
7	Subsystem Research Experiment and Development Plan	A/S	S	S	P	
8	Phase 2 Plan and Proposal (deleted)	P	S	S	S	
9	Reports and Data	P	S	S	S	R
10	Program Management	P	S	S	S	

A - Approve
P - Prime
R - Review
S - Support

Section 3

RS REQUIREMENTS SPECIFICATION

3.1 REVIEW OF SNLL SPECIFICATION

Team members reviewed the Preliminary RS Specification given in the RFQ with respect to design, fabrication, construction, and operation and to ensure that the specific requirements for the design, development, and commercialization of the proposed concept are appropriate and applicable. Appendix A contains a copy of this specification and comments and recommended changes provided to SNLL. Major recommended changes include:

- Addition of a requirement to drain
- Change in the minimum absorber thermal power from 30 to 80 MW
- Definition of thermophysical properties of receiver working fluid
- Addition of maximum insolation and minimum sun angle operating requirements
- Addition of the damping values given in Nuclear Regulatory Commission (NRC) Guide 1.61 to the earthquake requirements.

3.2 SYSTEM LEVEL DEFINITION

The conditions to which the molten salt RS is designed are defined in the RS Requirements Specification included in Appendix B. It was prepared based on the requirements in the revised specification from Task 1, the data obtained in the literature review, and the experience of the team members. It was updated at the end of Task 3 and was compiled in final form at the end of Task 4. The document defines the following:

- RS scope
- Applicable codes and standards

- Technical requirements
 - Design
 - Function
 - Performance
 - Operation
 - Safety
 - Control
 - Miscellaneous
- Interface requirements with the following subsystems:
 - Collector
 - Energy storage
 - Master control
 - Plant support services
- Environmental requirements
 - Design point
 - Operating limits
 - Survival

The format for the specification provides a comprehensive set of design data and requirements that will enable the RS designer to develop the receiver design in a consistent, unambiguous manner. Because of the variety of operating conditions, the requirements have been written (to the greatest extent possible) to guarantee acceptable receiver operation and performance over the total operating envelope and to provide acceptable control of receiver operation and performance from the perspective of overall system requirements.

The data contained in this document reflect the combined experience of the Barstow Solar 1 program, numerous studies of molten salt central receiver systems, and many analyses undertaken in the course of this Molten Salt Receiver SRE Phase 1 study.

3.2.1 RS Scope

The scope of the RS is discussed in Section 2.3.

3.2.2 Applicable Codes and Standards

The list of applicable codes and standards combines those identified in the preliminary specification provided by SNLL to the contractors and the more detailed list of applicable codes and standards developed for the Barstow Solar 1 program. Listed beside each of the codes is its area of applicability.

3.2.3 Technical Requirements

The RS requirements have been arranged in seven basic categories: design, function, performance, operation, safety, control, and miscellaneous.

Design. These include basic top-level requirements taken from the preliminary specification, general principles relating to thermal/hydraulics and structural design, and a limited number of specific requirements (e.g., pressure drop and corrosion allowance).

Function. These are similarly of a general nature and define the top-level functions that must be performed by the RS.

Performance. These requirements cover two basic areas:

- Receiver thermal efficiency during normal operating conditions, including cloudy periods
- Auxiliary power requirements during warm and overnight shutdowns (e.g., trace heating) and during normal receiver operations (e.g., pumping power requirements).

The approach to receiver performance requirements for normal operations has been to specify the interface conditions (e.g., incident flux and inlet/

outlet flow temperatures) and to place a requirement on the net thermal power to be delivered to the hot storage tank. With this approach, the total receiver efficiency requirement is defined, but the allocation of the overall efficiency to the different loss mechanisms (i.e., reflection, radiation, convection, and conduction) is left as an RS responsibility.

The design point conditions specified as the best collector field performance time occur at or near noon on February 19 (day 50 in DELSOL numbering), as shown in Figure 3.1. All design point analyses were based on this point. Maximum performance on February 19 rather than winter solstice (best field cosine time) results from decreased shadowing and blocking losses, which more than compensate for the reduction in field cosine.

The absorber surface contours rather than the aperture plane were chosen for the definition of incident flux because any projection of flux from one location to another requires both magnitude and vector direction for the flux distribution at a given location (e.g., the aperture plane). Also the data interface required would be extremely cumbersome, especially since the development of an aim strategy for the collector field can only be accomplished by looking at the fluxes on the absorber surfaces. Based on some limited analysis and limited test experience, monitoring of the flux in the aperture plane appears as difficult as monitoring the flux on the absorber surface, especially when the projection of the monitored flux, measured in magnitude only, is inevitably a source of controversy.

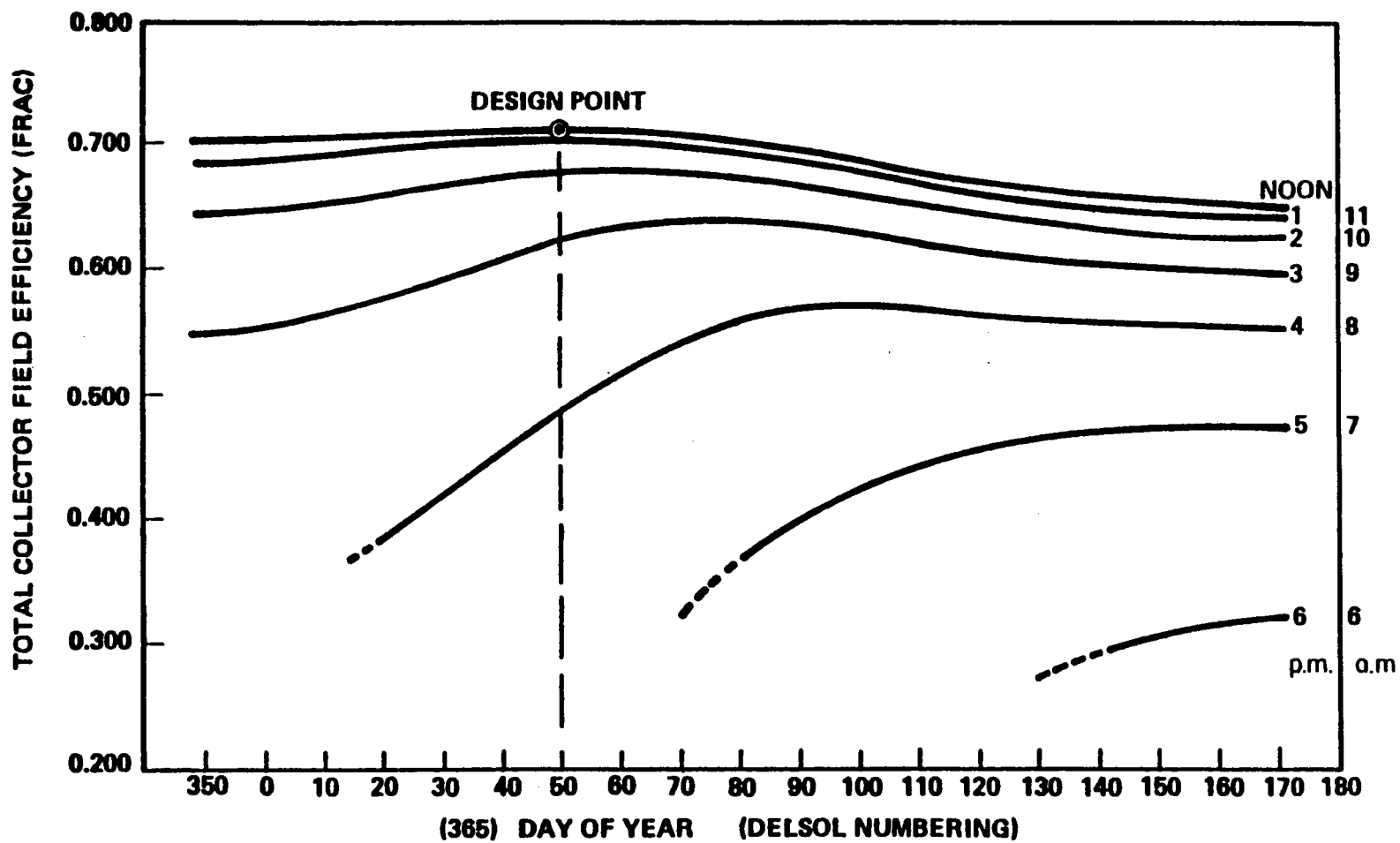


Figure 3.1 Collector Field Performance Design Point

At the design point, flux profiles and performance efficiency requirements are defined. At off-design points, only requirements regarding operating temperatures at specified fluxes are specified.

Because it is important for the RS to operate at sun elevations of 10 deg, operating flux profiles are provided which specify requirements to meet design point outlet temperatures for these off-design points. These requirements, along with similar requirements for operation with flux profiles associated with partly cloudy days, have been included to guarantee a minimum amount of operating time that will be lost during off-design operations.

The asymmetries of flux profiles relating to cloudy-day operations were based on asymmetries found during normal diurnal operation. The relatively stringent requirements are based on these data for all operations--including cloudy-day operations.

The rate of change of power for cloudy days was derived from field data; the representative transit times for clouds, from the preliminary specification.

The standby and overnight shutdown losses and auxiliary power requirements reflect analyses of losses, thermal cooldown rates, and typical yearly operations.

The remainder of the auxiliary power requirements reflect data on pumping power requirements and annual pump utilization. They include allowances for a horizontal pipe run of approximately 61 m (200 ft) for the cold-salt pipe leg. (No allowance is required for the hot-salt pipe leg because of the tower head.)

Operation. These requirements are intended to guarantee the integration of the RS into the overall system operation and to guarantee that inordinate amounts of operating time are not lost during start-up, shutdown, and transition. They, along with the control requirements, provide the flow-down of the functional requirements into the design.

The overall operating times are based on DELSOL analyses of clear-day operation modified by the ratios of measured cloudy-day insolation to DELSOL-estimated clear-day insolation.

The detailed operating times and ramp rates reflect preliminary analyses of collector field operations and ramping times that are reasonable and yet do not impose unduly stringent requirements on the RS.

The temperatures for flow diversion from the HST to the CST reflect considerations of temperature variations and tolerances of both tanks and a need to limit the temperature differences between the salt and related piping.

The emergency operation requirements reflect preliminary analyses of collector field operating capabilities, receiver door operating times, and the capacity of the IST. Detailed analyses of the flux profiles on the receiver doors and the measured properties of ablative materials in equivalent heat fluxes provide high confidence that ablative materials in replaceable sections attached to the front face of the door can protect the receiver in the event of total power failure.

Safety. These requirements relate primarily to four areas:

- General safety for utility power stations and tall structures
- Safety relating to use of molten salt
- Safety relating to high-temperature process piping and equipment
- Safety relating to operation with heliostats.

Based on extensive utility and industrial experience with power stations, high-temperature process equipment, and molten salt, we expect no unusual safety problems in these areas. Standard practices and codes provide a sound basis for safe operation. With respect to heliostat operation, the primary requirements for beam safety relate to the CS and the RS (i.e., responsibility is limited to controlling access to potentially dangerous areas).

Control. Together with the performance and operating requirements, these provide the design basis for the RS control system. The structure for these requirements reflects the detailed flow-down of general functional and operating requirements into numerical requirements that can be used for sizing and selecting RS control equipment and for developing RS software. The three general areas include the following:

- Variables to be controlled and control mode (e.g., active feedback and on-off)
- Sequencing, timing, and interlocking of transition operations
- Operator interface and integration with plant control system.

Miscellaneous. These requirements address the structural, civil, and thermal structural design requirements for the:

- Tower
- Aperture Door
- Piping
- Salt pumps
- Insulation and lagging
- Trace heating
- Fill and drain subsystem
- Support structure
- Foundation and dikes

They reflect general process plant, utility, and structural design practices and codes.

3.2.4 Interface Requirements

The RS interfaces with four other central receiver subsystems. For each of these subsystems, the following requirements are specified:

- Collector Subsystem: absorber geometry and location, incident flux profiles on the absorber surface, and heliostat operations and control relating to receiver protection against unacceptable fluxes.
- Energy Storage and Transport Subsystem: mechanical, physical, process flow, and transient interface requirements.
- Master Control Subsystem: physical, electrical, and data interface requirements.
- Plant Support Services Subsystem: mechanical, electrical, and process parameter interface data relating to electric power, instrument air, water, drainage, and wastewater disposal.

3.2.5 Environmental Requirements

These requirements are taken directly from the preliminary specification. Two requirements were added to the operating limits:

First, RS operation without defocus was limited to 1000 W/m^2 ($317 \text{ Btu/h}\cdot\text{ft}^2$). This limit results from analysis of 4 years of detailed direct normal insolation data for Barstow. These data show that, on the average, only 12.5 percent of the days have insolation above 1000 W/m^2 ($317 \text{ Btu/h}\cdot\text{ft}^2$), whereas over 50 percent of the days have insolation above 950 W/m^2 ($301 \text{ Btu/h}\cdot\text{ft}^2$), and none have insolation greater than 1069 W/m^2 ($339 \text{ Btu/h}\cdot\text{ft}^2$).

Results of a preliminary trade-off between the energy gained by increasing receiver size to accept higher powers and additional annual energy and the energy lost from increases in receiver losses because of its larger size indicated that the trade-off is very close between 950 and 1000 W/m^2 (301 and $317 \text{ Btu/h}\cdot\text{ft}^2$). Based on the West Associates data,¹¹ an increase in design-point insolation from 950 to 1000 W/m^2 (301 to $317 \text{ Btu/h}\cdot\text{ft}^2$) results in an increase in energy collection ranging between 1.5 and 3.0 GWht/yr (5.12 and $10.24 \times 10^9 \text{ Btu/yr}$). Conversely, the 5 percent increase in receiver radiation/convection losses because of the increased receiver area results in a decrease of approximately 2.5 to 2.7 GWht/yr (8.53 to $9.21 \times 10^9 \text{ Btu/yr}$). Thus the net change in annual energy between the design flux levels ranges from $+0.5$ to -1.2 GWht/yr ($+1.7$ to $-4.1 \times 10^9 \text{ Btu/yr}$). For fluxes above 1000 W/m^2 ($317 \text{ Btu/h}\cdot\text{ft}^2$), the increase in collectible energy is small as a result of the small time with insolation above 1000 W/m^2 ($317 \text{ Btu/h}\cdot\text{ft}^2$); therefore the net change in annual energy is likely to be negative (i.e., increased losses greater than increased energy collected). Because of the potential for operating errors and the reliability of measured insolation, 950 W/m^2 ($301 \text{ Btu/h}\cdot\text{ft}^2$) was chosen as the design point for a first-of-a-kind plant.

As a design margin, peak tubewall temperatures for stress analysis were also calculated at the maximum insolation conditions--1000 W/m² (317 Btu/h·ft²).

The second addition relates to start-up and shutdown sun elevations. MDC heliostat operations to 10-deg sun elevations have been validated. Flux analyses of collector field performance at these elevations for a north field indicate usable operating time can be gained without undue requirements on the heliostats, the receiver minimum power, or power asymmetry. Therefore, the minimum sun angle for normal operations was changed from "greater than 15 degrees above the horizon" to "greater than 10 degrees above the horizon."

3.3 SUMMARY OF RS REQUIREMENTS

A summary of the RS Requirements is given in Table 3.1.

Table 3.1 RS Specifications Summary

General:

Reference site	Barstow, California
Configuration	Partial cavity. Replaceable modular panels (20). Gravity-closing aperture door. All up-flow panels.
Aperture midpoint elevation	216 ±1.0 m (709 ±3.3 ft)
Heat-transfer fluid	Molten nitrate salt (60 wt% NaNO ₃ /40 wt% KNO ₃)
Service life	30 years
Availability and reliability	0.95, exclusive of insolation conditions
Maximum transportation length	35 m (115 ft)

Design Parameters:

Design point	Noon, February 19 (Day 50)
Design point insolation	950 W/m ² (301 Btu/h·ft ²)
Maximum insolation	1000 W/m ² (317 Btu/h·ft ²)
Absorbed power	320 MW (1092 × 10 ⁶ Btu/h)
Minimum absorbed power at rated conditions	80 MW (273 × 10 ⁶ Btu/h)
Maximum incident flux	0.65 MW/m ² (0.206 × 10 ⁶ Btu/h·ft ²)
Salt flow rate	760 kg/s (6.018 × 10 ⁶ lb/h)
Salt inlet temperature	288°C (550°F)
Salt outlet temperature	566°C (1050°F)
Overnight salt temperature	288°C (550°F)

Performance Limits:

Power range	25 to 100% of rated power
Ambient air temperature range	0 to 50°C (32 to 122°F)
Wind speed	12 m/s (26.8 mi/h)*

Operating Limits:

Power range	10 to 105% of rated power
Salt flow range	5 to 105% of rated flow
Sun angle	>10 deg
Ambient air temperature range	-9 to +50°C (+16 to +122°F)
Wind speed	16 m/s (35.8 mi/h)*

Survival Limits:

Ambient air temperature range	-30 to +50°C (-22 to +122°F)
Wind speed	40 m/s (90 mi/h)*
Rainfall	75 mm (3 in.) within 24 hours
	750 mm (29.5 in.) annually
Snowfall	0.3 m (1 ft) within 24 hours
Snow load	240 Pa (5 lb/ft ²)
Ice coating	50 mm (2 in.)
Hail - diameter	25 mm (1 in.)
Hail - specific gravity	0.9
Hail - terminal velocity	23 m/s (75.5 ft/s)
Earthquake - zone	3
Earthquake - accelerations	0.20 to 0.15 g (vertical and horizontal)

*Reference elevation 10 m (33 ft).

Section 4

SELECTION OF THE RS

During the MDC/SPP Repowering Study,⁶ a conceptual design for a north field Partial Cavity Receiver (PCR) configuration was developed for use with a molten salt SCRS Plant. In this section we discuss the evolution of this receiver concept, compare this concept with alternative concepts, and provide the rationale for the selection of the PCR as our baseline concept. We also describe the selection approach and the trade-off studies conducted in Task 3. At the end of the section, the selected RS configuration is briefly described. A detailed description of the final RS with a list of key design and operating data are given in Section 7.

4.1 SELECTION OF RECEIVER CONCEPT

The PCR concept, illustrated schematically in Figure 4.1, consists of 20 panels constructed of Incoloy 800 tubes welded lengthwise and arranged in an omega shape, as shown on the figure. The entire partial cavity was tilted 25 deg forward and mounted atop a concrete tower complete with interconnecting piping, surge tanks, trace heating, insulation, and an aperture door that closes for overnight conditioning and absorber protection in the event of a power failure. Also shown in the figure are the flow routes and control approach for each half of the absorber--a four-pass flow path and two parallel flow-control valves to regulate and distribute the flow and to control the outlet temperature.

This concept features an optimum combination of external and cavity absorber surfaces. It provides high efficiency, low weight, and low system cost

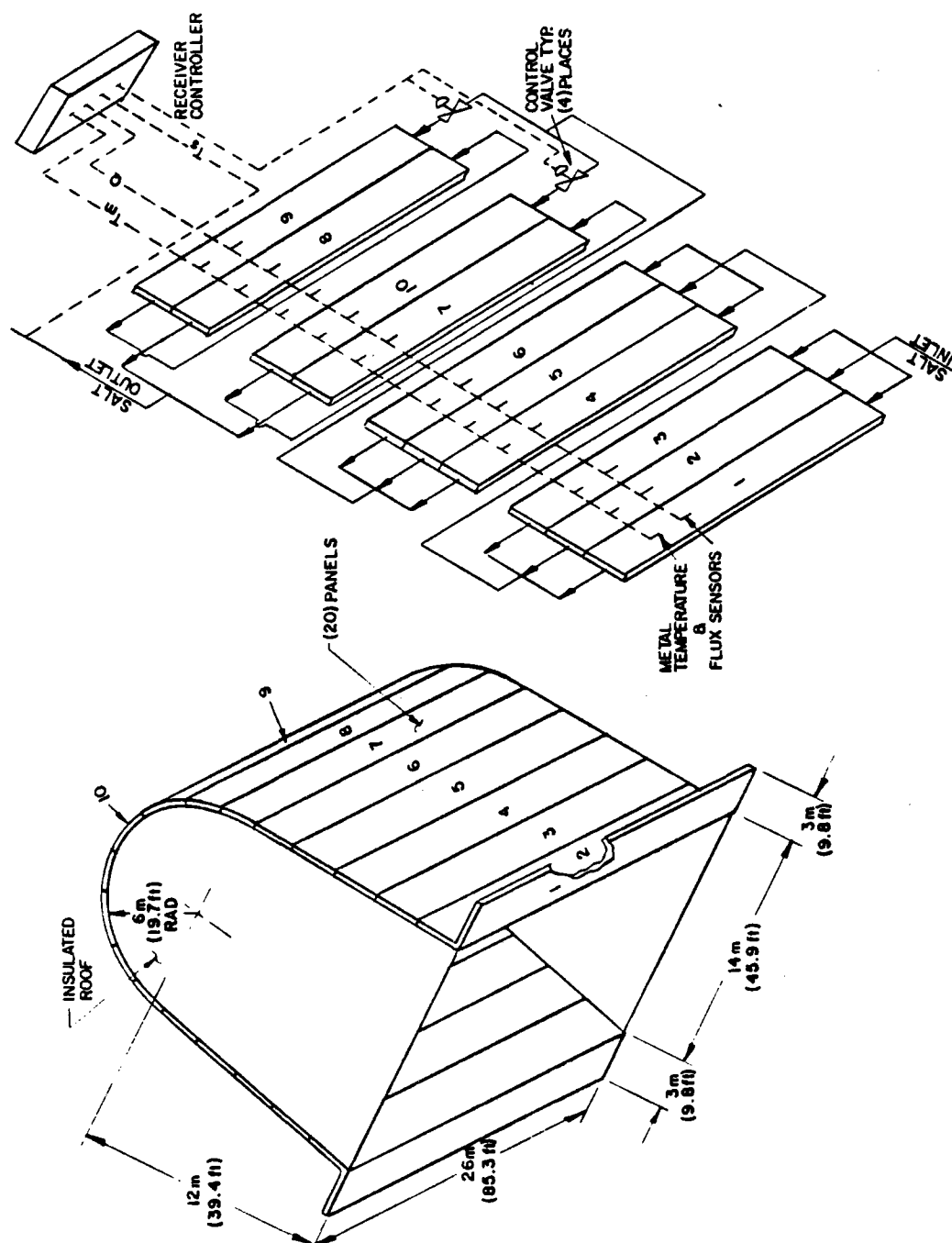


Figure 4.1 Proposal Baseline Configuration

with a design comprised of modular panels that are easily replaceable and that can be supported by a structure shielded from high incident fluxes.

The PCR concept evolved from three basic considerations:

- Typical solar flux profiles are high in the center with reducing flux around the edges. Therefore, a configuration that spreads the central portion of the flux profile over a greater area will keep the frontal area small while reducing the peak flux to the absorber surface.
- Single-surface heating permits the use of absorber panels that are easily removed for maintenance and utilize a supporting structure not needing active cooling.
- The reduced frontal area and partial cavity effect provide the high effective absorptivity and reduced reradiation and convection losses normally associated with cavity designs.

4.1.1 Comparison of PCR With Alternative Concepts

In the SPP Repowering Study, a comparison of the PCR with a surround-field, cylindrical, external receiver indicated a clear preference for the PCR. Because of the north latitude of the SPP site and the piping run differential dictated by site-specific requirements, we revised this trade-off study for a Barstow location with normal piping runs for both concepts. The results of this trade-off are shown in Table 4.1. Because overall plant cost/performance depend on the RS and the collector field and on the relationship between them, comparisons reflect cost and performance for both the RS and collector field. Thus further consideration of external receiver concepts was not warranted.

The second major comparison was between the PCR and the Quad-Cavity Receiver (QCR). Table 4.2 lists key parameters derived from the two final reports.^{6,10} Noteworthy in this comparison is the general similarity of many

Table 4.1 Cost/Performance Comparison Between PCR and Cylindrical External Receiver at Barstow Location--MDC Second-Generation Heliostats

Description	DELSOL Results	
	PCR (North Field)	External Receiver (Surround Field)
Design point	Noon--winter solstice	Noon--equinox
Number of heliostats	8,474	10,374
Optical height of receiver centerline [m (ft)]	210 (689)	200 (656)
Receiver efficiency, (%)	92.7	79.8
Overall efficiency (annual average)	0.603	0.511
Annual energy to bottom of tower (GWht)	750	779
Heliostat costs	\$135 to \$224/m ² *	\$135 to \$224/m ² *
Costs (\$ x 10 ⁶)		
Collector field	\$68.91 to \$111.79	\$79.60 to \$132.08
RS	\$24.39	\$20.00
Subtotal costs (\$ x 10 ⁶)	\$93.30 to \$136.18	\$99.60 to \$152.08
Capital cost/annual energy (\$/kWht)	0.124 to 0.182	0.128 to 0.195

*Range of values reflects uncertainty in projection of heliostat costs in 1981 dollars.

Table 4.2 Key Parameter Comparison Between PCR and QCR Concepts

Description	PCR (North Field)	QCR (Surround Field)
Delivered power (MWt)	333	316
Receiver efficiency (design point) %	91.6	91.6
Salt inlet/outlet temperature [°C (°F)]	288/566 (550/1050)	277/566 (530/1050)
Maximum salt film (tube I.D.) tem- perature [°C (°F)]	604 (1120)	598 (1108)
Salt flow rate [kg/s (10 ⁶ lb/h)]	767 (6.09)	707 (5.61)
Absorbed flux, peak/average (MW/m ²)	0.63/0.264	0.609/0.238
Pressure drop through receiver [kPa (lb/in ²)]	0.856 (124)	2.78 (402)*
Absorber tube dia x thickness [mm (in.)]	25.4 x 1.65 (1.0 x 0.065)	38.1 x 1.65 (1.5 x 0.065)
Absorber tube material	Incoloy 800	Incoloy 800
Number of panels/tubes per panel	20/118,94,92	20/64
Number of flow control valves	4	2
Absorber area [m ² (ft ²)]	1250 (13,450)	1327 (14,279)
Receiver weight, wet/dry [10 ³ kg (10 ³ lb)]	1007/839 (2221/1851)	964/823 (2126/1815)
Height of receiver centerline [m (ft)]	223 (732)	176 (577)

*Includes 1.36 MPa (196 lb/in²) for static head, control valve, surge tank, and margin not included in the pressure drop value for the PCR.

design (e.g., receiver weight) and performance (e.g., overall receiver efficiency) parameters. A review of the two concepts with respect to development and design risk indicated the following:

- Thermal Stress Considerations

- Two-sided heating of tubes in the QCR concept reduces absorber tubing, thermal stress and ΔT on tubewalls; however, diurnal flux variations and clouds will produce some daily thermal cycling and occasional periods of nearly one-sided panel heating.
- Flux gradients on wing panels of the QCR concept may create panel lateral stress problems, requiring a change in aim strategy and perhaps increasing the spillover.
- The QCR concept requires a precisely assembled, cooled, lateral support structure, which has significant thermal stress problems.

- Support Structure and Cavity Enclosures

- The nearly symmetrical cruciform shape of the QCR concept is better suited to withstand wind and seismic loads.
- The doors for the QCR concept are smaller and thus simpler; however, one single door should prove more reliable and easier to maintain than four separate doors.
- Assembly of the cavity enclosures, doors, and associated insulation and lagging for the QCR concept is more involved.
- Lateral supports for panels with two-sided heating in the QCR concept are completely untried and unproven. The design will require care to avoid undue "slop" in the support and consequent vibration in the wind. These supports need extensive design and testing and will significantly complicate the installation, removal, and maintenance of these panels.

- Receiver Performance Considerations

- Although precise estimates of comparative receiver performance were not made, the increased tube surface area and total aperture area of the QCR concept will likely lead to higher losses.
- Collector field/tower design analyses using DELSOL and based on receiver performance estimates in the two final reports indicate the comparative field/tower performance and costs shown in Table 4.3.

- Receiver Operation and Control

- In the QCR concept, interactions between the collector field and panels with two-sided heating will complicate flow control for two reasons:
 - If clouds are covering only one part of the field, the low flow rates called for by outlet temperature control algorithms may produce

Table 4.3 Cost/Performance Comparison Between PCR and QCR Concepts at Barstow Location--MDC Second-Generation Heliostats

Description	DELSOL Results	
	PCR (North Field)	QCR (Surround Field)
Design point	Noon--winter solstice	Noon--equinox
Number of heliostats	8,474	9,229
Optical height of receiver centerline [m (ft)]	210 (689)	172 (564)
Receiver efficiency, (%)	92.7	92.2
Overall efficiency (annual average)	0.603	0.580
Annual energy to bottom of tower (GWht)	750	784
Heliostat costs	\$135 to \$224/m ² *	\$135 to \$224/m ² *
Costs (\$ x 10 ⁶)		
Collector field	\$68.90 to \$111.79	\$74.88 to \$121.51
RS	\$24.39	\$22.50
Subtotal costs (\$ x 10 ⁶)	\$93.29 to \$136.18	\$97.38 to \$144.01
Capital cost/annual energy (\$/kWht)	0.124 to 0.182	0.124 to 0.184

*Range of values reflects uncertainty in projection of heliostat costs in 1981 dollars.

unacceptably low flow rates for those panels still receiving normal incident flux from the unshaded portion of the field. Conversely, if flow rates are increased to provide adequate cooling for panels receiving full flux, total flow rates may be too large to maintain design outlet temperature.

- Installation and maintenance of feed-forward control sensors on the two-sided heated panels of the QCR concept will be difficult at best. Experience at CRTF has shown that sensors exposed to direct radiation are difficult to keep in operation.
- The increased surface area of the QCR two-sided heated panels makes pre-heat of panels with the collector field more difficult, precludes the use of trace heaters, and increases losses during overnight hold.

4.1.2 Rationale for the Selection of the PCR Concept

The PCR was selected as the baseline concept for the following reasons:

- It offers the most flexibility in key areas of control, overnight conditioning, and structural support.
- One-sided panel heating at flux levels of interest has been demonstrated at CRTF without major problems. Tube-to-tube weld problems at CRTF during the ACR-Phase 2 testing¹⁰ resulted primarily from the combination of serpentine flow temperature differentials, panel flux gradients, and growth differentials between tubes. The PCR concept does not have these conditions.
- The absorber area provides flexibility to develop an aim strategy that distributes aim points around the collector field so that the distortions in flux distribution resulting from clouds are minimized.
- The panel design maximizes modularity and minimizes field work for installation and removal for maintenance.
- Cost/performance characteristics are comparable with the QCR design.

In Task 3 we identified, analyzed, and parametrically evaluated refinements and potential improvements to the PCR concept. In the following sections, the approach, trade-off studies, and final RS configuration will be discussed.

4.2 REFINEMENTS/IMPROVEMENTS SELECTION APPROACH

The development of a refinements/improvements selection approach included four basic steps:

- Review of key issues
- Identification of design options
- Development of a selection methodology
- Definition of selection criteria.

4.2.1 Review of Key Issues

The key issues for the RS ultimately revolve around cost and performance and around the risk that the estimates of either cost or performance are incorrect. Because cost involves not only capital cost but also operating and maintenance costs, many factors (e.g., lifetime) are important. Similarly, because performance involves not only design point and annual efficiencies, but also availability and the operating envelope of solar and meteorological conditions, factors not generally associated with efficiency (e.g., control during partly cloudy days when insolation is measurable, but possibly not usable) are equally important.

The key issues confronting the designer and fabricator of a successful commercial RS are summarized in Table 4.4. The issues listed include not only those directly related to this project (e.g., panel fabrication process development), but also those under intensive development in other DOE programs (e.g., solar components design criteria, molten salt data base, absorber material

Table 4.4 Key Issues for RS

● Panel Lifetime

- *- Design criteria
- *- Salt data base at high temperatures
 - Tubewall thickness
 - Tube-to-tube and structural support attachments
- Design flux profiles
 - Peak flux
 - Flux gradients
- *- Absorber material

● Receiver Performance

- *- Convection losses
 - Absorptivity of PYROMARK paint at elevated temperatures
 - Absorber geometry and view factors
 - Minimum operational power level
- Design flux profiles
 - Absorber area
 - Spillover
 - Impingement on uncooled surfaces

● Receiver Cost

- Receiver weight
 - Absorber area (design flux profiles)
 - Tubewall thickness
- Absorber material
- Receiver support structure
- Pump development and cost
- Aperture door
- Fabrication costs
 - Welding development
- Absorber modularity
- Erection costs
- Tower height
- Parasitic power
 - Pumping
 - Trace heaters/insulation

● Receiver Operations and Control

- Overnight hold and morning start-up
- Cloud transients
 - Instrumentation
 - Flow paths
 - Path lengths
 - Control flexibility
- Seasonal and diurnal variations in flux profile
 - Control flexibility
 - Aim point strategy
- Response to fault conditions

● Receiver Availability/Maintainability

- Panel replacement/repair

*Key issues that are being addressed in complementary DOE development programs.

compatibility with molten salt, and receiver convection losses). Critical data still to be forthcoming from these programs include:

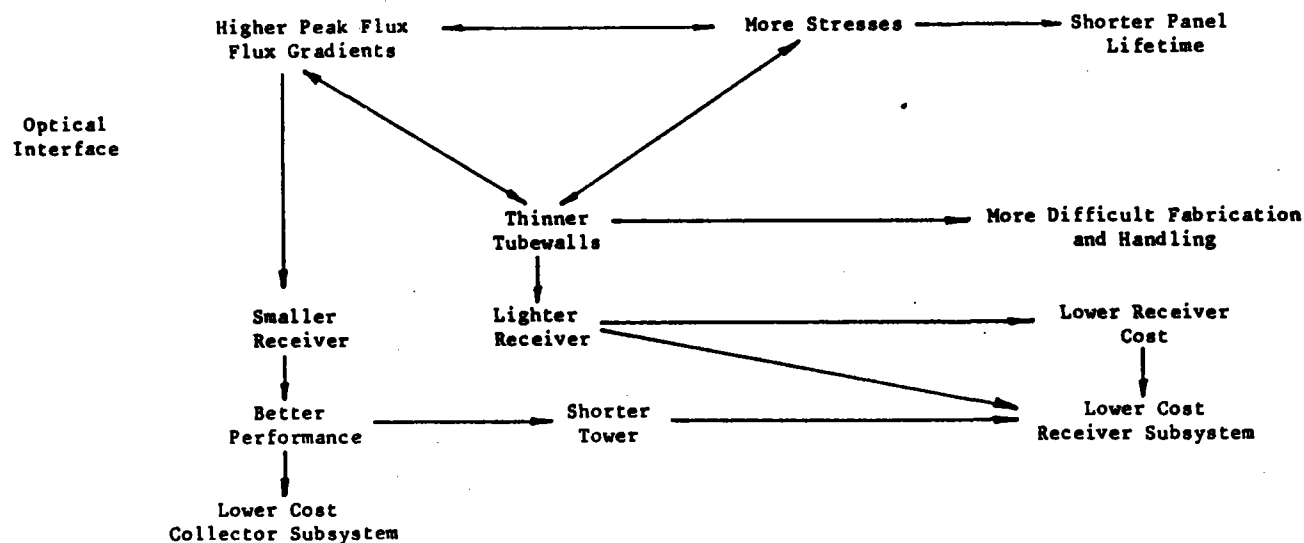
- Solar code design criteria
- Fatigue properties of various materials at high temperatures
- Resolution of controversies surrounding high-temperature salt properties
- Effects of impurities on salt stability and corrosion
- Analytical and experimental correlations of receiver convection losses.

Central to the RS design is the optical interface and absorber design. Because the conversion of reflected solar energy into thermal energy is the primary system function performed by the receiver, the driving elements in the RS design are the absorber and its optical interface and the interactions with the remainder of the RS elements.

Figure 4.2 summarizes the relationship of the optical interface requirements to the major receiver design issues. The design flux profiles appearing repetitively in Table 4.4 ultimately must reflect conflicting desires for both higher flux levels (higher performance, smaller absorbers, and lower cost) and lower flux levels (lower thermal stress, thicker tubewalls, easier panel fabrication, and longer panel lifetime). The trade-offs for these conflicting elements were one of the major activities of Task 3 and are discussed in Section 4.3.

Two other issues relating to optical interface are of major importance. First are the variations in design flux resulting from seasonal and diurnal motions of the sun and from clouds; second is the interaction between the collector field and the receiver during transient or abnormal conditions (e.g., warm-up of

A. Higher Peak Flux Reduces Cost but Increases Panel Fabrication Problems and Decreases Panel Lifetime



B. Lower Peak Flux Reduces Panel Fabrication Problems and Increases Panel Lifetime but Increases Cost

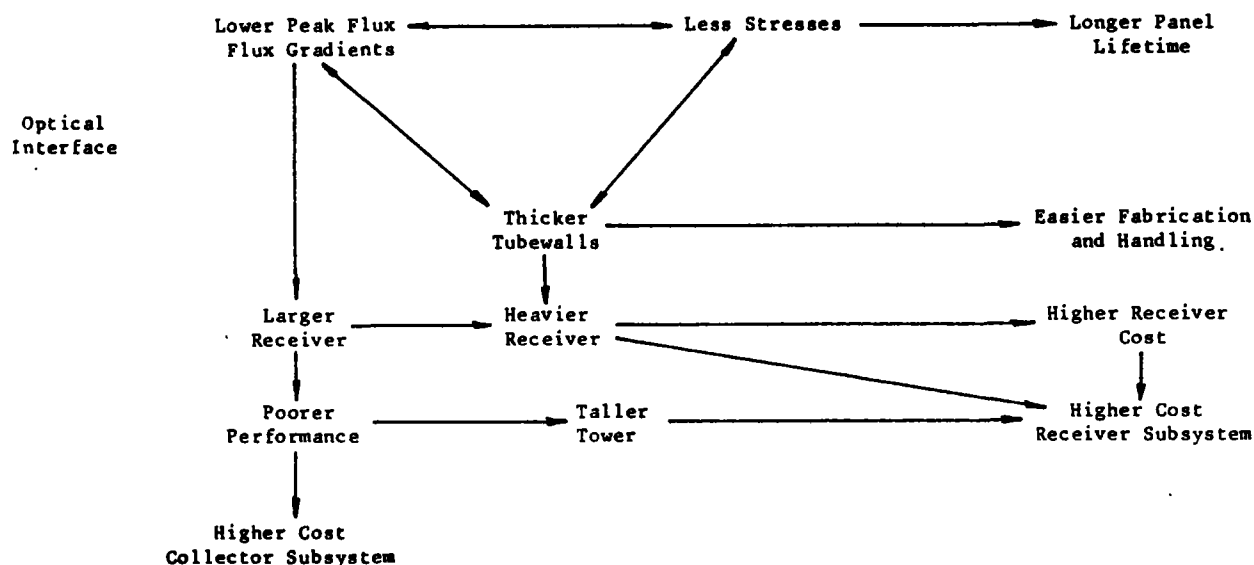


Figure 4.2 Effect of Optical Interface Requirements on Receiver Design

an unfilled receiver panel or overheating of the receiver panel following receiver pump failure).

The shifts in performance of local field areas with sun position and the changing image characteristics of heliostats in different field locations provide continuously varying fluxes, flux gradients, and thermal stresses on the receiver absorber panels. Cloud transients and the nonuniform effect of these transients that can result from certain aim strategies impose not only additional thermal stresses, but also additional control problems.

Detailed analyses for Barstow Solar 1 indicate that approximately 17 percent of the normal daylight hours will be partly cloudy. Clearly, the ability to capture a significant fraction of the available direct normal insolation during these periods is essential to the annual performance and economics of the central receiver system. Similarly, changing receiver start-up and shutdown from 15- to 10-deg sun elevation (as discussed in Section 3.2.5) results in a gain of annual energy greater than 3-1/2 percent. While this percentage may seem small, an additional 293 heliostats would be needed to compensate for the loss, which would add almost \$2.5 million to the CS cost (assuming heliostat costs of \$150/m²) without including required growth in receiver design power, size, and tower height.

Protection of the absorber from unacceptable heating is another major consideration relating to the optical interface, as discussed in Section 4.3.10.

4.2.2 Identification of Design Options

Among areas of major concern with the PCR concept were the following:

- Tilted cavity orientation
- Peak flux levels and tubewall temperatures, corrosion, creep fatigue, and salt stability
- Receiver door configuration
- Approach to overnight conditioning and receiver protection
- Requirement for all up-flow panels as opposed to serpentine flow.

Based on these concerns, the following six major design options were identified for further evaluation.

- Absorber configuration
 - Wing panel sizing and orientation
 - Cavity size and shape
 - Absorber orientation--tilted vs. vertical panels
 - External absorber panels above and below the cavity aperture
 - Cooled vs. uncooled cavity floor and ceiling
- Flow routing and control
 - Serpentine vs. all up-flow paths
 - Arrangement of panels in parallel and series flow paths; number and location of control valves
- Materials
 - Use of less-expensive materials
 - Availability
- Panel configuration
 - Tube diameters, wall thicknesses, and number of tubes per panel
 - Panel modularity
- Overnight and emergency operating procedures
 - Approach to overnight conditioning
 - Approach to receiver protection following pump, power, or collector field control failures

- Auxiliary equipment
 - Aperture door configuration
 - Salt feed pumps--type, number, and arrangement

Figure 4.3 illustrates four possible modifications to the PCR concept.

Key considerations with respect to these candidates include the following:

- Frontal area (spillover and thermal losses)
- Vertical vs. tilted
- Design criteria (materials and tube selection)
 - Salt film (tube I.D.) temperature limit (stability and corrosion)
 - Peak flux limits vs. temperature (30-year life)
 - Panel lateral gradients (flux and temperature).

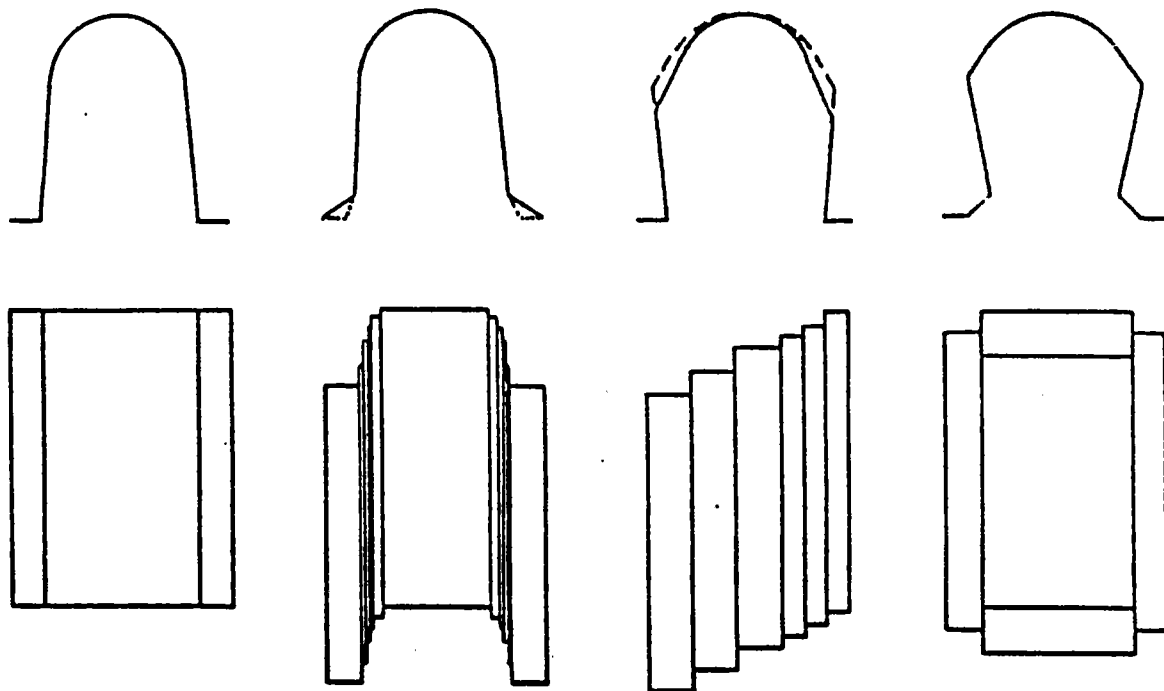


Figure 4.3 Candidate Absorber Configurations

In addition to serpentine flow routing, cursory consideration was given to different numbers and combinations of flow panels. Because of the obvious advantages of similar panels, only absorber geometries with identical panels were considered. Other items considered were:

- Four candidate panel materials: Type 304SS, Type 316SS, 9%Cr-1%Mo, and Incoloy 800
- Several tube diameters and wall thicknesses
- Panel fabrication both with and without spacers between the tubes.

Approaches considered for overnight conditioning were originally limited to receivers with an aperture door and receiver panels that remained full overnight. The candidate heating concepts considered included the following.

- Trace heaters attached to the back of the absorber tubes
- Radiant heaters on the receiver floor
- Immersion heaters in the surge tanks
- Fired heater in the surge tank
- Tower-mounted fired heater.

At SNLL's request, we investigated overnight drain and either preheat with an aperture door closed before fill and morning start-up or preheat with heliostats (no door required) before fill and start-up.

Among the receiver protection features considered were salt flow from the IST, a door with ablative front-face panels, a backup system for collector field defocus, and three half-capacity pumps (i.e., one backup pump).

Finally, the development of a preliminary receiver door design was identified as a major RS design issue.

4.2.3 Development of a Selection Process

The overall selection process and interrelationship of the different trade-off studies is illustrated in Figure 4.4. The top half of the chart relates to the development of the absorber configuration and the bottom half

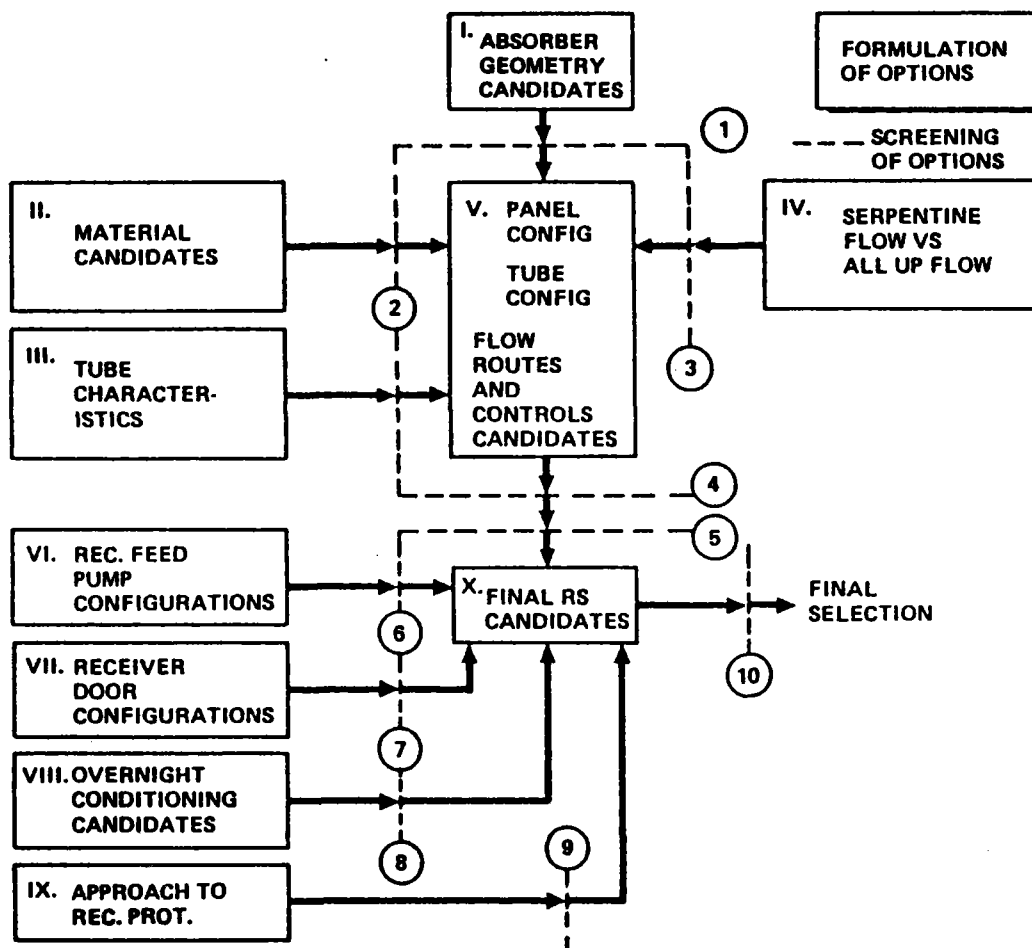


Figure 4.4 Concept Selection Process

relates to the selection of the equipment and operating approaches which allow the absorber to operate.

We evaluated four possible modifications to the PCR concept (Figure 4.3) using a simplified one-dimensional thermal model. This evaluation involved only the definition of absorber geometries and the calculation of flux profiles for these geometries. Based on the results of the evaluations of material candidates and tube characteristics, preliminary flux criteria were developed and used to screen absorber configurations. Considerations of panel fabrication from Task 6 were also a strong factor in these selections. Based on flow stability analyses, the requirement for all up flow was established and fed into the configuration of flow routes. Finally, all of these data were used to develop panel configurations, tube characteristics, flow routes, and controls.

Parallel to the absorber configuration analyses, but largely independent, were the other trade-off studies shown on the figure. Finally, at the completion of all of these trade-off studies, the final configuration was selected.

4.2.4 Definition of Selection Criteria

As discussed in Section 4.2.1, the most important evaluation criteria are ultimately cost, performance, and risk. Since it is possible to make comparative evaluations based on desirable/necessary attributes, the trade-off studies relied heavily on such comparisons wherever possible. The attributes used and their relationship to cost, performance, and risk issues are shown in Table 4.5. The table is based on our experience in receiver design and reflects important receiver attributes that are either desirable (e.g., low development risk) or necessary (e.g., ability to be drained).

Table 4.5 Concept Selection Criteria

<u>Criterion</u>	<u>Desirable/Necessary Attribute</u>
Cost	<ul style="list-style-type: none"> • Small absorber area • Low weight • Low-cost materials • Low-cost fabrication--all absorber panels the same (modularity) • Low-cost maintenance <ul style="list-style-type: none"> - Ease of panel removal - Low flux levels and thermal stresses - Low salt film (tube I.D.) temperatures <ul style="list-style-type: none"> -- Low corrosion -- Low salt regeneration/replacement • Low development cost/risk
Performance	<ul style="list-style-type: none"> • High thermal efficiency <ul style="list-style-type: none"> - Small frontal area - Cavity geometry--view factors • Operation with high-performance collector field • Low auxiliary power <ul style="list-style-type: none"> - Use stored thermal energy in OST - Careful door design - Low pressure drop in absorber • Large operating envelope <ul style="list-style-type: none"> - Low minimum power - Control and operation through cloud transients - Good thermal/hydraulic stability
Reliability, Availability, Response to Failures, and Safety	<ul style="list-style-type: none"> • Adequate design margins <ul style="list-style-type: none"> - Flux and tubewall temperatures - Film temperatures • Proven components • Reliable control sensors • Reliable door operation • Redundant pumps • Adequate receiver protection system • Ability to drain • Design simplicity

Not all attributes have equal weight. Low cost is important, but it must not be obtained at the expense of high technical risk or with a design that is difficult to maintain or repair.

Dominant factors in the initial screening of absorber configurations were minimum area consistent with peak flux levels, flux levels near the outlet where high salt film (tube I.D.) temperatures will occur, and flux gradients across the panels. With respect to materials selection, both corrosion resistance and high-temperature mechanical properties were the major factors. Additional considerations were given to material costs. Tube characteristics were selected by a combination of high-temperature thermal structural (i.e., peak flux) capabilities and ease of fabrication. Flow routing was governed primarily by the need for low flux in the high-temperature panels and to ensure a low pumping power requirement and good thermal hydraulic stability over a wide load range. The final absorber configuration ultimately embodied the combination of all these factors and included analyses of the pressure drop (low auxiliary power) and the tubewall, salt film (tube I.D.), and bulk fluid temperatures.

The receiver feed pump arrangement was chosen on the basis of reliability and auxiliary power--especially at the low loads common during early morning and evening operations.

The receiver door configuration selection was guided by consideration of low auxiliary power for overnight conditioning, absorber protection in the event of a power or control failure, and rapid morning start-up without the delays that would result from panel preheat and fill if the absorber needed to be drained every night.

The criteria most important in the evaluation of approaches to overnight conditioning were cost, reliability, ease of installation, and maintenance. Additionally, considerations of the operating envelope (i.e., performance) and auxiliary power, as well as the risk of operation without a door to protect the absorber, were included in the evaluation of overnight receiver draining.

The evaluation of the approach to receiver protection included considerations of redundancy, use of proven components, and cost.

The final selection resulted mostly from an accumulation of the individual selections.

4.3 TRADE-OFF STUDIES

In this section trade-off studies relating to the absorber configuration and to various receiver support equipment will be discussed. Details of these trade-offs are presented in Appendices C through H and the type of data used is summarized in Table 4.6.

Absorber configuration trade-off studies included parametric analyses of:

- Absorber surface arrangement, including tilted vs. vertical orientation
- Absorber materials
- Tube dimensions
- Allowable flux levels
- Thermal/hydraulic stability of all up and serpentine flow
- Panel geometry, arrangement, and flow routing

Other trade-offs that were made in parallel include:

- Aperture door configuration and size
- Overnight conditioning
- Feed pump arrangement
- Receiver protection

Figure 4.5 is the flowchart of the parametric analyses. We began by adjusting the candidate absorber configurations to obtain reasonable flux profiles and eliminate those configurations that were obviously undesirable. For those that were attractive based on considerations of flux profiles and absorber area, we defined panel configurations, flow paths, control valves, tubewall thicknesses, and absorber materials.

- The selection of panel configurations, flow paths, and control valves was based on ability to be drained and controlled, modularity, thermal/hydraulic stability, and the need to have relatively cooler fluid in high-flux regions and the highest temperature fluid in the panels with low thermal losses.

Table 4.6 Trade-Off Studies Selection Data

<u>Receiver Configuration Data</u>	<u>Panel Design Conditions</u>	<u>Receiver Performance Data</u>
Absorber area	Minimum power	Efficiency (design point and annual average):
Absorber panel configuration:	Maximum power	Convection
Number	Peak flux level	Radiation
Length	Maximum lateral flux	Conduction
Width	gradient	Spillover
Number of tubes	Peak wall temperature	Annual energy to storage
Tubewall thickness	Peak film temperature	Annual parasitic energy
Absorber weight	Minimum flow rate	
Support structure weight	Maximum flow rate	
Door configuration and weight	Pressure drop at maximum	
Total weight atop tower	flow rate	
	Flow velocity at maximum	
	flow rate	
	Flow velocity at minimum	
	flow rate	
<u>Auxiliary Equipment</u>	<u>Receiver Operation and Controls</u>	<u>RS Cost Data</u>
Collector field area	Maximum power	Receiver fabrication
Number of heliostats	Minimum power	Tower
Tower type	Maximum salt flow rate	Construction
Tower height	Minimum salt flow rate	Total subsystem
Receiver feed pump type:	Pressure drop at minimum flow	
Number	rate	
Head	Time to drain	
Flow rate	Number of control valves	
Auxiliary heaters for condi-	Control sensors	
tioning of salt equipment	Method for overnight condi-	
Number	tioning	
Rated power	Peak power requirements	
	Pumping power design point	
	annual power consumption	
		<u>Relative Receiver O&M Cost</u>
		<u>Collector Field Cost Estimate</u>
		<u>Cost of Energy to Thermal Storage</u>
		Capital
		Parasitic
		Relative O&M

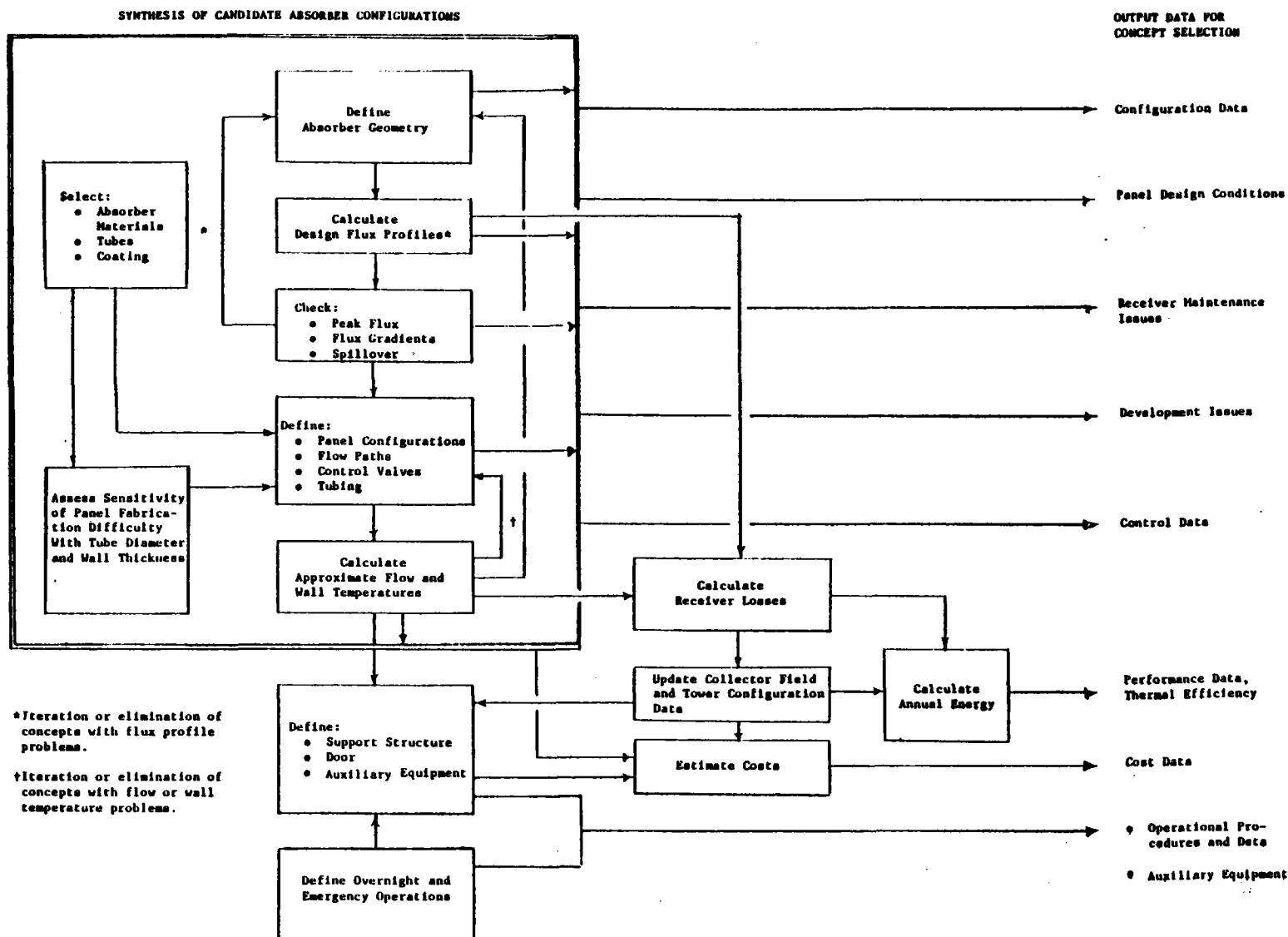


Figure 4.5 Flowchart of Parametric Analyses

- The selection of tubewall thickness reflects considerations of flux level, heat transfer, thermal stress, panel lifetime, and ease of fabrication.
- Absorber materials were selected on the basis of material properties, cost, and resistance to salt corrosion.

Approximate wall and fluid temperatures were generated for these configurations using simplified models. These data were used to screen further candidate configurations. If configurations were unacceptable they were either iterated, as shown on the figure, or eliminated.

The output of these analyses was used to complete the definition of the RS equipment, cost, and performance and to provide data for the final configuration selection. For those configurations that were most attractive, we estimated receiver losses, rescaled the collector field and tower configurations, and calculated annual energy delivered to thermal storage.

We defined the auxiliary equipment required for overnight conditioning, start-up, shutdown, and emergency operation. In these analyses we investigated options for keeping the panels hot overnight as opposed to draining them overnight and preheating them before early morning start-up. The requirements for overnight heating were assessed and the trade-offs between electrical trace and radiant heating of the panels and the circulation of heated salt were investigated. We compared the fill-and-drain of the downcomer with overnight hold. In all of these cases, we addressed both equipment costs and parasitic power requirements. Surge tanks and selected pumping or pressurizing schemes were sized to provide emergency coolant flow in the event of a power or receiver feed-pump failure. We also identified options for the aperture door.

4.3.1 Absorber Surface Arrangement

Four basic modifications to the PCR absorber geometry were considered.

- Cooled vs. uncooled cavity floor and ceiling
- External absorber panels above and below the aperture
- Wing panel size and orientation
- Cavity size, shape, and orientation (tilted vs. vertical).

Flux data were generated for each of these modifications and evaluated for desirable characteristics (i.e., low peak fluxes, reasonable flux gradients across panels, and reasonable utilization of absorber surface area). Details of these analyses are presented in Appendix C.

The cooled cavity floor and ceiling were eliminated because a substantial change in floor and ceiling slope is required to get adequate flux levels and because of the complexity of building and supporting unevenly shaped panels for the floor and ceiling. Panels above and below the cavity were also considered; however, they were eliminated because the steep vertical variation in flux level create serious lateral flux gradients for panels with horizontal tubes and, conversely, because panels with vertical tubes would have a large number of short tubes and problems with shielding the lower headers. Because there appeared to be no clear flux distribution advantage with variable panel widths, the final configuration was developed for a single panel width.

Tilted and vertical cavity orientations were considered. Key thermal/hydraulic characteristics for both orientations are compared in Table 4.7.

The vertical orientation was selected for the following reasons:

- Cost and performance are "equal"
- The vertical receiver is simpler and more conventional
 - Structural support
 - Design and construction
 - Door design, installation and operation
 - Panel inspection, maintenance, and replacement
- Thermal/hydraulic and tube stress performance are comparable to the tilted configuration.

Table 4.7 Comparison of Tilted and Vertical Orientations*

<u>Description</u>	<u>Tilted</u>	<u>Vertical</u>
Panel height, m (ft)	26.0 (85.3)	26.0 (85.3)
Incident power, MW	161.6	159.7
Peak flux, MW/m	0.616	0.648
Absorbed power, MW	150.2	148.7
Frictional P, kPa (lb/in)	697 (101.1)	642 (93.1)
Tubewall temperature, °C (°F)†		
O.D.	646 (1194)	657 (1215)
Mean	621 (1150)	632 (1170)
I.D.	603 (1117)	608 (1127)

*288°C (550°F) in, 566°C (1050°F) out, 950 W/m insolation; 8371 heliostats; Noon; one-half receiver.

†Maximum value at worst location.

Finally, considerable effort was expended to develop a cavity configuration that had a good utilization of absorber surfaces (i.e., reasonable flux levels everywhere) and still did not violate flux gradient, peak flux, or salt and tubewall temperature limitations.

4.3.2 Materials Selection

When designing the RS components, materials must be selected to meet the specific conditions of temperature and environment to which they will be subjected. The conditions considered in the selection of a material are:

- Operating temperature
- Possible maximum temperature
- Type of atmosphere or other corrosion conditions
- Expected life
- Type and magnitude of load
- Welding and fabrication
- Cost

The properties that were considered are:

- Creep strength
- Stress-rupture life
- Ductility
- Short-term tensile properties
- Surface stability
- Microstructural stability
- Thermal conductivity
- Thermal fatigue
- Thermal expansion
- Weldability
- Hot workability
- Cold workability

The criteria used were:

- Alloys must have documented mechanical properties which form a sound basis for design. Materials covered by the ASME Code or cases within the Code are regarded as preferred candidates. Materials which lack a widespread data base

may be considered as candidates for a future cost improvement program, but will not be selected for the first commercial plant.

- Alloys must be compatible with each other and with system working fluid.
- Alloys selected must be readily available and not overly difficult to fabricate. Preference will be given to metals frequently used in industry and available in a wide variety of product forms.

After a preliminary screening process, four materials were selected as candidates for panel fabrication:

- Type 304SS
- Incoloy 800
- Type 316SS
- 9%Cr-1%Mo

The material selection for the absorber panels and headers was based on a review of the high-temperature mechanical properties and a number of corrosion testing programs at SNLL, Martin Marietta Corporation (MMC), and Oak Ridge National Laboratories. These tests determined the degrees of susceptibility of various alloys to general corrosion and stress corrosion in a molten salt environment.

Thermal convection loop apparatus has been used at SNLL to study the corrosion behavior of Types 304SS, 316SS and Incoloy 800.¹²⁻¹⁵ The results of these thermal convection loop tests demonstrate that the general corrosion rates of both Incoloy 800 and Type 316SS are acceptable for long-term use in molten salt at temperatures as high as 600°C (1112°F). The corrosion rates measured by chemical descaling of corrosion coupons indicate 0.0135 mm (0.53 mil)/yr for Type 316SS and 0.0074 mm (0.29 mil)/yr for Incoloy 800 during isothermal exposure to 600°C (1112°F). Thus current data on the possible corrosion of metals

by molten nitrate salt, while limited, indicate that corrosion by the relatively pure salt should not be a major concern in materials selection.

Since the nitrate salts are strong oxidizers, oxidation resistance is a major consideration. All candidate materials oxidize by the outward diffusion of iron and the inward diffusion of oxygen to form a two-layer scale, with Fe_2O_3 comprising the outer layer. Accordingly, the material in contact with the molten salts is Fe_2O_3 ,--regardless of the materials being utilized. Pretreatment of the materials, particularly the ferritic steels, is important to produce a dense adherent scale in service. Depletion of chromium in surface layers has also been observed; however, the implication of these effects on corrosion rates, strength, and lifetime has not been established.

The microscopic examination and chemical identification of scales occurring on the outside surfaces of specimens subjected to nitrate-nitrite salts ($40\%\text{NaNO}_2$, $7\%\text{NaNO}_3$, $53\%\text{KNO}_3$) and nitrate salts ($60\%\text{NaNO}_3$, $40\%\text{KNO}_3$) in SNLL and MMC test programs indicate that the molten salt corrosion mechanism results primarily from oxidation processes.^{8,10}

Oxide flaking has been observed on carbon steel and 2-1/4%Cr-1%Mo steel alloys subject to relatively short-term exposure. However, evidence indicates that the films formed on these alloys become more stable after longer term exposure, producing an oxidation behavior similar to that observed on boiler tubing that has been exposed to water/steam environments.

A review of molten salt technology shows that carbon steel has been a satisfactory tubing material in over 500 commercial units where nitrate-nitrite salt has been used as the heat-transfer medium.¹⁶ While most of these industrial units operate in the 371 to 454°C (700 to 850°F) range, a number operate as high as 499°C (930°F), and at least two are still operating satisfactorily after 10 years between 510 and 538°C (950 and 1000°F).

In extended open-air immersion tests conducted by MMC, carbon steel suffered minor metal loss in nitrate salt after exposure for 16,000 cycles at 399°C (750°F). The surface loss was calculated at 6.5 mil based on a 30-year extrapolation of specimen weight-change data.¹⁰

In open beaker immersion tests conducted at SNLL, both carbon steel and 2-1/4%Cr-1%Mo steel suffered weight changes equivalent to slightly less than 1 mil after 4560 hours (190 days) of exposure to nitrate-nitrite salt, maintained at 550°C (1022°F).⁸

The literature survey indicated that Incoloy 800 is resistant to environmental cracking under a variety of loading conditions and, while more limited data show the corrosion rates for the lower cost Types 304SS and 316SS alloys are also acceptable, the results of environmental cracking studies for these alloys are not yet available.

Types 304SS and 316SS alloys are more susceptible to stress-corrosion cracking mechanisms than Incoloy 800 if contaminants (i.e., chloride ions) are inadvertently entrained in the system. The deposition/entrapment of chloride-containing residues and other contaminants on material surfaces can occur during

panel welding, handling, shipping, testing, storage, erection, and outdoor exposure as well as from the use of chloride-containing insulation.

The modified 9%Cr-1%Mo alloy is attractive because of its lower cost and its relative immunity to stress-corrosion cracking. However, it is not an ASME Code-approved material, is brittle in the as-welded condition, and requires pre-weld preheat and post-weld stress relief to prevent the formation of weld-induced cracking. These operations may be difficult and expensive to perform on a 27.5-m (90-ft)-long panel; thus material cost savings could be offset by higher fabrication costs. Furthermore, a substantial amount of welding development will have to be done before 9%Cr-1%Mo can be used for the absorber panel tubes.

Some creep-fatigue data are available on stainless steel Types 304 and 316, Incoloy 800H, and 2-1/4%Cr-1%Mo, and these data are used in the Elevated Temperature Code Case N-47.¹⁷⁻¹⁹ The tests listed in the cited references were not done in a molten salt environment. The results of creep-fatigue tests in a molten salt loop are not conclusive.⁹ Some creep-fatigue tests on tubes (Incoloy 800 and Type 316SS) were performed at Argonne National Laboratory,²⁰ with analytical support provided by Foster Wheeler.²¹

Uncertainty regarding creep-fatigue data exists not only for molten salt receivers but for all types of solar receivers. Lack of appropriate data will create uncertainty in the life of the receiver components, especially the absorber panels. Extensive creep-fatigue tests with hold times of 1 to 6 minutes on tubes of various materials in a molten salt loop are recommended. However, while these tests would be very useful in the long term, they would take too

long to generate data in time to meet the schedule for this program. In our opinion, the best alternative would be to design the receiver so that panels or individual tubes can be replaced easily and to accept the fact that tube life in certain critical, high-temperature zones in the receiver might be less than the desired design life.

In view of these considerations and to meet the 30-year design life requirement, Incoloy 800 material was selected for the high-temperature absorber panels. The Incoloy 800 was selected over the austenitic stainless steels because it is much stronger at elevated temperatures and has good low-cycle fatigue strength and ductility. Type 316SS could have been used in the high-temperature panels, but our analysis indicated that it would not meet the 30-year design life. For the low- and medium-temperature panels, Types 304SS and 316SS alloys were selected.

To have panel modularity in the molten salt receiver SRE, all absorber panels have to be made of Incoloy 800. This modularity would minimize the number of spares required by the utility. The other option was to have identical panels made of different materials: Types 304SS and 316SS and Incoloy 800 for the low-, medium-, and high-temperature panels respectively. Cost estimates made during Tasks 4 and 5 showed a possible savings of \$500,000 in material costs alone for the "multiple materials" option over the "all Incoloy 800" option. Because the requirement to have all panels made of Incoloy 800 imposes a very high cost penalty, during Task 4 we selected the "multiple materials" option--panels identical in all respects but materials. Thus the utility can still have a minimum number of spares made of Incoloy 800 to use as a replacement for any receiver panel.

Table 4.8 shows the RS materials selection based on the results of Tasks 3, 4, and 5. Based on our review of available data on molten salt corrosion, we recommend a corrosion allowance of 0.38 mm (15 mil) for Types 304SS and 316SS and 0.25 mm (10 mil) for Incoloy 800. These values are based on six scale exfoliation cycles every five years during the 30 years of operation at the maximum operating temperature of 566°C (1050°F). These corrosion allowances seem more than adequate when considering that the RS will operate at rated conditions during approximately half a day only.

Table 4.8 Material Selection*

<u>Location</u>	<u>Material</u>
Interconnecting piping:	
Primary riser	Carbon steel
Between Passes 1 and 2	1-1/4%Cr-1/2%Mo
Between Passes 2 and 3	2-1/4%Cr-1%Mo
Between Passes 3 and 4	Type 304SS
Between Passes 4 and 5	Type 304SS
Primary downcomer	Type 304SS
Panels and headers:	
Pass 1	Type 304SS
Pass 2	Type 304SS
Pass 3	Type 316SS
Pass 4	Incoloy 800
Pass 5	Incoloy 800

*Relative to material selection, we have assumed that the salt purity level will be maintained by a salt purification system, which is not within the scope of the RS.

4.3.3 Tube Size Selection

Because of cost the basic criterion for selection of tube size was to use the largest O.D. (fewer welds and lower fabrication costs) and thinnest wall (less weight, lower material cost, and higher allowable incident fluxes) possible within fabrication and stress constraints. As shown in Table 4.9, we considered 25.4, 31.8, and 38.1 mm (1, 1.25, and 1.5 in.) tube diameters. Smaller tubes were not commercially available with the desired wall thickness. These tubes were evaluated on the following basis:

- With the exception of 9%Cr-1%Mo, the minimum thickness required by the ASME Code, Section VIII-Division 1, is well below the 1.65 mm (0.065 in.) required for panel fabrication (see Section 6), even when the recommended corrosion allowances are added to values of Table 4.9.
- For similar pumping power requirements, analysis for 31.8 mm (1.25 in.) O.D. tubes indicated that the heat-transfer coefficients would be about 25 percent lower and the maximum allowable fluxes 17 percent lower than those values for 25.4 mm (1 in.) O.D. tubes.

Table 4.9 Minimum Wall Thicknesses*†

<u>Material</u>	<u>O.D. 25.4 mm (1 in.)</u>	<u>O.D. 31.8 mm (1.25 in.)</u>	<u>O.D. 38.5 mm (1.5 in.)</u>
Incoloy 800	0.297 (0.0117)	0.371 (0.0146)	0.447 (0.0176)
Type 316SS	0.310 (0.0122)	0.389 (0.0153)	0.465 (0.0183)
Type 304SS	0.396 (0.0156)	0.495 (0.0195)	0.594 (0.0234)
9%Cr-1%Mo	1.219 (0.048)	1.524 (0.060)	1.829 (0.072)

*These are purely code calculations. No corrosion allowance has been made.

†Temperature = 593°C (1100°F); Pressure = 2.069 MPa (300 lb/in²g).

- The ability to weld tubes with an O.D. larger than 25.4 mm (1 in.) was investigated. From a fabrication viewpoint, larger diameter tubes would present more fabrication problems. A greater amount of weld-induced distortion would occur because the weld is moved further from the neutral tube axis as the diameter increases.

Based on these considerations, 25.4 mm (1 in.) O.D. tubes with 1.65 mm (0.065 in.) wall thicknesses were selected for panel fabrication.

4.3.4 Allowable Flux Levels

To determine the maximum allowable flux levels, we did parametric thermal stress analyses on 25.4 mm (1 in.) O.D. tubes made of the candidate panel materials (Types 304SS and 316SS, Incoloy 800, and 9%Cr-1%Mo). The results are shown in Figure 4.6 as a function of the salt bulk temperature. The method used to

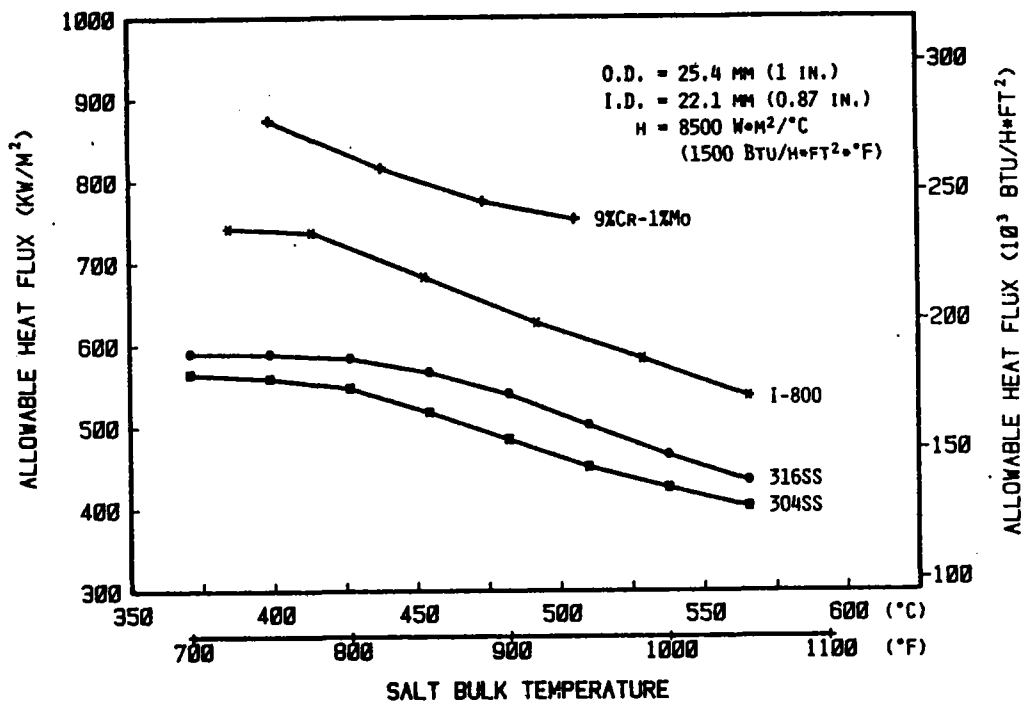


Figure 4.6 Allowable Heat Flux on Absorber Panel Tubes

arrive at these curves is given in Appendix D. From Figure 4.6, the allowable flux levels for Incoloy 800 are higher than those for Types 304SS and 316SS because of the higher creep-rupture strength of Incoloy 800. The allowable flux levels for 9%Cr-1%Mo, despite inferior creep-rupture properties, are even higher because of higher thermal conductivity, lower coefficient of thermal expansion and, consequently, lower thermal stresses.

The evaluation of panel/absorber candidate geometries and flow routes during Task 3 was guided by the following constraints:

- Maximum tubewall (tube O.D.) temperature should not exceed 649°C (1200°F)
- Allowable front-to-back tube temperature gradient should not exceed the values determined by stress analysis
- Maximum salt film (tube I.D.) temperature should not exceed 593° (1100°F).

The first two are a direct result of the parametric stress analysis; the third, because molten salt decomposition begins at ≈ 593 to 600°C (1100 to 1112°F).^{22,23}

4.3.5 Serpentine Flow vs. All Up Flow

An assessment was made of the stability of downflow panels (Appendix E).

The results indicate the following:

- Up-flow panels are stable at the design, maximum, and minimum load conditions; no instability is expected as a result of heat-flux variations.
- Downflow panels are unstable and could be subject to flow stagnation or reversal at the design and minimum load conditions.

Tube inlet flow restrictions could change the flow characteristics of the downflow panels, thus making them stable. However, such a restriction adds complexity to the control system and increases pumping power requirements. Given the highly fluctuating load conditions characteristic of a solar plant, the panels will be subjected to many load perturbations during the day, increasing the possibility of flow instability.

The bottom line is cost vs. risk. The total cost of downcomers between passes was estimated at \$250,000 (including installation and insulation). We believe that the saving by eliminating 10 downcomers does not justify the risk. Because we do not recommend the use of downflow panels until their stability is demonstrated by extensive testing, all up-flow panel circuitry was selected.

4.3.6 Panel Geometry and Flow Routes

Preliminary panel arrangements and flow routes were evaluated using the incident flux profiles and a simplified thermal/hydraulic computer model to estimate tubewall and salt temperatures and pressure drops. Details of this analysis are contained in Appendix F.

The key result from this analysis is that outlet pass flux levels are limited by salt film (tube I.D.) temperature rather than by tube creep-fatigue life. Therefore, the outlet pass must be located in regions of low flux.

4.3.7 Aperture Door Configuration

Because of its importance for the overnight conditioning approach (see Section 4.3.9), a preliminary evaluation of an aperture door was conducted. Details of this evaluation are presented in Appendix G.

Primary requirements for the door include good sealing to minimize heat loss through air convection and rapid closing (by gravity) to protect the absorber in the event of loss of salt flow and the inability to defocus the heliostat field because of either power or control system failures.

Based on these preliminary evaluations, the key issues for door design include the following:

- Insulation on the inside and outside with openings to allow the door structure to breathe and minimize thermal distortion
- Door seals, especially on the sides, where active seals that swing into place after the door is closed may be required
- Ablative tiles, replaceable to protect the door in the event of an emergency closing after a power failure
- Track and trolley system that will not bind from thermal expansion when the door is opened or closed
- Quick-close mechanism that will allow the door to close by gravity in less than 60 seconds.

The detailed door design was made during Task 5 (see Section 5.4).

4.3.8 Feed Pump Arrangement

To select the molten salt RS feed pumps, we contacted four vendors after a preliminary screening process: Lawrence, Byron Jackson, Bingham-Willamette, and Rockwell International.

The RS feed pump arrangement was chosen after considering cost, availability, reliability, part-load operation and power requirements. The selected arrangement consists of three half-capacity pumps (2 operating and 1 spare).

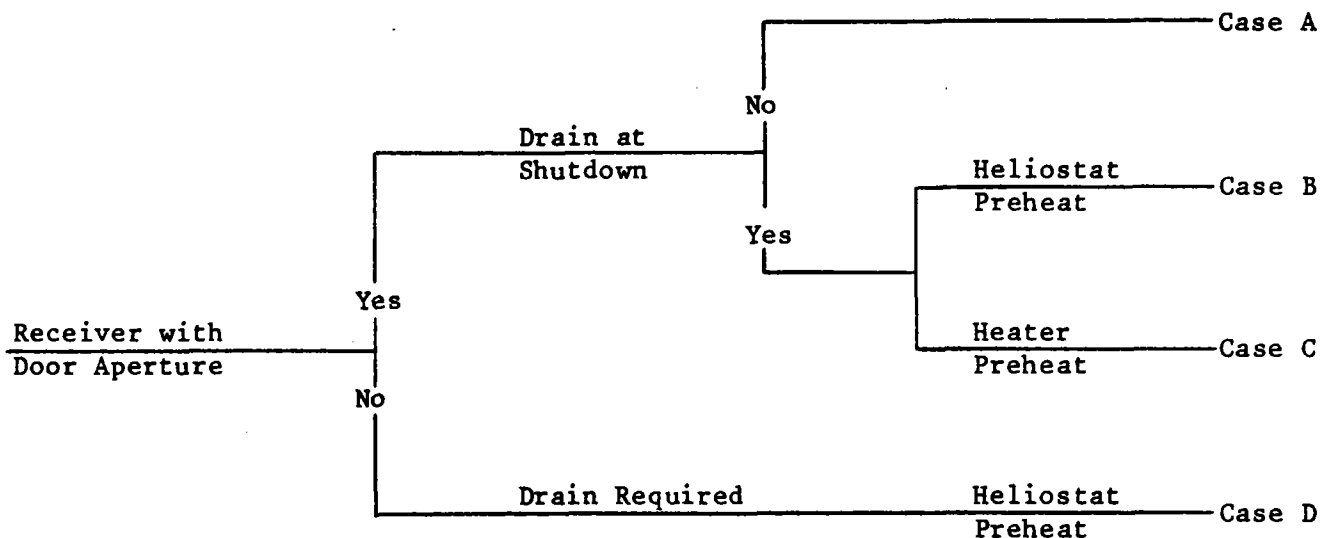
- For 50-percent capacity, there are several pumps available in the marketplace, allowing greater freedom of selection.

- Increased operating flexibility is ensured during part-load operation (i.e., part-load can be handled by one pump).
- There is increased reliability with three 50-percent pumps. One pump will be a backup; and even in the event of the failure of two pumps, there will still be a 50-percent flow through the receiver.
- Plant shutdown because of pump failure is practically nonexistent; one pump can be repaired while the other two are operating.
- Plant turndown capability is increased.

Bingham-Willamette vertical, centrifugal pumps, Type VCN were selected (Section 7.1.3).

4.3.9 Approach to Overnight Conditioning

The following matrix was investigated:



- Case A
 - Provide aperture door
 - Do not drain receiver
 - Keep warm overnight
- Case B
 - Provide aperture door
 - Drain at shutdown
 - Use heliostats for preheating
- Case C
 - Provide aperture door
 - Drain at shutdown
 - Use radiant heaters for preheat
- Case D
 - Omit aperture door
 - Drain at shutdown (mandatory)
 - Use heliostats for preheating

Each of these cases was evaluated, and the first (Case A) was selected. Table 4.10 highlights the major options evaluated. Details of the evaluation are given in Appendix H. Case A was selected because it offers the greatest flexibility, provides for morning start-up without heliostat preheat of the panels, and provides for protection of the receiver in the event of a power or control failure using the aperture door. Crucial to this selection is the design of a highly reliable aperture door with good seals (Section 5.4). A discussion of the advantages and disadvantages of the various options follows.

For a receiver without an aperture door, panel morning preheat with heliostats before fill and start-up is required. Heliostat beam distortion and cavity geometries generally cause nonuniform flux distribution during morning preheat and create the problem of providing adequate heat in some areas without overheating in others. The lack of thermal inertia and variable cooling provided by initial salt flow means that a careful balance must be kept between incident flux and losses so that panel overheating will not occur. These factors dictate a gradual heating up of panels, which reduces the operating time and usable annual energy.

Table 4.10 Overnight Conditioning Evaluation

<u>Option</u>	<u>Advantages</u>	<u>Key Issues</u>	<u>Recommendation</u>
Aperture door	<ul style="list-style-type: none"> • Receiver protection • Operate with receiver full overnight to minimize start-up delay 	<ul style="list-style-type: none"> • Reliability/availability • Cost 	Include door
Drain receiver overnight	<ul style="list-style-type: none"> • Save auxiliary power • Reduce risk of panel freeze 	<ul style="list-style-type: none"> • Morning start-up delay 	Do not drain panel
Electric heaters (radiant/trace)	<ul style="list-style-type: none"> • Low initial cost • Modular/redundant • Operational simplicity 	<ul style="list-style-type: none"> • Operating cost 	Select electric radiant heaters
Gas-fired heater with salt circulation	<ul style="list-style-type: none"> • Low operating cost 	<ul style="list-style-type: none"> • Initial cost • Operating complexity • Reliability/availability 	Do not select a gas-fired heater

The analysis in Appendix H indicates that by utilizing the heliostat field to preheat the panels a start-up delay of 19 minutes and thus a loss of 1.3 percent of the annual collected energy will result, compared with a saving of 0.7 percent in auxiliary electricity if the receiver is not heated overnight. Annual energy differences are not large--provided system availability penalties are equivalent. Specifically, the major impact on annual energy will be caused by time lost from either door problems in the heated case or fill problems in the unheated case. While door reliability/availability has not been assessed, the panel preheat analysis has shown that substantial differences in panel temperatures are likely for a partial cavity configuration and that a slow and careful heat up will be required to preheat the panels in a safe manner. The complexity of this procedure is such that its application to commercial practice is questionable. In addition, some fraction of operating time beyond initial morning hours may be lost as a result of inability to fill. Final resolution of this trade-off study appears to depend on the reliability and cost of the aperture door. In this study we decided to use the door/no-drain/heated option and proceed with the effort to generate a detailed door design and cost estimate. These data, along with door reliability data from Phase 2, will be used to reevaluate this trade-off for future commercial receiver designs.

Counterbalancing the advantages of the selections are the difficulties and expense of the door design, the need to guarantee reliable door operation or face lost operating time, and the auxiliary power required to keep the absorber warm overnight.

Within the selected case, the following methods for keeping the salt from freezing were considered:

- Electric immersion heaters in surge tanks
- Fired heaters in surge tanks
- Electric trace heaters attached to absorber panels
- Electric radiant heaters located on cavity floor
- Salt circulated through a tower-mounted fired heater

After a preliminary evaluation, we rejected the first two. The remaining three methods are compared in Table 4.11. Of these the radiant heaters have the lowest initial cost, weight, and maintenance. The gas-fired salt heater with salt circulation, while higher in initial cost, is lower in operating costs. However, there is some complexity associated with the operation of a gas-fired heater and its associated salt circulation pump and valves that is not present with the radiant heaters. Thus radiant heaters were selected because of operating simplicity, low capital cost, and inherent redundancy in the modularity of the units.

In summary, the selected thermal conditioning approach utilizes an aperture door, no overnight receiver drain, radiant heaters, and thermal energy of the hot salt from the OST. Radiant heating requirements were redefined during Task 4 (Section 5.2.3) when aperture door details and more accurate receiver heat loss estimates became available.

4.3.10 Approach to Receiver Protection for Fault Conditions

The receiver will be protected from damage by several design features. A pressurized IST will provide for full salt flow to the receiver for at least

Table 4.11 Comparison of Thermal Conditioning Methods

<u>Method</u>	<u>Cost (\$1000)</u>	<u>Weight kg (lb)</u>	<u>Operating Cost (\$1000/yr)</u>	<u>Maintain- ability</u>	<u>Disadvantages</u>
Panel tracing	45	900 (2000)	64	Difficult	<ul style="list-style-type: none"> ● Attachment difficult ● Not dependable ● Inaccessible
Radiant heaters (selected concept)	32	450 (1000)	77	Easy	<ul style="list-style-type: none"> ● Exposed during normal operation ● Highest operating cost
Gas-fired salt heater	118	1800 (4000)	21	Moderate	<ul style="list-style-type: none"> ● Highest initial cost ● Impact on tower ● Not usable for cold start

60 seconds and provide protection from full aperture flux with an ablative covering.

With normal auxiliary power the heliostat field will defocus from full power to 40 percent power in 1 minute and zero power in 2 minutes. An emergency diesel generator (part of the CS) will be available to defocus the heliostat field in the event of a power loss. All valves will have appropriate fail-safe positions to prevent flow through the receiver from being blocked during a power failure. All piping and equipment must be capable of draining to prevent freezing if trace heating is not operable. Three half-capacity pumps will permit operation to continue if one pump fails. Finally, the control system will provide for automatic failure operations.

The most serious failure is the loss of salt flow to the absorber panels under solar incident flux, which could result in tube failure, warping, or reduction in life. In this case, the heliostats must be defocused from the receiver while the emergency flow supply from the IST maintains some coolant flow. As long as the collector field can operate, such an approach is adequate; however, if it is impossible to defocus the heliostats because of either power or control system failures, the length of time required for the sun to drift enough to reduce incident fluxes is too long to prevent damage to the absorber panels. Protection during this combination failure is provided by the quick-closing door with ablative face and flow from the pressurized IST. In this case the aperture

door will experience a peak flux transient, as shown in Figure 4.7. Table 4.12 lists probable causes for and responses to these failures.

The second group of failures involves a reduction in required flow, which would lead to excessive salt and panel tubewall temperatures. Table 4.13 lists indicating signals for, and responses to, these failure modes.

The freezing of salt in the system can cause flow to be blocked or equipment to rupture. If electrical heaters fail, the receiver will be drained and shut down.

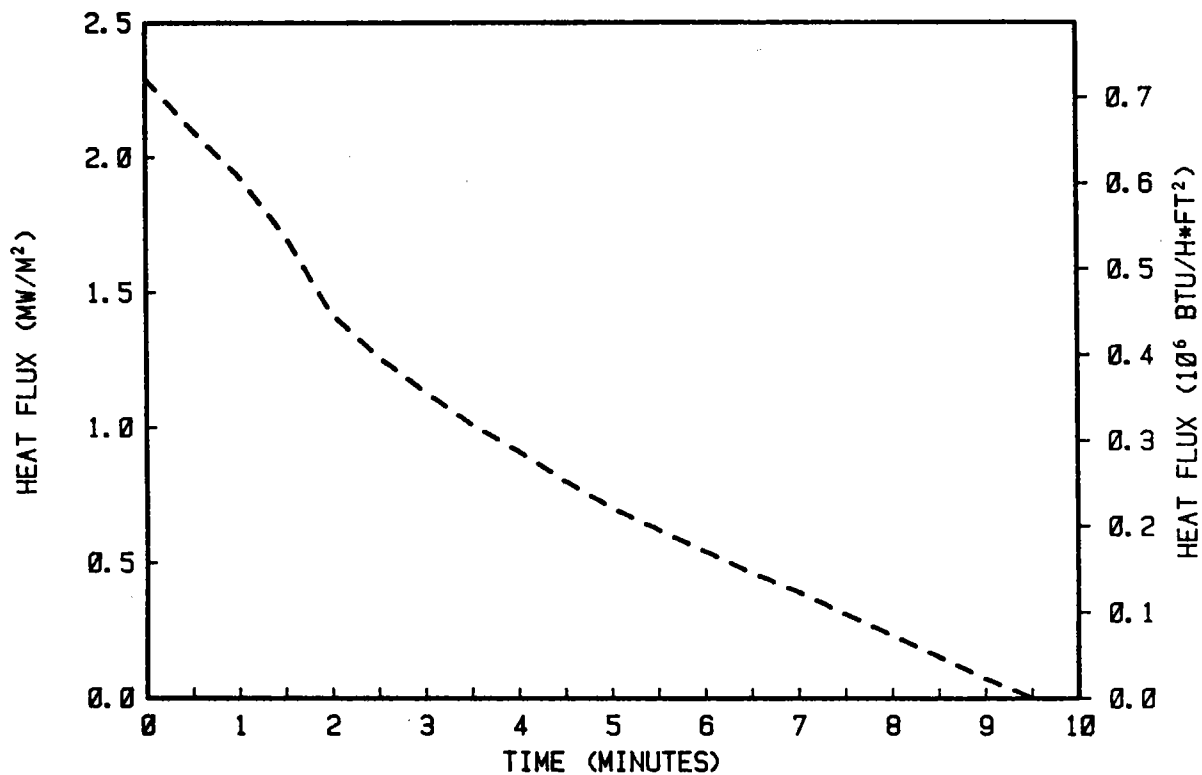


Figure 4.7 Aperture Plane Peak Heat Flux Decay

Table 4.12 Loss of Receiver Flow

<u>Failure</u>	<u>Indicating Signals</u>	<u>Response</u>
Valve does not close (Drag, control, or pump throttle valve)	● Inlet flow rate	● Defocus heliostats*
Line breaks	● Panel tube temperatures	● Close door
Controller fails	● Surge tank levels	● Institute warm standby
Two feedpumps fail		● Assess failure
Plant and grid power loss	● Inlet flow rate	● Close aperture door†
	● Panel tube temperatures	● Start diesel generator
	● Surge tank level	● Defocus heliostats
		● Institute cold shutdown

*IST provides 1 minute of full salt flow.

†Ablative covering protects door from full aperture flux.

Table 4.13 High/Low Temperature of Receiver Fluid

<u>Failure</u>	<u>Indicating Signals</u>	<u>Response</u>
1 feed pump	<ul style="list-style-type: none">● Panel temperatures● Pump discharge pressure● Flow rate decay	<ul style="list-style-type: none">● Start backup pump● Continue normal operation
Flow control	<ul style="list-style-type: none">● Panel temperatures● Flow rate error buildup	<ul style="list-style-type: none">● Defocus heliostats● Open control valves● Institute warm standby
Heliostat field control	<ul style="list-style-type: none">● Excessive local flux● Panel temperatures● Salt temperatures	<ul style="list-style-type: none">● Scram heliostats● Open control valves● Warm standby
Electric heaters	<ul style="list-style-type: none">● Panel and piping temperatures	<ul style="list-style-type: none">● Drain receiver● Institute cold shutdown

4.3.11 Single Tube Heat Flux Analysis

Detailed heat flux analysis of a single tube was performed. The simplified analysis provided by CONCEN, where the flux is resolved into its component normal to the plane of the local receiver panel has been found to lead to significant errors on some critical panels. These critical panels tend to be toward the back of the cavity. A special CONCEN run was made for a typical tube in this location. The results, presented in Appendix C, showed that the heat flux was not symmetrical, as had been assumed. Peak heat flux was up to 80 percent higher at some locations on the absorber surface (enhancement factor of about 1.80*), causing excessive tubewall and salt film (I.D.) temperatures. Using the increased flux data, we recalculated metal and salt temperatures for the V12 configuration (Appendix C). As a result of the higher heat flux values, calculated tubewall and salt film temperatures far exceeded the design limits (Section 4.3.4):

- The maximum front-to-back temperature gradient increased to 237.9°C (460.2°F).
- The maximum salt film (I.D.) temperature increased from 606.7 to 638.7°C (1124 to 1181.7°F).
- The maximum tubewall (O.D.) temperature increased from 642.5 to 695.7°C (1188.5 to 1284.2°F).

The solution to this problem basically requires:

- Reduction of peak flux levels by
 - Spreading the flux more uniformly via heliostat field aimpoint strategies
 - Increasing absorber surface area
 - Changing cavity shape by relocating the absorber panels

*Ratio of effective peak heat flux on the tube surface to heat flux normal to the plane of the panel.

- Change in salt flow paths to increase salt mass flow rate and thus the convective heat-transfer coefficient in the tubes (at the expense of pressure drop).

Because of budget and schedule constraints, we did not change the heliostat field aim strategy. That would have entailed extensive additional flux mapping analysis. Instead V12 geometry was revised, as shown in Figure 4.8, and the number of passes was changed from 4 to 5, thus increasing the convective coefficient in Panels 1 through 6. The revised panel circuitry is shown in Figure 4.9. With these modifications, the maximum tubewall (O.D.) and salt film (I.D.) temperatures were reduced by ≈ 63 and 38°C (≈ 113 and 68°F) to 633 and 601°C (1171 and 1114°F) respectively and the maximum front-to-back tube ΔT was reduced by $\approx 103^{\circ}\text{C}$ ($\approx 185^{\circ}\text{F}$) to 153°C (275°F).

Also, as shown in Figure 4.8, the wing panels were relocated inward to:

- Use the cavity radiant heaters to heat the wing panels during overnight conditioning. Thus trace heating is not required in any panel (except on the headers and piping).
- Keep Panels 7 through 10 as far from the aperture plane as possible to reduce heat flux levels on those hot panels.
- Reduce the heat imbalance in the wing panel.
- Reduce the required new width of the aperture door by about 2 m (6.6 ft).

4.3.12 Aperture Size Optimization

The proper sizing of the receiver aperture is important since absorber power is a function of aperture size. As the aperture size increases, the amount of power directed to the receiver that misses the aperture (spillover) decreases,

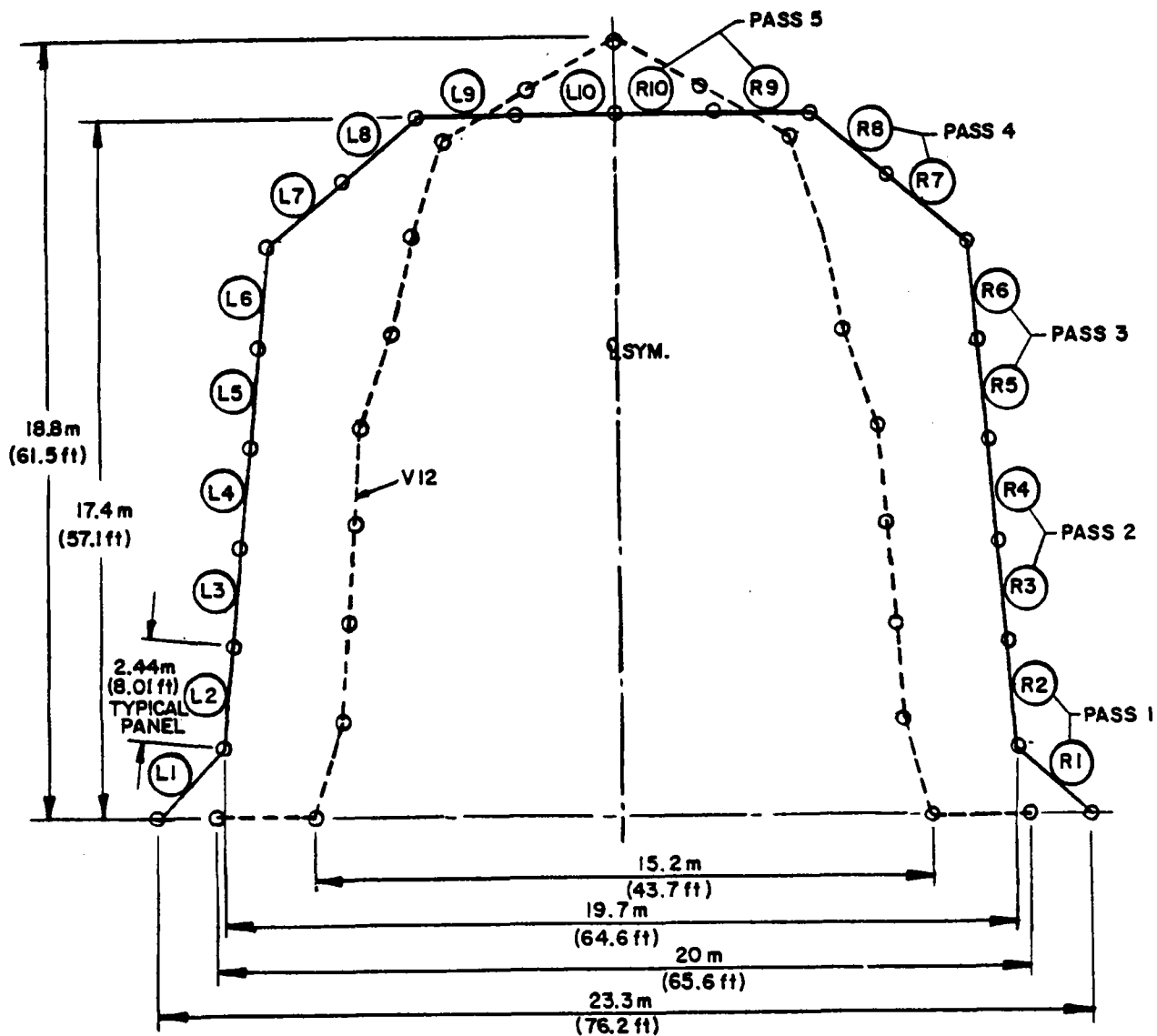


Figure 4.8 Modifications to V12 Geometry

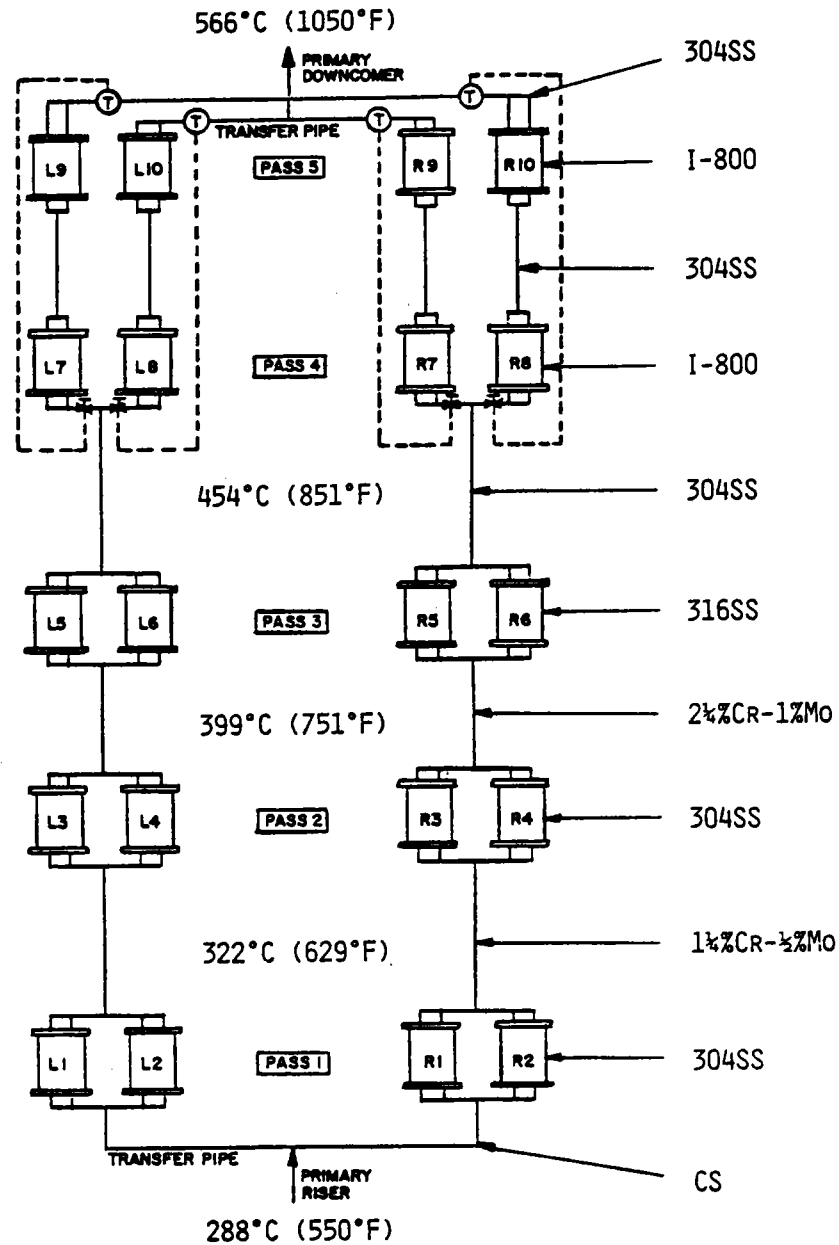


Figure 4.9 Revised Panel Circuitry

and the heat losses through the aperture by reflection, reradiation, and convection increase (see Figure 4.10). Thus there is an optimum aperture size to ensure that the receiver absorbs the maximum power. (Absorbed power is the solar power directed to the receiver from the heliostat field that reaches the aperture plane minus spillover and heat losses.)

To find the optimum exposed (active) panel length/aperture height, the net energy absorbed by the panels was calculated for panel lengths from 24.5 to 28.5 m (78.75 to 93.50 ft) in increments of 0.25 m (10 in.). Receiver thermal losses were assumed to vary in direct proportion to the panel active length/aperture height (area). Because of uncertainties in thermal loss estimates, curves were plotted for ± 25 percent spread (loss factors of 0.75, 1.0, and 1.25). As a

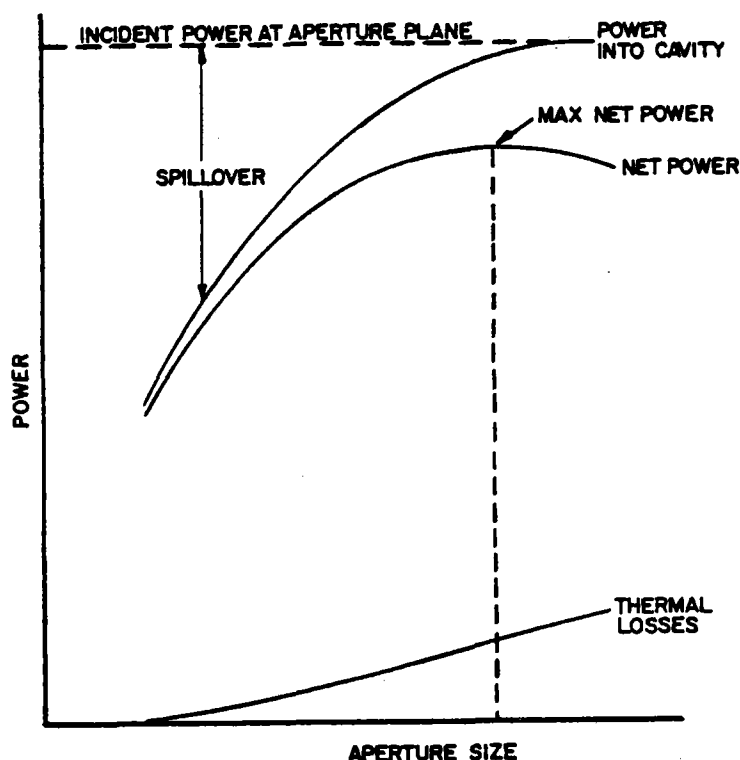


Figure 4.10 Typical Aperture Sizing Process

result of the aperture size optimization (Figure 4.11), the selected panel active length is 25.75 m (84.5 ft). As can be seen in the figure, the absorbed power curve is relatively flat near the optimum point, and even if assumed losses were changed by ± 25 percent, the location of the optimum point would change by less than 0.3 m (1 ft).

A similar trade-off was not done for the aperture width because the aperture width for a PCR configuration is determined not so much by a trade-off between spillover and thermal losses, but mainly by consideration of the magnitude of the heat flux next to the wing panel and the heat imbalance across the panel width.

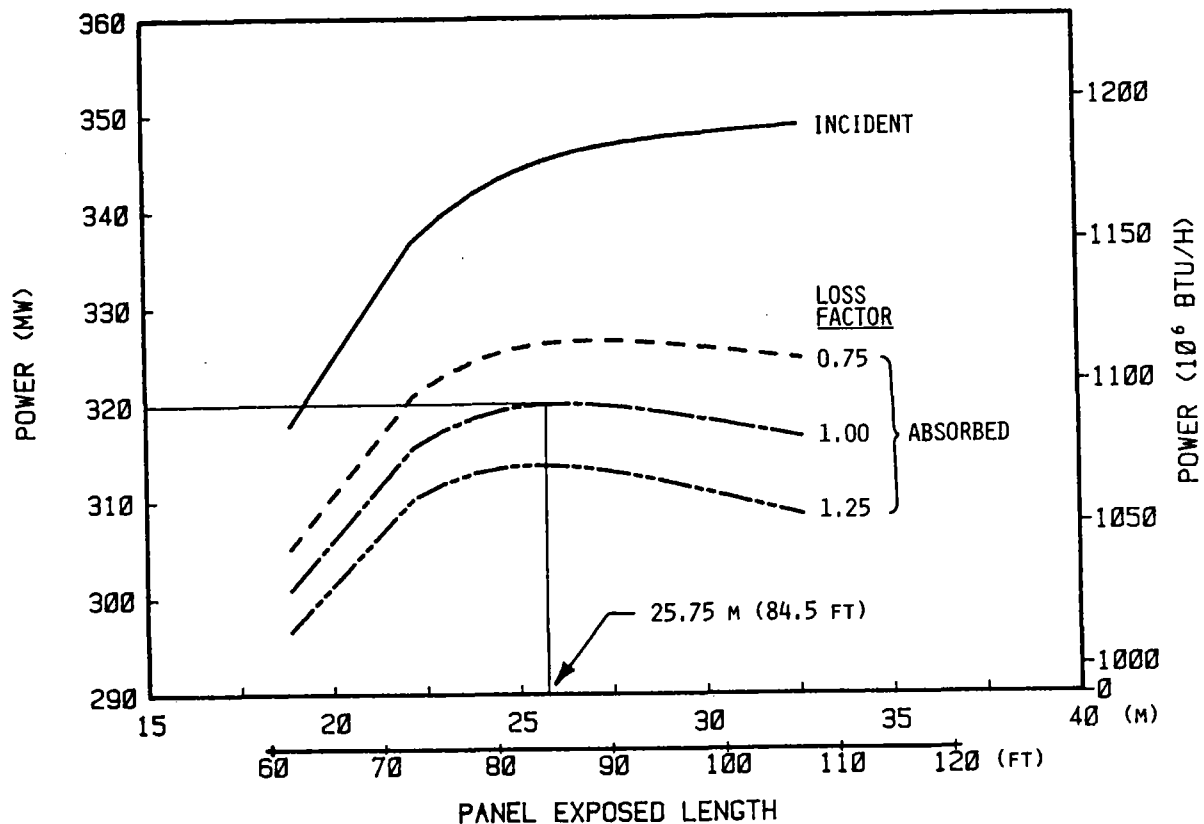


Figure 4.11 Optimum Aperture/Panel Length

The optimum vertical location of the panel--the vertical location that ensures the greatest amount of absorbed power of each panel--was determined concurrently with aperture size optimization. Each panel was "moved" up and down vertically in steps of 50.8 mm (2 in.), and its absorbed power was calculated at each location. The optimum vertical location was found to follow an angle of ≈ 12.1 deg (i.e., the panels should be stepped upward following an angle of ≈ 12.1 deg as shown in Figure 4.12).

REV	DATE	OR	DESCRIPTION
-----	------	----	-------------

REF.: 84-2292C
DATE: November 1982

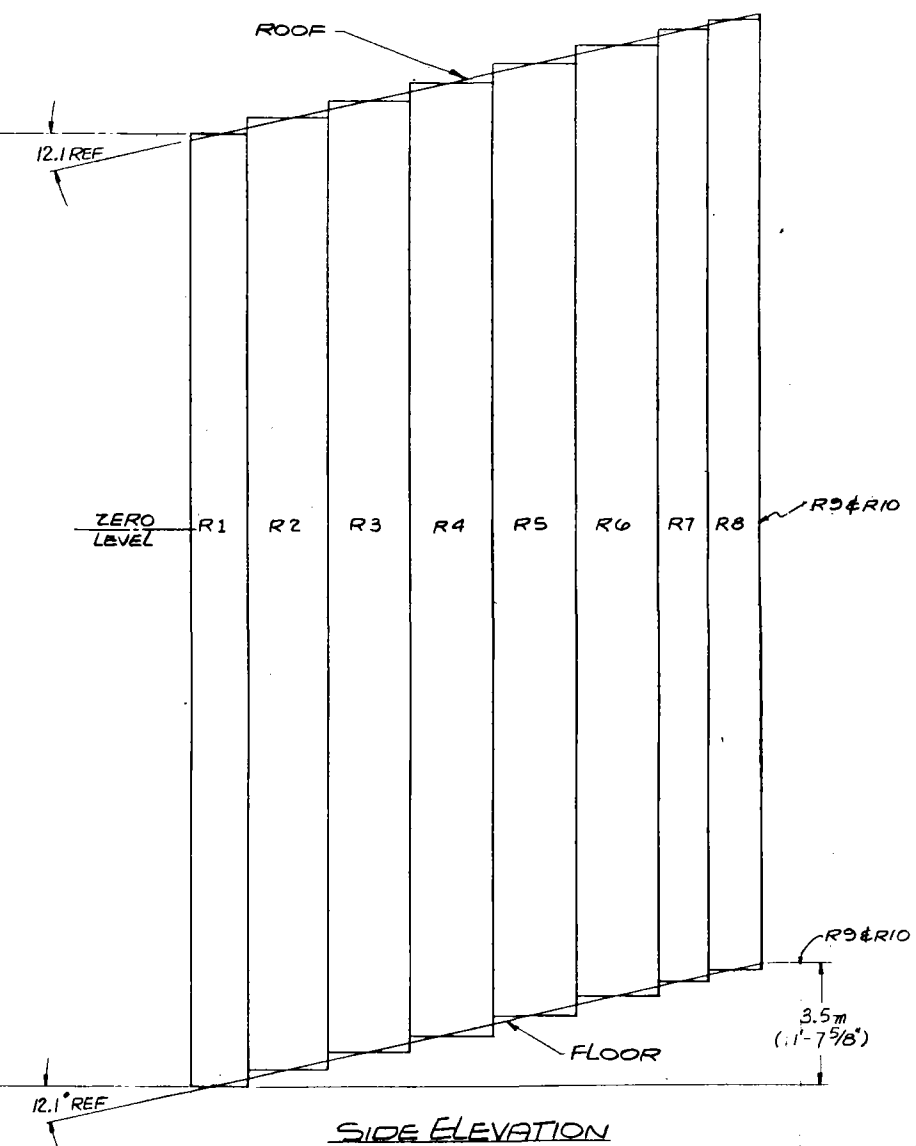
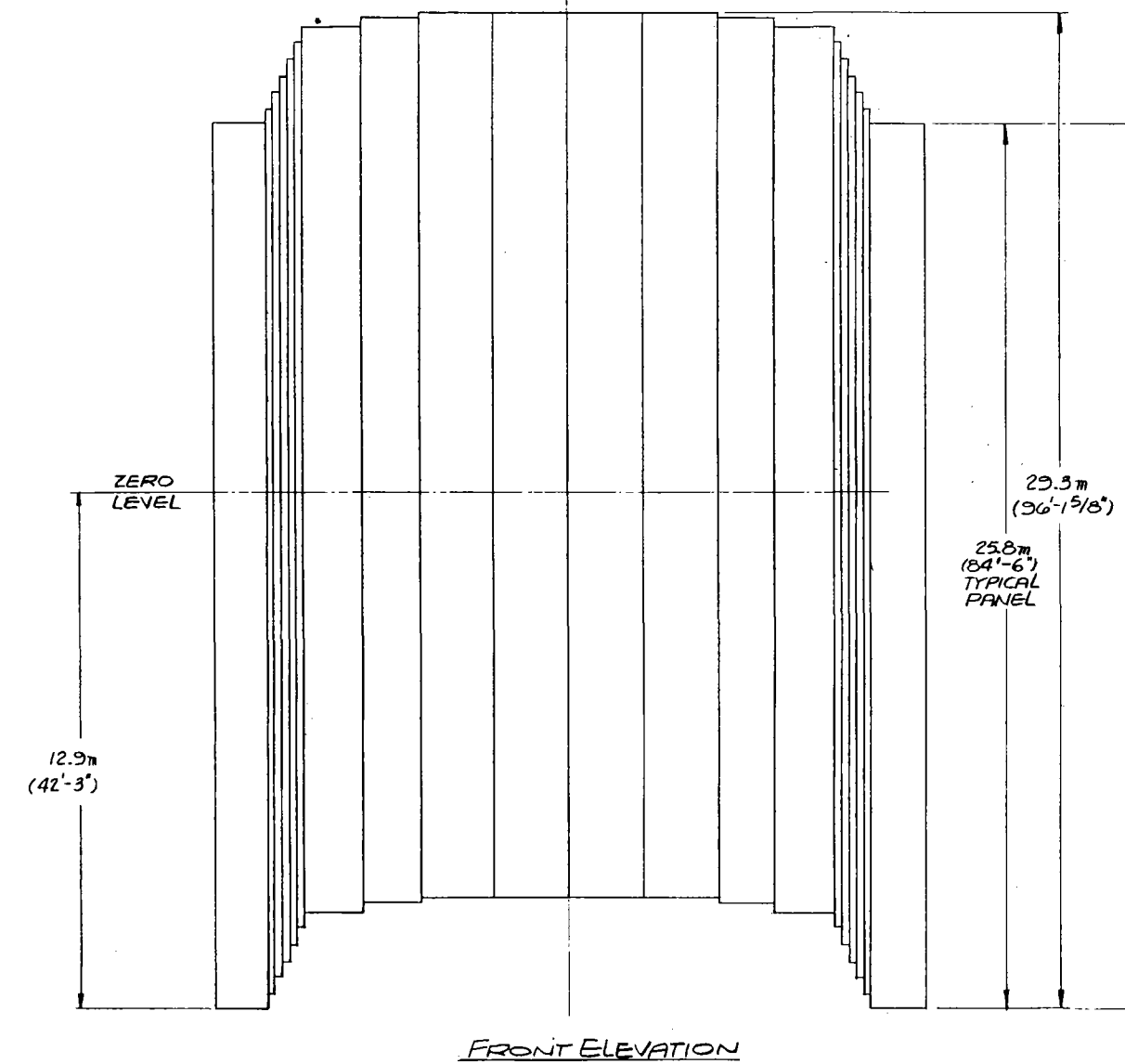
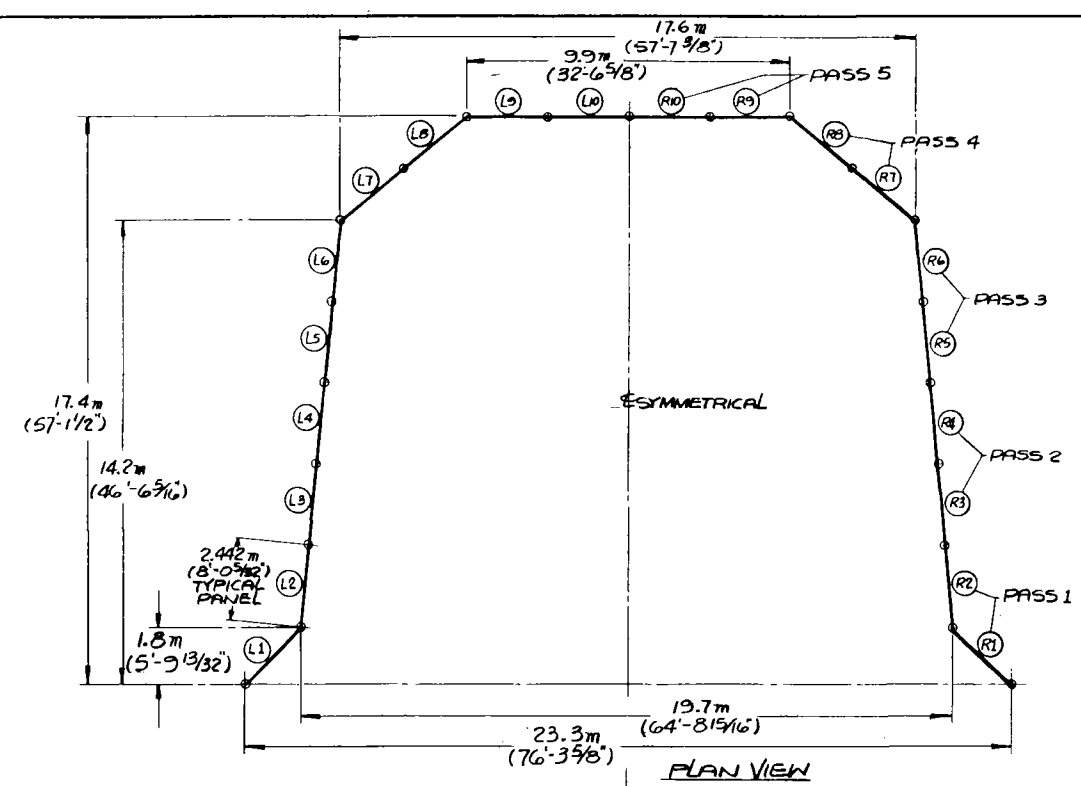


Figure 4.12

ITEM NO.	AMT REQD	DESCRIPTION/MATERIAL	SIZE
<div> FOSTER WHEELER DEVELOPMENT CORPORATION JOHN HILLARD RESEARCH CENTER 12 PEACH TREE HILL RD. LYNNSTON, N.J. </div>			
MOLTEN SALT SOLAR RECEIVER SRE CAVITY ARRANGEMENT			
DRAWN BY	ER 4/2	DWG NO	SCALE - 0.4" = 1m
CHECKED BY			
APPROVED BY			
RD-821-15			

4.4 SELECTED CONFIGURATION SUMMARY

The selected absorber configuration (Figure 4.13) is a partial cavity with 20 identical panels mounted vertically and stepped upward in elevation from front to rear. Figure 4.14 gives the dimensional relationships between the receiver, tower, and collector field. Configuration data are summarized in Table 4.14.

Figure 4.15 illustrates the overall flow schematic. Cold salt at 288°C (550°F) is pumped from the CST through the field supply piping* and tower riser to the receiver. At the inlet to the receiver, the salt flow is divided into two, one flow for each half of the absorber. Each proceeds through 10 panels in a combination of series and parallel paths, heating in the process to 566°C (1050°F). The hot salt then flows to the HST. Downcomers are provided after each pass through a panel or set of panels so that all panels are up-flow. Separate control valves are provided downstream of Pass 3 to control the outlet temperatures of Passes 4 and 5 by proportioning the flow.

In addition to outlet temperature data, flow control will use feed forward information on input power changes (either flux gage data or temperature data) to anticipate rapid flow changes required during partly cloudy conditions.

At the receiver exit, the flows are combined and returned by gravity through the tower downcomer, drag control valve, and field return piping* either

*Not part of the RS scope.

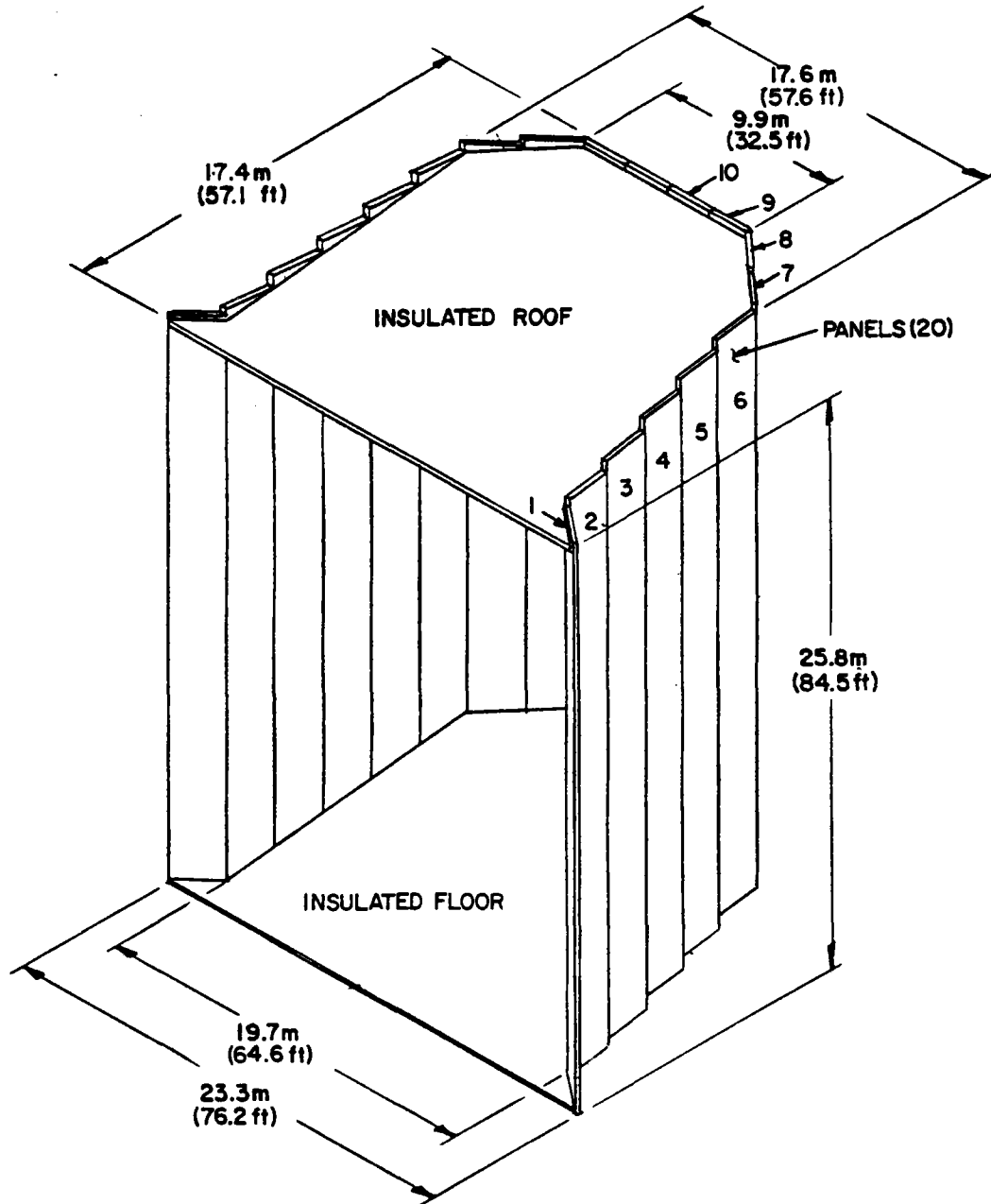


Figure 4.13 Cavity Isometric

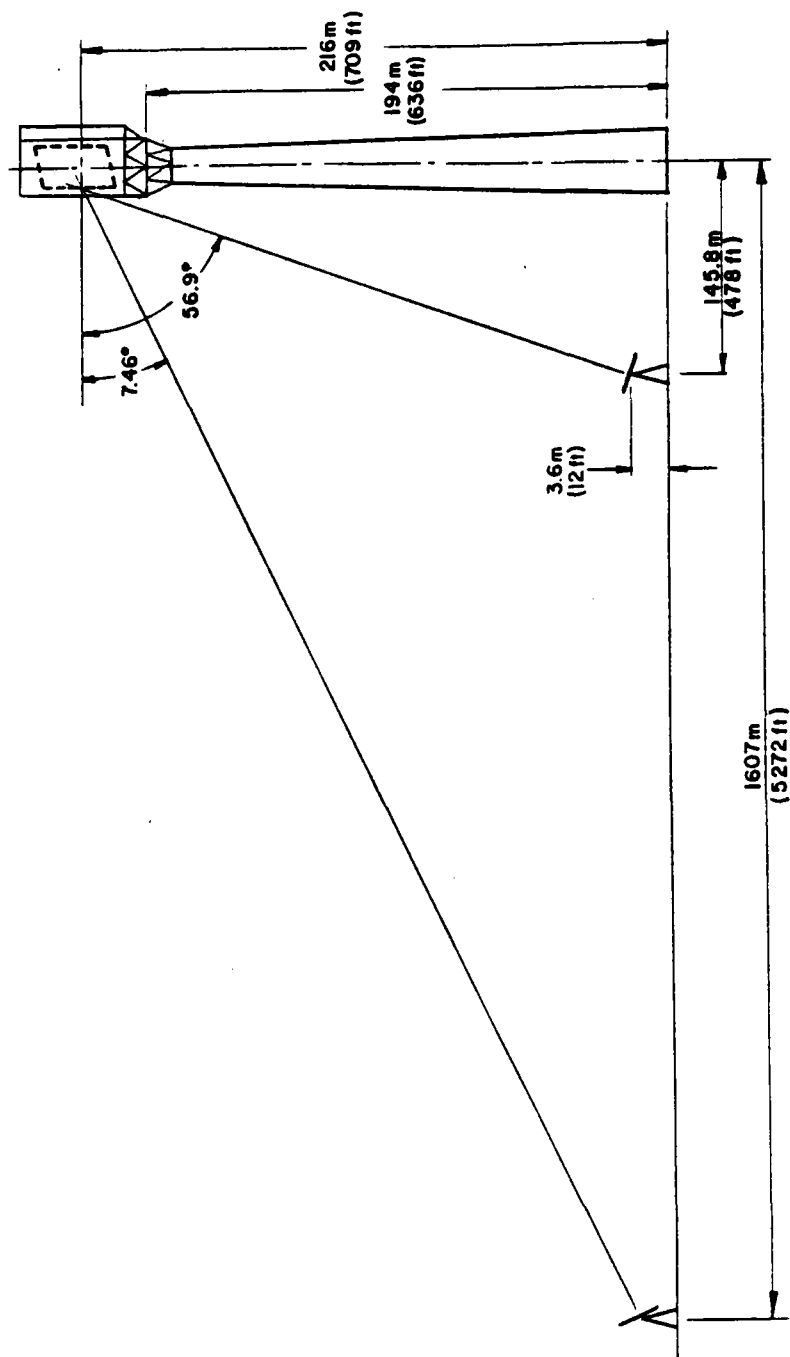


Figure 4.14 RS/CS Interface Drawing

Table 4.14 Selected Configuration Data Summary

Vertical absorber configuration	<ul style="list-style-type: none">● Aperture height = 25.8 m (84.5 ft)● Overall height = 29.8 m (97.75 ft)● Aperture width = 19.5 m (64 ft)● Overall width = 23 m (75.5 ft)
Modular panels (20)	<ul style="list-style-type: none">● Exposed (active) panel length = 25.8 m (84.5 ft)● Panel width = 2.442 m (8.01 ft)● 88 tubes: 2.54 cm (1 in.) O.D. 1.651 mm (0.065 in.) wall thickness● 87 spacers: 2.381 mm (0.094 in.) thick
All vertical up-flow panels (five passes per side)	<ul style="list-style-type: none">● Pass 1: Panels 1 and 2--Type 304SS● Pass 2: Panels 3 and 4--Type 304SS● Pass 3: Panels 5 and 6--Type 316SS● Pass 4: Panels 7 and 8--Incoloy 800● Pass 5: Panels 9 and 10--Incoloy 800
Two parallel control valves per side	<ul style="list-style-type: none">● Located downstream of Pass 3
Three half-capacity pumps	<ul style="list-style-type: none">● Bingham-Willamette, Type VCN
Aperture door	<ul style="list-style-type: none">● Internal blanket insulation● External ablator● Gravity close within 60 seconds
OST thermal energy with electric heating for overnight conditioning	<ul style="list-style-type: none">● 500 kWe radiant heaters for cavity● Trace heating for headers and piping
Tripartite system for receiver protection	<ul style="list-style-type: none">● 60 seconds full salt flow from IST● Heliostat defocus in 120 seconds● Diesel generator backup● Sacrificial ablator on quick-closing aperture door

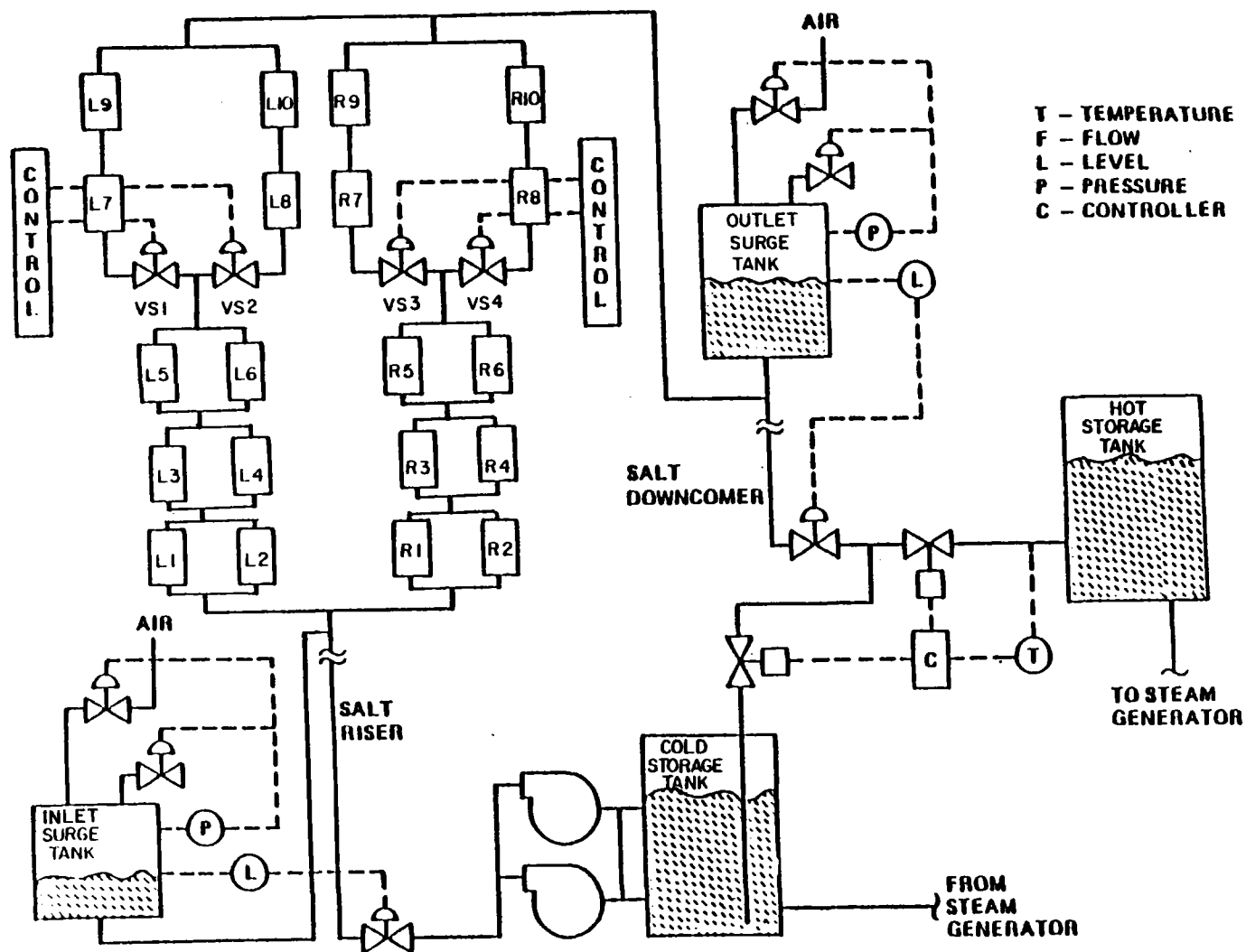


Figure 4.15 RS Flow Schematic

to the HST, when design salt outlet temperatures are achieved, or to the CST. The receiver IST and OST atop the tower buffer the fast-responding panel control valves from the slower responding salt pump and drag control valves.

Receiver protection includes surge tank salt flow, rapid heliostat field defocus, diesel generator backup power, and--as a last resort--sacrificial doors.

Key characteristics of the configuration and the rationale for its selection include the following:

- | | |
|---|---|
| ● North facing partial cavity | Best heliostat field performance
Smallest number of heliostats |
| ● Small frontal plane and small cavity aperture | Low radiation, convection, and reflection losses

Good efficiency, smaller number of heliostats |
| ● Large operating envelope with reasonable minimum power levels | Increased annual performance |
| ● Flow paths with good minimum power, flow control, and pressure-drop characteristics | Large operating envelope, increased annual performance

Acceptable pumping auxiliary power |
| ● Panel modules with identical geometry | Minimum fabrication cost |
| ● Easy early morning start-up with acceptable overnight thermal conditioning auxiliary power | Large operating envelope, increased annual performance

Acceptable auxiliary power loads |
| ● Excellent protection for receiver through surge tanks, redundancy of pumps, heliostat field backup power, and sacrificial doors | Reliable operation, low risk of catastrophic damage |

Section 5

RS DESIGN ANALYSIS

The RS was designed to meet the requirements defined in Section 3 and summarized in Table 3.1. The RS Preliminary Design Analysis was based on the configuration selected as the result of the trade-off studies conducted in Task 3 and described in Section 4. The RS design point as defined in Section 3.2 is noon, Day 50 (February 19), with an insolation of 950 W/m^2 ($301 \text{ Btu/h}\cdot\text{ft}^2$) and 320 MW ($1091.9 \times 10^6 \text{ Btu/h}$) rated power delivered at the base of the tower. The analysis was also based on the revised molten salt data received from SNLL during Task 3.²⁴

This section contains:

- Section 5.1--Design Analysis Plan (DAP)
- Section 5.2--T/H Design Analysis
- Section 5.3--Stress Analysis
- Section 5.4--Mechanical Design
- Section 5.5--Operation Analysis
- Section 5.6--Control Analysis

A detailed description of the final RS configuration and summary list of the key design and operating data are presented in Section 7.

5.1 DESIGN ANALYSIS PLAN

Before starting the design and analysis of the RS, a DAP was prepared. The DAP was reviewed and approved by SNLL before the detailed analysis of the subsystem and components was begun. The plan defines the required T/H and stress analyses, and shows the sequence in which they are performed and their interrelationships. Governing design criteria are identified, along with computer codes and correlations to be used. A copy of the DAP is given in Appendix I.

Primarily, the DAP is limited to the RS major components and constitutes the minimum effort required to demonstrate by analysis that the selected design complies with the design requirements. Guidelines and procedures in the DAP are used to demonstrate compliance with the RS requirements. Methods of analysis are given and types of documentation required are described.

Design criteria generally acceptable to the Architectural/Engineering industry were used for hardware selection to avoid detailed analyses for components, lines, and structural members whenever service requirements for the RS are similar to normal Architectural/Engineering requirements.

The flowchart shown in Figure 5.1 gives an overview of the design analysis process.

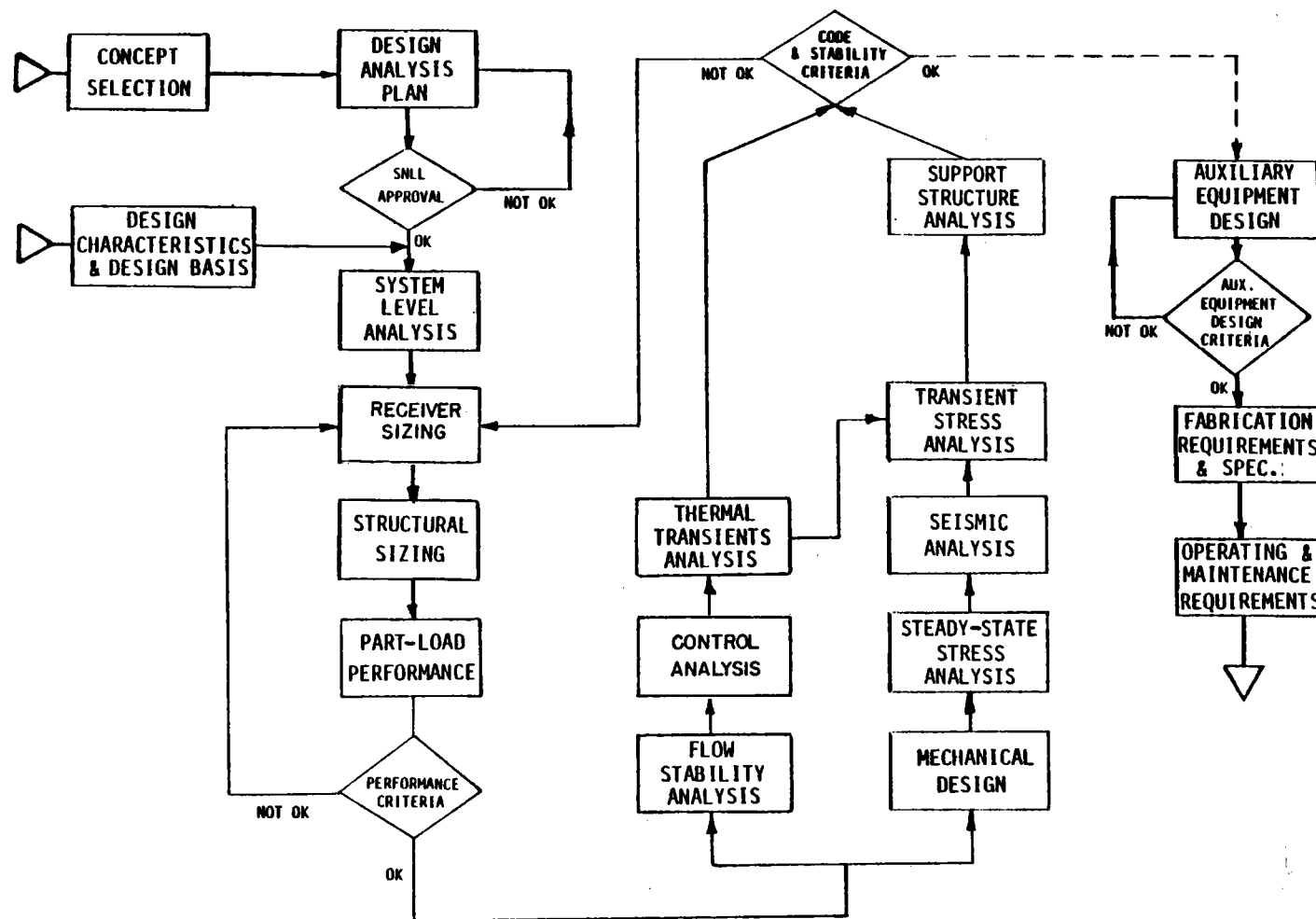


Figure 5.1 Flowchart--Design Analysis Process

5.2 THERMAL/HYDRAULIC DESIGN ANALYSIS

The major T/H design analysis tasks are:

- Steady state
- Transient
- Thermal conditioning
- Performance

T/H design analysis includes establishment of appropriate design bases, preliminary sizing and design, performance predictions, and the necessary analyses to substantiate the selected design.

The design bases included the T/H design conditions defined in Section 4 (e.g., salt inlet temperature, pressure, and flow as well as heat fluxes), thermophysical properties, and heat-transfer and pressure-drop correlations. (Updated molten salt properties received from SNLL before we began Task 4 were used throughout the T/H design analysis.²⁴)

The steady-state T/H analysis of the receiver was made using an in-house computer program called SOLAR. As shown in Figure 5.2, for the purpose of analysis each panel is divided into three regions (strips) with 17 nodal points (16 nodal elements) each along its length [51 nodes/panel (1020 nodal points for the whole absorber surface)]. Each element length is 1.716 m (5.63 ft) except for the top and bottom elements, which were adjusted to match the top and bottom ends of each panel. The exposed (active) length of each panel was established as a result of the aperture size optimization (Section 4.3.12). Incident heat flux values were specified for each nodal point in three columns per panel as shown in Table 5.1. The center column applies to the center half of the panel width; the left and right columns apply to the left and right quarters of the panel.

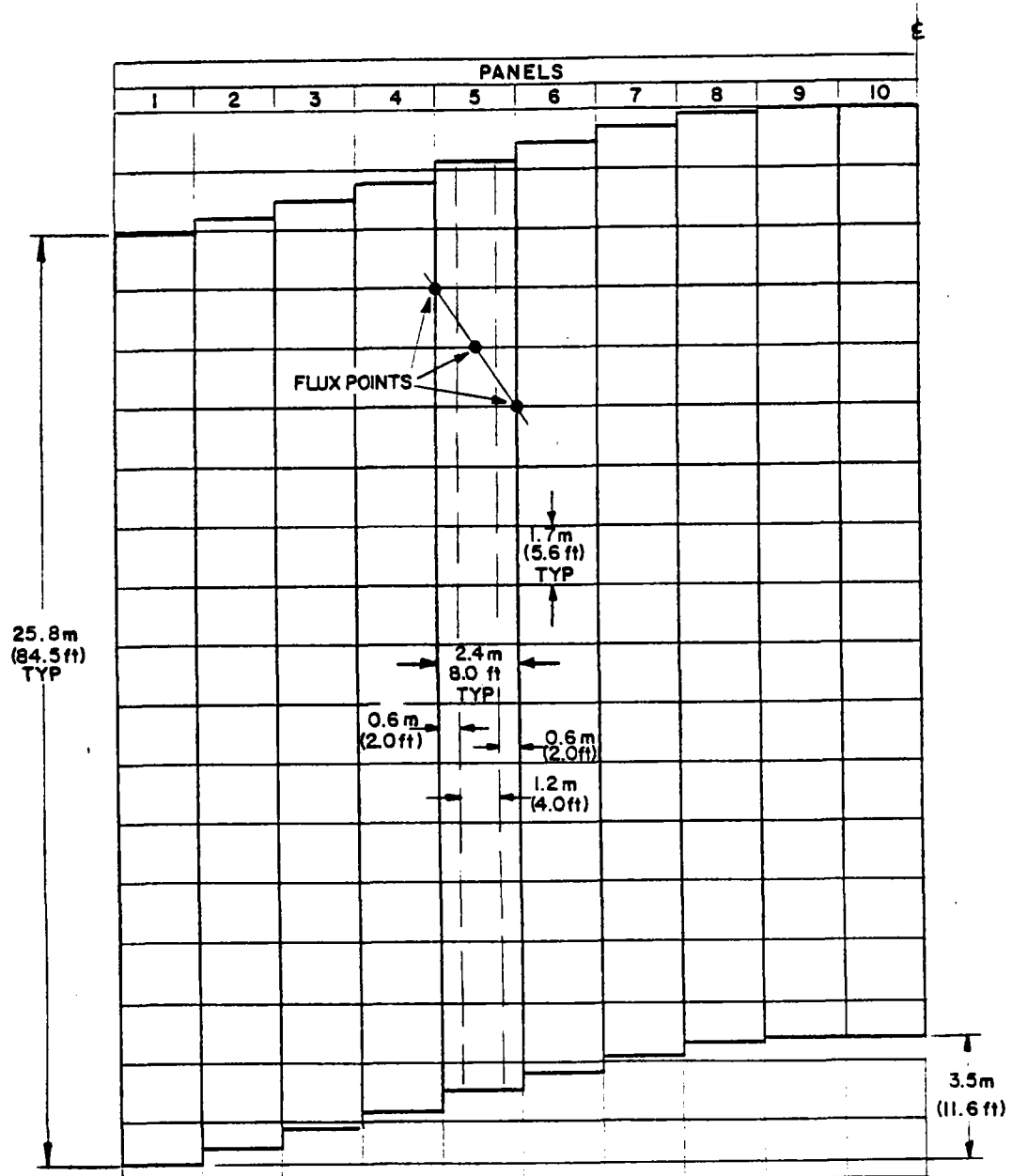


Figure 5.2 Developed View of Absorber Panels

Table 5.1 Typical Heat Flux Map, MW/m²

Pass	1		2		3		4		5	
Panel	1	2	3	4	5	6	7	8	9	10
	.000.000.030	.030.030.047	.047.036.019	.019.028.031	.030.020.018	.018.021.020	.020.009.026	.026.039.085	.028.024.017	.017.030.035
	.011.011.085	.085.080.162	.162.174.122	.122.111.133	.031.038.056	.056.044.059	.059.077.098	.098.108.198	.085.079.089	.089.094.110
	.038.039.166	.166.166.316	.316.356.366	.366.339.339	.133.146.168	.168.178.196	.196.179.204	.204.208.356	.198.181.185	.185.187.201
	.092.094.241	.241.238.440	.440.515.531	.531.483.497	.339.330.405	.405.384.364	.364.267.316	.316.287.466	.356.318.324	.324.310.286
	.111.125.295	.295.283.466	.466.527.570	.570.587.584	.497.464.543	.543.502.468	.468.368.393	.393.370.628	.466.470.462	.462.462.447
	.128.171.408	.408.380.573	.573.610.656	.656.678.639	.584.552.653	.653.592.503	.503.410.430	.430.408.669	.628.604.582	.582.586.563
	.137.210.488	.488.433.614	.614.649.659	.659.670.613	.639.562.654	.654.604.511	.511.411.436	.436.394.646	.669.618.607	.607.604.588
	.112.186.400	.400.312.526	.526.569.582	.582.576.551	.613.541.601	.601.560.498	.498.374.401	.401.364.585	.646.587.577	.577.577.550
	.096.136.298	.298.205.444	.444.483.532	.532.530.584	.551.481.595	.595.545.479	.479.362.387	.387.341.558	.585.552.532	.532.545.530
	.093.126.307	.307.245.515	.515.602.679	.679.716.671	.584.542.650	.650.583.523	.523.385.400	.400.356.583	.558.574.554	.554.549.524
	.111.173.426	.426.386.635	.635.700.721	.721.701.631	.671.604.692	.692.604.515	.515.356.367	.367.330.515	.583.577.533	.533.498.487
	.124.169.393	.393.354.569	.569.593.565	.565.530.466	.631.533.585	.585.493.419	.419.288.301	.301.256.380	.515.498.458	.458.432.406
	.117.133.275	.275.228.357	.357.355.351	.351.328.281	.466.379.425	.425.359.308	.308.218.215	.215.175.266	.380.377.353	.353.331.310
	.054.077.142	.142.089.146	.146.146.155	.155.139.122	.281.230.246	.246.215.181	.181.126.124	.124.099.154	.266.252.246	.246.226.203
	.027.043.075	.075.028.044	.044.043.041	.041.039.034	.122.103.116	.116.104.087	.087.058.054	.054.046.071	.154.150.137	.137.121.107
	.009.016.032	.032.007.011	.011.009.009	.009.006.007	.034.030.035	.035.029.025	.025.018.018	.018.015.021	.071.066.059	.059.051.043
	.002.005.003	.003.001.001	.001.001.001	.001.001.000	.007.006.007	.007.006.006	.006.003.003	.003.002.003	.021.018.016	.016.013.010

Normal incident heat flux values, multiplied by an absorptivity factor to account for reflection, reradiation, and convection losses are used by SOLAR to determine the nodal element absorbed power and salt bulk temperature change within the element. Absorbed power in each element is determined from the product of the average normal absorbed heat flux and the flat projected element area. Peak heat flux values are obtained by increasing the normal heat flux values by an enhancement factor that accounts for nonuniform heat flux distribution around the tube (Section 4.3.11). The peak incident heat flux values are used by SOLAR to calculate tubewall and salt film (I.D.) temperatures.

Using the normal and peak absorbed heat flux values, inlet salt bulk temperatures and flow rates, salt and tube material properties, and panel geometry, the program evaluates the left, center, and right tubes in each panel. Tubewall and salt temperatures are calculated at each nodal point; absorbed power, salt bulk temperature change, and frictional and gravitational pressure drops are calculated for each nodal element. The program utilizes one of three correlations to predict the salt conductance, depending upon the flow regime--Seider-Tate (laminar),²⁵ Hausen (transition),²⁶ or Dittus-Boelter (turbulent).²⁷ The outlet salt conditions from the first element are used as the inlet salt conditions for the next element, and the calculation is repeated. The calculation continues upward through all nodes, finally giving the outlet salt temperature of the panel.

SOLAR can perform T/H analysis for all five passes continuously, one after the other, using the outlet conditions of the previous pass as inlet conditions for the next pass.

To perform the flow distribution analysis (Section 5.2.1), it was necessary to modify SOLAR. Initially, the program assumed the same salt flow for tubes connected to a common header. SOLAR was then modified to adjust the flow through each tube by an iterative procedure until the same total pressure drop was obtained for all tubes in parallel. Appendix J contains a more detailed description of SOLAR and the design point computer printout.

5.2.1 Steady-State T/H Analysis

The absorber full- and part-load T/H analyses were based on incident flux maps (Appendix K) for 10-deg sun elevation (≈ 7 a.m.), 8 a.m., 10 a.m., and noon for the design day. Afternoon heat flux values at 2 p.m., 4 p.m., and 10-deg sun elevation (≈ 5 p.m.) are identical to morning values except for being reversed from one side of the receiver to the other [left (east) values become right (west) values].

Absorbed Power. Calculated receiver absorbed power vs. time of day is plotted in Figure 5.3, the plot being a mirror image around noontime. At noon with the sun directly to the south, the heat flux is symmetric around the north-south centerline of the unit and each half of the receiver (left or right) absorbs one-half of the power.

Analysis of SOLAR computer runs for these cases indicates that the noon condition is the most critical, since it results in the highest tubewall and salt film (I.D.) temperatures. Thus the noon condition was chosen for detailed stress analysis (Section 5.3). The T/H results for this condition are presented in this section for one half of the receiver only because of the noon symmetry.

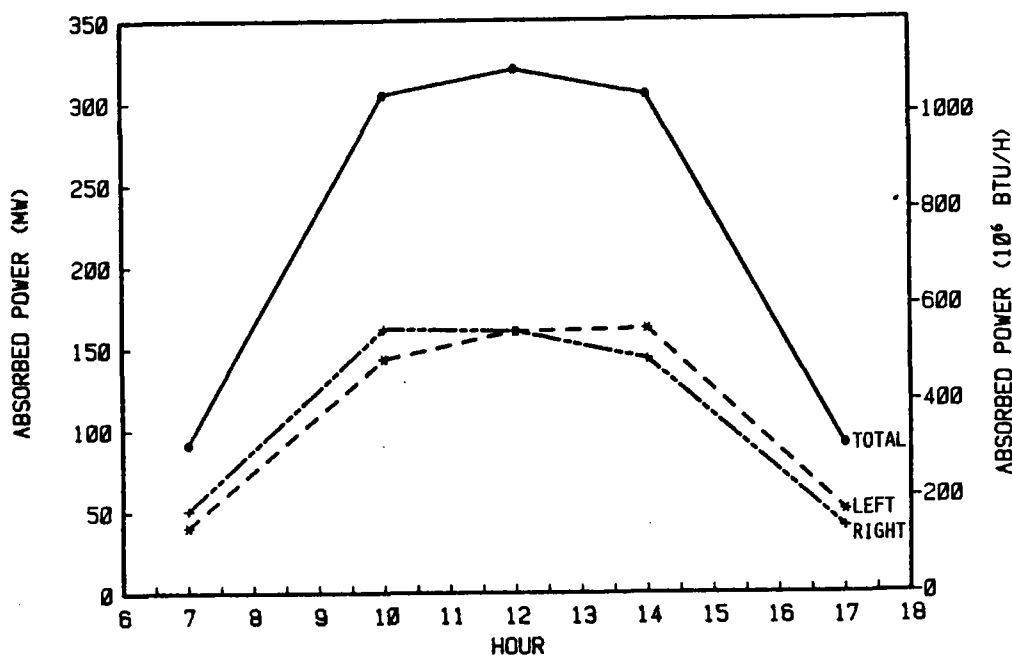
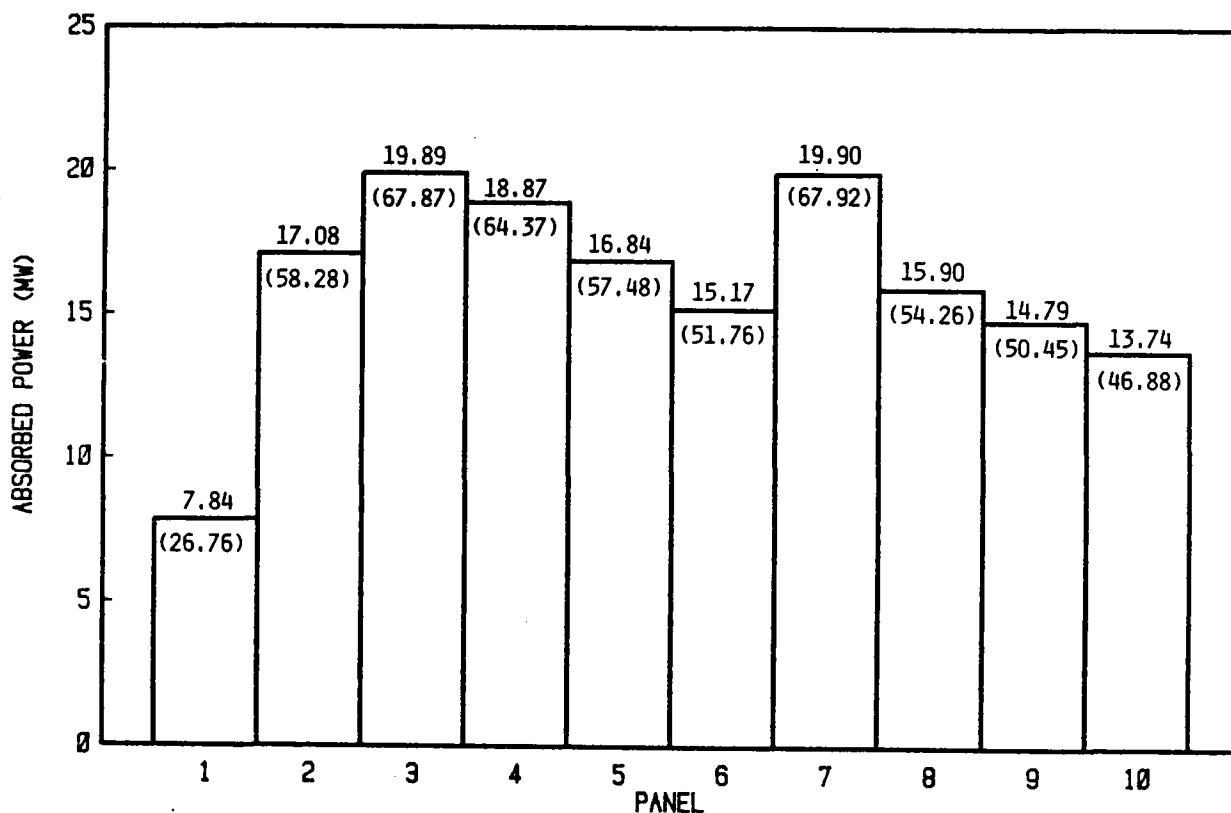


Figure 5.3 Receiver Absorbed Power vs. Time of Day

RS performance was calculated for the design point at the design insolation condition-- 950 W/m^2 ($301 \text{ Btu/h}\cdot\text{ft}^2$). As a design margin, tubewall temperatures for stress analysis were calculated at the maximum insolation conditions-- 1000 W/m^2 ($317 \text{ Btu/h}\cdot\text{ft}^2$) as defined in Section 3.2.5. Absorbed power per pass is given in Table 5.2 and per panel, in Figure 5.4. As indicated in the table, at the design point heat flux the receiver's power output is 320.04 MW ($1092.04 \times 10^6 \text{ Btu/h}$). Performance calculations (Section 5.2.4) show that the required receiver output to meet the RS rated power of 320 MW ($1091.88 \times 10^6 \text{ Btu/h}$) is 318.3 MW ($1086.08 \times 10^6 \text{ Btu/h}$); the difference is made up by 1.7 MW ($5.8 \times 10^6 \text{ Btu/h}$) of viscous dissipation in the downcomer and drag valve.

Table 5.2 Absorbed Power per Pass

Pass	Design Point		Maximum Insolation		Percent
	MW (10 ⁶ Btu/h)		Conditions		
	MW (10 ⁶ Btu/h)		MW (10 ⁶ Btu/h)		
1	24.92	(85.04)	26.23	(89.50)	15.6
2	38.76	(132.24)	40.79	(139.18)	24.2
3	32.01	(109.23)	33.69	(114.97)	20.0
4	35.81	(122.17)	37.68	(128.58)	22.4
5	28.53	(97.33)	30.02	(102.44)	17.8
Total per side	160.02	(546.02)	168.42	(574.67)	100.0
Total absorber	320.04	(1092.04)	336.84	(1149.34)	

Figure 5.4 Absorbed Power per Panel at Design Point--Left or Right Side
[MW (10⁶ Btu/h)]

Tube Temperatures. Steady-state panel salt inlet and outlet temperatures are shown in Figure 5.5 and are plotted in Figure 5.6. The salt flow per panel is approximately equal in Passes 1 through 3. At the Pass 4 inlet, the salt flow splits as it enters Panels 7 and 8 (as shown in Figure 5.4) in a 52.3:47.7 percent ratio, in direct proportion to the power absorbed in Panels 7/9 and 8/10. Salt flows per panel are given in Table 5.3, which summarizes the T/H characteristics calculated by SOLAR for the design point. Detailed results are given in Appendix J.

Figure 5.7 gives the peak absorbed heat flux for the hottest tube in each pass at maximum insolation condition. This figure shows that the greatest heat flux occurs in Passes 2 and 3, where the salt temperature is relatively low. This combination of factors helps to reduce tubewall temperatures and thermal stresses.

The temperature profiles for the hottest tube in each pass at maximum insolation condition are illustrated in Figures 5.8 through 5.12. The peak tube O.D. and I.D. temperatures shown are based on peak heat flux values (Figure 5.7) with the enhancement factor included. Maximum tubewall thickness was used.

Table 5.4 gives the average tubewall temperature* and average peak tube surface (O.D.) temperature for each panel. SOLAR calculates these temperatures

*The average tubewall temperature was calculated using the equation in Section 5.3.7, which takes into account the nonuniform heat flux distribution around the tube (Section 4.3.11). The equation gave us the average tubewall temperature for the cross-sectional area at a specific point along the tube.

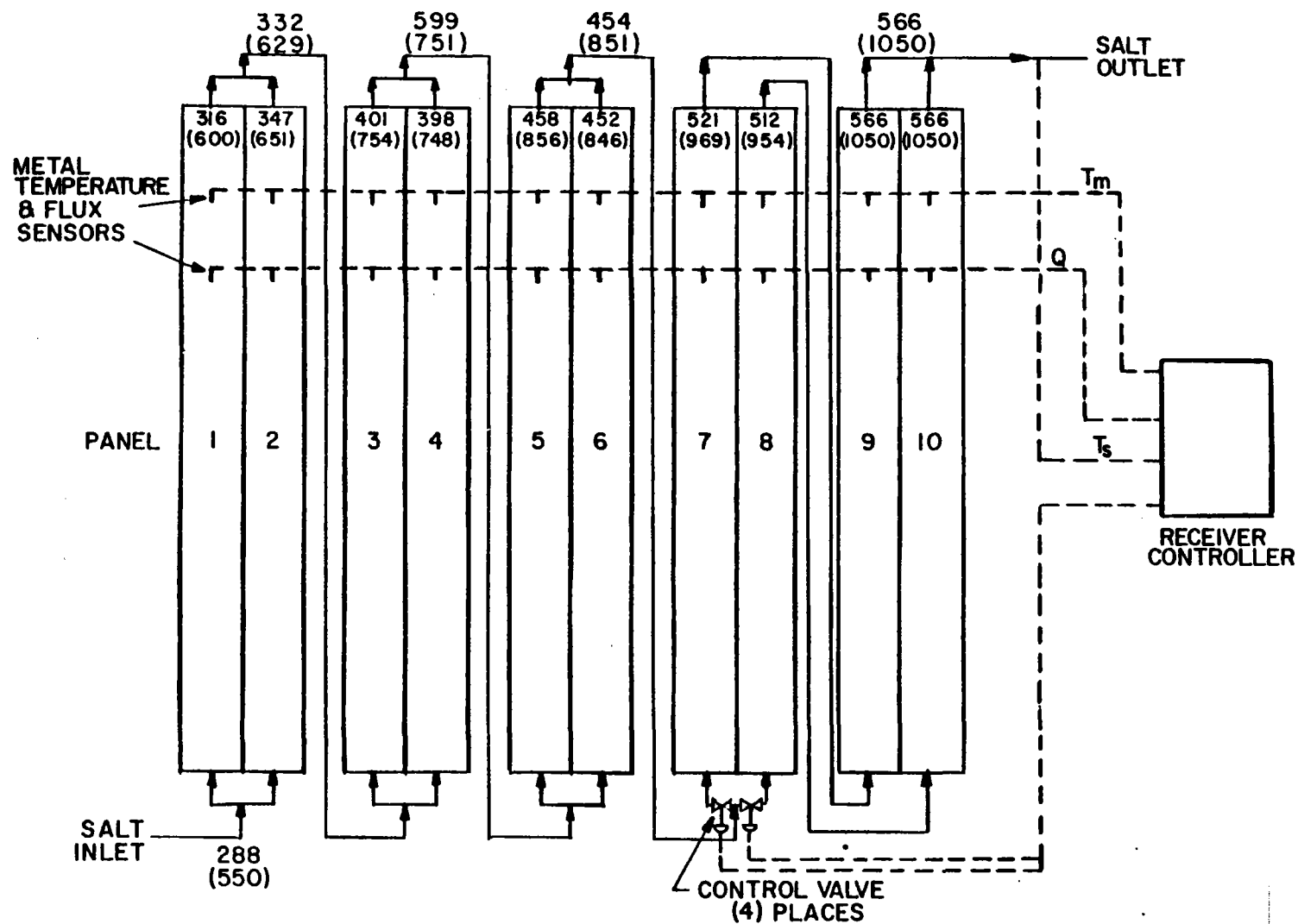


Figure 5.5 Panel Flow Diagram Showing Salt Outlet Temperature, °C (°F)

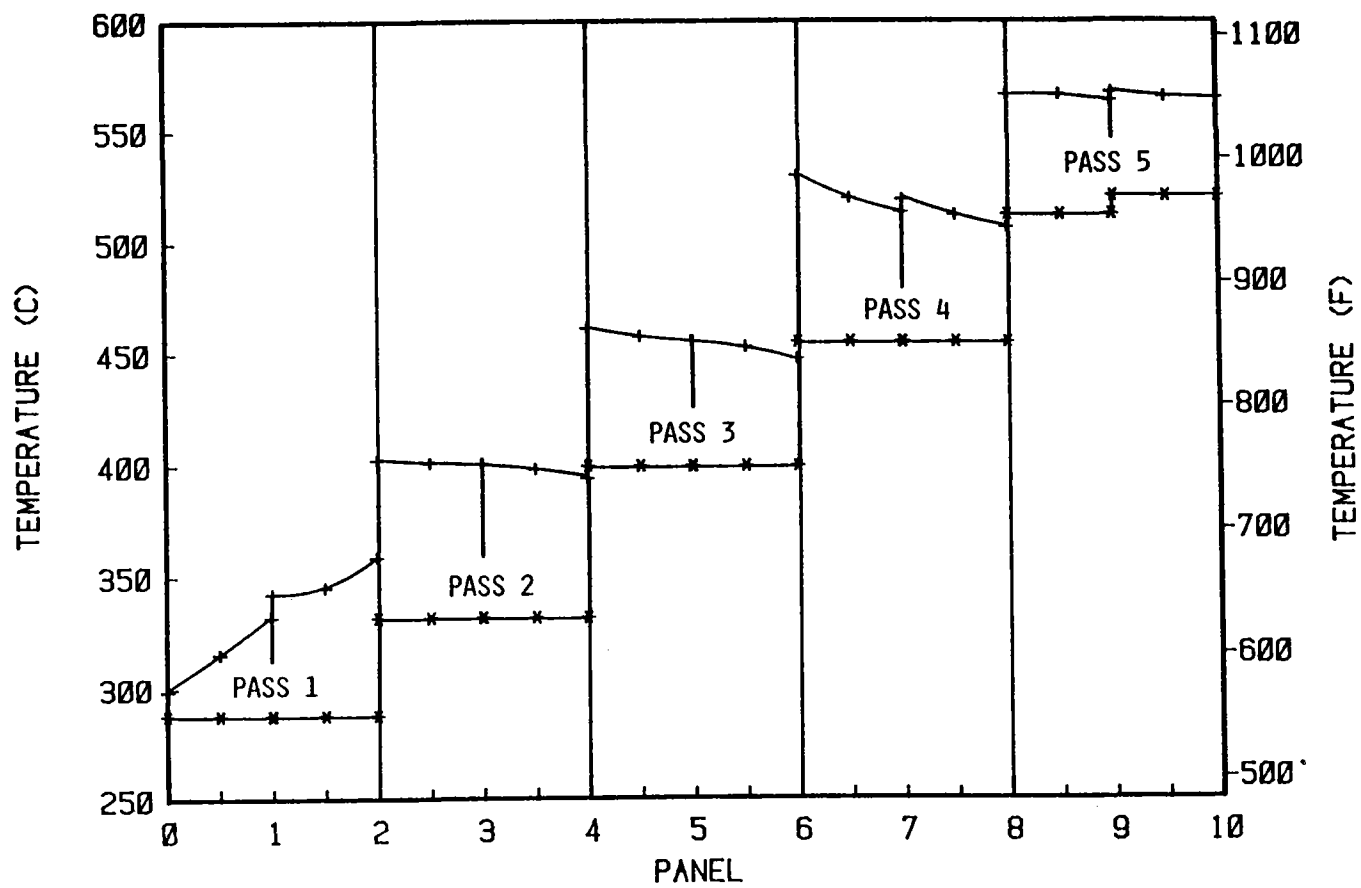


Figure 5.6 Salt Inlet/Outlet Temperature Profile

Table 5.3 T/H Characteristics--Design Point Conditions

Pass	Panel*	Temperature °C (°F)		Salt Flow kg/s (10 ⁶ lb/h)	Average Frictional ΔP kPa (lb/in ²)
		In	Out		
1	L1, R1	288 (550)	316 (600)	188.0 (1.492)	239.6 (34.75)
	L2, R2		347 (657)	191.1 (1.516)	242.3 (35.14)
2	L3, R3	332 (629)	401 (754)	189.6 (1.505)	227.9 (33.06)
	L4, R4		398 (748)	189.5 (1.504)	227.7 (33.03)
3	L5, R5	399 (751)	458 (856)	189.7 (1.506)	221.1 (32.07)
	L6, R6		452 (846)	189.4 (1.503)	220.6 (32.00)
4	L7, R7	454 (851)	521 (969)	198.3 (1.574)	237.0 (34.37)
	L8, R8		512 (954)	180.8 (1.435)	200.8 (29.13)
5	L9, R9	512 (954)	566 (1050)	180.8 (1.435)	199.7 (28.97)
	L10, R10	521 (969)	566 (1050)	198.3 (1.574)	235.9 (34.22)

*See Figures 4.8 and 4.9 for panel numbering sequence.

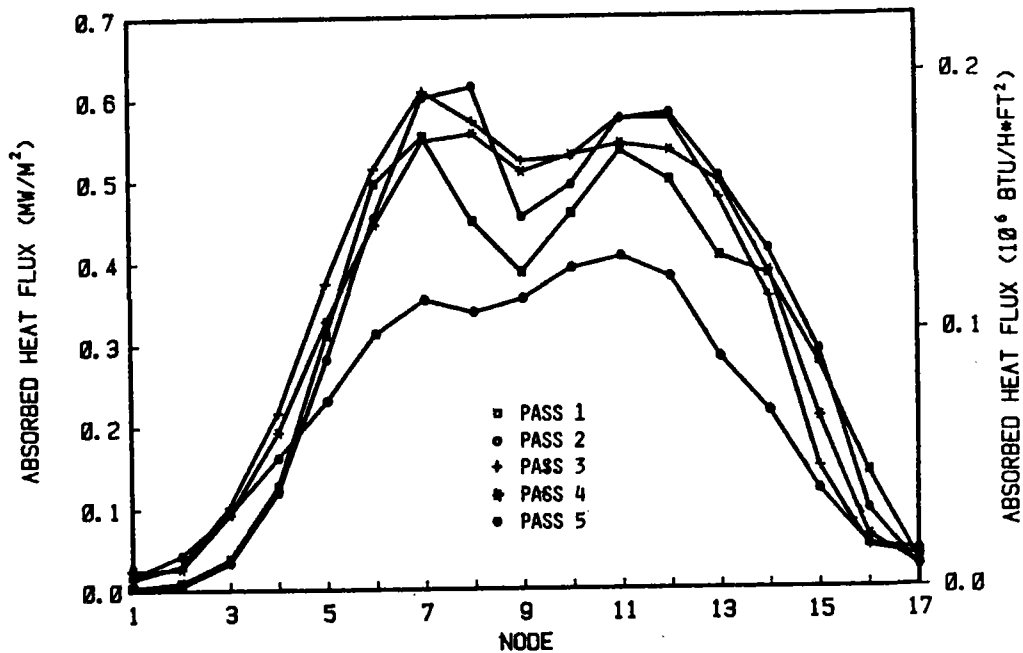


Figure 5.7 Peak Heat Flux

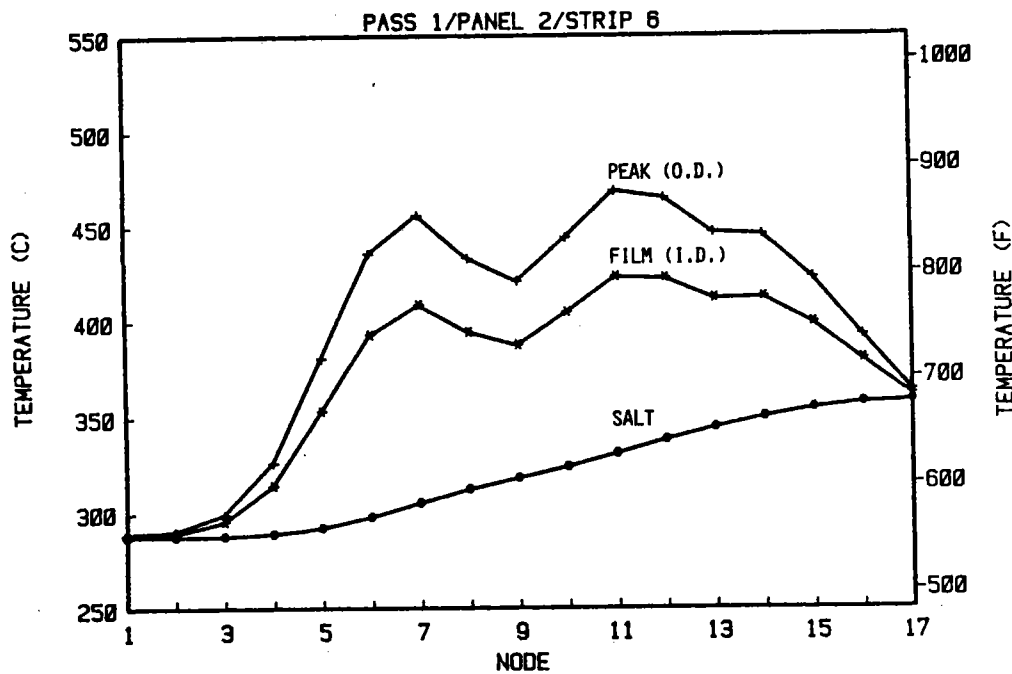


Figure 5.8 Temperature Profile of Hottest Tube in Pass 1

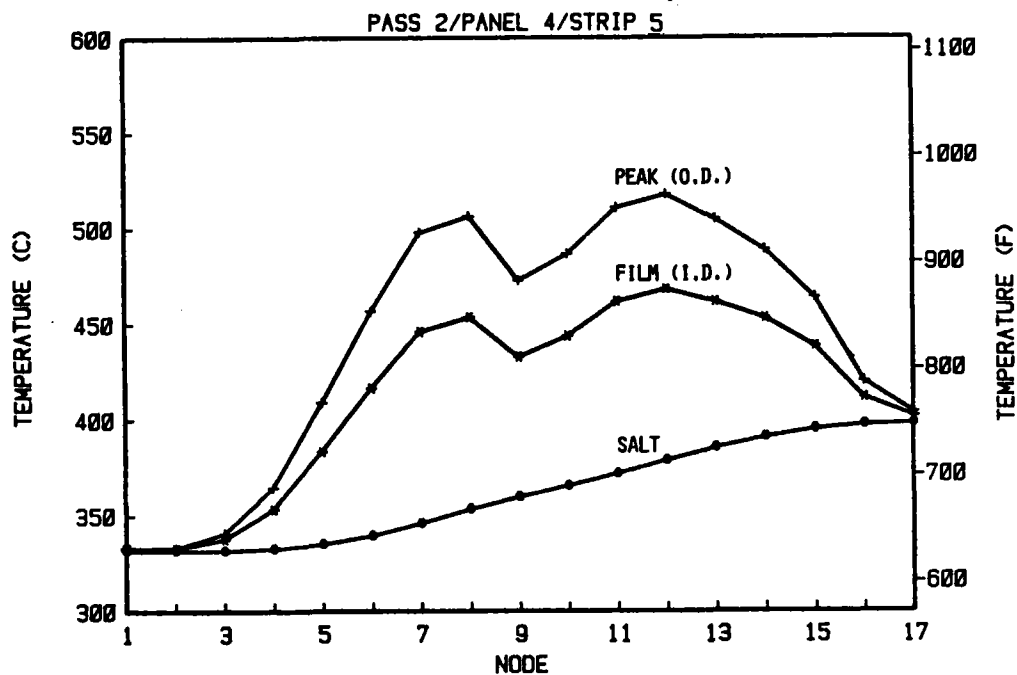


Figure 5.9 Temperature Profile of Hottest Tube in Pass 2

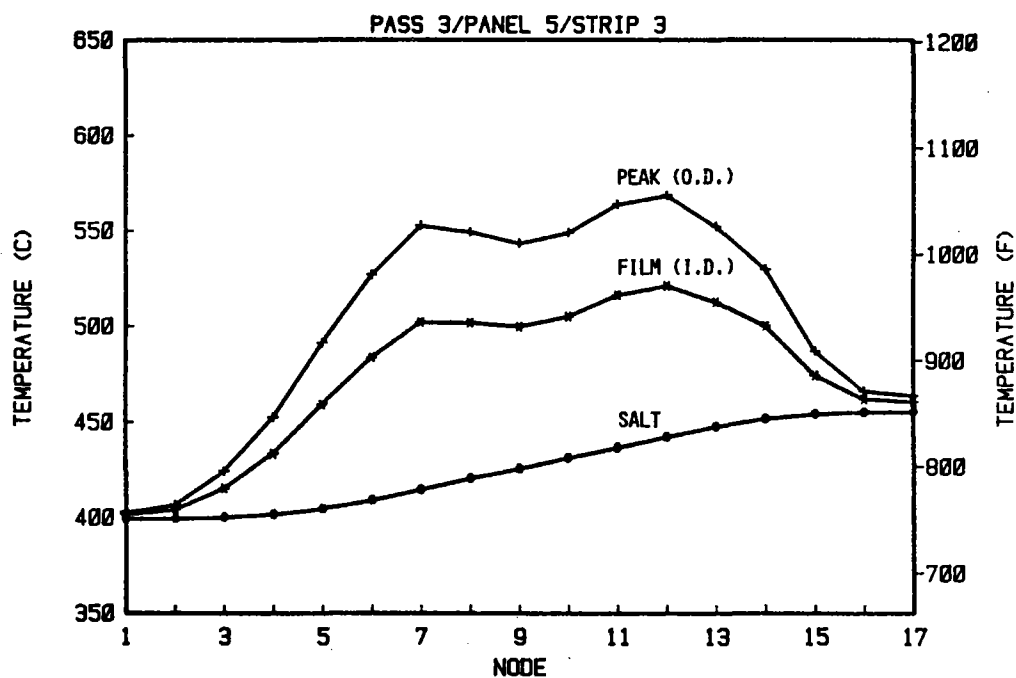


Figure 5.10 Temperature Profile of Hottest Tube in Pass 3

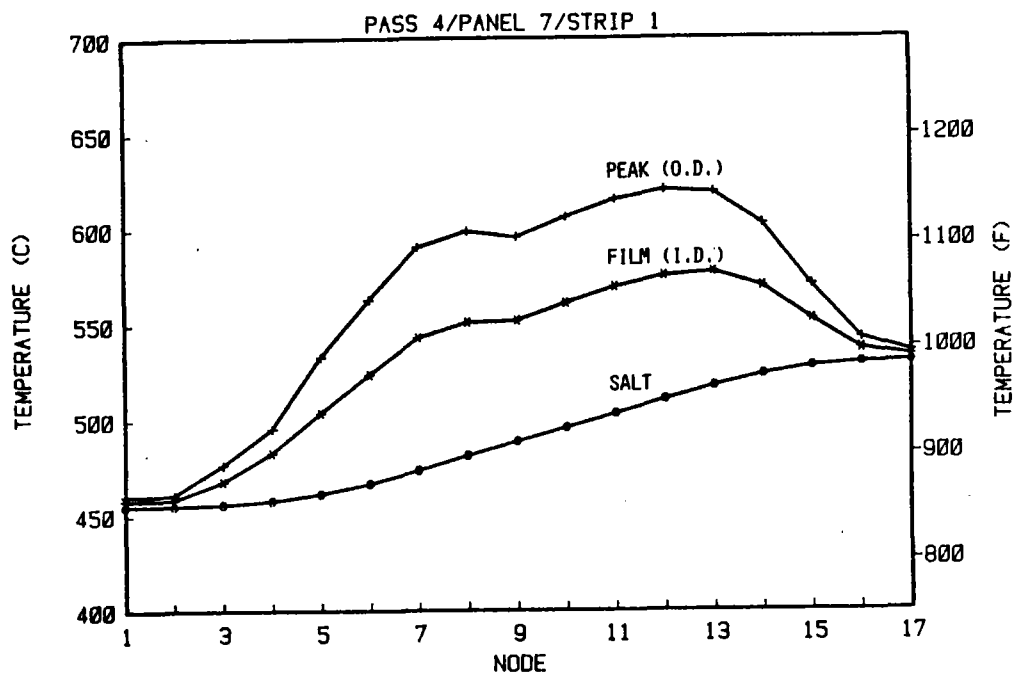


Figure 5.11 Temperature Profile of Hottest Tube in Pass 4

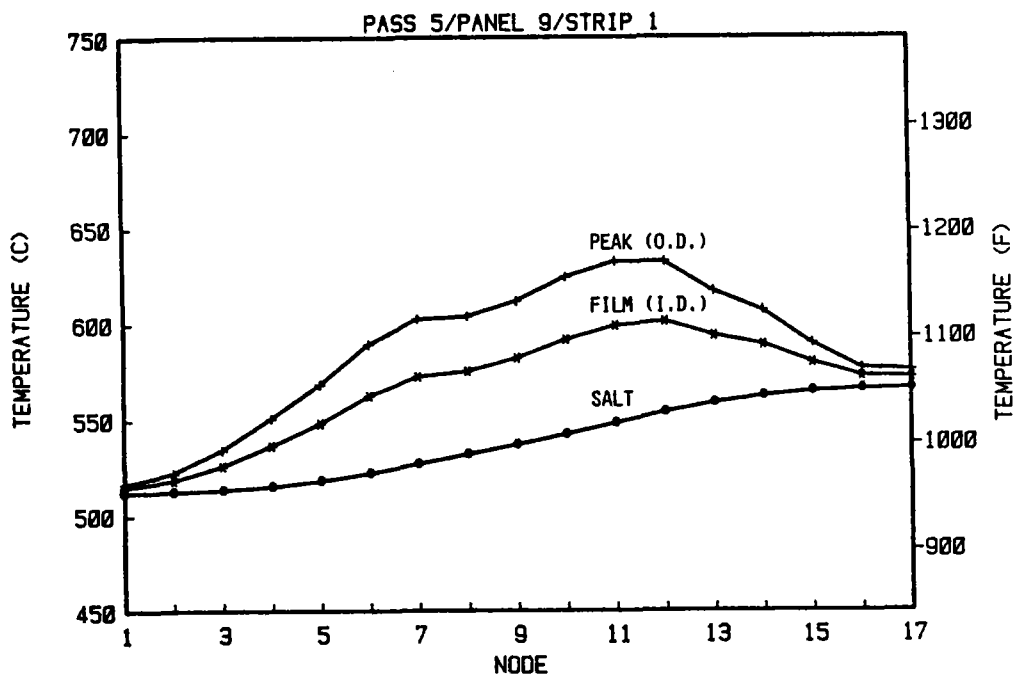


Figure 5.12 Temperature Profile of Hottest Tube in Pass 5

Table 5.4 Average Tubewall and Surface Temperatures, °C (°F)

<u>Panel</u>	<u>Average Tubewall</u>	<u>Average Peak Tube Surface (O.D.)</u>
1	314 (597)	347 (656)
2	337 (639)	392 (737)
3	389 (732)	452 (846)
4	389 (732)	455 (852)
5	451 (844)	513 (955)
6	449 (840)	551 (952)
7	506 (943)	557 (1035)
8	499 (930)	544 (1010)
9	552 (1026)	590 (1094)
10	554 (1029)	587 (1088)
Overall	444 (831)	494 (922)

starting with the average for each node; continuing to each strip, panel, and pass; and finally calculating the overall average for the absorber. The average tubewall temperature was used to calculate the panel thermal expansion. The average peak (O.D.) temperature is useful when estimating absorber thermal losses (Section 5.2.4). The calculated average tubewall temperatures were stored on a disk in matrix form for use in the shear stress analysis (Section 5.3.7).

Panel thermal expansion (Table 5.5) was calculated using the average tubewall temperature matrix. At maximum insolation condition, the longitudinal expansion ranges from 113 mm (4.46 in.) in the coldest tube of Panel 1 (wing panel) to 232 mm (9.12 in.) in the hottest tube of Panel 10. The maximum difference in thermal expansion among tubes [12.7 mm (0.5 in.)] occurs in Panel 1. This growth difference will induce an in-plane panel distortion, which has been estimated at as much as 63.5 mm (2.5 in.). The axial stress analysis in Section 5.3.5 addresses this in more detail. As discussed in that section, each panel was divided into three subpanels to reduce distortion and stresses to acceptable levels.

Table 5.5 Panel Thermal Expansion, mm (in.)

Panel	Longitudinal Expansion			Maximum Expansion Across Width
	Left Tube (Strip 1)	Center Tube (Strip 2)	Right Tube (Strip 3)	
1	113 (4.46)	120 (4.72)	126 (4.96)	12 (0.47)
2	129 (5.06)	129 (5.08)	134 (5.28)	13 (0.53)
3	153 (6.04)	153 (6.03)	154 (6.05)	16 (0.62)
4	154 (6.07)	154 (6.05)	153 (6.01)	16 (0.62)
5	183 (7.21)	182 (7.17)	182 (7.15)	18 (0.72)
6	182 (7.17)	181 (7.14)	180 (7.07)	18 (0.72)
7	212 (8.34)	208 (8.17)	205 (8.08)	21 (0.82)
8	207 (8.16)	204 (8.05)	202 (7.97)	21 (0.81)
9	230 (9.07)	230 (9.07)	229 (9.02)	23 (0.90)
10	232 (9.12)	231 (9.09)	231 (9.08)	23 (0.90)

Transverse thermal expansion across the panel was also calculated. It ranges from 11.9 mm (0.47 in.) in Panel 1 to a maximum of 22.9 mm (0.90 in.) in Panels 9 and 10. The gap between panels is designed to accommodate this thermal expansion, panel manufacturing tolerances, and in-plane panel distortion because of differences in longitudinal thermal expansion within a panel (Section 5.4).

Peak Values. Table 5.6 lists peak tubewall (O.D.) temperatures and front-to-back tube temperature gradients (ΔT) for critical nodes in each pass. The peak tubewall (O.D.) temperatures and ΔT s in the table do not necessarily occur at the same location. The peak ΔT and peak heat flux locations always coincide. The location of the peak tubewall (O.D.) temperature depends on a combination of salt bulk temperature and heat flux values. As indicated in the table, the maximum absorbed heat flux and peak front-to-back tube ΔT --0.614 MW/m² (195 x 10³ Btu/h·ft²) and 153°C (275°F) respectively--occur in the center tube of Panel 4 (Pass 2, Strip 5, Node 8). The peak tubewall (O.D.) and salt film (I.D.)

Table 5.6 Maximum Values per Pass

Description	Pass Number				
	1	2	3	4	5
Material	304SS	304SS	316SS	I-800	I-800
Location (panel/strip/node)	2/6/7	4/5/8	5/3/7	7/1/8	9/1/11
Peak absorbed flux, MW/m ² (10 ⁶ x Btu/h·ft ²)	0.554 (0.176)	0.614* (0.195)	0.609 (0.193)	0.557 (0.177)	0.406 (0.129)
Front-to-back tube ΔT, °C (°F)	149 (269)	153* (275)	138 (248)	117 (211)	84 (151)
Location (panel/strip/node)	2/6/11	4/5/12	5/3/12	7/1/12	9/1/12
Peak tubewall (O.D.) temperature, °C (°F)	467 (873)	517 (963)	568 (1055)	620 (1148)	633* (1171)
Salt film (I.D.) temperature, °C (°F)	422 (792)	468 (874)	521 (970)	577 (1070)	601* (1114)

*Maximum for absorber.

temperatures--633°C (1171°F) and 601°C (1114°F) respectively--occur in the left tube of Panel 9 (Pass 5, Strip 1, Node 12). At this location the absorbed peak heat flux is 0.381 MW/m² (121 x 10³ Btu/h·ft²). Thus the recommended maximum salt film (I.D.) temperature--593°C (1100°F) (see Section 4.3.4)--is exceeded in Pass 5. Figure 5.13 shows the panel areas where this recommended maximum is exceeded.

At the point of maximum salt film (I.D.) temperature, the salt bulk temperature is 554°C (1029°F), which results in a salt ΔT (I.D. temperature minus

320 MW MOLTEN SALT RECEIVER						
TEMPERATURE SUMMARY						
FILM (I.D.) TEMPERATURE (F)						
PEAK (O.D.) TEMPERATURE (F)						
FRONT-TO-BACK TEMPERATURE DIFFERENCE (F)						
PASS 5						
	PANEL 9			PANEL 10		
17	1061.2 1068.1 16.6	1060.3 1066.8 15.7	1056.1 1063.1 16.8	1061.9 1068.8 16.0	1059.0 1066.4 17.0	1060.2 1069.1 20.5
16	1062.5 1070.5 19.2	1061.5 1069.1 18.2	1057.8 1066.0 20.0	1063.4 1071.6 19.1	1060.3 1068.8 19.7	1061.8 1072.0 23.7
15	1075.2 1093.6 44.6	1073.2 1090.4 41.6	1068.2 1085.4 41.5	1073.1 1090.2 39.6	1069.3 1086.2 39.1	1070.6 1089.3 43.3
14	1091.9 1124.6 80.0	1087.8 1117.6 73.0	1082.6 1112.3 72.6	1086.4 1116.1 69.3	1080.5 1108.2 64.7	1077.5 1103.9 61.6
13	1100.4 1142.8 106.7	1102.2 1146.0 107.8	1094.8 1136.8 103.5	1097.8 1139.7 98.7	1093.3 1134.3 96.4	1092.1 1132.9 96.1
12	1113.9 1170.7 141.2	1112.2 1168.1 138.7	1102.9 1151.5 130.6	1105.2 1157.8 124.3	1101.0 1152.7 122.4	1099.3 1150.5 121.2
11	1109.9 1170.8 151.2	1104.8 1162.1 142.8	1097.2 1152.2 136.9	1100.1 1155.0 130.5	1095.1 1148.4 126.7	1094.3 1147.8 127.1
10	1097.0 1155.9 147.0	1091.2 1146.0 136.6	1084.1 1136.7 131.0	1088.1 1140.6 124.8	1083.7 1134.9 121.8	1081.5 1131.9 119.7
9	1079.6 1133.3 134.2	1077.5 1129.4 129.3	1069.5 1118.4 121.6	1074.7 1123.4 115.8	1072.1 1120.7 115.7	1071.3 1120.1 116.0
8	1067.3 1118.9 128.8	1071.8 1125.9 135.1	1064.2 1115.2 127.2	1069.8 1120.7 121.1	1065.0 1114.2 117.1	1063.1 1111.5 115.2
7	1062.2 1116.3 135.2	1063.4 1117.9 136.6	1053.0 1102.3 123.2	1059.5 1108.7 117.2	1051.4 1096.4 106.9	1051.1 1096.3 107.7
Q LEVEL						
6	1044.5 1092.7 120.3	1043.7 1091.3 118.8	1034.9 1077.6 106.6	1042.9 1085.5 101.3	1036.8 1076.0 93.3	1034.3 1072.3 90.4
5	1018.8 1054.8 89.5	1019.5 1055.9 90.7	1013.9 1047.2 82.8	1023.7 1056.9 78.7	1018.8 1049.1 71.9	1016.7 1046.1 69.4
4	997.7 1023.2 63.1	996.4 1021.1 61.1	994.2 1017.7 58.0	1005.5 1028.9 55.2	1001.6 1022.6 49.4	999.1 1018.5 45.7
3	978.6 993.6 36.8	978.5 993.3 36.6	975.8 989.0 32.5	988.7 1001.8 30.9	985.9 997.2 26.6	984.4 994.7 24.2
2	965.1 972.0 17.0	964.5 971.1 16.1	963.2 969.0 14.1	977.1 982.8 13.3	975.8 980.6 11.2	974.9 979.1 9.8
1	958.7 961.7 7.4	958.3 961.1 6.7	957.8 960.2 5.8	972.1 974.5 5.5	971.5 973.5 4.5	971.1 972.7 3.7

Figure 5.13 Pass 5 Temperature Summary (Crosshatching indicates panel area where salt temperature limit is exceeded), °F [$^{\circ}\text{C} = (^{\circ}\text{F} - 32) / 1.8$]

bulk temperature) of $\approx 47^{\circ}\text{C}$ ($\approx 84^{\circ}\text{F}$). To meet the recommended maximum, the heat flux at this location will have to be reduced by about 17 percent--a reduction that could be difficult to achieve within acceptable cost limits. (See following section for further discussion.)

Uncertainty Analysis. With a given heat-transfer area and heat flux,* our main concern with uncertainties associated with thermal design parameters (because of the spread in data from which they are based) is the tubewall temperature variation. In this analysis we considered uncertainties in tubewall thickness (t), tubewall thermal conductivity (k), and salt convective heat-transfer coefficient (h). We also assessed fouling, as discussed in the next section.

We investigated the standard deviations for salt convective coefficient, tubewall thermal conductivity, and tubewall thickness, which are indicative of the spread of the data distribution, and the respective values of 8.3, 1.67, and 3.03 percent were used in this uncertainty study. The root of the sum square (RSS) method was adopted to calculate the variation in tubewall temperature with a 90 percent confidence level, which corresponds to a design parameter variation of 1.282 standard deviation.

*Calculation of the uncertainties in heat flux values, which are the responsibility of the heliostat field designer, were beyond the scope of work.

The increase in peak tubewall (O.D.) temperature because of uncertainties in salt convective coefficient and tubewall thermal conductivity and thickness is computed from the following equation:

$$\Delta T = \sqrt{(\Delta T)_h^2 + (\Delta T)_k^2 + (\Delta T)_t^2}$$

where

(ΔT) = Total increase in peak tubewall (O.D.) temperature (and in average front-to-back temperature gradient) because of uncertainties

$(\Delta T)_h$ = Increase in ΔT because of uncertainty in salt convective coefficient (h)

$(\Delta T)_k$ = Increase in ΔT because of uncertainty in thermal conductivity of tube (k)

$(\Delta T)_t$ = Increase in ΔT because of uncertainty in tubewall thickness (t).

The calculated results are shown in Table 5.7. These results show that the peak front-to-back tube ΔT and the salt film (I.D.) and peak tubewall (O.D.) temperatures could be 12.1°C (21.8°F), 5.6°C (10.0°F) and 5.8°C (10.4°F) higher respectively than the values given in Table 5.6. This predicted increase is particularly critical in the peak salt film (I.D.) temperature, which was calculated at 601°C (1114°F), or 8°C (14°F) higher than the recommended limit (see Section 4.3.4). The uncertainty analysis shows that the estimated peak salt film (I.D.) temperature could reach 607° (1124°F), necessitating a 25.5 percent reduction in the heat flux at this location to meet the recommended limit. We believe this too big a reduction to be achieved by means at the designer's disposal (i.e., changed heliostat field aim strategy, selective relocation of the panels within the cavity, or increased absorber area).

Table 5.7 Effect of Uncertainties on Peak Tubewall (O.D.)
Temperatures, °C (°F)

Description	Location (Pass/Panel/Strip/Node)	
	2/4/5/8	5/9/1/12
(ΔT) _h	11.9 (21.4)	5.6 (10.0)
(ΔT) _k	1.1 (2.0)	0.7 (1.2)
(ΔT) _t	2.2 (3.9)	1.3 (2.4)
ΔT	12.1 (21.8)	5.8 (10.4)
Front-to-back temperature gradient	165 (297)	89 (161)
I.D. temperature	468 (896)	607 (1124)
O.D. temperature	527 (985)	638 (1181)

Experimental programs at Olin show that some alternatives exist that should solve the salt decomposition problem, such as physically adding nitrates or oxidizing the nitrites to nitrates to restore the original salt composition. These molten salt stabilizer research methods have been demonstrated by Olin under laboratory test conditions,²⁸ but further testing is required under conditions at pilot plant scale.

The quantity of salt exposed to this temperature is only a small fraction of the total salt flow rate, and it is exposed for only a short period of time because of the velocity of salt through the tubing [about 3 m/s (10.1 ft/s) in the outlet panels] and the resultant turbulent mixing.

As a solution, we recommend that the required salt outlet temperature be reduced by 14°C (25°F) to 552°C (1025°F) for the first commercial plant, unless methods to make the salt fully compatible with the higher temperature limit have been fully demonstrated by that time.

Fouling Assessment. Molten salt fouling data within the heat flux and temperature ranges experienced by the absorber panels do not exist.²⁹ The molten salt fouling resistance recommended in the Standards of the Tubular Exchanger Manufacturer's Association (TEMA)³⁰ is $88 \text{ m}^2 \cdot ^\circ\text{C}/\text{MW}$ ($0.0005 \text{ h} \cdot \text{ft}^2 \cdot ^\circ\text{F}/\text{Btu}$). It is used in the chemical process industry, where the low heat fluxes, thick walls, and low convective coefficients make the fouling resistance a small part of the overall heat-transfer resistance. This is not the case in the absorber panels, which have very high heat fluxes, thin walls, and high convective coefficients.

SOLAR runs were made with different fouling factors, and the results are shown in Table 5.8 and Figure 5.14. They indicate that, if the TEMA fouling factor is used, the temperature gradient as a result of fouling will be larger than the tubewall temperature gradient, increasing the peak front-to-back tube ΔT (Pass 2) by 39.4 percent to 213°C (383°F) and the peak tubewall (O.D.) temperature (Pass 5) by 6.1 percent to 673°C (1243°F)--well above the design limits established in Section 4.3.4. Thus TEMA values are too conservative. If they are used to design the receiver, severe constraints will be placed on the absorber design:

- To get the peak tubewall (O.D.) temperature within the design limits, the peak heat flux in Pass 5 would have to be reduced by at least 25 percent or the required outlet temperature by about 28°C (50°F) to 538°C (1000°F).
- To get the peak front-to-back tube ΔT within the design limits, the heat flux in Pass 2 would have to be reduced by at least 38 percent.

Until fouling data are available, we recommend that the detailed design of the first commercial plant in Phase 2 be made with a fouling factor of $18 \text{ m}^2 \cdot ^\circ\text{C}/\text{MW}$ ($0.0001 \text{ h} \cdot \text{ft}^2 \cdot ^\circ\text{F}/\text{Btu}$). Tests will have to be made to determine how

Table 5.8 Effect of Fouling on Calculated Tubewall Temperatures

Fouling Resistance $\text{m}^2 \cdot ^\circ\text{C}/\text{MW}$ ($\text{h} \cdot \text{ft}^2 \cdot ^\circ\text{F}/\text{Btu}$)	Front-to-Back Tube ΔT Pass 2, $^\circ\text{C}$ ($^\circ\text{F}$)	Peak Tubewall (O.D.) Temperature Pass 5, $^\circ\text{C}$ ($^\circ\text{F}$)
None	153 (275)	633 (1171)
17.6 (0.0001)	165 (297)	641 (1185)
35.2 (0.0002)	177 (318)	649 (1200)
88.0 (0.0005)	213 (383)	673 (1243)

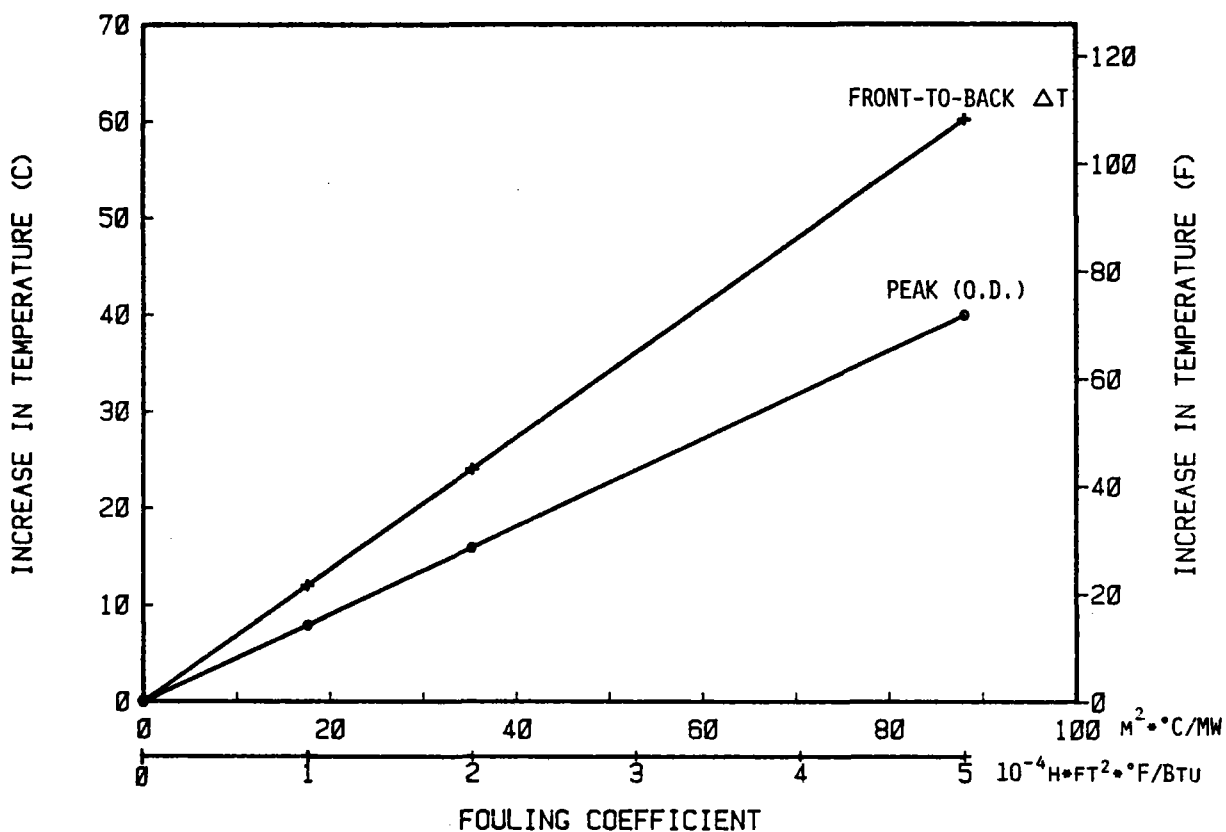


Figure 5.14 Effect of Fouling Factor on Tubewall Temperatures

often the panels will have to be cleaned so that the recommended fouling factor is not exceeded. [Note: The salt film (I.D.) temperature is not affected by fouling.]

Salt Reynolds Number and Convective Coefficient. The panel tube Reynolds Number and convective heat-transfer coefficient vs. percentage of rated salt flow are given in Figures 5.15 and 5.16 for the range of salt temperatures of interest [288 to 566°C (550 to 1050°F)]. A salt flow less than 5 percent could be in the laminar or transition region, as shown in Figure 5.17, depending on the salt bulk temperatures. This will only occur during start-up or shutdown periods, since the RS operating range as defined in the Requirements Specification (Section 3 or Appendix B) is from 10 to 105 percent of rated flow. Salt flows between 5 and 25 percent could be in the transition or turbulent region, again depending

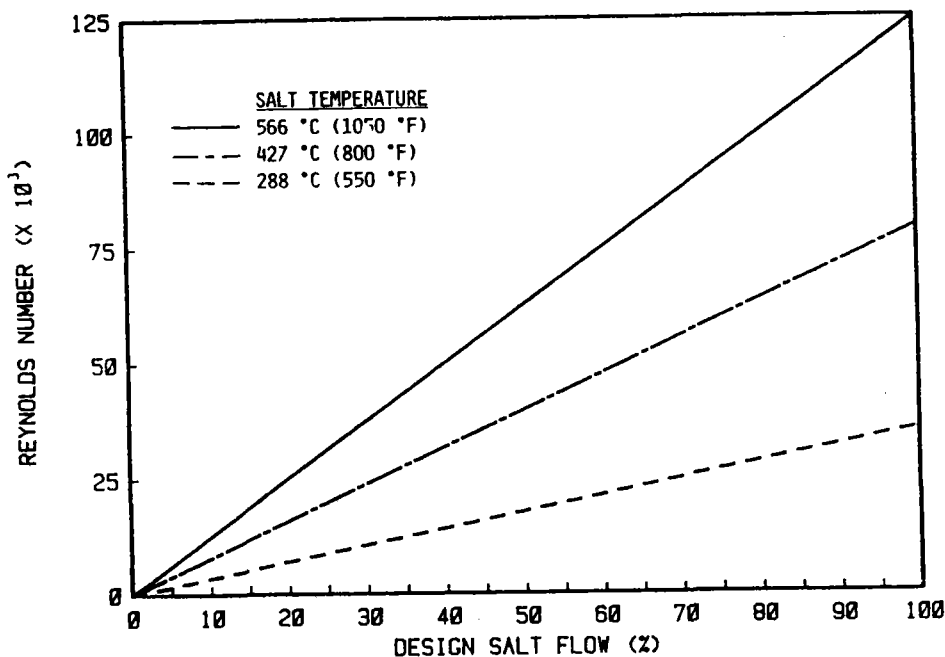


Figure 5.15 Reynolds Number vs. Percent Mass Flow

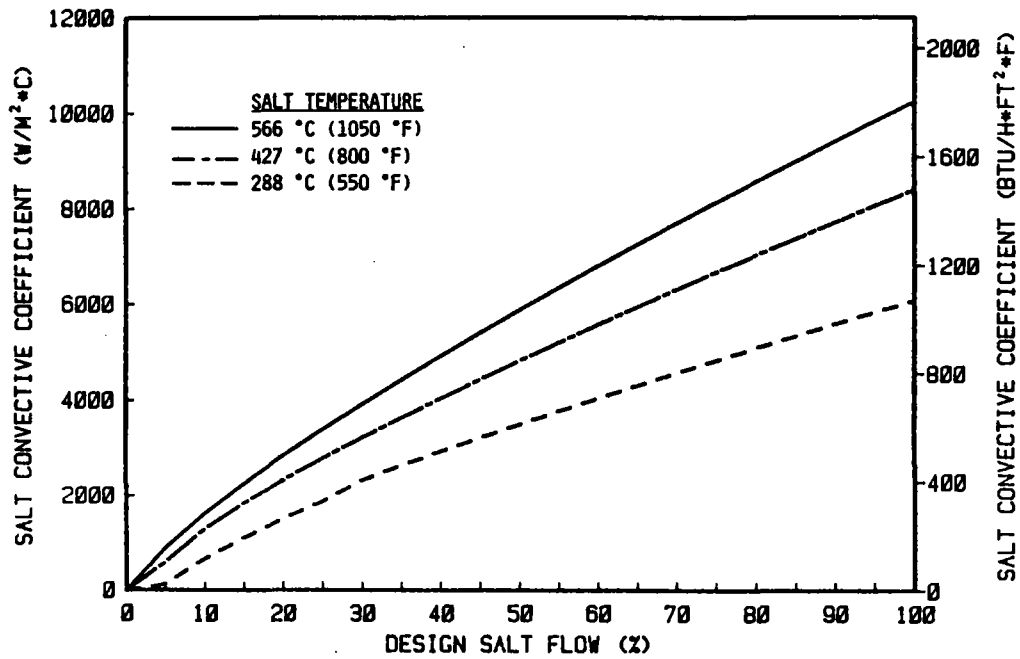


Figure 5.16 Convective Coefficient vs. Percent Mass Flow

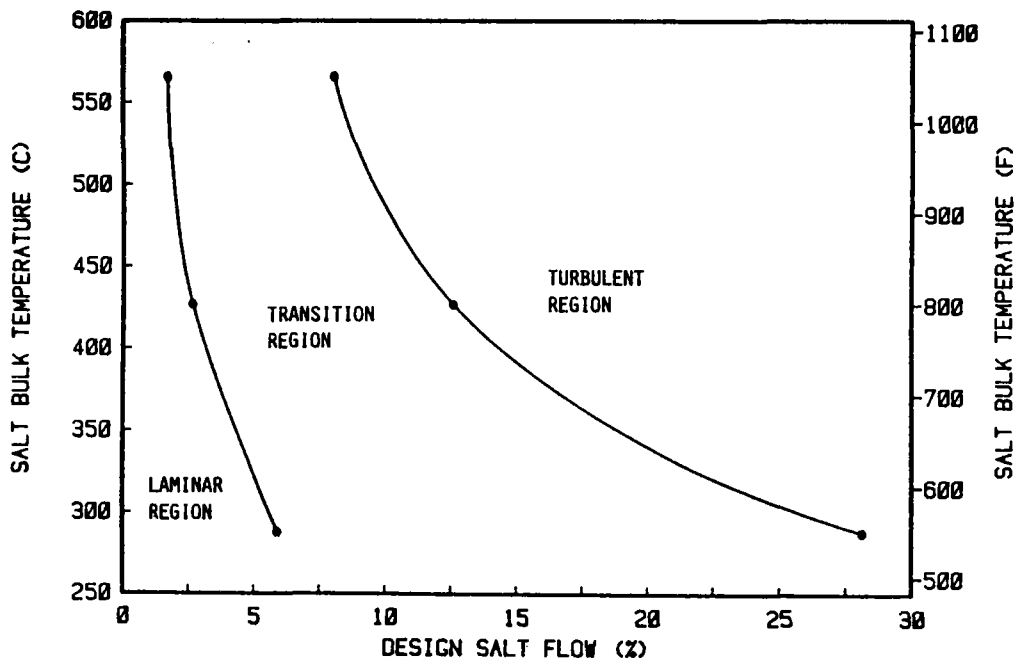


Figure 5.17 Salt Flow Regimes

on the salt bulk temperature. For the RS required performance range (25 to 105 percent of rated flow), the flow is turbulent.

As stated before, SOLAR uses one of three correlations to calculate the molten salt convective coefficient, depending upon the flow regime--Seider-Tate²⁵ (laminar, $Re \leq 2100$), Hauzen²⁶ (transition, $2100 < Re \leq 10,000$) or Dittus-Boelter²⁷ (turbulent, $Re > 10,000$). The ACR tests reported turbulent flow at $Re > 4000$.¹⁰ Details of these correlations are given in Appendix J. The salt convective coefficient at the design point condition increases from about $5686 \text{ W/m}^2 \cdot ^\circ\text{C}$ ($1000 \text{ Btu/h} \cdot \text{ft}^2 \cdot ^\circ\text{F}$) at the inlet of Pass 1 to about $10,200 \text{ W/m}^2 \cdot ^\circ\text{C}$ ($1800 \text{ Btu/h} \cdot \text{ft}^2 \cdot ^\circ\text{F}$) in Pass 5--and in so doing, its contribution to the overall thermal resistance on a clean tube (no fouling) diminishes from 68 to 57 percent.

Table 5.9 lists the ranges of several T/H variables of interest at the design point conditions.

Table 5.9 Average T/H Values at Rated Flow

Pass	Panel	Reynolds Number	Salt Velocity m/s (ft/s)	Convective Coefficient (h) $\text{W/m}^2 \cdot ^\circ\text{C}$ ($\text{Btu/h} \cdot \text{ft}^2 \cdot ^\circ\text{F}$)
1	Left	38,974	3.0 (9.8)	6061 (1066)
	Right	43,554	3.0 (9.9)	6336 (1116)
2	Left	58,618	3.1 (10.0)	7205 (1270)
	Right	58,058	3.1 (10.0)	7183 (1265)
3	Left	77,150	3.1 (10.2)	8184 (1442)
	Right	76,296	3.1 (10.2)	8148 (1434)
4	Left	94,476	3.3 (11.0)	9192 (1620)
	Right	85,166	3.0 (10.0)	8490 (1496)
5	Left	97,656	3.1 (10.2)	9164 (1613)
	Right	107,980	3.4 (11.1)	9903 (1745)

Flow Distribution. The flow distribution of salt through the receiver is governed by controlled and uncontrolled variables. The controlled variables are the salt flow-control valves at the inlet to all Pass 4 panels. These valves control the amount of salt that passes through their respective circuits to ensure that the average bulk salt temperature leaving the circuit is maintained at 566°C (1050°F). The amount of heat absorbed in each circuit dictates how the control valves proportion the flow. The uncontrolled variables include heat flux variations from tube to tube within a given pass as well as variations in physical geometry, such as tubewall thickness, jumper tube layout, location of a tube within a panel, and feeder/riser pipe configuration.

For identical physical geometries, variations in flow among the tubes are caused by variations in heat flux across a panel. For a given total pressure drop between headers, the tube that absorbs more heat carries more salt because salt density and thus gravity head are reduced.

The sensitivity of salt flow and of salt outlet and tubewall temperatures to variations in heat flux across the panels was investigated at full- and part-load conditions at the design point. By an iteration procedure, SOLAR calculates the flow distribution from variations in heat absorption. The program adjusts the flow in each tube (left, center, and right) until the calculated total pressure drops (frictional and gravity head) through the tubes are "equal" [within 6.9 Pa (0.1 lb/in²)]. A similar technique is used to obtain the flow distribution between two separate panels connected to a common header (as in Passes 1 through 3). In this case six tubes (three for each panel) are used simultaneously for the flow distribution iteration. As expected, maximum salt flow

variations were obtained for Pass 1 (wing panel), where the heat flux variations are the greatest. The results are given in Table 5.10. As the table shows, changes in salt flow rate and outlet temperatures for the worst variation in heat absorption (Pass 1) are not significant at or near full load. The coldest tube within that pass has approximately 1.8 percent less flow than the average tube. Consequently, salt flow through the panel tubes is very insensitive to heat flux variations across the panel width, and each tube within a given panel has essentially the same salt flow rate. This is not the case for 10-percent

Table 5.10 Effect of Flow Distribution--Pass 1

<u>Receiver Power and Flow (Per- centage of design point)</u>	<u>Absorption Variation (Percentage from average)</u>	<u>Flow Variation (Percentage from average)</u>	<u>Salt Outlet Temperature Change* °C (°F)</u>
105	-75.0	-1.67	+0.2 (0.4)
	+60.0	+1.17	-0.8 (1.5)
100	-75.0	-1.75	+0.2 (0.4)
	+60.0	+1.26	-0.9 (1.6)
75	-75.0	-2.18	+0.3 (0.5)
	+60.0	+1.50	-1.1 (2.0)
50	-75.0	-3.33	+0.4 (0.7)
	+60.0	+2.35	-1.7 (3.0)
25	-75.0	-6.31	+0.8 (1.4)
	+60.0	+4.59	-3.3 (5.9)
10	-75.0	-22.39	+3.1 (5.5)
	+60.0	+15.43	-10.1 (18.1)

*Resulting from flow change only.

flow, where the assumption of equal flow per tube is no longer valid. Because of this and the possibility of being in the transition region, we do not recommend operation with less than 25-percent full flow. From 0 to 25 percent is considered start-up (Section 3.1).

The variation in outlet salt temperature in Panel 1 from variation in heat absorption and salt flow rates per tube results in large salt outlet and average tubewall temperature gradients across the panel, 45°C (80°F) and 28°C (50°F) respectively. Therefore, as explained in Sections 5.3.5 and 5.4.1, each panel was divided in three separate subpanels within common inlet and outlet headers to reduce the ΔT across the panel and the resultant shear stresses.

Pressure Losses. Panel pressure drop between headers [including tube entrance and exit losses and the unheated inlet and outlet jumper tubes used to connect the panel tubes with the headers (Section 5.4.1)] was computed by SOLAR using maximum tubewall thicknesses and the Darcy-Weisbach formula with friction factors from the Colebrook equation.¹¹ SOLAR computes the pressure drop through each nodal element based on local salt conditions. The sum of the individual pressure drops gives the total tube pressure drop. Pressure drop through the interconnecting piping between panels is calculated separately by manual methods based on Moody diagram friction factors, average pipe lengths estimated from pipe layout drawings, and bend and tee loss factors according to Foster Wheeler design standards.

Terminal points for the receiver used for piping pressure-loss calculations were at the connection of the primary riser to the IST and at the connection of the primary downcomer to the OST. The primary downcomer from the OST

to the top of the tower is within the scope of the RS. However, it was not included in pressure-loss calculations because it does not affect the sizing of the salt feed pumps and is sized to absorb ≈ 75 percent of the gravity head by friction and thus to minimize the pressure loss that must be taken across the drag valve (Section 5.4.7). A summary of frictional pressure losses based on minimum tube I.D. is presented in Tables 5.11 and 5.12.

The total frictional pressure drop through the absorber panels--not including the interconnecting piping--is shown in the following chart as a function of salt flow.

Percentage of full salt flow	10	25	50	75	100	105
Pressure drop through absorber panels, kPa (lb/in ²)	20.5 (3.0)	97.8 (14.2)	329 (47.7)	675 (97.9)	1132 (164.2)	1239 (179.2)

At full flow the frictional pressure drop accounts for 35 percent of the total pressure drop between headers in a panel. At 10 percent load, it accounts for less than 1 percent. Thus the gravitational pressure drop component governs, especially at low loads.

Panel Insulation Thickness. A relationship was developed between insulation thickness and heat loss through the insulation at the design operating condition. Considering cost and weight, we selected insulation that ranges from 0.15 to 0.25 m (6 to 10 in.) thick, depending on the panel temperature. With the selected insulation thickness (Table 5.13), total heat loss through the back of the panels is estimated at 0.2 MW (0.7×10^6 Btu/h).

Table 5.11 Frictional Pressure Drop Through Receiver
at Design Point, kPa (lb/in²)*

<u>Pass/Pipe</u>	<u>ΔP</u>	
1	245.7	(35.6)
2	228.1	(33.1)
3	220.9	(32.1)
4 >	438.0	(63.5)
5		
Total through panels	<u>1130.3</u>	<u>(164.0)</u>
Interconnecting piping	<u>289.6</u>	<u>(41.9)</u>
Total	1419.9	(205.9)

Table 5.12 Frictional Pressure Drop Through Receiver
vs. Time on Design Day, kPa (lb/in²)*

<u>Time</u>	<u>Left Side</u>	<u>Right Side</u>
7:00 a.m.	200 (29)	138 (20)
10:00 a.m.	1503 (219)	1220 (177)
Noon	1482 (215)	1482 (215)
2:00 p.m.	1220 (177)	1503 (219)
5:00 p.m.	138 (20)	200 (29)

*Includes interconnecting piping, but does not include control valve.

Table 5.13 Insulation

<u>Pass</u>	<u>Material</u>	<u>Average Temperature on Back Surface of Panel, °C (°F)</u>	<u>Insulation Thickness mm (in.)</u>
1	Forty-Eight ETR	310 (590)	152.4 (6.0)
2	Forty-Eight ETR	360 (680)	177.8 (7.0)
3	Durablanket	427 (800)	203.2 (8.0)
4	Durablanket	488 (910)	228.6 (9.0)
5	Durablanket	543 (1010)	254.0 (10.0)

Drainage. To estimate the required time to drain salt from the receiver by gravity the following equation was derived by combining continuity and Bernoulli's equation.

$$\text{Time} = \sqrt{h[(K_p - 1) + (A_t/A_d)^2(K_d + 1)]/2g}$$

where

- h: Absorber panel height, m (ft)
- K_p: Salt velocity head lost in panel tube
- A_t: Panel tube flow area, m² (ft²)
- A_d: Drainpipe flow area, m² (ft²)
- K_d: Salt velocity head lost in drain pipe
- g: 9.817 m/s² (32.2 ft/s²)

With a given drainpipe size and the initial assumed values of K, the required time to drain salt can be computed from this equation. Since this result was based on the assumed values of K, an iterative scheme was employed to improve accuracy. From the initial calculated result, we estimated the average salt velocity and modified the values of K to take it into account. Substituting for the modified K values in the equation, we obtained a more accurate result. Repeating this procedure until the change was insignificant, we estimated that it

would take approximately 30 minutes to drain salt from the absorber panels, interconnecting piping, and surge tanks.

5.2.2 Transient Analysis

The following cases were investigated:

- Morning hot start-up
- Noon hot start-up
- Hot shutdown
- Emergency shutdown
- Cloud-cover

A computer model using SINDA-3G, which employs a network-type analysis to solve multidimensional transient or steady-state temperature distribution problems, was prepared for the receiver transient analysis. In this model the selected tubes from each pass are modeled with 19 nodes (17 for the exposed length and one each for inlet/outlet jumper tubes). As the fluid introduced into the bottom node of the model flows upward, each node temperature resulting from a heat transfer between metal node and fluid node responds to the time-dependent heat flux and salt flow rate. The time-dependent salt temperatures and heat-transfer coefficients resulting from this study were used for the transient stress analysis of selected nodes critical on the receiver (Section 5.3.6).

Morning Hot Start-Up. We assumed that the receiver is in a hot standby mode at 288°C (550°F) and that the available power increases linearly in 50 minutes from zero to the value corresponding to 10-deg sun elevation, which is assumed to occur at 7 a.m. To arrive at the desired start-up approach, we varied the start-up salt flow and the time at which focusing of the heliostat field

begins until the outlet salt asymptotically approached the design outlet temperature of 566°C (1050°F). In the selected approach, morning start-up takes about 20 minutes. Salt flow rate is kept constant at 70 percent of the value corresponding to 7 a.m. power for 8 minutes and then is increased linearly to 94 percent in 12 minutes, as shown in Figure 5.18. Heliostat focusing, which starts at 6:40 a.m., is assumed to take 5 minutes. Thus power is assumed to increase linearly from zero to the available value in 5 minutes and then follow the available power distribution curve. The resultant salt outlet temperature is plotted in Figure 5.18. With this approach the design outlet temperature of 566°C (1050°F) will be reached at about 7 a.m., as shown.

Noon Hot Start-Up. Assuming that the receiver is initially in a hot standby mode, as is the case during morning start-up, we tried a few different approaches. In the first two, we used the same power distribution--linear increase from zero to full power in 15 minutes and two different salt flow distributions:

- Salt flow rate kept constant at 30 percent of the design flow rate (DFR) for 5 minutes and then increased linearly to the DFR in 10 minutes
- Salt flow rate kept constant at 50 percent of the DFR for 8 minutes and then increased linearly to the DFR in 7 minutes.

The results show that design outlet temperature is reached in approximately 14 and 17 minutes respectively. The second method, although taking 3 minutes longer to reach the design outlet temperature, was preferable because start-up with 50 percent of full flow is less risky. However, since start-up

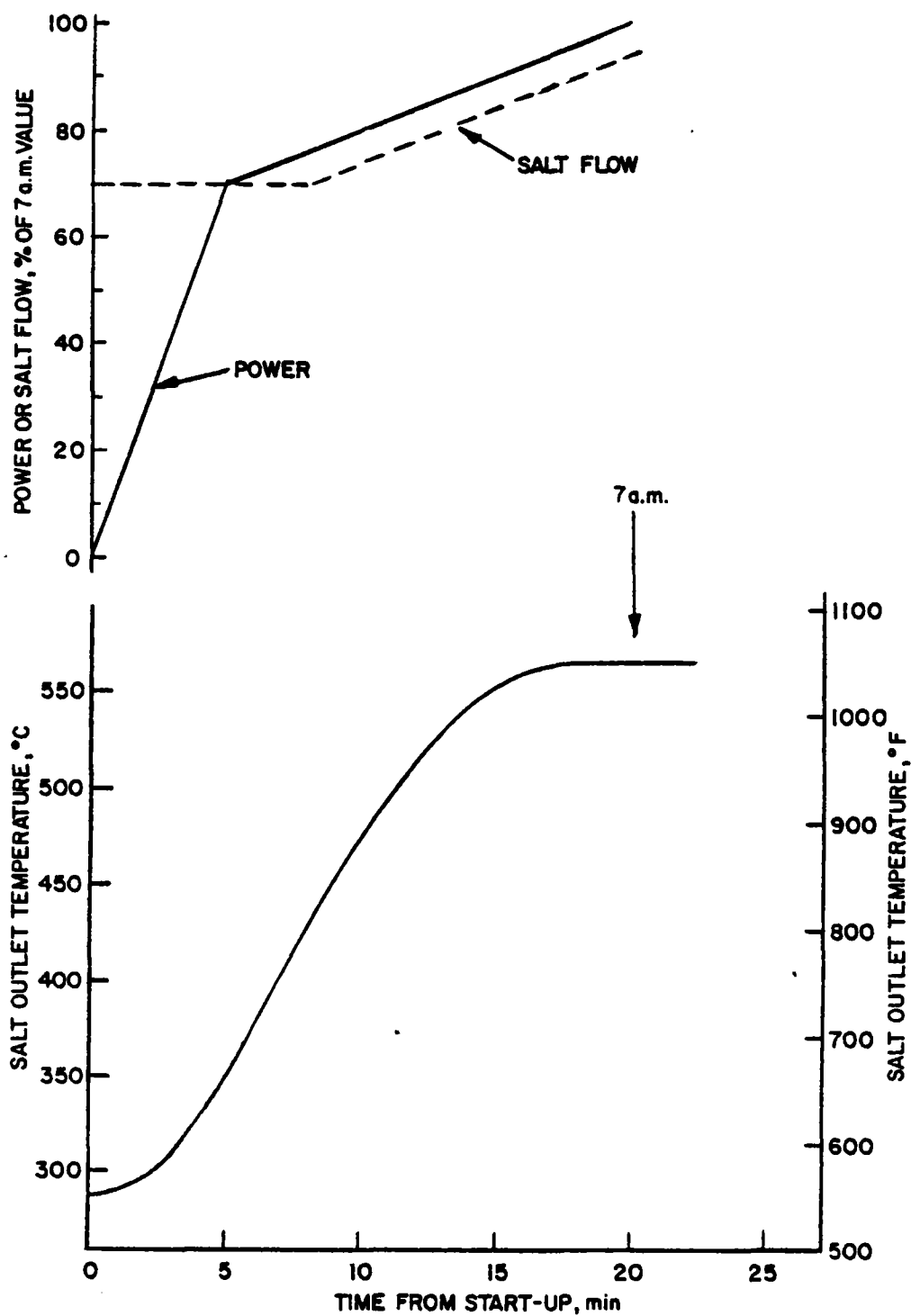


Figure 5.18 Morning Start-Up Transient

takes too long with this method, we tried another method to achieve completion of start-up in less time. In this third method, shown in Figure 5.19, power increases linearly from zero to full power in 6 minutes; salt flow is kept constant at 50 percent of DFR for 3 minutes and 15 seconds, and then flow is increased linearly to 96 percent in 2 minutes and 45 seconds. As shown in the figure, noon start-up can be completed in approximately 12 minutes.

Hot Shutdown. In this transient, power is assumed to decrease linearly from the value corresponding to 10-deg sun elevation (which is assumed to occur at 5 p.m.) to zero in 3 minutes, as specified in the Requirements Specification (Appendix B). In determining salt flow, we made an effort to minimize salt temperature drop during the transient to achieve the greatest possible utilization of absorbed heat by the receiver. Thus the salt flow was assumed to vary in proportion to the available power. However, this assumption resulted in a high salt outlet temperature of 571°C (1060°F), because the heat-absorption rate per unit mass of salt increases during the transient. To correct this problem, we kept the salt at a flow corresponding to 5 p.m. power for 15 seconds and then decreased it linearly to zero in 3 minutes. The outlet salt temperature from each pass and the distributions for power and salt flow are shown in Figure 5.20. A salt outlet temperature drop of $\approx 6^{\circ}\text{C}$ ($\approx 11^{\circ}\text{F}$) from each pass can be seen in that figure.

Emergency Shutdown. Among the various events to which this transient applies, we analyzed auxiliary power failure (no power to pump salt, no power to defocus the heliostat field, and no power to close the door), which is expected

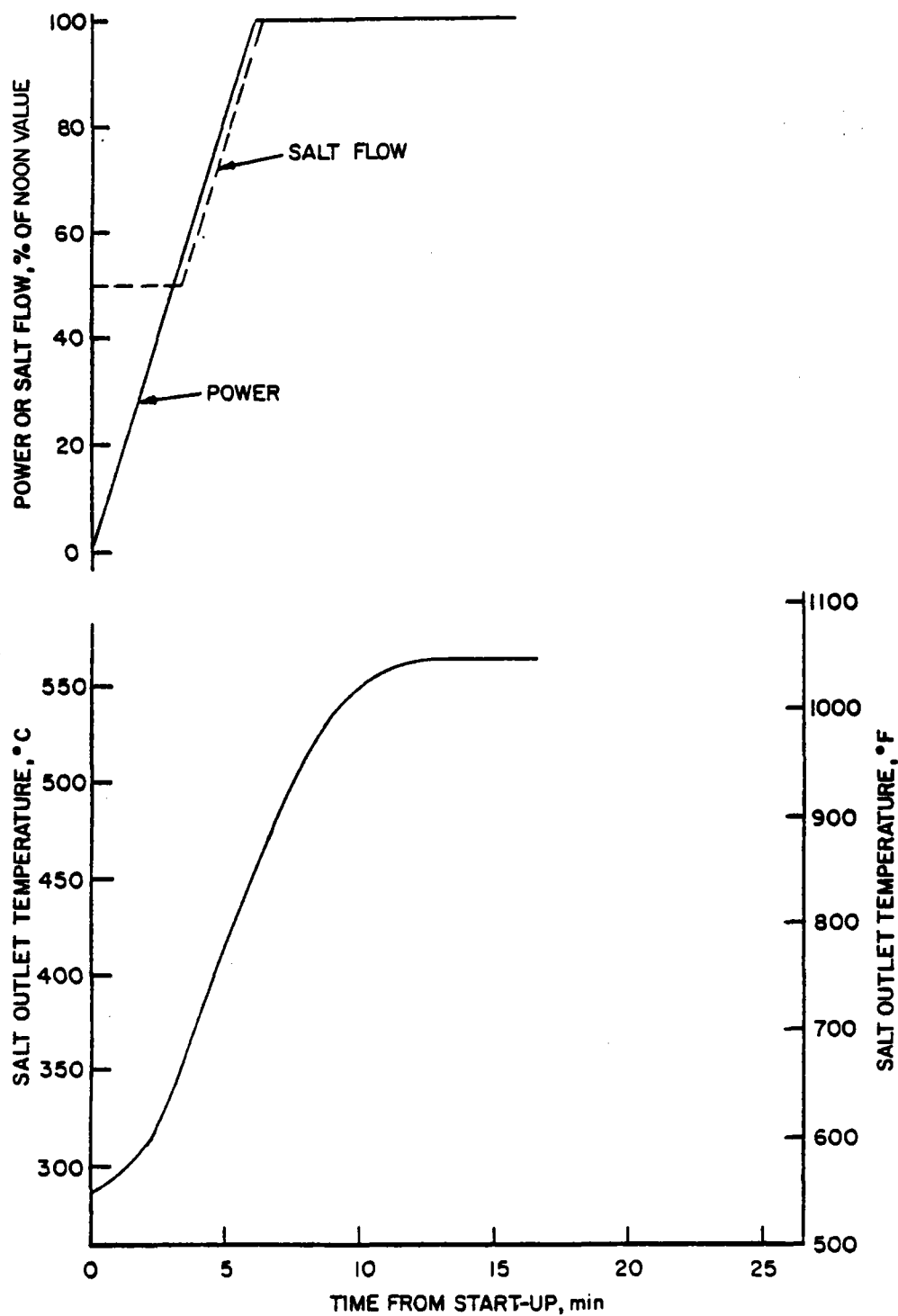


Figure 5.19 Noon Start-Up Transient

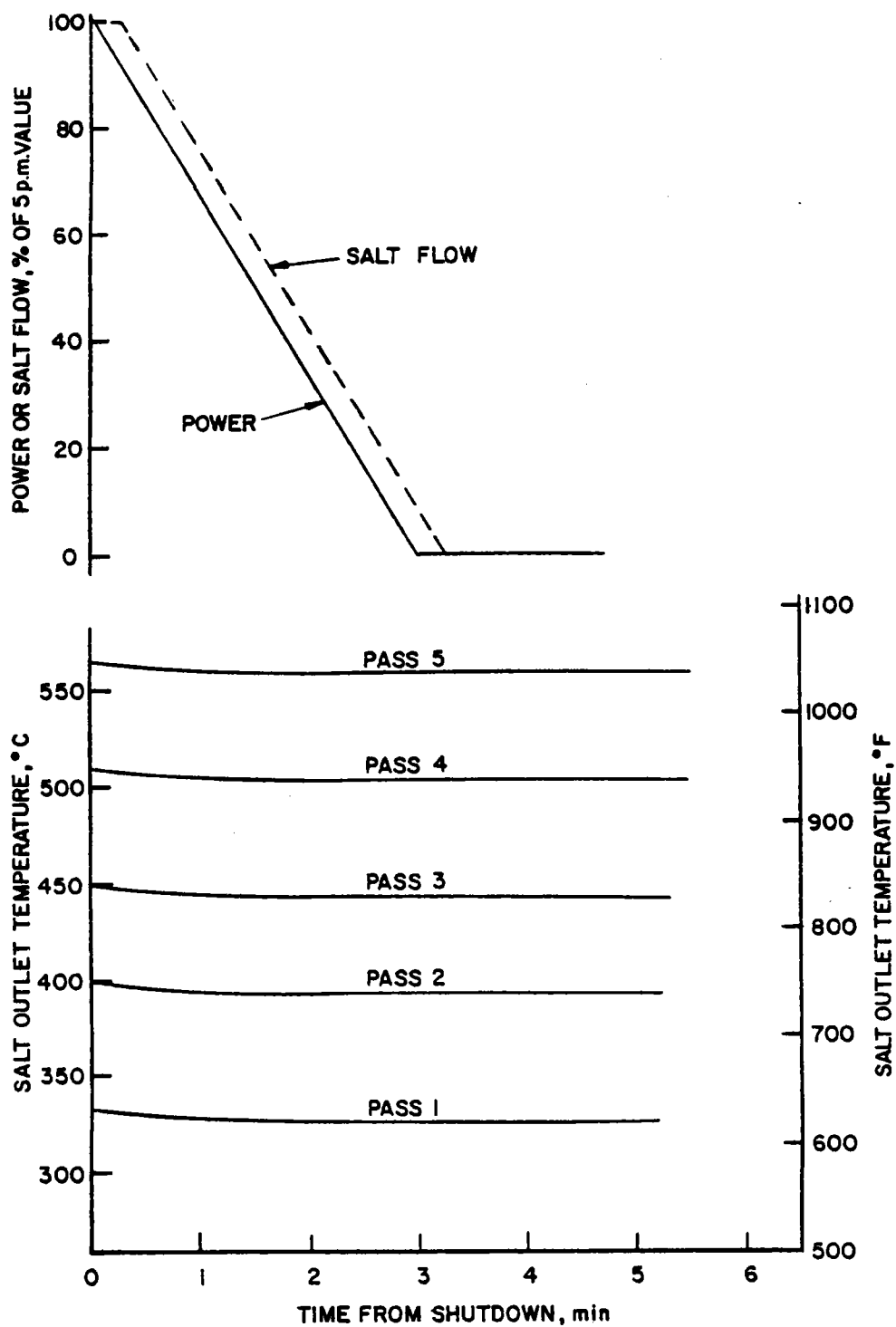


Figure 5.20 Hot Shutdown Transient

to have the most severe transient effect on the receiver. In this event, the salt in the pressurized IST will be used to supply emergency salt flow while the aperture door closes by gravity. With the receiver initially in a normal operating condition, absorbed power is assumed to decrease linearly from the noon value to zero in 30 seconds as the door closes. The salt flow from the IST is adjusted to decrease linearly from a full flow to zero in 2 minutes to avoid a drastic drop in tubewall temperature during the transient. The results of this event, shown in Figure 5.21, indicate that the receiver outlet temperature drops to 439°C (820°F) in about 2 minutes.

Cloud Cover. Among three cloud cover transients (east, south, and north halves of field obscured by clouds), the east half case was chosen for analysis because we expect it to have the most severe transient effect on the receiver. In this scenario, with the east half of the heliostat field covered by clouds, the total power absorbed by the right half of the receiver is only 7 percent of full power, while that of the left half is 93 percent. Therefore, we investigated the more critical right half only. In our analysis the absorber salt flow was maintained at full flow during the transient,* and the power absorbed by Passes 1 through 5 decreased linearly from the full power to the respective values of 16.6, 0.1, 0.6, 1.9, and 21.4 percent in 30 seconds. The results of this transient, shown in Figure 5.22, indicate that the outlet temperature of the right half of the receiver drops to about 288°C (550°F) in about 2 minutes.

*Worst case: when the control system fails. Normally, the receiver control system will reduce the salt flow to follow the decrease in power.

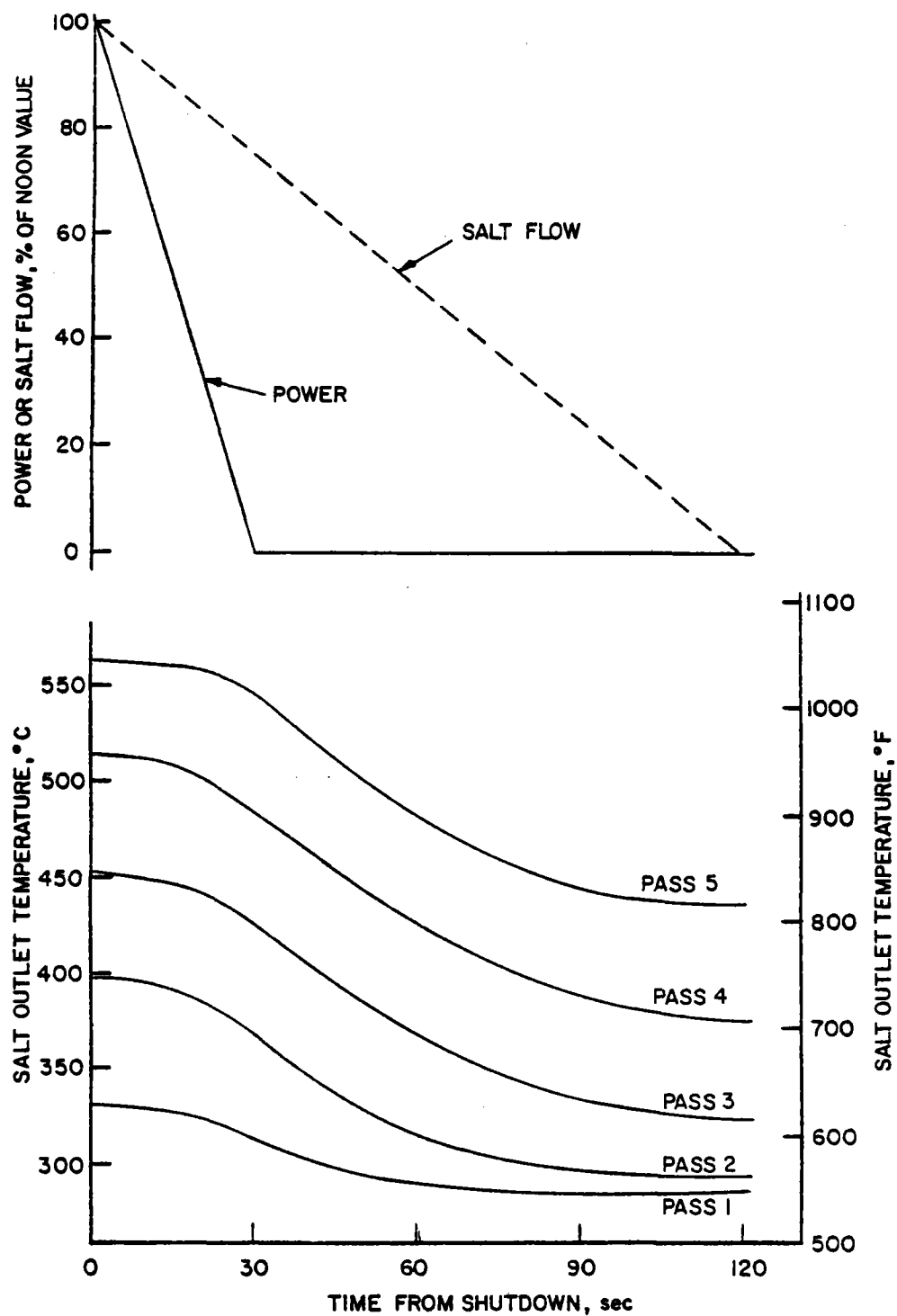


Figure 5.21 Emergency Shutdown Transient

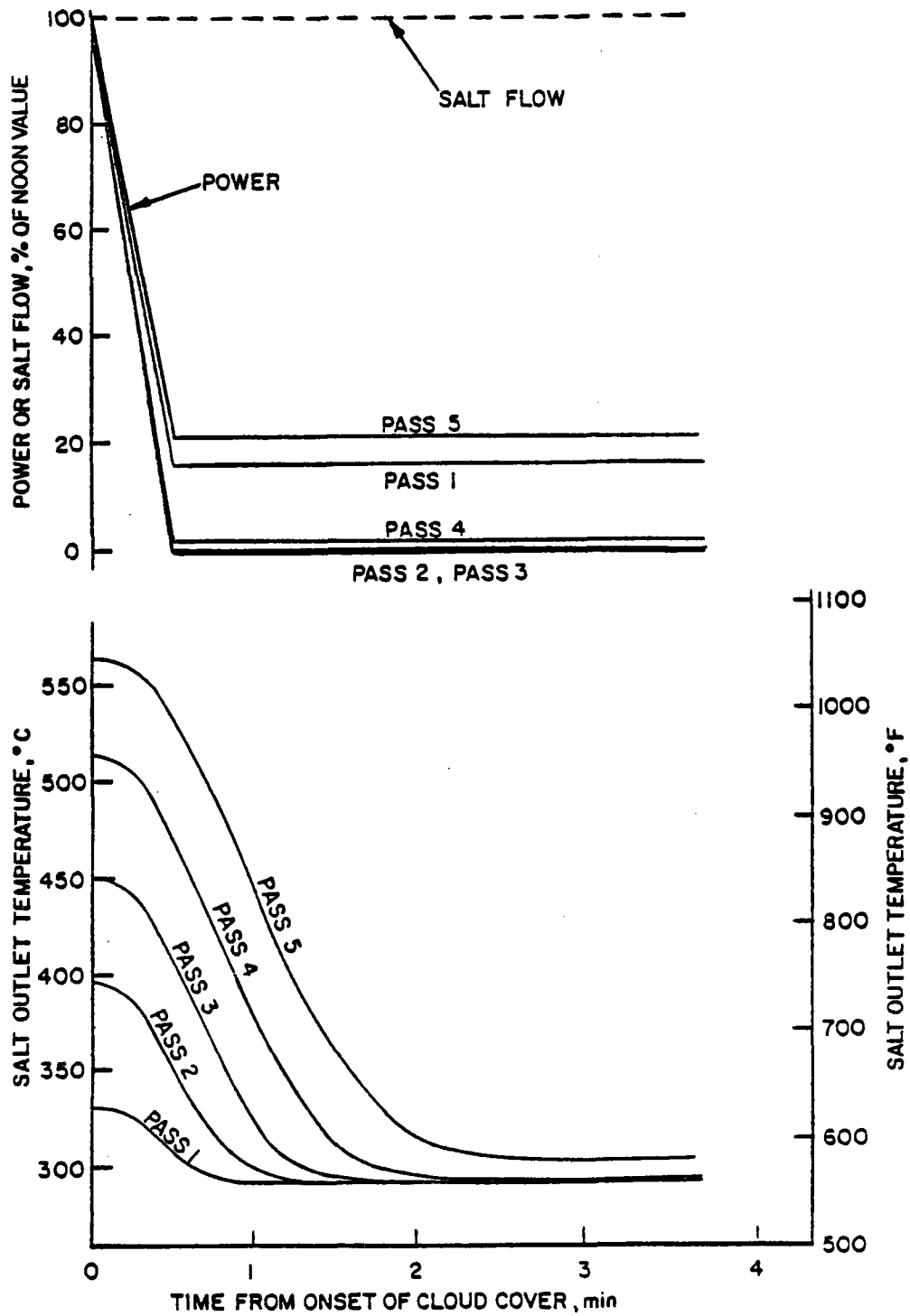


Figure 5.22 Cloud Cover Transient

5.2.3 Overnight Conditioning

The approach to overnight conditioning selected during Task 3, Concept Selection (Section 4.3.9), included radiant heaters for the cavity and hot salt drained from the OST back into the panels to reduce the total amount of electric heating required. The selected approach offers a system with minimal complexity and with inherent redundancy in the modularity of the heaters. Thus it offers greater reliability.

To establish the final heating requirements, losses were reevaluated, and the radiant heater configuration was defined. The losses for overnight conditioning come from two major elements:

- Conduction through door panel insulation, floor and ceiling insulation, and from heat shorts through structural supports
- Convection through gaps in door seals.

The conduction losses were estimated using natural-convection cooling and one-dimensional conduction through the insulation and structure.

For convection losses through door gaps, the estimate was based on a driving pressure resulting from the gravity head difference between the inside and outside of the cavity, which sets up a natural-circulation path with half the pressure difference at the top and half at the bottom. The effect of wind was not considered. The average gap for all seals was assumed to be 1 mm (0.04 in.). This small value was selected because of seal redundancy in the door design. Using these assumptions, an airflow rate was calculated for convective flows from the cavity to the atmosphere, and the energy contained in this flow was considered as a loss.

Inevitably, there will also be some losses resulting from infiltration of cold air entering (and hot air leaving) the casing. These losses are not amenable to calculation and thus were not considered. They must be minimized by careful design and construction.

The results of the loss calculations are summarized in Table 5.14.

Table 5.14 Heat Losses During Overnight Shutdown

Surface	Heat Loss kW (10 ³ Btu/h)	
Aperture door	36.7	(125.2)
Panel insulation	172.5	(588.6)
Floor and ceiling	95.6	(326.2)
Heat shorts	59.9	(204.4)
Total conduction losses	364.7	(1244.4)
Convection losses	195.0	(665.4)
Total losses	559.7	(1909.8)

Based on a rated heater power of 18 kW (61,420 Btu/h) per heater, approximately 31 heaters are required to maintain a steady heat balance. To provide for a timely heat-up and design margin and provide some level of redundancy, 50 heaters have been included in our design. These heaters, illustrated in Figure 5.23, are located as shown in Figure 5.24 and are inclined 45 deg toward the panels except for the outer ring heaters, which are inclined 30 deg.

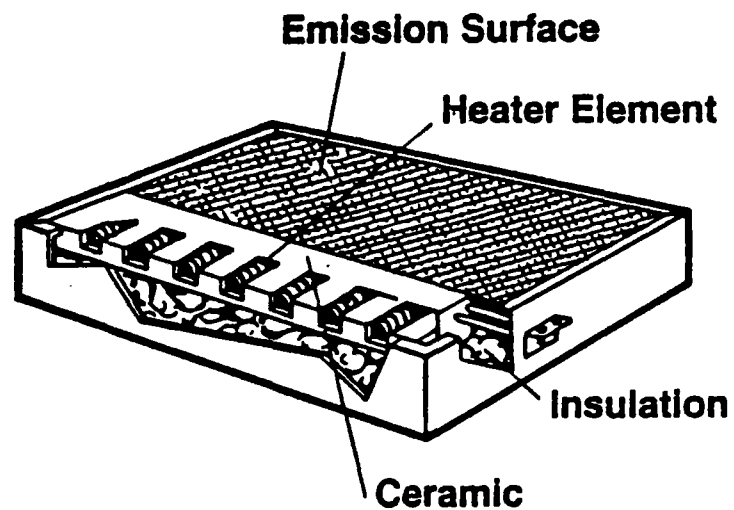


Figure 5.23 Radiant Heater Configuration (Made by Chromalox Heating Products)

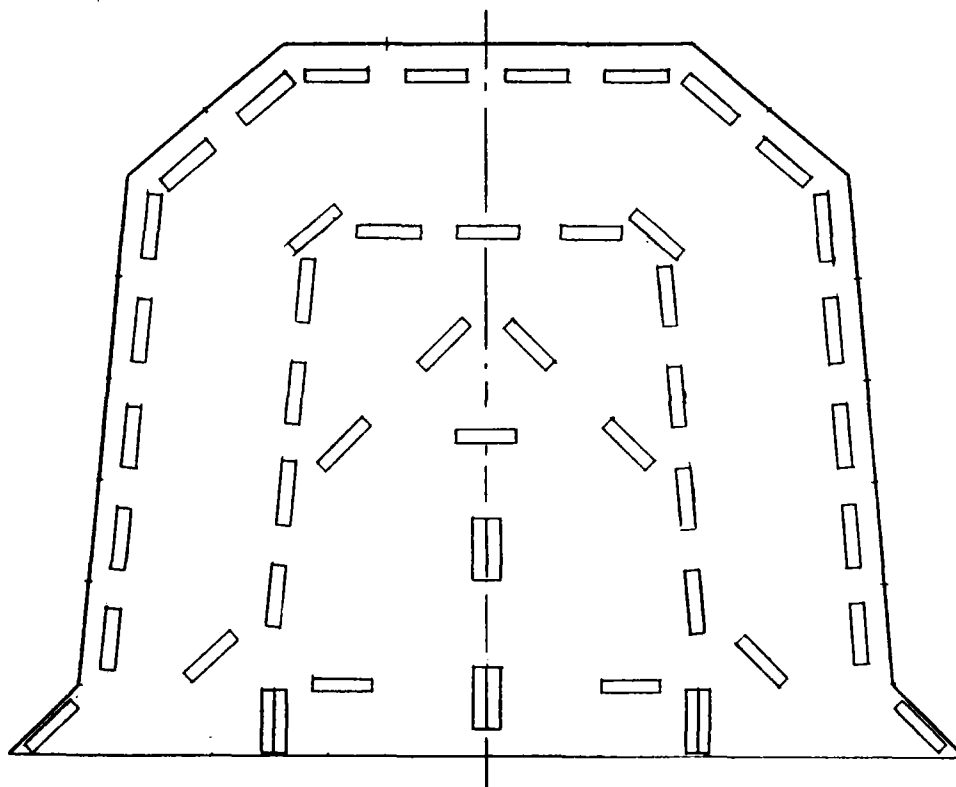


Figure 5.24 Location of Cavity Radiant Heaters

As proposed in Appendix H, once the panel temperatures fall to $\approx 343^{\circ}\text{C}$ ($\approx 650^{\circ}\text{F}$), 2.3 hours after shutdown, hot salt from the OST will be drained back into the panels by gravity by reducing the pressure in the IST. By draining over a 5-minute period, temperature ramp rates can be limited to acceptable levels. By draining approximately 34,000 kg (74,960 lb) of salt, eight panels (Passes 4 and 5) can be filled and an additional 1.046 MWh (0.307×10^6 Btu) energy can be supplied to the cavity, reducing the required nightly cavity radiant heater operating time by approximately 1.9 hours. In the morning before start-up, the extra inventory in the IST will be returned to the OST tank by repressurizing the IST.

The overnight duty on the cavity radiant heaters, using this approach, is summarized in Table 5.15.

Table 5.15 Overnight Duty for Cavity Radiant Heaters

Month	Hours			
	Shutdown Period	Cooldown Period (No Heating)	Cooldown Period After Salt Fill	Heating Time Required
June	11.4	2.3	1.9	7.2
May/July	11.8	2.3	1.9	7.6
April/August	12.6	2.3	1.9	8.4
March/September	13.7	2.3	1.9	9.5
February/October	14.8	2.3	1.9	10.6
January/November	15.9	2.3	1.9	11.7
December	16.3	2.3	1.9	12.1

Based on nominal Barstow weather data extracted from 5 years of detailed insolation data,¹¹ the radiant heaters will operate for ≈ 3900 h/yr, including approximately 1440 hours of operation in poor weather. The total auxiliary power required will be ≈ 2200 MWhe/yr (7506.6×10^6 Btu/yr).

5.2.4 Performance

The RS performance was calculated for both annual average operating conditions and design point conditions for the reference site location--Barstow, California--using the environmental conditions defined in the RS Requirements Specification (Appendix B). The resultant RS performance data are shown in the form of stair-step charts in Figure 5.25. The overall thermal efficiency for the complete RS and the receiver thermal efficiency, which normally excludes piping and viscous dissipation losses, are both shown in Table 5.16. As shown in the table, the RS net output at the design point is 320 MW (1091.9×10^6 Btu/h) at the base of the tower.

Design Point Thermal Losses. The cavity receiver configuration was selected primarily to minimize receiver thermal losses during operation and overnight or cloudy-day shutdown. Reflection, reradiation, and convection losses are minimized by the cavity during operation and the reflection and reradiation losses are eliminated entirely by the aperture door during overnight shutdown.

The receiver was analyzed for spillover, reflection, reradiation, convection, and conduction losses; using the results of these analyses, the RS efficiency was calculated.

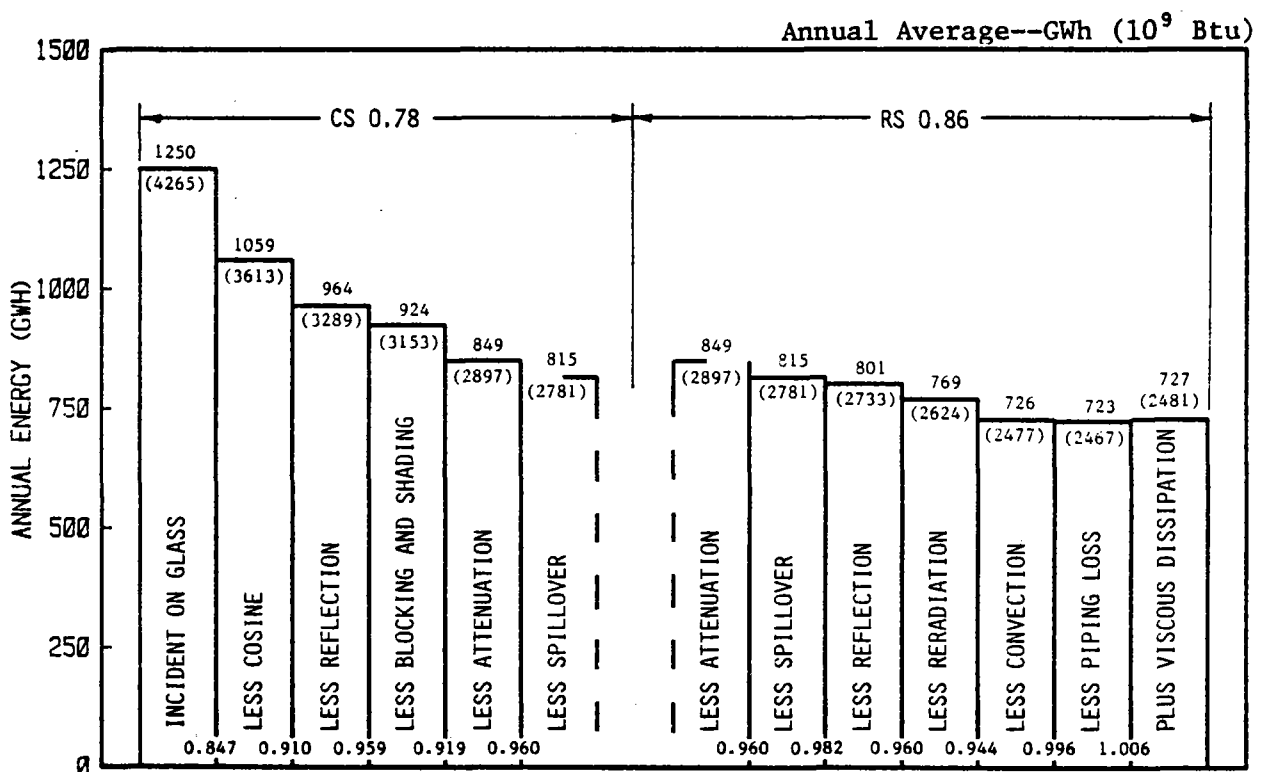
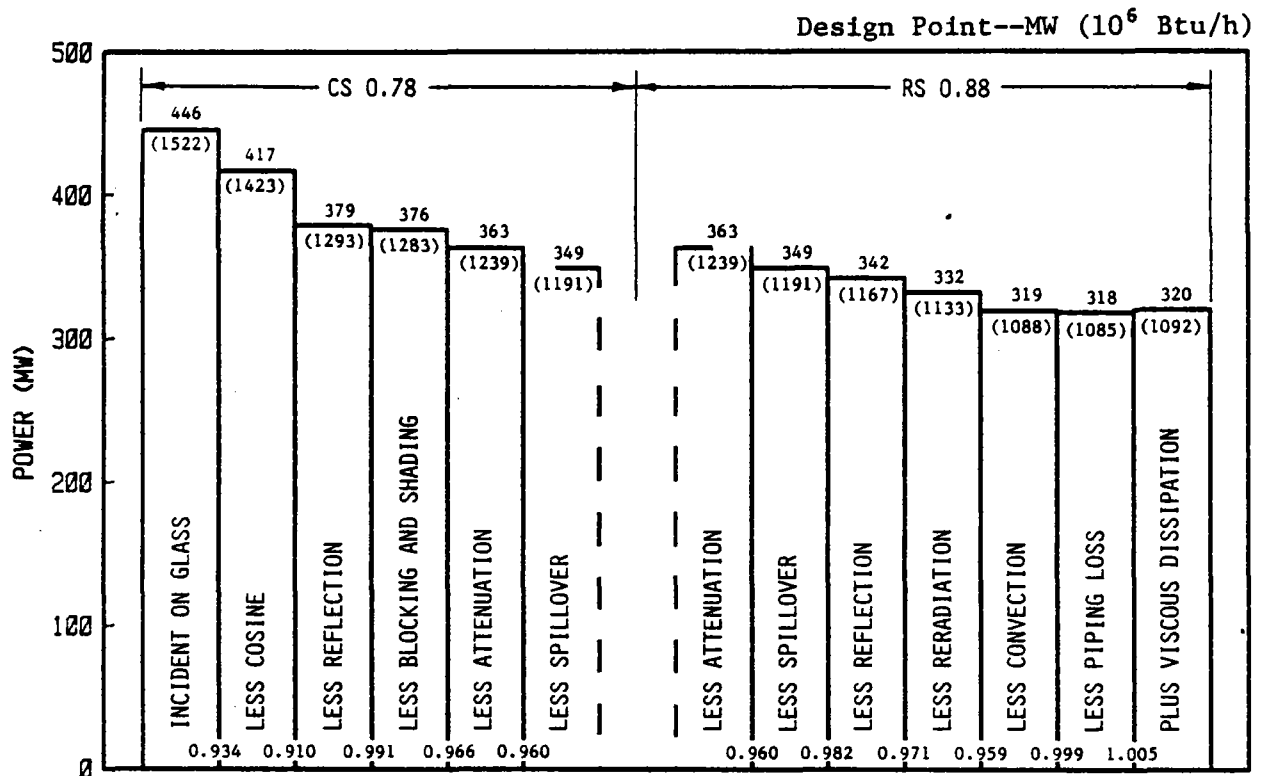


Figure 5.25 Molten Salt Receiver Efficiency

Table 5.16 RS Performance Train

Description	Design Point			Annual Average		
	Input Power (MW)	Loss (MW)	Step Efficiency	Input Energy ($10^3 \times \text{MWh}$)	Loss ($10^3 \times \text{MWh}$)	Step Efficiency
Spillover	363.6	14.7		849.0	34.0	
Reflection	348.6	6.4		815.0	14.0	
Reradiation	342.2	10.0		801.0	32.1	
Convection	332.2	<u>13.6</u>		768.9	<u>42.9</u>	
Receiver output and efficiency	318.6	44.7	0.877	726.0	123.0	0.858
Conduction/piping	318.6	0.3		726.0	2.6	
Viscous dissipation	318.3	<u>-1.705</u>		723.4	<u>-4.0</u>	
RS output and overall efficiency	320.0	43.3	0.881	727.4	124.2	0.859

Specific losses were calculated as follows:

- Spillover losses were calculated using the detailed MDC flux-mapping code, CONCEN. They represent the true value of the spills at the design-point flux profiles, including the effects of aim strategy, mirror surface waviness, cant errors, and gimbal errors. The errors which are statistically in nature are modeled with a Monte Carlo technique.
- Reflection and reradiation losses were calculated with the NASA-developed TRASYS program. This program calculates the reradiation interchanges within the cavity for incoming reflected solar energy and thermal radiation. This nodal program computes both direct (i.e., Node "I" direct to Node "J") and indirect (i.e., Node "I" to intermediate nodes to Node "J") reradiation paths. For the SRE baseline receiver, all absorber surfaces are diffuse reflectors with a surface absorptivity of 0.95 and a surface emissivity of 0.90. The floor and ceiling are also diffuse reflectors with surface absorptivity of 0.36 and an emissivity of 0.47. Details of the calculations are presented in Appendix L.
- Convection losses were evaluated for both natural and forced convection, and the final estimates represent an RSS of these two loss mechanisms. Natural convection was evaluated using the techniques of Abrams³² and those of Kraabel.³³ Forced convection was evaluated using correlations of Achenbach³⁴ and Jacob.³⁵ The results from these different techniques generally agreed, and the final values used were based on the correlations of Kraabel (natural) and Jacob (forced). The results are summarized below; details of the calculations are presented in Appendix L.

	Heat Loss	
	MW (10 ⁶ Btu/h)	
Natural convection (Kraabel model)	13.2	(45.1)
Forced convection (Jacob model)	3.3	(11.5)
RSS combination (combined heat losses)		
Design point value	13.6	(46.4)
Annual average	13.4	(45.7)

- Conduction and piping losses were estimated using simple one-dimensional heat conduction equations with the full ΔT between the salt and ambient air temperatures taken across the insulation.

The viscous dissipation term represents the conversion of static head into heat through viscous dissipation in the drag valve.

The calculated receiver losses are shown in Figure 5.26. Figure 5.27 shows RS output power vs. time of day on the design point day (February 19) for maximum insulation conditions.

Annual Average Performance. The annual average performance given in Table 5.16 has been estimated using DELSOL, with the spillover modified to reflect the effects of aim strategy as calculated by CONCEN and by estimates of thermal losses (i.e., salt temperature decay in the receiver, OST, and downcomer) which occur during shutdown. Only overnight thermal losses not compensated for by trace heating or radiant heaters have been included directly. These amount to approximately 7.6 MWh (25.9×10^6 Btu) on an average operating day and 15.2 MWh (51.9×10^6 Btu) during total shutdown.

In addition to these effects, DELSOL assumes that reflective losses are a constant fraction of incoming radiation and that reradiation, convection, and piping losses are all constant values during plant operating hours. Plant operating hours were computed using DELSOL with a 0.87 weather factor to correlate DELSOL annual insolation with the Aerospace Corporation model derived from Barstow data.³⁶

Part-Load. Part-load performance for the SRE receiver is presented in Table 5.17. Because losses from reradiation and convection are determined by wall temperatures, which are relatively constant as long as the outlet temperature is at the design value, they are independent of power.

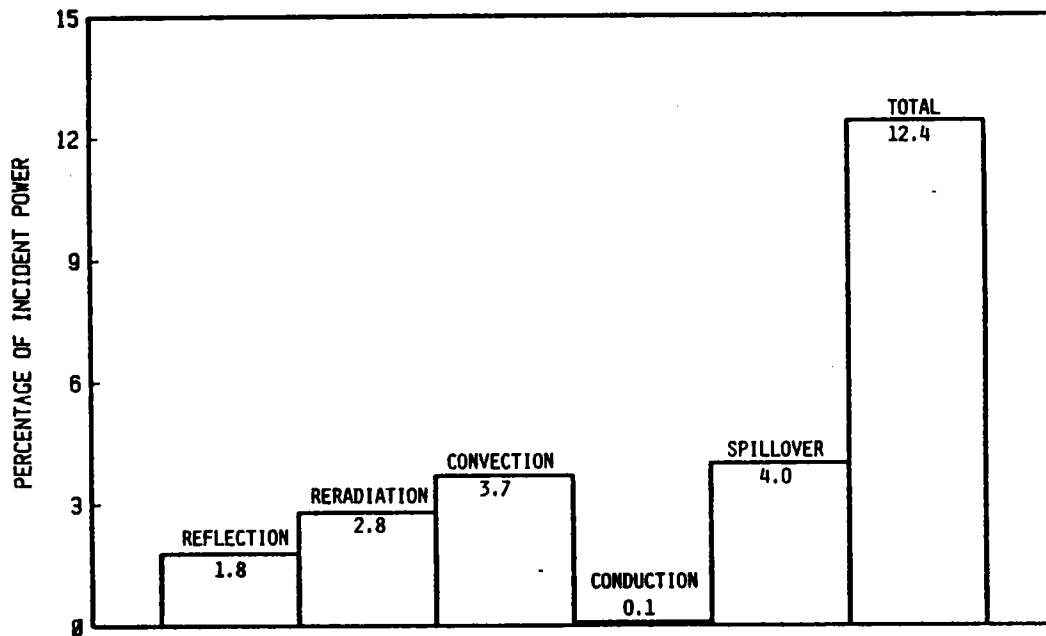


Figure 5.26 Receiver Design Point Losses

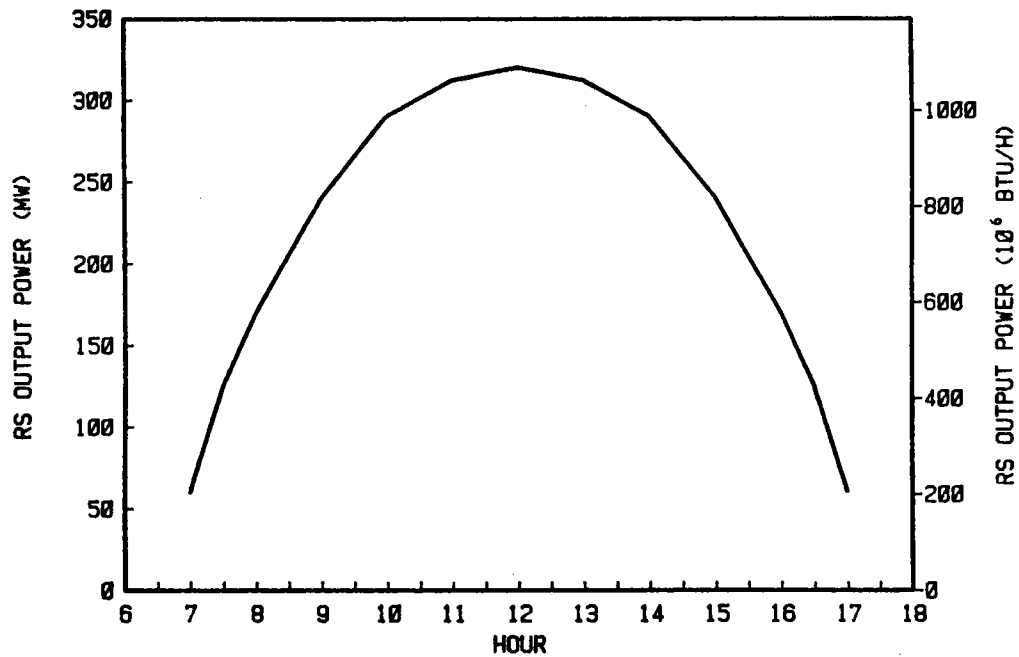


Figure 5.27 RS Output Power for Design Point Day (February 19)

Table 5.17 Part-Load Performance - Molten Salt SRE Receiver

Loss	25% Load			50% Load			75% Load		
	Input Power (MW)	Loss (MW)	Step Efficiency	Input Power (MW)	Loss (MW)	Step Efficiency	Input Power (MW)	Loss (MW)	Step Efficiency
Spillover	109.8	4.4		194.3	7.8		278.5	11.1	
Reflection	105.4	1.9		186.5	3.4		267.4	4.8	
Reradiation	103.5	10.0		183.1	10.0		262.6	10.0	
Convection	93.5	<u>13.6</u>		173.1	<u>13.6</u>		252.6	<u>13.6</u>	
Receiver output and efficiency	79.9	29.9	0.728	159.5	34.8	0.821	239.0	39.5	0.858
Conduction/piping	79.9	0.3		159.5	0.3		239.0	0.3	
Viscous dissipation	79.6	<u>-0.4</u>		159.2	<u>-0.8</u>		238.7	<u>-1.3</u>	
RS output and overall efficiency	80.0	29.8	0.729	160.0	34.3	0.823	240.0	38.5	0.862

FOSTER WHEELER SOLAR DEVELOPMENT CORPORATION

REF.: 84-2292C
DATE: November 1982

RS Auxiliary Power Requirements. The RS auxiliary power requirements are summarized in Table 5.18. In addition to requirements for electricity, the equivalent thermal energy required (assuming an electrical to thermal conversion factor of 2.342) is also shown.

In determining receiver trace heating requirements, we have assumed that the salt in the OST is used once to rewarm the receiver before the cavity heaters must be turned on. The total heat loss is estimated at ≈ 560 kW ($\approx 1.911 \times 10^6$ Btu/h) (Table 5.14), with radiant heaters sized to provide 900 kW (3.071×10^6 Btu/h). This means the heaters should operate either at derated power or on a 60-percent duty cycle.

In addition to radiant heating, the major auxiliary power consumers are the receiver salt feed pumps. The feed pumps are half-capacity feed pumps that operate with two pumps on for 80 percent of the normal operating day and with only one pump on during early morning and late evening hours (the other 20 percent).

Table 5.18 RS Auxiliary Power Requirement

<u>Receiver Trace Heating</u>	<u>Average Power (kWe)</u>	<u>Clear Day (h/yr)</u>	<u>Cloudy Day (h/yr)</u>	<u>Annual Electric Energy Required (MWhe)</u>	<u>Equivalent Thermal Energy Required from RS (MWht)</u>
Cavity heaters	560	2460	1440	2184	
Receiver pipework					
>427 °C (>800°F)	12	4227	1440	88	
<427 °C (<800°F)	14	---	1440		
Riser/downcomer	20	4227	1440	<u>132</u>	
	13	---	1440		
Annual total for trace heating				2404	5,630
<u>Receiver Feed Pumps</u>		<u>Operating (h/yr)</u>			
Single pump	1109	3266		3621	
Second pump	1049	2613		<u>2741</u>	
				6362	<u>14,899</u>
					20,529

Auxiliary Electric Energy Required x 2.342 = Equivalent Thermal Energy Required.

5.3 STRESS ANALYSES

In this section we present the results of stress analyses of the absorber panels, including elevated-temperature creep and fatigue evaluation. The major stress analyses concerned:

- Tube-to-tube joints
- Creep-fatigue
- Buckling
- Transients
- Shear
- In-plane ΔT

During the life of the plant, the receiver and support structure will be subjected to various thermal and mechanical loads. The thermal loads consist of steady-state thermal gradients and start-up and shutdown transients. The mechanical loads include self-weight, pressure, external reaction, seismic, and wind loads. Thermal loads are cyclic in nature because of diurnal start-up, shutdown, and operating transients. The failure modes caused by these loads include ductile rupture, creep rupture, fatigue failure, thermal ratcheting, buckling, and vibration.

Those sections of the receiver subjected to radiant heating (i.e., the absorber panels) are the most critical component from the thermal-stress and creep-fatigue point of view. Hence we analyzed the panels extensively to determine the severity of the thermal stresses and their impact on the structural integrity and creep-fatigue life of the receiver.

5.3.1 Design Standards and Criteria

The objective of the stress analysis is to ensure the structural integrity of the receiver within the requirements of the RS specification

(Appendix B), the ASME Boiler and Pressure Vessel Code, the UBC, and other applicable codes and standards. There are no well-accepted criteria for creep-fatigue evaluation of solar components except those set forth in the ASME Code (Section III and Code Case N-47).³⁷ Because Section III and Code Case N-47 were written for nuclear components, their use in solar component design could lead to excessively conservative designs in some areas, and the receiver might suffer significant cost penalties. A Solar Energy Standards Committee appointed by the ASME is presently working on a Solar Code. FWSDC team personnel are active on this committee. FWSDC has also developed an "Interim Structural Design Standard for Solar Energy Applications,"³⁸ under contract from SNLL. Thus structural evaluation of the receiver in the high-temperature regime was guided by the rules of Code Case N-47, the consensus being generated by the Solar Energy Standards Committee, and the conclusions from the "Interim Structural Design Standard."

In the design of the pressure boundary, we satisfied all requirements of the ASME Boiler and Pressure Vessel Code, Section VIII-Division 1. In addition, because of the highly cyclic nature of receiver operations, we satisfied the fatigue criteria of Section VIII-Division 2 for temperatures in the sub-creep regime. For elevated temperature design, we analyzed for creep-fatigue based on the linear damage addition approach of Code Case N-47. As discussed before strict adherence to Code Case N-47, however, is too conservative for solar applications and will result in severe economic penalties. Hence we used the approach in Code Case N-47 with some modifications. One modification that

we have proposed for use with solar applications is the use of inelastic fatigue curves (Figure T-1420-1C of Code Case N-47) in conjunction with inelastic strains approximated from an elastic analysis.

We did an elastic analysis and estimated the inelastic strain ranges from the elastic analysis. Since the stress state at the tubewall crown (the critical point in our design) is very nearly uniaxial--the axial stresses being far higher than hoop stresses--one would expect that the elastic and inelastic strain ranges are very close. To verify this we did elastic and inelastic analyses (Appendix M).

We used our in-house computer program NONAX^{3,4} in this analysis. NONAX is a special-purpose program developed by Foster Wheeler Development Corporation to perform thermal and stress analyses on thick-walled cylinders made of homogeneous and isotropic materials. The loading may be axisymmetric or nonaxisymmetric. It may consist of an arbitrary combination of internal and external tractions, axial load, axial bending, and an arbitrary temperature distribution. Elastic, elastic-plastic, and creep analyses under varying load cycles and hold times can be done using this program. NONAX is considerably less expensive to run than a multipurpose finite-element program.

The inelastic analysis was carried up to 10 cycles. Both creep and plasticity were included. The results of these analyses are shown in Figure 5.28, where the elastic, elastic-plastic, and elastic-plastic-creep strain ranges for diurnal cycling are plotted. The calculated inelastic strains are 9.09 percent higher than the elastic strains. Hence in the creep-fatigue evaluation, we

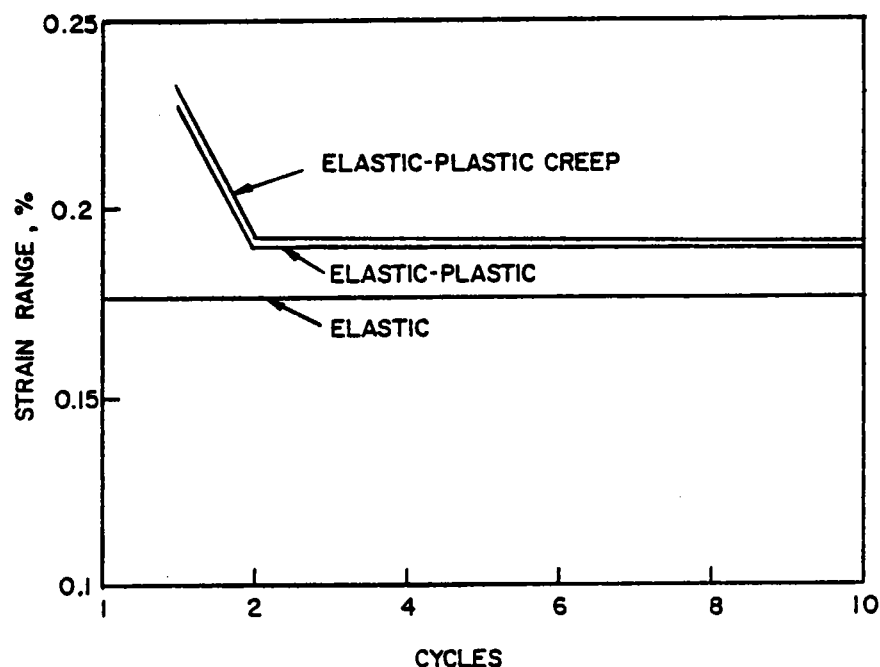


Figure 5.28 Comparison of Elastic and Inelastic Analyses
on 25.4 mm (1 in.) O.D. Incoloy 800 Tube

estimated the inelastic strains by increasing the elastic strains by 10 percent. This approach permits considerable economy in both design analysis and hardware without sacrificing reliability or safety. Using this estimated inelastic strain and using the inelastic fatigue curves of Code Case N-47 (Figure T-1420-1C), we evaluated the fatigue damage.

We estimated the creep-rupture life using the rupture life curves of Code Case N-47. However, we used only the pressure stresses (as opposed to thermal plus pressure stresses as recommended in Code Case N-47) in evaluating

the rupture life.³⁷ We added the creep and fatigue damage fractions and limited this value to 1.

With regard to material properties, both Types 304SS and 316SS are qualified materials under the Code, and their creep and fatigue properties are well documented.⁴¹ Although Incoloy 800 is an accepted Code material, the Code does not list its creep and fatigue data. However, the Code has rupture life and allowable cycles graphs for Incoloy 800H. Because the material properties are very similar for Incoloy 800 and 800H at the absorber panel design temperatures, the creep-fatigue data for 800H were used.³⁷

5.3.2 Joining and Attachment Methods

Tube-to-Tube Joints. The steady-state thermal stress analysis of the longitudinal tube-to-tube weld joints was done using the finite-element model shown in Figure 5.29. Because we assumed the flux to be symmetric, only one-half of it was considered in the analysis. The finite-element model consisted of 152 isoparametric two-dimensional solid elements. The ANSYS finite elements STIF55 and STIF42 were used for the thermal stress analysis. ANSYS is a multi-purpose finite-element program widely used in the nuclear power industry. It is capable of transient and steady-state heat-transfer analyses as well as static and dynamic stress analyses. Elastic, elastic-plastic, and creep analyses can be done using this program. A preprocessor was developed for an automated generation of the ANSYS input data, including the finite-element mesh and the boundary conditions. The input for the preprocessor consist of the tubewall geometry and material properties, peak heat flux, salt film (I.D.) coefficient and

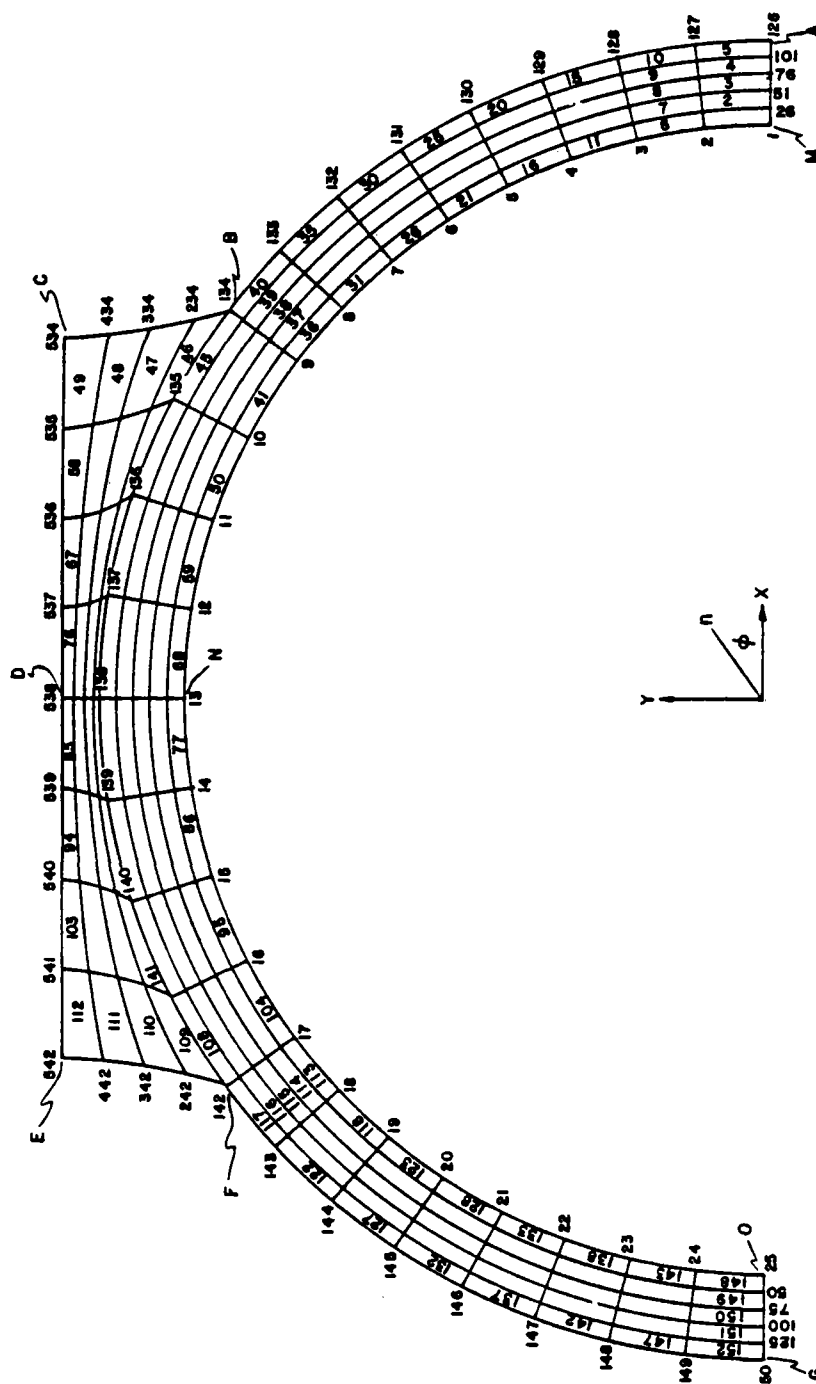


Figure 5.29 Finite Element Model

bulk temperature. The preprocessor generates the ANSYS model flux input values by using numeric integration of the flux distribution along the heated boundary. The boundary conditions used for the thermal stress analyses are shown in Table 5.19.

Table 5.19 Boundary Conditions for Half Tube Model

<u>Boundary</u>	<u>Thermal Analysis</u>	<u>Stress Analysis</u>
M-A	$\partial T / \partial n = 0$	$v = 0, \tau_n = 0$
A-B-C	$k(\partial T / \partial n) = q_{\max} \cos \phi$	$\sigma_n = \tau_n = 0$
C-D-E	$\partial T / \partial n = 0$	$v = \text{Constant},$ $\tau_n = 0$ $u_E = 0$
E-F-G	$\partial T / \partial n = 0$	$\sigma_n = \tau_n = 0$
G-O	$\partial T / \partial n = 0$	$v = 0, \tau_n = 0$
O-N-M	$k(\partial T / \partial n) = -h(T - T_b)$	$\sigma_n = \tau_n = 0$

where

- n = Local coordinate in the outward direction normal to the surface (the direction varies from point to point)
- ϕ = Angle between n and x
- T = Temperature
- σ_n = Normal stress on surface
- τ_n = Shear stress on surface
- u = Displacement in X-direction
- v = Displacement in Y-direction
- q_{\max} = Peak heat flux
- h = Salt film (I.D.) coefficient
- T_b = Salt bulk temperature
- k = Tubewall thermal conductivity

In addition, the boundary conditions in the axial direction of the tube are:

- Thermal Analysis--No heat flow in the axial direction
- Stress Analysis--Axial stress is constant and net axial force is zero (generalized plane strain).

Since the ANSYS finite element STIF42 does not have a generalized plane-strain option, the plane-strain option (axial strain = 0) was used in the analysis. The results were then modified by using a post-processor to determine the generalized plane strain solution and isolate the secondary and peak components of the stresses.

Using this model, computer runs were made for several tube-to-tube joints of 25 mm (1-in.) O.D. Incoloy 800 tubes. Six of the many cases studied are shown in Figure 5.30 and Table 5.20. In these six cases, the material properties and heat flux levels were held constant. Only the geometry varied as follows:

- Case 1: Reference case, single tubes not welded
- Case 2: Tube welded symmetrically on both sides (front and back), 1.59-mm (1/16-in.) spacer
- Case 3: Nonsymmetrically welded tube with weld in the front of the panel (flux side), 1.59-mm (1/16-in.) spacer
- Case 4: Nonsymmetrically welded tube with weld in the back of the panel (no-flux side), 1.59-mm (1/16-in.) spacer
- Case 5: Same as Case 2 but with a thicker spacer [3.175 mm (1/8 in.)]
- Case 6: Same as Case 5 but with a smaller weld radius [5.08 mm (0.2 in.)].

The results of this study are shown in Table 5.21. They indicate that there are no significant differences in stresses between the symmetrically and

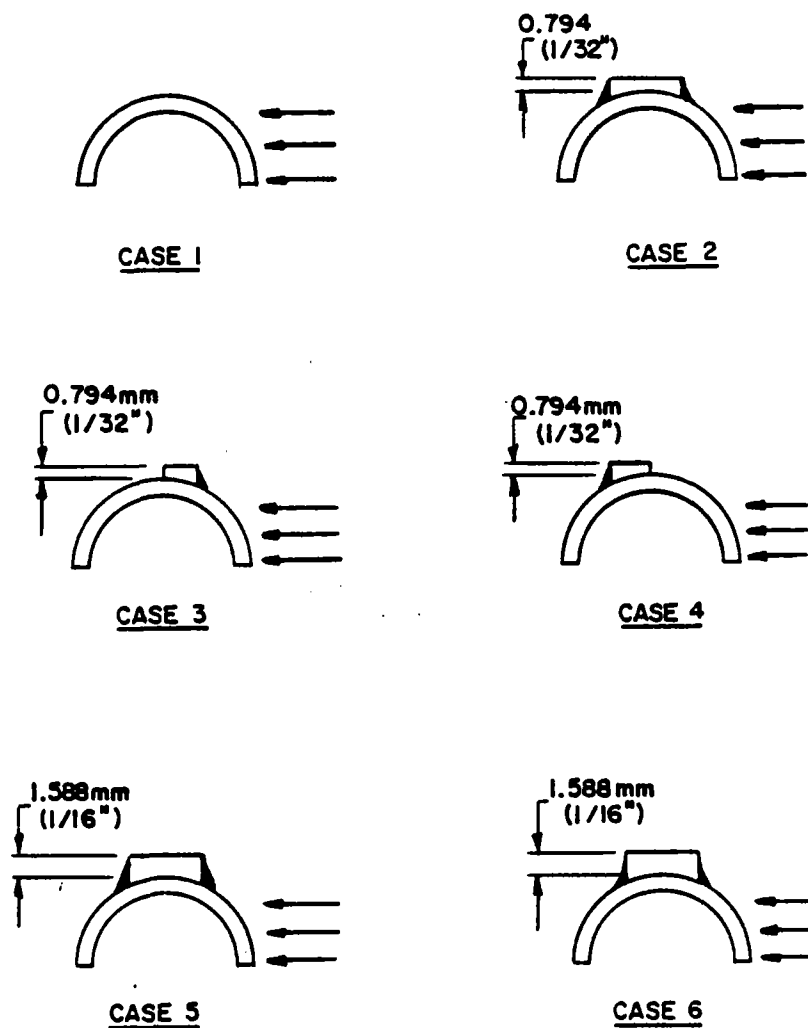


Figure 5.30 Tube-to-Tube Joint Configurations (Thickness shown is for half of the spacer)

Table 5.20 Input Conditions for Tube Joint Analyses (Incoloy 800 Material)

	Case 1	Case 2	Case 3	Case 4	Case 5	Case 6
Internal radius, R_i mm (in.)	11.05 (0.435)	11.05 (0.435)	11.05 (0.435)	11.05 (0.435)	11.05 (0.435)	11.05 (0.435)
External radius, R_o mm (in.)	12.7 (0.5)	12.7 (0.5)	12.7 (0.5)	12.7 (0.5)	12.7 (0.5)	12.7 (0.5)
Spacing mm (in.)	26.99 (1.0625)	26.99 (1.0625)	26.99 (1.0625)	26.99 (1.0625)	28.58 (1.125)	28.58 (1.125)
Weld radius mm (in.)	---	11.11 (0.4375)	11.11 (0.4375)	11.11 (0.435)	11.11 (0.435)	11.11 (0.2)
Weld angle (degree)	---	± 36	36	-36	± 36	± 36
Heat flux, q_{max} MW/m^2 (Btu/h \cdot ft 2)	0.631 (200,000)	0.631 (2000,000)	0.631 (200,000)	0.631 (200,000)	0.631 (200,000)	0.631 (200,000)
Salt conductance, h $MW/m^2\cdot^\circ C$ (Btu/h \cdot ft $^2\cdot^\circ F$)	8.517 (1500)	8.517 (1500)	8.517 (1500)	8.517 (1500)	8.517 (1500)	8.517 (1500)
Bulk temperature, T_b $^\circ C$ ($^\circ F$)	482 (900)	482 (900)	482 (900)	482 (900)	482 (900)	482 (900)
Thermal conductivity $W/m\cdot^\circ C$ (Btu/h \cdot ft $^2\cdot^\circ F$)	20.77 (12.0)	20.77 (12.0)	20.77 (12.0)	20.77 (12.0)	20.77 (12.0)	20.77 (12.0)
Modulus of elasticity, E MPa (lb/in 2)	157,890 (22.9×10^4)	157,890 (22.9×10^4)	157,890 (22.9×10^4)	157,890 (22.9×10^4)	157,890 (22.9×10^4)	157,890 (22.9×10^4)
Poisson's ratio, ν	0.3	0.3	0.3	0.3	0.3	0.3
Coefficient of thermal expansion, α $^\circ C^{-1}$ ($^\circ F$) $^{-1}$	5.28×10^{-6} (9.5×10^{-6})	5.28×10^{-6} (9.5×10^{-6})	5.28×10^{-6} (9.5×10^{-6})	5.28×10^{-6} (9.5×10^{-6})	5.28×10^{-6} (9.5×10^{-6})	5.28×10^{-6} (9.5×10^{-6})

FOSTER WHEELER SOLAR DEVELOPMENT CORPORATION

REF.: 84-2292C
DATE: November 1982

Table 5.21 Temperatures and Stresses in the Panel Tube (Incoloy 800)

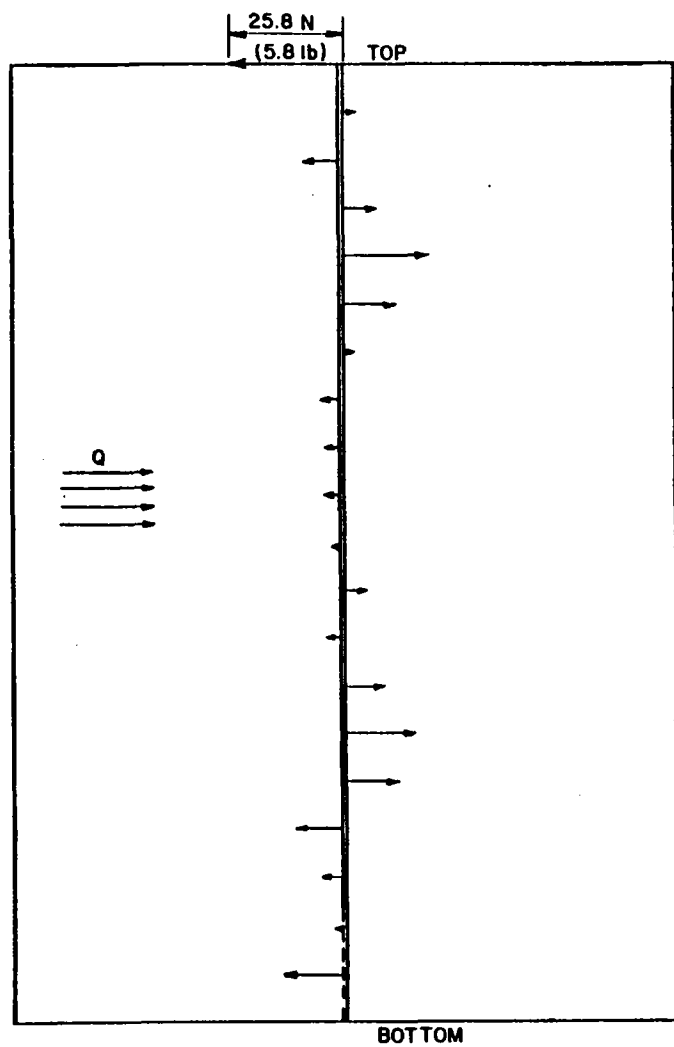
	<u>Case 1</u>	<u>Case 2</u>	<u>Case 3</u>	<u>Case 4</u>	<u>Case 5</u>	<u>Case 6</u>
Temperature at Node 126 °C (°F)	612 (1134)	617 (1142)	617 (1142)	617 (1142)	617 (1142)	617 (1142)
Temperature at Node 134 °C (°F)	---	561 (1042)	561 (1042)	569 (1057)	567 (1052)	564 (1047)
Temperature at Node 534 °C (°F)	---	605 (1121)	605 (1121)	---	626 (1159)	619 (1146)
Temperature at Node 538 °C (°F)	---	494 (922)	498 (928)	523 (973)	502 (936)	507 (944)
Temperature at Node 138 °C (°F)	---	494 (921)	496 (924)	513 (955)	500 (932)	503 (938)
Effective stress in Element 5 MPa (kip/in ²)	248.2 (36.0)	253.7 (36.8)	237.9 (34.5)	247.5 (35.9)	246.1 (35.7)	242.0 (35.1)
Effective stress in Element 46 MPa (kip/in ²)	---	96.5 (14.0)	78.6 (11.4)	---	108.2 (15.7)	113.8 (16.5)
Effective stress in Element 49 MPa (kip/in ²)	---	140.7 (20.4)	133.1 (19.3)	---	180.0 (26.1)	162.7 (23.6)
Effective stress in Element 85 MPa (kip/in ²)	---	66.9 (9.7)	---	228.9 (33.2)	55.8 (8.1)	48.3 (7.01)
Effective stress in Element 82 MPa (kip/in ²)	---	68.9 (10.0)	---	39.3 (5.7)	61.4 (8.9)	55.8 (8.1)

nonsymmetrically welded cases. The metal temperatures and stresses at the crown (Node 126) are not significantly different for these cases. However, the temperatures at the center of the weld (Node 534, Figure 5.29) vary significantly. The temperature for a 2.38 mm (3/32 in.) spacer was approximately equal to that at the crown. Hence a spacer thickness of 2.38 mm (3/32 in.) was chosen as the optimum.

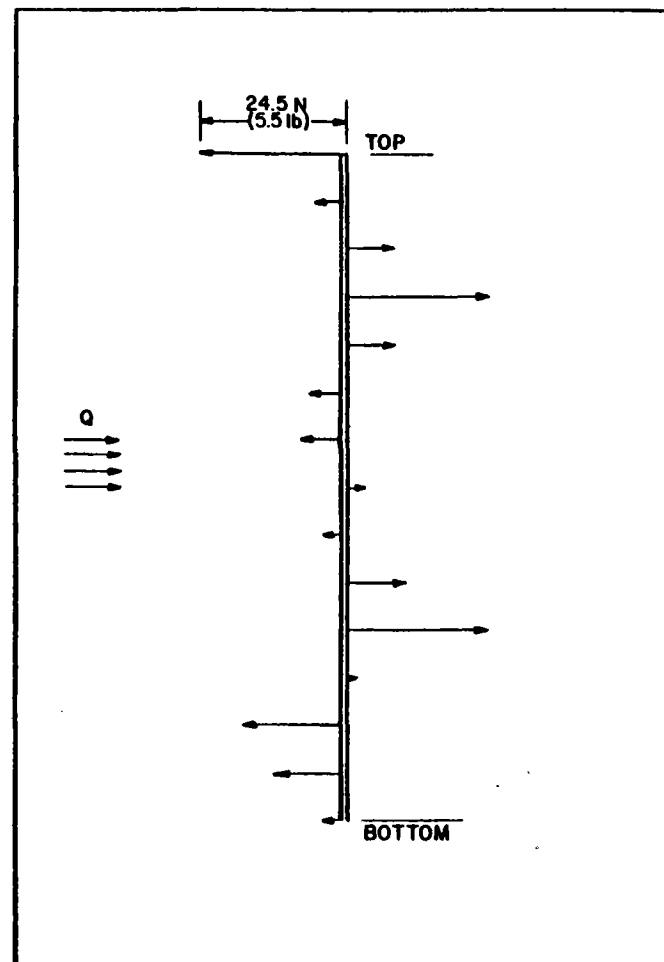
The effect of the weld radius on initial temperatures was also studied. We observed that, by reducing the weld radius to approximately 5.08 mm (0.2 in.), the metal temperatures in the welded area can be held to a minimum. However, this is a parameter that is difficult to control during manufacturing. For analytical purposes, the weld radius was assumed to be 11.11 mm (7/16 in.).

Panel Attachment Lug. Panel support lug configuration and spacing were determined. The lugs were designed to withstand wind and seismic loads and loads caused by thermal expansion constraints. The lug and buckstay arrangements (Section 5.4.1) permit in-plane panel expansions. The panel is restrained from bowing out.

The lug reactions and the deflections in the panel because of the front-to-back thermal gradient were studied parametrically. These are shown in Figures 5.31 and 5.32 for two typical lug spacings of 2.13 m (7 ft) and 1.52 m (5 ft). The reactions and deflections are very low. The fact that these deflections are very low also justifies the generalized plane-strain model assumed subsequently for the panel creep-fatigue analysis (Section 5.3.4). The lug spacing itself was optimized from the standpoint of thermal buckling, as described later in this section.



Lug Spacing 1.5 m (5 ft)



Lug Spacing 2.1 m (7 ft)

Figure 5.31 Buckstay Lug Reactions Per Tube (Pass 1)

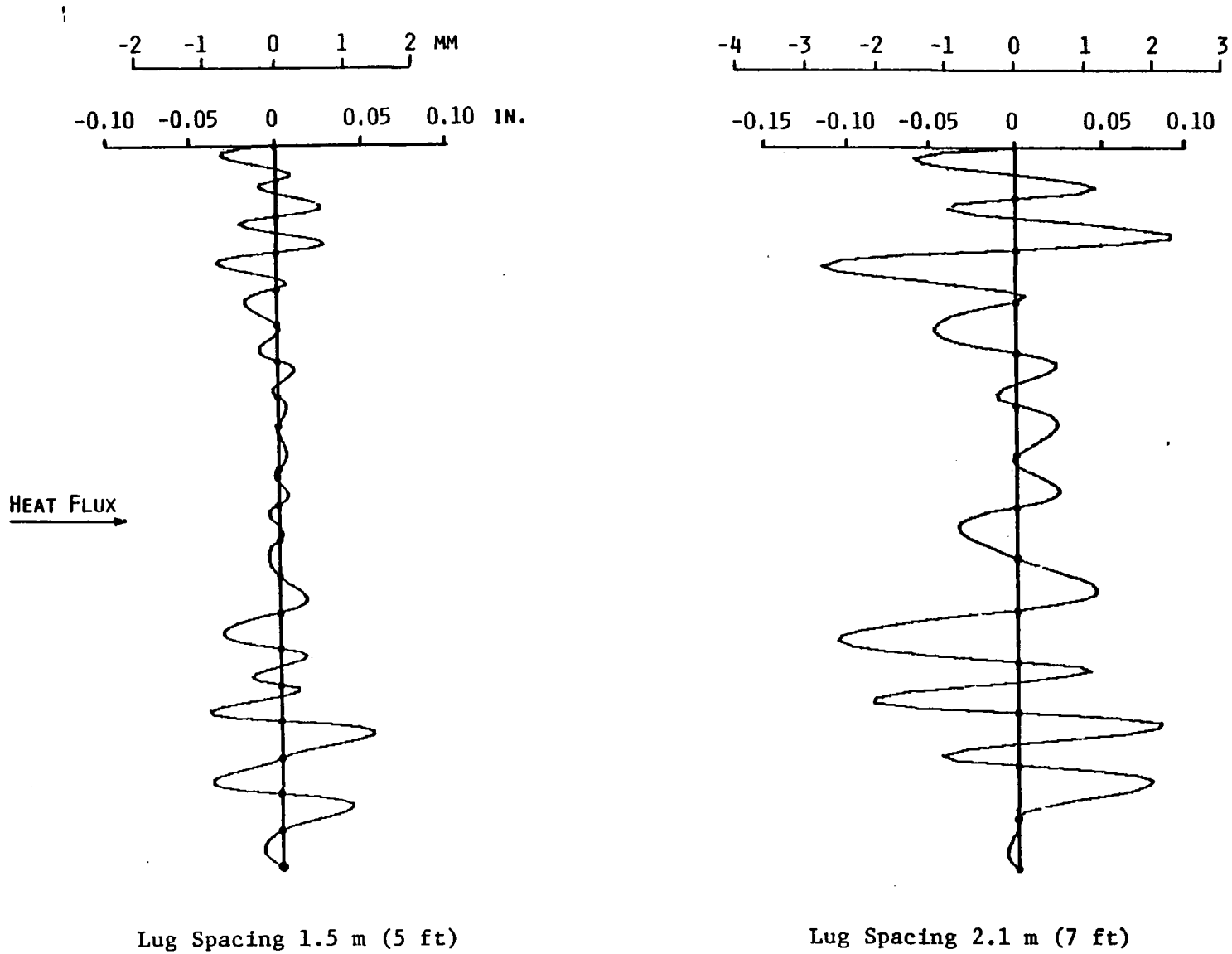


Figure 5.32 Absorber Panel Deflections (Pass 1)

5.3.3 Effect of Incident Heat Flux Angle on Absorber Panels

The finite-element model shown in Figure 5.29 assumed that the heat flux was symmetrical and normal to the plane of the panel. However, heat flux analysis of single tubes showed that the flux were not symmetrical (Section 4.3.11). Thus it became necessary to develop a new finite-element model. In this new model, shown in Figure 5.33, the tube-to-tube spacing, weld angle, and incident angle of the flux vector can be varied. The model consists of 304 isoparametric solid elements. Again the ANSYS finite-elements STIF55 (thermal) and STIF42 (stress) and the preprocessor were used for the analysis.

The boundary conditions for the thermal stress analyses are shown in Table 5.22. The notation used is the same as that used for Table 5.19. As before, the boundary conditions in the axial direction of the tube are:

- Thermal Analysis: No heat flow in axial direction
- Stress Analysis: Axial stress is constant and net axial force is zero (generalized plane strain).

Again, the plane strain option (axial strain = 0) was used in the analysis and the results were then modified by using the post-processor to determine the generalized plane strain solution and isolate the secondary and peak components of the stresses.

To study the effect of the non-normal incident heat flux, we made a computer run with a peak flux intensity of 0.631 MW/m^2 ($2 \times 10^5 \text{ Btu/h}\cdot\text{ft}^2$) and an incident angle of 40 deg (Figure 5.34). The resultant temperature and stress

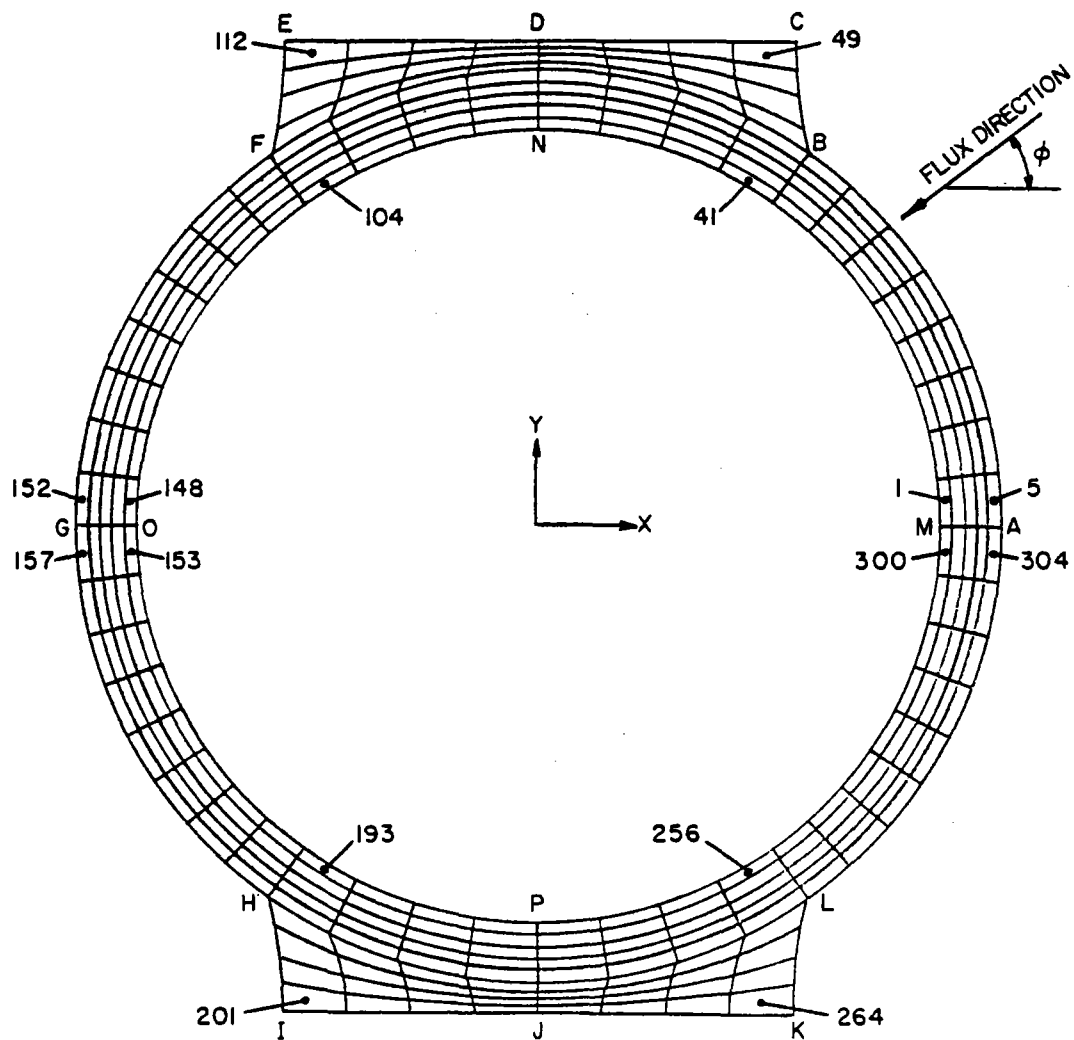


Figure 5.33 Finite-Element Model of Full Tube

Table 5.22 Boundary Conditions for Full Tube Model*

Boundary	Thermal Analysis	Stress Analysis
K-L-A-B-C	$k(\partial T / \partial n) = q_{\max} \cos \phi$ (not shadowed) $= 0$ (shadowed)	$v_A = 0$ $\sigma_n = \tau_n = 0$
C-D-E	$T_{CDE}(x) = T_{KJI}(x)$	$u_{CDE}(x) = u_{KJI}(x)$ $v_{CDE}(x) + v_{KJI}(x) = \text{Constant}$
E-F-G-H-I	$\partial T / \partial n = 0$	$u_G = v_G = 0$ $\sigma_n = \tau_n = 0$
I-J-K	$T_{CDE}(x) = T_{KJI}(x)$	$u_{CDE}(x) = u_{KJI}(x)$ $v_{CDE}(x) + v_{KJI}(x) = \text{Constant}$
M-N-O-P-M	$k(\partial T / \partial n) = -h(T - T_b)$	$\sigma_n = \tau_n = 0$

*See Table 5.19 for notation.

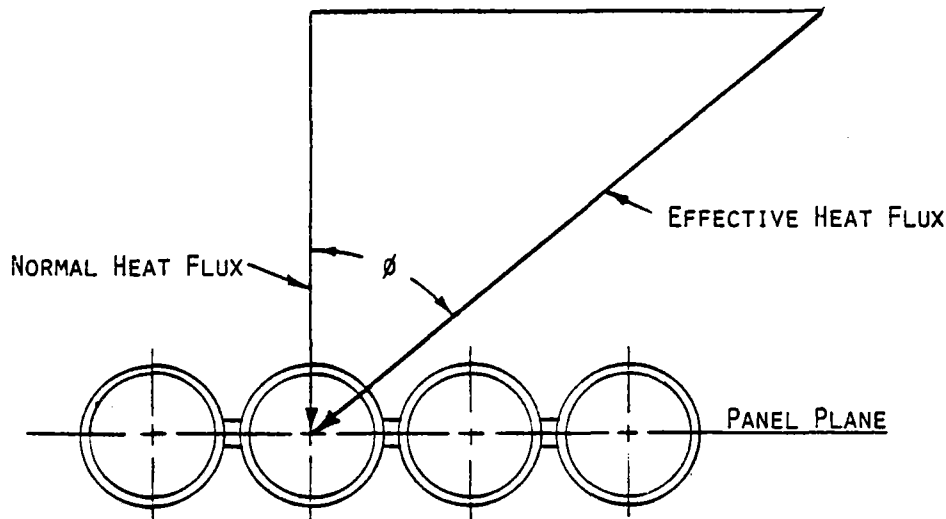


Figure 5.34 Definition of Incident Angle

distributions are given in Figure 5.35; tubewall I.D. and O.D. temperature profiles, in Figure 5.36.

We compared this with a symmetrical case, where the same peak flux intensity falls normal to the panel plane. The half-tube model described in Section 5.3.2 was used in this analysis. Table 5.23 compares the peak tubewall (O.D.) temperatures and thermal stresses for these two cases. As the results show, if the flux intensities are equal, the equivalent stresses are very nearly equal in both cases. The maximum tubewall (O.D.) temperature and equivalent stress always occur at the location where the heat flux is at the peak.

5.3.4 Creep-Fatigue Evaluation of Absorber Panels

To determine the critical locations in the absorber panels for further analysis and creep-fatigue evaluation, the worst combination of tubewall temperatures and thermal gradients (which are proportional to thermal stresses) was compared (Table 5.24). This table shows that the critical locations are in Pass 2 (Type 304SS), Pass 3 (Type 316SS), and Pass 4 (Incoloy 800). Two-dimensional temperature distribution analyses and generalized plane-strain analyses were performed at these locations. The finite-element model described in the last section was modified to account for the changes made in the spacer shape and dimensions during the welding development task (Section 6).

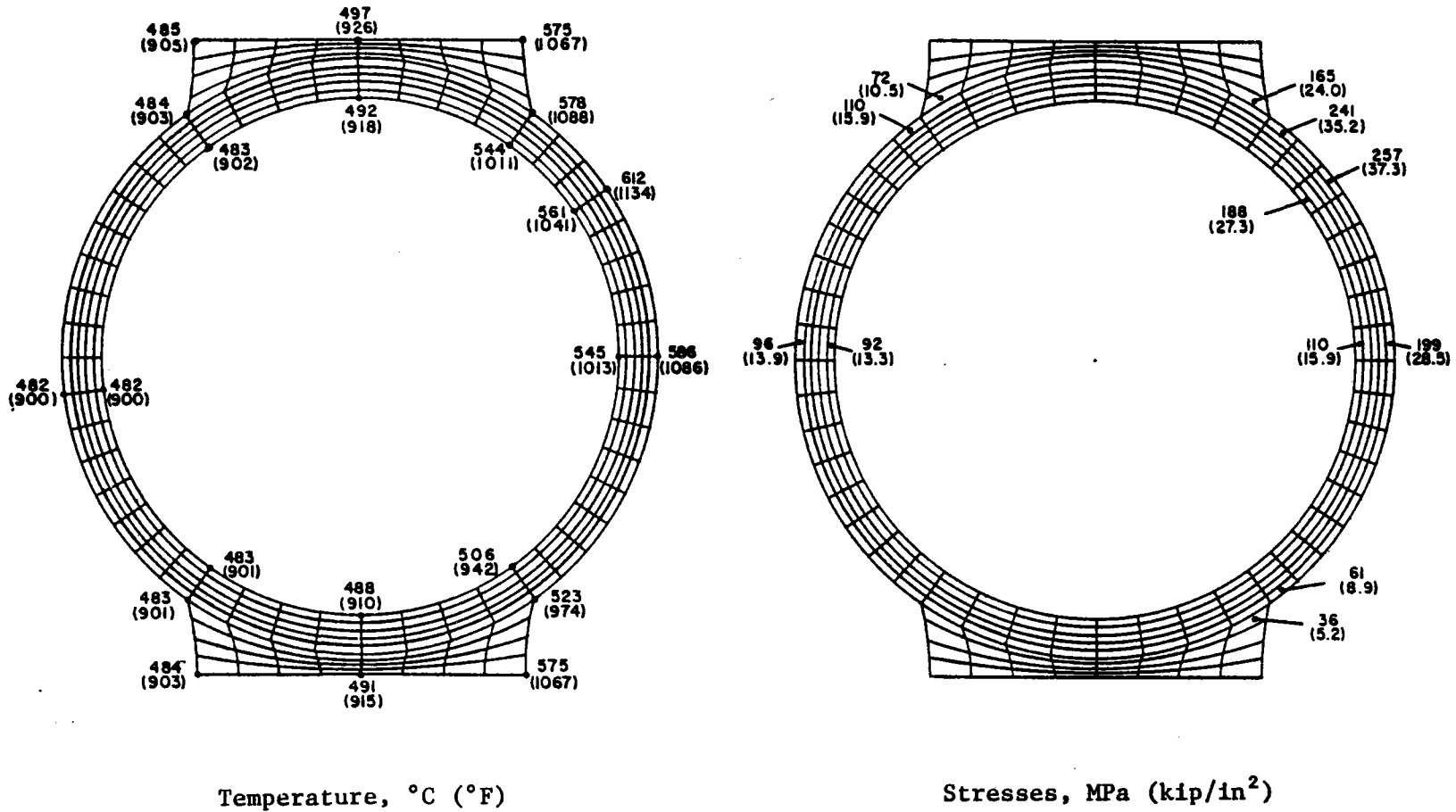


Figure 5.35 Temperature Distribution and Equivalent Stresses in the Tube

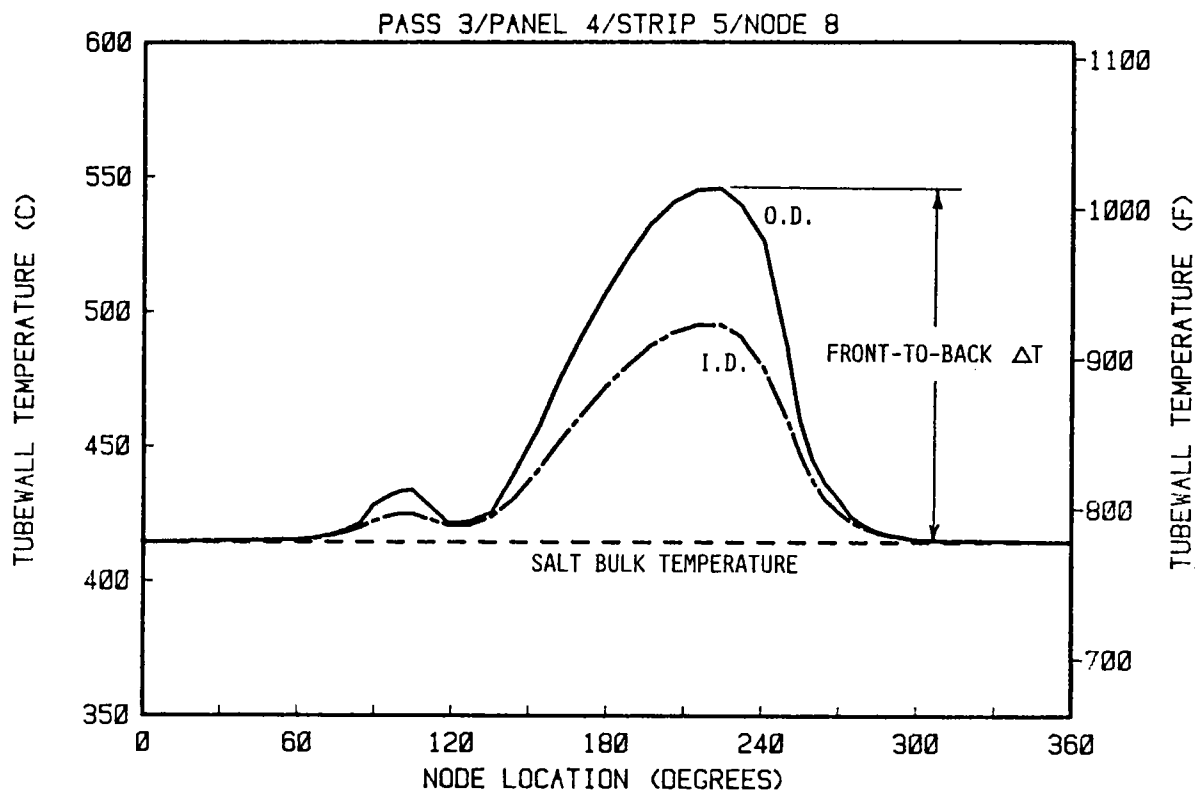


Figure 5.36 Tubewall Temperature Profile

Table 5.23 Comparison of Normal vs. Non-Normal Incident Heat Flux

Item	Peak Heat Flux Normal to Panel Plane	Peak Heat Flux Not Normal to Panel Plane
Maximum tubewall (O.D.) temperature, °C (°F)	616.8 (1142.2)	612.1 (1133.7)
Maximum fin temperature °C (°F)	604.7 (1120.5)	593.2 (1099.8)
Maximum axial stress MPa (kip/in ²)	-261.17 (-37.88)	-291.86 (-42.33)
Maximum equivalent stress MPa (kip/in ²)	253.59 (36.78)	257.11 (37.29)

Table 5.24 Maximum Tubewall Temperatures and Thermal Gradients

<u>Pass</u>	<u>Maximum Tubewall Temperature °C (°F)</u>	<u>Maximum ΔT °C (°F)</u>
1	467 (873)	149 (269)
2	517 (963)	153 (275)
3	568 (1055)	138 (248)
4	620 (1148)	117 (211)
5	633 (1171)	84 (151)

The new model is shown in Figure 5.37. Boundary conditions from Table 5.22 were also modified for the new model. The input conditions, taken from T/H analysis results (Section 5.2.1), are given in Table 5.25.

The resultant temperature contours in the tube cross section and the Von Mises' effective stress at critical locations in the cross section are shown in Figures 5.38, 5.39, and 5.40. The key results of the analysis and creep-fatigue evaluation are summarized in Table 5.25. The elastic strain range was obtained directly from the analysis; the inelastic strain range was estimated as explained in Section 5.3.1. The allowable number of cycles (N_d) was obtained from Fatigue curves T-1320 of Code Case N-47. The creep-rupture time (T_d) was obtained from the rupture-life curves of Code Case N-47.

Assuming that the panel will be subjected to 50,000 cycles, all of a severity equivalent to that obtained in diurnal operation through the full temperature range, and the total operating time is 100,000 hours, we determined the total creep-fatigue damage in Pass 2/Panel 4/Strip 5/Node 8,* as:

$$D = \Sigma t/T_d + \Sigma n/N_d = 0.2 + 0.667 = 0.867$$

*Similar analyses were done for Pass 3/Panel 5/Strip 3/Node 7 and Pass 4/Panel 7/Strip 1/Node 12.

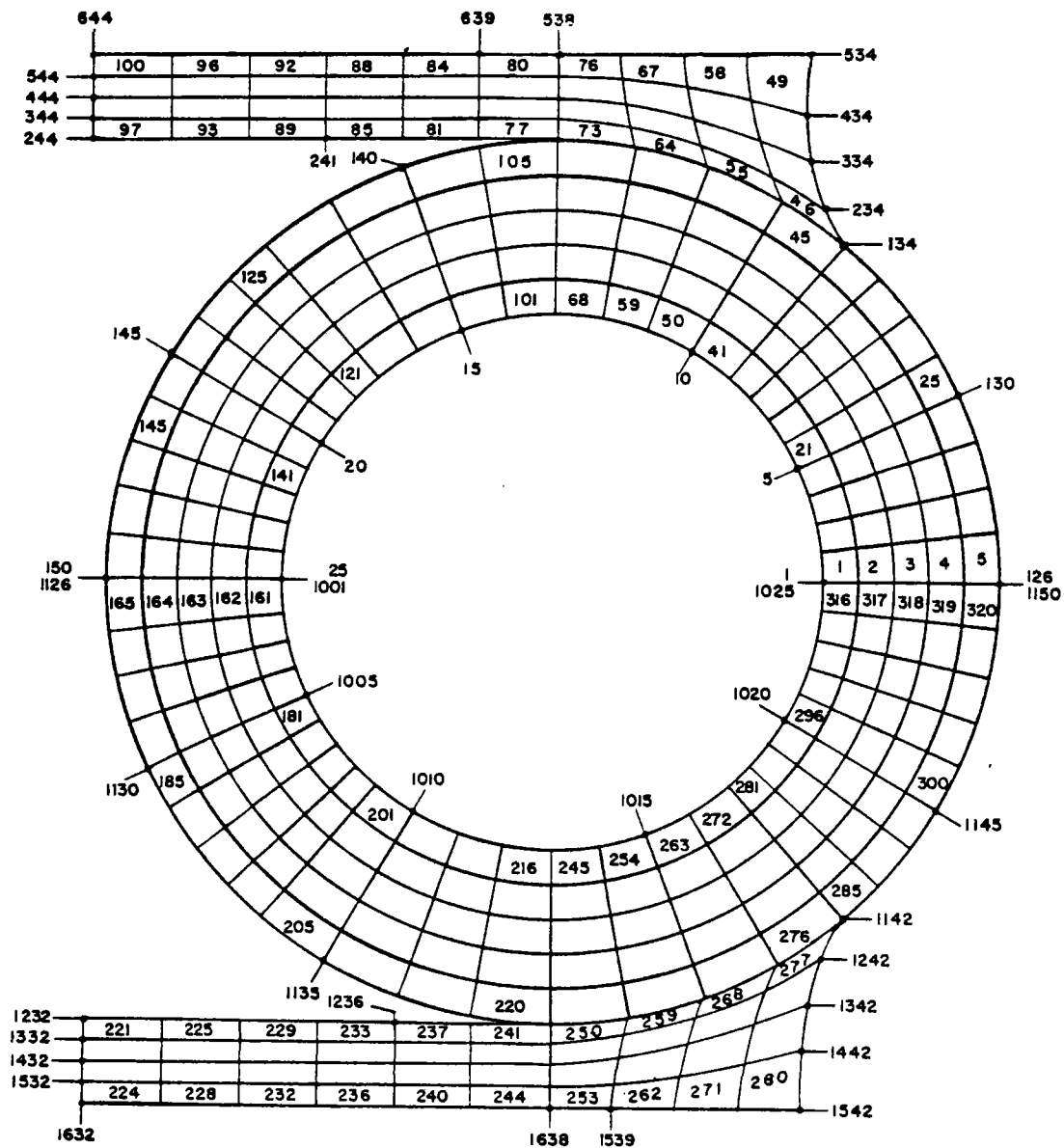
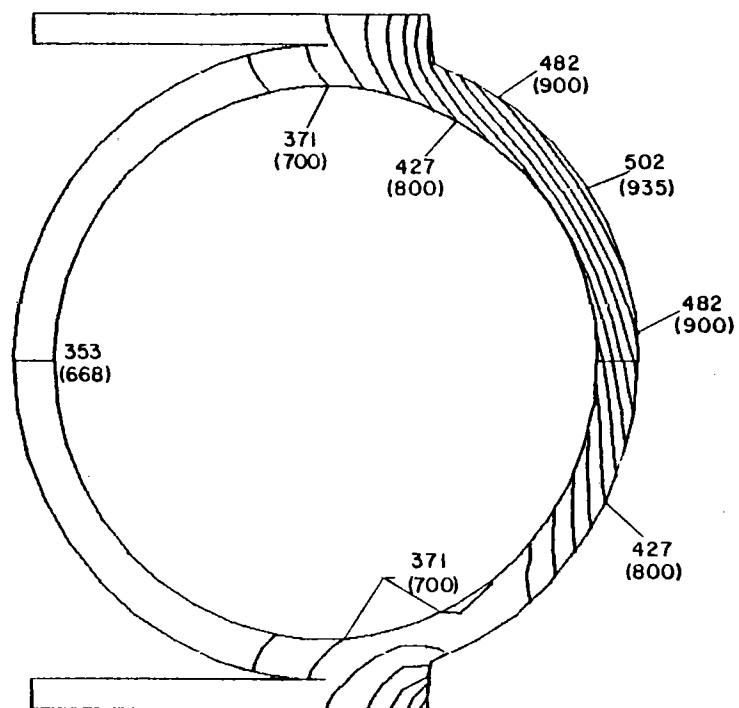


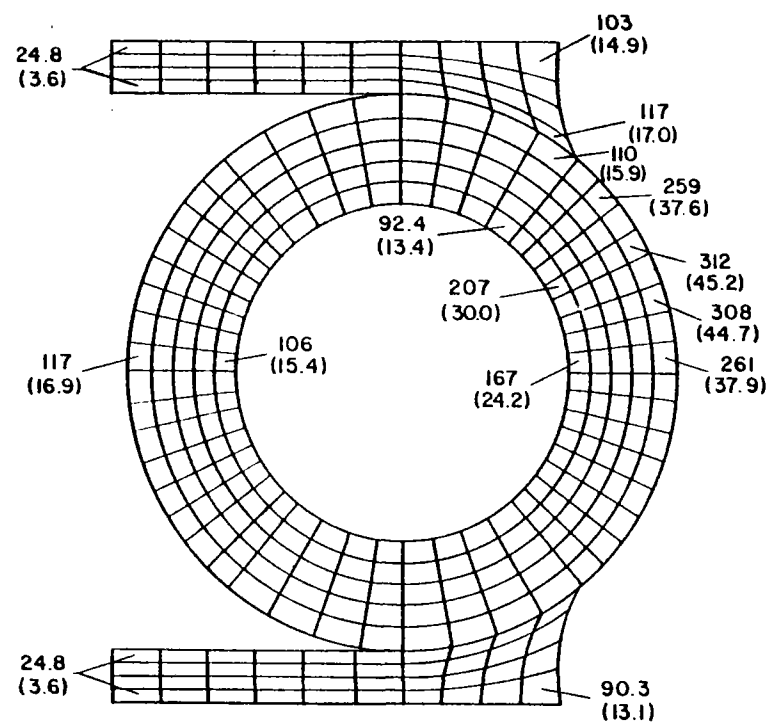
Figure 5.37 Revised Finite Element Model of Full Tube With Spacer Strips

Table 5.25 Creep-Fatigue Analysis

Description	Location (Pass/Panel/Strip/Node)		
	2/4/5/8	3/5/3/7	4/7/1/12
<u>Input Conditions:</u>			
Tubewall material	Type 304SS	Type 316SS	Incoloy 800
Heat flux (q), MW/m ² (Btu/h·ft ²)	0.614 (194,600)	0.609 (192,900)	0.536 (169,800)
Salt conductance (h), kW/m ² ·°C (Btu/h·ft ² ·°F)	7.06 (1243)	8.02 (1412)	9.49 (1672)
Salt bulk temperature (T _b), °C (°F)	353 (668)	414 (778)	511 (951)
Incident flux angle (φ), deg	35	47	8
<u>Results of Analyses:</u>			
Maximum front-to-back ΔT, °C (°F)	148 (267)	131 (235)	107 (192)
Maximum metal temperature, °C (°F)	502 (935)	545 (1013)	617 (1143)
Maximum effective stress, MPa (kip/in ²)	316.5 (45.9)	291.6 (42.3)	160.7 (23.3)
Elastic strain range	0.00177	0.00167	0.000936
Inelastic strain range	0.00195	0.00183	0.00103
Fatigue life (N _d), cycles	75,000	100,000	1,000,000
Creep-rupture time (T _d), hours			
based on S _y :	>500,000	>300,000	48,000
based on pressure stress:	>>1,000,000	>1,000,000	>1,000,000
Damage fraction (D), based on S _y :	0.867	0.9333	2.13
based on pressure stress:	0.667	0.5	0.15



Temperatures, °C (°F)



Stresses, MPa (kip/in²)

Figure 5.38 Temperature Contours and Effective Stresses--Pass 2

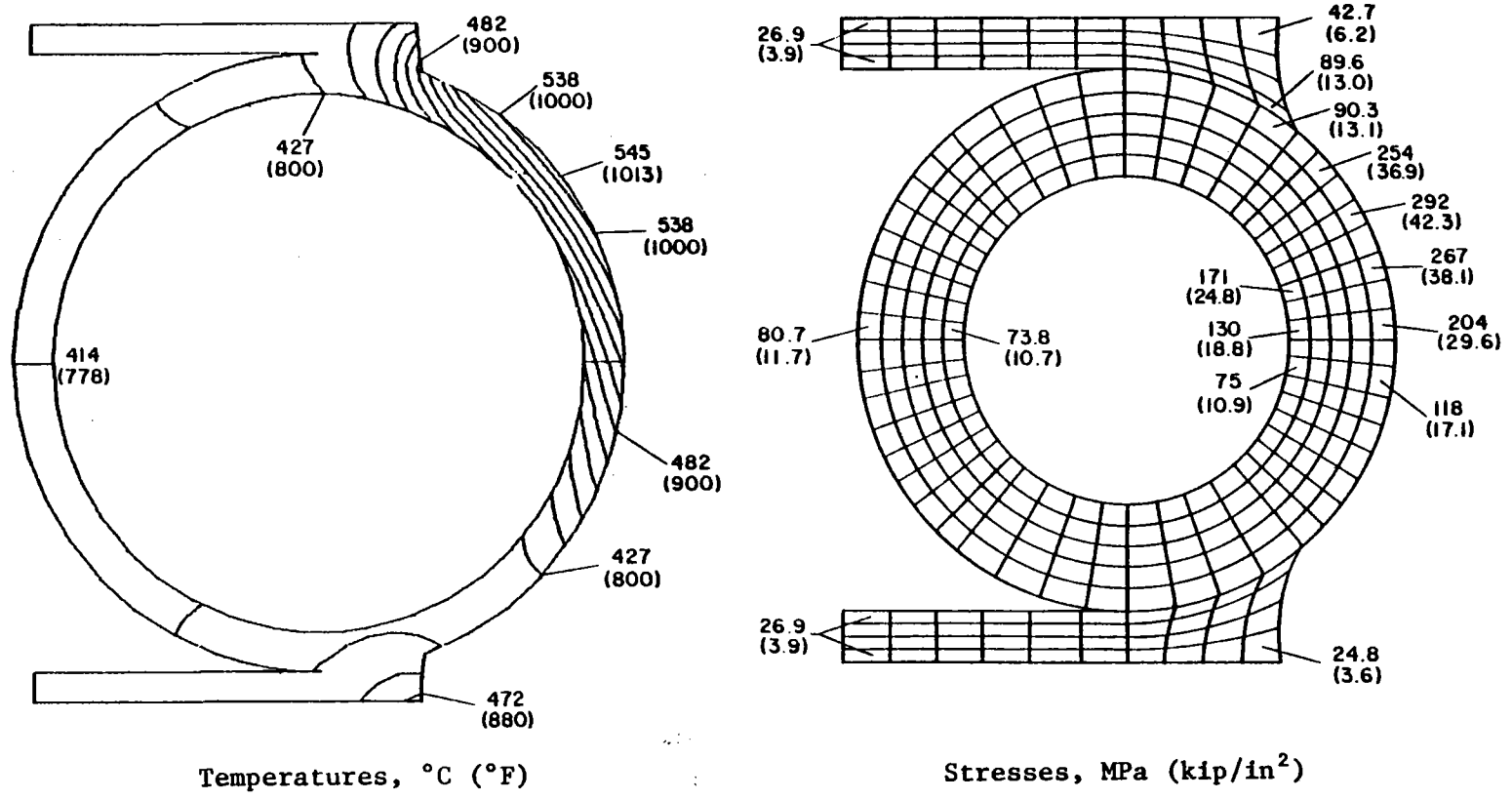


Figure 5.39 Temperature Contours and Effective Stresses--Pass 3

5-83

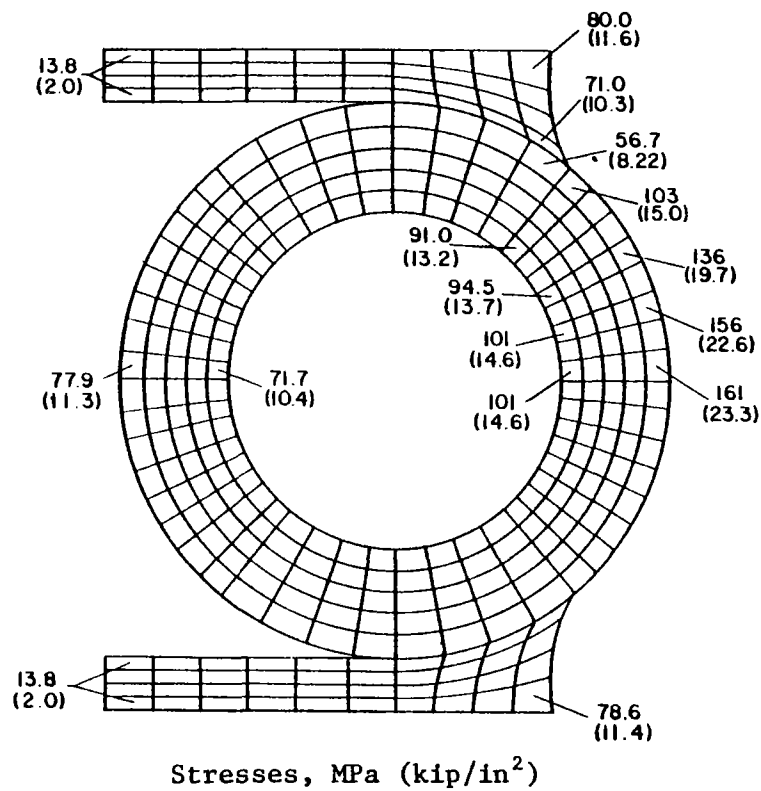
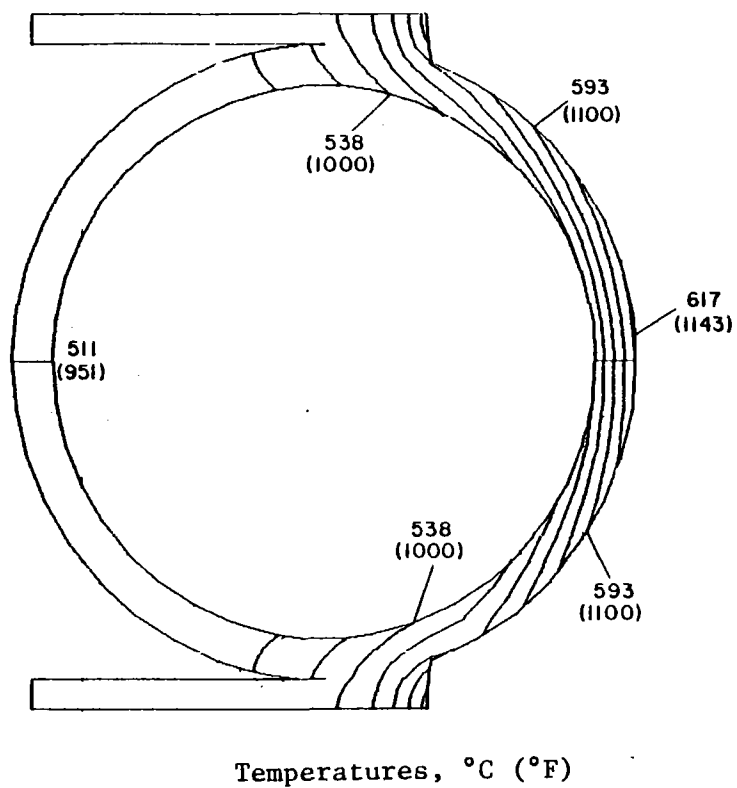


Figure 5.40 Temperature Contours and Effective Stresses--Pass 4

where the creep rupture life (T_d) is based on the yield stress (S_y). T_d based on pressure stress alone is more than a million hours, and the corresponding creep damage fraction (t/T_d) is negligible. Thus if the creep damage were based on pressure stress alone the total damage would be 0.667. In the second case (i.e., creep damage based on pressure stress), the total damage is within the allowable limits. If the creep damage is based on S_y , the total damage exceeds the limit by a small amount. The allowable damage envelope for Types 304SS and 316SS and Incoloy 800 from Code Case N-47 is shown in Figure 5.41. Considering the conservatism of Code Case N-47, the creep-fatigue life projected for the panel is adequate. Results for the other two critical locations were similar.

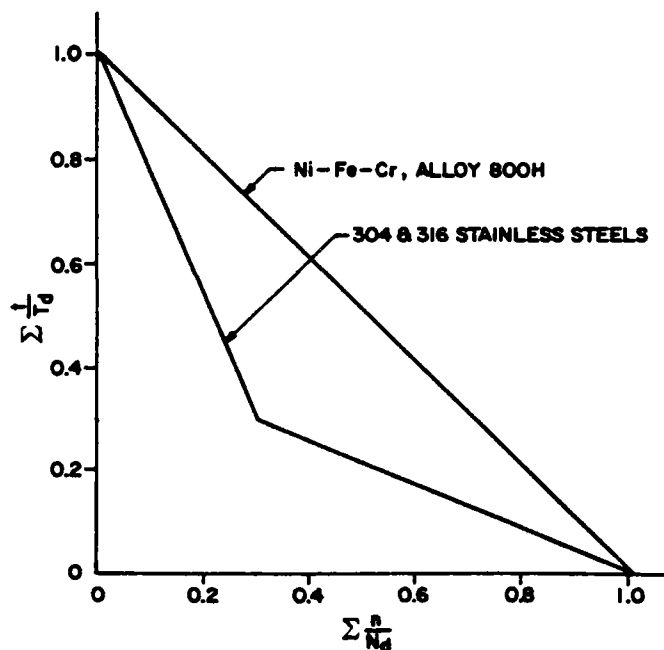


Figure 5.41 Creep-Fatigue Damage Envelope

5.3.5 In-Plane Temperature Gradient

Axial Stresses in the Panel Because of Transverse In-Plane ΔT . As discussed in Section 5.3.7, the maximum in-plane ΔT is 50°C (90°F), and this occurs in the wing panels (L1, R1). The axial stress because of this ΔT would be 70.2 MPa (10.18 kip/in²) if the panel were not allowed to bend in its own plane. This stress would also cause panel buckling and a lateral force of 6230 N (1400 lb) in the lugs. If a panel were allowed to bend in its own plane, it would interfere at its edges with the edges of adjacent panels. To solve this problem, we divided the wing panels into three sections or subpanels. Each of these three subpanels is connected to the same headers as before, reducing axial stresses in the panel by a factor of three and lateral forces in the lugs to 445 N (100 lb). To maintain the modularity and to provide for any uncertainty in the in-plane ΔT values, all other panels are also divided into three subpanels.

Panel Buckling and Maximum Allowable In-Plane ΔT s. The maximum allowable in-plane ΔT in a subpanel (i.e., 1/3 of the panel) is governed by thermal buckling considerations. The axial stress in the panel is given by:

$$\sigma = E\alpha\Delta T/2 = 113.15\Delta T$$

The Euler buckling stress is given by:

$$\sigma_c = k\pi^2 EI/L^2 A$$

where

k = A factor depending upon the support conditions

L = Vertical spacing of lugs

A = Cross-sectional area of tube and spacer

I = Moment of inertia of tube and spacer

Assuming hinged support conditions at the lugs ($k = 1$) and a vertical spacing of lugs [$L = 1.83 \text{ m (6 ft)}$], $\sigma_c = 30.8 \text{ MPa (4.47 kip/in}^2\text{)}$. Using Code Case N-47 criterion for thermal buckling of heat-exchanger tubes:

$$\sigma = 2\sigma_c/3$$

The allowable ΔT is $14.6^\circ\text{C (26.3}^\circ\text{F)}$. However, the nuclear criterion may be too conservative for our application. Unlike heat exchanger tubes, where collision damages may occur if tubes are allowed to buckle, thermal buckling is not so critical in the panel. Furthermore, because of the strain-controlled nature of thermal stresses, even if the panel starts buckling, the stresses relax and the buckling cannot continue. Thus we relaxed the criterion to:

$$\sigma = \sigma_c$$

With this criterion, the maximum allowable ΔT in a subpanel is $22^\circ\text{C (39.53}^\circ\text{F)}$. The actual maximum ΔT in the subpanel is $16.7^\circ\text{C (30}^\circ\text{F)}$.

5.3.6 Transient Analysis

Transient temperature distribution and stress analyses were done for the receiver panels for several start-up and shutdown transient conditions. Section 5.2.2 describes the transients. The finite-element program ANSYS was used in the analysis. The finite-element model used is the same one described in steady-state analysis (Figure 5.37). The input for the stress analysis came from the transient T/H analysis also described in Section 5.2.2. The input consisted of the incident heat flux and the salt bulk temperature and film

conductance as functions of time, tube material properties, and thermal and stress boundary conditions. Essentially, five transients were evaluated:

- Morning hot start-up
- Noon hot start-up
- Hot shutdown
- Emergency shutdown
- Cloud-cover

Of the three locations chosen for creep-fatigue evaluation (Pass 2--304SS, Pass 3--316SS, and Pass 4--Incoloy 800), we selected Pass 2 and Pass 4 for transient analysis. We did not perform the analysis for Pass 3 because the effect of transient stresses is primarily on fatigue, and Pass 2 fatigue conditions are more severe than those in Pass 3. [The fatigue properties of Type 304SS (Pass 2) and Type 316SS (Pass 3) are identical.] The analysis and results are discussed in the following paragraphs. Appendix N contains details of the results of the transient analysis.

Morning Hot Start-up. From the viewpoint of creep fatigue, the maximum tubewall temperature and the temperature differential (ΔT) between the maximum and average tubewall temperatures are important since stresses are proportional to ΔT . These values and the minimum and average temperatures for Pass 2 are plotted in Figures 5.42 and 5.43. In these figures ΔT -Maximum stands for the maximum minus the average tubewall temperature and ΔT -Minimum stands for the minimum minus the average. At no time during the transient event do the tubewall temperatures and ΔT s--and thus the stresses--exceed the corresponding steady-state values. The tubewall temperatures and stresses in Pass 4 during the morning start-up are also within acceptable limits.

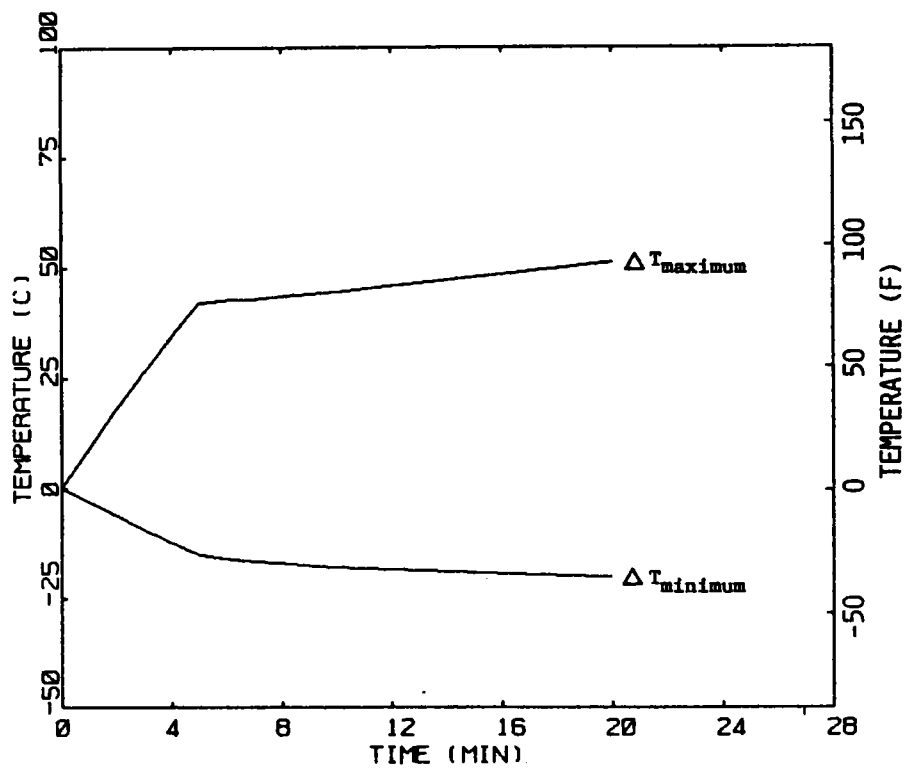


Figure 5.42 Temperature Differential--Morning Start-Up, Pass 2

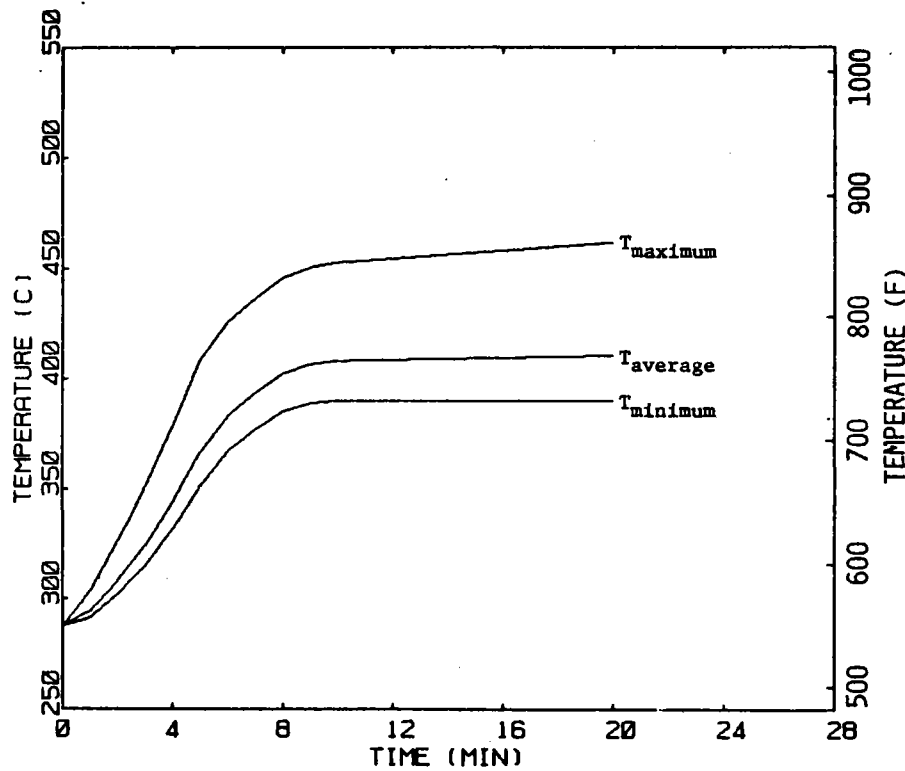


Figure 5.43 Tubewall Temperatures--Morning Start-Up, Pass 2

Noon Hot Start-Up. As explained in Section 5.2.2, two approaches were tried for noon start-up. The first approach is designated as NS17 (Noon start-up in ≈ 17 minutes); the second approach is designated as NS12 (Noon start-up in 12 minutes). For Pass 2 (NS12), the maximum ΔT is 85°C (153°F) at 6 minutes; for Pass 4 (NS17), the maximum ΔT is 96.1°C (173°F) at 17 minutes. These ΔT s are within acceptable limits.

Hot Shutdown. We observed that the hot shutdown transients are less severe than the emergency shutdown transients (see Emergency Shutdown). Hence separate temperature and stress analyses were not done for this transient.

Emergency Shutdown. As explained in Section 5.2.2, emergency shutdown takes place in 2 minutes. Typical tubewall temperatures and ΔT s in Pass 2 during this transient are shown in Figures 5.44 and 5.45. The maximum ΔT s occur at the beginning of the transient, and their values are 98.3°C (177°F) and 104.7°C (188.5°F) in Passes 2 and 4 respectively. Nowhere are the steady-state stresses exceeded.

Cloud-Cover. As described in Section 5.2.2, cloud-cover transient takes place in ≈ 2 minutes. Similar to the emergency shutdown, the maximum ΔT s occur at the beginning of the transient. The values are 97.8°C (176°F) and 103.9°C (187°F) in Passes 2 and 4 respectively. These values are almost equal to those for emergency shutdown.

5.3.7 Shear Stress Analysis of Absorber Panel

One of the concerns regarding receiver design has been the shear stresses caused by transverse in-plane ΔT s (i.e., left to right) in the panels. To solve

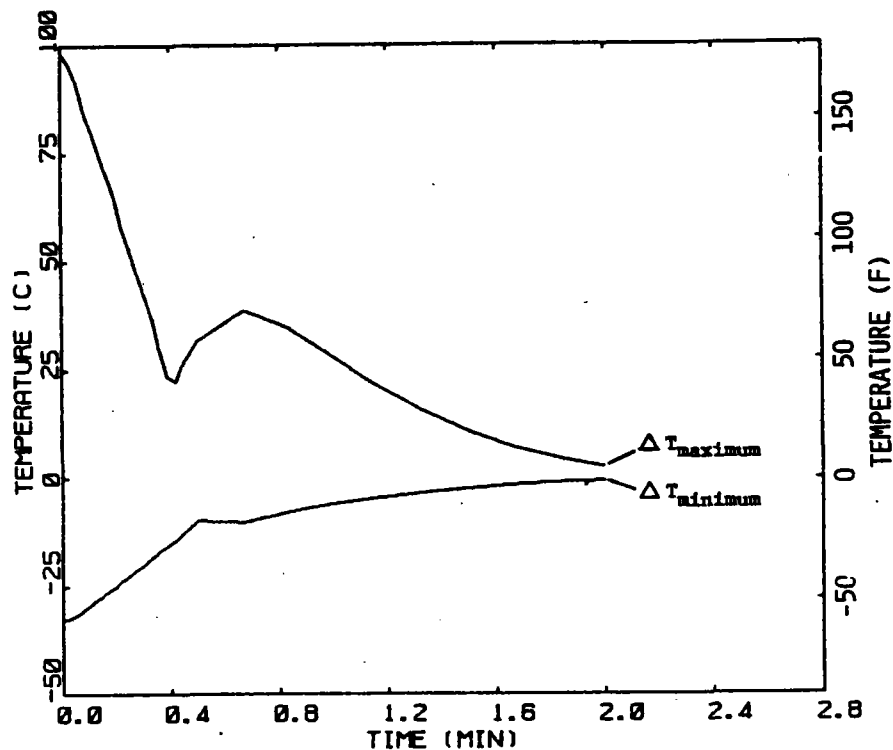


Figure 5.44 Emergency Shutdown--Temperature Differentials, Pass 2

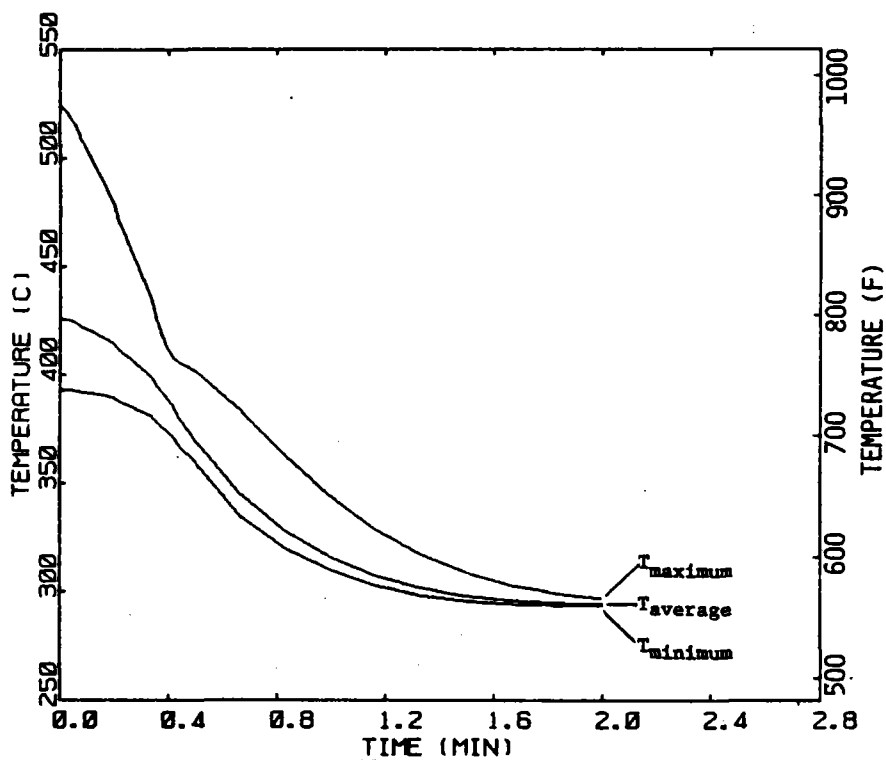


Figure 5.45 Emergency Shutdown--Metal Temperatures, Pass 2

this problem, we modeled the panel as an orthotropic plate. The orthotropic properties were determined by performing microanalyses of the tube-spacer-weld combination using the finite-element program ANSYS. As is shown in Figure 5.46, the plate model is divided into 376 elements (432 nodes).

Average Tubewall Temperature. One of the inputs to the program is the nodal temperature. The nodal temperature is assumed to be the average tubewall temperature, which is obtained by integrating the tubewall temperatures over the tube cross-sectional area and then dividing by the cross-sectional area. As shown in Appendix O, the average tubewall temperature is given by:

$$\bar{T} = T_b + (Qr_o/\pi k) \left[k/hr_i - 0.5 + \left\{ r_o^2/(r_o^2 - r_i^2) \right\} \ln (r_o/r_i) \right]$$

where

r_i, r_o = Inner and outer radii of the tube respectively

Q = Peak absorbed heat flux

h = Salt conductance

T_b = Salt bulk temperature

k = Tubewall thermal conductivity.

The average tubewall temperature, an input to the shear stress model, was generated at a number of locations in each panel. The temperature contours were then plotted, as shown in Figure 5.47. From these plots it was obvious that the wing panel has the highest transverse in-plane ΔT of 50°C (90°F). Hence we chose this panel for shear stress analysis.

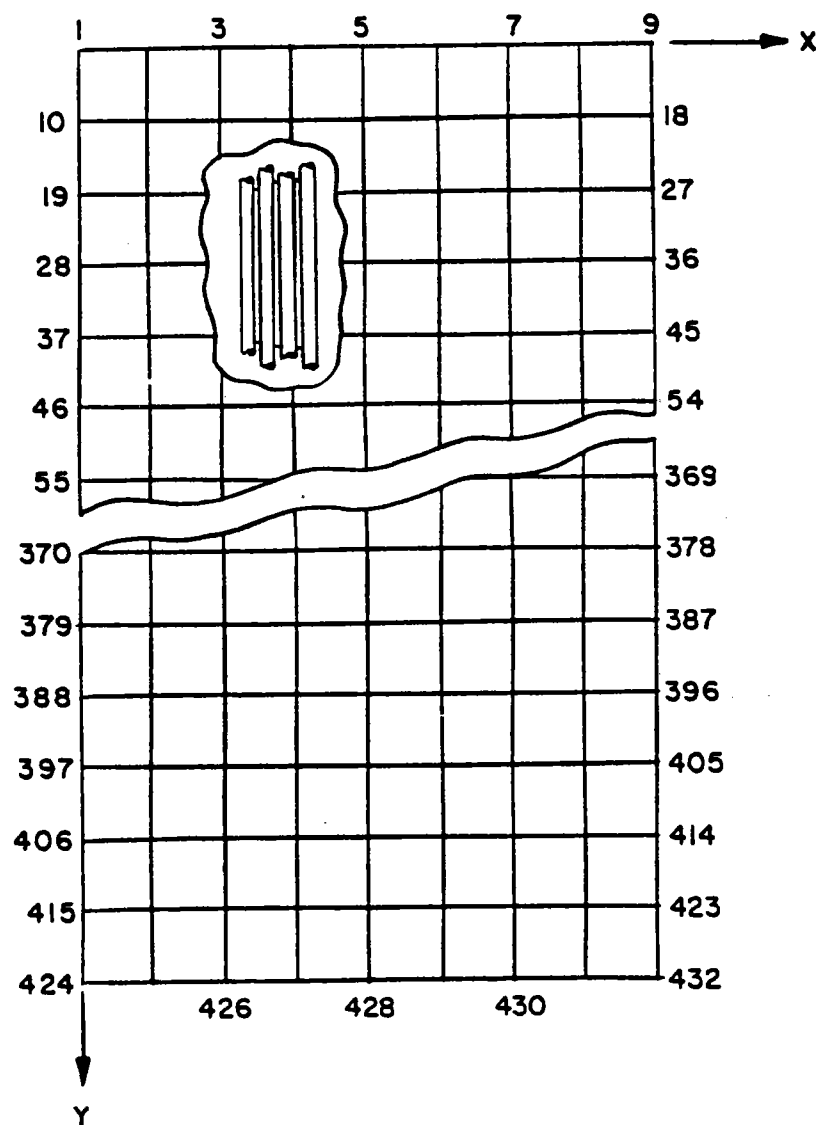


Figure 5.46 Finite-Element Model of the Panel

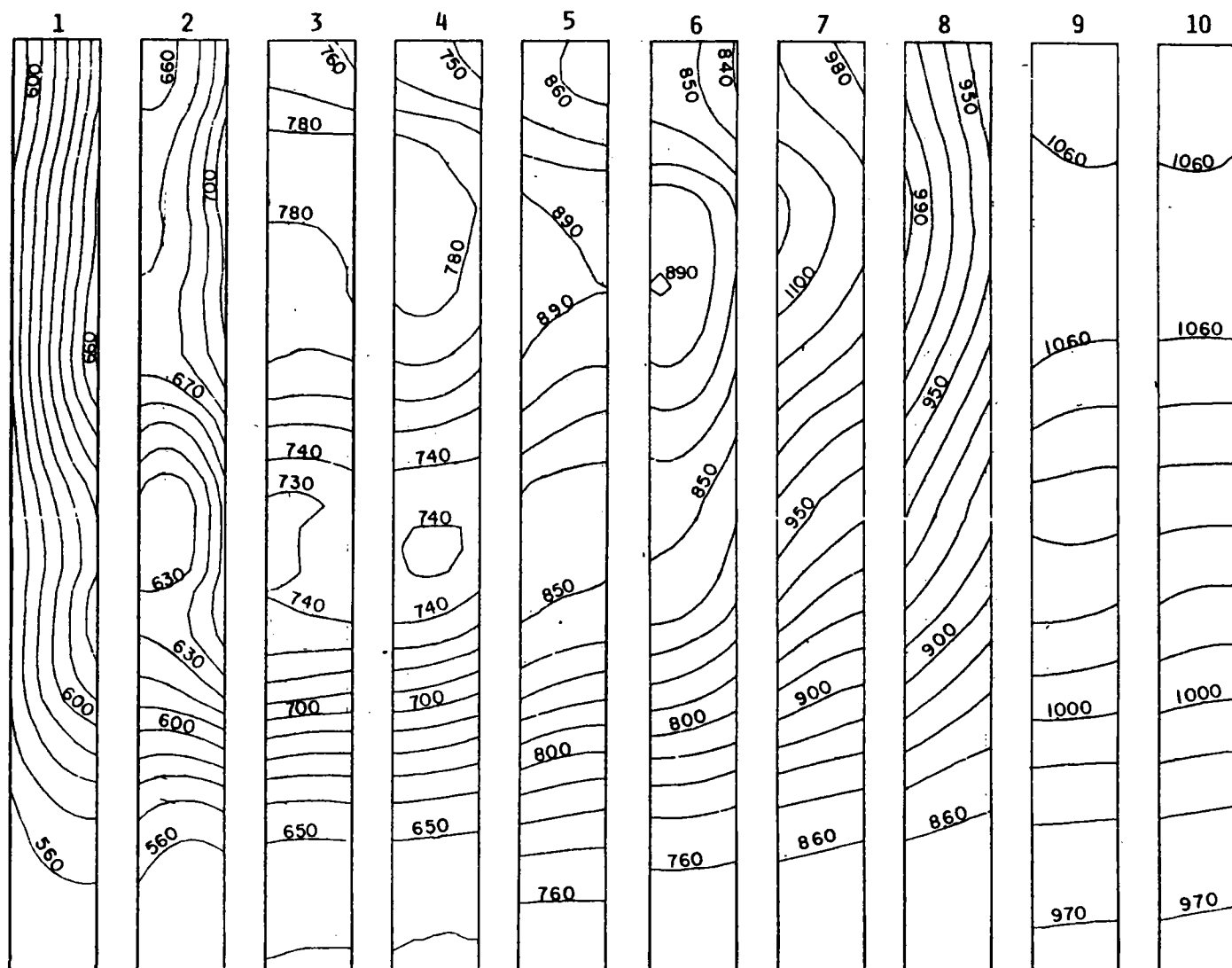


Figure 5.47 Temperature Contours in Absorber Panels, °F
[°C = (°F - 32)/1.8]

Orthotropic Plate Properties: The orthotropic elastic properties of the equivalent plate were determined by microanalyses using ANSYS. The finite-element model used is shown in Figure 5.37. Note that the coordinate system shown in Figure 5.37 is the local coordinate system rather than the global coordinate system shown in Figure 5.46.

As shown in Appendix O, the equivalent properties for a wing panel, referring to the global coordinate system in Figure 5.46 are:

$$\bar{E}_x = 248.58 \text{ MPa (34 kip/in}^2\text{)}$$

$$\bar{E}_y = 160,648 \text{ MPa (23.3 x 10}^3 \text{ kip/in}^2\text{)}$$

$$\nu_{xy} = 0.31$$

$$G_{xy} = 30,120 \text{ MPa (4.37 x 10}^3 \text{ kip/in}^2\text{)}$$

Using these properties and the finite-element model shown in Figure 5.46, the stresses in the equivalent plate were obtained. The boundary conditions are free-free on all four sides. The stresses obtained are shown in Figure 5.48. They are the stresses in the equivalent panel. The actual stresses in the real panel can be obtained by multiplying them by appropriate concentration factors developed by microstress analysis. As shown in Appendix O, the maximum stresses anywhere in the plate for the free-free boundary conditions are:

$$\sigma_x = 1082 \text{ kPa (157 lb/in}^2\text{)}$$

$$\sigma_y = 5212 \text{ kPa (756 lb/in}^2\text{)}$$

$$\sigma_z = 621 \text{ kPa (90 lb/in}^2\text{)}$$

$$\tau_{xy} = 793 \text{ kPa (115 lb/in}^2\text{)}$$

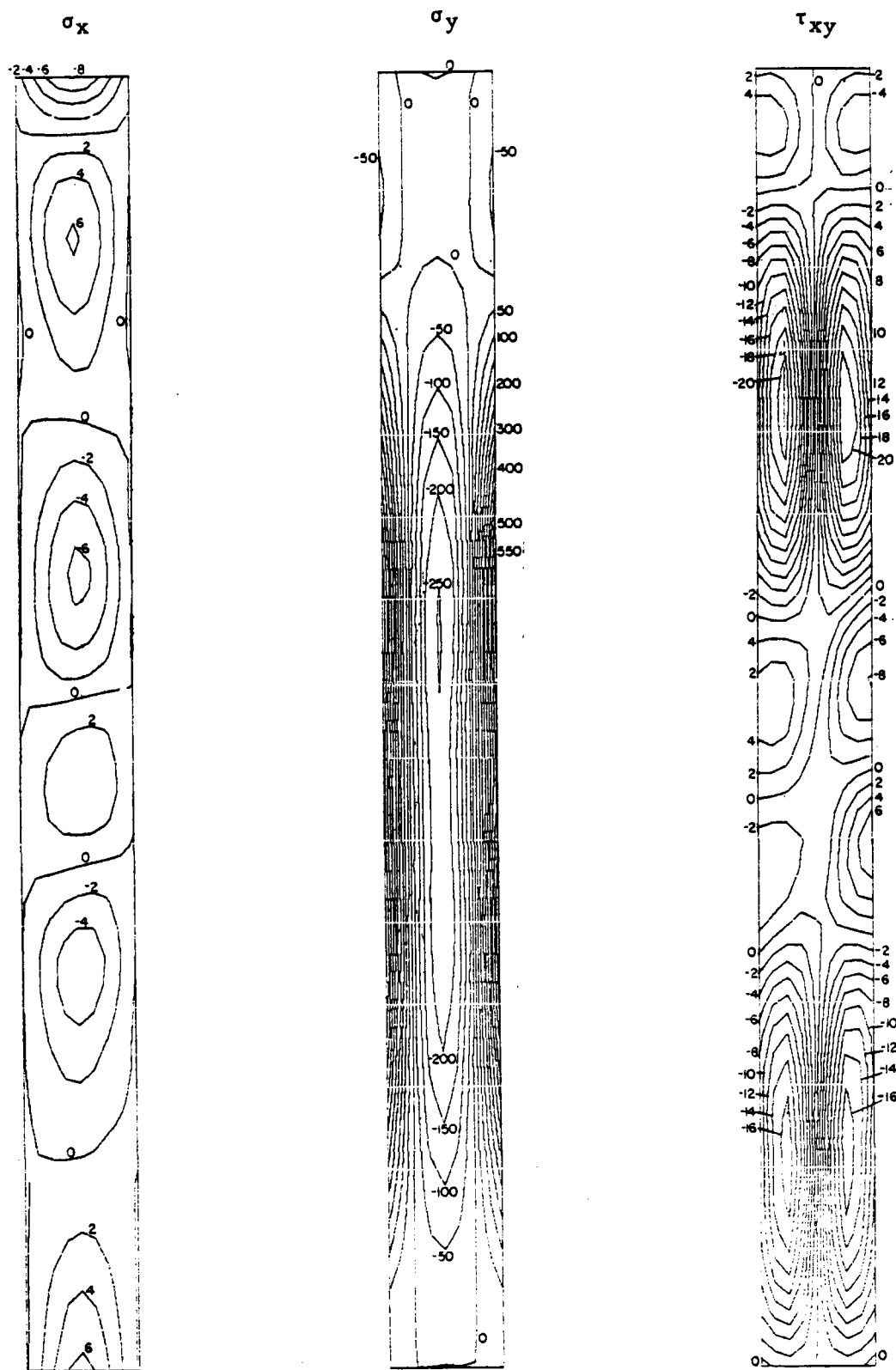


Figure 5.48 Stress Contours in Wing Panel as Shown in lb/in^2
($1 \text{ lb/in}^2 = 6.895 \text{ Pa}$)

The actual panel does not have the same boundary conditions as assumed in the previous analysis. The actual conditions are closer to spring supports at the bottom and top. Furthermore, the panel is not allowed to bend in its own plane. This latter condition will result in additional stresses in the (y) direction (global):

$$\sigma_y = \alpha \Delta T / 2 = 25.3 \text{ MPa (3664 lb/in}^2\text{)}$$

Thus the stresses caused by the in-plane ΔT s are very small. They will not have a significant impact on the structural integrity of the panel.

5.4 MECHANICAL DESIGN ANALYSIS

This section contains the results of the mechanical design analysis.

The major tasks were:

- Absorber panels
- Surge tanks and interconnecting piping
- Absorber door
- Receiver structure
- Tower and tower foundation
- Riser and downcomer piping

Component-level drawings were prepared in sufficient detail to allow preparation of RS fabrication and construction/erection plans and cost estimates. A complete set of RS drawings is given in Section 7 with the detailed description of the RS. Portions of those drawings are used in this section to support the mechanical design description.

The RS mechanical design was performed in accordance with the RS Requirement Specification (Appendix B). All pressure parts were designed in accordance with the ASME Boiler and Pressure Vessel Code. The structural analysis complies with all the requirements of the UBC, AISC, and all other applicable codes and standards.

5.4.1 Absorber Panels

As discussed in Section 4, the absorbing surface of the cavity is made of 20 panels--each with 88 tubes. The mechanical design of the panels was guided by the following constraints:

- Sufficient flexibility to absorb the thermal expansion of the panel and the thermal differentials between various portions of the panel
- Ease of fabrication, installation, and replacement of panels
- Economical design--minimum weight, low fabrication costs, easy and inexpensive operation and maintenance

- Maximum transportable length = 35 m (115 ft)
- Panel top-supported and guided to grow downward
- Surfaces not exposed to main flux protected
- Heat tracing on headers and piping
- All piping sloped 3 deg for drainage
- 30-year cyclic design life
- Operation/survival requirements (Appendix B)
- Minimum field labor/welding
- Handling loads of 5g
- Shipping loads
 - 2g vertical
 - 5g direction of travel.

The final panel configuration,* shown schematically in Figure 5.49, provides the best answers to constraints posed by the design requirements. To satisfy the first requirement (i.e., flexibility to accommodate large thermal expansions) four tube-to-header configurations were considered. In the first three, shown in Figure 5.50, the header is in the same plane as the panel; thus the panel weight is carried by the jumper tubes (bent end portions connecting the panel tubes with the headers) to the header. This arrangement results in very high stresses in (a) and (b). The stresses in (c) are acceptable, but fabrication (bending) of the jumper tubes is difficult and costly because of the tight tolerances required by the automatic welding torch for butt-welding jumper tubes to panel tubes and header stubs. Figure 5.51 shows the selected

*Panel tube size and materials were selected on the basis of the analysis performed in Task 3 (Section 4).

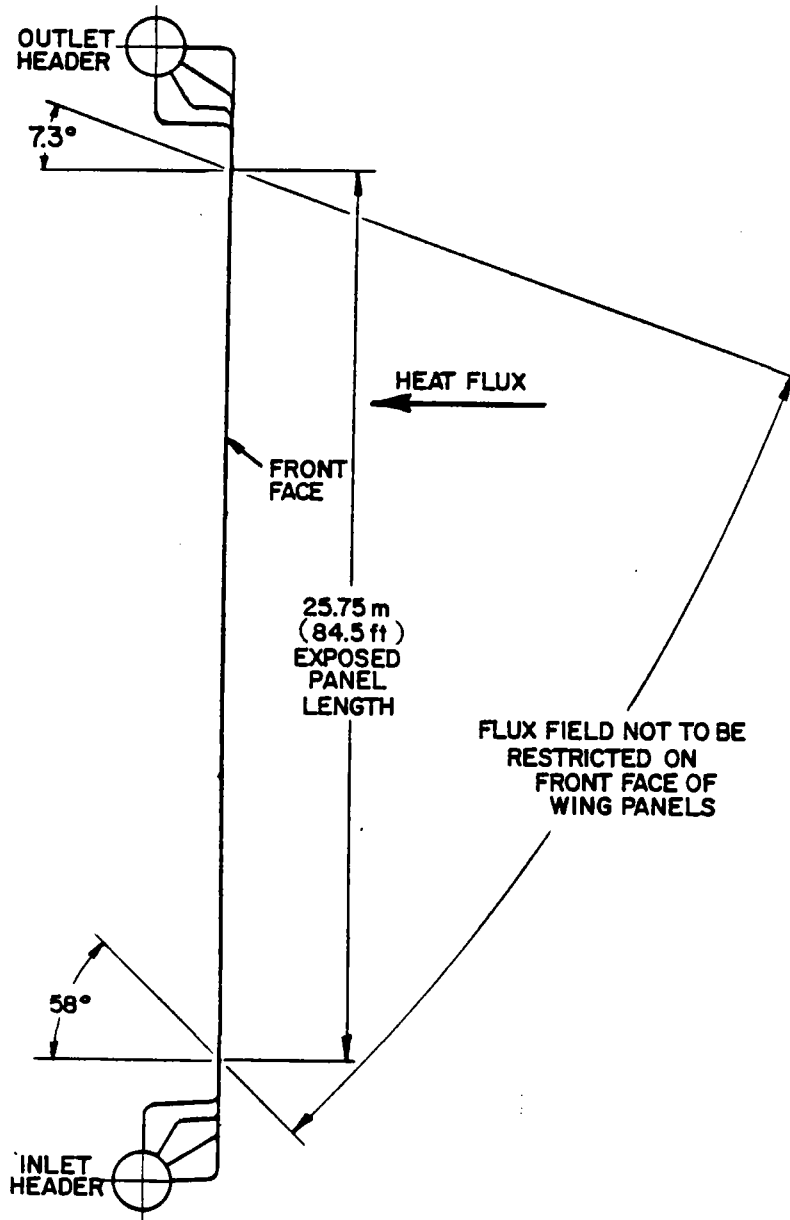


Figure 5.49 Side Elevation of Absorber Panel Showing Configuration and Governing Dimensions

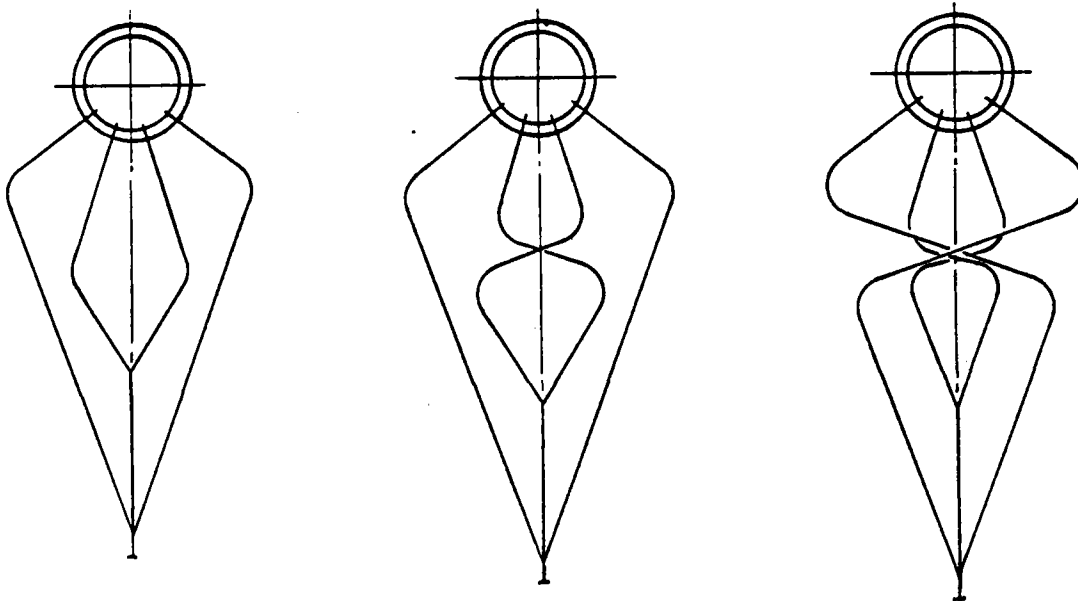


Figure 5.50 Preliminary Jumper-Tube Configurations

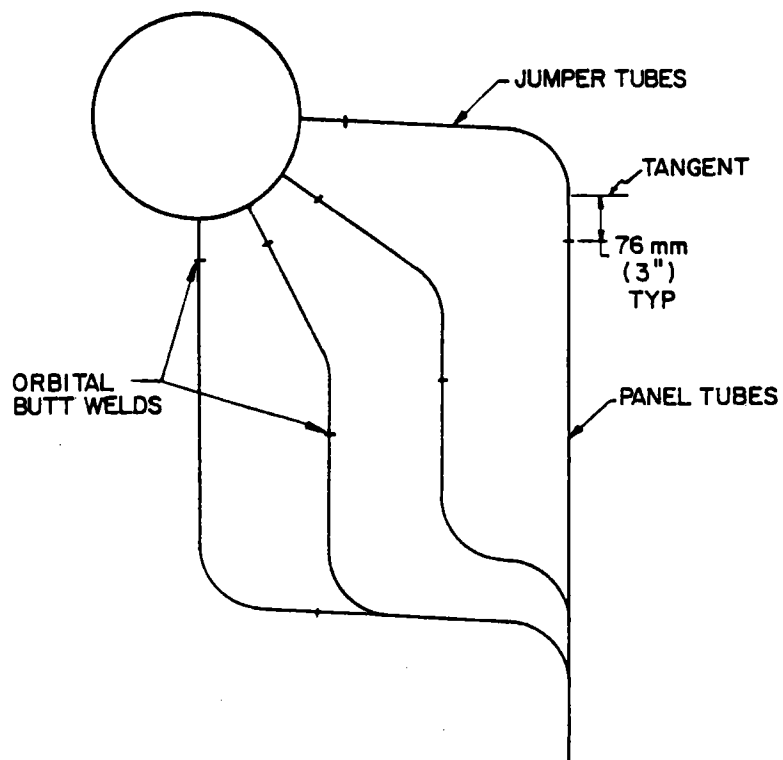


Figure 5.51 Selected Jumper-Tube Configuration

configuration in which the headers are shifted off plane. This configuration was selected for the following reasons:

- Adequate flexibility to accommodate differences in thermal expansion of tube sections within the same panel
- Panel weight supported by tie-rods, not by header/jumper tube--panel support arrangement is simpler and more reliable
- Less stresses in jumper tubes
- Easier to fabricate (bend), thus less expensive.

The results of welding a test panel section (Section 6) have shown that we should expect a difference in length up to 25.4 mm (1 in.) for tubes within the same panel because of variations in thermal expansion of tubes during welding. As a consequence, the final configuration of the jumper tubes provides, in addition to the required flexibility, a straight longitudinal portion (Figure 5.51) for final fit-up for every tube and the needed clearance for the automatic orbital butt welder. The tubes are attached to only 1/4 of each header (90 deg), to satisfy the requirement that the panel be completely drainable.

Figure 5.52 shows four possible ways of attaching tubes to headers. The header with stubs was selected because it is the least expensive to fabricate, and the thinner headers can better accommodate the thermal transients of the receiver. The stubs are attached to the header as shown in Figure 5.53.

After the stub is welded to the header in a semifinished condition, its I.D. is enlarged by drilling to match the I.D. of the jumper tubes, cutting away the portion of the fitting shown extending into the header port and providing a full-penetration welded joint that can be x-rayed.

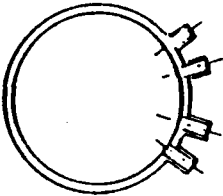
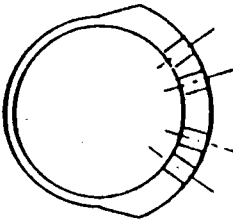
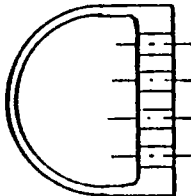
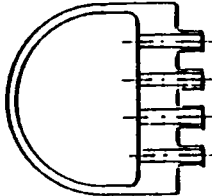
Arrangement	Method of Tube Attachment	Comments
 <p>Pipe With Stubs (selected)</p>	Tubes orbital Welded to stubs	Tube weld can be x-rayed but stub cannot
 <p>Combination thick- and thin-walled header</p>	Tubes fillet welded and rolled into 25.4-mm (1-in.)-thick section	Tube weld cannot be x-rayed but fit-up is simplified
 <p>Flat tubesheet</p>	Tubes fillet welded and rolled into 25.4-mm (1-in.)-thick section	Tube weld cannot be x-rayed but fit-up is simplified
 <p>Flat tubesheet with spigots</p>	Tubes orbital or internal bore welded to spigots	Tube weld can be x-rayed

Figure 5.52 Candidate Header Arrangements

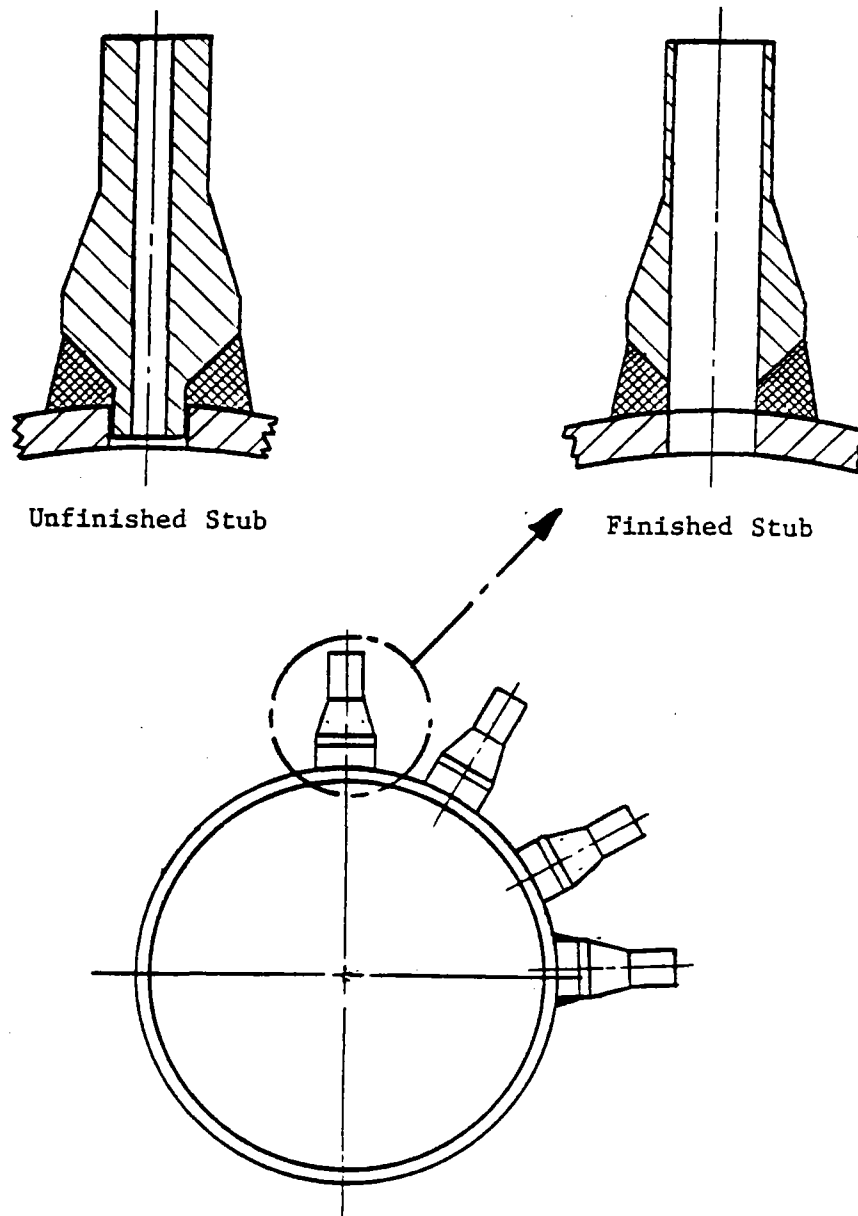


Figure 5.53 Selected Tube-To-Header Attachment Configuration

During the earlier part of the design effort, the maximum length of Incoloy 800 tube that vendors could supply was about 21 m (70 ft). Thus a butt weld in the exposed section of the tubes would be required to weld two pieces together to meet the required panel length. However, when doing the cost estimates during Task 5, a vendor was found that could supply tubes up to 30 m (100 ft) in length, which eliminated the need for the middle butt weld. Cost trade-off studies indicated that the savings in labor costs by eliminating these middle butt welds far outweigh the extra cost of the longer tubes. Thus only three butt welds are required per tube: at one end the tubes are bent and butt welded directly to the header stubs; at the other end, an additional butt weld is required for fit-up as explained before.

The inlet and outlet headers (Figure 5.54) are 0.25 m (10-in.) Sch 40 pipe with two 0.15 m (6-in.) nozzle connections for feeders and risers. They are supported by rigid hangers. As shown in Figure 5.55, the upper outlet header is tied by rods to the supporting steel above and also braced laterally into the panel strongback; the lower inlet header is permitted to move with the longitudinal expansion of the panel. It is tied to the panel with the help of a light structure connected to the lowest buckstay/lug assembly. The large displacements caused by thermal expansion would not permit supporting the lower header from "cold" steel. The small expansion difference between the lowest portion of the panel and the inlet header is easily accommodated by the flexibility of the jumper tubes.

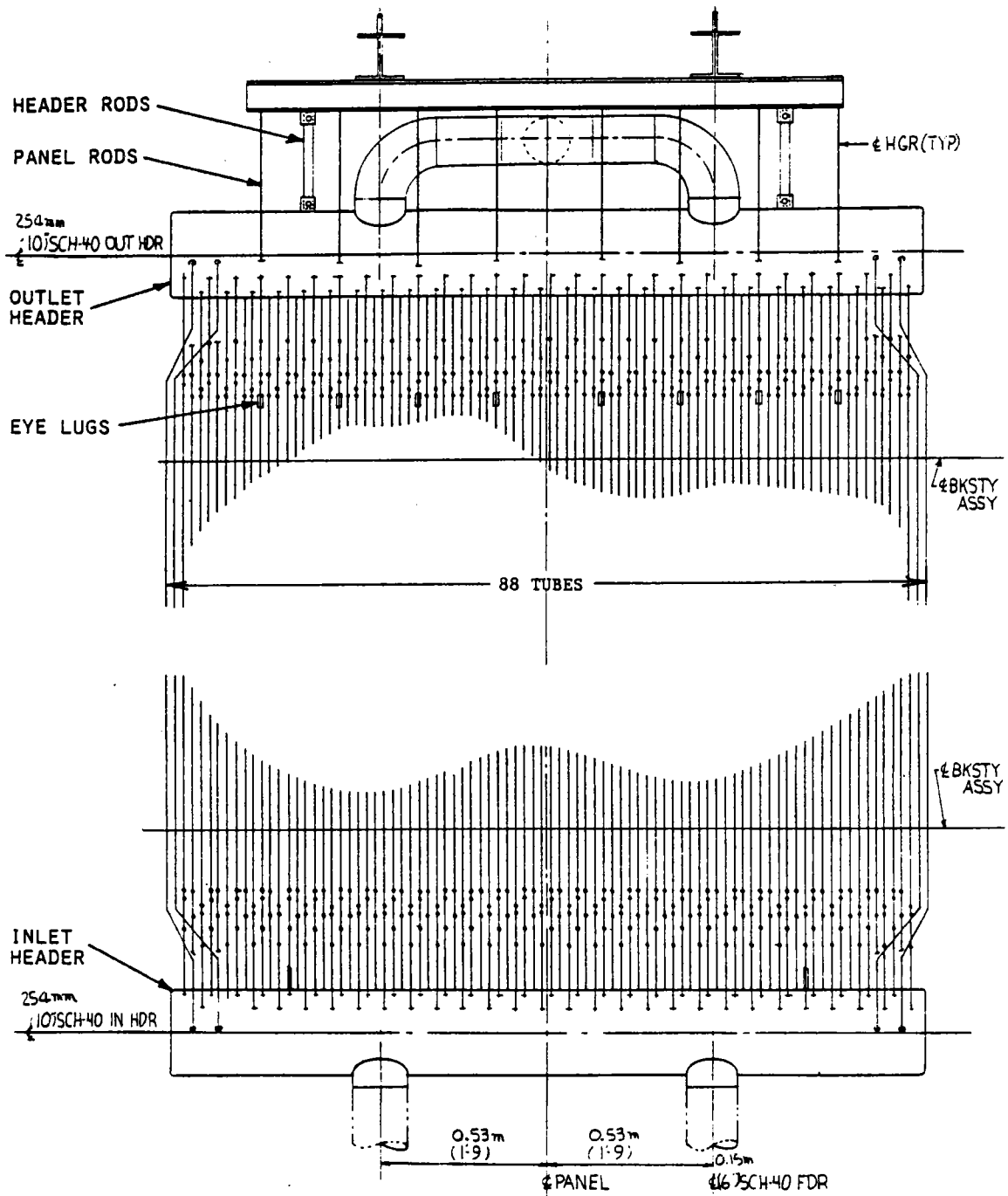
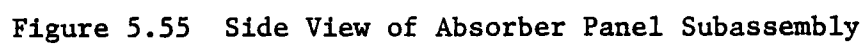


Figure 5.54 Front View of Absorber Panel Subassembly

REF.: 84-2292C
DATE: November 1982



To permit easy removal/replacement of the panels and to reduce the gap between panels, the headers are shorter than the overall width of the panel. Thus the tubes at the periphery of the panel must be bent out of plane to connect to the header. By using flat heads on the headers, the number of these peripheral tubes is kept to a minimum. The flat heads permit easier and more economical fabrication than the hemiheads normally used and also allow for a more even distribution of the panel support rods.

The weight of the panel is supported by nine eye lugs welded on the straight portion of the tubes (see Figure 5.54). This arrangement is widely used in boiler panels, and our experience indicates it is very reliable; distributes the loads well into the walls of the supporting tubes; minimizes the deformations and deflections of the panel; and reduces installation, maintenance, and replacement problems. As shown in Figure 5.56, an eye lug consists of a pair of plates bent around the tube (welded to the tube at their lower ends just below the tube bend) and a typical eye lug plate (welded to the plates at their upper ends), which connects the lug to adjustable support rods. These panel support rods are tied together with the upper header rods into a spreader-beam system that connects into the main vertical support beams, as shown in Figure 5.55.

The panel in-plane distortion--caused by welding during fabrication and by transverse temperature gradients during operation--determines the required gap between two adjacent panels, which should be kept to a minimum. The in-plane post-weld distortion was practically eliminated by using a deeper spacer strip [11.1 mm (7/16 in.)] between tubes (Section 6.4). The in-plane distortion (because of the temperature differences across the panel) is unavoidable. The

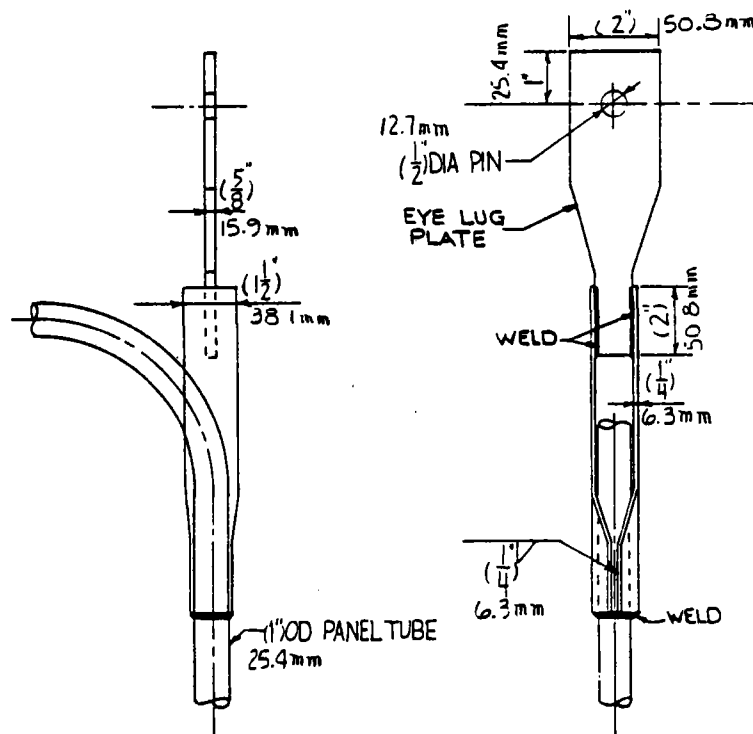


Figure 5.56 Panel Support Eye Lug

maximum mean ΔT across a panel width was estimated at 28°C (50°F), as discussed in Section 5.3.7, and the maximum in-plane displacement of the lower end of the top-supported panel would be approximately 67 mm ($2\text{-}5/8$ in.). Such a displacement is unacceptable from a practical standpoint; the forces required to limit it, and consequently the stresses induced in the panel and the supporting structure, would be excessive.

The most practical solution to alleviate this problem--and the one finally selected--was to fabricate the panel in three independently expanding subsections--28, 32, and 28 tubes wide* (i.e., to omit the spacer strip and the welding

*The subpanels must be in multiples of four tubes because symmetry is needed for panel welding (Section 6).

of tubes to each other, for their entire length, at two places across the panel width). For this configuration the maximum reaction force to prevent the panel from deflecting against the adjacent panel is approximately 9785 N (2220 lb), producing a stress in the tubes of approximately 6.55 kPa (950 lb/in²). The maximum temperature difference across a panel occurs only in the two wing panels; all other panels experience less severe conditions.

To facilitate handling, shipping, and installation, the tubes and headers are a part of a subassembly that also comprises the buckstays and ties; top horizontal beam with hangers and lifting lugs; vertical supporting beams (strongback), which attaches to the receiver support structure; insulation; etc.

The panel buckstays perform the following functions:

- Transmit the wind and seismic loads on the panel into the strongback and to the supporting steel structure
- Keep the panel straight in a transverse direction while permitting free thermal expansion--vertical and lateral (in the plane of the panel)
- Absorb and transmit in-plane loads imposed on the panels by earthquakes
- Act as stiffening members for the panels to resist shipping forces.

The longitudinal out-of-plane tube distortion (bowing) is limited by the buckstay spacing, determined to be 1.8 m (6 ft) maximum (Section 5.3.2). Each buckstay is held in place by nine buckstay lugs welded directly to the tube spacers (Figure 5.57), as discussed in Section 6, and rigidly tied to three of them--one in the center of each of the three subpanel sections--to ensure a controlled and predictable lateral thermal expansion of the panel as well as

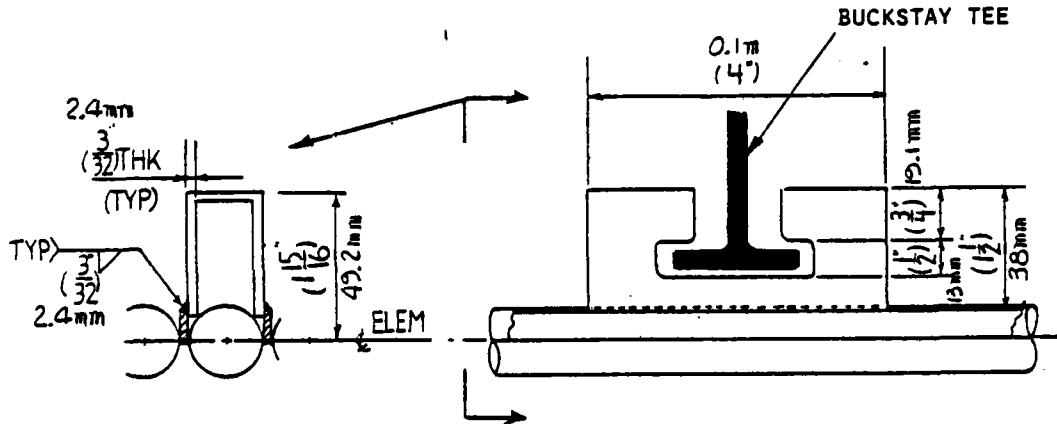


Figure 5.57 Buckstay Lug

to minimize out-of-plane distortion. Both lugs and buckstays are fabricated of stainless steel plate. Since the buckstays are adjacent to or in contact with the tubes and are also covered by the insulation on the back of the panels, we assumed a design temperature equal to the highest mean tubewall temperature.

The loads exerted on the panel and buckstays are transmitted by a system of tie-bars or links to the panel strongback. This load path is characterized by pinned connections (Figure 5.58) that allow vertical panel expansion. As discussed in Section 5.2.1, the maximum vertical displacement is expected to be approximately 232 mm (9.12 in.). As a result of this longitudinal thermal growth, the bottom end of the panel moves forward approximately 6.4 mm (0.25 in.) between the cold and hot positions (Figure 5.59).

Blanket-type insulation is applied to the back of the tube panels with stainless steel retaining pins. Insulation thickness varies between 0.15 m (6 in.) for Pass 1 and 0.25 m (10 in.) for Pass 5 (Table 5.13). Insulation

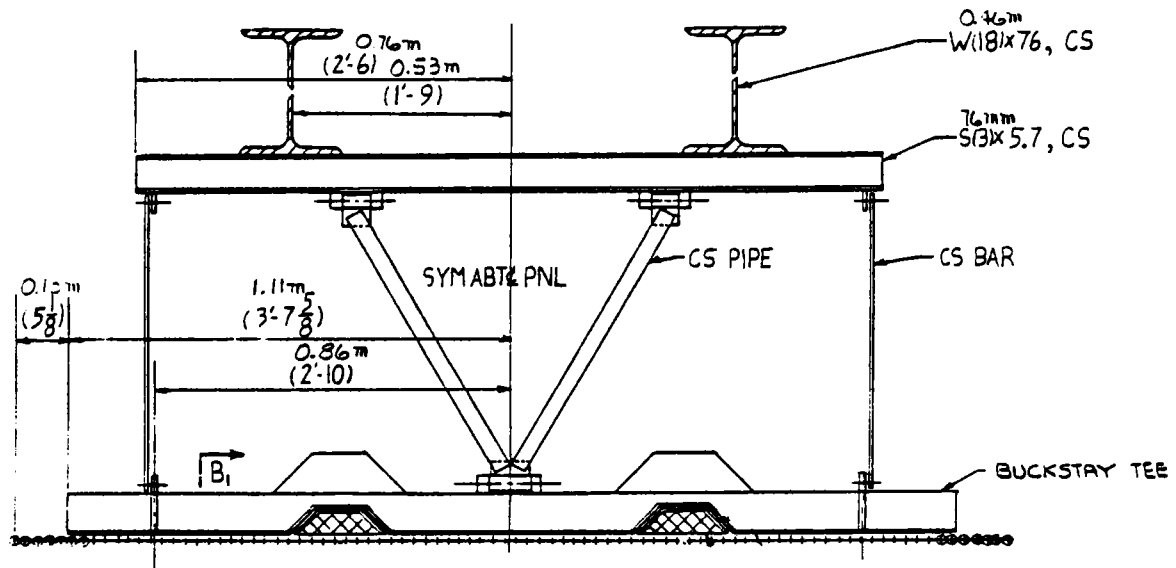


Figure 5.58 Link Support Arrangement

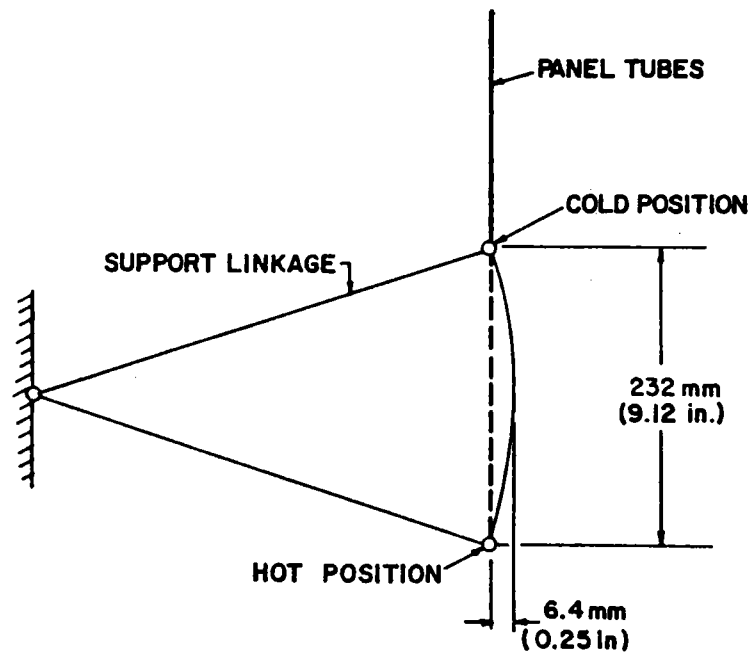


Figure 5.59 Movement at Bottom End of Panel 10 as a Result of Thermal Expansion

between the subsections of each panel and between panels is rigid ceramic Fiberfrax board in overlapping pieces, backed by soft ceramic fiber (Figure 5.60). Fiberfrax insulation--made by Carborundum Company of Niagara Falls, New York--offers low thermal conductivity, high-temperature stability, and excellent resistance to thermal shock. It has a 1260°C (2300°F) continuous use limit and a melting point of 1760°C (3200°F).

Key features of the absorber panel are summarized below:

- Modular shop assembly simplifies transportation, erection, and replacement.
- All panels are identical except for tube/header materials and insulation thickness.
- Swing links eliminate frictional restraint of expansion, but provide excellent strength.
- Vertical splits in panel reduce forces required to keep panel straight and in plane.
- Horizontal expansion movements are controlled by limit stops between buckstays and tube lugs.
- Jumper tubes permit differential thermal expansion.

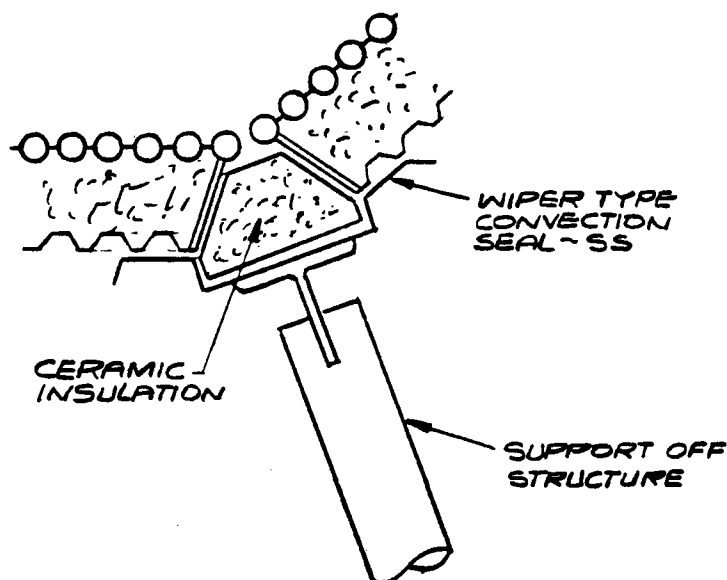


Figure 5.60 Arrangement of Insulation Between Absorber Panels

5.4.2 Interconnecting Piping and Surge Tanks

Dimensions, layout, and materials for all risers, downcomers, and transfer lines were selected on the basis of the design conditions (pressure, temperature, flow, etc.) and the need for flexibility. Materials used for all of these piping sections were discussed in Section 4.3.2. All connections, collecting headers, bend radii, and other details are typical for boiler piping design and are in accordance with our standard practice and all applicable power piping codes. Flexibility studies and stress analyses ensured feasibility of the selected arrangements and safe operation of the unit under all conditions.

The receiver piping--atop the tower--consists of the main riser and downcomer portions, feeders, risers and transfer piping, and drain and vent piping. The absorber inlet and outlet piping arrangements are shown in Figures 5.61 and 5.62. All piping is completely drainable, insulated, and trace heated. Pipe sizes are given in Table 5.26.

Table 5.26 Receiver Pipe Sizes

	<u>O.D. m (in.)</u>	<u>Schedule</u>
Feeders	0.15 (6)	40
Risers	0.15 (6)	40
Transfers	0.30 (12)	40
Primary riser	0.40 (16)	60
Primary downcomer	0.30 (12)	10*
Secondary downcomers		
Between first 4 passes	0.30 (12)	40
Between Passes 4 and 5 (2 required)	0.25 (10)	40
Drain and vent piping	0.10 (4)	40

*Changes from 10 at the top to 80S at the base of the tower.

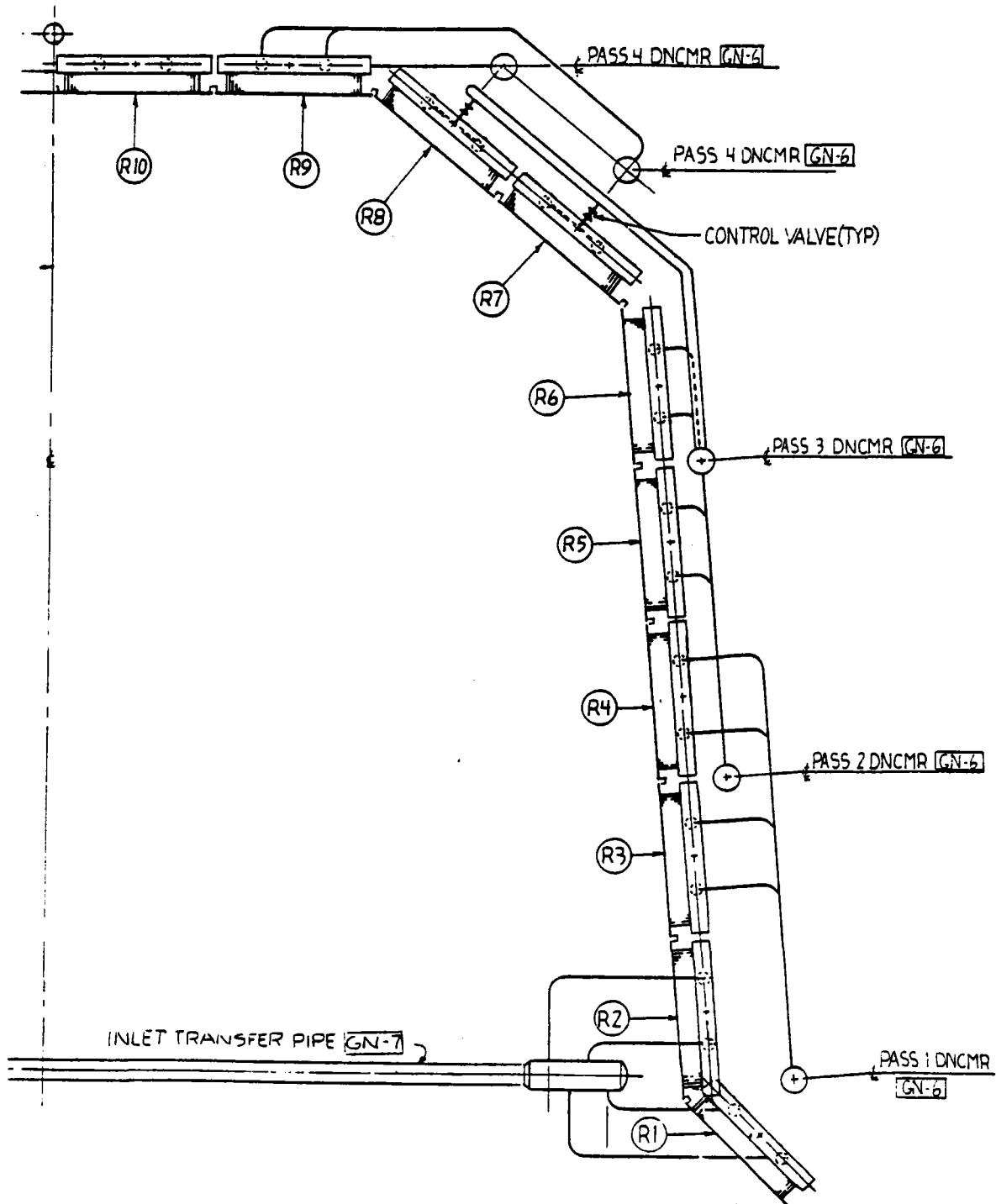


Figure 5.61 Absorber Inlet Piping Arrangement

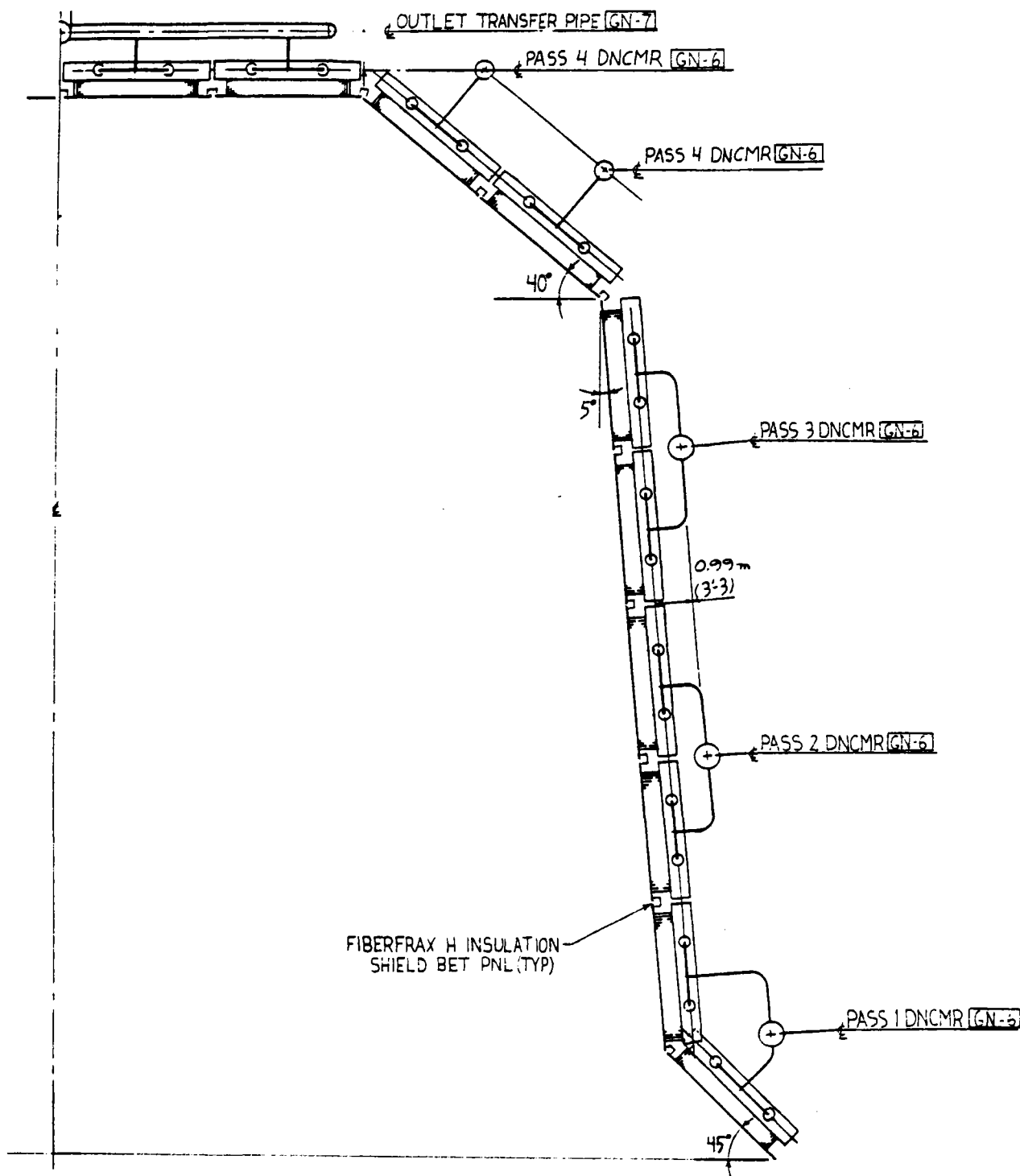


Figure 5.62 Absorber Outlet Piping Arrangement

Sizes were selected to minimize header flow imbalance, pressure drop, and length required for flexibility. To prevent leaks, welded rather than flanged piping connections are used wherever possible. Piping and valves are located for easy access for maintenance and removal. All valves are self draining globe-type with internal bellows seals, capable of both manual and pneumatic operation.

Figure 5.63 illustrates the location of the surge tanks in the receiver structure. They are located on the north-south centerline at the rear of the receiver structure--which helps to counterbalance the weight of the aperture door. The OST is located at an elevation above the highest absorber panel header. This location provides for positive filling of all of the absorber panel tubes and interconnecting piping. The tank is pressurized above the salt vapor pressure to ensure positive pressure at all times.

The IST capacity was determined by the requirement that when at the half-full set-point level it has to provide 60 seconds of emergency full salt flow for receiver protection in case of a feed pump or power failure (Section 4.3.10). It is pressurized to provide the driving force for emergency salt flow. Both the IST and OST have the same outside dimensions (Table 5.27). The capacity (volume) of the IST is slightly less because its higher design pressure requires a thicker wall. Both tanks are completely insulated to reduce heat losses.

5.4.3 Receiver Aperture Door

The door design requirements and key issues were discussed in Section 4.3.7 and Appendix G are summarized in Table 5.28.

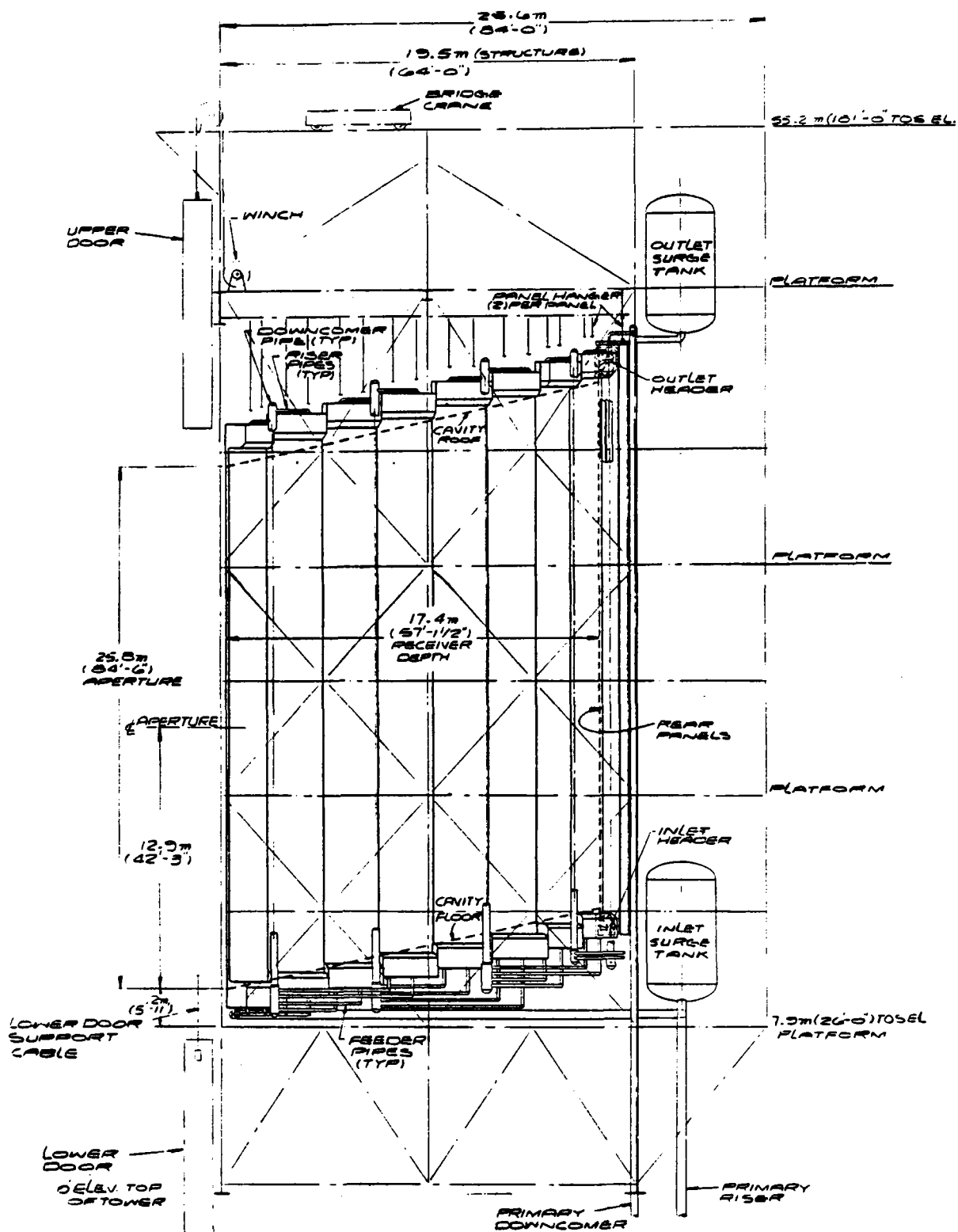


Figure 5.63 Side Elevation for Receiver

Table 5.27 IST/OST Tank Specifications

	IST		OST	
Operating temperature, °C (°F)	288	(550)	566	(1050)
Design temperature, °C (°F)	316	(600)	593	(1100)
Operating pressure, kPa gage (lb/in ² g)	2410	(350)	103	(15)
Design pressure, kPa gage (lb/in ² g)	2760	(400)	207	(30)
Outside diameter, m (ft)	3.2	(10.5)	3.2	(10.5)
Overall height, m (ft)	7.0	(23.0)	7.0	(23.0)
Wall thickness, mm (in.)	44.5	(1-3/4)	9.5	(3/8)
Volume, m ³ (ft ³)	51.5	(1818)	52.8	(1866)
Salt capacity, kg (lb)*	49,100	(108,100)	45,800	(100,700)
Insulation thickness, mm (in.)	152	(6)	229	(9)
Material	CS		304SS	
Weight (empty), kg (lb)	27,000	(59,500)	5,900	(13,000)

*At operating level (half-full).

Table 5.28 Aperture Door Design Considerations

Requirements
Minimize heat losses from cavity
Close by gravity in less than 1 minute during power failure
Withstand thermal transients when closed over hot absorber with heliostats focused
Withstand a 40 m/s (90 mi/h) wind (at reference elevation)
30-year lifetime
Key Issues
Insulation system
Edge seals
Deflections and roller loads
Structure expansion or warping
Thermal protection of support cables
Quick-close system
Reliability and availability
Cost

Preliminary Selection Procedure. Anticipating the many difficult problems a receiver door system will have to overcome, we studied several possible arrangements. The final choice is the most reliable and economical, while also ensuring relatively simple, low-cost maintenance. Some of the systems considered and analyzed were:

- Horizontally Sliding Doors ("closet" type) With Horizontal Straight Tracks at Top and Bottom. This system has simple tracks and door weight supported on one of the tracks only (either top or bottom)--the other having some provision for the expansion of the doors. The door mechanism can be located at the bottom of the receiver aperture. The main disadvantages are:
 - Need for shielding of the door tracks--the top track from convection currents from the receiver cavity, the bottom track from direct radiation from the heliostats.
 - Doors must be made of at least four sections and would occupy much space at the side of the structure.
 - Door tracks must be designed to take wind and earthquake loads.
 - Since the entire weight of the doors is supported by the roller assembly, the mechanism is more likely to jam during operation.
- Sliding Doors on Curved Tracks With Doors Stored at Sides of Receiver (in open position). This system minimizes the exposure of the doors to wind (in open position) and provides good weight distribution for the door sections. The lower track can be eliminated in front of the receiver (where it is difficult to protect it from direct radiation), but provision must be made to secure the doors at this location against rattling in the wind. Some of the disadvantages for this system are:
 - Need for thermal protection for top track in front of receiver cavity.
 - More complicated closing/opening mechanism.
 - More difficult to seal at top and bottom of aperture.
 - Door must be in four or six sections.
- Roll-Up ("garage-door type") System. This door is similar to others described; its main disadvantages are:
 - Interference with the steel structure on the receiver
 - Need for six or more door sections.

In addition to these door designs, we looked at some types of hinged doors. Their main problem was the high wind loads they may have to resist

during closing or opening. Most or all of these options need a counterweight to close the doors during a power failure. Such a weight would add to the cost of the tower and receiver structure.

Selected Door Configuration. We selected a two-piece, vertically sliding door ("guillotine" type), mainly because of the fewer problems presented by such a system in designing for the "no power" closing requirement and because wind and earthquake loads on the doors are directly transmitted to the main columns of the structure. The assembly consists of two sections, each of which span the receiver aperture horizontally (Figure 5.64). When opening and closing by a cable drum-type hoist, the door sections move up and down parallel to the receiver aperture on vertical door tracks. The lower section counterbalances the upper section, minimizing the power required for opening and closing. The vertical door tracks are located at the sides of the receiver aperture, directly in front of (and attached to) the main columns of the steel structure. The two sections of the door are similar in construction, but the upper section is larger and heavier to permit closing by gravity in the event of a power failure.

Each door section is made of a series of girders 2.44 m (8 ft) apart (horizontally) that carry the wind load (which is the controlling design factor) into the main columns over the 27.4-m (90-ft) span between them. These girders are made of two tee sections (WT5 x 24.5) joined by angle braces and connected at each end to a piece of W18 x 35. All girders are tied together by vertical beams (W18 x 40) in line with the main columns of the steel structure.

The most important feature of this construction is the hollow core of the door, shown in Figure 5.65, which allows a relatively free flow of air for heat

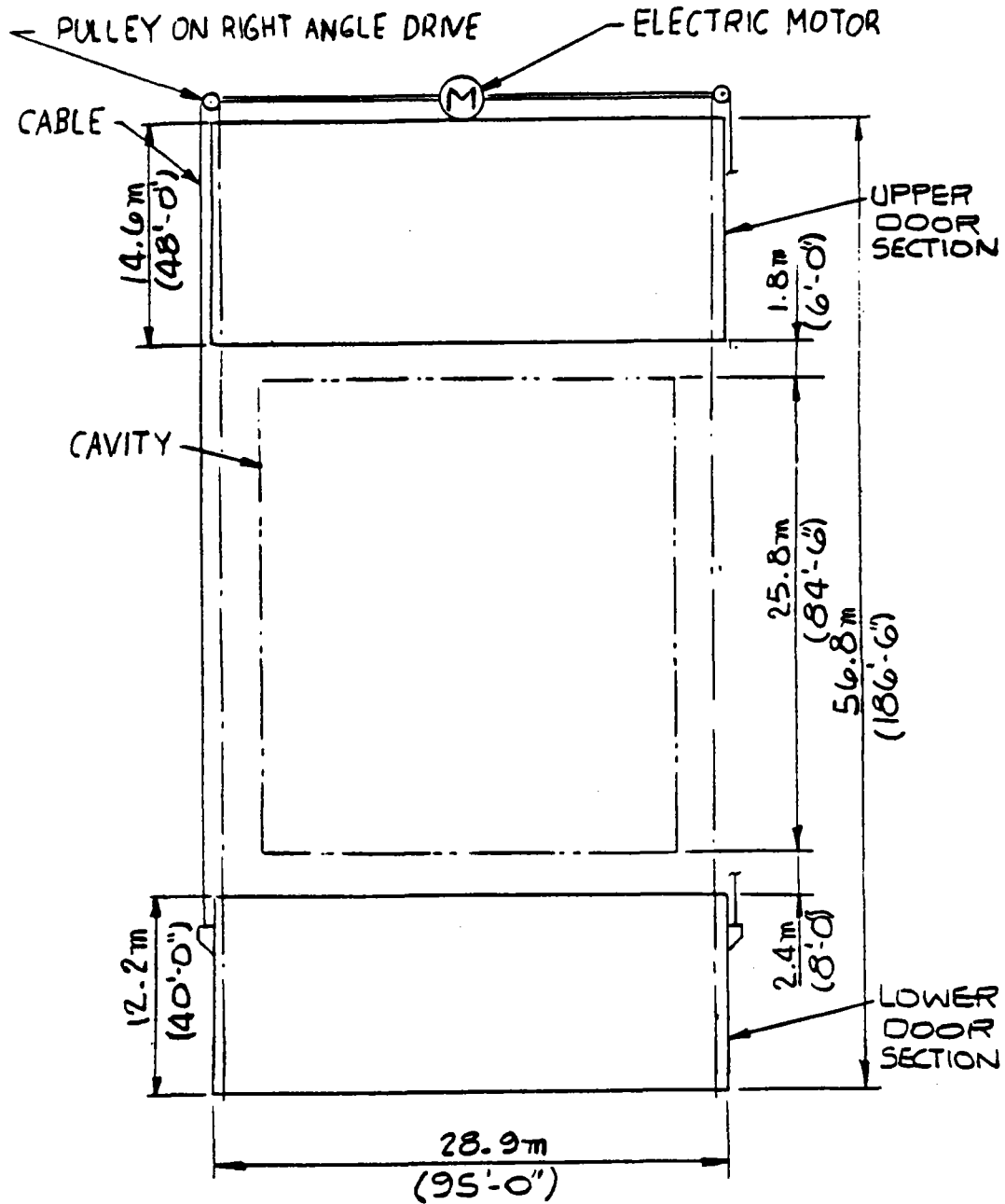


Figure 5.64 Front Elevation of Aperture Door

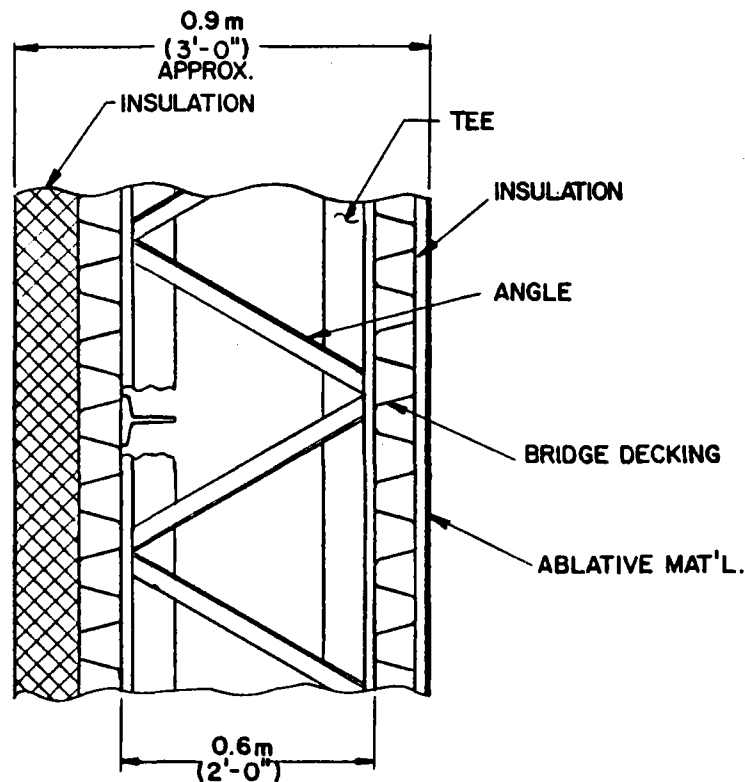


Figure 5.65 Cross Section of Aperture Door

dissipation within the door structure to ensure a minimum temperature difference between members. By limiting the temperature variations within the door, the distortions expected during operation or in an emergency are minimized. On both sides of the door, the girders are covered by corrugated plate (with corrugations running vertically) covered by insulation (see Figure 5.65). The corrugated plate (Robertson Section 21 noncomposite floor decking) was chosen because of the need for a lightweight member capable of carrying wind loads over the 2.44-m (8-ft) span between girders and suitable for installing the insulation. The inside face of the door (facing the receiver cavity) has a 152-mm (6-in.) layer of Fiberfrax (blanket-type) insulation. The outside is protected by a 51-mm (2-in.)

layer of Fiberfrax blanket insulation covered by a 38-mm (1.5-in.) layer of ablative material* to protect the door (and the receiver) during an emergency until the earth's rotation moves the incident solar flux away from the receiver or the heliostats are otherwise defocussed (Section 4.3.7).

To minimize heat losses by convection during cloudy periods and overnight, the door has two sets of seals:

- Stationary ("passive") seals attached to the door and to the frame around the aperture. At the top and bottom and between door sections, they are simple, flexible, stainless steel strips (Figures 5.66 and 5.67); at the sides they are wedge-shaped blocks with a profile intended to minimize friction when the door moves (see Figure 5.68).
- Movable ("active") seals attached to the receiver (top, bottom, and sides). These are cam-actuated spring-loaded flaps, made of many independent segments to provide good sealing even when the door is subjected to large distortions (see Figure 5.66).

The vertical tracks on which the doors move are made of two wide-flange beams (W14 x 82) welded to each other and tied back into the main columns. This box-type construction facilitates and simplifies the design of the roller assemblies while offering high rotational stiffness. The roller assemblies (Figures 5.69 and 5.70) must not only carry the wind loads normal to the door and (at least on one side) the lateral earthquake loads, but also allow for any and all expected thermal distortions of the door. These considerations led to the selection of Lubrite spherical bearings, which are capable of taking high loads while accepting limited angular displacements. Each assembly was designed for a maximum normal (wind) load of 345,000 N (78,000 lb) and a maximum temperature difference between the inside and outside door surfaces of 222°C (400°F). These values

*Ablative material data is given in Appendix G.

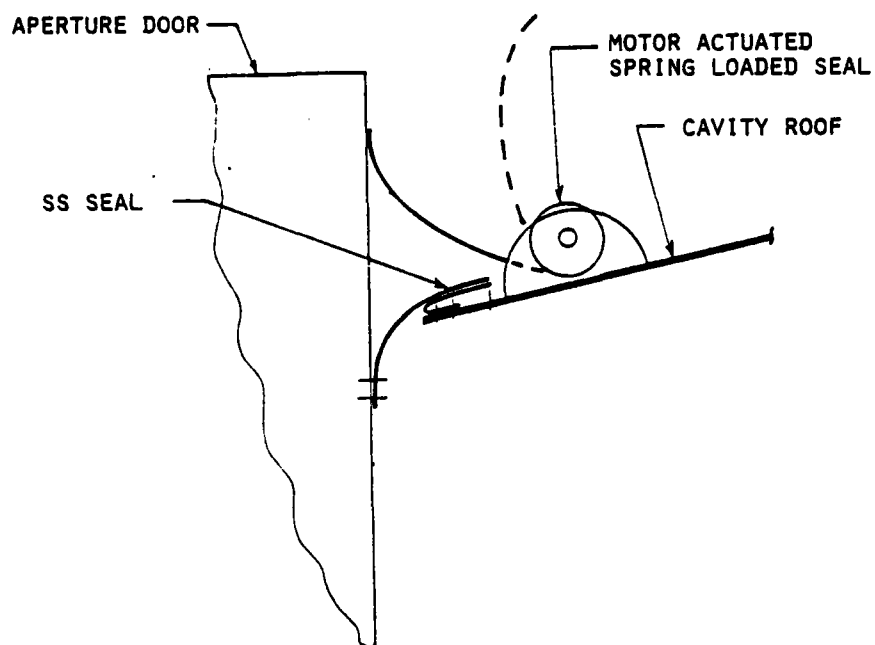


Figure 5.66 Top Door Seals (Reversed for lower door section)

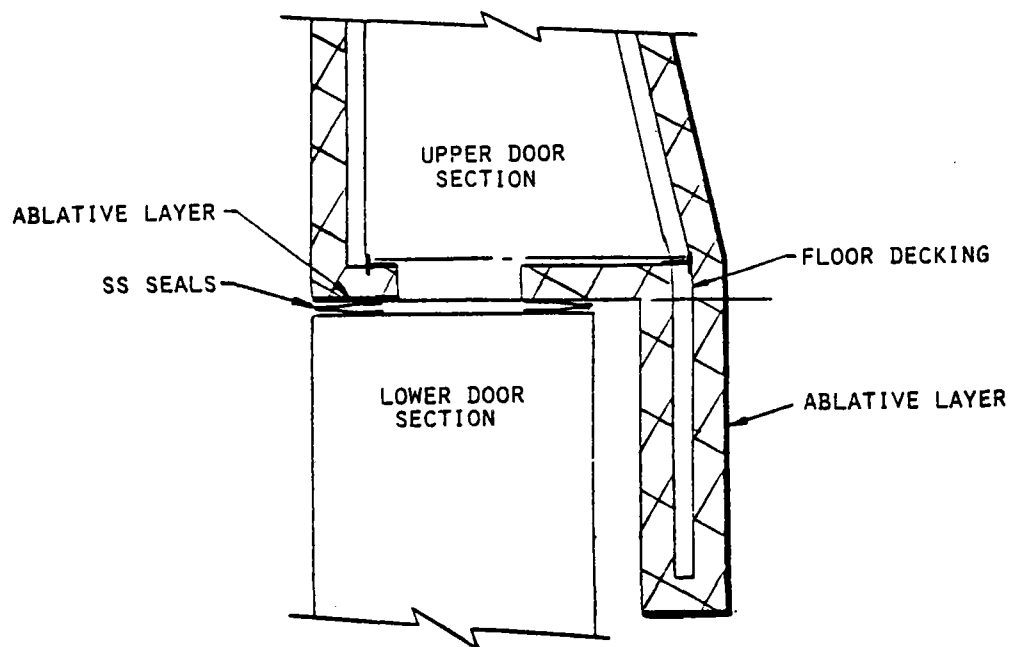


Figure 5.67 Seals Between Door Sections

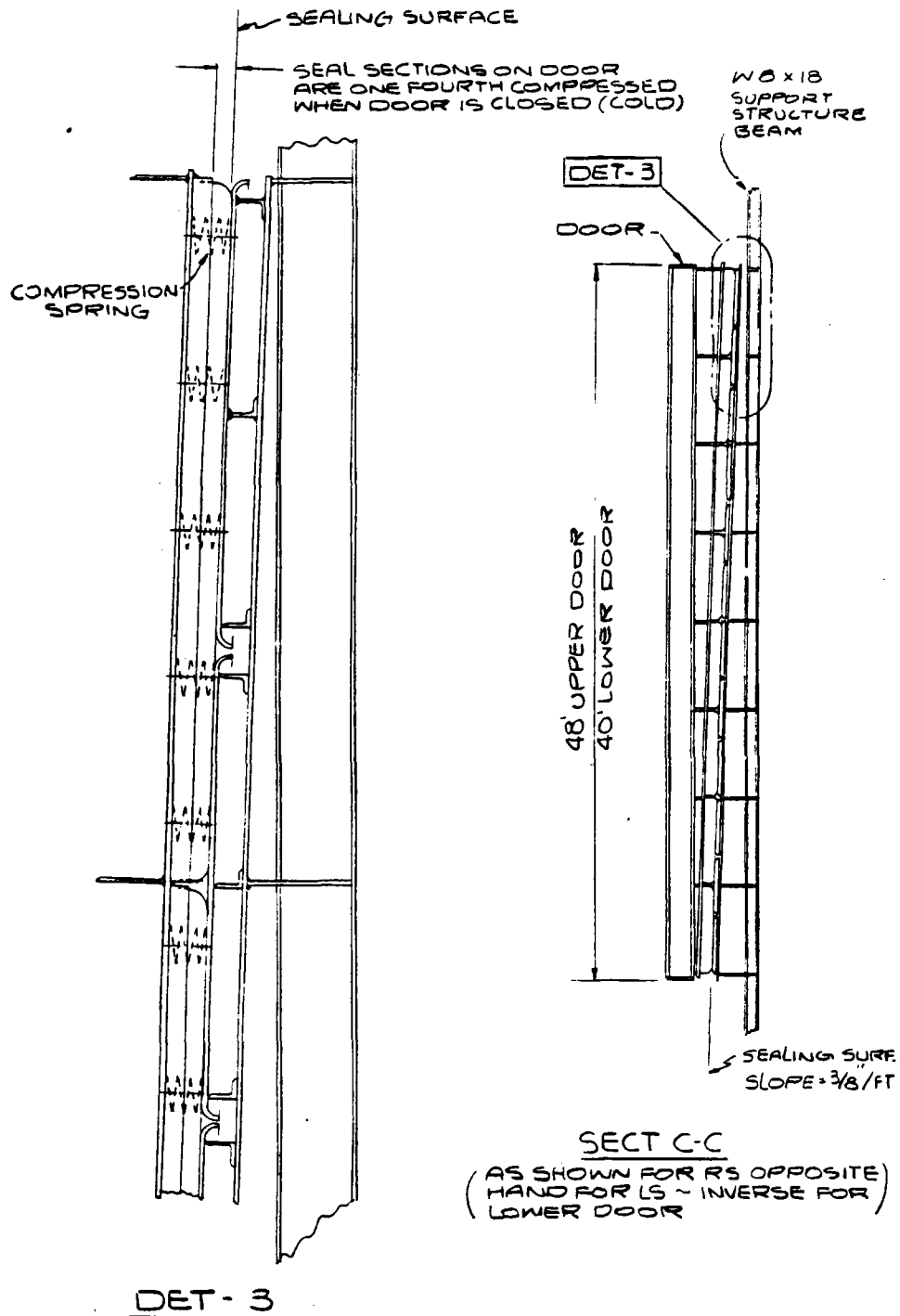


Figure 5.68 Side Seal of Aperture Door

are very conservative, but are justified because the door must be highly reliable. On this basis, the maximum deflection of the door (at the center, when bowing from side to side) is approximately 127 mm (5 in.), corresponding to a rotation of 2.5 deg at each end. These values are well within the acceptable limits for the type of construction being considered.

Key features of the door are summarized below:

- Fabricated truss plus corrugated sheet surface give light and rigid door.
- Maximum free area through door structure assists convection currents.
- Four-point spherical bearing attachment to trolleys eliminates binding because of distortion.
- Double seal minimizes convection losses when receiver is "bottled up."
- Short and direct load path exists from door rails to structural steel.
- Operation is simple and reliable compared with multiple-section or "up and over" doors.

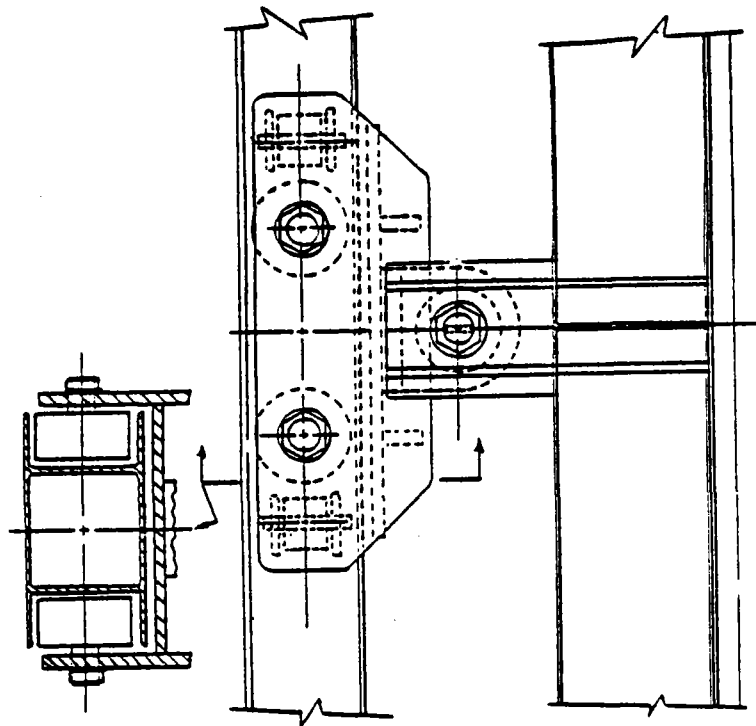


Figure 5.69 Side View of Door Trolley

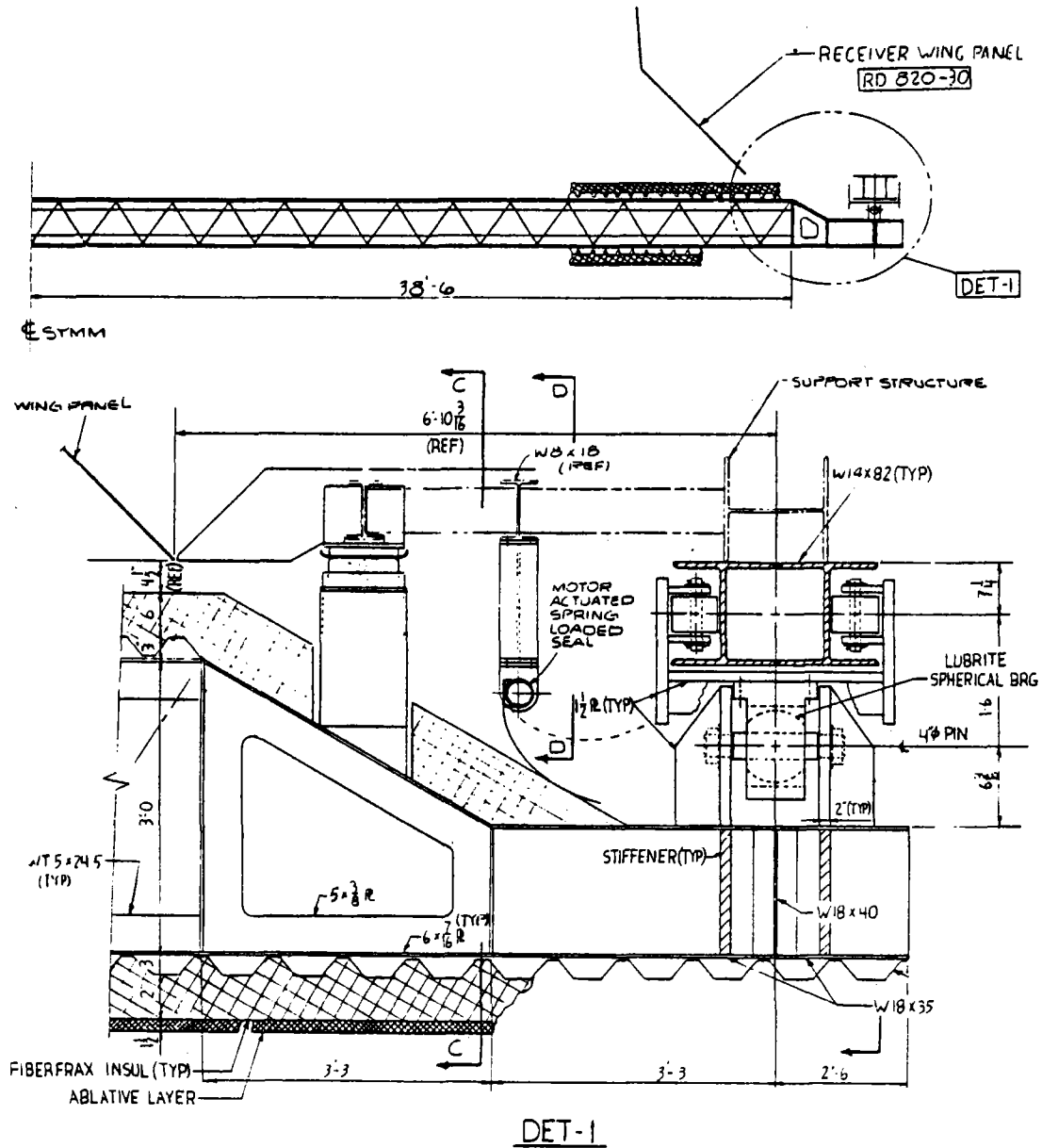


Figure 5.70 Plan View of Door Edge and Trolley (Right Side)

5.4.4 Receiver Support Structure

The receiver unit utilizes a skeletal structure to support the absorber and associated equipment (panels, piping, surge tanks, aperture door and door hoist mechanism, cavity floor and ceiling, service elevator, overhead crane, etc.). The structure surrounding the absorber on three sides is shown in Figures 5.71 and 5.72. It consists of six major functional elements:

- Door Support. The door is hung from the uppermost level of the structure.
- Bridge Crane Girder. A crane girder is also supported at the uppermost level of the structure.
- Absorber Support. The absorber panels are hung from the next lower level of the structure. This level also supports the top platform (Figure 5.73) and cavity roof.
- Access Platforms. There are two main platform levels (at top and bottom) and two intermediate platforms (Figure 5.71). They are reached by stairs and a service elevator. The cavity floor is supported by posts attached to the lowest platform. Portions of the roof and floor are removable so that panels can be removed.
- Guides. In addition to the support given by the platforms, horizontal loads on the receiver, including those from wind and earthquake, are absorbed by intermediate guides at three levels.
- Base. The steel structure is supported at four points by the concrete tower.

Loading Data.

Gravity. For a summary of weight components see Load Summary (Table 5.29). The roof and floor of the cavity weigh ≈ 1.20 kPa (25 lb/ft²), based on an estimated composition of decking, insulation, open joist support, and a post/hanger system. The live load of the floor was assumed at 4.79 kPa (100 lb/ft²) with a 50-percent reduction to columns. No uniform piping load on the platform was considered. Grating on platforms is estimated at 0.48 kPa (10 lb/ft²).

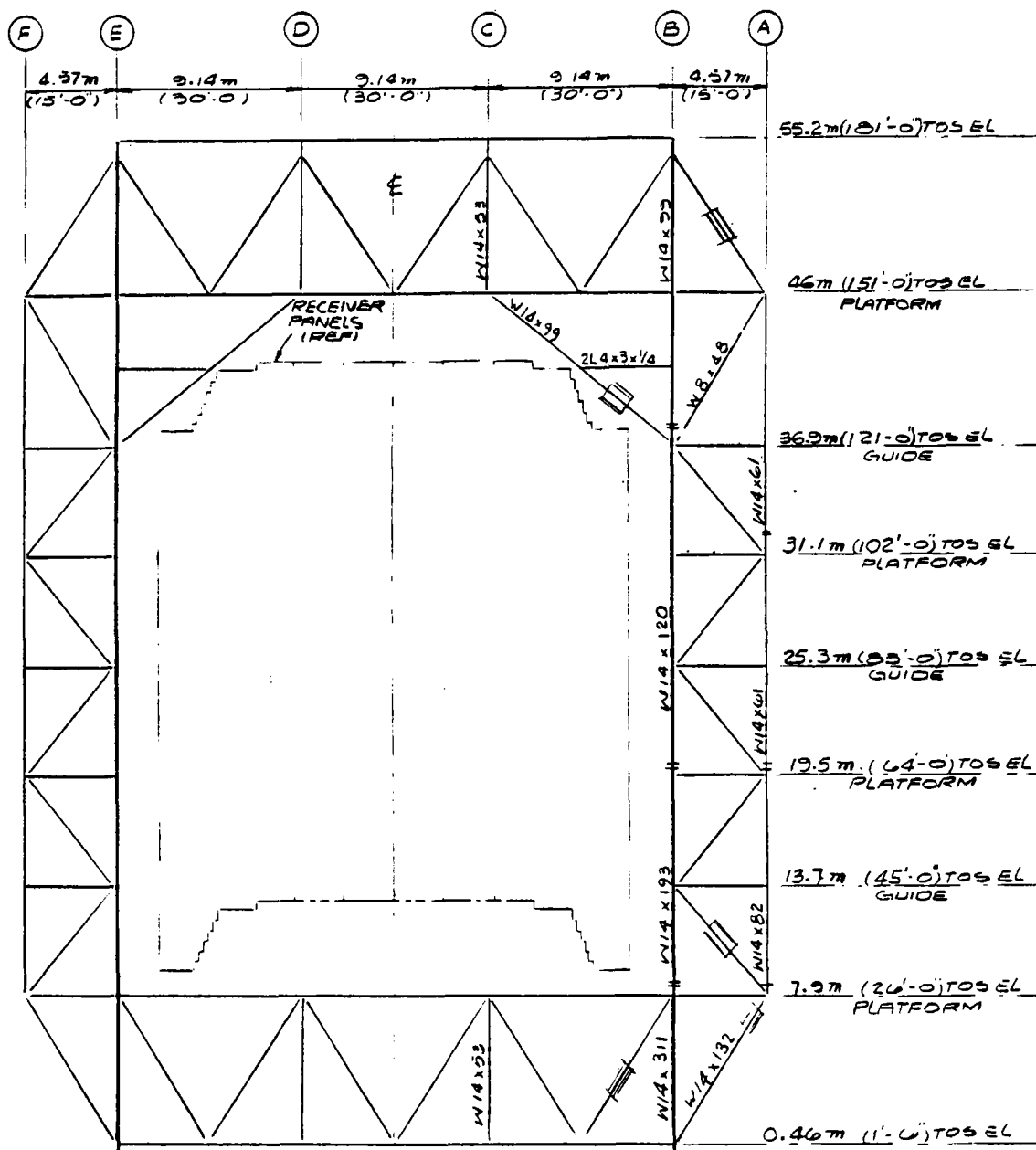


Figure 5.71 Front Elevation of Receiver Structure--Bent 1

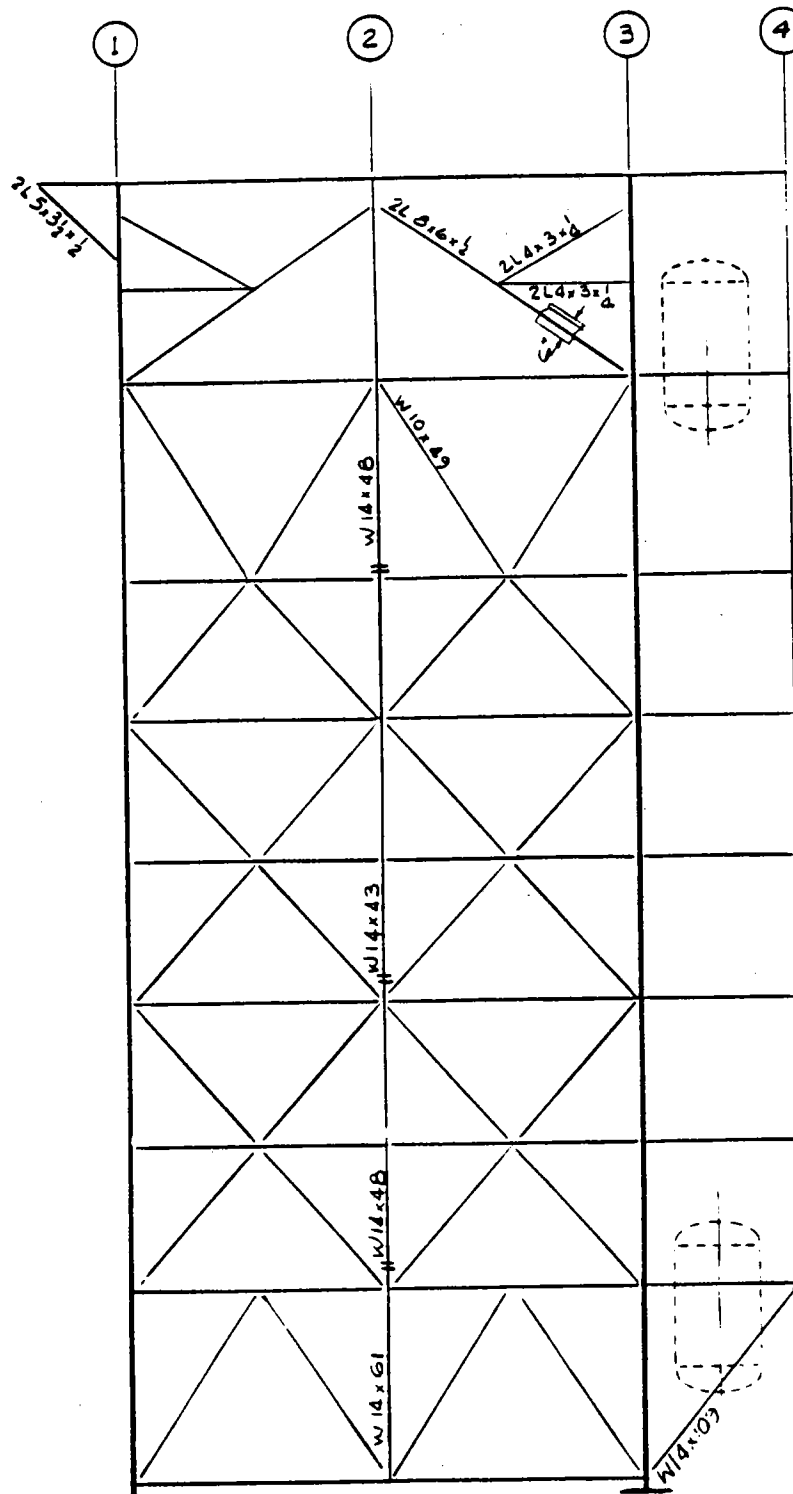


Figure 5.72 Side Elevation of Receiver Structure--Bents B and E

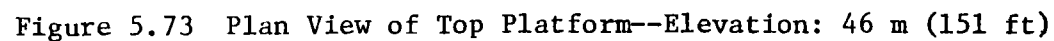


Table 5.29 Load and Reaction Summary, kip (1 kip = 6895 kPa)

Gravity	Bent				Total
	B1	E1	B3	E3	
A. Dead					
I. Structural					
Members	195	195	340	340	1070
Grating	5	5	30	30	70
Subtotal	200	200	370	370	1140
II. Nonstructural					
OST					15
IST					45
Panels and Piping					540
Roof					100
Floor					100
Door, Rail, and Machinery					200
Subtotal	250	250	250	250	1000
Total	450	450	620	620	2140
B. Live					
I. Structural					
Platforms	25	25	150	150	350
II. Nonstructural					
OST					150
IST					175
Panels and Piping					375
Subtotal	50	50	300	300	700
Total	75	75	450	450	1050
C. Dead and Live _{max}					
I. Structural	225	225	520	520	1490
II. Nonstructural					
OST					165
IST					220
Panels and Piping					915
Roof					100
Floor					100
Door					200
Subtotal	300	300	550	550	1700
Total	525	525	1070	1070	3190

Gravity	Bent				Total
	B1	E1	B3	E3	
D. Dead and Live (Earthquake)					
I. Structural	200	200	370	370	1140
II. Nonstructural					
OST					165
IST					220
Panels and Piping					915
Roof					100
Floor					100
Door					200
Subtotal	300	300	550	550	1700
Total	500	500	920	920	2840
E. Earthquake* (Operational)					
North-South ±V	300	300	650	650	1000
±H _{N-S}	150	150	350	350	
±H _{G-W}	10	10	10	10	
East-West ±V	650	650	650	650	1000
±H _{G-W}	250	250	250	250	
F. Earthquake* (Erect/Empty)					
North-South ±V	300	300	400	400	750
±H _{N-S}	150	150	225	225	
±H _{G-W}	8	8	8	8	
East-West ±V	500	500	500	500	750
±H _{G-W}	188	188	188	188	
G. Wind*					
North-South ±V	150	150	400	400	630
±H _{N-S}	85	85	230	230	
±H _{G-W}	5	5	5	5	
East-West ±V	650	650	650	650	1000
±H _{G-W}	250	250	250	250	

*V = Vertical
H = Horizontal

Earthquake. The assumptions for horizontal acceleration were refined after preliminary design, when the structural weight was determined. The weight drop favorably affected cost, since the magnitude of the horizontal acceleration at the top of the tower was decreased. A horizontal acceleration of 0.35 g was uniformly applied to the structure. This loading and the results of an elastic analysis were used to design members under allowable elastic stresses and deflections. An average ground-level acceleration of 0.25 g was used as input to the SNLL formulas^{1,2} for both concrete and steel towers. This approach was considered a reasonable method to produce a design that fairly approximated the receiver "survival" criteria. These loads produce reactions comparable to wind loading.

Wind. The following design data and assumptions were used in the wind analysis.

- ANSI A58.1 1972, Exposure C at 40.2 m/s (90 mi/h) = 2.63 kPa (55 lb/ft²)
- Shape factor
 - Receiver--1.3
 - Steel--2.0 for (net additional) exposed area (i.e., around receiver); solidity = 0.4
 - Tanks--0.8.

Receiver doors were assumed closed at maximum design wind speeds.

Major Design Considerations.

Location of Guides. Guide locations were based on a design assumption used for the panel strongbacks (i.e., a beam over three supports for horizontal loading). In addition, because the floor and roof masses need guiding for the forces of earthquake and wind acting on them, the uppermost guide is as close to the roof as possible and the lowest guide is close to the cavity floor. Thus

a staggered arrangement of platform, guide, platform, etc., developed, and it was considered for stair arrangements and bracing layout.

Structure Height. The overall height of the structure is determined by the upper travel limit of the "guillotine" door. The structure extends above this highest point, and a hanging door support cable system is employed. A bridge crane runway and machine room for the elevator are located at the top level of the structure (Figure 5.63).

Column Location and Orientation. Initial design criteria included a structure supported at four points, since it was redundant to have additional supports, and fewer than four was impractical. Thus a rectangular plan was chosen with intermediate columns at approximately 9.1 m (30 ft) on center, based on span restrictions for framing members. Preliminary analysis showed that axial loads in struts were larger on Bents 1 and 3 (Figure 5.72) and therefore eccentricity in the bottom struts was to be avoided. We decided to orient the strong direction of the major columns (B1, B3, E1, and E3) along these bents so that columns instead of struts take the eccentricity moment caused by vertical bracing work points. In the other direction, the struts have been designed for an eccentricity moment, and no weak axis bending occurs in the columns.

Receiver Panel Lifting. A basic design concept called for the weight of the receiver to be taken via hangers to a support level above. The 20 individual panel/strongback subassemblies are supported by hangers. Each subassembly can be removed through the center of the receiver/tower by an overhead bridge crane, which must travel across the cavity, pick up each subassembly and lower it through the center of the receiver. The requirement that the center

of the receiver remains clear for panel removal is met at the 43 m (141 ft) panel support elevation because we do not anticipate that the bridge crane will necessarily have to cross either Bent 2 or the receiver centerline; thus struts on these lines can be used to brace the panel support girders near their midpoint. At the lowest two levels of the structure, a 9.1 m (30 ft) square opening is provided.

Bracing. Initially, braced bents seemed to be the most cost-effective way to handle horizontal loads. As originally conceived, two bents in each direction straddled the cavity, with an additional, completely braced bent on the side of the tanks away from the cavity, transverse to the receiver centerline. Since horizontal loads are transmitted by horizontal braces across to Bent 3, most of this additional bracing was eliminated, saving considerable cost. As verified by computer analysis, gravity loads are taken by vertical bracing from the intermediate columns to main columns on Bents 1, 3, 4, B, and E, eliminating the need for bending members to transfer these loads to the main columns. Additional gravity loading transmitted by these braces does not substantially affect their design.

Originally conceived for a sloping receiver, a "U" shaped structure was investigated. It had two "wings" tied to a strong "back-bone" that was torsionally stiff enough to transmit transverse horizontal loads to one vertical bent with two side bents straddling the receiver to resist the torsional couple. This system was not used after computer analysis proved the feasibility of a "box" system, avoiding the increased cost of the heavy horizontal bracing required for the "U" system. Any concern about deflection interaction of

Bents 1 and 3 through the horizontal truss guide was eliminated when computer analysis showed that both bents deflect almost equally, assuming horizontal shear is shared between them and such deflection is limited to 0.5 percent of the total structure height (see Figure 5.74).

Key features of the receiver structure are:

- Four major support columns comprising part of the four major braced bents
- Bent arrangement that minimizes torsional loading on rear of structure
- No obstruction to lifting and positioning of panel modules
- A service crane to complete receiver installation when basic structure is erected.

5.4.5 Cavity Floor and Ceiling

The cavity floor and roof (Figure 5.75) are uncooled surfaces consisting of 102 mm (4 in.) of duraboard Fiberfrax weatherproof insulation anchored to carbon steel plate. The duraboard insulation is a rigid, high-temperature material. It was selected because of its strength and rigidity. It will stand up to the handling involved during maintenance. The floor and roof are made of sections that can be lifted out by the overhead crane to permit removal and replacement of the absorber panels through the center of the receiver/tower structure.

A flexible seal between the floor and absorber panels (Figure 5.76) minimizes thermal losses from the cavity. A seal is also required between the ceiling and the panels but it need not be flexible because the tops of the absorber panels are fixed. As stated in the previous section, the roof is hung from the upper main platform. The floor is supported by posts from the lowest platform (Figure 5.77).

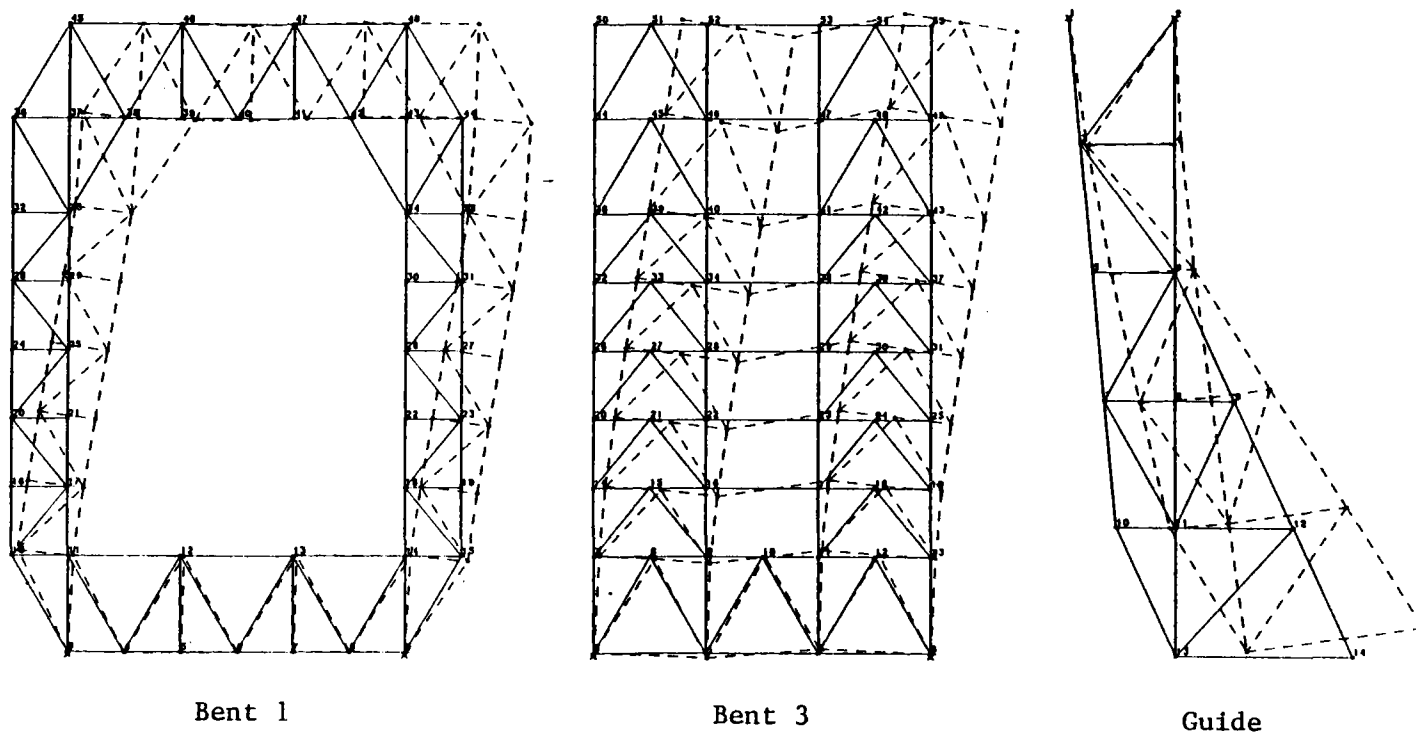


Figure 5.74 Deflection Analysis of Receiver Structure

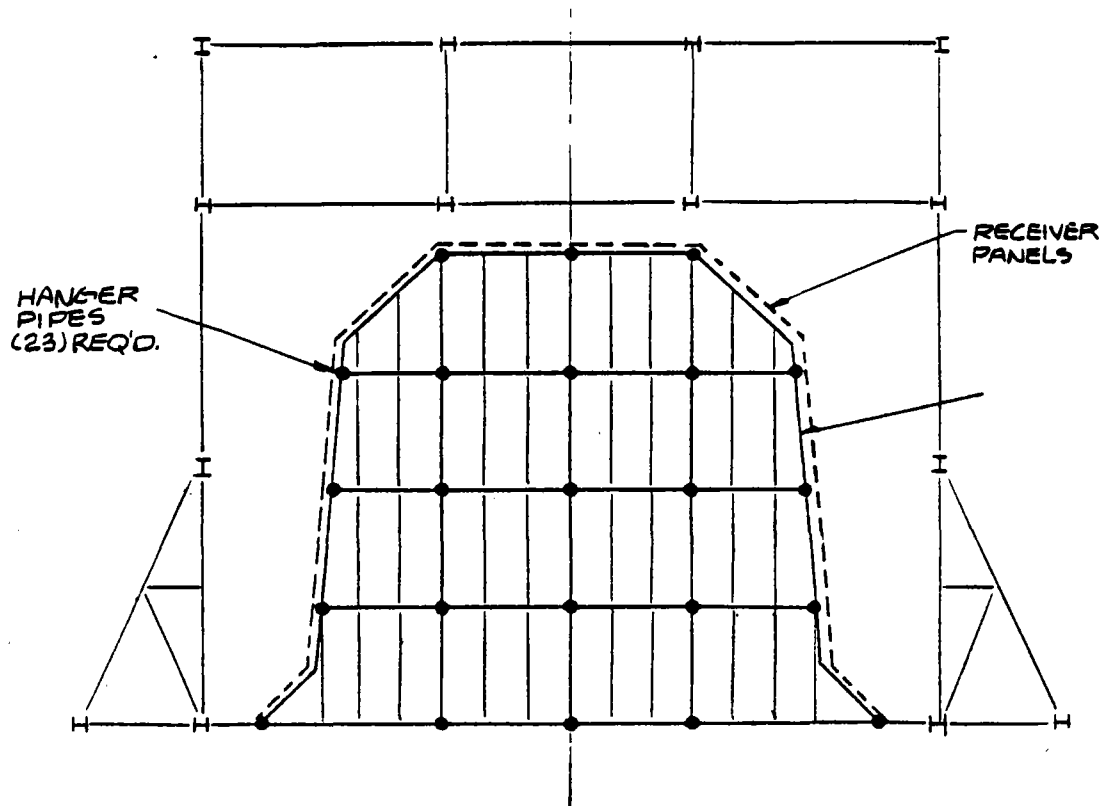


Figure 5.75 Plan View of Cavity Floor/Roof

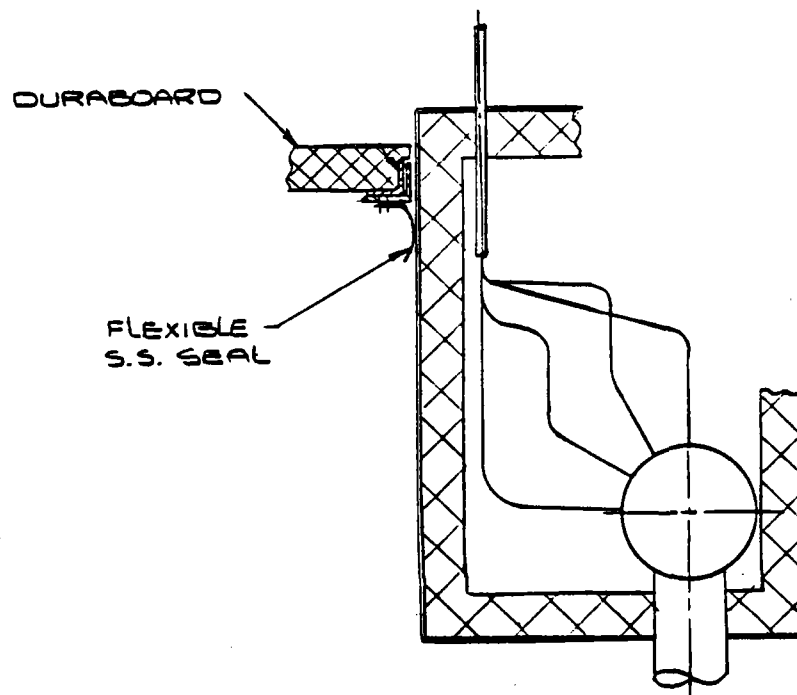


Figure 5.76 Seal Between Cavity Floor and Absorber Panels

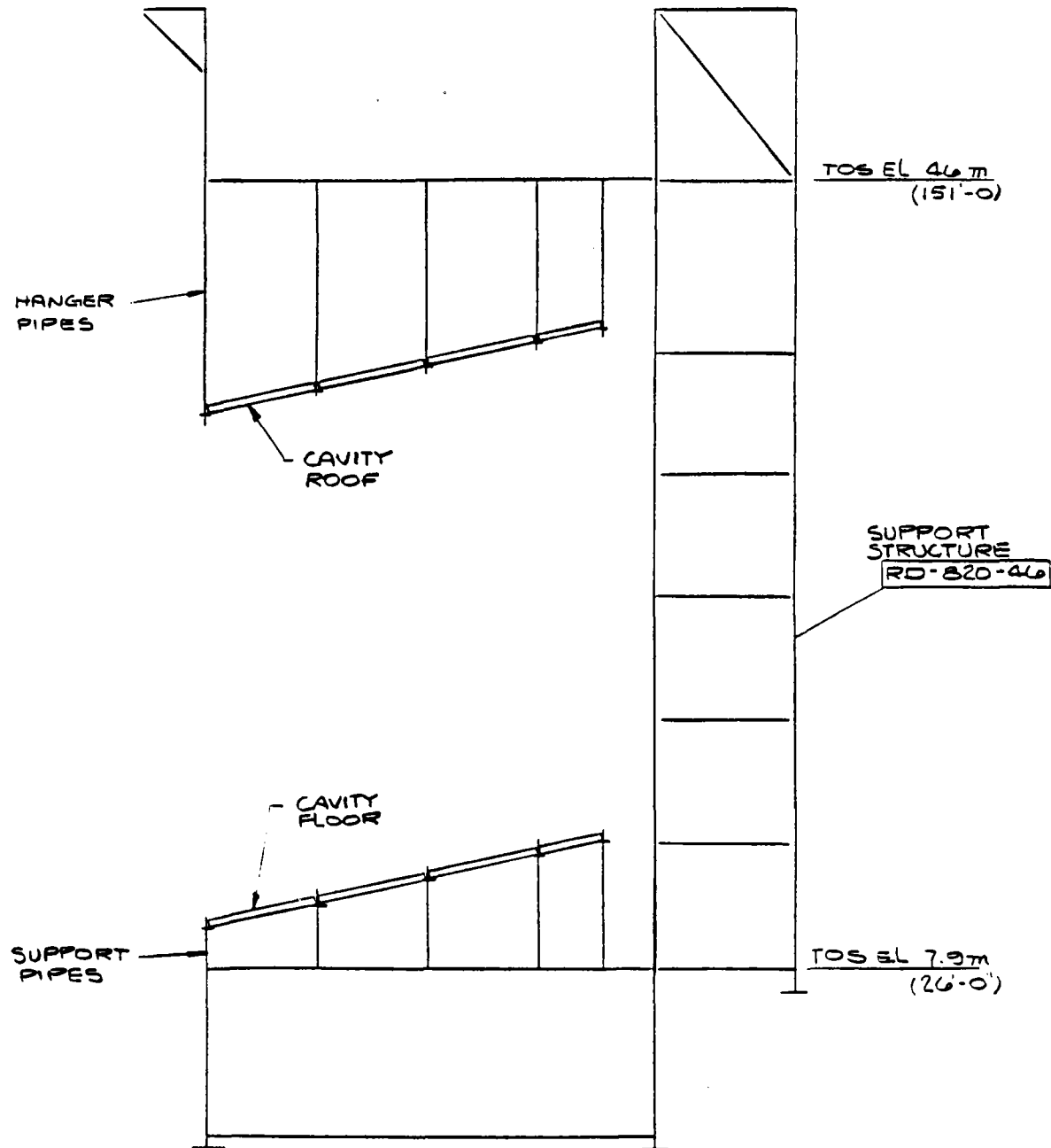


Figure 5.77 Attachment of Cavity Roof and Floor to Structure

5.4.6 Receiver Tower Design

The objective of this task was to select and design the receiver tower configuration that would be most cost-effective and would meet the design requirements while utilizing accepted construction practice. The main design requirements for the receiver tower are:

- Support for receiver weighing $\approx 1,300,000$ kg (2,860,000 lb)
- Receiver displacement in wind that does not exceed 1 m (3.3 ft)
- Support for the riser and downcomer piping
- Access to the receiver and piping for maintenance and absorber panel removal through the center
- Tower 200 m (656 ft) high
- 30-year life
- Lightning protection and aircraft warning
- Soil-bearing capacity (Barstow data)
- Site: Barstow, California
- Structural integrity during the following postulated survival seismic and wind conditions:
 - Wind speed: up to 40 m/s (90 m/h) at 10 m (33 ft) reference elevation
 - Earthquake: 0.25 g peak ground acceleration (UBC Zone 3)
 - Temperature: -30 to +50°C (-22 to +122°F)

The following loads were used for the conceptual design of the tower and its foundations:

- Dead Loads. These include weights of framing and permanent equipment such as receivers, piping, and controls.
- Live Loads. These are superimposed loads from use and occupancy (not including wind, earthquake, or dead loads).

- Wind Loads. These are based on wind speeds of 16 m/s (36 m/h) under operating conditions and 40 m/s (90 m/h) under survival conditions at a reference height of 10 m (33 ft) above ground. Wind loads are calculated in accordance with the requirements of ANSI A58.1.
- Seismic Loads. A peak ground acceleration of 0.15 g under operating conditions and 0.25 g under survival conditions was used. The tower was assumed to be located in UBC Zone 3. This peak ground acceleration was combined with the response spectrum given by NRC Req. Guide 1.6 and damping values given for the operating basis earthquake in NRC Req. Guide 1.61.

Conceptual designs were made for construction of steel and concrete towers (Figures 5.78 and 5.79). Results of tower cost analyses for these two concepts are given below. These results were confirmed using the SNLL tower cost equations,² which are based on studies performed by Stearns Roger.³

<u>Item</u>	<u>Concrete (10⁶\$)</u>	<u>Steel (10⁶\$)</u>
Tower	1.693	3.470
Foundation	1.75	3.167
Total	4.679	8.695

The concrete tower, constructed of reinforced concrete and utilizing slip-form techniques, was selected for the following reasons:

- Less expensive--by a factor of nearly two.
- Lower operating and maintenance costs.
- More construction experience. There are more than a dozen towers, equally high, that have been constructed using slip-form reinforced concrete. This technique is widely used in concrete chimneys and cooling towers for power plants.

5.4.7 Riser/Downcomer Piping

The design requirements for the riser/downcomer piping were taken from the RS Requirements Specification (Appendix B); they are summarized in Table 5.30.

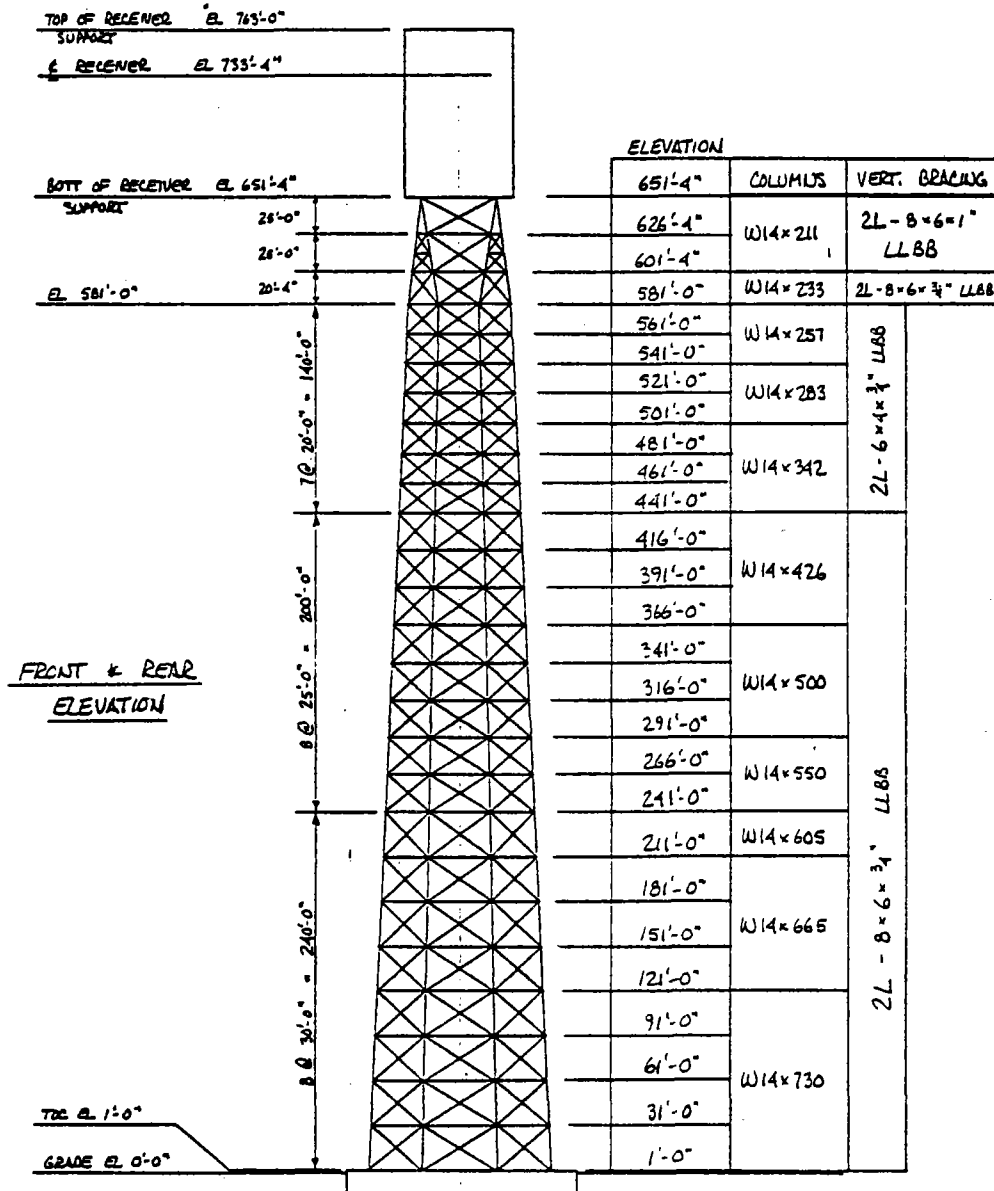


Figure 5.78 General Arrangement of Steel Tower

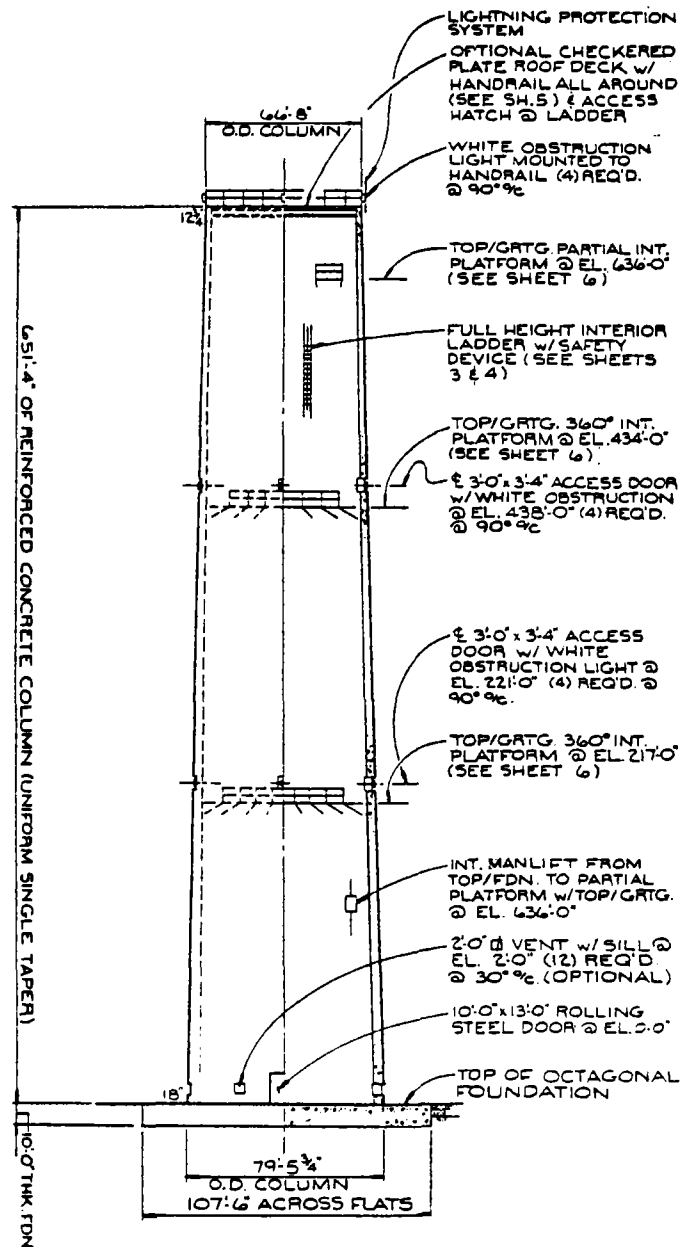


Figure 5.79 General Arrangement of Concrete Tower

Table 5.30 Riser/Downcomer Piping Characteristics

Characteristic	Riser	Downcomer
Design pressure MPa gage (lb/in ² g)	6.9 (1000)	4.1 (600)
Design temperature °C (°F)	316 (600)	593 (1100)
Material	SA-106-B	SA-376-304H
Code	ANSI B31.1	ANSI B31.1
Size, m (ft)	0.41 (16) Sch 60	0.3 (12) Sch 10 top Sch 80S bottom
Weight, kg/m (lb/ft)	161 (108)	97 (65)
Insulation type	Calcium silicate	Calcium silicate
Insulation thickness m (in)	0.15 (6)	0.10 (4)

The primary riser was sized to minimize combined costs for both pumping and piping. Piping costs increase as pipe size increases; conversely, pumping costs decrease as pipe size increases. Pipes from 0.25 m (10 in.) to 0.64 m (25 in.) O.D. were investigated, and the optimum pipe was found to be 0.41 m (16 in.) O.D. Since pumping costs are independent of downcomer size, the downcomer was sized to dissipate a large percentage of the gravity head at the design flow rate. A 0.30 m (12 in.) O.D. was selected; it will dissipate 75 percent of the gravity head by friction. The remainder is dissipated by the drag valve.

Piping materials were selected based on results of the material selection (Section 4.3.3). The carbon steel riser carries cold salt at 288°C (550°F). The Type 304SS downcomer carries hot salt at 566°C (1050°F). Piping wall thickness was calculated in accordance with the ANSI B31.1 Power Piping Code. Insulation thickness was chosen from Foster Wheeler design manuals.

The design salt flow rate was used to size the riser/downcomer pipes. It is a conservative assumption, since the average salt flow rate will be less than the design value. The riser design pressure was calculated by adding the salt gravity head and friction losses (receiver and riser) to the operating pressure of the OST [105 kPa gage (15 lb/in²g)] and then adding 5 percent as a design margin.

5.5 OPERATION ANALYSIS

The analysis of operation described in this section is based on the normal and emergency operating modes described in detail in the RS Requirements Specification (Appendix B).

5.5.1 Operating Modes

The plant must be capable of starting up from an ambient or hot 288°C (550°F) condition, collecting energy by heating molten salt flowing through the receiver, and shutting down at night without draining. It must also be able to stop and start during various weather conditions and to drain and shut down for extended periods. To accomplish these objectives, the system can operate in six modes. All operations are executed by changing mode, as illustrated in Figure 5.80.

Cold Drained. The entire salt inventory is in the CST. All other components are at ambient temperature. Heliostats are stowed. The system is in this mode before initial start-up, during extended shutdowns, and for various repair or maintenance operations.

Hot Drained. The condition is similar to the preceding mode, but electric heaters keep the salt-loop temperatures at ≈288°C (550°F) and the sump pump tank is filled. The system must be in this mode before the piping can be filled with molten salt.

Hot Standby. The entire salt loop is filled with salt at about 288°C (550°F), and heliostats track the standby aim points. In this mode the system is prepared to begin flow for energy collection or to shut down for the night.

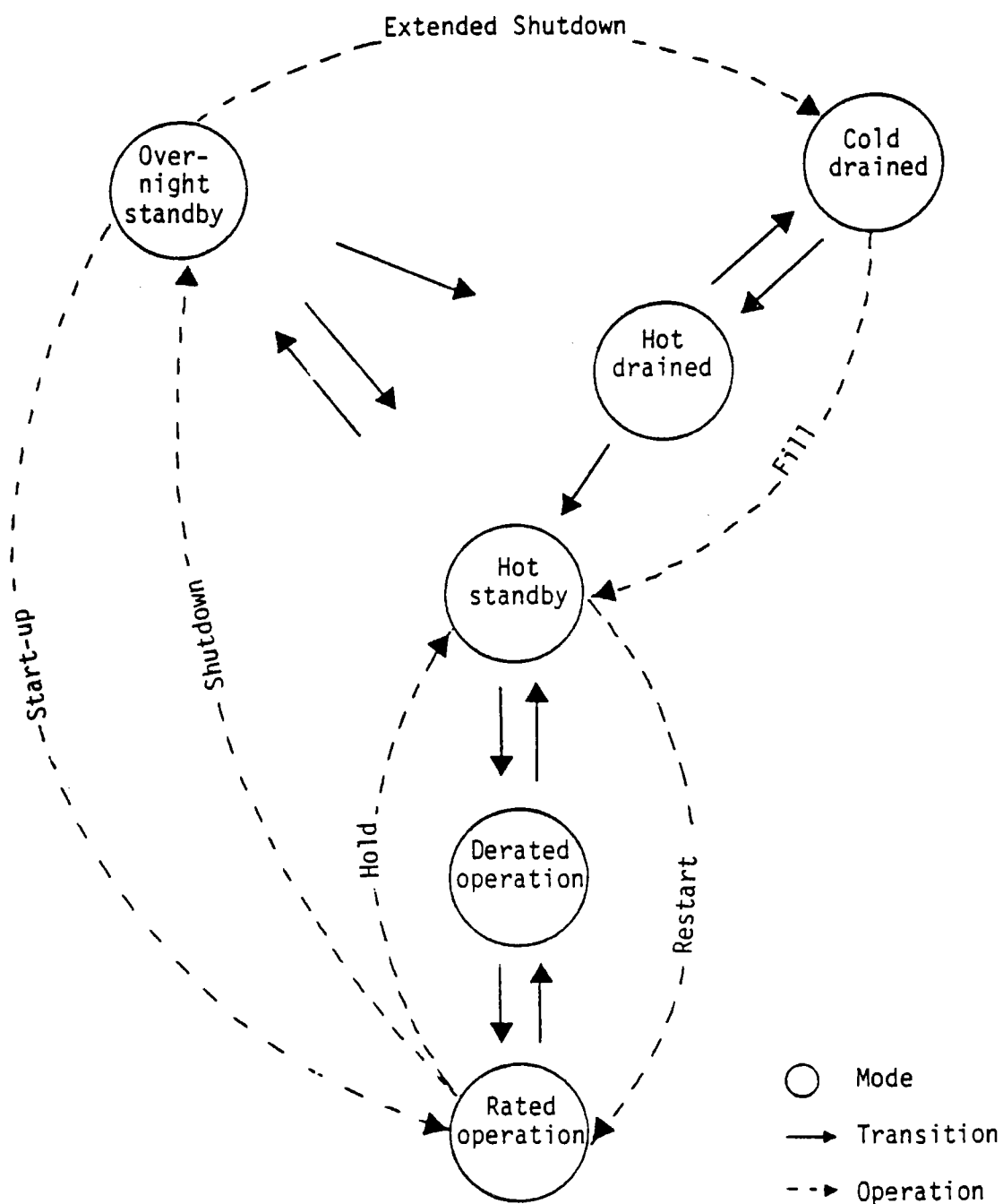


Figure 5.80 Operating Modes and Transitions

Derated Operation. Heliostats track receiver aim points. Molten salt is pumped through the receiver, but flux levels are not high enough to produce rated outlet temperatures, and flow is diverted back to the CST.

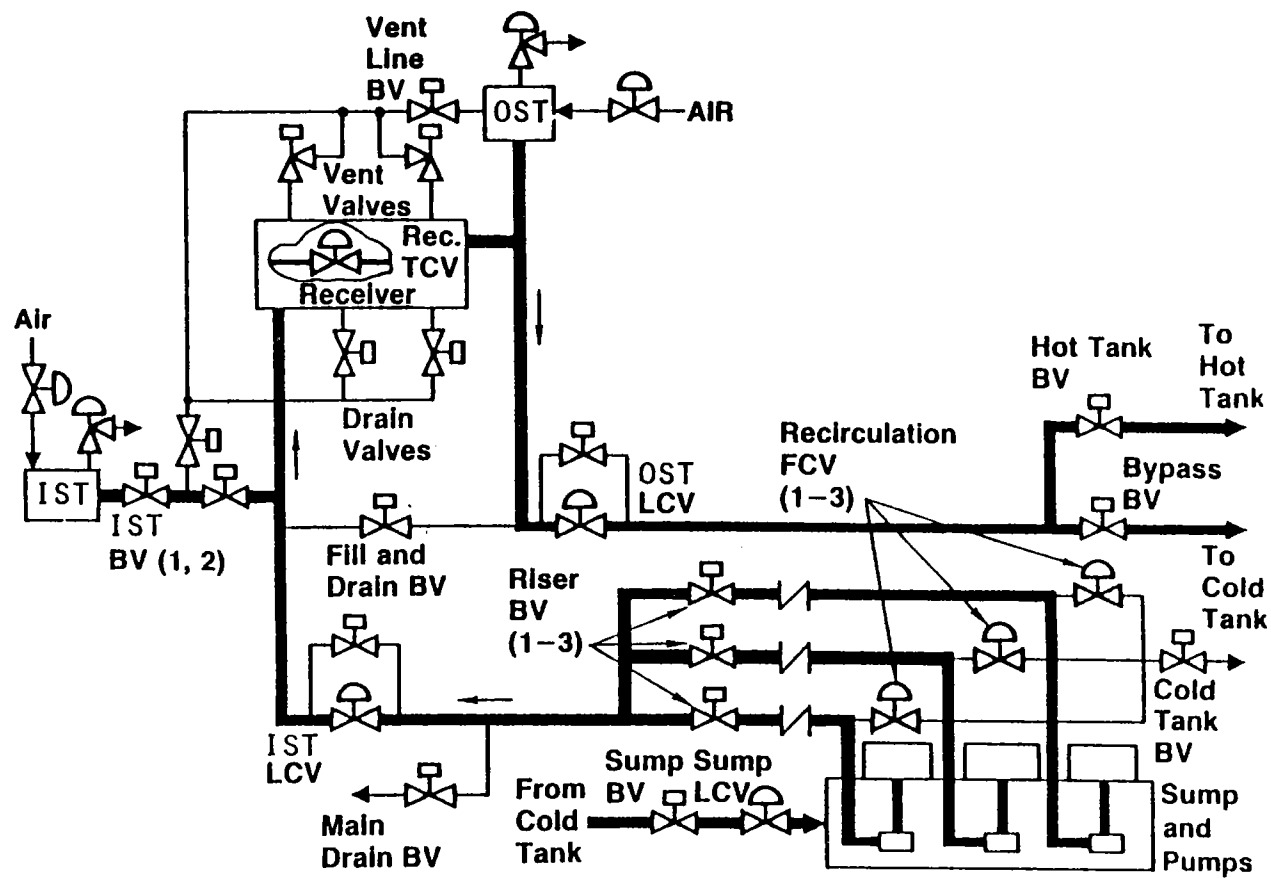
Rated Operation. This is the normal operating mode for energy collection. Flow through the receiver is controlled to maintain an outlet temperature of 566°C (1050°F) and is discharged to the HST.

Overnight Standby. Salt flow is stopped, and the system is bottled up. Electric heaters keep salt-loop temperatures at ≈288°C (550°F) so that morning start-up can begin as soon as adequate insolation is available. If required, the system can be drained from this mode.

An operating schematic, Figure 5.81, shows the location of pumps and valves used to control plant operation. In addition to pumps and valves, the heliostats, electric heaters, and aperture door are controlled. The state of the critical components during each mode is given in Appendix P. The control valves, which are normally open when deactivated, must be commanded to the closed position ("Closed"), if required. When activated, the parameter being controlled is indicated (e.g., level, temperature). All electric heaters are thermostatically controlled to maintain parts in contact with salt at ≈288°C (550°F).

5.5.2 Mode Transitions

To perform various operations, the system must change from one mode to another. The sequence of events used to accomplish these transitions is given in Appendix P. The available transitions follow.



BV Bypass Valve
LCV Level Control Valve
TCV Temperature Control Valve

Figure 5.81 Operating Schematic

- Cold drained to hot drained
- Hot drained to hot standby
- Hot standby to derated operation
- Derated to rated operation
- Overnight standby to hot standby
- Rated operation to derated operation
- Derated operation to hot standby
- Hot standby to overnight standby
- Overnight standby to hot drained
- Hot drained to cold drained

5.5.3 Major Operations

As indicated in Figure 5.80, various operations are accomplished by cycling through the modes using the transition sequences described in Section 5.5.2. The major operations are:

Fill. The fill operation completely fills the salt loop and prepares the system for salt flow and energy collection. Cavity radiant heaters or selected heliostats preheat the receiver panels. This operation takes place during the initial plant start-up as well as during restarts from extended cold shutdowns. The transitions are as follows:

Cold drained → Hot drained → Hot standby

Restart. Restart brings the system back on line for energy collection. This is the secondary operation for a cold start-up, but it is used primarily to resume operation from temporary standbys resulting from poor weather. The following transitions are required:

Hot standby → Derated operation → Rated operation

Hold. Daylight cloudy periods will cause the system to transfer to hot standby until the weather clears or the sun falls below 10 deg elevation. Transitions are just the reverse of a restart.

Start-Up. A normal start-up occurs every morning when the weather is good. The loop is maintained at $\approx 288^{\circ}\text{C}$ (550°F) at night. The heliostats are brought to standby. Flow is begun and the heliostats track receiver aimpoints. When outlet temperatures reach 566°C (1050°F), flow is diverted to the HST. Transitions are:

Overnight standby \rightarrow Hot standby \rightarrow Derated operation \rightarrow Rated operation

Shutdown. Daily shutdowns occur as insolation levels fall below acceptable collection values. Essentially the opposite of a start-up, flow is first diverted to the CST and finally terminated. Heliostats are stowed, and the receiver is bottled up. When the panels cool to 343°C (650°F), salt from the OST is drained to selected receiver panels, forcing cooler salt to the IST. Electric heaters maintain temperatures above freezing until start-up is begun. The transitions are as follows:

Rated operation \rightarrow Derated operation \rightarrow Hot standby \rightarrow Night standby

Extended Shutdown. If the system must be cooled to ambient temperature because of a failure or for maintenance, this operation is initiated. Salt is drained from the system, and all heaters are turned off. The sequence is as follows:

Night standby \rightarrow Hot drained \rightarrow Cold drained

5.5.4 Emergency Operations

Single failures result in automatic procedures to prevent equipment damage in the safest manner while minimizing down time. In most cases the system is placed in a standby mode to assess the problem. It can then be put in a

drained mode for repair, or restarted if the situation can be resolved while in a hot condition. Single failures are assumed to occur during rated operation. The emergency sequence is shown in Appendix P.

Loss of Receiver Flow. If flow through the receiver is lost or substantially reduced with heliostats focused on the receiver, excessive salt and tube temperatures with possible tube failure or shortened life may occur. A loss of flow could result from several sources:

- Salt flow control loss
- IST pressure loss
- Power/salt pump failure
- Receiver piping/tube failure

Salt Flow Control loss. Flow to the receiver could be blocked by a failure of the control system, which closes the riser block valve or control valve. Although the valves fail open, they may also stick in a semiclosed condition. This condition is sensed by a rapidly falling IST level and pump outlet flow rate. The flow is continued from the IST while the heliostats are defocused.

As in inlet flow failure, a similar condition could result in the flow path from the receiver to the HST. In this case, a rapidly rising OST level causes heliostats to be defocused and the door to be closed. The IST is then vented and the pumps are tripped.

IST Pressure Loss. A loss of pressure in the IST would most likely be the result of a vent valve failure, but could result from a ruptured tank. An excessive rise in IST level or panel tube temperatures, or drop in

IST pressure initiates the emergency sequence. Heliostats are defocused, and the door is closed while the IST is isolated. Flow continues until the system is brought to standby.

Power/Salt Pump Failure. If salt flow is stopped because of a power failure or the failure of two pumps, the aperture door will close by gravity. An ablative cover protects the door until an emergency generator can supply power to defocus the heliostats or until the earth's rotation moves the incident solar flux away from the receiver aperture. If a single pump fails, a spare pump starts without discontinuing operation.

Receiver Piping/Tube Failure. A ruptured pipe or tube reduces downstream salt flow and results in excessive tubewall temperatures and loss of salt. These temperatures, in addition to flow and pressure fluctuations, cause the heliostats to defocus and the aperture door to close. Receiver flow is stopped as rapidly as possible so that the receiver can be drained.

Loss of Heliostat Field Control. In the event of a heliostat field failure, the maximum salt flow is passed through the panels to prevent overheating. Operating heliostats are focused away from the receiver. Panel and salt temperatures are monitored to determine whether an unsafe condition exists that requires closing of the receiver door.

5.5.5 Operating Timelines

Timelines are presented in Appendix P for the following major operations:

- Fill. This operation allows the system to be transferred from an ambient condition to a hot standby mode. From this mode, the plant can proceed to rated operation or overnight standby.

- Start-Up. This operation is required every morning when the weather is good. The plant is brought from an overnight standby condition to a fully operational state for energy collection.
- Shutdown. At night or when weather prevents further energy collection, the plant is placed in an overnight standby mode and maintained at 288°C (550°F).
- Extended Shutdown. To drain the system and cool it to an ambient condition free of salt, this operation is implemented. A small drain system empties lines blocked by check valves and drains the sump below the impeller level.

5.6 CONTROL ANALYSIS5.6.1 RS Control System

Introduction. The RS control system has two primary functions:

- To maintain a constant outlet temperature during normal operations
- To operate and protect the receiver during transient and emergency conditions such as start-up, shutdown, and feed-pump failure.

Because of input power and flux distribution changes caused by diurnal and meteorological conditions, an active control system must vary receiver flow rate to maintain a constant outlet temperature. Additionally, because of the long flow paths and flow times, this control system must receive feed-forward information to anticipate outlet temperature changes before they are actually detected by the outlet temperature sensors. Outlet temperature control and some preliminary simulation results are presented later in this section.

The proposed control system is based on the distributed digital system successfully developed for Solar One at Barstow. All process control elements for the RS are centralized in a common control room using shared color CRTs. Figure 5.82 is a block diagram of a typical control-valve scheme in the process control system. It is representative of any control loop. Details of the receiver control loops are presented later in this section.

Control and display are centralized at a color picture tube with piping and instrumentation diagram, historical trending, and alarm summary graphic displays for ease, fast response, and reliability of operator actions. Data multiplexing and digital transmission significantly reduce the amount of copper wire needed and electricians' labor.

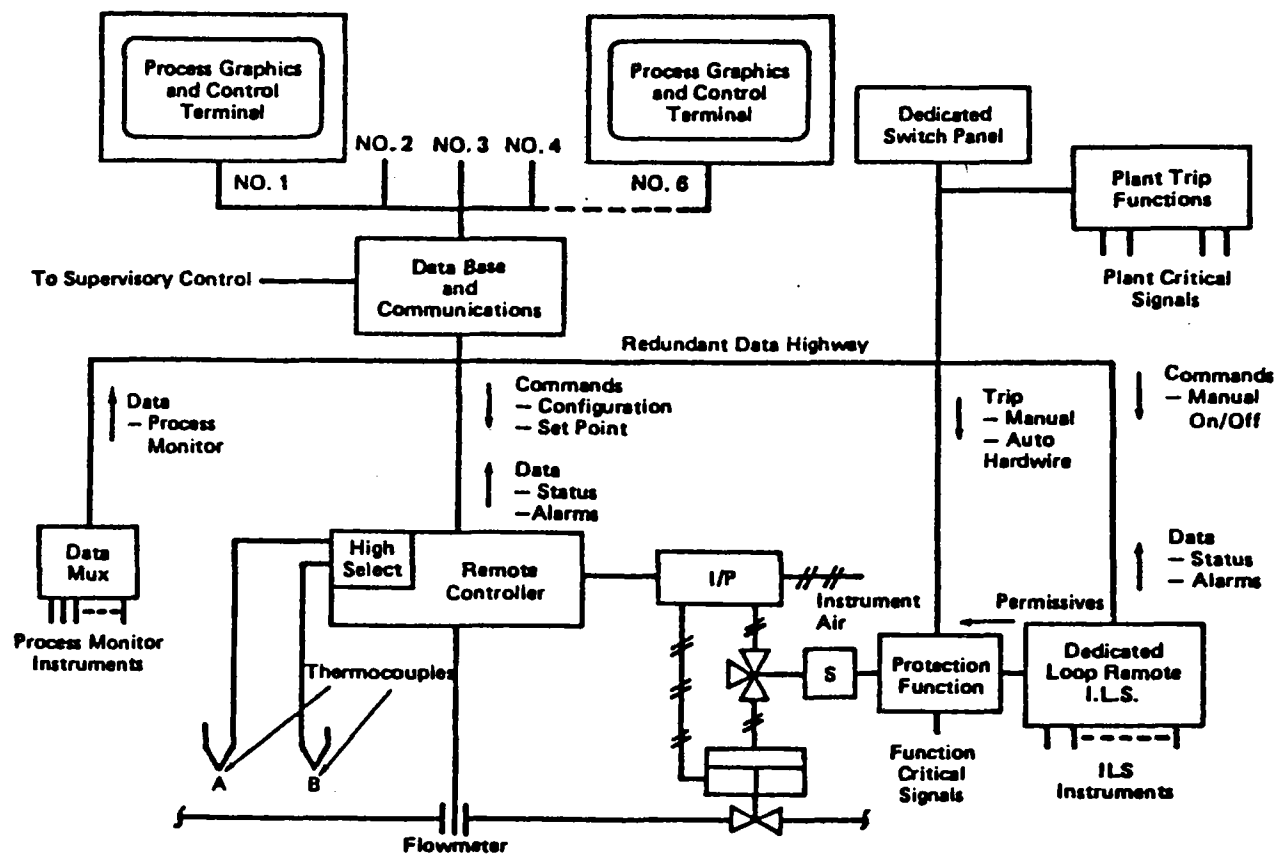


Figure 5.82 Process Control Elements

Key instruments are installed in redundant pairs with electronic circuitry capable of selecting the functional instrument. Electronic redundancy is used in data transmission process controllers and logic.

Loop controllers are microprocessor systems which accept analog sensor data, process it digitally, and send analog signals to the valve actuators. These controllers, used on Solar One, have proved highly reliable.

Functional Description. During normal energy collection operations, the RS control system uses a valve to control IST level, four parallel valves to control outlet salt temperatures, and a drag valve to control OST level. It also operates a level control valve at the inlet to the RS sump pump tank and regulates cover gas pressure in the IST and OST and the sump pump tank.

If the RS control system is unable to maintain design outlet temperature at 25 percent of design flow rate during low-power operation because of clouds or low insolation, the RS is changed to alternative flow control. As a result the flow rate is increased to 30 percent of design value and the outlet temperature drops below 538°C (1000°F). In alternative flow control, the temperature control valves are used solely to control flow rate at 30 percent of design value as long as the outlet temperature remains below 538°C (1000°F). Should the outlet temperature rise above 538°C (1000°F), the flow rate is decreased to bring it back to 566°C (1050°F) and the RS reverts to normal energy collection operation.

During overnight operations, the RS control system must monitor system temperatures to protect against salt freeze and must operate valves and modulate surge tank pressures to permit salt flow from the OST into the absorber panels.

Finally, the RS control system must sequence valves, pumps, receiver door operation, and thermal conditioning heaters during start-up, shutdown, and emergency transients. Detailed sequences of events and timelines are presented in Appendix P.

RS control variables and setpoints are given in Table 5.31. RS equipment with on-off control is listed in Table 5.32.

Table 5.31 RS Control Variables and Setpoints

<u>Control Variable</u>	<u>Nominal Setpoint</u>	<u>Setpoint Range</u>
Outlet temperature, °C (°F)	565 (1050)	287 to 565 (500 to 1050)
IST Pressure, kPa gage (lb/in ² g)	2410 (350)	Atmospheric to 2586 (375)
Level	Half full	1/4 to 3/4 full
OST Pressure, kPa gage (lb/in ² g)	103 (15)	Atmospheric to 207 (30)
Level	Half full	1/4 to 3/4 full
Thermostatic controls for radiant, immersion, and trace heaters, °C (°F)	293 (560)	288 to 316 (550 to 600)
Salt flow rate, kg/s (10 ⁶ lb/h)	---	0.0 to 836 (0.0 to 6.6)

Table 5.32 RS Equipment With On-Off Control

- Salt feed pump motors (3)
- Aperture door activation system
- Flow diversion valve for diverting outlet flow to CST
- HST inlet blocking valve for diverting outlet flow from HST
- Drag valve bypass-line blocking valve
- IST level control valve bypass-line blocking valve
- Pump outlet blocking valves (3)
- Riser drain line blocking valve
- Pump sump inlet blocking valve
- Pump recirculation line blocking valve
- Drain line to surge tank blocking valve
- Riser-downcomer drain/fill interconnect blocking valve
- Air cover gas blocking valve for OST
- Air cover gas blocking valve for IST
- Air cover gas blocking valve for sump pump tank
- Absorber salt drain valves (10)
- Absorber salt vent valves (13)
- High-pressure air compressor motor with high-/low-pressure switch control
- Shop/instrument air compressor motor with high-/low-pressure switch control.

Elements. The RS control system includes instruments, wiring, electronic controllers, logic and protection, and equipment that interfaces with the plant control system.

Table 5.33 lists the RS control areas and the types of control involved. Figures 5.83 through 5.85 show the detailed control block diagrams for salt outlet temperature and for surge tank (accumulator) pressure and level control. Table 5.34 summarizes the number and types of control instruments.

The primary interface with the plant control system is at the data highway J-boxes.

Table 5.33 Types of Control

<u>Area</u>	<u>Analog Control Loops</u>	<u>Interlock Logic Loops</u>	<u>Independent Protection Loops</u>
Salt pumps	Accumulator level control (2 loops)	On/off to master control Cooling Lubrication Recirculation valves Miscellaneous (12 loops)	Pump shutdown (2 loops)
Surge tanks (Accumulators)	Pressure control (4 loops)	Level/pressure (2 loops)	
Salt tempera- ture control	Flow valves (4 loops)	Flow valves (4 loops)	Receiver shutdown (1 loop)
Doors		Open Close Miscellaneous (4 loops)	Door closing (1 loop)

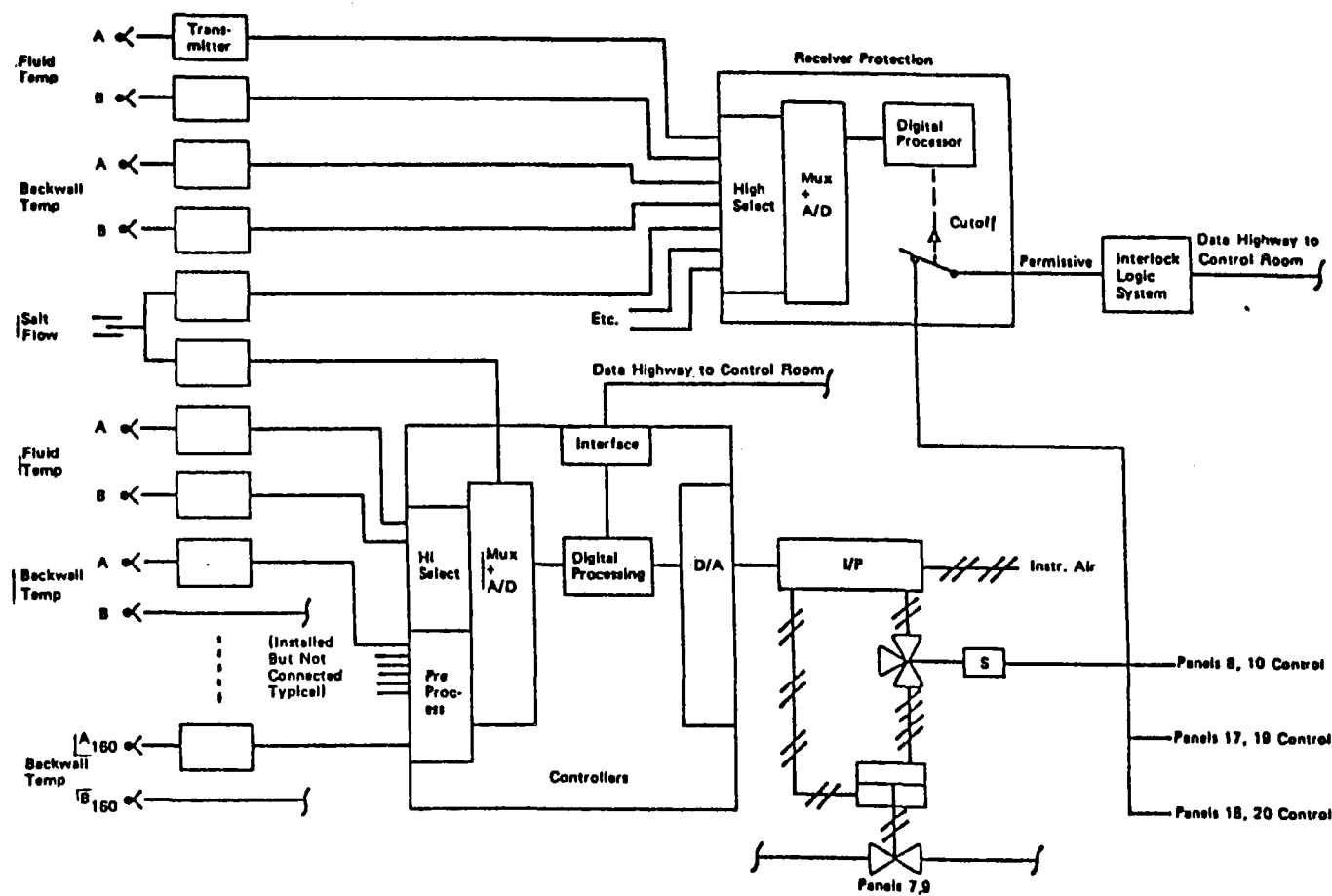


Figure 5.83 Salt Temperature Control (Typical 4 Places)

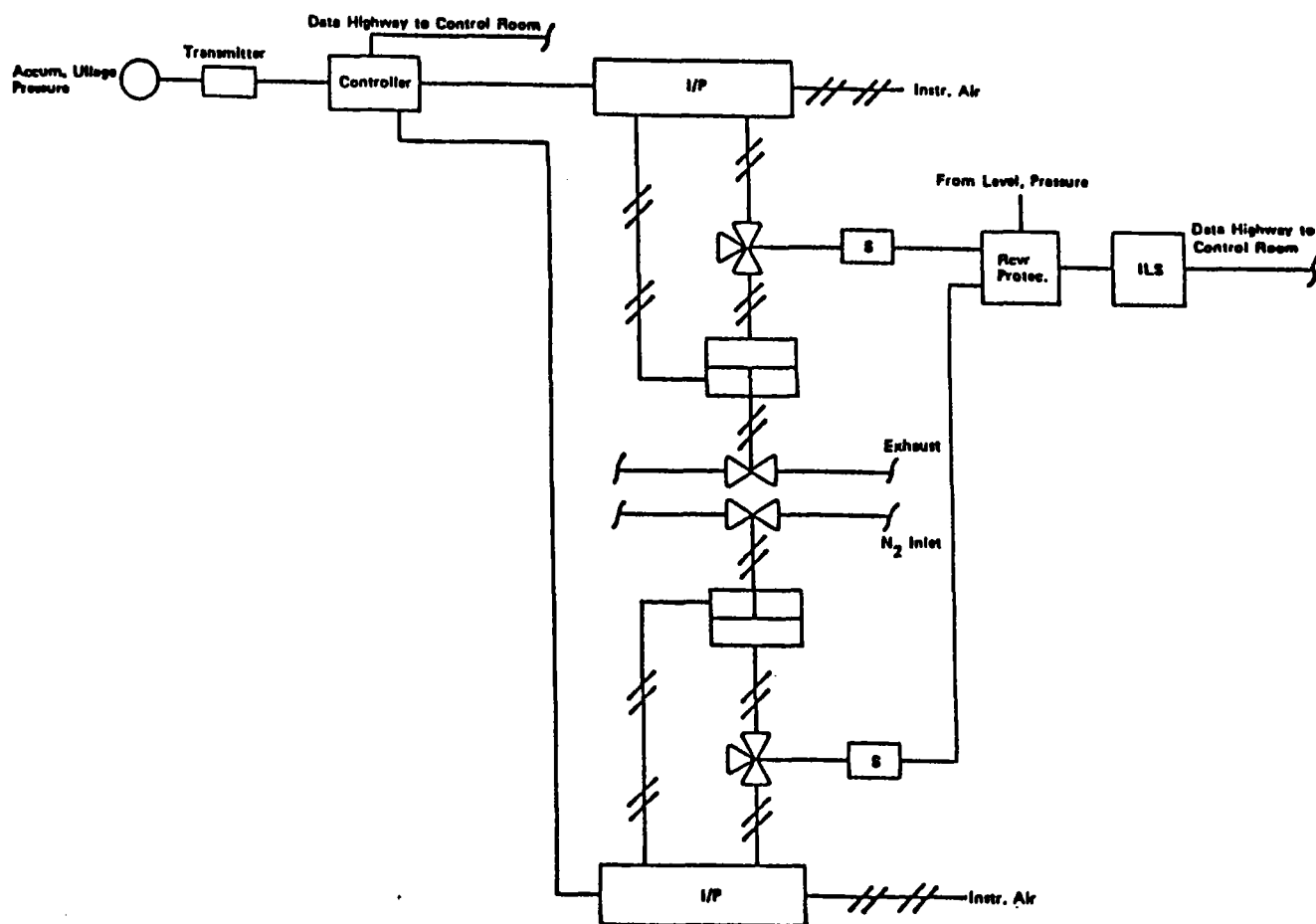


Figure 5.84 Surge Tank (Accumulator) Pressure Control (Typical 2 Places)

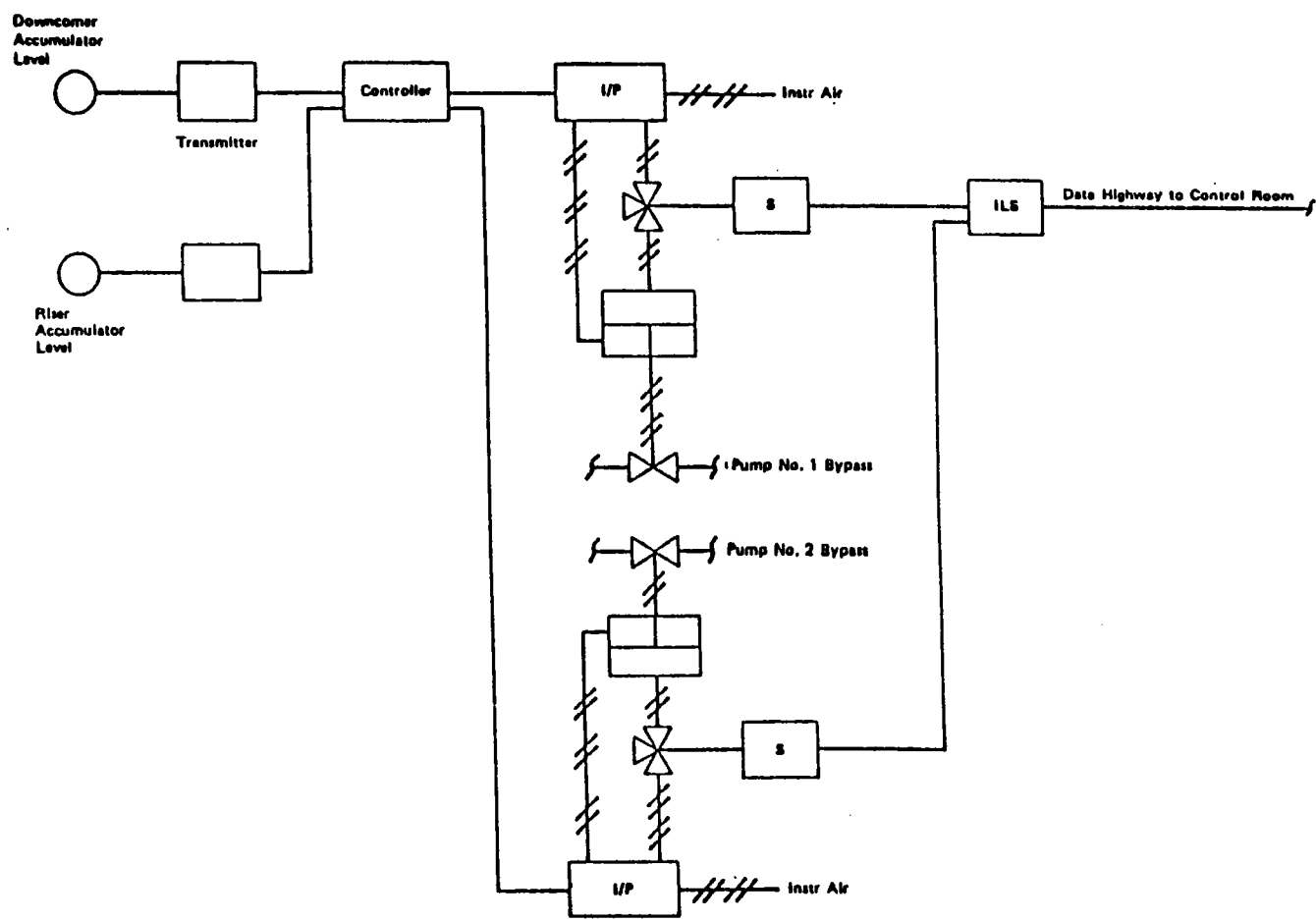


Figure 5.85 Surge Tank (Accumulator) Level Control

Table 5.34 Control Instruments

<u>Type of Instruments</u>	<u>Number of Instruments</u>				
	<u>Temperature</u>	<u>Pressure</u>	<u>Flow</u>	<u>Level</u>	<u>Flux</u>
Control Instruments and Transmitters					
Active	184	2	6	2	---
Spares	160	---	---	---	---
Measurement Instruments* and Transmitters	240	4	---	---	80

*These instruments are for evaluation. They may not be required for operation after the first unit is successfully tested.

Simulation. One key operation in the RS control system is the control of outlet temperature during cloud transients.

Because of the importance of using the greatest amount of measured insolation, maximum operation during partly cloudy periods is essential to RS economics. Previous results at Solar One and at the receiver test at CRTF have shown that feed-forward data are required for operation during periods of rapidly varying insolation. Two alternatives have been proposed for the feed-forward information:

- Flux sensors mounted in, or adjacent to, the receiver panels
- Backwall tube temperatures.

Flux sensors offer the fastest indication of power changes; however, they have not always been reliable. Backwall temperature sensors are considered to be more reliable; however, they are not as fast and require substantial processing to define power transients.

We constructed a model and investigated control system behaviors using backwall temperatures and a digital simulation of an analog controller. These results were initially promising, but the investigation was ended before achieving final gains that might have been acceptable. Subsequently, the digital simulation of the analog controller was replaced with a digital simulation of the proposed digital microprocessor controller. Using the revised simulation, we investigated control using feed-forward information--both from backwall temperature sensors and from flux sensors. In general, the flux sensor data provided a small improvement. A description of both the initial simulation model and results and the revised model and results is presented in the next section.

Although final resolution of control system gains and the selection of flux sensors vs. backwall temperature data for feed-forward cannot be made at this time, acceptable receiver control can clearly be achieved, and actual test data will provide important information on the relative merits of the feed-forward sensor.

5.6.2 Overall Model

The system model consists of:

- Receiver
- Riser and downcomer
- IST and OST
- Associated valves
- Air supply systems
- Interconnecting piping

The receiver model is made of 20 absorber panels arranged in a cavity configuration (Figure 5.86). The panels are connected by 15 interconnecting piping sections (headers, downcomers, feeders, risers, and transfer piping) to complete the two flow paths of the receiver half, as illustrated in Figure 5.87. The interconnecting piping section models also provide for the time lag resulting from the flow rate and the length of interconnecting piping. There are four salt flow-control valves (one for each parallel outlet pass) that control the receiver salt outlet temperatures. The valves are located downstream of Pass 3. The number listed on each panel or by each header is keyed to a matrix in the mathematical model used to perform the heat-transfer equations and determine transport lag that simulates the receiver dynamically.

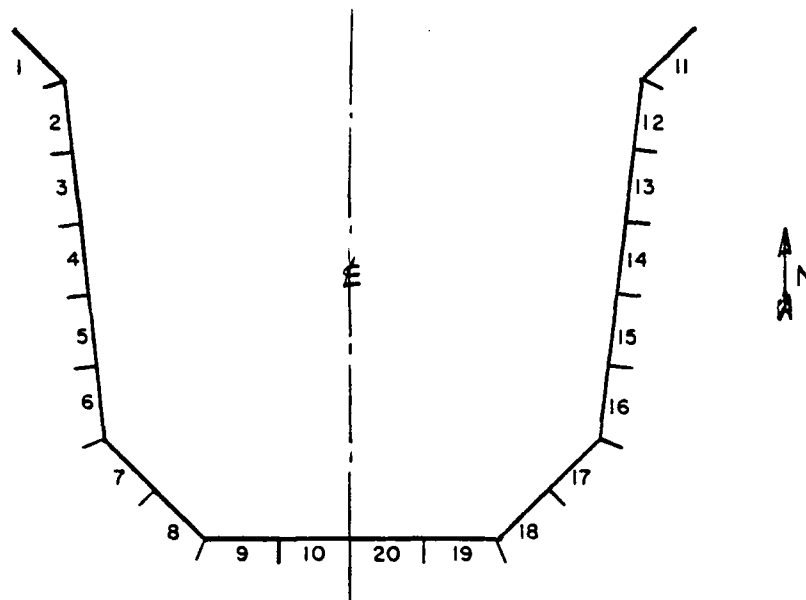


Figure 5.86 Receiver Model Panel Numbering

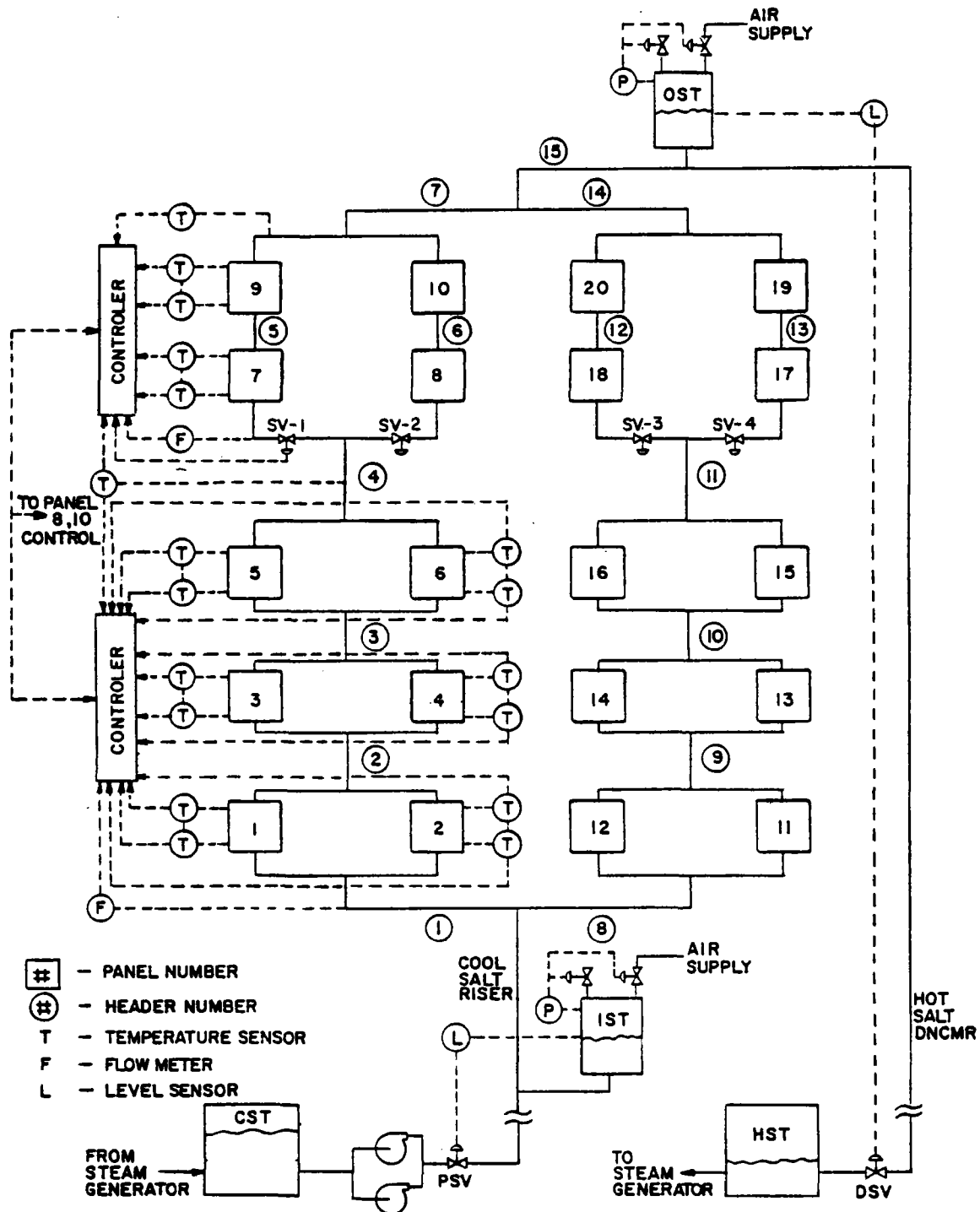


Figure 5.87 RS Model Diagram

As shown in Figure 5.88, each panel in the model is further subdivided into eight equal-length segments (nodes). The standard heat-transfer equations for each panel tube node are given in Appendix Q. The salt convective coefficient is calculated by using the Dittus-Boelter equation for fluids heated in smooth tubes with fully developed turbulent flow.²⁷ Each panel node has its own unique solar flux heating the tubes. The flux matrix can be manipulated by a cloud subroutine to provide system disturbances.

The four receiver controllers, one for each salt flow-control valve, are identical and independent of each other. In the basic control strategy, an outer loop is used for outlet-salt temperature control. The receiver back tubewall temperature heat and mass balance equations are used in an inner flow-control loop as shown in Figure 5.89--a common cascade controller arrangement with the exception of the heat and mass balance equations. The addition of the back tubewall temperature equation (Appendix Q) was necessary to keep the fluid transport lag in the receiver between 1 and 2 minutes at maximum flow and longer as the flow is reduced from maximum. The reaction time of the calculation is rapid (2 to 4 seconds), compared with that of the fluid transport lag.

Since each last salt pass/receiver half is hydraulically coupled to the other, the outer flow loop serves two purposes: to help decouple each half of the receiver from the other and to compensate for long-term changes in system flow characteristics.

The receiver salt riser and downcomer lengths are so great that the mass momentum of the salt flowing in them must be considered. This is done by using

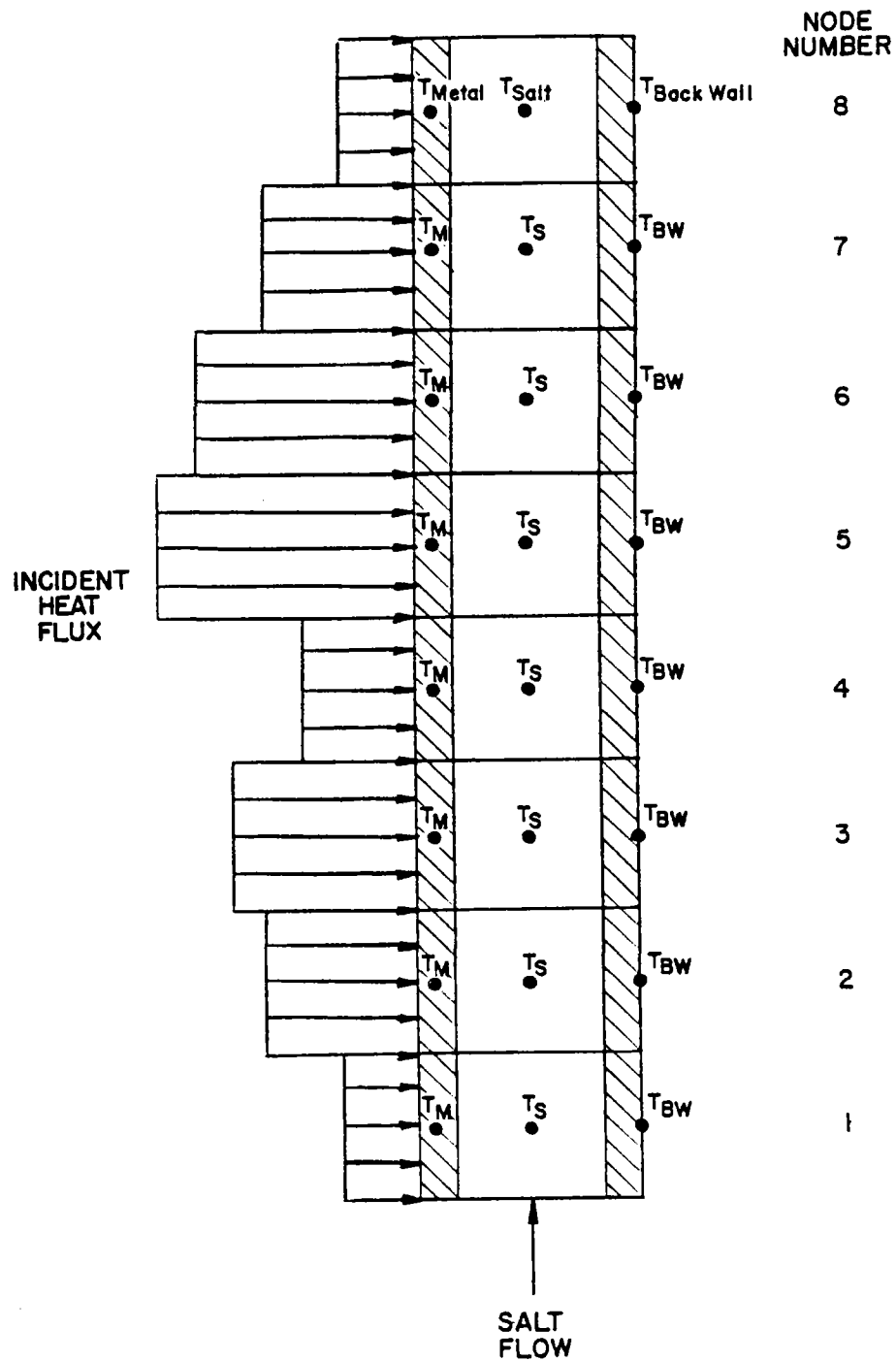


Figure 5.88 Panel Model Configuration

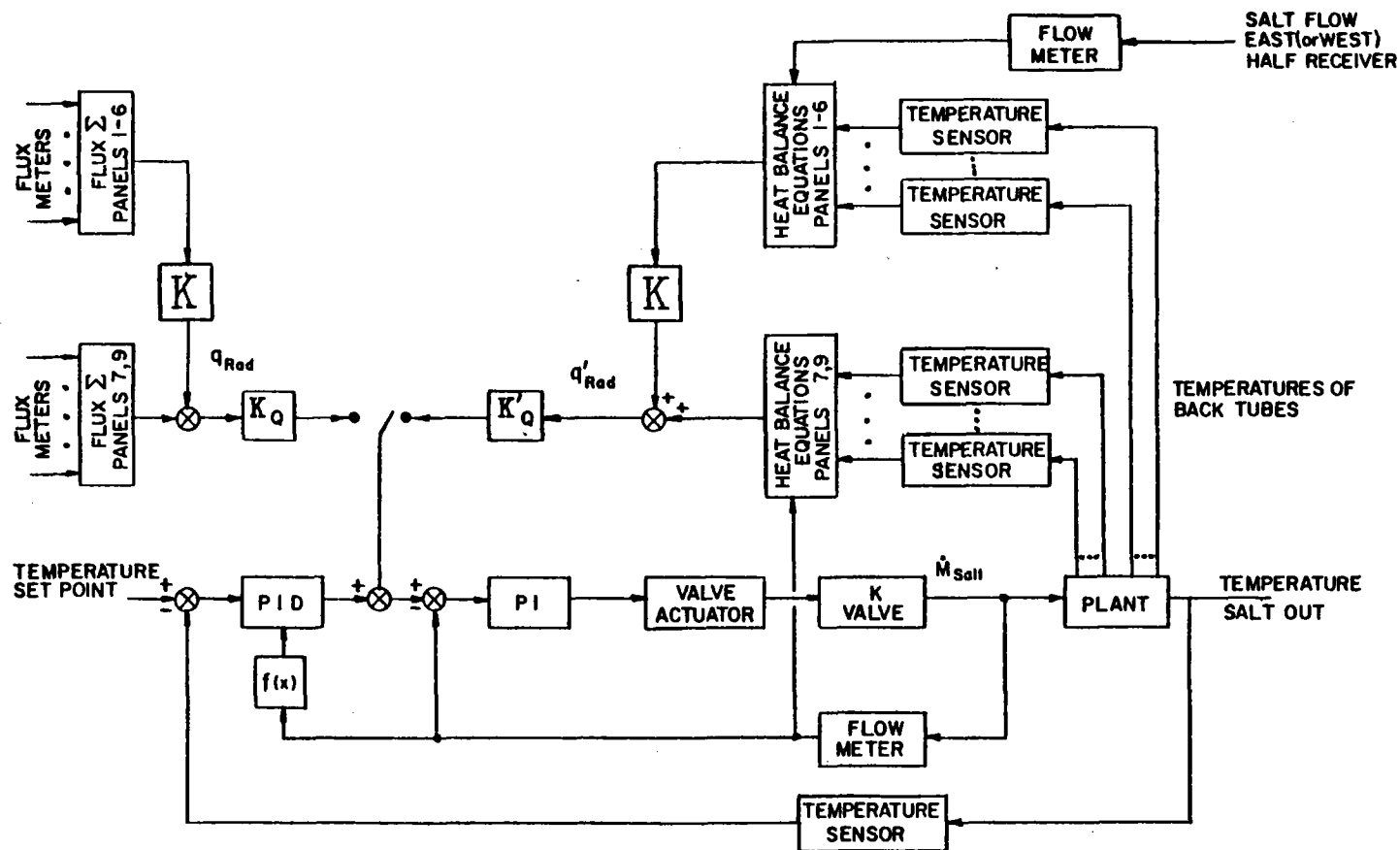


Figure 5.89 Panel Salt Valve Control (TYP) Block Diagram

standard fluid flow calculations and momentum equations for incompressible flows. The sonic velocity of the salt is unknown, but will most likely be sufficiently high so that the incompressible approximation is adequate.

The salt surge tanks serve two purposes: to provide a supply of salt to cool the receiver in case of pump failure and to help remove large pressure transients induced by the receiver flow control valves as they react to clouds. Each surge tank consists of a tank with air vent and supply valves. Approximately 50 percent of the tank is filled with molten salt; the rest is compressed air. The surge tank model illustrated in Figure 5.90 accommodates the compression of the air and the mass momentum of the salt. Basic pressure, temperature,

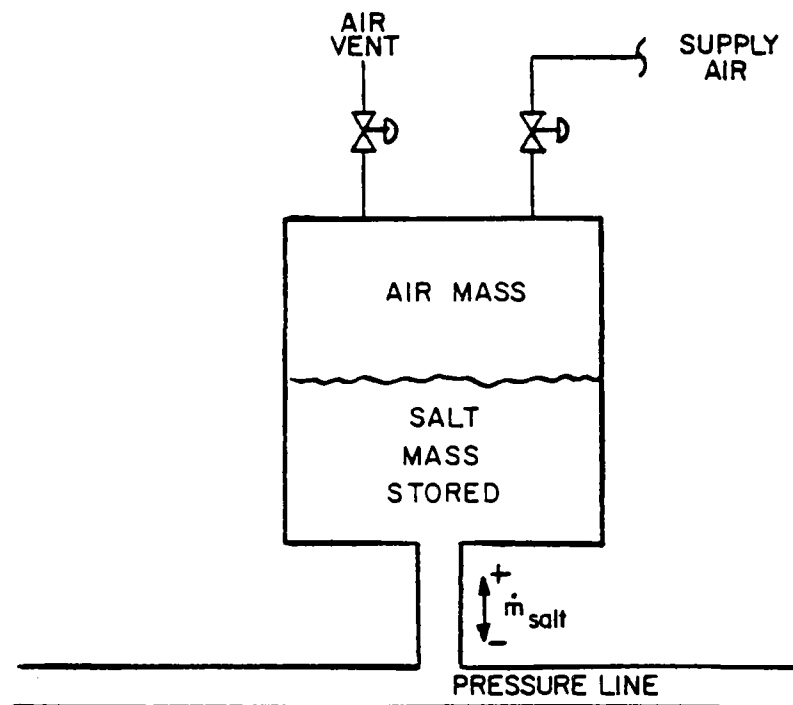


Figure 5.90 Accumulation/Surge Tank Model

and mass equations are given in Appendix Q. Surge tank level and pressure were controlled as shown in Figure 5.91.

The salt level in the IST is controlled by a valve at the pump end of the salt riser. The OST level is controlled by a pressure-reducing (drag) valve at the bottom of the downcomer. The drag valve serves two functions: it controls salt level in the OST and dissipates part of the static head pressure in the downcomer. Each tank has an air vent and an air-supply valve for a positive pressure in the tanks and protection from excess pressure. The control of these air valves is such that neither is open at the same time.

5.6.3 System Response

The control system response was analyzed in three sequential stages. The controller was modeled using a state variable representation of an analog controller. During this stage only a 10-percent cloud variation was modeled using back tubewall temperatures for feed-forward information. Subsequent to this analysis, the controller models used in the simulation were updated to represent more accurately the type of controller proposed for the RS. The new controller model simulates a Beckman controller with simple derivative filtering (Figure 5.92). Using this updated controller model, we considered both a 10- and a 50-percent cloud and looked at both back tubewall temperatures and flux gages for feed-forward information. Because the results were preliminary, a final analysis of a 50-percent cloud was performed. Details of these analyses are given in Appendix Q.

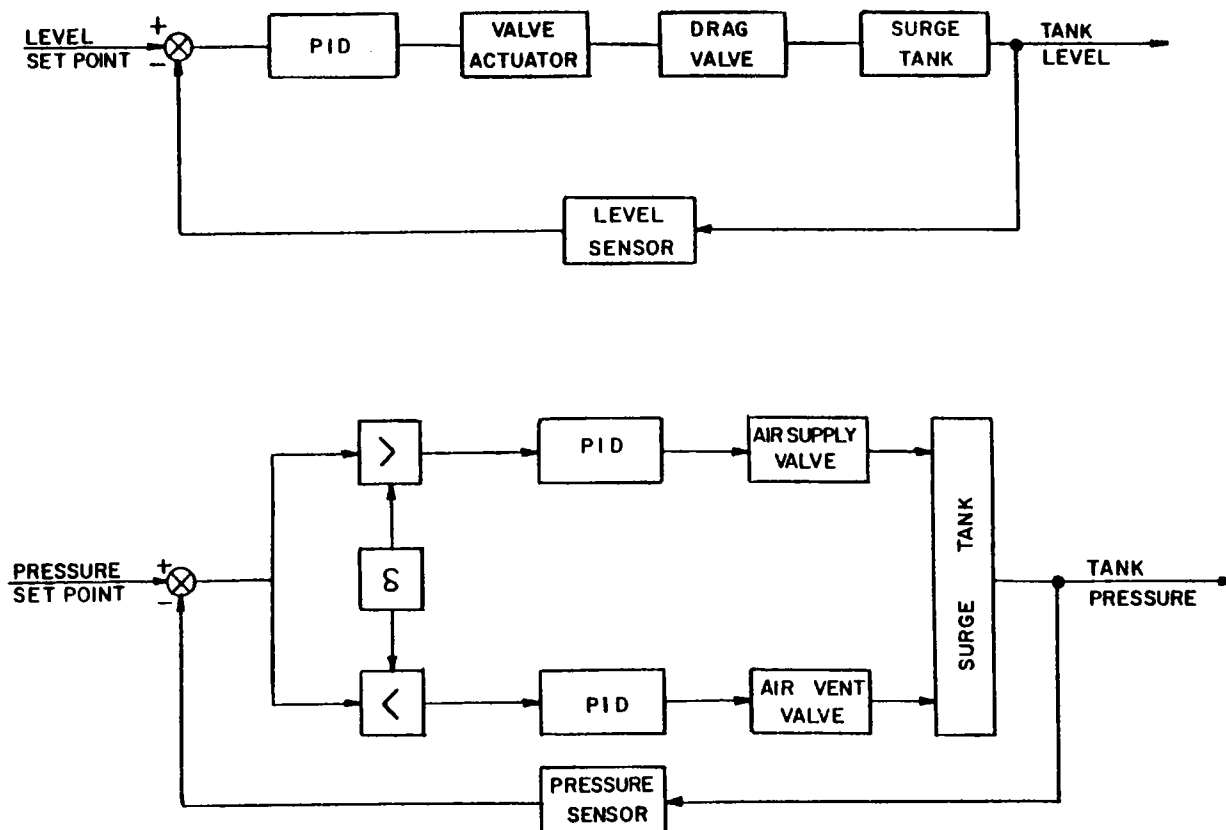


Figure 5.91 Accumulator/Surge Tank Control Block Diagram

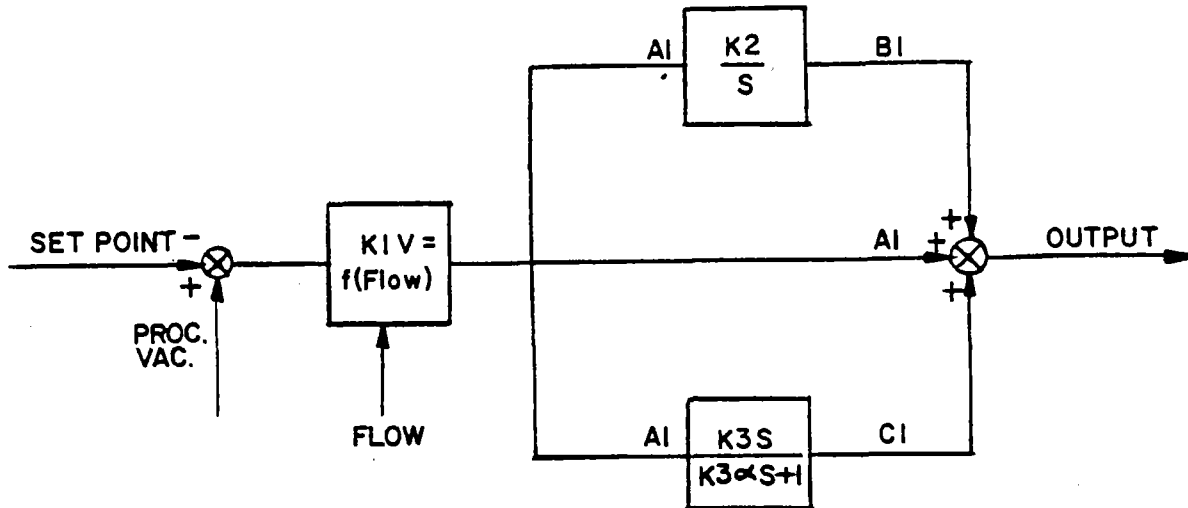


Figure 5.92 Beckman PID as Used in Valve Controllers

The results indicate that 50-percent step changes in power level will produce transient temperature variations of approximately $+10/-15^{\circ}\text{C}$ ($+18/-27^{\circ}\text{F}$) damping down to $\pm 3^{\circ}\text{C}$ ($\pm 5.4^{\circ}\text{F}$) in approximately 150 seconds. The flux gage data showed a slight advantage [$\approx 3^{\circ}\text{C}$ ($\approx 5.4^{\circ}\text{F}$) less undershoot in temperature]. Both systems appear promising based on the simulation results. Actual test data will be essential to validate the simulation models for the key physical processes and the simulation results.

Section 6

PANEL FABRICATION DEVELOPMENT

6.1 BACKGROUND

Task 6 was established to resolve the fabrication issues and to develop the basic fabrication methods for the continuous longitudinal welding of thin walled tubes to form flat panels and for attachment of support lugs to the panels.

6.2 FABRICATION PROCESS DEVELOPMENT PLAN

Before starting Task 6, a detailed Fabrication Process Development Plan (FPDP) was prepared and submitted to SNLL for comments and approval. SNLL's comments were received and incorporated into an amended FPDP, Appendix R. This FPDP outlines FWSDC's welding plan and describes in detail the qualification tests that were to be conducted to ensure satisfactory component performance. It was used as the basic guideline for the development work and testing that followed to establish the optimum methods for joining tubes to tubes and attaching support lugs to tube panels. With the exception of the thermal cycle test, all tests outlined were completed. The thermal cycle test was deleted at SNLL's request and the man-hours saved were used for further fabrication welding development.

As stated in our proposal to SNLL,** Foster Wheeler conducted a successful welding development program before this contract. During welding development and mock-up fabrication for the test panel of the DOE/General Electric sodium receiver program, Foster Wheeler made successful tube-to-tube orbital welds using 19 mm (3/4 in.) O.D. Incoloy 800 tubes with 1.65 and 1.27 mm (0.065 and 0.050 in.)

thick walls. A special miniature version of the inert-gas-shielded tungsten arc (GTA) torch, shown in Figure 6.1 was used. We demonstrated the welding process acceptability and completed the welding procedure qualification by making over 80 orbital welds and then 12 jumper tube-to-panel tube and 12 jumper tube-to-header stub welds in the full-scale mock-up. As a result of the success of this welding development program, no further orbital weld development was required for tubes with similar characteristics (and none was performed under this contract).

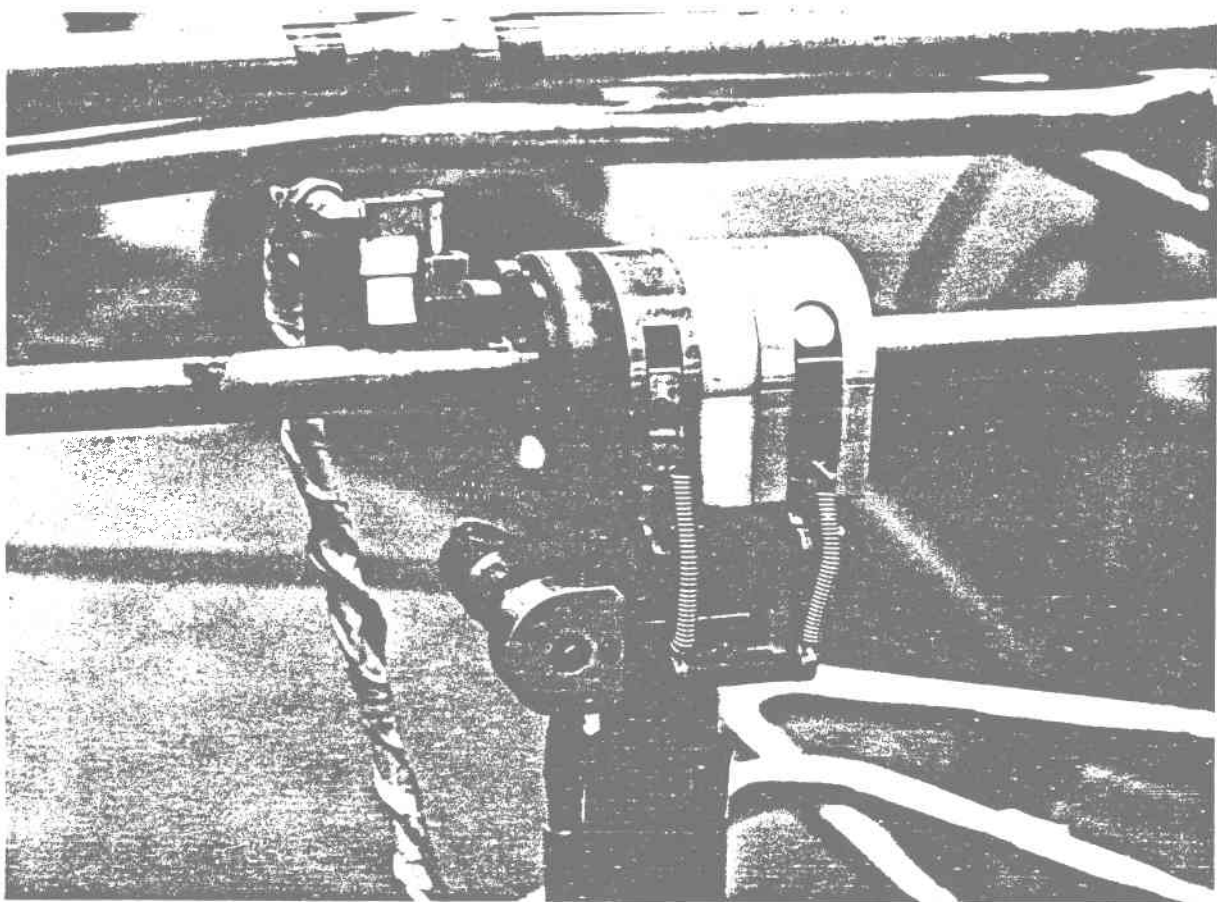


Figure 6.1 Automatic Welding Torch for Butt-Welding Thin-Walled Tubes

6.3 PANEL WELDING DEVELOPMENT

The process for longitudinally welding thin tubes to form panels must meet several basic requirements. It must:

- Be as automatic as possible because of the large quantity of weldment required in a full size panel
- Have a low heat input to prevent burn-through of the thin tubewall
- Minimize weld-induced panel distortions.

As shown in Figure 6.2, there are two types of possible weld-induced plane distortion: out-of-plane distortion (bowing) and in-plane distortion, consisting of transverse necking (which results in an "hourglass" shape) and general bowing/cambering.

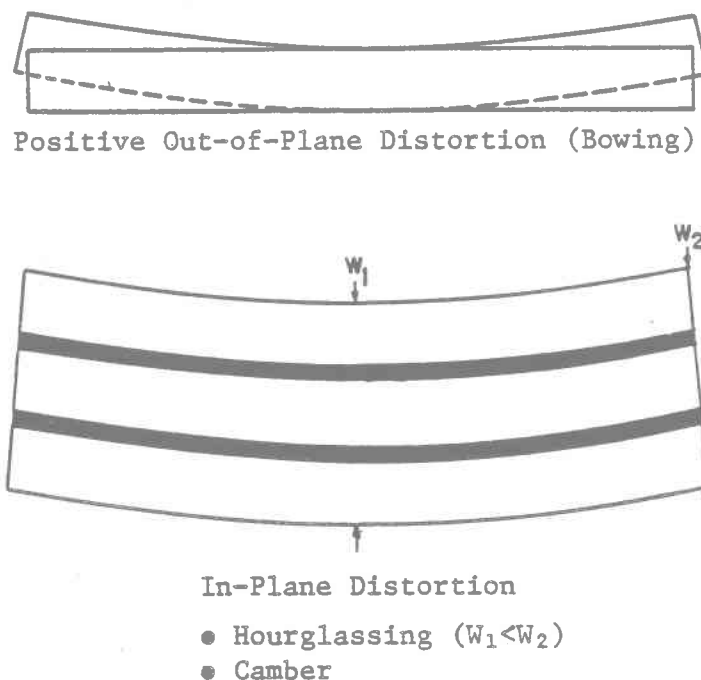


Figure 6.2 Weld-Induced Panel Distortion

6.3.1 Welding Process

A semiautomatic short-circuiting arc (dip transfer) MIG welding process was chosen for longitudinally welding tubes to form a panel. This process was chosen because of its ability to produce sound welds in thin sections with minimal tubewall penetration.

6.3.2 Welding Head and Power Supply

A MIG welding head (Figure 6.3) was designed and fabricated to feed a consumable bare electrode into the weld zone at a constant rate and supply a continuous blanket of inert gas to shield the weld zone from atmospheric contamination. Welding power was supplied by a Linde type SVI-300 constant potential power supply, which maintains a constant arc length by varying the current delivered to the arc. Electric current and voltage were recorded by Esterline Angus instruments (Figure 6.4).

6.3.3 Welding Head Travel and Tracking

The welding head was mounted on a horizontal cross-beam carriage (Figure 6.5). A drive mechanism moved the head along the carriage at a constant, predetermined rate. A concave roller (Figure 6.6) near the welding tip rested on one of the tubes being joined, to guide and position the welding head relative to the tubes being welded. Bearings allowed the head to move a limited amount both vertically and horizontally. Precise positioning of the welding head was considered essential to prevent tubewall burn-through and to provide consistent weld geometry and soundness.

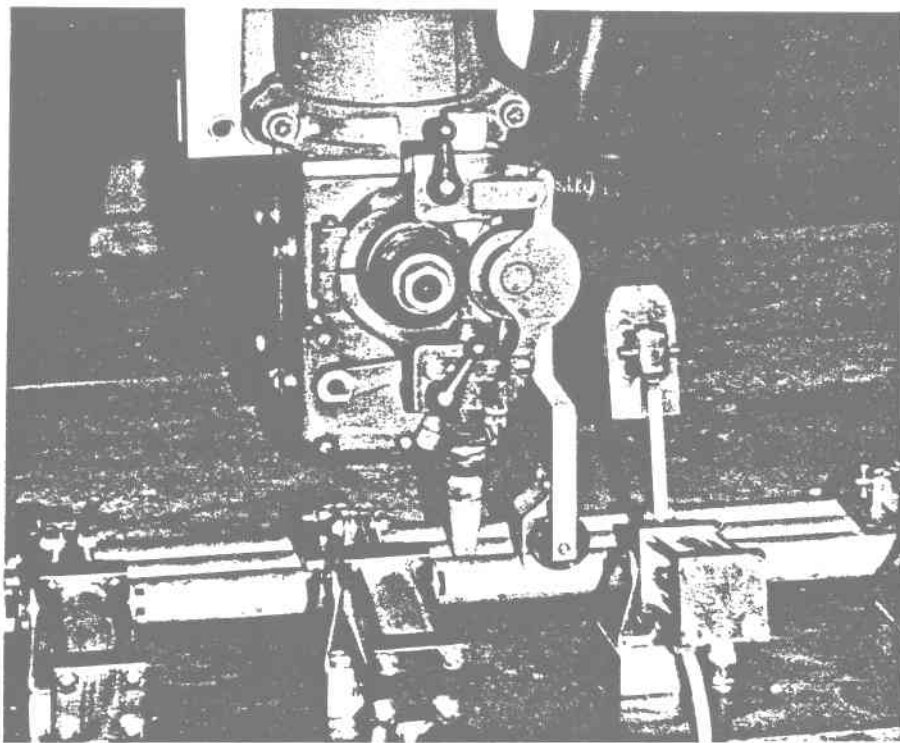


Figure 6.3 Metal Inert Gas (MIG) Welding Head

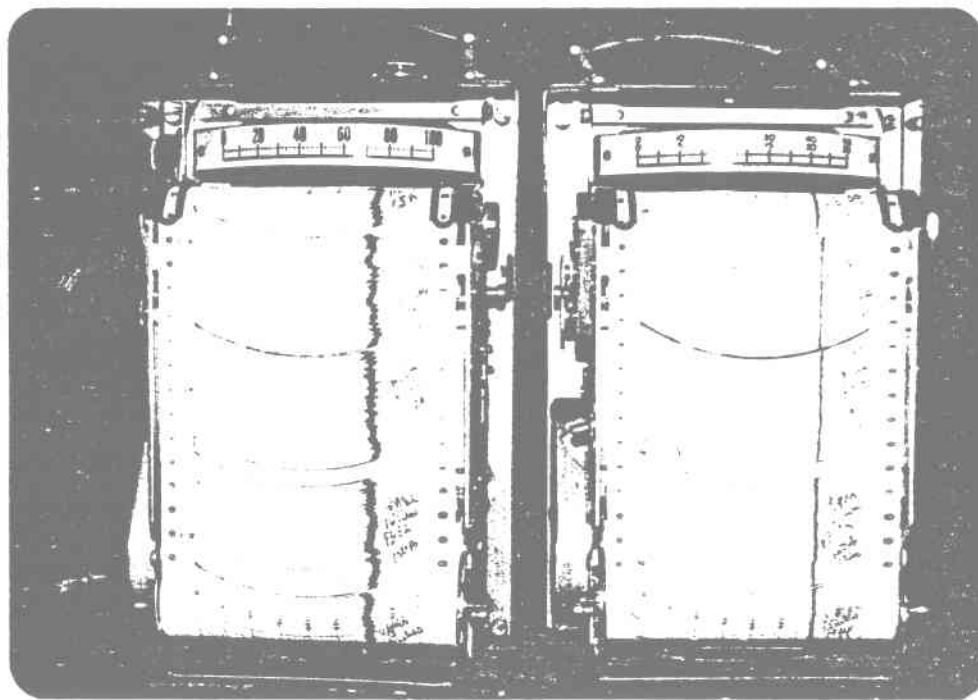


Figure 6.4 Esterline Angus Recorders Used To Record Current (Amps) and Voltage

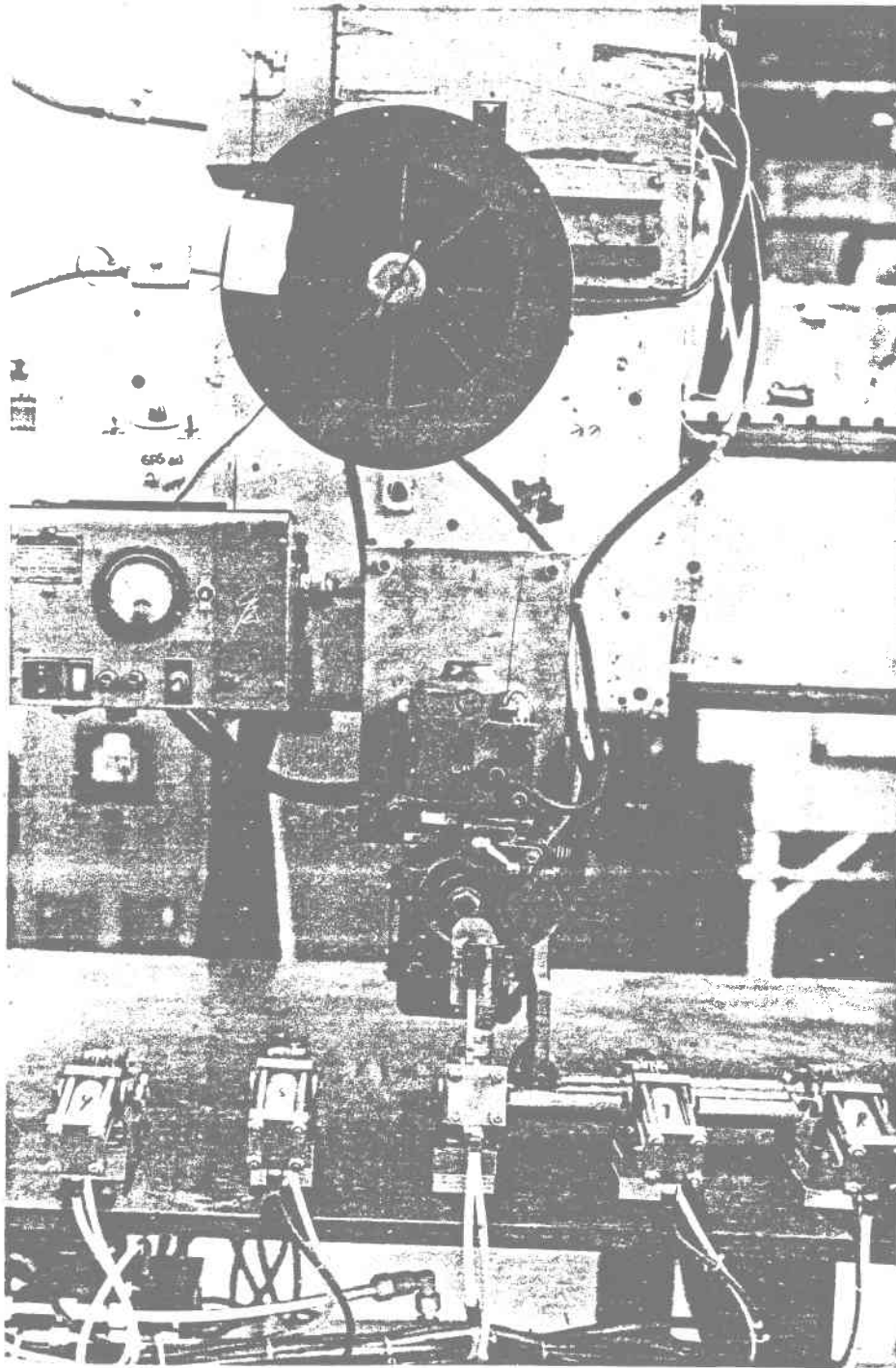


Figure 6.5 Welding Head With Wire Reel and Controls
Mounted on Cross-Beam Carriage

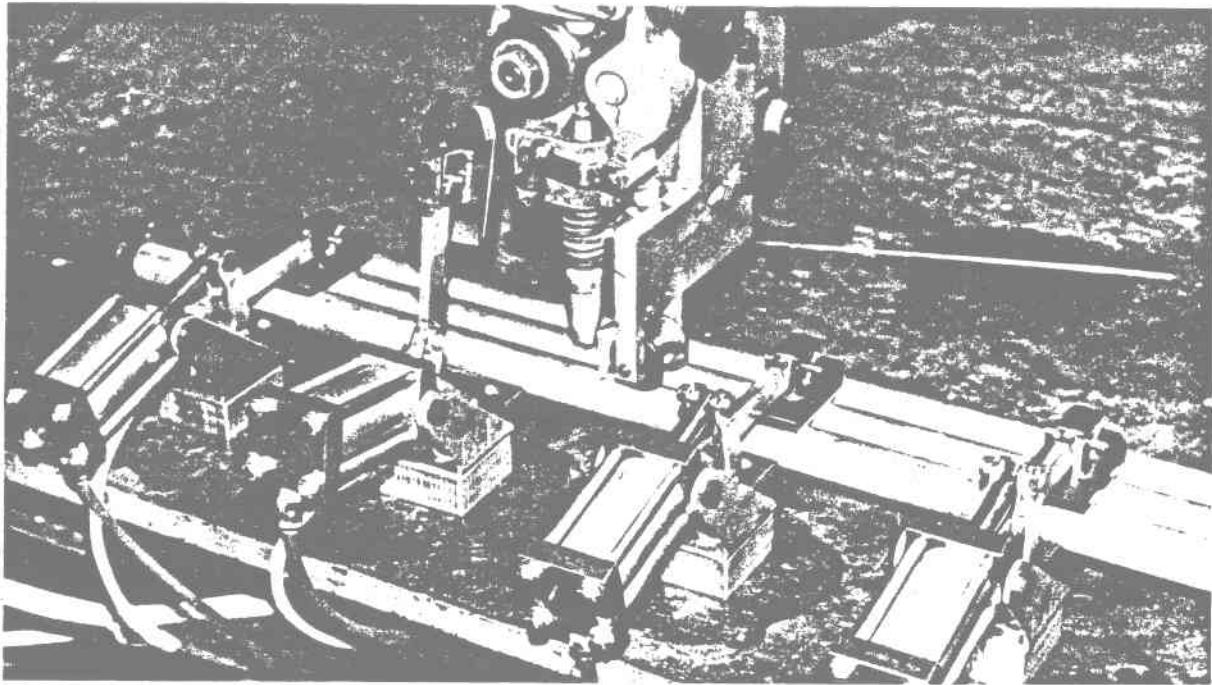


Figure 6.6 Pneumatically Actuated Toggle Clamps and Roller Guide

6.3.4 Welding Fixture

A rigid table with a flat 3-m (120-in.) long x 1-m (39-in.) wide x 19-mm (3/4-in.) thick steel top was placed beneath the cross-beam carriage and securely welded to the upright columns supporting it. This table provided the surface for panel fabrication.

For trial welding, we bolted a series of scalloped support blocks (Figure 6.7) to the table. These blocks supported three tubes on the table at 0.15-m (6-in.) intervals. Pneumatically activated toggle clamps (Figure 6.6) held the tubes firmly on the support blocks and prevented them from moving during welding. The clamps were automatically activated to open at each clamp site as the welding head traversed the length of the tubes. The opening of the clamps

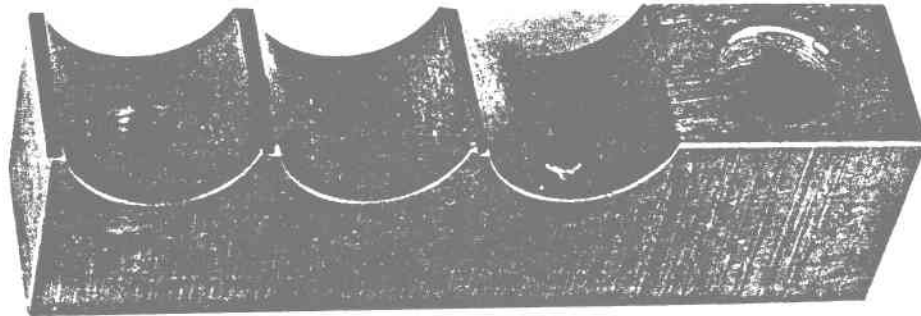
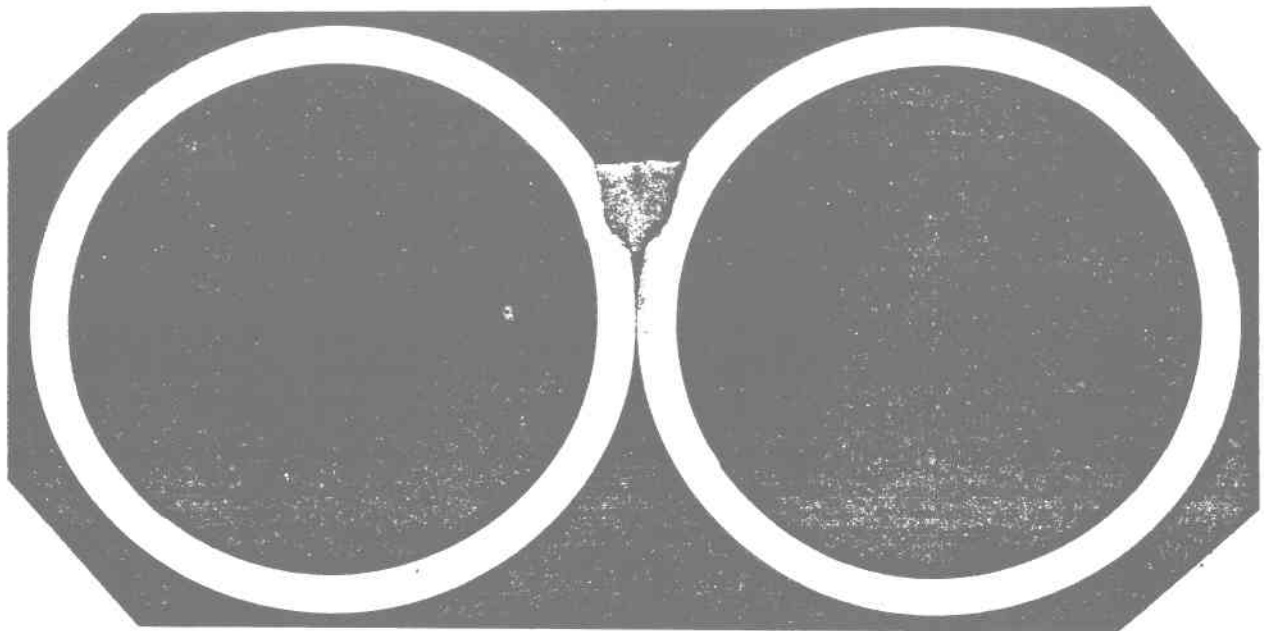


Figure 6.7 Scalloped Support Block Used During Fabrication of First and Second Development Panels

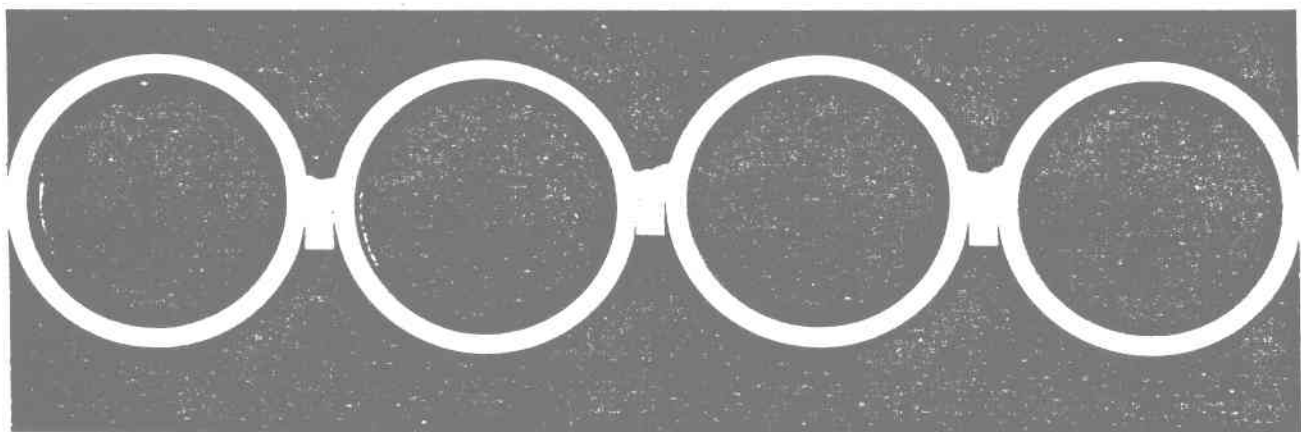
was controlled by microswitches contacted by a cam mounted on the travel carriage (Figure 6.5). The switches, in turn, operated solenoid valves that directed the supply air to the toggle clamps. Since one clamp was always in the open position for passage of the welding torch (Figure 6.6), the effective hold-down span at the welding site was 0.30 m (12 in.). This same basic approach was employed in development panel fabrication, but it was supplemented with the additional fixtures described in Section 6.4.

6.3.5 Trial Welding

Trial welds (Figure 6.8 and Table 6.1) were made using 0.46 to 0.61-m (18- to 24-in.) lengths of Type 304SS welded tubing of prototypical size [i.e., 25.4-mm (1-in.) dia x 1.65-mm (0.065-in.) wall thickness]. The welding electrode used was 0.51-mm (0.02-in.)-dia Inconel 82. The shielding gas was 99.99 percent argon.



First Trial 3X



Third Trial 1.5X

Figure 6.8 Cross Sections of Trial Welds for Joining Tubes

Table 6.1 Trial Welds

First trial welds, tubes touching	Third trial welds, spacer strip added
<ul style="list-style-type: none">● Sound welds● Excessive bowing	<ul style="list-style-type: none">● Bowing reduced, not eliminated● Good weld geometry● Sound welds
Second trial welds, tubes separated	Fourth trial welds, removable backing strip
<ul style="list-style-type: none">● Bowing reduced● Poor weld geometry● Poor weld quality	<ul style="list-style-type: none">● Water-cooled copper spacer● Welds cracked● Backing strip hard to remove

Welds were first made with the tubes touching longitudinally at the tangential lines. The approach produced an acceptable welded joint but promoted extreme out-of-plane distortion (bowing). This distortion was attributed to a combination of weld metal shrinkage and weld location, which was well above the neutral axis of the tubes.

The second series of trial welds was made with the tubes 1.59 mm (1/16 in.) apart, so that the weld could be placed nearer the neutral tube axis. This configuration lessened the out-of-plane distortion but promoted erratic welding behavior, inconsistent weld geometry, poor weld quality (soundness), and poor appearance. These observations were attributed to the open gap between the tubes.

The third series of trial welds was made with a 1.59-mm (1/16-in.) wide x 3.18-mm (1/8-in.) deep, rectangular, Type 304SS spacer strip sandwiched between

the tubes. The top of the spacer strip was placed 0.79 mm (1/32 in.) below the neutral axis of the tube to enable the weld to form near the neutral axis. A lip was added to the roller guide to restrain the spacer strip during welding (Figure 6.9). The separation provided by this spacer strip was too narrow; the weld bridged the gap between the tubes without fusing into the spacer strip. A gap was often evident between the bottom of the weld and the top of the spacer strip, and the weld location was still too high, causing axial weld-induced bowing. By increasing the width of the spacer strip to 2.38 mm (3/32 in.), we solved the lack-of-fusion problem and allowed the weld to form nearer the neutral axis of the tube (Figure 6.8). Sound welds were produced that fused the tubes and spacer strip with minimum (up to 25 percent) tubewall penetration. However,



Figure 6.9 Roller Guide With Lip Used to Position Welding Head and to Restrain Spacer Strip During Welding

some out-of-plane distortion was still present, since the minimum weld height obtainable was 3.18 mm (1/8 in.), which placed the center of the weld about 0.79 mm (1/32 in.) above the neutral axis of the tube. Lowering of the spacer strip relative to the neutral axis of the tube to lower the weld centerline again prevented fusion. No practical solution to better placement of the weld was found.

In a fourth series of trial welds, we used a 2.38-mm (3/32-in.) wide spacer strip of water-cooled copper. Our objective was to develop a nonfusible, removable, reusable backing strip to form the back side of the weld. The welds were reasonably well centered and well-shaped, but they contained numerous small transverse cracks--most likely caused by the too rapid solidification of the weld metal by the chilled copper strip and by possible copper pickup. Removal of the spacer strip was also a problem because the tubes shrank and bound the strips between them. Because of time and funding limitations, this effort was not pursued further.

6.4 DEVELOPMENT PANEL FABRICATION

Three 2.44-m (96-in.)-long development panels were fabricated (see summary in Table 6.2). The following sections describe the fabrication of each panel.

6.4.1 Development Panel 1

The first panel was fabricated using the weld design described in the third set of trial welds (Figure 6.8). The panel was fabricated from prototypical [25.4-mm (1-in.)-dia x 1.65-mm (0.065-in.)-wall thickness Incoloy 800 seamless tubing] and 2.36-mm (0.093-in.) wide x 3.18-mm (1/8-in.) deep rectangular Incoloy 800 spacer strip. Most of the welds were made with a 0.89-mm (0.035-in.)-dia Inconel 82 welding electrode after feeding problems were experienced with the 0.51-mm (0.020-in.)-dia electrode used for trial welding. This modification not only solved the electrode feeding problem, but also permitted us to increase welding head travel speed by 50 percent with no appreciable change in weld geometry or decrease in weld quality. Argon gas shielding was used. The top of the spacer strip was positioned 0.76 mm (0.030 in.) below the neutral axis of the tube and the separation between tubes was 2.38 mm (3/32 in.).

The fixture for welding the tubes was essentially the same as that used for trial welding. Scalloped support blocks with rectangular grooves for the spacer strip were spaced 0.15 m (6 in.) apart. Pneumatic clamps and end clamps restrained the tubes. Weights and 'C' clamps kept the in-process panel flat (Figure 6.10). Using welding parameters developed from trial welds, two-tube subassemblies were fabricated; these subassemblies were then joined to form a panel 30 tubes wide. A 31st tube was added separately.

Table 6.2 Panel Fabrication

Panel 1: 31 Tubes Wide, Incoloy 800

- Fixture basically the same as in trial welds
- Third trial weld configuration used
- 1 tube → 2 tubes → panel
- Major problems:
 - Strip bowing
 - In-plane distortion (hourglassing)
 - Out-of-plane distortion (bowing)

Panel 2: 31 Tubes Wide, Incoloy 800

- Third trial weld configuration again used
- Additional support blocks
- Plastically elongated strip $\approx 1\%$
- Tubes wedged apart
- 222 N (50-lb) load applied to strip
- Edge tube of panel preheated
- Major problems: Same as for Panel 1, but reduced in magnitude

Panel 3: 28 Tubes Wide, Type 304SS

- Spacer strip depth increased
- 2 tubes → 4 tubes → Panel
- Fixture modified and strengthened
- Major problems:
 - Spacer strip induced negative bowing
 - Excessive tubewall penetration
- Distortion
 - In-plane: None measured
 - Out-of-plane
 - Transverse: None measured
 - Longitudinal: ≈ 7.94 mm ($\approx 5/16$ in.)

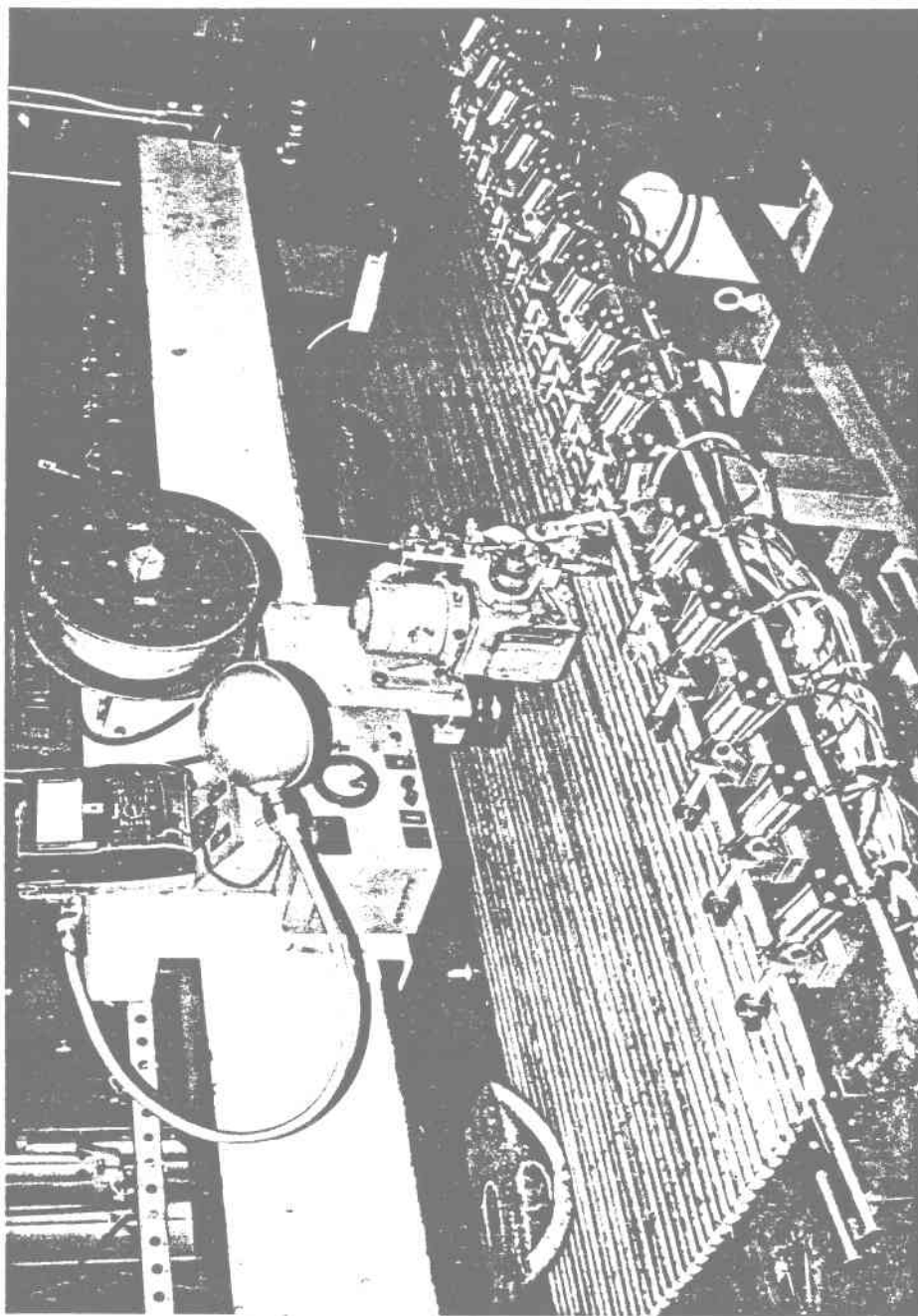


Figure 6.10 Fixture Employed During Fabrication of First Development Panel

Two major problems were encountered during panel fabrication. First, the spacer strip often bowed in the vertical plane during welding, causing erratic welding behavior and also contributing to panel distortion. The bowing was attributed to a combination of the differential expansion of the tubes and the strip and to the tubes pinching the strip ahead of the weld. Because of its lower mass, the spacer strip became appreciably hotter than the adjacent tubes; thus it expanded at a greater rate. Although a small gap was present between the tubes and the spacer strip to allow for unrestricted relative motion, transverse weld metal shrinkage drew the tubes together, eliminating the gap and causing pinching.

The second problem was differential expansion of adjacent tubes during welding, which contributed significantly to in-plane distortion in the form of "hourglassing" (i.e., the panel was narrower at the midpoint than at the ends). The prime cause was the asymmetrical nature of the assembly process (i.e., the welding of two-tube subassemblies of relatively small mass with respect to the mass of the in-process panel).

Distortion of the first panel was much greater than anticipated. Measurements taken were as follows:

● Out-of-plane distortion

- | | |
|-----------------------|----------------------------|
| - Longitudinal bowing | Ends: 26.9 mm (1.06 in.) |
| | Center: 28.7 mm (1.13 in.) |
| - Transverse bowing | Ends: 28.7 mm (1.13 in.) |
| | Center: 29.7 mm (1.17 in.) |

- In-plane distortion

- Width at ends	End A: 924 mm (36.38 in.)
	End B: 926 mm (36.44 in.)
- Width at center	911 mm (35.88 in.)
- Width differential	13.5 mm (0.53 in.)

6.4.2 Development Panel 2

Aside from the following fabrication changes, the second development panel (Figure 6.11) was fabricated of the same materials and in the same manner as the first panel.

- An additional set of scalloped support blocks was placed between the existing support blocks, decreasing their spacing to 76 mm (3 in.).
- The spacer strips, which were fully annealed, were elongated plastically approximately 1 percent to impart some cold work and to remove minor kinks.
- Wedges were placed between the tubes at 0.61 m (24 in.) intervals to maintain tube separation during welding. These wedges were removed just ahead of the weld zone as welding progressed.
- A 222-N (50-lb) tensile load was initially applied to each spacer strip before welding, but the idea was later abandoned.
- The edge tube of the in-process panel was preheated to $\approx 120^{\circ}\text{C}$ ($\approx 250^{\circ}\text{F}$) to pre-expand the tube before welding on a two-tube subassembly.

The first four of these changes were intended to eliminate spacer strip bowing. The last modification was intended to eliminate, or at least significantly reduce, the differential expansion of adjacent tubes. These fabrication modifications were partially successful; spacer strip bowing still occurred occasionally and panel distortion was decreased, but was still considered too great.

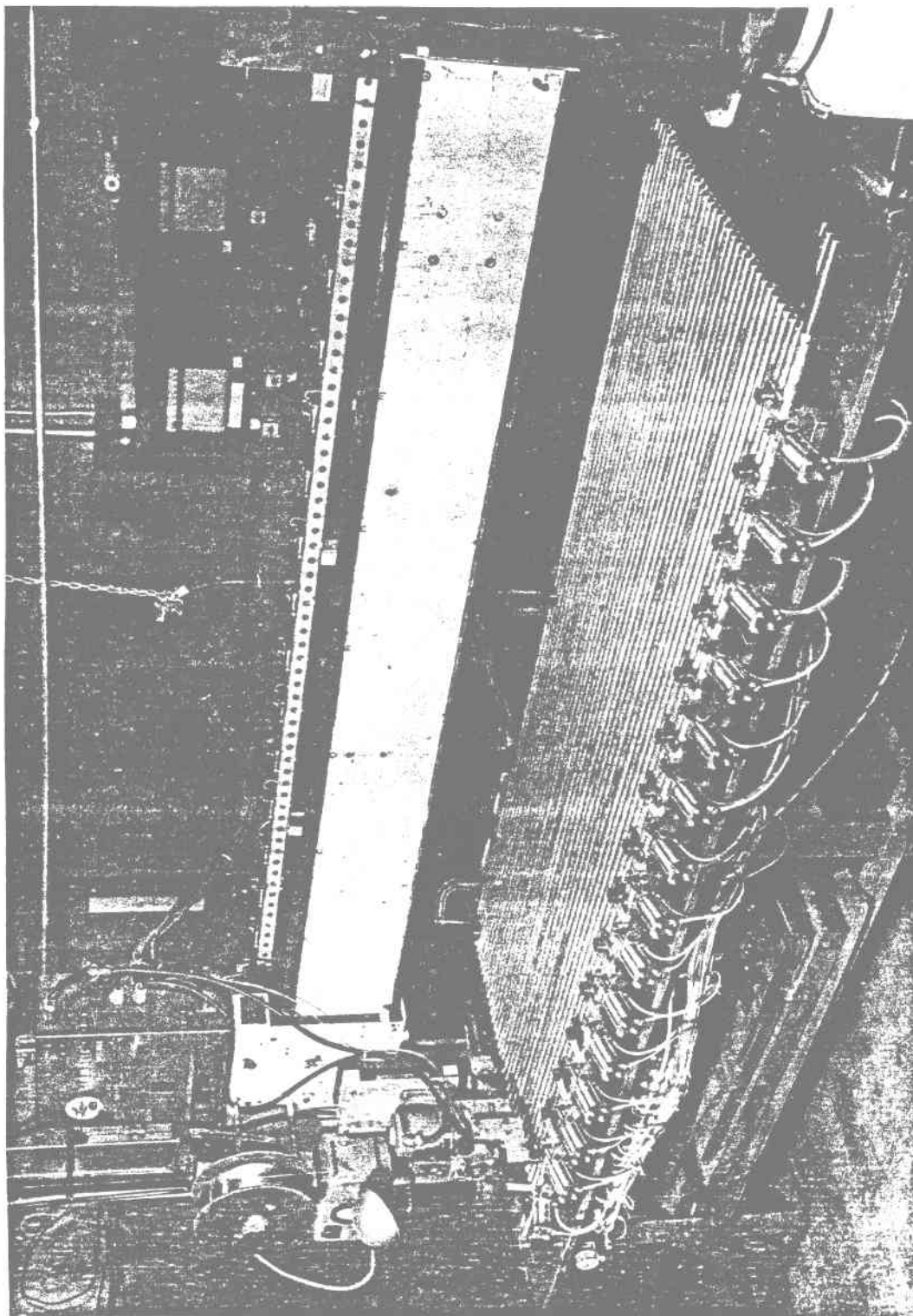


Figure 6.11 Fixture Employed During Fabrication of Second Development Panel

6.4.3 Development Panel 3

The third and last development panel was 28 tubes wide and was constructed of Type 304SS welded tubing of prototypical size and wall thickness, 11.11-mm (7/16-in.) deep x 2.34-mm (0.092-in.)-wide Type 304SS rectangular spacer strip, and 0.89-mm (0.035-in.)-dia Inconel 82 electrode. Tube separation was 2.38 mm (3/32 in.), and the shielding gas used was 95 percent argon, and 5 percent hydrogen. We had to use Type 304SS in lieu of Incoloy 800 because of an unacceptable procurement delay for Incoloy 800 tubes and strip. Spacer strip depth was increased (with Designer/Stress Analyst approval) to retard bowing; the added mass reduced the differential expansion between the tube and the spacer strip and the added depth stiffened the strip in the vertical plane.

Preheating of the in-process edge tubes was abandoned. Instead, differential tube expansion was reduced by increasing symmetry of mass during welding. This reduction was accomplished by making two-tube subassemblies joining these into four-tube subassemblies, then joining the four-tube subassemblies to make up the 28-tube panel (Figures 6.12 through 6.14).

A two-tube subassembly [2.44 m (96 in.) long] was welded using the same welding parameters as those used to weld the two previous test panels. Because of the increased mass of the deeper spacer strip, the front face of the spacer strip did not fuse. Thus a slightly hotter weld was required to fuse the deeper spacer strip and produce a void-free weld-base metal interface. With argon shielding gas, tubewall penetration was often as high as 50 percent at the hotter setting. By substituting a mixture of 95 percent argon and 5 percent hydrogen for pure argon, we were able to reduce tubewall penetration while still promoting adequate fusion of the spacer strip (Figure 6.15).

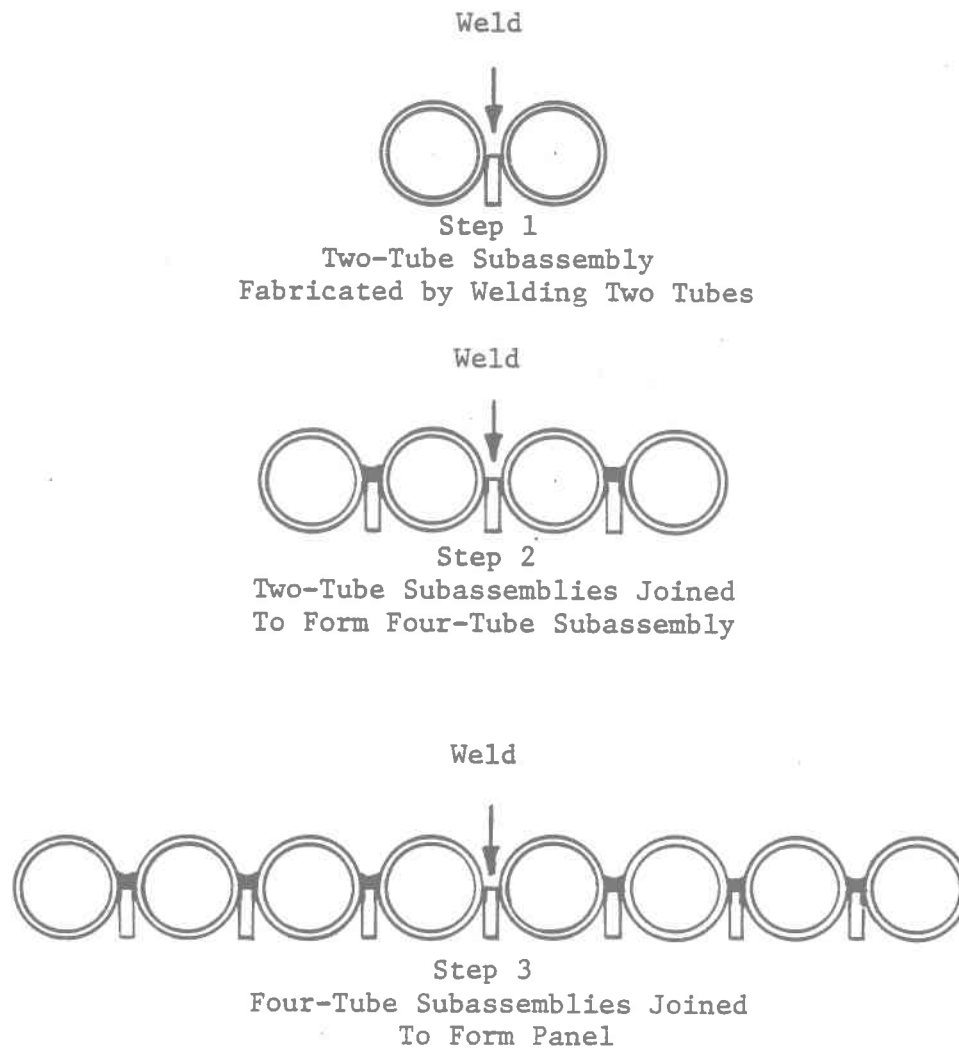


Figure 6.12 Procedure Used for Fabricating Third Development Panel

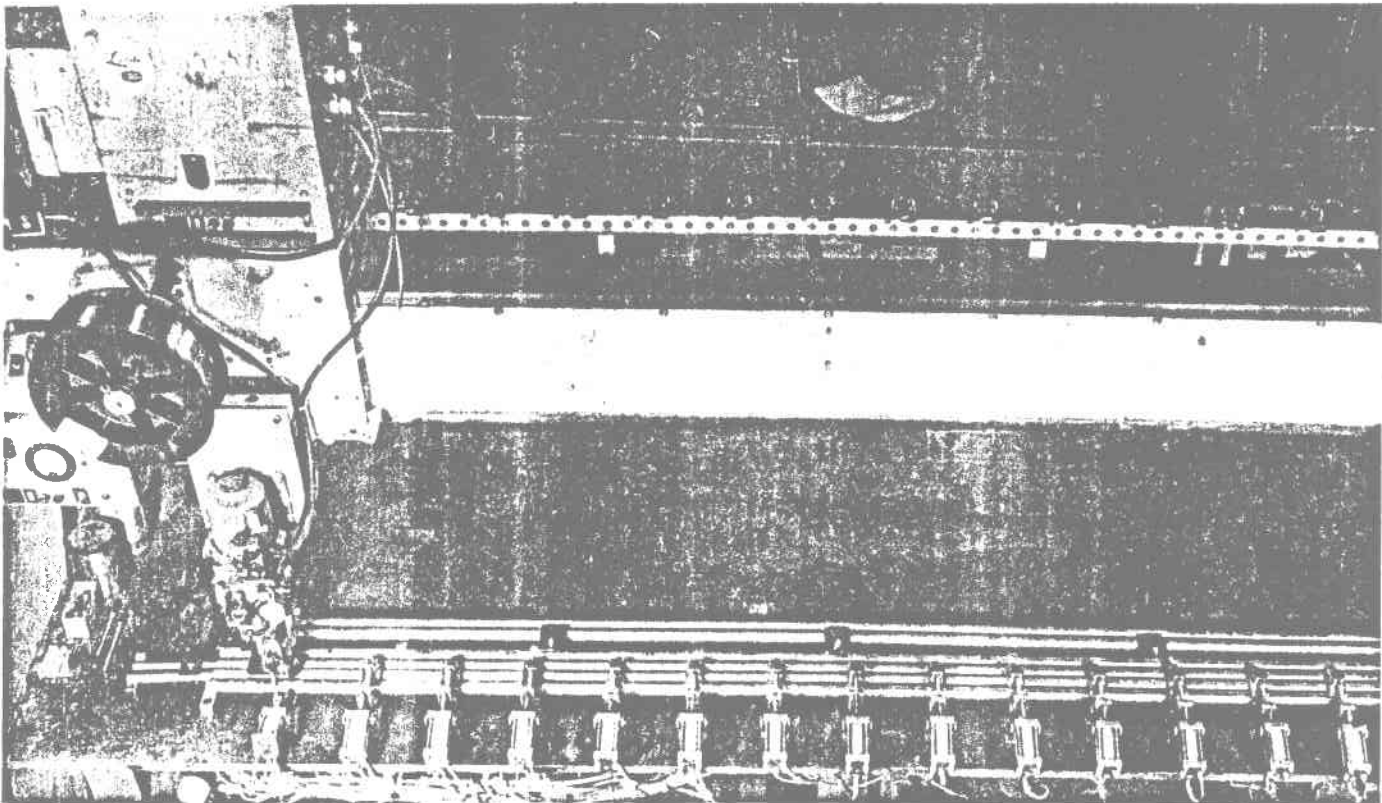


Figure 6.13 Welding of Four-Tube Subassemblies for Third Development Panel

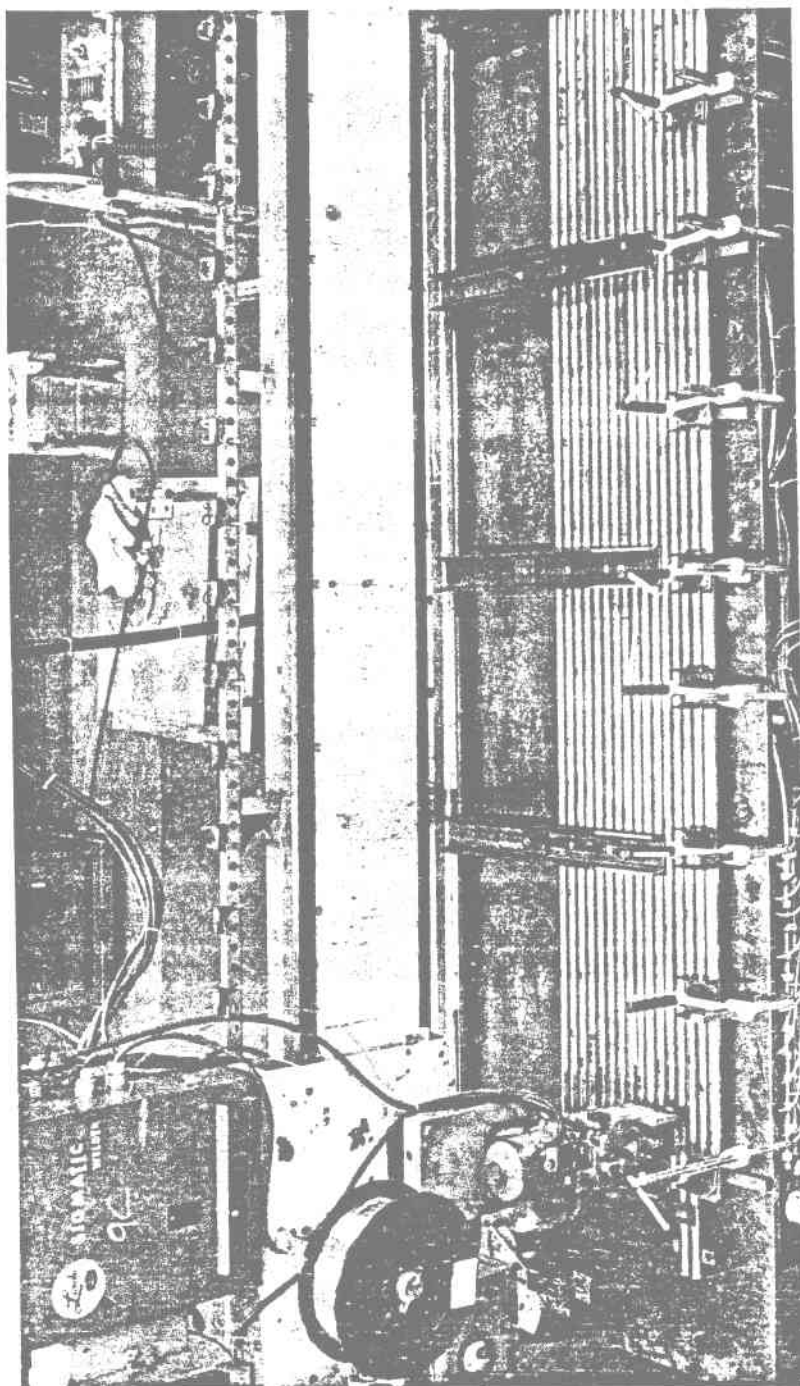


Figure 6.14 Welding of Four-Tube Subassembly to In-Process Panel

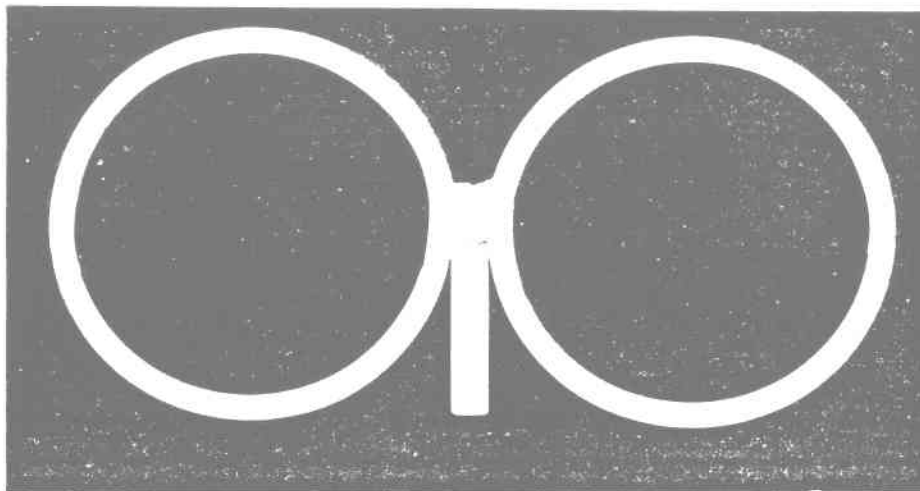


Figure 6.15 Macroscopic Cross Section of Typical Tube-to-Tube Weld in Third Development Panel

The fixture for the third panel was modified and made more rigid in an additional attempt to reduce panel distortion. The following changes were made:

- The supplemental support blocks used in fabricating Panel 2 were eliminated.
- The number of scallops in the remaining support blocks was reduced from three to two.
- Supplemental clamping was used during the fabrication of four-tube subassemblies.
- Clamping of four-tube subassemblies for making the panel was accomplished by sturdy "C" clamps and by "U" channel bars bolted to the table or held in place by jacking bolts.

Having three scallops in the support blocks was judged unnecessary and created problems when we tried to weld the subassemblies. The pneumatic clamps, too weak to restrain four or more tubes, were thought to be a significant factor in earlier panel distortion.

While waiting for the drawn spacer strip to arrive, a full-length [2.44 m (96 in.)] four-tube trial subassembly was made with spacer strip machined from annealed sheet. This trial subassembly displayed very little distortion. However, a subsequent subassembly utilizing the drawn spacer strip displayed 7.9-mm (0.31-in.) negative out-of-plane distortion. The only major difference between the machined and drawn strip was yield strength; the drawn strip was procured 1/4 hard. Resistance annealing of the 1/4-hard strips solved the distortion problem; the assemblies showed no measurable out-of-plane distortion. It is our theory that the negative bowing observed when using 1/4-hard strip was caused by differential expansion across the depth of the strip during welding. This differential expansion caused the strip to bend downward. The annealed strip, having a lower yield strength, experienced compressive yielding or "upset" as a result of the opposing force from the fixture. Consequently, the annealed spacer strip remained straight, and out-of-plane distortion was eliminated.

No serious problems were experienced during the fabrication of the third panel (Figures 6.16 through 6.19). The strip bowing problem previously encountered was completely eliminated.

Figure 6.20 shows an end view comparison between the first and third development panel. As shown by the following measurements of the third panel, out-of-plane distortion was considerably reduced and no measurable in-plane distortion was present.

● Out-of-plane distortion

- Longitudinal bowing	Ends: +7.9 mm (0.313 in.)
	Center: +7.9 mm (0.313 in.)
- Transverse bowing	Ends: None measurable
	Center: None measurable

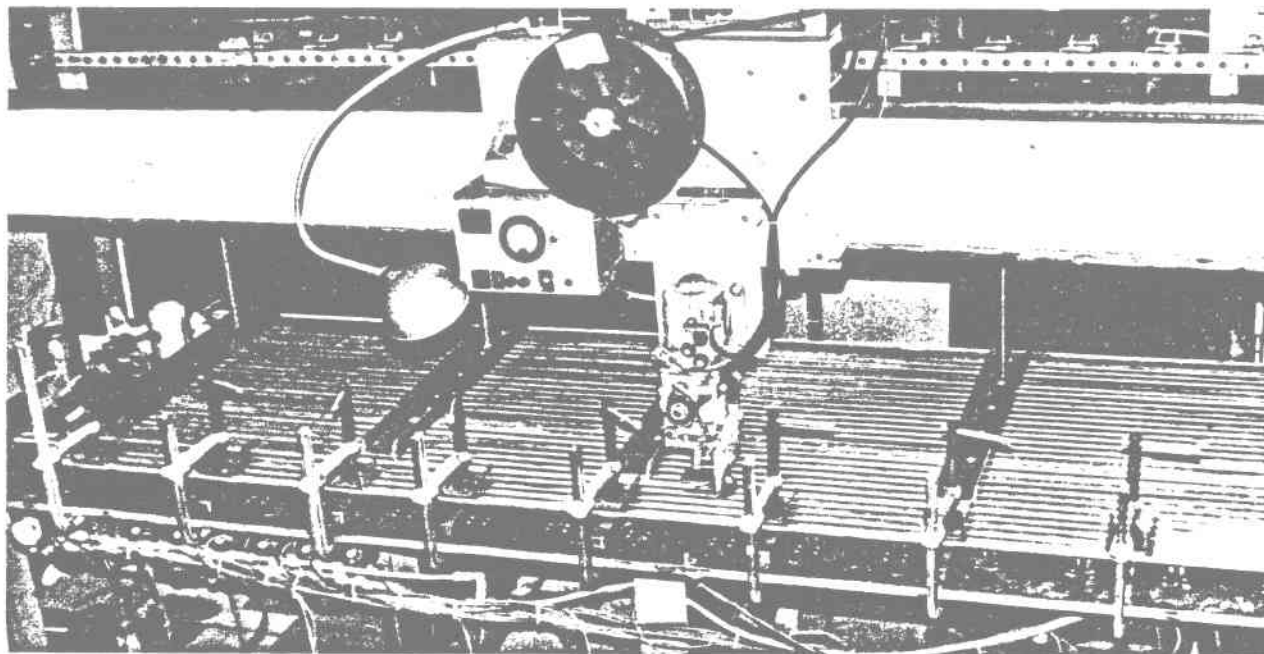


Figure 6.16 Fixture Employed During Fabrication of Third Development Panel

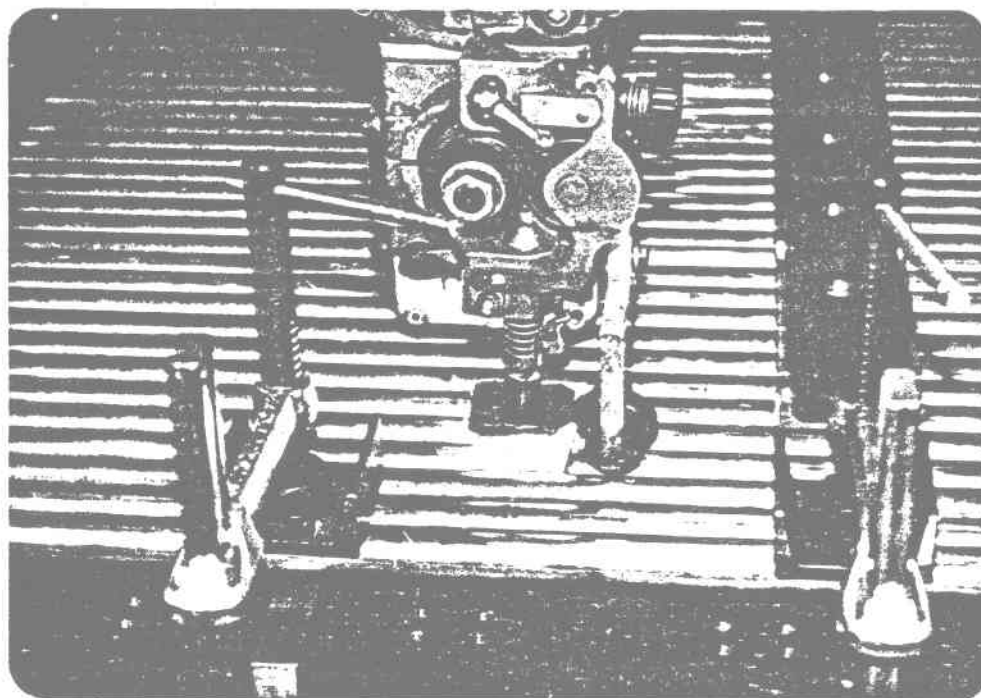


Figure 6.17 In-Process Welding of Last Four-Tube Subassembly

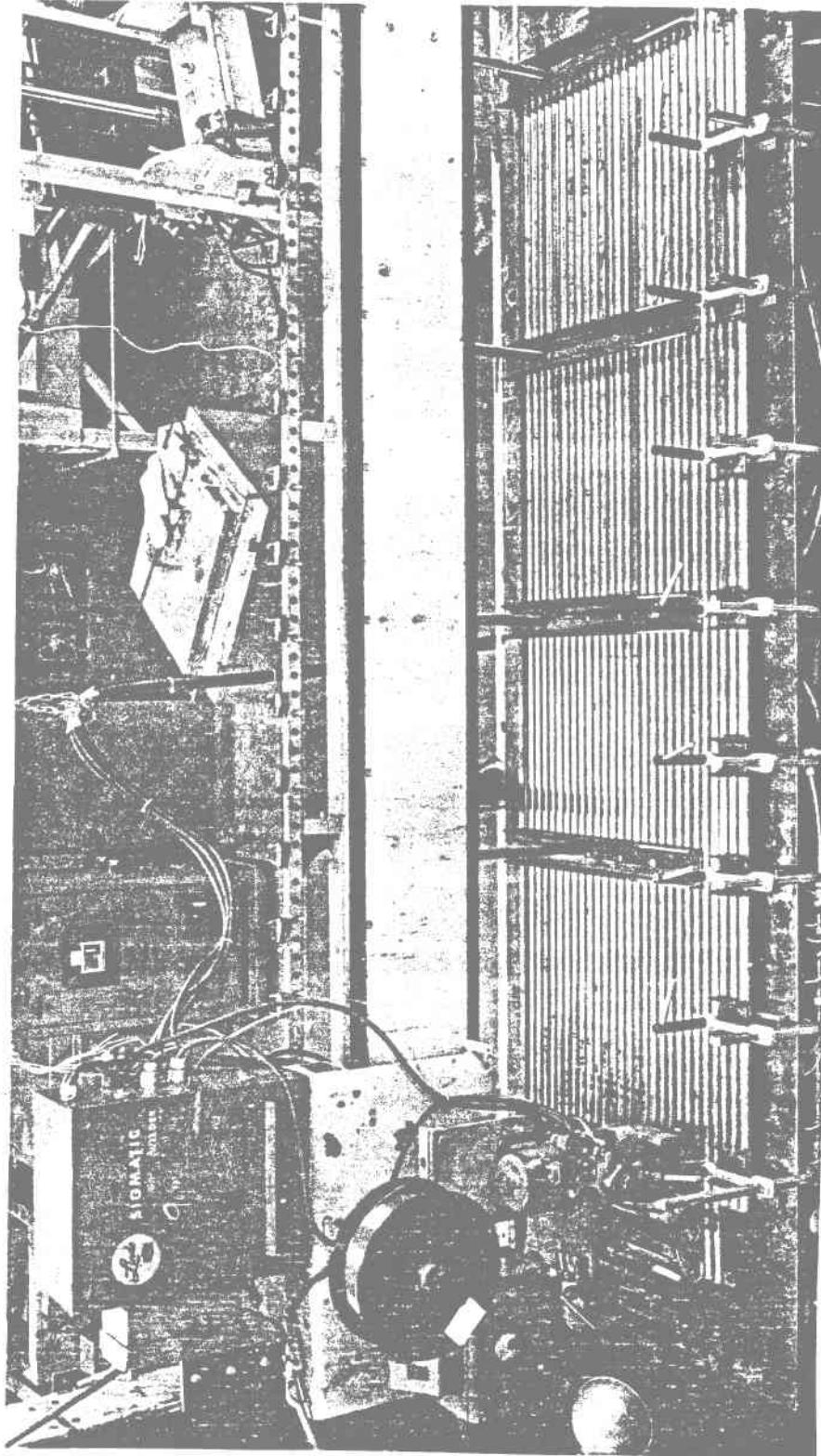
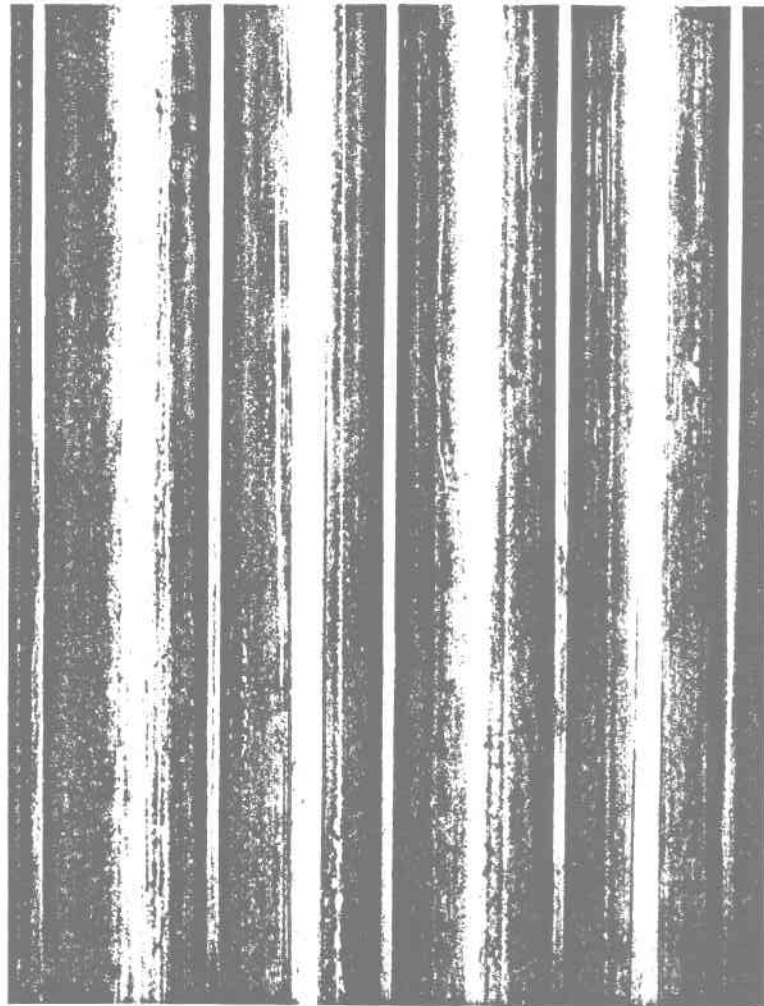


Figure 6.18 Last Stage of Third Development Panel Fabrication

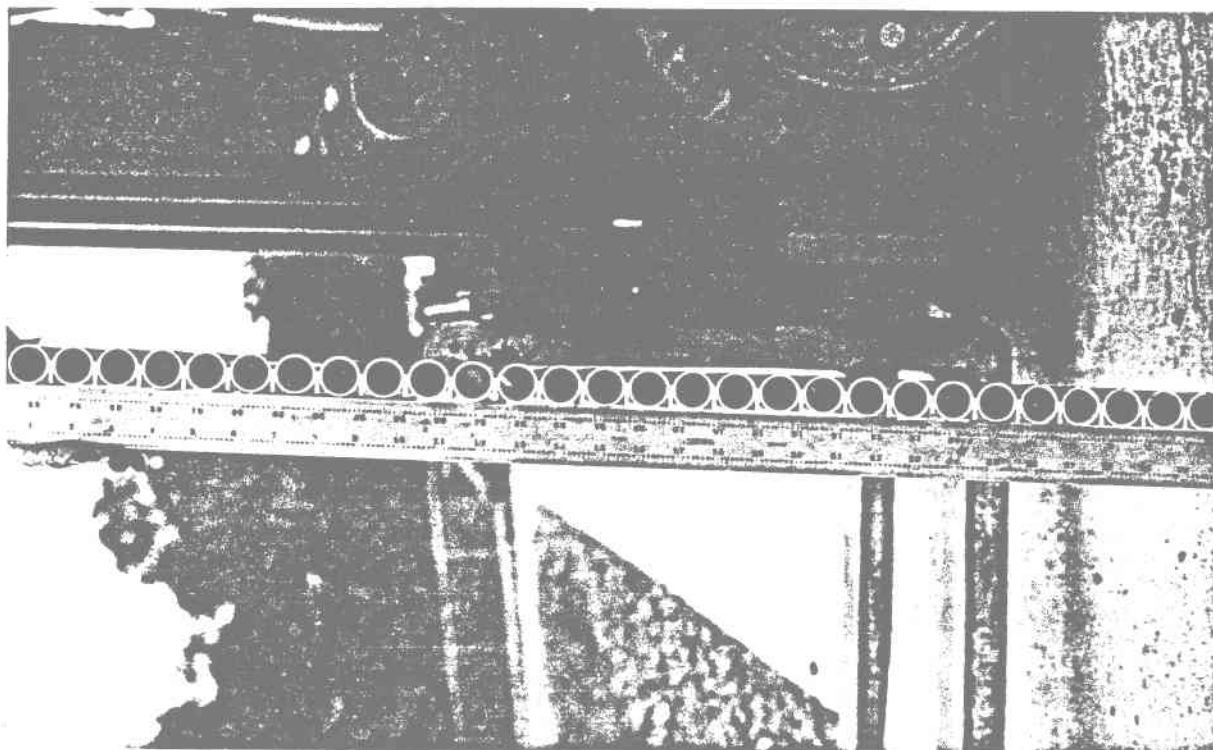


Back

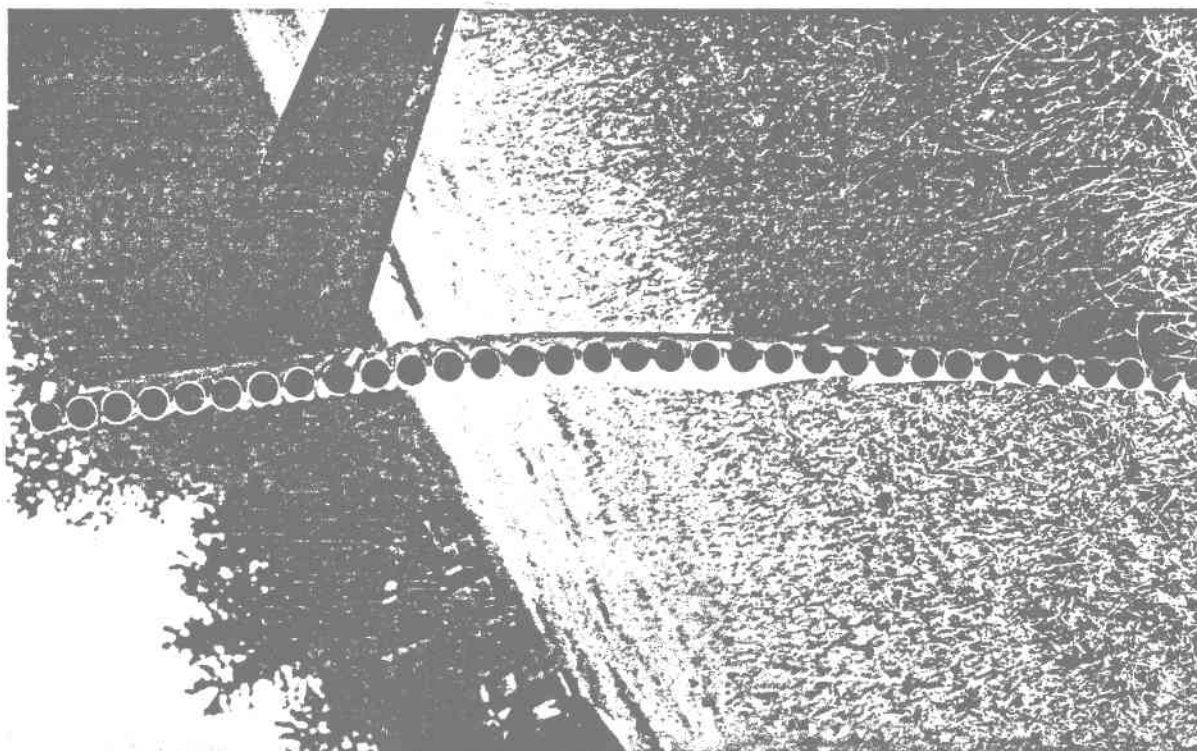


Front

Figure 6.19 Typical Front and Back Close-Up of Third Development Panel Before Welding Last Spacer Strip (Middle of front view)



Third



First

Figure 6.20 Comparison of End Views of First and Third Development Panels

● In-plane distortion

- Width at panel ends: 774 mm (30.47 in.)
- Width at panel center: 774 mm (30.47 in.)
- Width differential: None measurable
- Edge camber (longitudinal): None measurable

At the request of our Manufacturing Engineering Department, longitudinal shrinkage of the panel tubes was measured during the fabrication of the third panel. The shrinkage varied, but it averaged as follows in 2.44 m (96 in.):

Two-tube subassembly:	3.97 mm (0.156 in.)
Four-tube subassembly:	3.17 mm (0.125 in.)
Eight-tube subassembly:	<u>1.57 mm (0.062 in.)</u>
Total	8.71 mm (0.343 in.)

Negligible transverse shrinkage was calculated based on an unwelded panel width of 775 mm (30.53 in.).

The following welding parameters were used to fabricate the third development panel:

- Potential, VDCRP 19 to 20
- Current, amps 150 to 155
- Travel rate, m/min (in./min) 0.76 (30)
- Wire feed rate, m/min (in./min) 9.52 (375)
- Contact tip to work distance, mm (in.) 9.5 (0.375)
- Shielding gas, flow rate, m³/h (ft³/h) 0.71 (25)

6.5 SUPPORT LUG ATTACHMENT

Three methods of attaching support lugs to the panel were evaluated (Figure 6.21). The first method utilized integral welding of the lug and tubes. The lug spanned a tube, and the lug legs replaced a section of the spacer strip. Trial welds were made using the welding parameters used to weld the third development panel (Figure 6.22). Cross-sectional examination showed the welds to be acceptable.

The second method utilized the spacer strip as a point of attachment. A prototypical lug was full-penetration butt-welded its full length to adjacent spacer strips of a panel section. The tungsten inert gas (TIG) method, 1.57-mm (0.062-in.)-dia filler rod, and argon shielding gas were used. The full-length weld induced some negative out-of-plane panel distortion because of a combination of weld metal shrinkage and weld location [≈ 12 mm (≈ 0.47 in.) below the tube neutral axis]. The welds of a second lug were limited to 25.4 mm (1 in.) long full-penetration welds placed at the four corners of the lug. This reduction in weld length lessened panel distortion to a barely perceptible level.

In the third method, spacer strips were also used as a point of attachment. The lug legs were placed inside and in contact with two adjacent spacer strips and were fillet welded to the spacer strips. A prototypical lug was attached to a panel section via 25.4-mm (1-in.)-long fillet welds at the four corners of the lug. TIG welding was again employed, using 1.57-mm (0.062-in.)-dia 308 filler rod and argon shielding gas. Only slight panel distortion was observed.

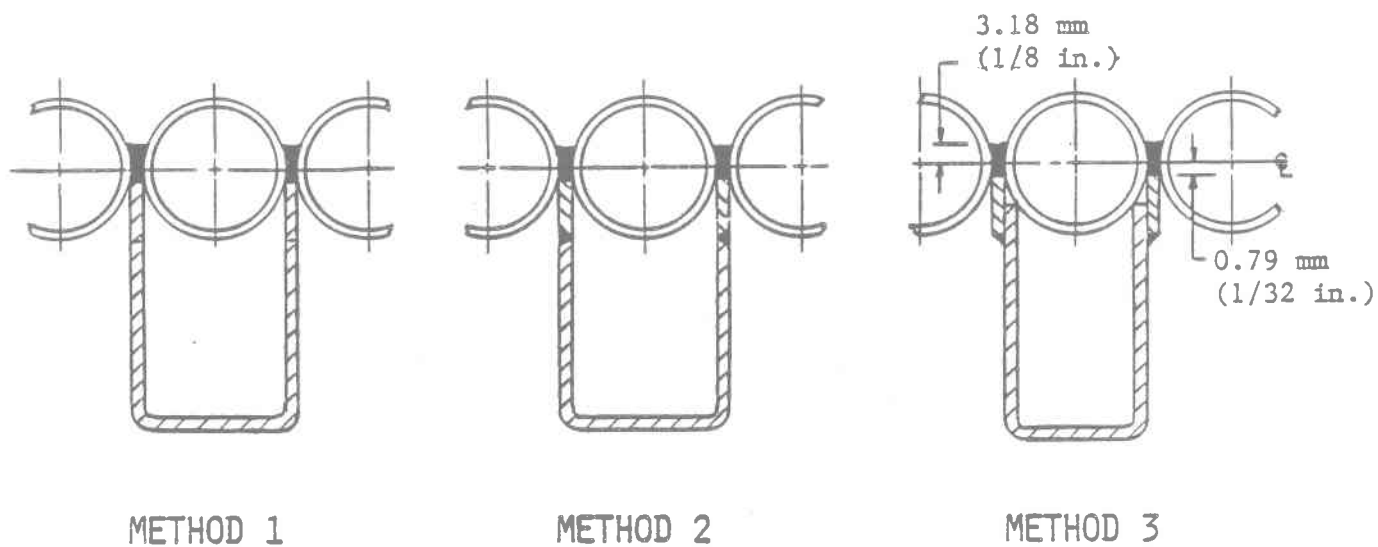


Figure 6.21 Candidate Methods for Attaching Support Lugs to Panel Tubes

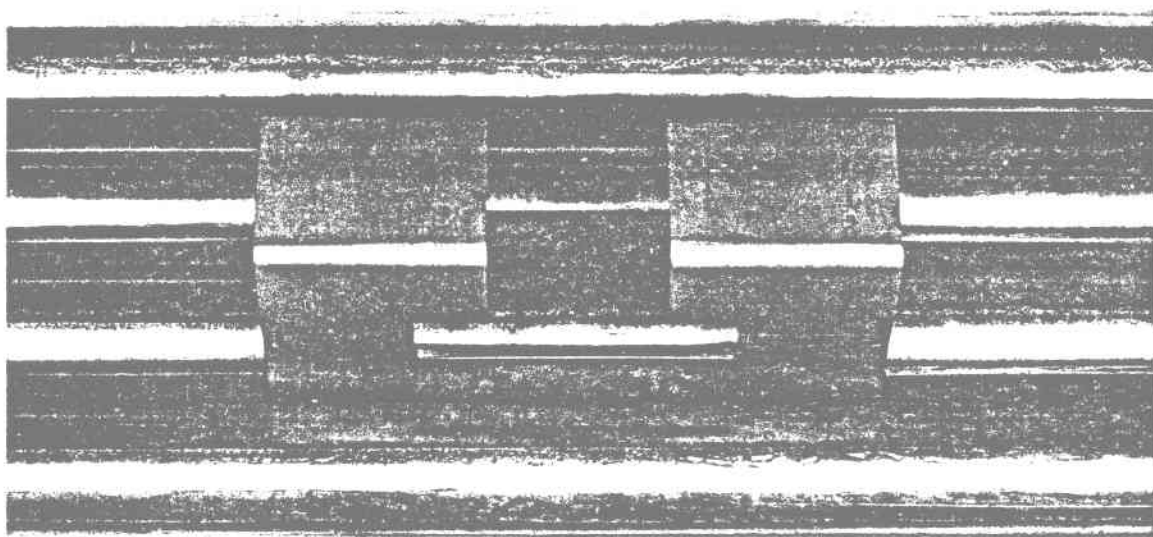


Figure 6.22 Prototypical Panel Support Lug Integrally Welded With Panel Tubes

The second and third attachment methods (Figure 6.23) were selected for further evaluation. The first method was discarded because:

- Precise positioning of lugs would be difficult in a full-size panel because of longitudinal weld-induced panel shrinkage
- Attachment of lugs at this point in the fabrication process would make panel flattening difficult, if required
- Cost of fabrication would increase.

The third attachment method was selected by Manufacturing Engineering because it is easier to position and to weld.

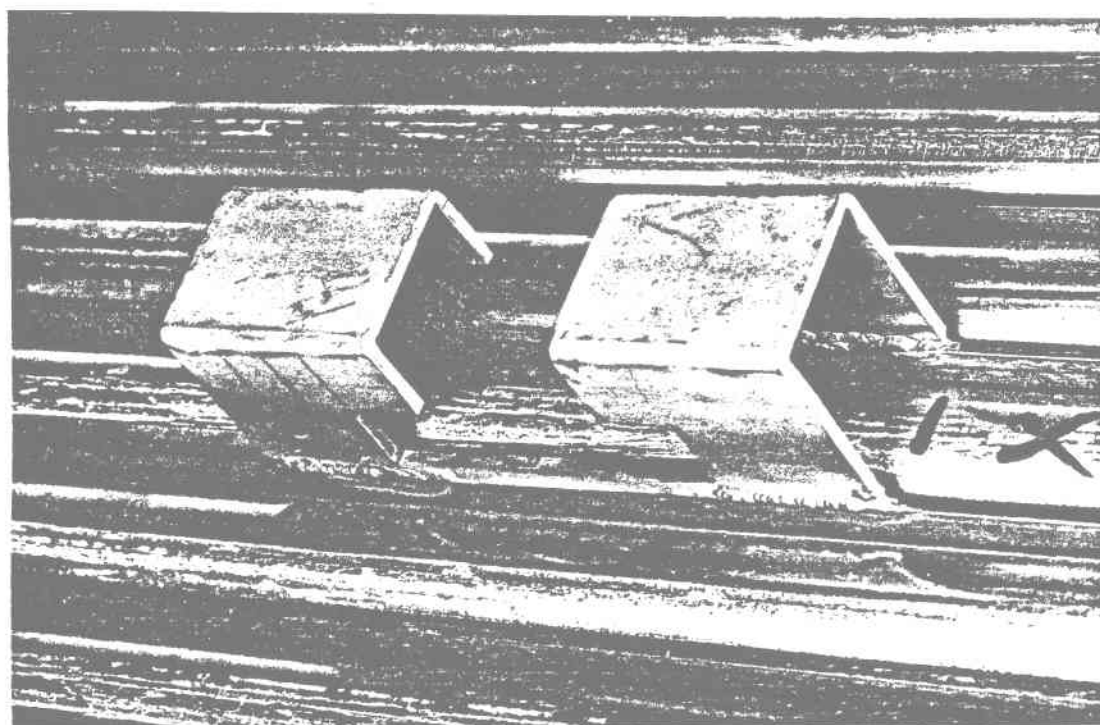
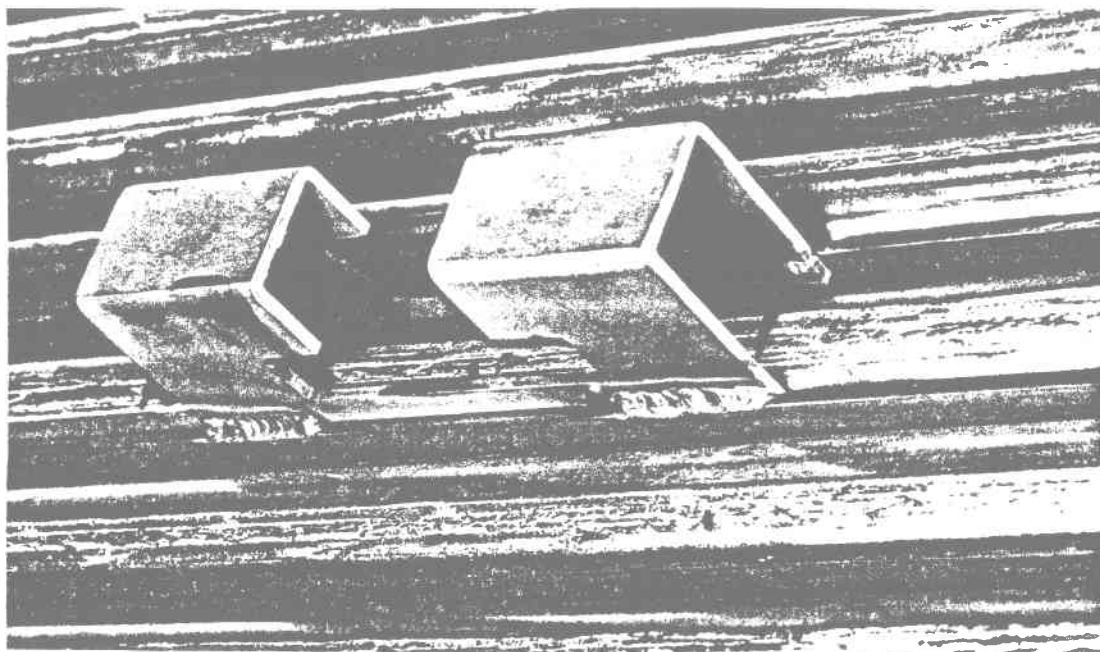


Figure 6.23 Close-Up of Prototypical Support Lugs Welded to Spacer Strip

6.6 EVALUATION AND TESTS

6.6.1 Weld Evaluation

Weld quality, tubewall penetration, and overall weld geometry were continuously monitored during trial welding and development panel fabrication by destructive and nondestructive tests and examinations.

The nondestructive tests were conducted as follows:

- The surface of the welds was visually examined at up to 10X magnification and were also subjected to liquid dye-penetrant examination for evidence of porosity, cracking, or lack of fusion.
- The inner surface of welded tubes was visually examined for evidence of tubewall burn-through.

No anomalies were observed.

Destructive tests were performed on cross-sectional samples removed from 0.3-m (1-ft)-long two-tube or four-tube subassemblies prepared for this purpose. Tests and examinations conducted were:

- Microhardness measurements of the heat and the heat-affected zone (HAZ)
- Macroscopic examination via stereo-microscope from 10X to 70X for weld soundness, degree of tubewall penetration, and overall weld geometry
- Microscopic examination at up to 500X for lack of base metal fusion and for small defects such as shrinkage cavities, microporosity, or microfissuring
- Hammer bend tests to evaluate for weld metal embrittlement and lack of fusion.

The welds produced were sound and tough and they displayed adequate base metal fusion without excessive tubewall penetration. Figure 6.24 is macroscopic and microscopic views of typical welds for Development Panel 1.

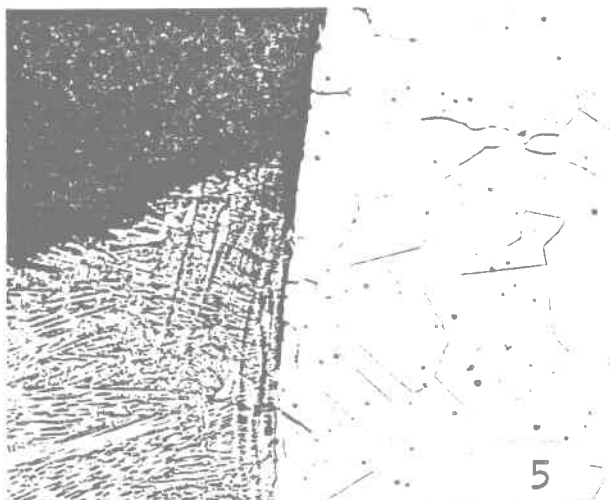
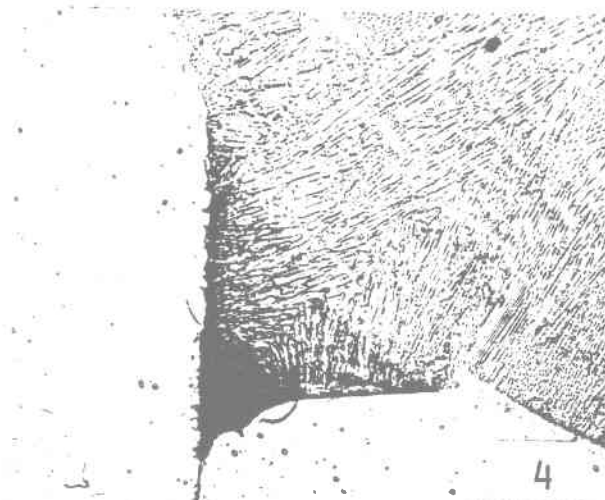
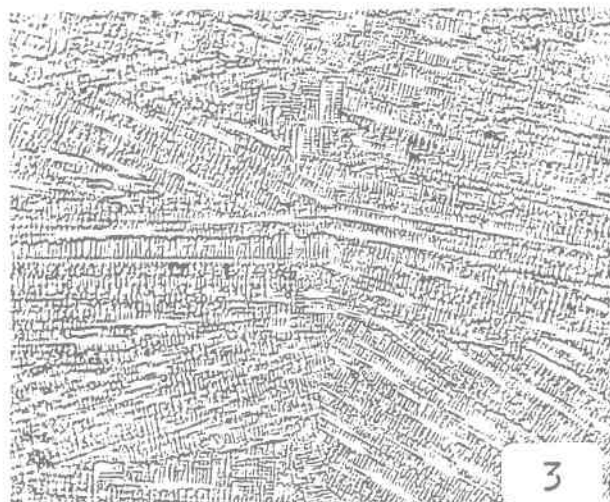
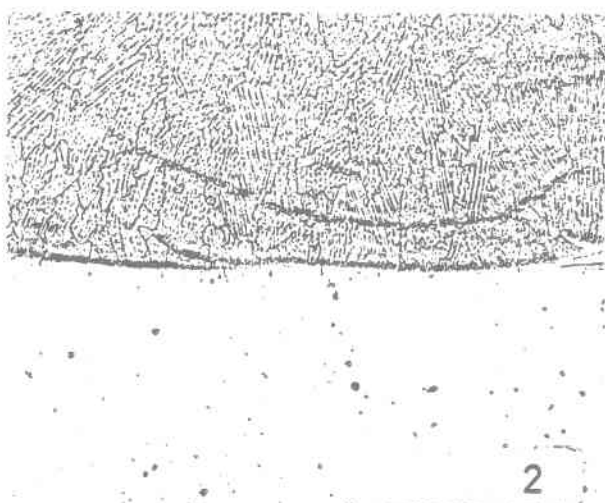
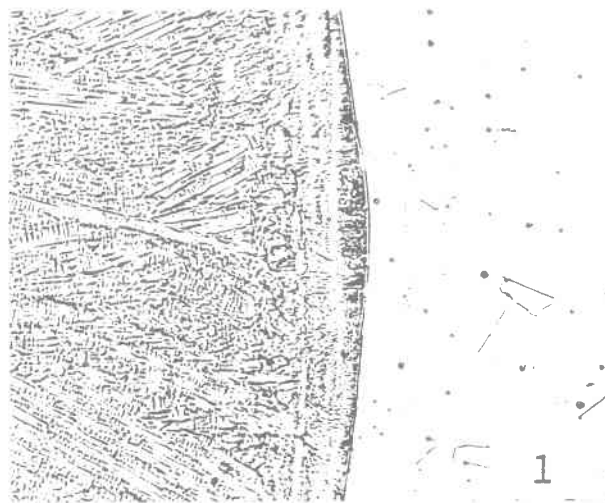
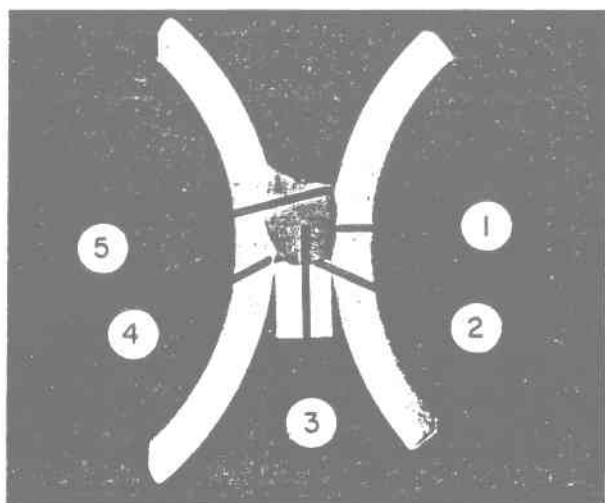


Figure 6.24 Macroscopic Cross Sections of Panel Weld Cut From First Development Panel

6.6.2 Panel Weld Strength Tests

A series of strength tests described in the FPDP (Appendix R) were conducted at ambient temperature on specimens removed from the first development panel. The tests were designed to subject the specimens to loading and bending conditions exceeding those anticipated during normal panel operation and thus to demonstrate the adequate safety factor of the tube-joining method. The first panel, made of Incoloy 800, was used for testing.

Longitudinal Bend Test. Two specimens, three tubes wide by 1.2 m (48 in.) long, were bent 180 deg longitudinally at a radius of approximately 0.15 m (6 in.). The weld face was located at the outer surface of the bend (Figure 6.25). The tubes were filled with sand and the ends were sealed before bending to prevent the tubewall from collapsing. The welds and the HAZ of the tube were liquid dye-penetrant examined both before and after bending. No cracking of the welds or tubes was observed.

Transverse Bend Test. Two specimens, 20 tubes wide by 0.15 m (6 in.) long, were bent 180 deg at a radius of 0.15 m (6 in.) in the transverse direction. The weld face was again located at the outer surface of the bend (Figure 6.26). Both the welds and the HAZ of the tube were liquid dye-penetrant examined before and after bending. No cracks were observed in the welds or tubes.

Transverse Panel Tensile Test. One specimen, six tubes long (Figure 6.27), was subjected to a transverse tensile test (Figure 6.28) to failure

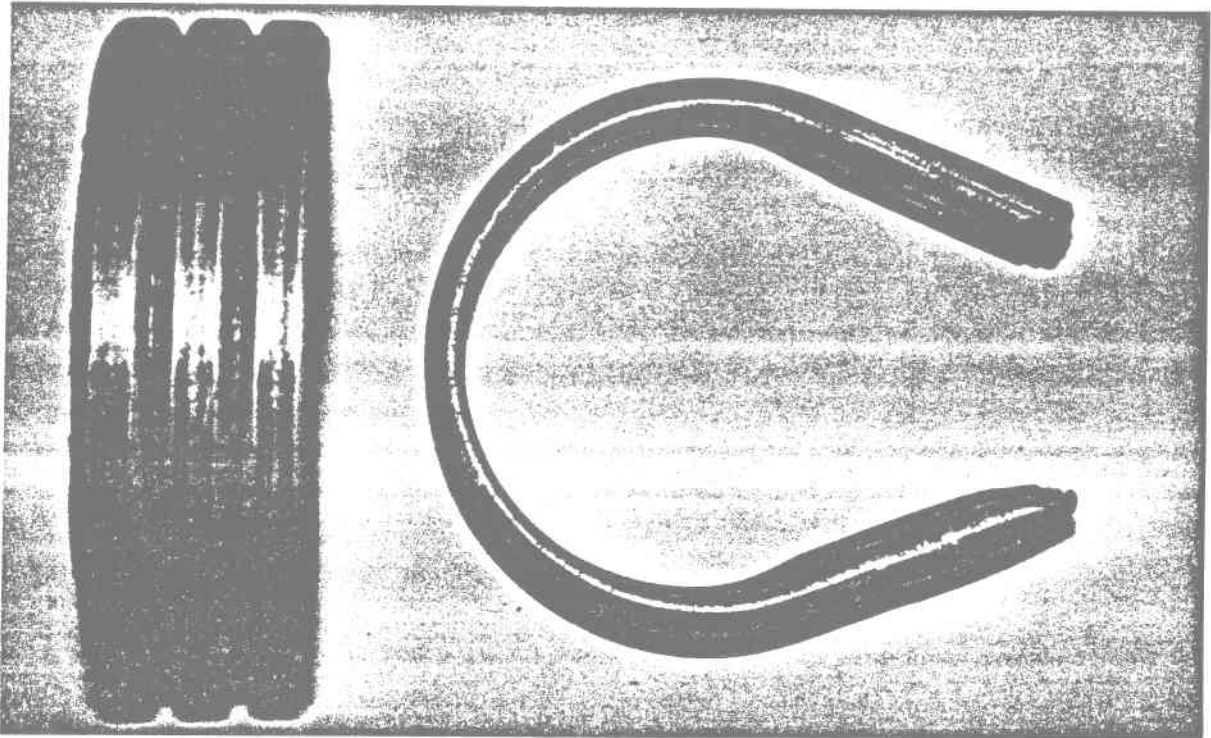


Figure 6.25 Top and Side Views of One of Two Longitudinal Bend Test Specimens

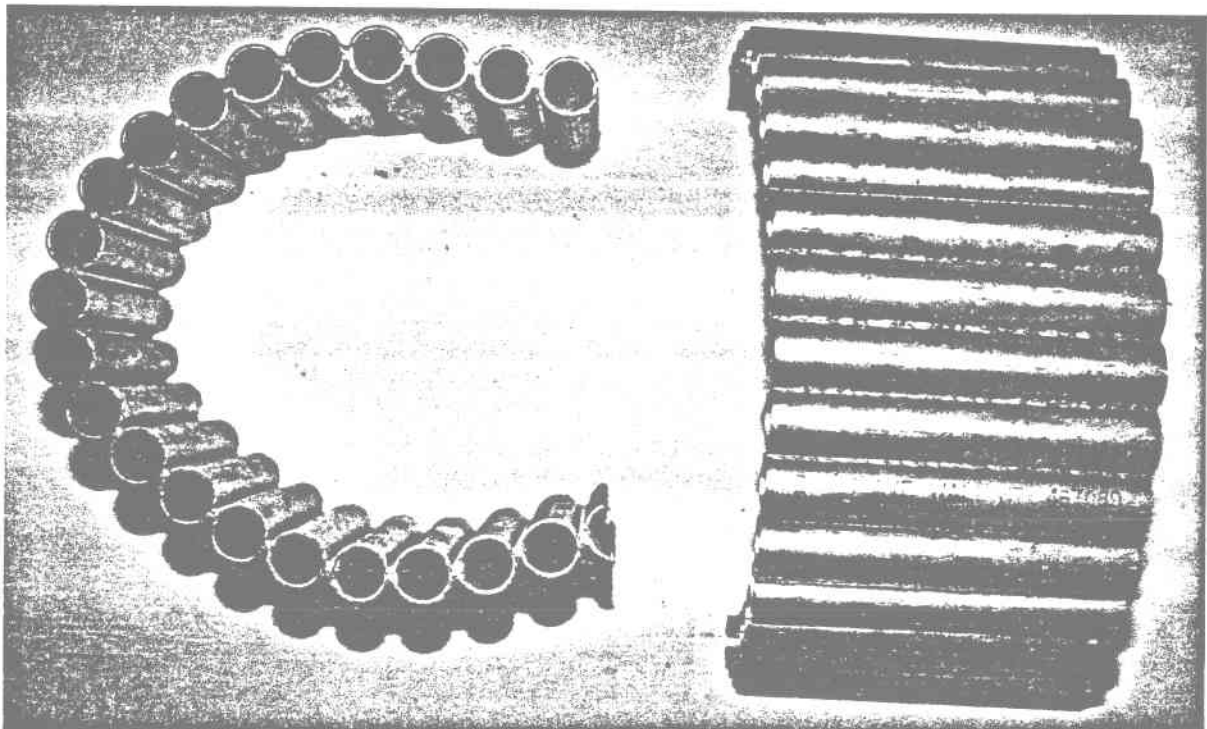


Figure 6.26 Top and Side Views of One of Two Transverse Bend Test Specimens

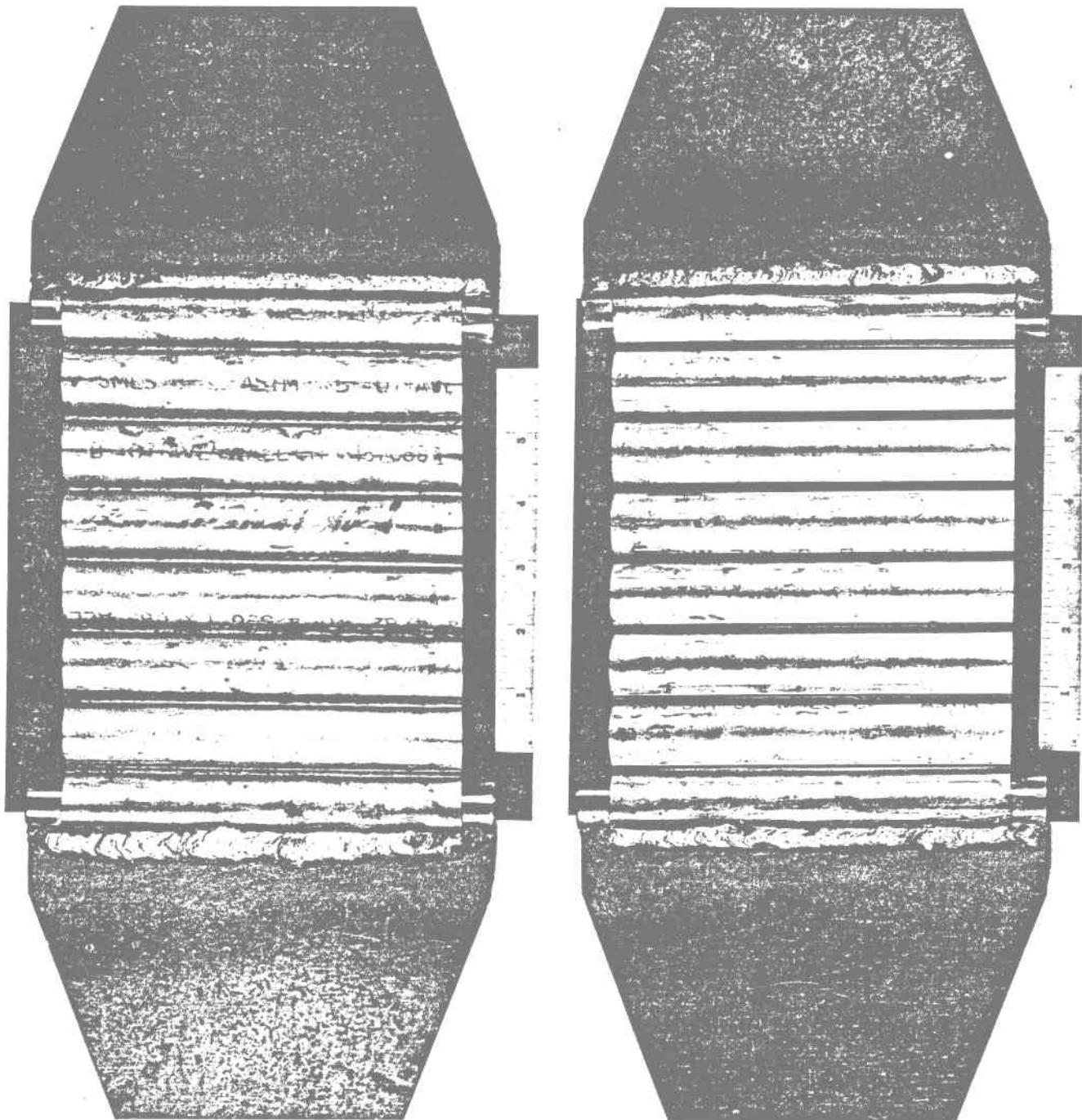


Figure 6.27 Front and Back Views of Transverse Tensile Test Specimen Before Test

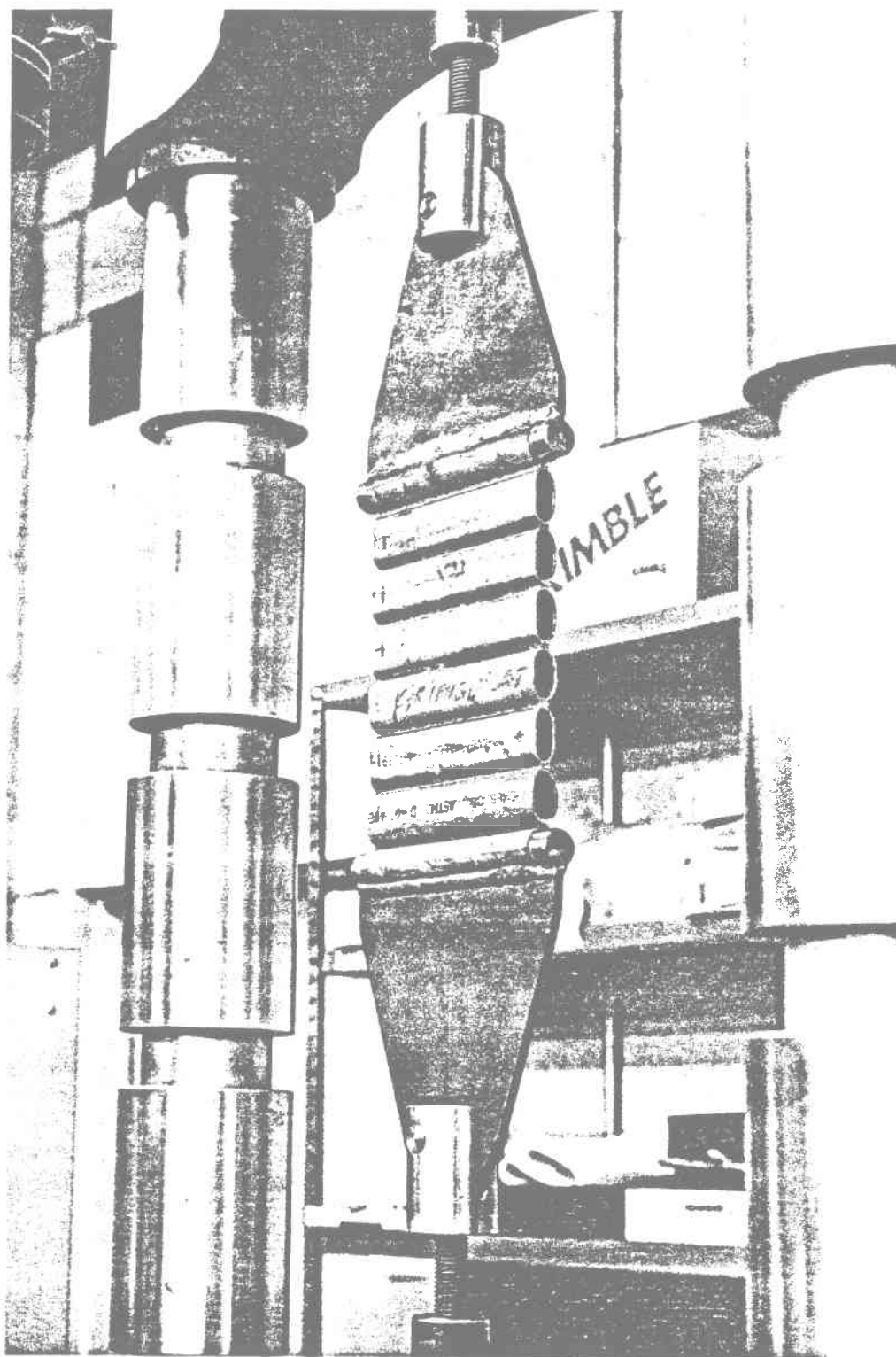


Figure 6.28 Transverse Tensile Test Specimen During Testing

to determine the ultimate tensile strength of the welds. The specimen was liquid dye-penetrant examined before testing to ensure that there were no weld defects. The specimen failed in the HAZ of the middle tube (Figure 6.29) at a tensile load of 126.9 kN (28.5×10^3 lb). Using the cross-sectional area of the fracture, the ultimate tensile stress was estimated at approximately 529 MPa (76.7×10^3 lb/in²).

The strength tests demonstrated that the panel welds are at least as strong as the tubes and that they should satisfy the ASME Code Criteria.

6.6.3 Panel Lug Strength Test

Two prototypical panel lugs were subjected to a tensile strength test to show that the lug design would prevent tube distortion under maximum design load conditions and to determine the maximum load-carrying capacity of lugs, attachment welds, or both.

A 16-tube wide x 0.45-m (17.5-in.)-long test panel was fabricated in the same manner as Development Panel 3. The two lugs were attached to the center of the panel lengthwise at tube positions 4 and 13 using the two attachment methods selected (i.e., butt- and fillet-welding the lugs to adjacent spacer strips). Both lugs were attached using a 25.4-mm (1-in.)-long welds at the four corners of the lug legs. TIG welding using argon and 1.57-mm (0.062-in.)-dia 308 filler rod was used.

The test panel (Figure 6.30) was fastened to the cross head of a 0.89-MN (2×10^5 -lb)-capacity Baldwin Universal Tensile Test Machine (Figure 6.31). The

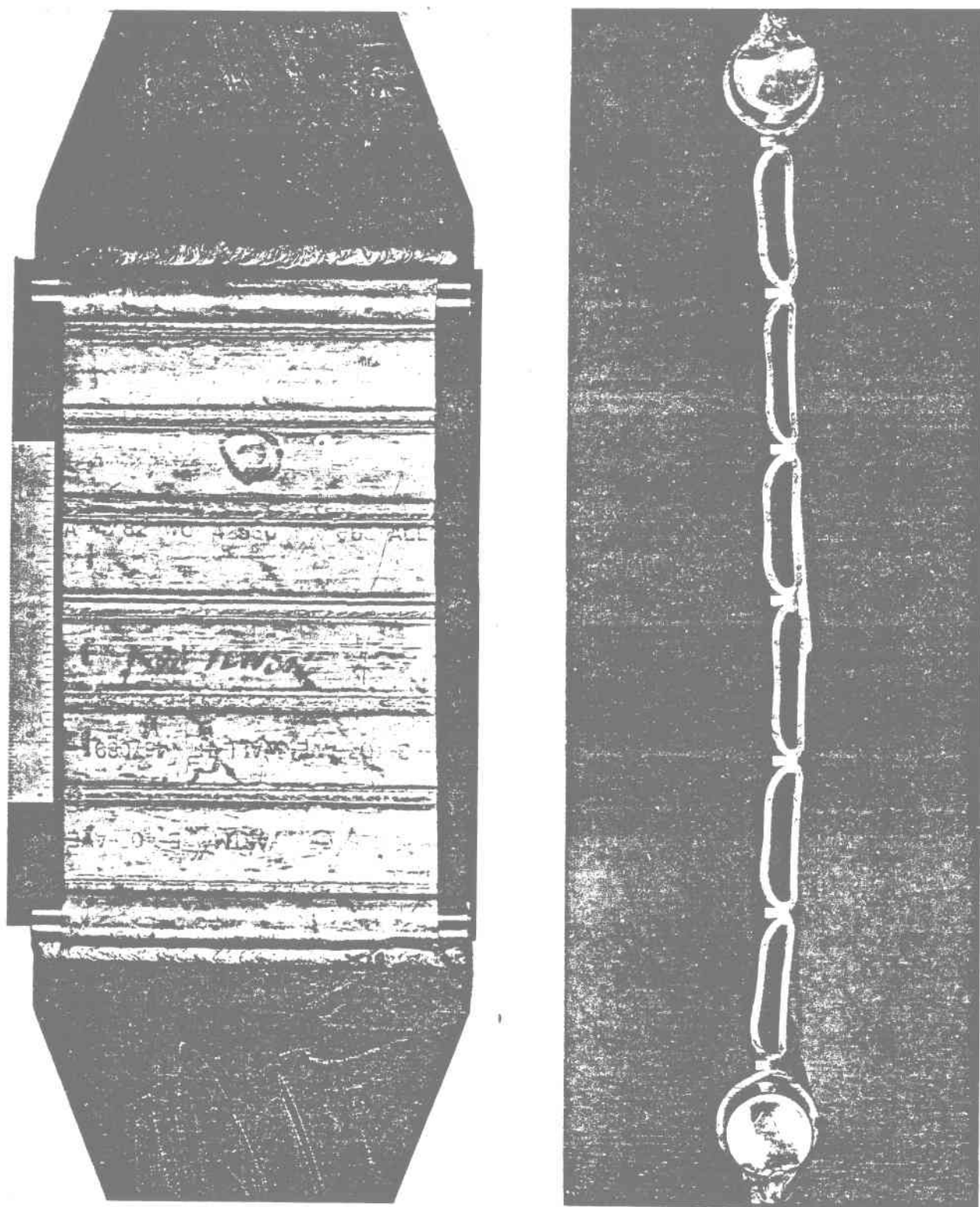


Figure 6.29 Front and Edge Views of Transverse Tensile Test Specimen After Test (Note fracture in adjacent-to-middle weld in HAZ of Tube)

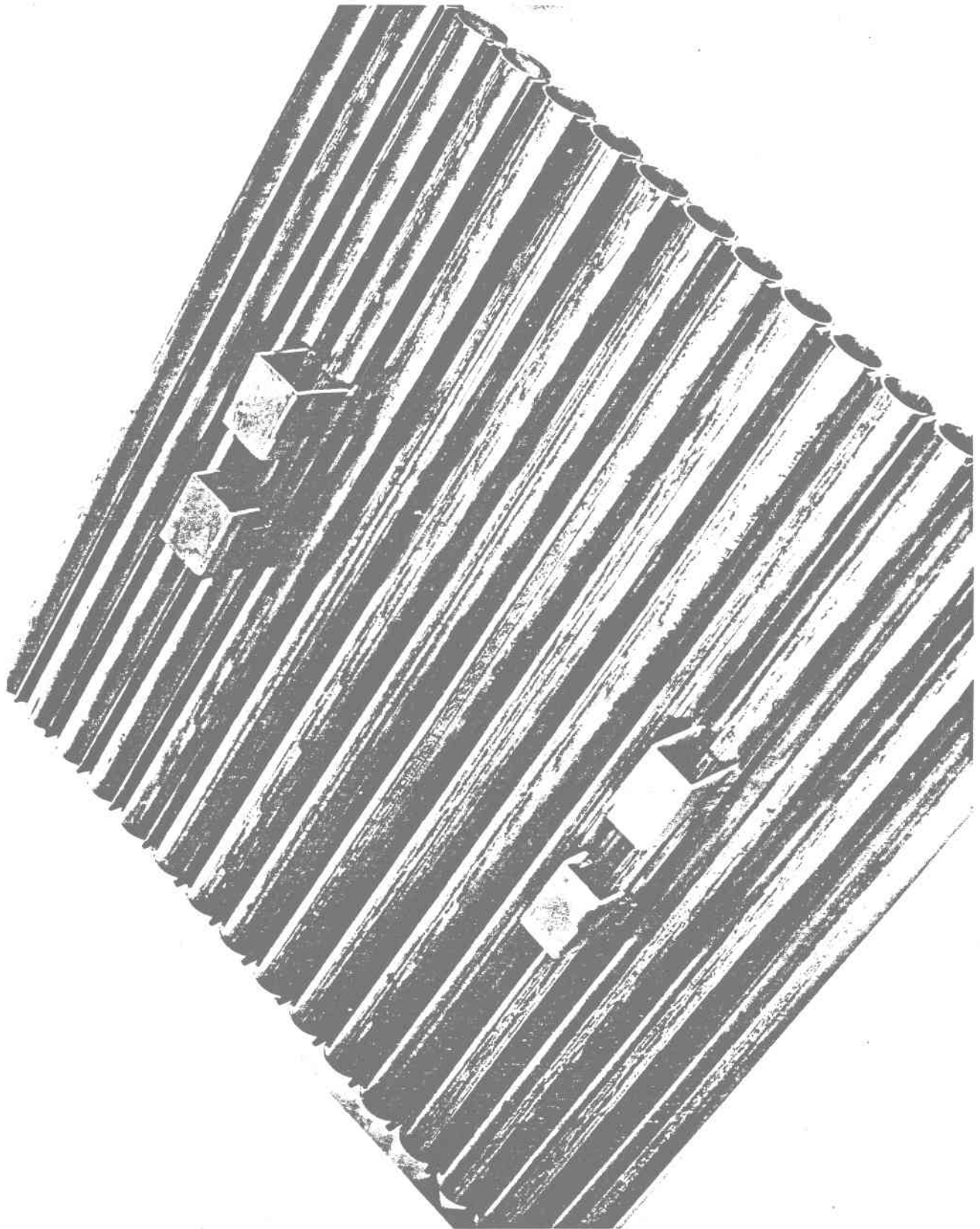


Figure 6.30 Panel Support Lug Test Panel Before Test

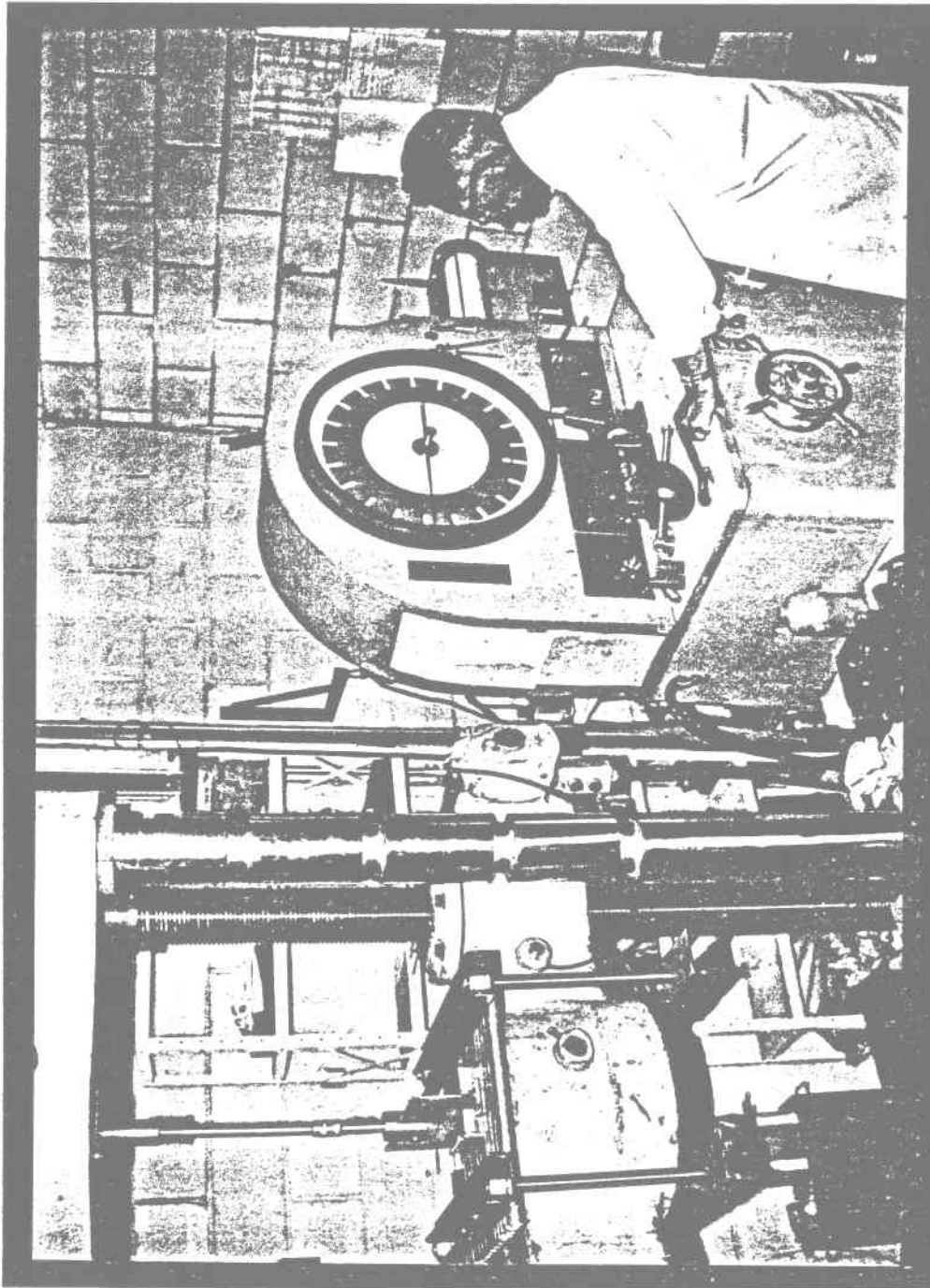


Figure 6.31 Baldwin Universal Tensile Test Machine Used for Tensile Tests

lugs were tensile loaded by means of a 50.8-mm (2-in.)-wide x 0.1-m (4-in.)-high "T" bar placed through the lugs. The bar/lug/test panel combination was loaded via a pinned bar located at the top center of the "T" bar (Figure 6.32).

The lugs were first loaded to 2224 N (500 lb) [i.e., 1113 N (250 lb) each, which is the design load]. No tube or lug distortion was observed. The lugs were then slowly loaded until failure occurred at 72.3 kN (16,250 lb) which is approximately 32 times the design load. Failure occurred through two of the fillet welds (Figures 6.33 and 6.34). Obviously, the lugs had adequate reserve strength.

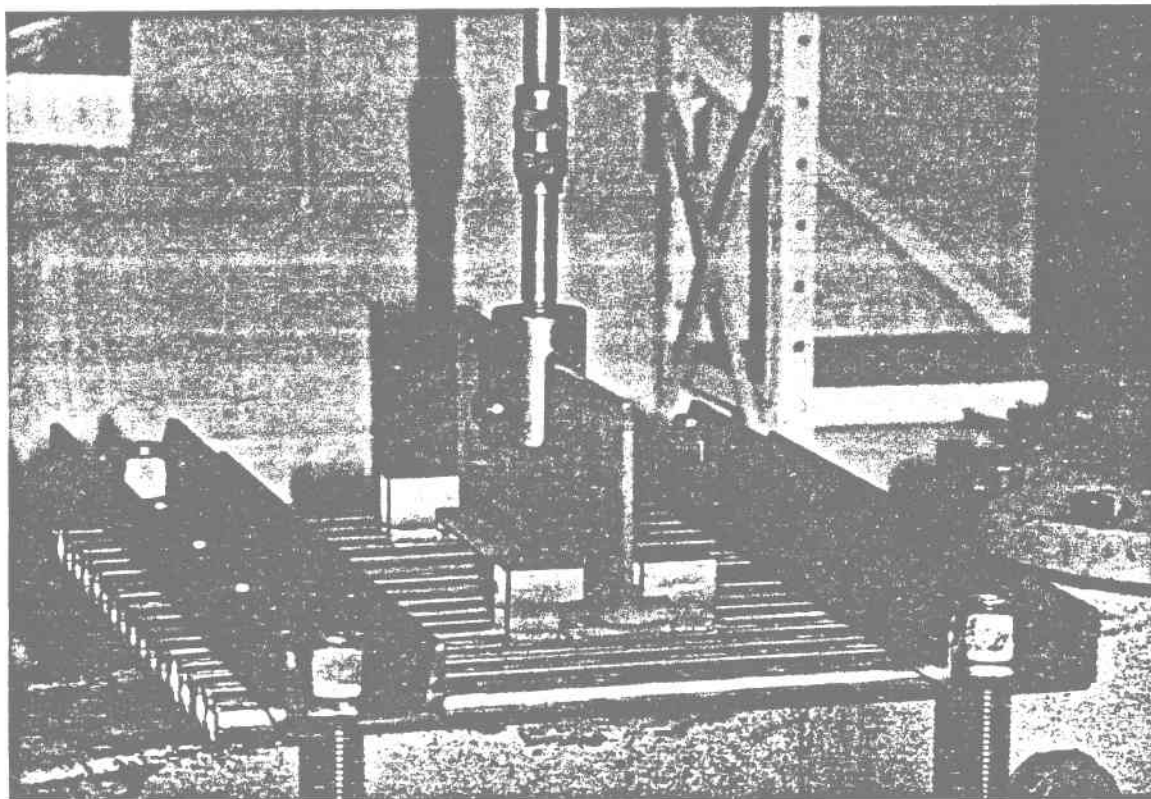


Figure 6.32 Close-Up of Test Rig Used to Tensile Load Prototypical Panel Support Lugs

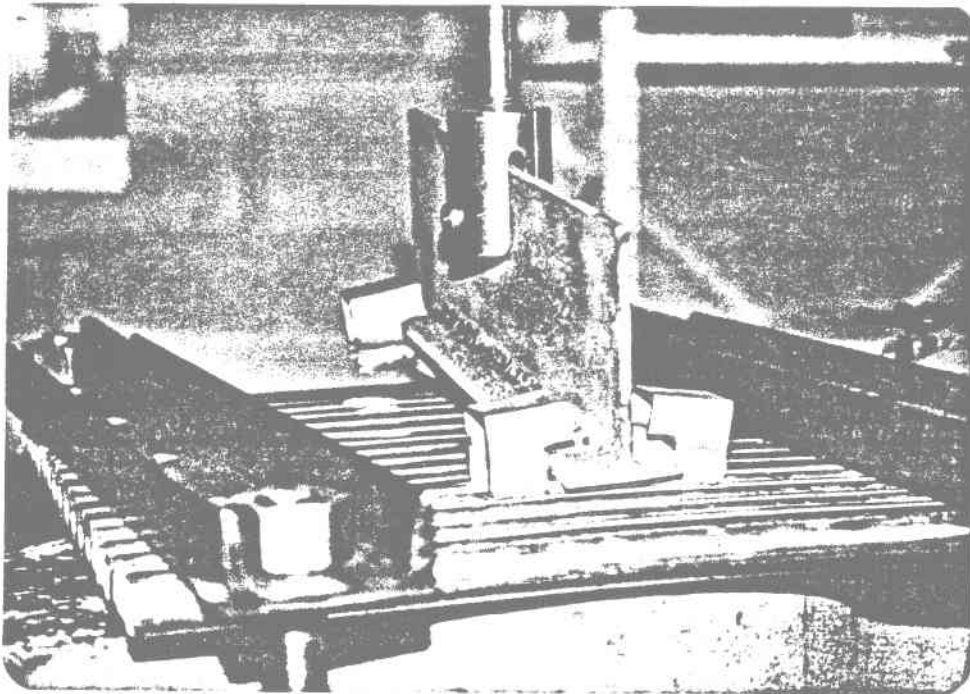


Figure 6.33 Failed Prototypical Support Lug

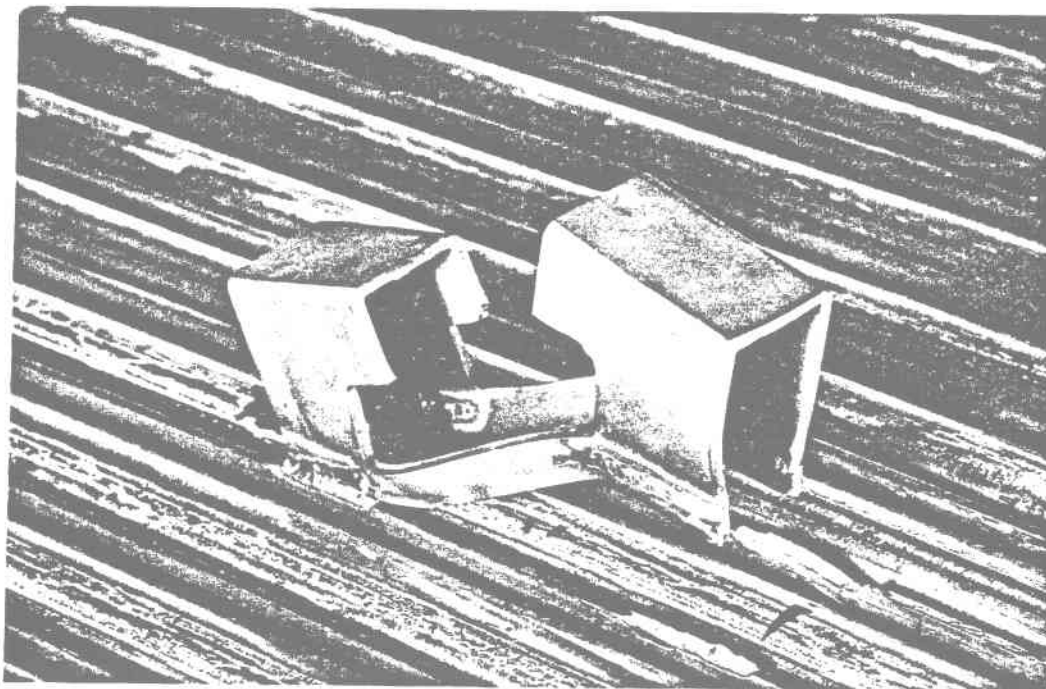


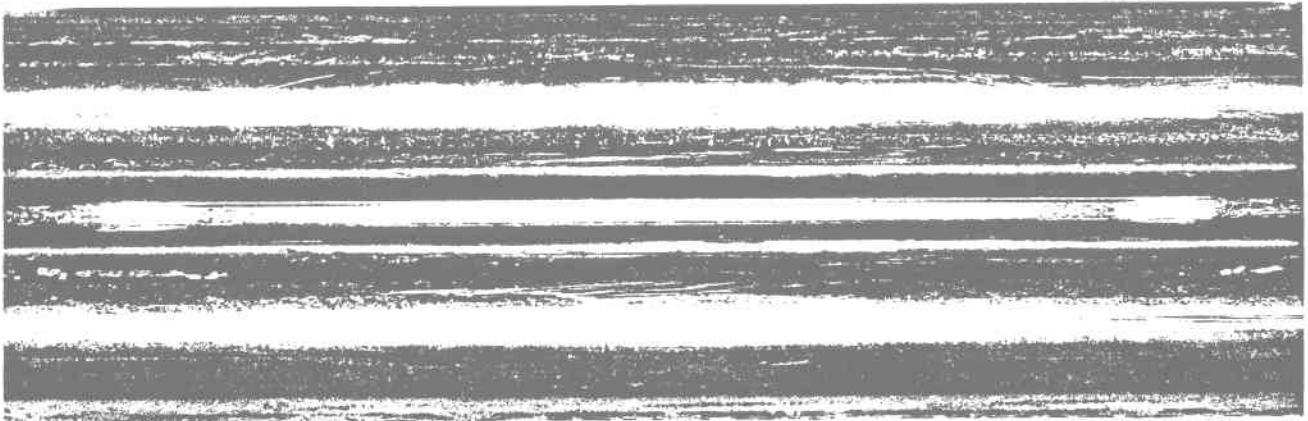
Figure 6.34 Close-Up of Failed Support Lug

6.7 REPAIR WELDING

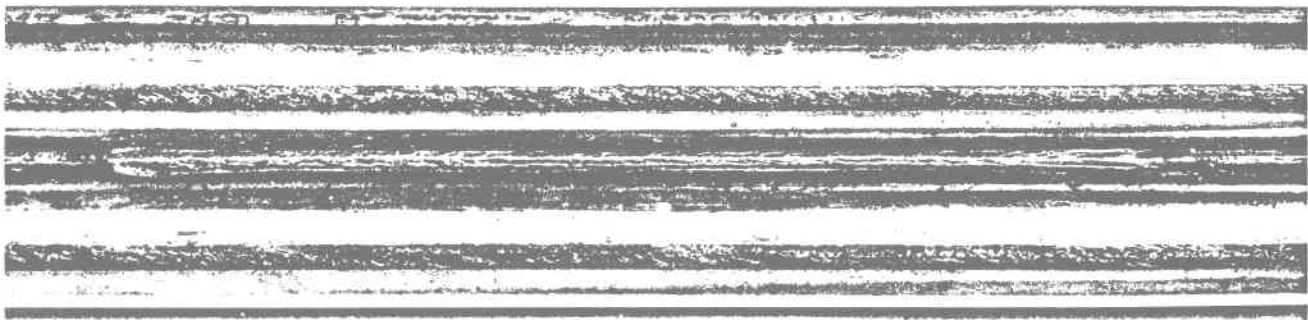
Weld repairs were performed on 30.5-mm (1-ft)-long two-tube welded specimens prepared from Type 304SS tubes and spacer strip, and Inconel 82 electrode. The cross-sectional geometry of the specimen was the same as that of Development Panel 3.

Approximately 0.15 m (6 in.) of weld was removed down to the original top edge of the spacer strip. The cavity created was cleaned and rewelded; the weld was visually examined. The rewelded specimens were then cut through their cross sections, and the rewelds were further examined using the techniques previously described (Section 6.6.1).

Welds were initially removed by grinding using a 76-mm (3-in.)-dia x 1.59-m (1/16-in.)-thick fiberglass-reinforced cutoff disc chucked in a hand-held rotary air tool. Cavities produced by this method varied in cross-sectional profile and depth, making consistently acceptable weld repairs difficult to obtain. Also, residual binder from the cutoff wheel was suspected of causing weld metal porosity. Milling was then substituted for grinding. Specimens were chucked in a Bridgeport milling machine and the weld metal was milled away using a 0.1-m (4-in.)-dia x 2.38-m (3/32-in.)-thick profile cutter. A lubricant was used initially during the milling operation but was later discarded (i.e., the milling was done dry); residual lubricant was suspected of causing weld metal porosity. Using the latter method, cavities with consistent profiles and depth were created, and with proper cleaning, acceptable repair welds could be consistently produced (Figure 6.35).



(a) Specimen Prepared for Rewelding by Milling Away "Defective" Weld



(b) Typical Weld-Repaired Specimen

Figure 6.35 Weld Repair

Repair welds were made using the same parameters and fixtures employed to fabricate Panel 3, except that the original roller guide was replaced with a roller guide without a protruding lip. However, rewelding at these settings tended to distort the tubewalls (bowed inward). Therefore, repair welds were made with a slightly colder setting (lower voltage) than used originally to minimize distortion.

6.8 PREPARATION OF DEVELOPMENT PANEL 3 FOR SHIPMENT

The third development panel was prepared for shipment to SNLL in the following manner:

- The unwelded extremities of the panel were removed by saw cutting, reducing the length of the panel to 2.2 m (86.5 in.).
- Six support lugs were fillet-welded at each of their corners to the panel spacer strips, as shown in Figure 6.36. Welding was performed by the TIG process using argon shielding gas and 308 filler rod. The lug positions on the development panel were the same as in a full-size panel.
- The finished third panel (Figure 6.37) was encased for shipment in a container fabricated from 19-mm (3/4-in.) plywood and 51- x 101-mm (2- x 4-in.) pine studding (Figure 6.38).

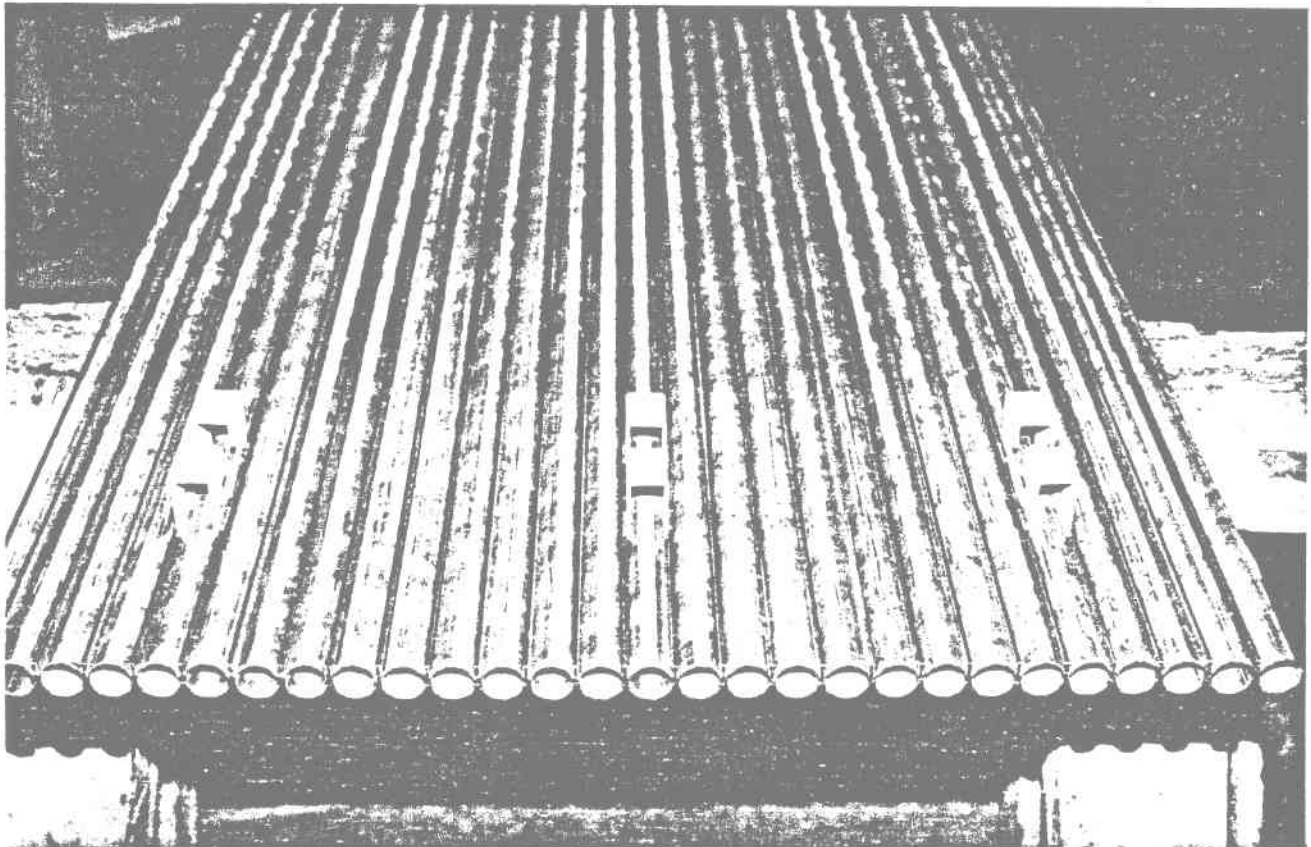


Figure 6.36 End View of Third Development Panel Showing Support Lugs

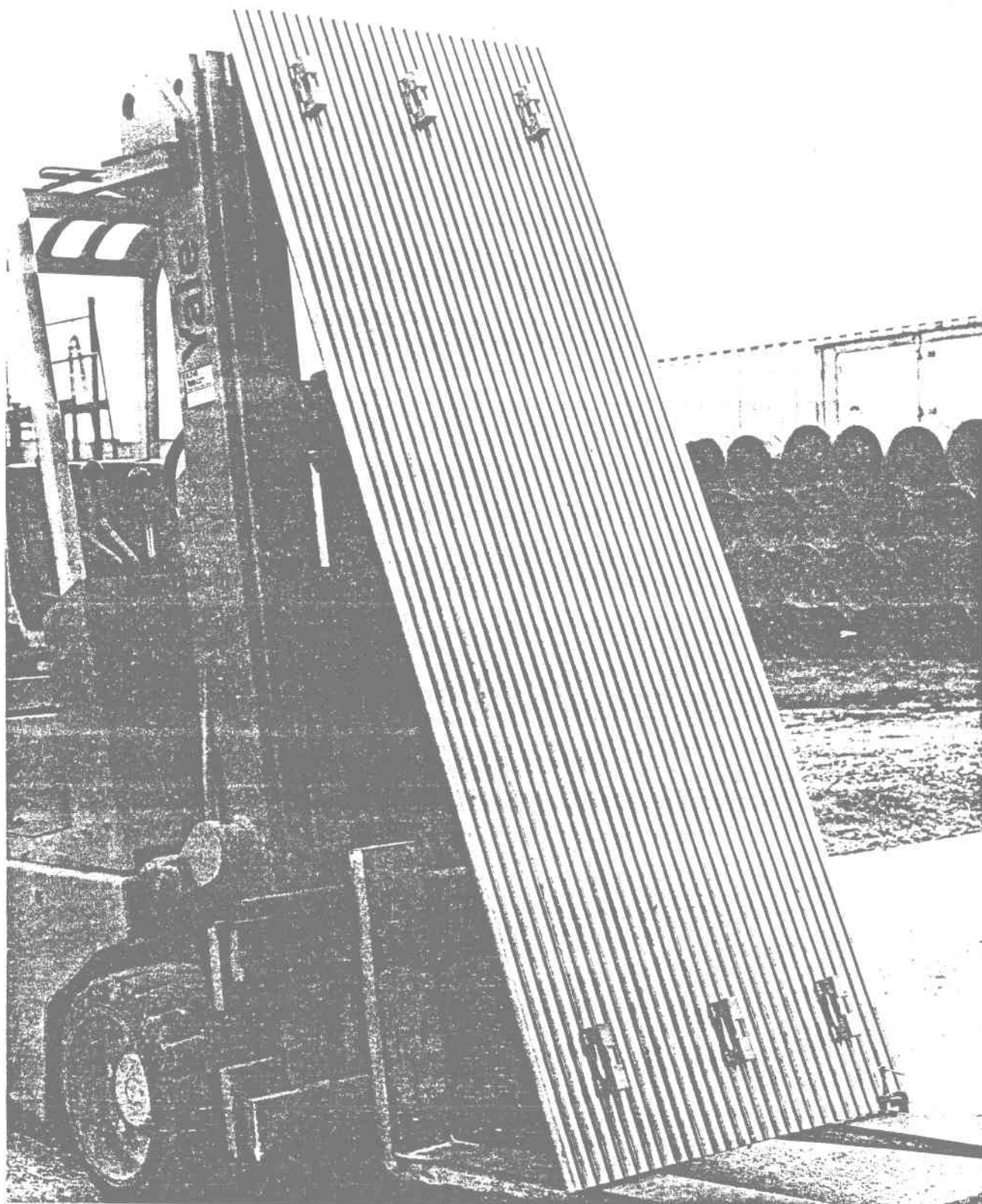


Figure 6.37 Finished Third Development Panel With Lugs

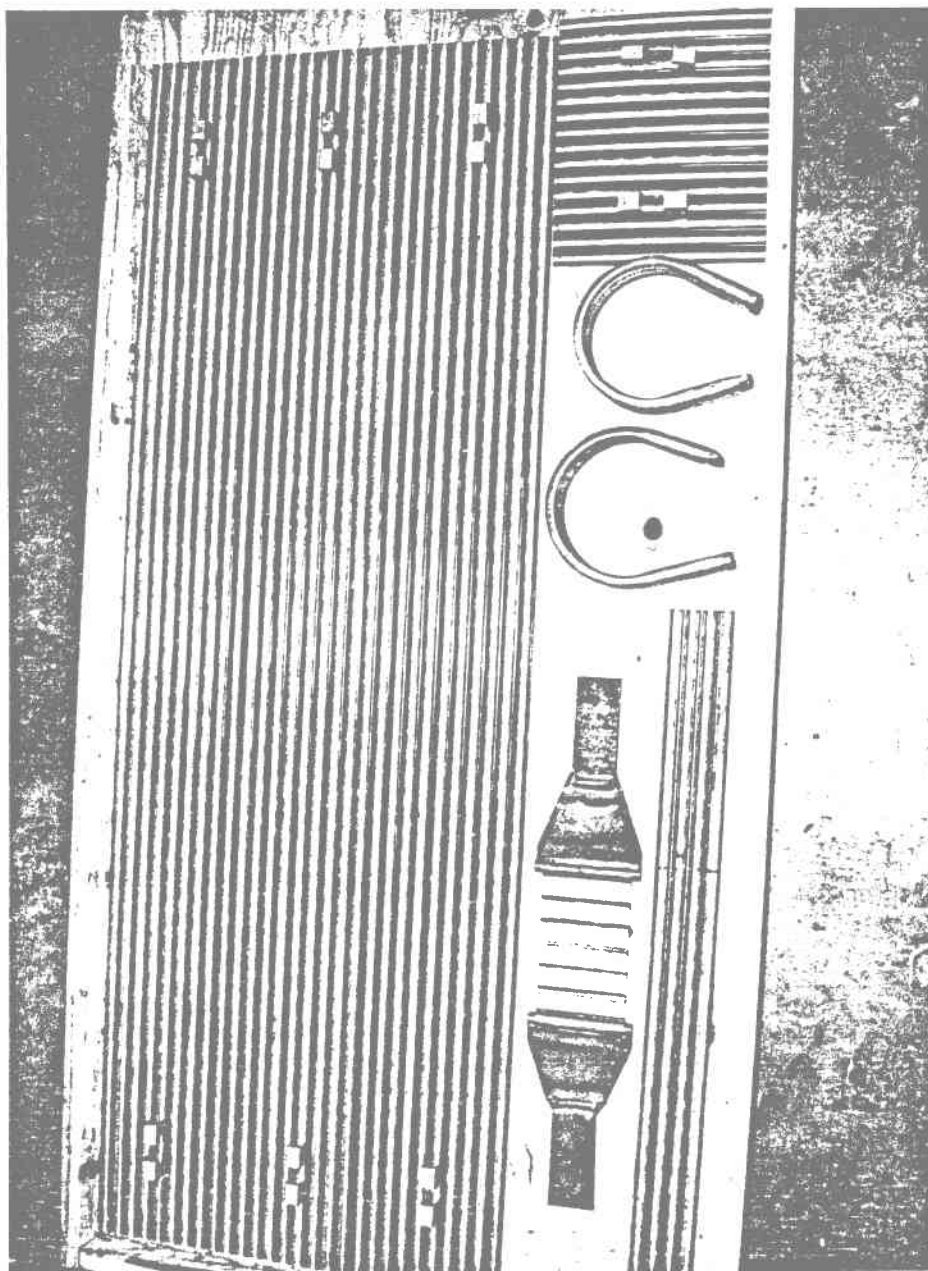


Figure 6.38 Third Development Panel Ready for Shipment to SNLL

6.9 DISCUSSION AND CONCLUSION

The fabrication of a 27.4-m (90-ft) by 28- or 32-tube-wide panel from Incoloy 800 (or Types 304SS/316SS) production solar panels appears feasible using the basic methods used to make the third development panel. However, to minimize production problems, the following recommendations are offered:

- The tubes for a given panel should be from the same heat and production lot to ensure that they all have the same yield strength. The tubes strain plastically during welding, and all tubes must strain equally to avoid in-plane distortion.
- The tubes and spacer strip should be purchased to tight dimensional and straightness tolerances. This requirement is imperative to ensure proper component alignment when placing them in the fixture.
- The tubes and spacer strip should be procured solution-annealed and free of cold work. (This ties in with the first recommendation.)
- The fixture must be strong enough to resist tube/spacer strip distortion during welding, which can occur because of differential expansion across and between a component and from weld shrinkage.
- The tube/spacer strip support blocks must be aligned in a straight line to ensure the fabrication of straight subassemblies and a straight panel.
- Tubes and spacer strip must be cleaned thoroughly before welding to avoid weld porosity. Shielding gas must be dry [$<-40^{\circ}\text{C}$ (-40°F) dewpoint] for the same reason.
- Precise alignment of the weld contact tip with respect to the work surface is necessary to ensure uniform, high-quality welds and prevent tubewall burn-through.
- Symmetry of mass during welding must be maintained as discussed in Section 6.4.3, Figure 6.12.

Weld repairs should not be difficult provided the cavity created when the weld is removed is fairly precise dimensionally and the cavity is thoroughly cleaned. Weld repairs should be performed while the in-process panel is still

FOSTER WHEELER SOLAR DEVELOPMENT CORPORATION

REF.: 84-2292C
DATE: November 1982

in the welding fixture. A milling machine could be adapted to ride on the same cross-beam carriage as the welding head. The welding head used to make the original weld could also be used to make the repair weld with minimum modification.

Section 7

RS DESCRIPTION AND COST ESTIMATE

7.1 RS DESCRIPTION

The RS includes the receiver unit, tower and foundation, control system, and energy transport loop (salt feed pump, riser and downcomer piping, drag valve, and ancillary equipment--including instrumentation and control elements). Key design and operating data are given in Table 7.1.

7.1.1 Receiver Unit

The receiver is a tower-mounted heat exchanger that converts the radiant solar energy reflected from the heliostat field into thermal energy in the receiver coolant. The receiver coolant is a molten nitrate salt that is heated in the receiver from 288 to 566°C (550 to 1050°F).

The receiver includes the absorber panels, cavity floor and ceiling, support structure, aperture door, surge tanks, and interconnecting piping. It is located south of the heliostat field, atop a 194-m (636-ft) reinforced concrete tower. The optical elevation of the cavity aperture is 212.5 m (697.2 ft) above the heliostat centerline elevation [216.1 m (709 ft) above grade]. The top structural member is 249 m (817 ft) above grade. Figure 7.1 shows the overall arrangement of the receiver unit. As shown in the figure, the receiver is symmetrical around the north-south centerline.

The heart of the receiver unit is the absorber, which comprises 20 individual replaceable panels (18 internal and two semi-external "wing" panels--one

Table 7.1 RS Data Summary

General

Reference site	Barstow, California
Configuration	Partial cavity. Replaceable modular panels (20). Gravity-closing aperture door. All up-flow panels.
Aperture optical elevation	216 m (709 ft)
Heat-transfer fluid	Molten nitrate salt (60 wt% NaNO ₃ /40 wt% KNO ₃)

Design Parameters:

Design life	30 years
Design point	Noon, February 19 (Day 50)
Design point insolation	950 W/m ² (301 Btu/h·ft ²)
Maximum insolation	1000 W/m ² (317 Btu/h·ft ²)
Output power at base of tower	320 MW (1092 x 10 ⁶ Btu/h)
Minimum absorbed power at rated conditions	80 MW (273 x 10 ⁶ Btu/h)
Salt flow rate	760 kg/s (6.018 x 10 ⁶ lb/h)
Salt inlet/outlet temperature	288/566°C (550/1050°F)
Overnight salt temperature	288°C (550°F)

Receiver

Overall [height x depth (N-S) x width (E-W)]	55.2 x 25.6 x 32.0 m (181 x 84 x 105 ft)
Cavity (width x height x depth)	19.8 x 25.8 x 17.4 m (65 x 84.5 x 57 ft)
Aperture (width x height)	19.8 x 25.8 m (65 x 84.5 ft)
Aperture area	510.2 m ² (5492 ft ²)
Total frontal area including wing panel	592.2 m ² (6375 ft ²)
Total exposed (active) area	1258 m ² (13,542 ft ²)
Total wet weight	1341 x 10 ³ kg (2950 x 10 ³ lb)

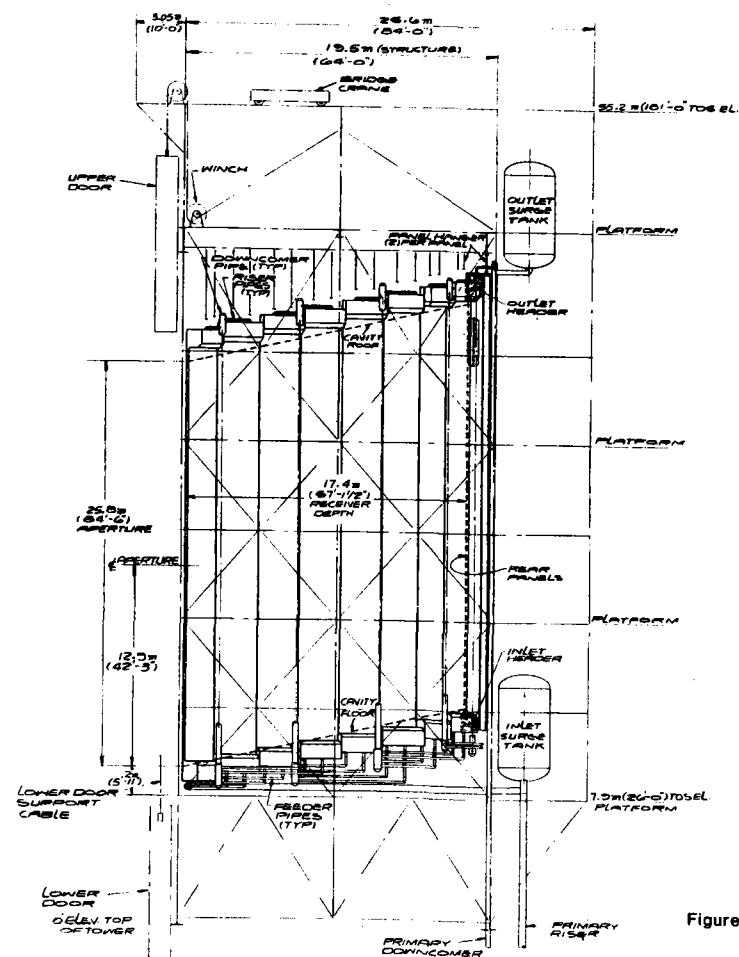
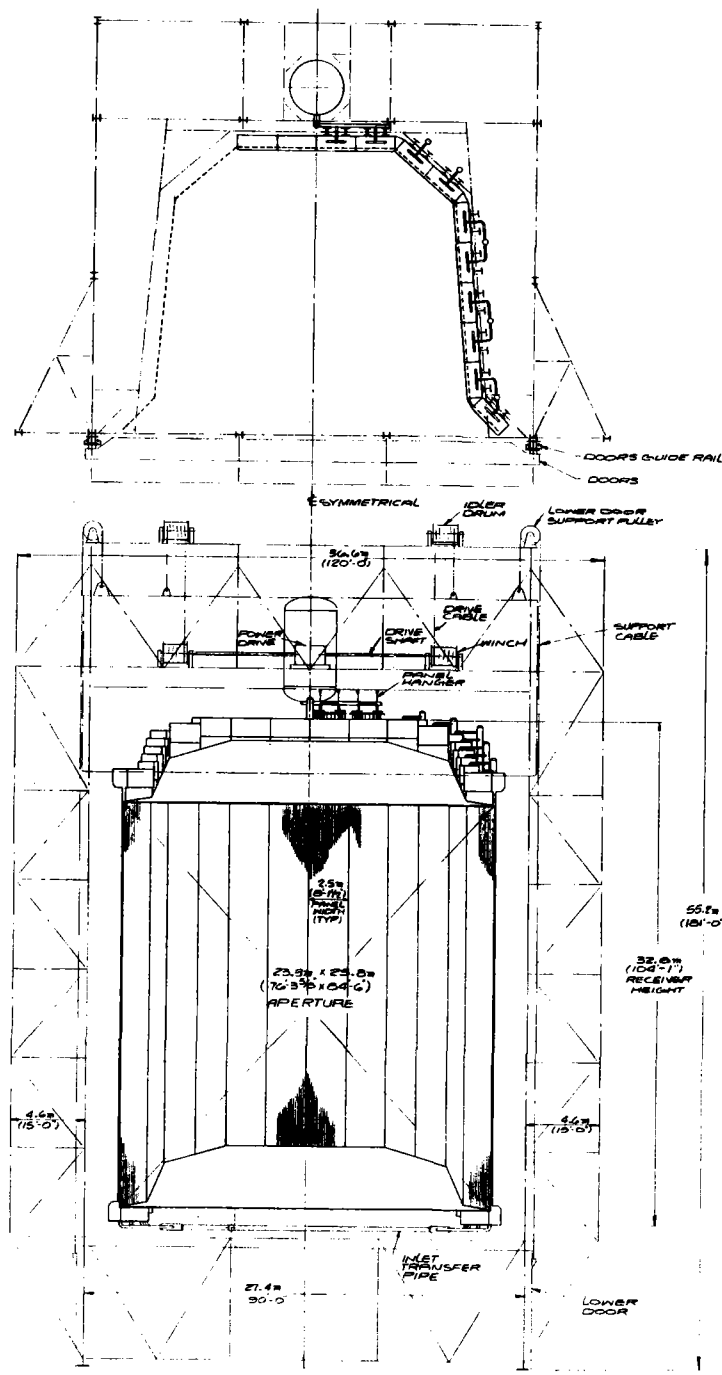
Absorber Panels

Construction type	Continuously welded tubes with a spacer strip between.
Tube material	304SS/316SS/Incoloy 800
Number of panels	20
Number of tubes per panel	88
Overall length x width	28.4 x 2.44 m (93.4 x 8.01 ft)
Distance between header centerlines	27.5 m (90.25 ft)
Exposed (active) length	25.8 m (84.5 ft)
Exposed (active) surface	62.9 m ² (677.1 ft ²)
Tube O.D. x wall thickness	25.4 x 1.65 mm (1.0 x 0.065 in.)
Spacer strips, thickness x depth	2.381 x 11.1 mm (3/32 x 7/16 in.)
Design pressure	3463 kPa (350 lb/in ² g)
Panel weight (empty)	10,000 kg (24,000 lb)
Maximum frictional pressure drop at rated flow (header-to-header)	242.3 kPa (35.14 lb/in ²)

Performance

Maximum absorbed power	336.8 MW (1149.3 x 10 ⁶ Btu/h)
Nominal absorbed power	320.0 MW (1092.0 x 10 ⁶ Btu/h)
Peak absorbed heat flux	0.614 MW/m ² (195 x 10 ³ Btu/h·ft ²)
Average absorbed heat flux	0.254 MW/m ² (81 x 10 ³ Btu/h·ft ²)
Design point RS efficiency	0.881
Annual average RS efficiency	0.859
Peak tubewall (O.D.) temperature	633°C (1171°F)
Peak salt film (I.D.) temperature	601°C (1114°F)
Peak front-to-back tube ΔT	153°C (275°F)
Salt Reynolds number, minimum to maximum	34,800 to 114,700
Salt velocity, minimum to maximum	3.0 to 3.4 m/s (9.7 to 11.2 ft/s)
Salt film coefficient, minimum to maximum	5780 to 10,250 W/m ² ·°C (1020 to 1800 Btu/h·ft ² ·°F)
Receiver frictional Δp	1517 kPa (220 lb/in ² g)
Feed pump inlet pressure	345 kPa (50 lb/in ² g)
Feed pump outlet pressure	6895 kPa (1000 lb/in ² g)
Inlet surge tank operating pressure	2410 kPa (350 lb/in ² g)
Outlet surge tank operating pressure	103 kPa (15 lb/in ² g)

REF.: 84-2292C
DATE: November 1982



NOTE
REFERENCE DIMS:
CIRCUIT ARRANG: RD-820-30
TYPICAL PANEL - RD-820-25
SUPPORT STRUCTURE RD-820-45
RD-820-40
DOOR ARRANG: RD-820-44

Figure 7.1

<p>FOSTER WHEELER DEVELOPMENT CORPORATION 1000 WEST 10TH AVENUE DENVER, COLORADO 80202</p>	
<p>MOLTEN SALT SOLAR RECEIVER SRE GENERAL ARRANGEMENT</p>	
<p>DESIGNED BY: <i>[Signature]</i> CHECKED BY: <i>[Signature]</i> APPROVED BY: <i>[Signature]</i></p>	<p>DATE: 11/1/82 SCALE: AS SHOWN PROJECT: RD-820-47</p>

on each side of the aperture and located at an angle 45 deg to the aperture plane). These 20 panels enclose three sides of the 17.4-m (57-ft) deep cavity. The open side of the cavity forms a 19.9-m (65-ft)-wide x 25.8-m (84.5-ft)-high aperture. A structural steel skeleton supports all the receiver components. The overall dimensions of the receiver structure are: 25.6 m (84 ft) wide in the north-south direction, 32 m (105) wide in the east-west direction, and 55.2 m (181 ft) high. The cavity is 17.4 m (57.1 ft) deep x 25.75 m (84.5 ft) high. Figure 7.2 shows the flow circuitry and how the individual absorber panels are assembled to form the absorber cavity.

Figure 7.3 shows the piping and instrumentation diagram (P&ID). As shown in the figure, cold salt from the CST is pumped through the primary riser to the top of the tower, where the piping branches to feed each side of the absorber. Panels on each side of the absorber form two independent parallel-flow circuits, with the flow through each proportional to the amount of heat absorbed in its side of the receiver. Each circuit comprises 10 panels connected into five passes.

The 88 vertical tubes in each panel are fed from a common header at the bottom and discharge into a common header at the top. Absorber panels are connected through transfer lines that interconnect the headers. Flow for each pass is upward through the absorber panels, with downcomers to return the flow from the top outlet headers of one pass to the bottom inlet headers of the next pass. The salt leaving Pass 5 flows into the primary downcomer.

Passes 1, 2, and 3 of each circuit have two upward flowing panels connected in parallel. Flow leaving these passes mixes in the interpass downcomers,

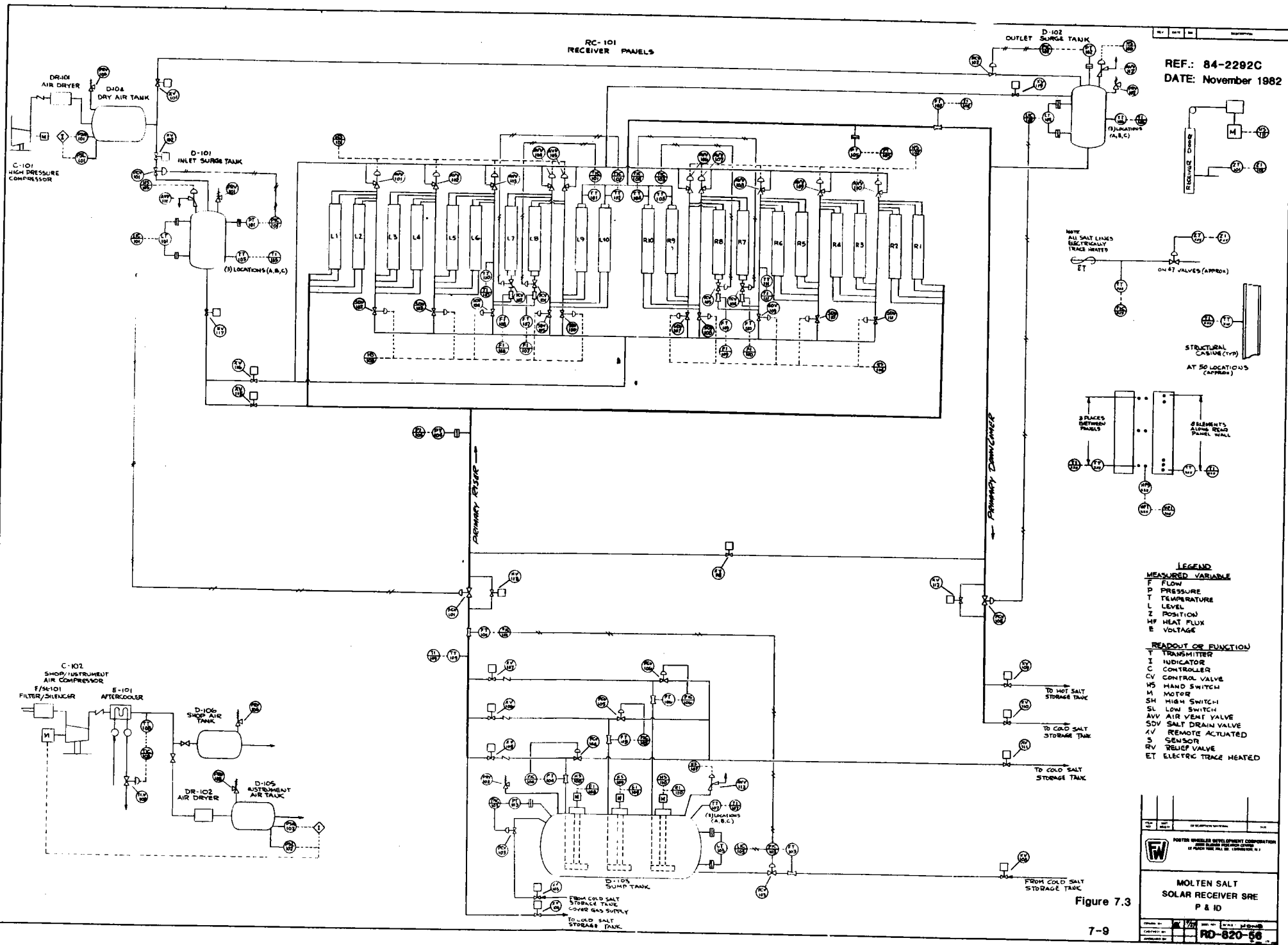


Figure 7.3

which deliver salt at a uniform temperature to the downstream pass. Pass 4 of each circuit has two panels in parallel, connected in series to specific Pass 5 panels. The salt flow rate through each series of panels is controlled by valves at the Pass 4 inlet to maintain the exiting salt temperature at 566°C (1050°F). High-absorption panels in Pass 4 are connected in series to low-absorption panels in Pass 5 to minimize the variation in flow rate through the outlet pass panels.

Cold inlet Pass 1 is positioned at the front of the receiver to minimize ambient heat losses. Hot outlet Pass 5 is positioned within the cavity in a low-heat-flux zone to minimize thermally induced stresses.

Absorber Panels. The absorbing surface of the cavity consists of 20 panels with a 25.75-m (84.5-ft) exposed (active) panel length and a 2.442-m (8 ft-5/32 in.) panel width. The panels are made of 88 tubes--each with 25.4-mm (1-in.) O.D. and 1.65-mm (0.065-in.) maximum wall thickness. The tubes are continuously welded with 2.381-mm (3/32-in.) spacer strips to form three solid sub-panel sections--each 28, 32, and 28 tubes wide. At the top and bottom, the tubes are connected to 0.25-m O.D. (10-in.) Sch 40 headers of the same material as the tubes (i.e., Type 304SS for Passes 1 and 2, Type 316 for Pass 3, and Incoloy 800 for Passes 4 and 5) with two 0.15-m (6-in.) nozzle connections for feeders and risers. The distance between header centerlines is 27.5 m (90.25 ft).

The absorber panels are fabricated in individual modules or subassemblies to facilitate handling during fabrication, shipment, and erection. The modules are designed to be completely interchangeable except for tube material. Panel

configuration, shown in Figure 7.4, is basically very similar to that of a typical, conventional utility boiler panel. Each module consists of the panel tubes, inlet and outlet headers, buckstays, support struts, and strongbacks. Insulation and sheathing are added to all modules in the field during erection.

The panel modules are designed to be hung vertically from the receiver unit support structure, using nine support rods connected to the panel tubes by eye lugs welded directly to the tubes. This arrangement permits unrestricted vertical thermal expansion throughout the length of the panel. The horizontal support for the panel is provided by buckstays which traverse the panel width and are vertically spaced 1.8 m (6 ft) apart. Each buckstay is held in place by nine buckstay lugs welded directly to the spacer strips. The buckstays are attached to the panel strongbacks by support links or struts. The central strut positions the center of the buckstay. Each module has two full-length strongbacks. Before erection these strongbacks, in conjunction with temporary shipping struts, provide the rigidity required to handle the module without damage to the relatively flexible tube panel. When the module is installed, the strongbacks are attached to the receiver unit support structure, thereby providing lateral restraint for the struts.

The panel is treated to optimize its absorptivity by spray painting high-absorptivity black Pyromark paint on the exposed panel surface after preparing the surface by sand blasting. The paint must be cured at 249°C (480°F) after drying and then baked at 538°C (1000°F).

Near the ends of the panels, outside the absorption area, the tube-to-tube longitudinal welds are terminated and the individual tubes are joined to jumper

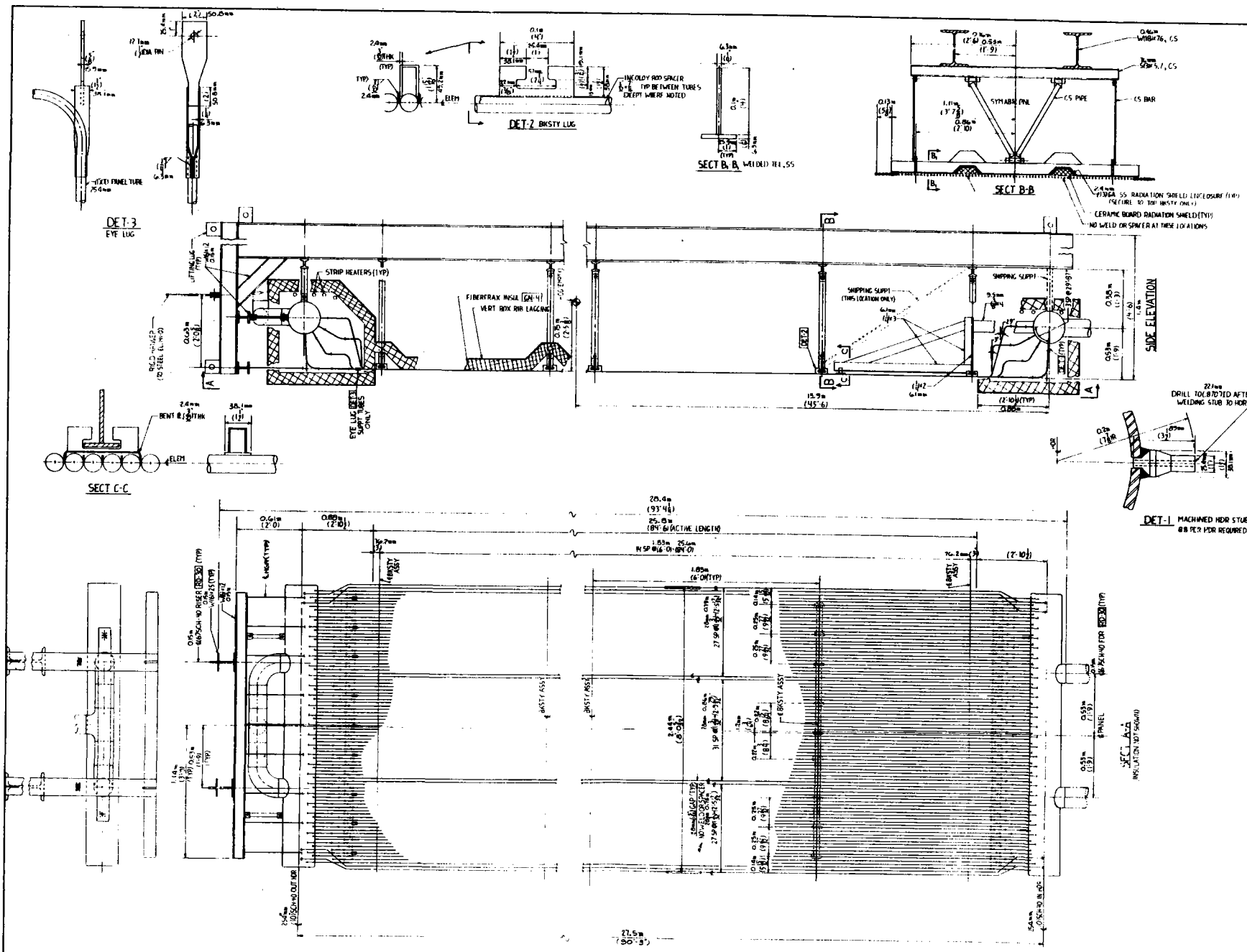


Figure 7.4

tubes (bent end tube portions) connecting the panel tubes with the headers and providing flexibility to accommodate differential thermal expansion. The header has stub fittings to receive each jumper tube.

The entire subassembly--comprising panel tubes, inlet and outlet headers, buckstays, supporting structure, and strongback--is shop-built and shipped as a unit. Insulation and sheathing are added during erection. Including insulation, the gross (empty) weight of an entire subassembly is 10,900 kg (24,000 lb). The fabrication is simplified by using the same jumper tube geometry for both headers and, as previously mentioned, making all panels identical (except for the tube material and insulation thickness). Thus erection and panel replacement are simplified and the number of spares needed is kept to a minimum.

Cavity Floor and Ceiling. In addition to the absorber panel modules, uncooled surfaces are required to complete the absorber cavity enclosure in areas not directly exposed to radiant flux (i.e., the floor and roof of the cavity). These areas must be effectively closed and insulated to minimize heat loss and to protect the jumper tubes, headers, and structure from the incident solar flux.

The cavity floor and roof consist of 0.1 m (4 in.) duraboard Fiberfrax weatherproof insulation anchored to carbon steel plate (Figure 7.5). The floor supports radiant heaters that are used to prevent salt from freezing during shutdown. The floor and roof are made of sections that can be lifted out by the overhead crane to permit removal and replacement of the absorber panels through the center of the receiver/tower structure.

REF.: 84-2292C
DATE: November 1982

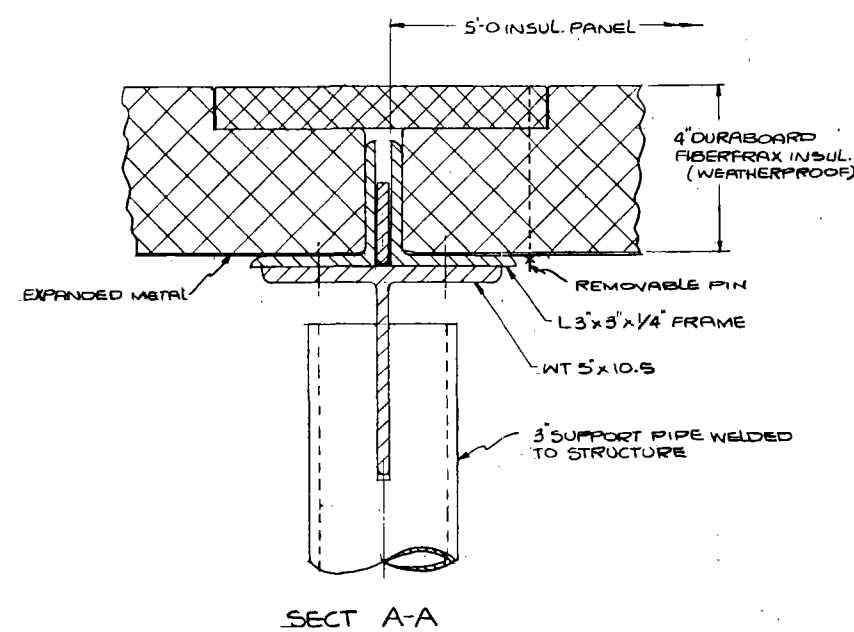
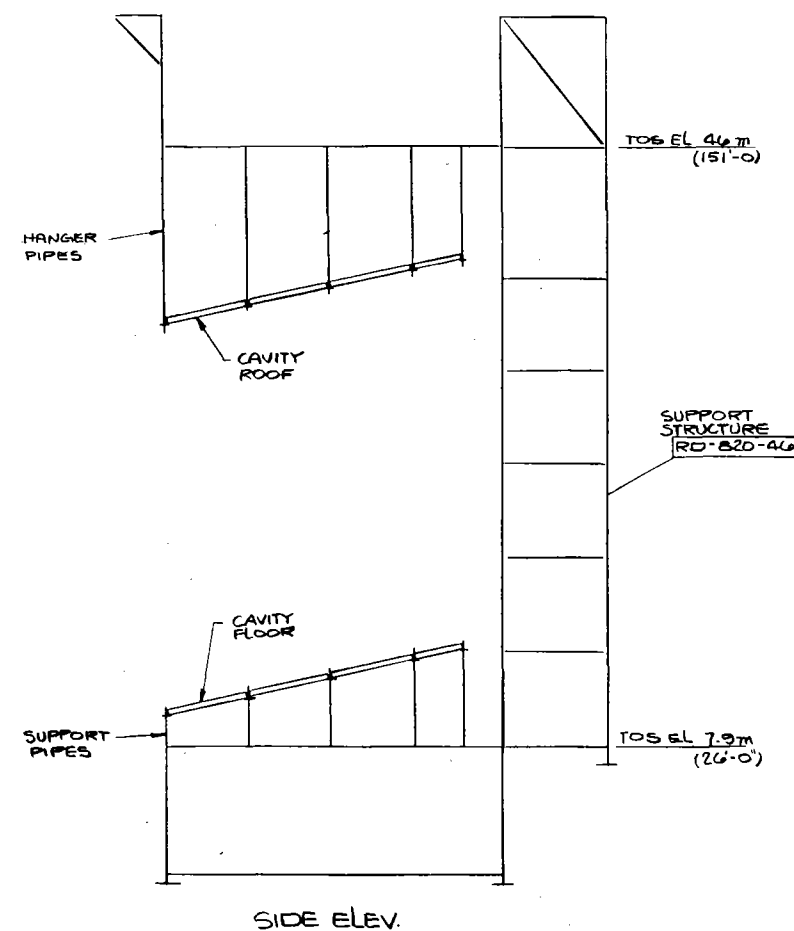
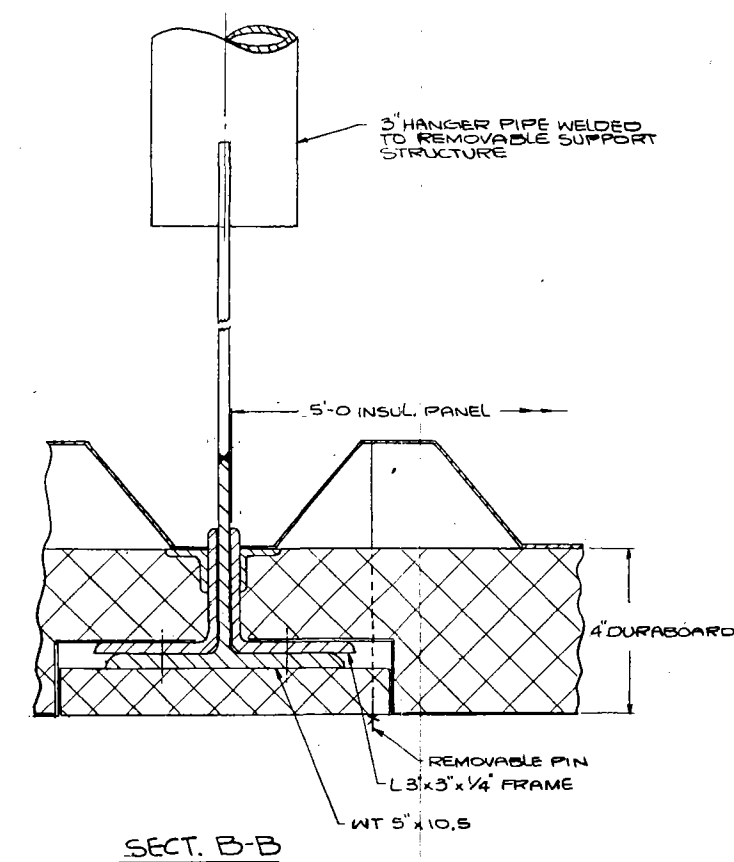
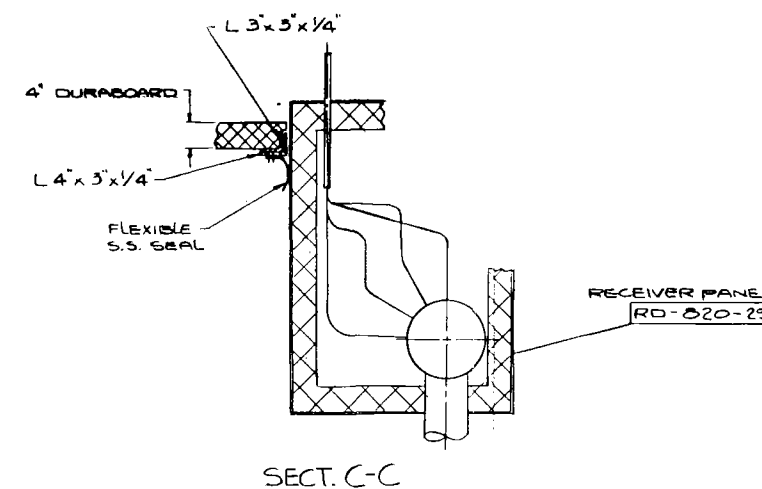
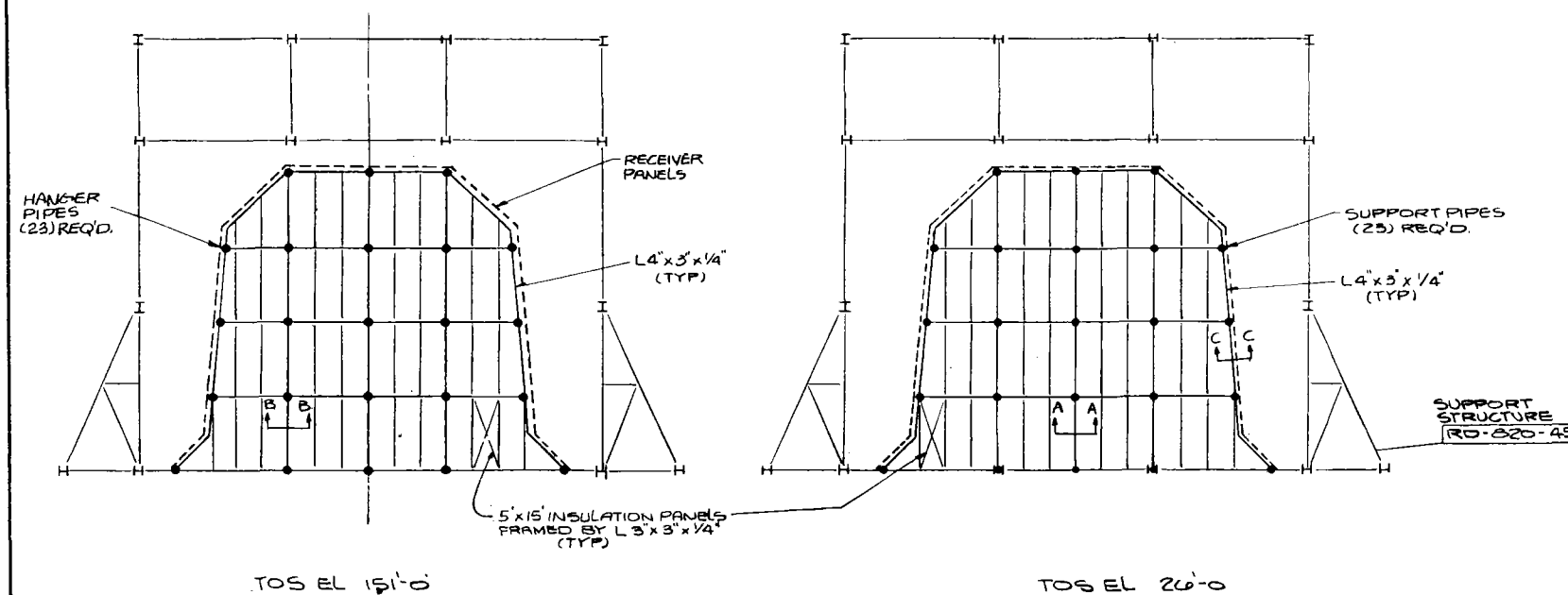


Figure 7.5

ITEM NO.	AMT. REQ'D	DESCRIPTION/MATERIAL	SIZE

FW FOSTER WHEELER DEVELOPMENT CORPORATION JOHN BLZARD RESEARCH CENTER 12 PEACH TREE HILL RD. LIVINGSTON, N.J.	
MOLTEN SALT SOLAR RECEIVER SRE ROOF & FLOOR DETAILS	
DRAWN BY: ER CHECKED BY: APPROVED BY:	DWG. NO: RD-821-63 SCALE: 1/4" = 1'-0" 7-17

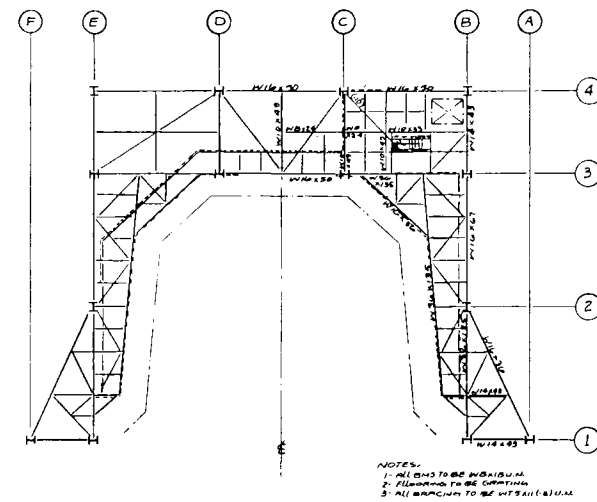
Receiver Structure. The receiver unit utilizes a skeletal structure to support the absorber and associated equipment. This structure is shown in Figures 7.6 and 7.7.

The support structure surrounds the absorber on three sides and is joined to the absorber strongbacks to support lateral absorber loads. Structural members extending over the upper headers and panel ends carry the weight of the absorber unit. Additionally, the piping to and from the receiver unit as well as the absorber downcomers and transfer lines are supported from the structure. Pipe hangers were selected for these applications on the basis of anticipated displacements, so that excessive stresses are not induced in the piping.

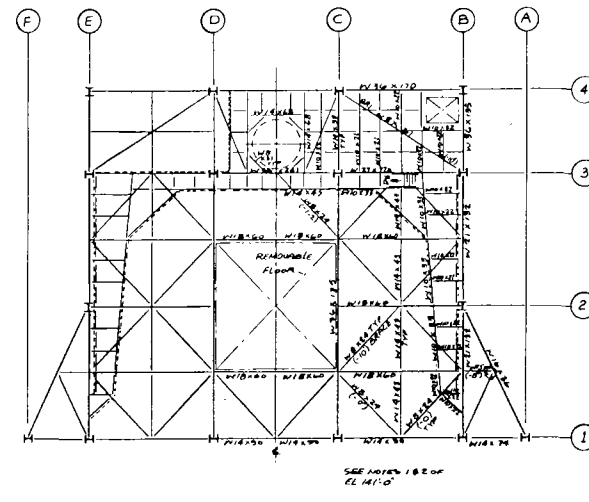
The upper level of the structure was designed to accommodate a permanent 15-ton overhead crane. Walkways are provided at four levels between the base of the absorber and its roof level. Ladders are furnished between walkway levels and an elevator services all levels of the receiver unit.

Other features of the receiver unit structure include:

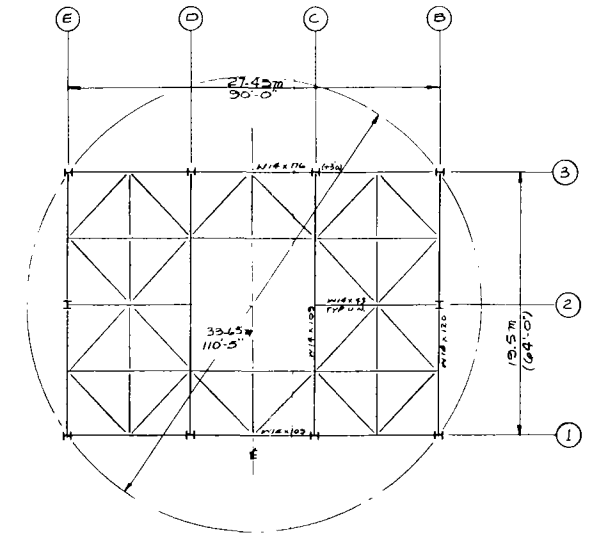
- Equipment decks behind the absorber unit at two platform levels
- Standpipes for fire and flushing operations at each level where personnel have access
- Eye-wash fonts and emergency showers connected to these water systems
- Illuminated walkways and ladders to permit safe night-time use
- Permanent and portable work lights so that as much maintenance as possible can be performed at night.



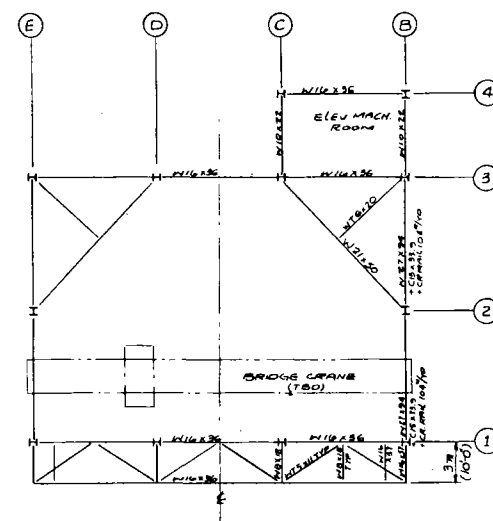
TOS EL 31.1m (102'-0") & 19.5m (64'-0")



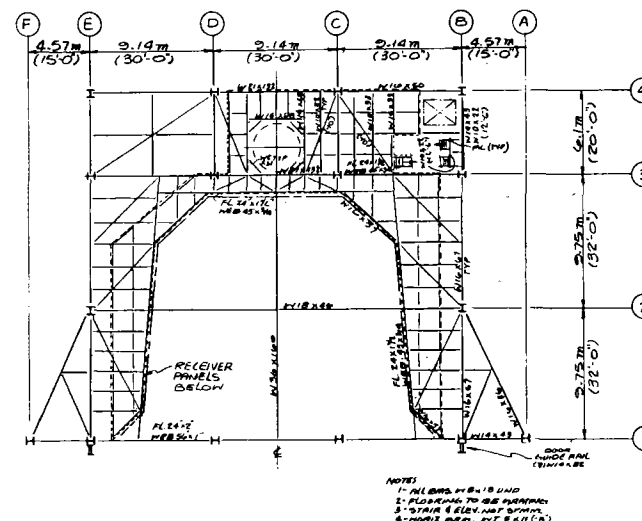
TOS EL 7.0m (23'-0")



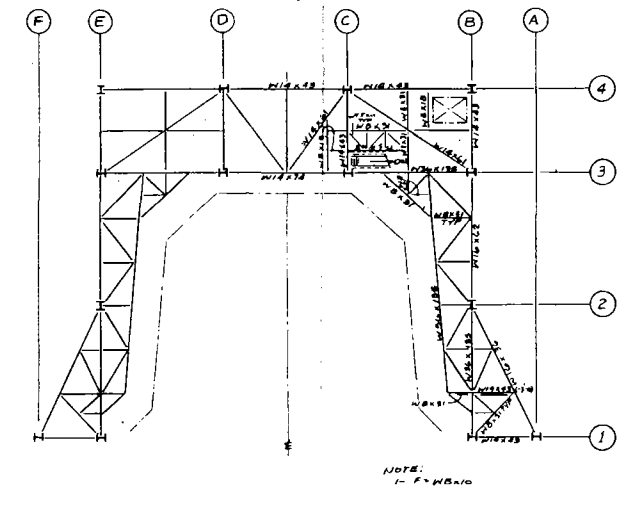
TOS EL 0.90m (1'-6")



TOS EL 35.2m (115'-0")



TOS EL 46m (151'-0")

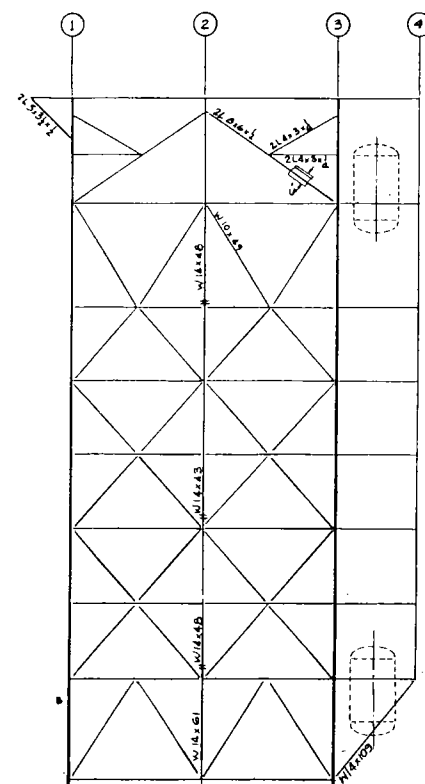


TOS EL 36.9m (121'-0") 25.5m (83'-0") & 13.7m (45'-0")

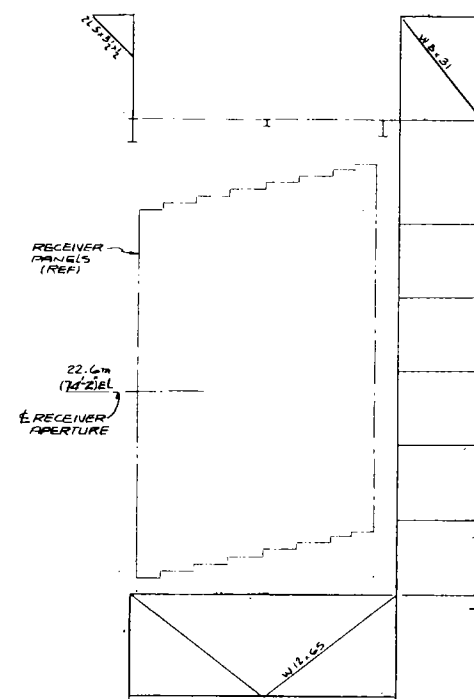
- NOTES:
1- SEE DWG. RD-820-46 FOR
RECV. VIEWS
2- REF. DWG.: CIRCULAR ARRANGEMENT
DWG. RD-820-30
TYPICAL PANEL & SUPPORT
DWG. RD-820-25
OVER ARRANGEMENT
DWG. RD-820-44
3- MATERIAL: A36, Fy = 36 KSI

Figure 7.6

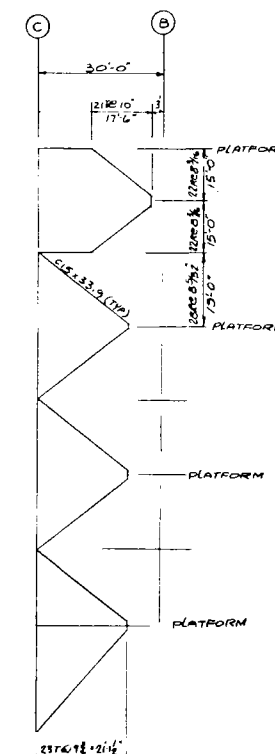
ITEM NO.	REV.	DESCRIPTION	DATE
<p>FORSTER WHEELER DEVELOPMENT CORPORATION SOLAR RESEARCH CENTER 12 PINE TREE HILL RD. LYNNSTON, N.J.</p>			
<p>MOLTEN SALT SOLAR RECEIVER SRE SUPPORT STRUCTURE PLAN VIEWS</p>			
DESIGNED BY	ER	DATE	SCALE
CHECKED BY			
APPROVED BY			
RD-820-45		FORM D-28	



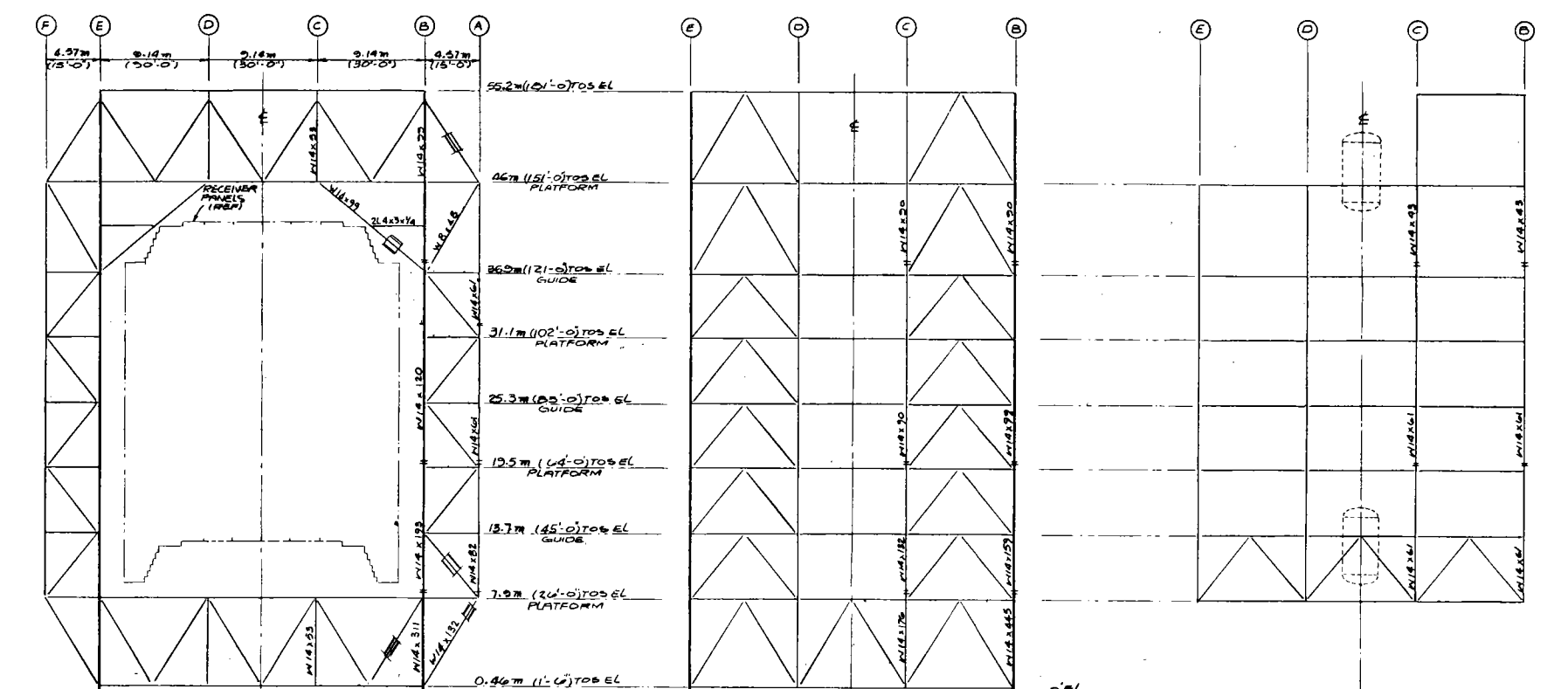
BENT B & E



BENT C&D




STAIRS

BENT 1BENT 3BENT 4

NOTES:
1- SEE DWG. # RD - B20 - 45 FOR
PLAN VIEWS
2- REF DWGS: CIRCUITRY ARRANGEMENT
DWG. # RD - B20 - 30
TYPICAL PANEL & SUPPORT
DWG. # RD - B20 - 10
DOOR ARRANGEMENT
DWG. # RD - B20 - 44
3- MATERIAL: A36, $F_y = 36$ KSI

YEAR	APPT	DESCRIPTION/ANALYTICAL	DATE
NO	NO/20		



FOSTER WHEELER DEVELOPMENT CORPORATION
JOHN HILAND RESEARCH CENTER
12 PINE TREE HILL RD., LIVINGSTON, N.J.

MOLTEN SALT
SOLAR RECEIVER SRE
SUPPORT STRUCTURE
ELEVATION VIEWS

DESIGNED BY: **ER** **ER-8** DWG NO. **SCALE 1/8" = 1'-0"**

CHECKED BY: **RD**

APPROVED BY: **RD-820-46**

Figure 7.7

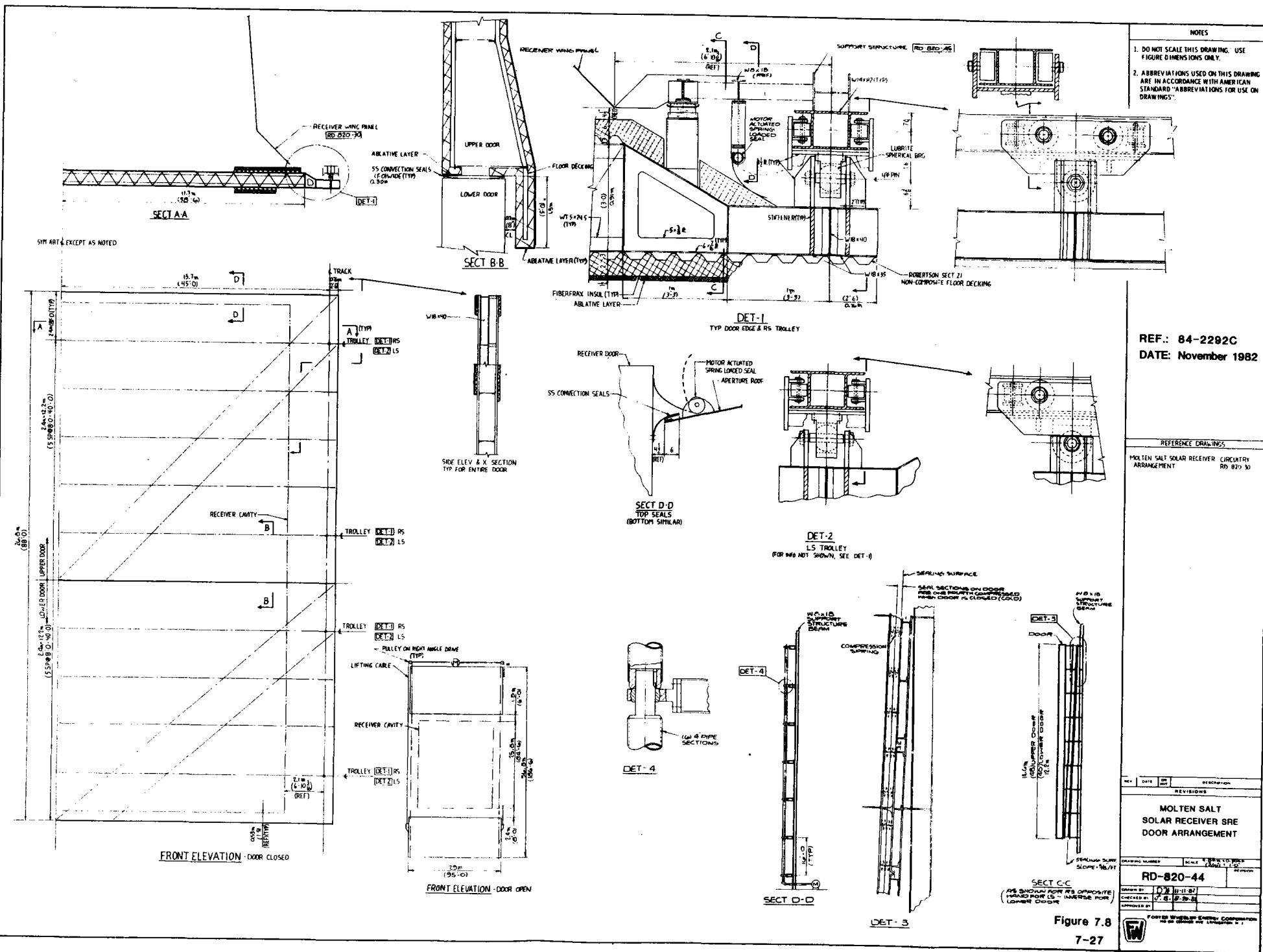
All members of the support structure that may be exposed to solar flux are insulated and covered with a stainless steel radiation shield painted with white Pyromark paint. Because the fluxes around the aperture are normally low, radiation shields and convective air are sufficient protection for the load-bearing structural members. Those members that could receive higher-than-normal fluxes during a heliostat field failure (control or power) are insulated with Fiberfrax ceramic fiber covered with an ablative material.

Aperture Door. The receiver includes an aperture door to minimize thermal losses when the receiver is not in operation and to protect the receiver in the event of feed pump or power failure.

The door assembly consists of two sections, each of which spans the receiver aperture horizontally (Figure 7.8). The lower section partially counterbalances the upper section, minimizing the power required for opening and closing. The two sections of the door are similar in construction, but the upper section is larger and heavier to permit closing by gravity in the event of a power failure.

To minimize cavity heat losses by convection during cloudy periods of overnight operation, the door has a system of seals to close the gaps between the door and aperture and between door sections.

Each door section is made of modular panels designed for in-place assembly during erection. The aperture side of the door is faced with a layer of Fiberfrax blanket insulation. The outside is covered by a layer of ablative material



to protect the door (and the receiver) during an emergency until the earth's motion moves the incident solar flux away from the receiver or the heliostats are otherwise defocused.

Surge Tanks. The inlet and outlet surge tanks atop the tower buffer the fast-responding temperature control valves from the slower responding salt feed pump recirculation and drag valves, permitting rapid response to flux change. During the transition from normal operation to a standby condition, these tanks also accommodate the change in salt and piping volumes resulting from temperature change. Set points for both tank level controls are set at one-half full.

The IST provides a reservoir of salt that can be passed through the receiver for a short period of time (approximately 60 seconds) if the salt pumps fail. An air compressor with storage tank maintains a constant pressure in the IST for this purpose. Salt level is maintained by adjusting the feed pump recirculation valve.

The OST is located at the highest point in the salt-flow circuitry, providing a means for monitoring the salt level in the RS to ensure that the panels are filled with salt. Salt level is maintained by adjusting the drag valve (at the base of the tower) which controls the amount of salt leaving the RS.

Interconnecting Piping. The panels in each receiver pass are connected by a series of feeders, risers, downcomers, and transfer pipes (Figure 7.2). All piping is designed with adequate flexibility for thermal expansion and in an arrangement that can be fully drained. Drain lines equipped with drain valves extend from the bottom of each downcomer and feed into a common manifold that is

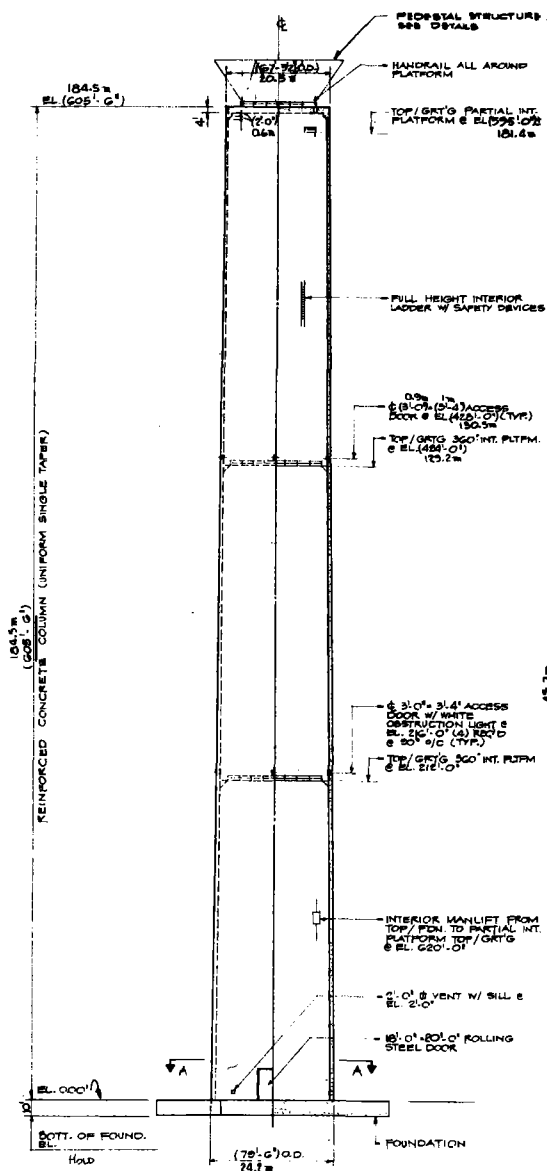
connected to the primary riser. Vent lines equipped with vent valves extend from the top of each downcomer and feed into a common manifold that extends to the OST. During salt fill, air trapped in the pressure-part circuitry is vented through these lines to the OST. When draining the receiver, the vent valves are opened.

7.1.2 Receiver Tower and Foundation

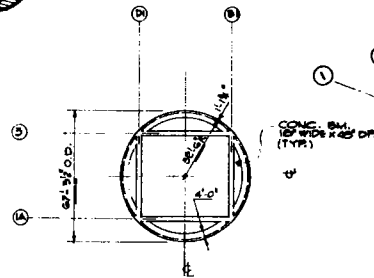
The tower that supports the receiver is a slip-formed, reinforced-concrete structure rising 184.5 m (605.5 ft) above ground level, supported by an integral octagonal mat foundation 45.7 m (150 ft) wide and 3 m (10 ft) thick (Figure 7.9). With an O.D. of 24.2 m (79.5 ft) at the base and 20.5 m (67.3 ft) at the top, the walls are tapered ≈ 0.6 deg. Wall thickness of the concrete shaft tapers from 0.76 m (30 in.) at the base to 0.35 m (13.75 in.) at the top. A 9.1-m (30-ft) high transition steel structure is located between the top of the concrete tower and the bottom of the receiver structure.

The tower has an internal staircase, an internal service elevator, lightning protection equipment, aircraft warning lights, and worker protection restraints. A work platform is also provided atop the tower. The primary riser and downcomer are supported along the inside of the tower shell with expansion loops--two for the riser and five for the downcomer--to accommodate thermal expansion (Figure 7.10). As shown in this figure, room has been provided at ground level inside the tower for the sump pump tank, which contains the three salt feed pumps, and for other receiver support machinery such as the air compressors and air storage tanks.

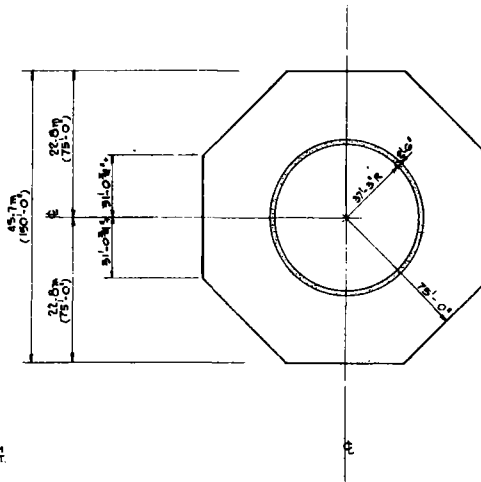
REF.: 84-2292C
DATE: November 1982



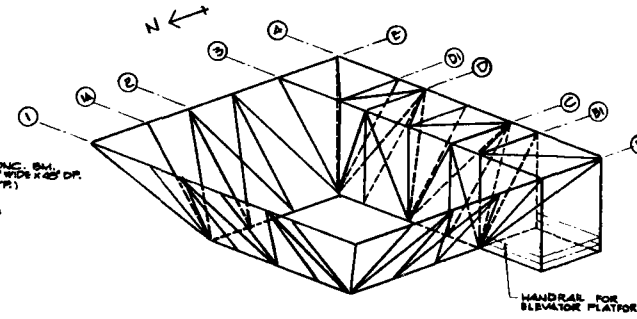
ELEVATION - SECTION
SCALE: 1" = 40'



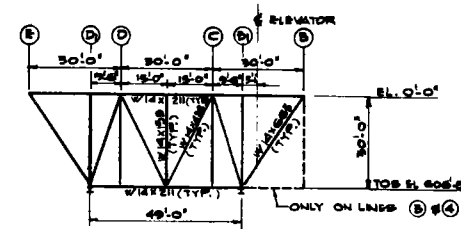
PLAN @ EL. 605'-0"
SCALE: 1/2" = 1'-0"



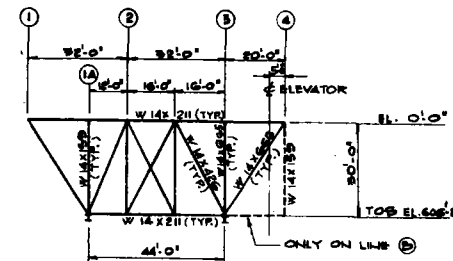
SECTION A-A
SCALE: 1/2" = 1'-0"



PEDESTAL STRUCTURE
SCALE: 1" = 20'



ELEVATION ON LINES 1, 3, & 4
NOTE: VERTICALS ON LINES 1, 3, & 4 SLANT IN N-S DIRECTION
SCALE: 1" = 20'



ELEVATION ON LINES 2 & 5
NOTE: VERTICALS SLANT IN EAST-WEST DIRECTION
SCALE: 1" = 20'

LETTER	DATE	DESCRIPTION
REVISIONS		
1		FIELD CONSTRUCTION
2		FABRICATION
3		PREPARATION OF SHOP DETAILS
4		CUSTOMER COMMENTS
5		PURCHASE OF ALL MATERIALS
6		PURCHASE OF MAJOR MATERIALS
7		PRELIMINARY ARRANGEMENT
REV	REV	DATE
		ISSUED FOR

MOLTEN SALT
SOLAR RECEIVER SRE
TOWER DETAILS



FOSTER WHEELER S P E C INC.
110 SOUTH ORANGE AVE. LIVINGSTON, N.J.

Figure 7.9

7-31

ORDER NO.
8771

DRAWN BY: B. J. H. SCALE: 1/2" = 1'-0"

CHECKED BY: APPROVED BY: RD-820-76

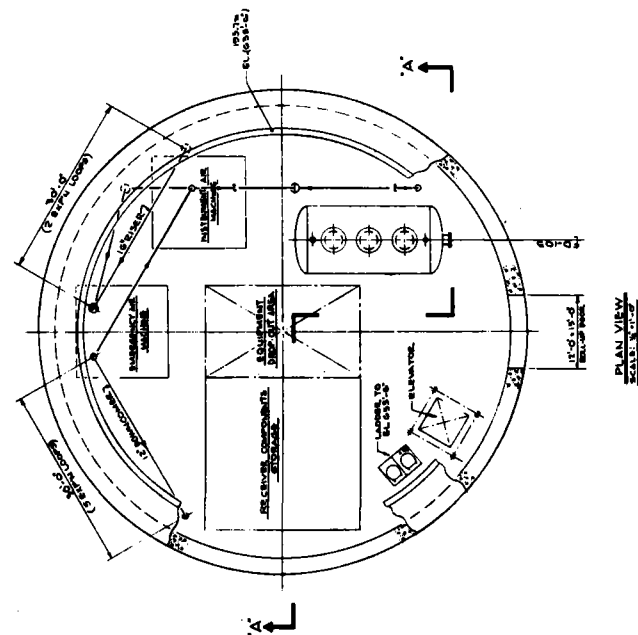
DWG. No.

THIS DRAWING SUPERSEDES
THIS DRAWING SUPERSEDED BY

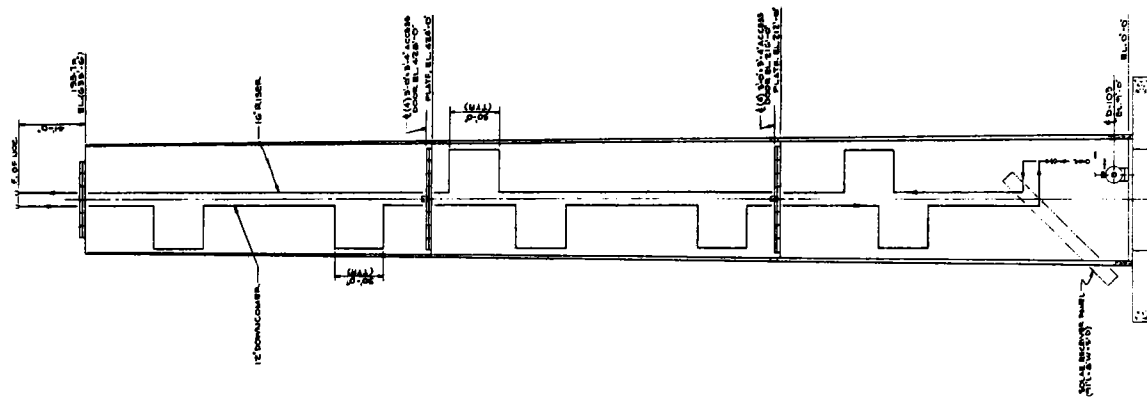
1-10-11218



REF.: 84-2292C
DATE: November 1982



PLAN VIEW
SCALE 1"=5'-0"



SECTION A-A
SCALE 1"=5'-0"

Figure 7.10

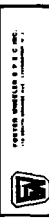
7-33

5771

DWG. NO.

LETTER	DATE	DESCRIPTION
1		REVISION
2		REVISION
3		REVISION
4		REVISION
5		REVISION
6		REVISION
7		REVISION
8		REVISION
9		REVISION
10		REVISION

MOLTEN SALT
SOLAR RECEIVER SRE
TOWER PLOT PLAN



RD-820-77

The area along the tower centerline has been kept clear for removal and maintenance of panel subassemblies and other large parts.

7.1.3 Energy Transport Loop

The energy transport loop consists of the primary riser and downcomer piping, receiver feed pumps, drag valve, and associated instrumentation and control elements.

With the exception of the feed pumps, the design flow for the loop was chosen to be the RS design flow rate [398 L/s (6300 gal/min)] which is a conservative value since the average salt flow rate is less than the design flow rate.

All energy transport loop equipment is fully drainable, heat traced, and insulated. It is capable of delivering molten salt at all flow rates from 5 to 110 percent of design flow.

The carbon steel primary riser was sized to minimize combined pumping and piping costs. The Type 316SS primary downcomer was sized to dissipate a large percentage of the gravity head at the design flow rate. The remainder of the gravity head is dissipated across the drag valve and in the field return piping to the HST. The drag valve is a self-draining turbo-cascade control valve required to dissipate between 25 and 100 percent of the tower static head by splitting the main flow into multiple streams through a labyrinth of successive 90-deg turns.

The receiver feed pumps are Bingham-Willamette Type VCN (vertical, centrifugal, wet-pit, closed-impellers) heavy duty, high-temperature-service salt pumps. Each pump delivers a 305-m (1000-ft) head, which ensures a minimum pressure of 10³ kPa gage (15 lb/in²g) at the OST to prevent gas formation. The pumps are located inside the receiver tower about 3.7 m (12 ft) above ground level. Their characteristics are:

Type	VCN
Number	3 (1 spare)
Material	Type 316SS
Design flow, L/s (gal/min)	209 (3300)*
Minimum flow, L/s (gal/min)	41.8 (660)
Turndown ratio	10:1
Operating pressure, MPa gage lb/in ² g)	
Suction	0.35 (50)
Outlet	5.9 (850)
Operating temperature, °C (°F)	
Maximum	302 (575)
Minimum	260 (500)

*10 percent higher than the RS design point flow rate.

Temperature, pressure, flow-rate, flux, position, and level sensors are provided on the receiver panels, piping, valves, and tanks, as shown in the P&ID (Figure 7.3), to monitor the receiver for safe, stable operation.

Air-cooled flux sensors and rear-wall thermocouples will provide data to the valve controllers. Header salt thermocouples at intermediate locations and at the receiver unit exit are also provided. Thermocouples are distributed throughout the pipework, headers, and valves to indicate cold spots so that appropriate actions (e.g., trace heating adjustment, draining) can be taken to prevent salt freeze-up. Salt flow rates are measured by a wedge-type flow meter, which can be completely drained. Pressure is measured using silicone-oil-filled lines with diaphragms to isolate the sensing units from the high-temperature salt.

All control, drain, and vent valves shown in the P&ID (Figure 7.3) are self-draining globe-type valves with internal bellows seals. All valves can be manually and pneumatically actuated.

7.1.4 Auxiliary Equipment

Electrical System. There are two power-supply circuits--one 480 V, 3 phase and the other 110 V, single phase. Both are fed from the plant power supply via connections atop the tower. The 480-V circuit supplies the major power users such as heaters, pumps, compressor, elevator, hoisting equipment, and door actuator; the 110-V circuit is for lighting, service outlets, and controls. In the event of plant power failure, the 480-V circuit would be fed by a central plant emergency diesel generator, which may be somewhat delayed in coming on line. The more critical 110-V circuit, which supplies the emergency lighting and receiver controls, is fed by an emergency battery pack so that control power is always available to accomplish safe emergency receiver shutdown.

Service and Safety Equipment.

Service Crane. One of the major advantages of our design is the ability to remove complete panel/strongback subassemblies for maintenance. A permanent 15-ton overhead crane can travel across the receiver, remove sections of the roof and floor, pick up any subassembly, and lower it through the center of the receiver/tower to the ground. As soon as the structure is erected, the overhead crane can also be used for construction. During receiver operation, the crane will be stored at the rear of the structure, away from the hot air coming from the cavity aperture.

Service Elevators. The receiver elevator facilitate access to all levels of the receiver. It transports personnel and small equipment. A terminal room is located at the tower top, just below the receiver unit interface level. The tower elevator terminates on a deck that also serves as the starting point for the receiver elevator. Adequate space is provided on this deck for handling and transfer of equipment between elevators.

Fire Protection. During normal operation or standby of the receiver, the only combustible materials present will be in the electrical and instrumentation/control systems. Therefore, no fire protection is needed other than strategically located CO₂ fire extinguishers. When the receiver is undergoing maintenance or repair, relatively small amounts of combustible materials such as wood scaffolding, rope, oil, grease, cartons, and packaging may be present. Standpipes and hoses are provided for flushing and are available to extinguish this type of fire.

Personnel Protection.⁴³ Personnel protection is an important consideration while working with nitrate salt. The solid salt should not get in eyes, on skin, or on clothing. Breathing of dust should be avoided. Liquid salt is hot enough to cause third-degree burns. If skin or eyes come in contact with the salt, they should be immediately flushed with running water for at least 15 minutes. Eye baths and showers for this purpose are located at the rear of each major platform, one on each side of the receiver. These are connected to the 25.4-mm (1-in.) pipe headers that feed the service water connections described later. In cleaning up solidified spills, personnel should wear NIOSH/MSHA-approved dust respirators, goggles, coveralls, and boots. After as much of the salt as possible is cleaned up and isolated in suitable containers, the residual salt should be flushed away with water. When the salt is involved in a fire, personnel fighting the fire should wear NIOSH/MSHA-approved self-contained breathing apparatus and protective clothing. Personnel working around the receiver should wear standard safety gear (i.e., hard hat, glasses, long-sleeved shirt, gloves, and safety shoes). Maintenance personnel who work on or inspect the absorber, piping, valves, or instrumentation when the receiver is out of service but still hot should wear suits and gloves that protect against burns.

Service Air. Three 19-mm (3/4-in.), 0.7 MPa (100 lb/in²) air connections, suitable for air-tool operation, are provided on each major platform, one at the rear and one on each side of the receiver. These are fed from 38.1-mm (1-1/2 in.) pipe headers.

Service Water. Two service water connections at the rear of each major platform, one on each side of the receiver, are fed from 25.4-mm (1-in.) pipe headers that are heat-traced to protect them from freezing.

Comfort Facilities. Drinking water and toilets are provided in connection with the terminal room beneath the receiver atop the tower.

Drains. To collect possible salt spills or water and dilute salt solutions resulting from hosing down or cleaning operations, a large pan spanning the width and length of the receiver is located approximately at elevation 1.5 m (5 ft). This pan is drained through a single 0.15-m (6-in.) line that connects to a line similar in size at the receiver deck interface elevation.

Water drain lines 51 mm (2 in.) diameter are provided for the eye baths and showers described earlier. These lines are manifolded and connected to a single 51-mm (2-in.) drain that connects at the interface elevation to a drain running down the tower.

Communications. Although no personnel will be in the vicinity of the receiver while it is in operation, communications are needed during maintenance and repair activities. The communications system for the receiver consists of a multichannel hard-wired system with two paging loudspeakers and one soundproofed phone booth on each major platform. The phone booths are located at the rear of the receiver near the elevator. The loudspeakers are located at the rear outboard corners of each platform and directed so that they can be heard from any point on each platform. Separate channels connect the speakers

and phones to the plant control room, maintenance office, and plant main office. In addition, for efficient maintenance (particularly of instrumentation) an FM radio system with a master in the control room and individual portable two-way units for personnel outside are provided.

Table 7.2 gives the receiver weight breakdown including salt and all components located above the tower.

Appendix S lists the major auxiliary equipment components of the RS.

Table 7.2 Receiver Weight

	Weight	
	<u>10³ kg</u>	<u>(10³ lb)</u>
Absorber panel modules	109	240
Roof and floor	65	144
Casing and insulation	93	204
Aperture door	109	240
Piping	50	110
Salt and air storage tanks	57	126
Controls and miscellaneous equipment	25	56
Platforms and ladders	173	380
Structural steel	327	720
Overhead crane	50	110
Normal charge of salt	<u>282</u>	<u>620</u>
Total estimated receiver weight (wet)	1341	2950

7.1.5 RS Interfaces

The RS interfaces with the Collector, Storage, and Master Control Sub-systems.

Functional/Service Interfaces. The functional/service interfaces between the receiver unit and other portions of the overall plant include:

Salt supply line:	0.4 m (16 in.) dia, Sch.80 pipe, insulated
Salt return line:	0.3 m (12 in.) dia, Sch. 60 pipe, insulated
1400 kVA supply trunk at 480 V:	3 phase, 60 Hz, P.F. = 0.9
Potable water supply:	0.1 m (4-in.) Sch. 60, insulated
Gravity-fed wastewater drain:	0.15 (6-in.) Sch. 40, insulated
Lightning rod ground cables:	4 cables, 2/0 woven copper

Electrical Interfaces and Instrument and Control Interfaces. The receiver unit interfaces with plant electrical power and the instrumentation/control system through the J-boxes atop the tower.

Electrical Interfaces. All electrical requirements for receiver equipment are drawn from the 480-V main line through the circuit breakers on the ground and connected to the equipment through J-boxes located on the tower. A pad-mounted transformer steps down the 480 V to 208 V/120 V for the trace heater system. The elevator draws 40 amps from the 480-V line to drive the 18.6-kW (25-hp) motors. The radiant cavity heaters, trace heaters, hoist, crane, and door actuator are also connected to their respective circuit breakers.

The lights and receiver control draw their power from the 110-V line and are interfaced through the J-box located on the receiver tower.

Instrument/Control Interfaces. All instruments and control signals used to monitor and control the receiver unit are interfaced with the plant control system through the J-boxes located on the tower. The instrument analog input signal is 4 to 20 mA. All instrument signals are connected to the plant data logger located in the main control room. The 40 control signals from the DCS System are 4 to 20 milliamps and interface with the controller through pneumatic converters.

7.2 COST ESTIMATE

The receiver is a shop-fabricated unit that will be shipped to the job-site and erected on top of a concrete tower. Appendix T contains the shop fabrication and field fabrication/erection plans for RS.

The shop fabrication plans describe a step-by-step fabrication sequence, including all significant fabrication and inspection operations. Taken into consideration are the tools, jigs, fixtures, equipment, floor space, and special supplies required. Welding procedures, weld qualification requirements, and nondestructive examination and inspection requirements are identified. Also included are shop fabrication schedules showing fabrication of subassemblies. Schedules for tool design and fabrication, welding development, and mock-ups are also included. The fabrication schedule is shown in Figure 7.11.

The field fabrication/erection plans include a schedule (Figure 7.12) that identifies the interrelationship between and time periods required for preparing the site; pouring foundations; erecting the tower; assembling structural supporting steel; installing the receiver, piping, heat tracing, pump, drain tanks, instrumentation and controls; and applying insulation.

Tables 7.3 and 7.4 give the cost estimate in 1982 dollars for the complete RS including the receiver, concrete tower, riser and downcomer piping, feed pumps, and auxiliary equipment.

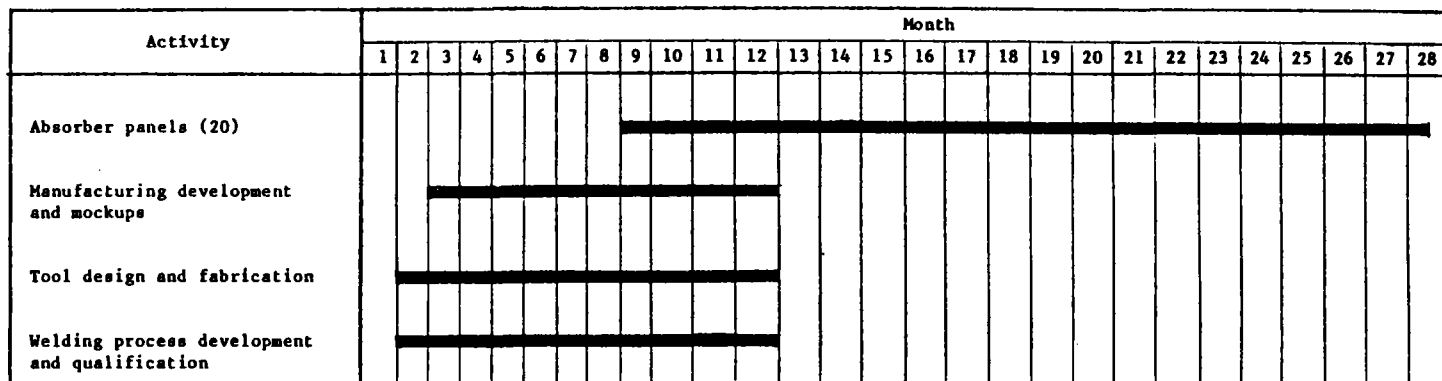


Figure 7.11 Fabrication Schedule of Receiver

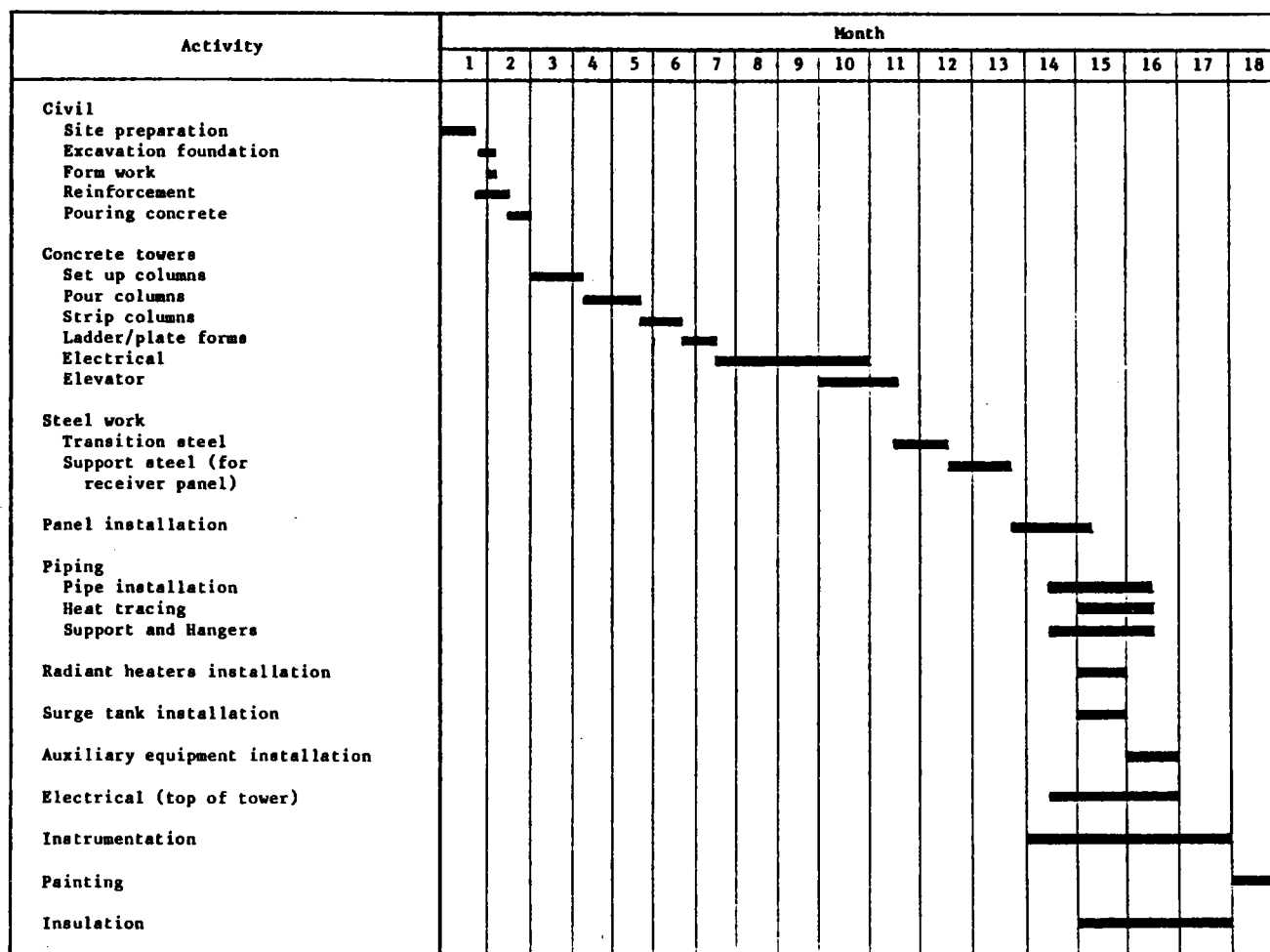


Figure 7.12 Master Project Construction Schedule

Table 7.3 320-MWt Molten Salt Receiver Subsystem Construction Cost Estimate (\$ 1982)

Item and Description	Labor Hours	Labor (\$)	Subcontracts (\$)	Materials (\$)	Subtotal (\$)	Total (\$)
Excavation and civil	700	13,200	40,000		53,200	
Tower and foundation			5,373,400		5,373,400	
Structural steel	8,800	164,000		1,113,500	1,277,500	
Machinery and equipment	11,210	237,600		10,506,100	10,743,700	
Piping and valves	26,550	498,700		2,432,000	2,930,700	
Electrical	5,290	100,500		207,600	308,100	
Instruments	4,310	81,200		538,900	620,100	
Painting			300,000		300,000	
Insulation			288,300		288,300	
Direct field costs		1,095,200	6,001,700	14,798,100	21,895,000	21,895,000
Construction facilities, services, and supplies	985	41,300	62,900	21,000	125,200	
Field staff, subsistence, and expenses		217,500		95,000	312,500	
Indirect field costs		258,800	62,900	116,000	437,700	437,700
Total field costs						22,332,700
Engineering and management	34,030	2,043,000		55,000	2,098,000	
Start-up and checkup		150,000		35,000	185,000	
Total office costs		2,193,000		90,000	2,283,000	2,283,000
Total field and office costs						24,615,700
Contingency						3,047,300
Fee 8%						2,213,000
Total construction cost						29,876,000

Table 7.4 Direct Field Cost Breakdown

<u>Item and Description</u>	<u>Labor Hours</u>	<u>Labor (\$)</u>	<u>Subcontracts (\$)</u>	<u>Materials (\$)</u>	<u>Subtotal (\$)</u>
Part 1: Top of Tower					
Structural steel	4,940	92,000		491,500	583,500
Machinery and equipment	9,120	173,340		9,846,400	10,019,740
Piping and valves	440	6,550		1,432,350	1,438,900
Electrical	1,630	30,750		72,250	103,000
Instruments	3,340	62,950		400,170	463,120
Painting			100,000		100,000
Insulation			88,550		88,550
Direct field costs		365,590	188,550	12,242,670	12,796,810
Part 2: Tower and Balance					
Excavation and civil	700	13,200	40,000		53,200
Tower and foundation			5,373,400		5,373,400
Structural steel	3,860	72,000		622,000	694,000
Machinery and equipment	2,090	64,260		659,700	723,960
Piping and valves	26,110	492,150		999,650	1,491,800
Electrical	3,660	69,750		135,350	205,100
Instruments	970	18,250		138,730	156,980
Painting			200,000		200,000
Insulation			199,750		199,750
Direct field costs		729,610	5,813,150	2,555,430	9,098,190
Total direct field costs (Parts 1 and 2)		1,095,200	6,001,700	14,798,100	21,895,000

Section 8

RECEIVER DEVELOPMENT

The major development issues for the molten salt receiver cover four broad areas:

- Design
- Performance
- Operation
- Molten salt and receiver technology

A considerable amount of development activity has been devoted to these issues and, based on these activities, a molten salt receiver can be designed, constructed, and operated. However, residual risks remain relating to absorber panel design, fabrication, and lifetime; receiver operation, availability, and maintenance; receiver performance and auxiliary power use; molten salt stability and corrosion; and creep-fatigue design requirements.

In this section, the verification status will be reviewed, and verification options will be identified and correlated with the verification issues. Based on these reviews and a review of test capabilities and requirements, test programs for each of the major verification options and the risk reductions resulting from these programs will be identified. Finally, a baseline test program with several options will be proposed.

8.1 VERIFICATION STATUS

While considerable analysis, testing, and industrial experience have been accumulated for molten salt RS components, operating scenarios and conditions have generally been simulated to limited degrees. Hence, demonstration of component designs in realistic operating scenarios with actual operating conditions (e.g., temperature, pressure) is not available. Key areas lacking demonstration include:

- Continuously welded, thin-wall tube panel with intermediate lateral supports operating in a representative flux and temperature environment
- Aperture door and heated cavity operating in hot/overnight shutdown mode
- Outlet temperature control in a multipass series/parallel cavity configuration
- Receiver operation and utilization of available insolation
- Receiver availability
- Receiver performance
- Receiver auxiliary power requirements
- Molten salt feed pump efficiency and reliability--especially the lifetime of the submerged bearings
- Drag valve lifetime and reliability, in particular; control valves in general
- Salt stability in a representative operating environment of fluxes and temperatures.

8.1.1 Design Issues

- Absorber Panels. Absorber panels have been tested at CRTF for water/steam, sodium, and molten salt receivers. These tests were limited in duration and simulated portions of panel operating regimes, but not all the operating regimes (i.e., duplication of local fluxes, flow rates, and local temperatures simultaneously). Additional testing of water/steam panels throughout

their full operating regimes is currently under way at Solar One. Testing of a different type of receiver tubing arrangement with horizontal rather than vertical tubes is currently under way in the IEA sodium receiver at Almeria, Spain, and is scheduled for an alternative horizontal tube arrangement at THEMIS in Targassonne, France, in the near future.

- Tube Materials. The ACR molten salt receiver SRE (ACR-SRE) and Solar One use Incoloy 800, the IEA receiver uses austenitic steel, and the THEMIS receiver uses Type 316SS. Other receiver tube materials have been proposed (e.g., Types 316SS and 304SS), but Incoloy 800 has been selected because of its greater corrosion resistance and its better creep-fatigue life.
- Tube Size. The ACR-SRE receiver used 19-mm (0.75-in.) x 1.65-mm (0.065-in.)-wall tubes. The present receiver SRE weld development program has concentrated on 25.4-mm (1.00-in.) x 1.65-mm (0.065-in.)-wall tubes as the best selection for a full-scale receiver. Testing completed to date has been too short to provide useful data on tube life.
- Construction. Test panels have been fabricated for molten salt, sodium, and water/steam (Solar One) receivers. Additional fabrication development took place during the current receiver SRE programs, as reported in Section 6.
- Tube-to-Tube Joining. Both tack-welded (ACR-SRE) and continuously welded (Solar One) panels have been built and tested. While concerns with lateral temperature gradients and the attendant thermal stresses for continuously welded panels have not been completely eliminated, the panels have held together so far and are still in operation. Test operations led to numerous failures of the tack welds; however, panel operation continued acceptably despite these failures. Operation with continuously welded, thin-walled substantially long panels with appropriate flux levels, flux gradients, and temperatures has not been demonstrated.
- Attachment of Support Structure. For the thicker tubewall Solar One configuration, welding of support structure attachments has been demonstrated. The ACR-SRE thin-walled receiver test unit required no support structure attachments because of its short panel length. The present receiver SRE weld development programs are developing appropriate support-structure attachments; however, these have not been demonstrated in either actual or simulated solar service.
- Header Arrangements. The Solar One thick-walled tube panels with cantilevered headers have been fabricated and are currently in service. The ACR-SRE thin-walled tube panel tested at CRTF had in-plane headers. Attachment of tubes to headers follows well-established techniques from the boiler industry.
- Support Arrangement. The ACR-SRE receiver test panel was suspended from its upper header and allowed to grow downward with no lateral support. Solar One panels are supported both at the tubing bends in the plane of the panel and at the top header. Both of these supports tie into

the strongback, which is tied to the main core structure. A separate hanger attached to the strongback provides support for the lower header. Lateral support for the Solar One panel is provided by lateral slides and a vertical pipe-and-roller system, which permits expansion both laterally and vertically. The proposed SRE support structure uses eye lugs for vertical panel support and buckstays for lateral support. Eye lugs and buckstays are used in boilers, but have not been demonstrated on thin-walled tube configurations.

- Installation and Removal. Both Solar One and the proposed SRE receiver utilize strongback panel supports, which are used for shipping (with appropriate auxiliary beams) and are attached directly to the main structure. Solar One experience with installation was favorable, but to date there is no experience relating to panel removal for strongback-mounted panels. Additionally, there is no experience with mounting large panels in a partial cavity configuration with all of the problems relating to interference between cranes and support structure.
- Insulation. Numerous approaches to rear-wall panel insulation--both with and without light-tight tube welds--have been successful.
- Aperture Door. Doors have been built for three small central receivers--two-piece horizontally moving doors for the ACR-SRE test and for the IEA sodium receiver, and a single-piece vertically moving door for the THEMIS project. Operating difficulties have been experienced with both horizontally moving doors, more severe for the ACR-SRE. The THEMIS door has not been tested during normal receiver operations.
- Actuating Mechanism. The doors are moved by a cable-and-pulley arrangement on rollers inside a channel track. Sticking problems (probably because of thermal distortion of the door and tracks) frequently made the ACR-SRE door inoperable without a manual assist to get it moving. Although a vertical cable pulley with trolleys has not been demonstrated, there should be fewer problems because of sticking. A lubrite spherical bearing to remove thermal distortion loads from the trolley has not been demonstrated in this type of application. The ACR-SRE used two pneumatic actuators to drive the cable that opened and closed the door. As mentioned earlier, the actuators were unable to overcome the sticking resistance, and manual assistance was needed. The electric motor in the proposed design was not used on any previous door design.
- Seals. The ACR-SRE door had no true seals. To date, there has been no adequate demonstration of door sealing for this application.
- Thermal/Structural Design. The ACR-SRE door was simple--a frame filled with 7.6 cm (3 in.) of insulation and covered with thin stainless steel plate. This arrangement was subject to thermal distortion and was inadequate. The proposed door design with vented structure between both internal and external layers of insulation appears promising, but has not been demonstrated.

- Reliability/Redundancy. Of main interest are the reliability and redundancy requirements, if any, for the door actuator mechanism. Because of the relative inaccessibility of the door, its failure to open would substantially reduce operating time and its failure to close would necessitate system drain. High reliability in door operations is essential.
- Uncooled Surfaces. Various insulations such as 3000 board have been demonstrated with only minor problems (e.g., problems with covers on 3000 board during the recently completed Rockwell ESG sodium panel test).
 - Design Temperatures and Fluxes. These values are currently estimated using analytical codes. Higher-than-predicted values can be used for design to provide adequate protection.
 - Surface Optical Properties. Values for these properties will affect temperatures in the cavity. Values available from the manufacturers and the literature should be acceptable.
- Control Valves. While numerous on-off valves have been used in process plant molten salt service, modulating control valves are not in general use. During the ACR-SRE tests, a control valve was used; however, there were some problems with flow-control instabilities because of the valve characteristics.
 - Seals and Seal Life. While valves with bellows seals have been used extensively, there is some concern with bellows life in cyclic service. Valve service in an SRE receiver environment has not been demonstrated.
 - Wear on Drag Valve. Demonstration of a drag valve in solar plant service is limited to the IEA sodium plant, which has a shorter tower and less dense fluid. While corrosion tests on a Stellite valve trim material are encouraging, operation of a drag valve in SRE-type service has not been demonstrated.
 - Fill and Drain Valve (On-Off). These valves have proved acceptable in the process flow industry and have operated without problems during the ACR-SRE program.
- Control Sensors (Back Tubewall Temperatures vs. Flux Gages). Utilizing flux gages, Solar One has demonstrated acceptable flow control during transients. Initial problems with water-cooled flux gages have been largely overcome by using air-cooled flux gages with careful design and installation. Panel flow control during transients, based on back tubewall temperatures, has been demonstrated in a limited way, but has not been verified with respect to deep power transients.
- Feed Pumps. Low-head molten salt pumps with a range of capacities extending beyond our receiver requirements are common in the process industry. Pumps with the required head and high capacity have not been demonstrated.
 - Multistage Pumps. These pumps have been used for many years; however, they have not operated at our full-scale receiver head requirements [maximum of 76 m (250 ft) vs. approximately 350 m (1000 ft)].

- Submerged Bearings. These have also been in use for many years; however, they have a history of wearing out in about 9 months in continuous service (approximately 6000 hours).
- Thermal Conditioning Equipment. Thermal conditioning equipment for lines, tanks, pumps, and valves has been demonstrated in many installations and, most notably, in nuclear-related sodium loops.
 - Cavity Radiant Heaters. Performance, reliability when exposed to receiver radiant operating environment, and distribution of heat without cold spots have not been demonstrated, especially in an environment sealed with a large door.
 - Tracer Heaters. Although there have been some developmental problems with trace heaters, good service has been demonstrated when there was proper design and installation.

8.1.2 Operating Issues

- Availability. Availability data on operating receiver systems are too sparse and are not representative of normal operating cycles and overnight conditioning with door operation. Availability estimates are largely based on component data and lack verification of key systems such as door and thermal conditioning equipment.
- Use of Available Sunlight. While data are beginning to be accumulated for Solar One, its external cylinder receiver with surround field and water/steam coolant makes it questionable that these data have any significance for a north field molten salt receiver.
- Draining and Requirements for Continuous Trace Heating of Drain Lines. The ACR-SRE receiver demonstrated draining with the door open and closed. Because trace heating was continuous, the possibility of providing adequate draining without continuous trace heating was not demonstrated.
- Control of Receiver. Solar One has demonstrated control of a water/steam external receiver over a wide operating range. The ACR-SRE test demonstrated limited control of a salt test panel over a limited operating range. Control of a partial cavity receiver under start-up, shutdown, and transient conditions has not been demonstrated.

8.1.3 Performance Issues

- Surface Optical Properties. Information about Pyromark paint is available and, except for possible effects of temperature on absorptivity and emissivity, is acceptable. Measurements have not been made in the field under normal operating conditions.

- Cavity Optical Properties. These have been predicted by optical analysis codes (e.g., TRASYS). Although the theory and analysis are generally well understood, actual verification is not available.
- Convection Losses. Numerous models, data correlations, and tests have been devised to determine convective losses. While promising approaches have been identified, the problem of combining forced and free convection and the accuracy of measurements to date limit confidence in current correlations. Extensive performance testing at the IEA facility in Almeria may provide data that will help to corroborate or improve current projections.
- Conduction Losses. Estimates of these have been made analytically, and limited instrumentation was used in the ACR-SRE test; however, detailed verification of conduction losses, especially through "heat shorts," is not available.
- Pressure Drop. Measurements of pressure drop in the ACR-SRE were slightly higher than predicted; however, given the complexity of the system, this is not of great concern.
- Overnight/Hot Shutdown Losses. No data for a closed and sealed cavity are known to be available.
- Auxiliary Power Requirements. Pump power requirements are generally well understood and predictable, provided pressure drops and salt properties are accurately predicted. Actual trace heating power requirements have not been demonstrated for cyclic operation of a solar power plant. Cavity radiant heater power requirements have not been verified, nor has the sensitivity of these requirements to the sealing characteristics of the aperture door been established.

8.1.4 Technological Issues

- Salt Corrosion. Extensive salt corrosion testing has been conducted. Based on these data, acceptable corrosion levels are likely in Incoloy 800 tubes. Questions remaining relate primarily to the effects of long-term cyclic operations and the effects of impurities.
- Salt Stability. With a dry air cover, without carbon dioxide, and for temperatures less than 593°C (1100°F), salt stability appears to be acceptable. Questions remaining relate primarily to the effects of impurities and regeneration of salt when impurity levels become unacceptable.
- Surface Fouling. Existing data indicate that pure salt tends to create a thin, oxide layer which is resilient and self-inhibiting; however, impurities such as calcium and magnesium can precipitate out and form a scale.

- Creep-Fatigue Life. Elastic estimates of creep-fatigue life for Solar One were conservative when compared with full inelastic estimates. Data verifying these analyses are not available.
- Film Coefficients. Limited validation of salt film coefficients was obtained in the ACR-SRE receiver test. Detailed validation of these coefficients and salt properties is not currently available.

8.2 VERIFICATION OPTIONS

The verification options that have been identified include the following:

- Analysis. Some form of analysis can provide acceptable verification, provided techniques and inputs are well established.
- Existing Data. Previous testing or industrial experience can provide acceptable verification of SRE receiver design performance, operation, or technology.
- Laboratory-Scale Testing. For phenomenological-type information (e.g., surface absorptivity), laboratory scale testing may be the most appropriate verification option.
- Component Testing. For some developmental issues (e.g., pumps, valves), either scale-model or full-scale component testing may be required.
- Molten Salt Loop Testing. Molten salt loop testing can provide important information on process flow equipment design and operation, on molten salt stability and corrosion in a temperature cycling, flowing environment and--if so configured and operated--on tube stress and corrosion at various operating points.
- Scaled CRTF Receiver Testing. Using CRTF and a scaled or nearly scaled receiver configuration, information relating to cavity operation, flux distributions, flow and temperature control, and overnight conditioning can be obtained. By operating the flow loop from ground level, it is possible to obtain information on pump, surge tank, and drag valve operation in addition to basic receiver operation, which can be simulated with a tower-mounted flow loop.
- CRTF Panel Testing. Because of the 64:1 scaling in power (8:1 in dimension) between the full-scale receiver and the CRTF scaled configuration, better information about larger panels can be obtained for individual panels by using the entire CRTF field to illuminate a single panel. While such a panel would be significantly smaller than a full-size panel, it could be significantly larger than a scaled CRTF receiver panel. Through this panel scale-up, better information about panel support and panel behavior with flux profiles and gradients can be obtained.

8.3 SUMMARY OF TEST REQUIREMENTS AND TEST CAPABILITIES

Development test requirements are dictated by the full-scale receiver configuration and the condition and scenarios in which this configuration must operate. Verification of receiver design requires simulation of as many as possible of:

- Size
- Configuration
- Materials and fluids
- Operating conditions
- Operating scenarios

Limiting any development program with respect to achieving these simulations are:

- Collector Field. Size and availability of existing collector fields (CRTF and Solar One), cost of building a new field.
- Instrumentation. State-of-the-art limitations on flux and front-face tube temperature measurement technology.
- Test Time. Clearly there are conflicts between the timely accumulation of data and the length of time required to get good data pertaining to panel life; operability and availability; and salt stability and corrosion, which may result from salt breakdown at high temperatures. When considering the available test options, it is clear that short of a full-scale cavity configuration test, no option is able to simulate all of the key parameters listed. Therefore, only through a combination of tests can a reasonable development program be established.

8.3.1 Simulation Requirements

In planning RS testing, investigations must consider:

- Size. Important in simulating cavity performance; overnight conditioning operation, including heater design and aperture door design; panel support and integrity in flux gradients; and pump and valve design, performance, and operation. It also strongly influences the salt transit times and the response times of the outlet temperature control equipment.

- Configuration. Important for simulating performance, overnight conditioning equipment and aperture door, panel support, and pump and valve designs. Some similarity in flow routes is important for control system simulation.
- Materials and Fluid Similarity. Required for panel design, both from thermal and corrosion standpoints, and also for pumps and valves. Clearly, materials and fluid similarities are essential for evaluating molten salt technology issues.
- Process Variables. Simulation of process variables--temperature, pressure, heat flux, and flow velocity--goes along with the use of similar materials and operating fluid, and is important for the evaluation of performance and molten salt technology.
- Operating Scenarios. The simulation of operating scenarios--diurnal cycles and partly cloudy weather--is important to demonstrate control, utilization of available insolation, receiver availability, receiver performance over its operating envelope, and receiver auxiliary power requirements. Also, because of the issues of cyclic operation, the simulation of operating scenarios is important for molten salt technology evaluation.

8.3.2 Test Limitations

Three major limitations that must be considered in test planning are:

- Available Collector Fields. There are currently two collector fields of substantial size operating in the U.S.--a 5.5-MW north field at the CRTF in Albuquerque, New Mexico, and a 45-MW surround field at Solar One in Barstow, California. The CRTF was designed and is operated as a test facility; Solar One was designed and is being operated as a pilot plant for a 100-MWe commercial utility plant. Because of the expense involved in heliostat production either on a limited basis or in the substantial quantities required for a 1/4 or greater scale, RS testing is essentially limited to an existing collector field.

The proposed SRE configuration, a north-facing partial cavity, is naturally suited for testing at CRTF. Testing at Barstow would involve one of two options:

- Put the receiver on the existing tower below the Beam Characterization Subsystem targets and use only part of the existing field (approximately 20 MW).
- Construct a new tower south of the existing field to increase the available power to approximately 40 MW.

The advantages of testing at Solar One are all size related. Power scaling can be increased from the 64:1 at CRTF to 16:1 (first option) or 8:1 (second option). The disadvantages are obviously cost and the impact of any RS testing of Solar One operation as a pilot plant.

- Instrumentation. While there is much interest in detailed measurements of various receiver losses, instrumentation available for measuring details of incident flux and absorber surface temperatures is quite limited. Aperture flux meters, flux gages mounted in or near the absorber surfaces, and the traveling reflecting bar developed by the Swiss provide measurements of flux, but all have error bands on the order of 5 to 10 percent. Since receiver radiation and convection losses are on the order of 5 to 10 percent or less of the incident flux, it is clear that without more accurate measurements of the incident flux, allocation of losses among spillover, reflection, reradiation, and convection will remain highly speculative.

Similarly, the great difficulty in measuring front-wall tube surface temperature further reduces the confidence of any breakdown of losses.

While imaging infrared radiometers offer good capabilities with respect to temperature and flux distributions, good reference point temperatures and flux information are required to provide absolute rather than relative values.

A related issue in instrumentation is the need for good correlations of fluxes and temperatures to provide valid receiver design criteria relating to requirements imposed by salt stability. The current upper limit on salt film temperature [i.e., 595°C (1100°F)] is based primarily on test data from bulk samples. Unfortunately, the determination of the local flux and temperature in an operating cavity receiver is currently limited by flux and temperature measurements and thus leaves considerable uncertainty regarding the proper design criteria.

- Time Scale. Because of the long-term nature of creep-fatigue and corrosion damage, it is desirable to run tests for investigating these issues for a substantial period of time. On a lesser but still significant time scale is the seasonal operation of the plant, both with respect to sun position and meteorological conditions. And finally, because of the nature of plant development, regular operations after infant mortality problems are discovered and solved means that tests directed at operating issues (i.e., availability, insolation use, and maintenance costs) must run for approximately 1 to 2 years before meaningful operating data are available.

8.3.3 Test Capabilities

When evaluating the test options in the context of the parameters mentioned earlier, we can draw these conclusions:

- Laboratory-Scale.
 - No simulation of size except for small details.
 - Only very fine details of configuration are likely to be simulated (e.g., Pyromark paint on a small bank of welded tubes to assess absorptivity data).

- Materials and fluids can be simulated.
 - Pressures and temperatures can be simulated as can fluxes and flow velocities (the latter two variables only within certain constraints).
 - Operating scenarios--some cyclic effects can be evaluated within the overall limitations described.
- Component. In general, component testing is limited by the available support equipment and by cost. Large component test loops such as the sodium test loops at Energy Technology Engineering Center are candidates for testing large salt components (e.g., pumps and valves); however, the costs of such tests are high.
 - Simulation of size is primarily limited by cost rather than capability. Experience in nonsolar development of pumps and valves has consistently demonstrated that designs acceptable when small may not be acceptable when large.
 - Simulation of configuration is possible; however, configuration problems are not independent of size and so great care must be taken whenever size or other important variables is not also simulated in a configuration test.
 - Materials and fluids can be simulated.
 - Temperature and pressure can be simulated, as can flow velocities, with some interdependence on size. Fluxes can be simulated within limitations.
 - Operating scenarios within the limitations of flux capabilities can generally be simulated.
- Molten Salt Loop. In the context being considered, molten salt loop testing will be limited to a rather small scale, with large-scale component testing considered only in the context of "Component" testing.
 - In general, molten salt loop testing will not simulate full size; however, it can simulate a small section of a full-scale panel for irradiation, as previously considered by SNLL.
 - In general, a molten salt loop can simulate the configuration within the context of reduced size. Unfortunately, because small components are not always similar to the larger components in design, there may be considerable expense to get salt loop components that are similar to full-scale components.
 - One of the primary functions of the salt loop is the simulation of materials and fluids.

- A second important function is the simulation of pressures, temperatures, flow rates and heat fluxes within the context of a small section of a full-scale panel.
- Finally, a third important function of a salt loop is the simulation of operating scenarios.

- CRTF Cavity Configuration.

- Because of the limited power available (approximately 5 MW), size cannot be simulated at CRTF.
- Configuration simulation at CRTF appears feasible with respect to geometry (approximately 1/8 scale) and flux maps. It is not feasible for T/H simulation because of the combined requirements for absorber and flow areas. Scaled tubes of approximately 3.2 mm (1/8 in.) are not practical either from full-scale heat transfer or pressure-drop considerations. Further, because an alternative flow routing is necessary, even though the flux profile can be simulated to a degree, the cavity temperature distribution, and thus reradiation and convection heat losses, will be somewhat different.

Nevertheless, by routing the fluid in series back and forth across the cavity, and by splitting the last passes into two parallel flows--one on each side of the cavity, an approximate correlation between cavity temperatures for the CRTF and full-scale configurations is possible, as is simulation of a series/parallel control for the salt flows. Because of the scale and transit times, detailed simulation of actual control system gains is clearly impossible.

Because of the large scale factor and, to a lesser degree, T/H requirements which mandate some passes with 19 mm (3/4 in.) tubing, the panels can simulate the welded construction and to some degree the intermediate support approach, but cannot provide simulation of a full-scale panel.

With respect to the aperture door and the overnight conditioning equipment, it is possible within the constraints of scale to simulate the basic approach--however, without the effects of large scale on thermal structural behavior of the door or on cavity internal heat transfer.

- Materials and fluids can be simulated.
- Process variables in general can be simulated; however, pressure drops, detailed cavity temperature distributions, and flow velocities will all vary somewhat from the full-scale configuration.
- Operating scenarios can be simulated.

- CRTF Panel. A CRTF panel test, while not able to simulate a full-scale panel with full-scale flux, can provide full-scale panel flux levels for a panel ranging from approximately 1.8 by 9 m (6 x 30 ft) to 2.4 by 6 m (8 x 20 ft).

Such a panel is large enough, up to full scale in width, to provide a good evaluation of panel thermal structural design and behavior over the panel operating ranges. However, to do this, salt must be delivered to the panel inlet at 285 to 555°C (545 to 1031°F).

- Panel tubes, welding, and structural supports can be simulated effectively
- Fluids and materials can be simulated
- Process variables for a panel can be simulated
- Operating scenarios as they relate to panel operating environment, except for overnight operations, can be simulated.

8.4 TEST PROGRAM OPTIONS AND RISK REDUCTIONS

Of the five options discussed (i.e., laboratory-scale, component, salt-loop, cavity-configuration, and panel testing), all but laboratory-scale testing offer the potential for substantially reducing risk; however, only full-scale component testing for pumps and valves offers the potential for actual qualification and verification of final RS designs.

Because of the extensive history of laboratory-scale testing and the attendant limitations, further testing at this level will not substantially reduce the risk of the current design. If new candidate materials or salt compositions are proposed, laboratory-scale testing will be a valid screening function; however, such testing should rightfully be done by the commercial industry proposing these changes; it is not recommended as part of a follow-on SRE Phase 1 development program.

As mentioned earlier, full-scale component testing of receiver pumps and control valves offers the potential for full qualification of these components. Because of their continual thermal cycling and the experience at Solar One, careful design and testing of these components will greatly reduce the possibility of lost operating time because of failures that may result from thermal cycling. Unfortunately, these thermal effects are critically size dependent; hence subscale testing can provide only limited confidence in pump and valve designs. Further, although design, fabrication, and testing of these components will span several years, the combination of these tests with the development of an operating plant in which the components are used after successful testing is both possible and cost effective. Therefore, while these component tests are

recommended as part of the overall development of a commercial scale receiver, they are not recommended as part of an SRE development program. The other receiver component that may benefit substantially from component tests is the aperture door. A reduced-scale version of one section can provide meaningful data that will greatly increase confidence in the thermal structural design of the door, trolley, and seals. Radiant heaters will be needed to create the appropriate thermal loads. Pending an estimate of the cost and availability of funds for such a test, we will retain it as an option.

Current plans for molten-salt-loop testing at CRTF are unsettled. Basic corrosion testing would supplement existing data; however, corrosion may not be a great enough risk to warrant future testing. Components in a salt loop are generally too small to provide accurate component data. However, data relating flux, tube temperature, salt stability, and corrosion at relatively high salt bulk temperatures [510°C (950°F) or higher] would greatly reduce the operating risks (salt stability and corrosion) associated with a 565°C (1050°F) outlet temperature and normal operating excursions, which can raise inner tubewall temperatures to 593°C (1100°F) and higher. Because of the potential value of this testing, a salt loop with provisions for radiant heating of a small panel test section will be retained as an option. Should a salt loop be included, additional tests relating to fill/drain operations and requirements for fill/drain system trace heating could also be run.

The remaining two test options--a cavity configuration and a panel test--require the use of either CRTF or Solar One. While either facility offers reasonable panel section size test capability, both offer significant size

constraints for cavity configuration testing. The 1/8 power scaling and 35 percent linear size scaling available with a new tower south of the existing Solar One do not permit a full T/H simulation of the receiver; however, they do allow for panel testing at reasonable scale. Additionally, such a test should provide useful data on door design and operation. Unfortunately the cost is high and there is the possibility of interference with Solar One operation and testing.

Because neither thin-walled, continuously welded panel tests nor partial cavity configuration tests (including an aperture door and thermal conditioning equipment) have been conducted to date, performance of these two tests at CRTF will offer valuable data relating to panel design and cavity operation at small scale and are recommended for final consideration. The panel tests, by verifying thermal structural design, will reduce the risk of early catastrophic failures associated with absorber panels. The cavity configuration tests will provide important data on the utilization of available sunshine and receiver control and operation, as well as limited data on receiver performance.

In summary, test elements to be considered in defining the baseline test program and options are:

- Subscale component testing of an aperture door section with trolley and seals and including effects of radiant heating.
- Salt-loop testing, which includes radiantly heated small panel sections, to evaluate the interrelationship of flux, tube temperature, salt stability and corrosion at high [$>510^{\circ}\text{C}$ ($>950^{\circ}\text{F}$)] bulk salt temperatures.
- A cavity configuration test at CRTF.
- A panel test at CRTF.

8.5 PROPOSED TEST PROGRAM

Candidate test program options include these at CRTF using the basic salt loop elements (with appropriate modifications) of the MSEE:

- Absorber Panel Test. Of relatively short duration to verify the panel structural design and support system under realistic flux/temperature conditions.
- Cavity Test. Would follow the panel test and be longer. It would investigate RS operability and utilization of available sunshine, overnight conditioning and door operation, outlet temperature control, receiver auxiliary power use, performance, and availability.
- Salt Loop Irradiated Panel Test. Would be a small sub-loop of the MSEE and would have the capability for radiant heating of small test panel sections to investigate high bulk temperature/flux level phenomena in a tightly controlled environment.

In addition to these CRTF tests, a scale model section of the aperture door should be constructed and tested in an appropriate test facility. This test should include extensive thermal cycling of the door, seals, and trolley mechanism.

The priority for these program options is:

- Cavity Test
- Absorber Panel Test
- Salt Loop Panel Section Irradiation Test
- Aperture Door Test.

The cavity test was given first priority because it is the most comprehensive of the tests and it offers important information relating to operability and use of insolation and receiver salt control experience--especially verification of physical modeling of salt flows. Additional data relating to the

aperture door and overnight conditioning, performance, and auxiliary power use will also be obtained; however, because of the limitations of instrumentation and scale, these data will verify methods of analysis more than design.

The absorber panel test is second in priority because it will provide a meaningful scaling test of the panel and its support structure. By preheating the inlet salt, it is possible to operate the panel over the entire panel operating envelope. While past panel tests have provided only limited thermal structural data, because of limited test time and competing test objectives (e.g., control), this panel would be operated purely to simulate realistic flux/temperature environments and cycles, which should result in the maximum of useful thermal structural design data.

Supplementing the panel test is the salt loop panel section irradiation test. This test would use the mixed HST/CST tank salt bleed flows in panel test sections with radiant heaters. Both salt decomposition and panel corrosion would be monitored to provide better design criteria for receiver outlet pass flux limits.

Finally, there is an option for a subscale aperture door test. This test, which has not yet been designed, would supplement the cavity configuration door test in the same way that the panel test supplements the small-scale cavity panel tests. By combining the cavity test at small scale with the larger scale component tests (i.e., panel and door), both the overall integration and individual component problems can be investigated and corrected.

While these tests all offer useful information, detailed cost analyses of each are beyond the scope of this study. Of the tests considered, the most general and the one that will provide the best overall data is the cavity configuration test. The others, which are optional, can only be evaluated after better cost estimates are available.

The next three sections present a preliminary test description for the cavity configuration tests and cursory descriptions for the panel and salt loop irradiated panel section tests. Finally, test objectives and test requirements are identified for aperture door tests.

8.5.1 CRTF Cavity Test Program

- Test Objectives.

- Demonstrate systematic reliable operation of a molten salt partial cavity receiver, including the operation of the aperture door and overnight conditioning equipment
- Demonstrate high utilization of the available insolation
- Demonstrate a series-parallel molten salt control system
- Provide data relating to receiver thermal performance, auxiliary power use, and availability.

- Test Requirements.

- Simulate a full-scale cavity flux environment including average flux [0.25 to 0.28 MW/m² (79,000 to 89,000 Btu/h·ft²)] and flux distributions--especially for outlet passes [\approx 0.4 to 0.45 MW/m² (\approx 127,000 to 143,000 Btu/h·ft²)] with high bulk salt temperatures--and simulation of flux conditions during start-up, shutdown, and cloud-induced transients.
- Simulate full-scale panel designs, flow velocities, and flow routes to the greatest degree possible. Panel design and flow velocities are important for verification of panel construction and structural support in a realistic T/H environment. Flow route simulation is important for providing realistic local temperature/flux correlations and for flow-control simulation. Because of requirements for total panel absorber area and for panel flow area, it is not possible to simulate all of the relevant conditions.

- Simulate inlet 288°C (550°F) and outlet 566°C (1050°F) salt temperatures.
 - Simulate aperture door design and cavity thermal conditioning approach and operations.
 - Provide special instrumentation designed to measure flux and cavity temperature data for evaluation of performance data.
 - Provide instrumentation for measuring receiver net power and for monitoring receiver auxiliary power users.
- Test Hardware. The combined design-point thermal rating of the CRTF cavity absorber is 5.33 MW (18.19 x 10⁶ Btu/h), with a salt flow rate of 12 kg/s (95,300 lb/h). The absorber heat-transfer surface is made of tubular panels assembled to enclose three sides of the absorber cavity with major dimensions ≈3 m (≈9.9 ft) wide x 2.3 m (7.5 ft) deep and 4.7 m (15.4 ft) high. The open side of the cavity forms a 3-m (9.9-ft) wide x 3.7-m (12-ft) high aperture equipped with a door to retain heat during periods without insolation. Absorber panels are heavily insulated on the outside; a sheet-metal casing that protects the absorber is insulated. A structural steel skeleton, which supports the absorber panels and casing, is the connecting interface with the tower. Figure 8.1 shows the absorber arrangement; Figure 8.2, the receiver flow path arrangement; and Figure 8.3, the developed view of the absorber area.

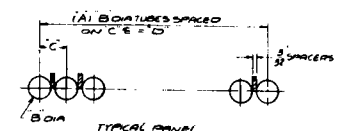
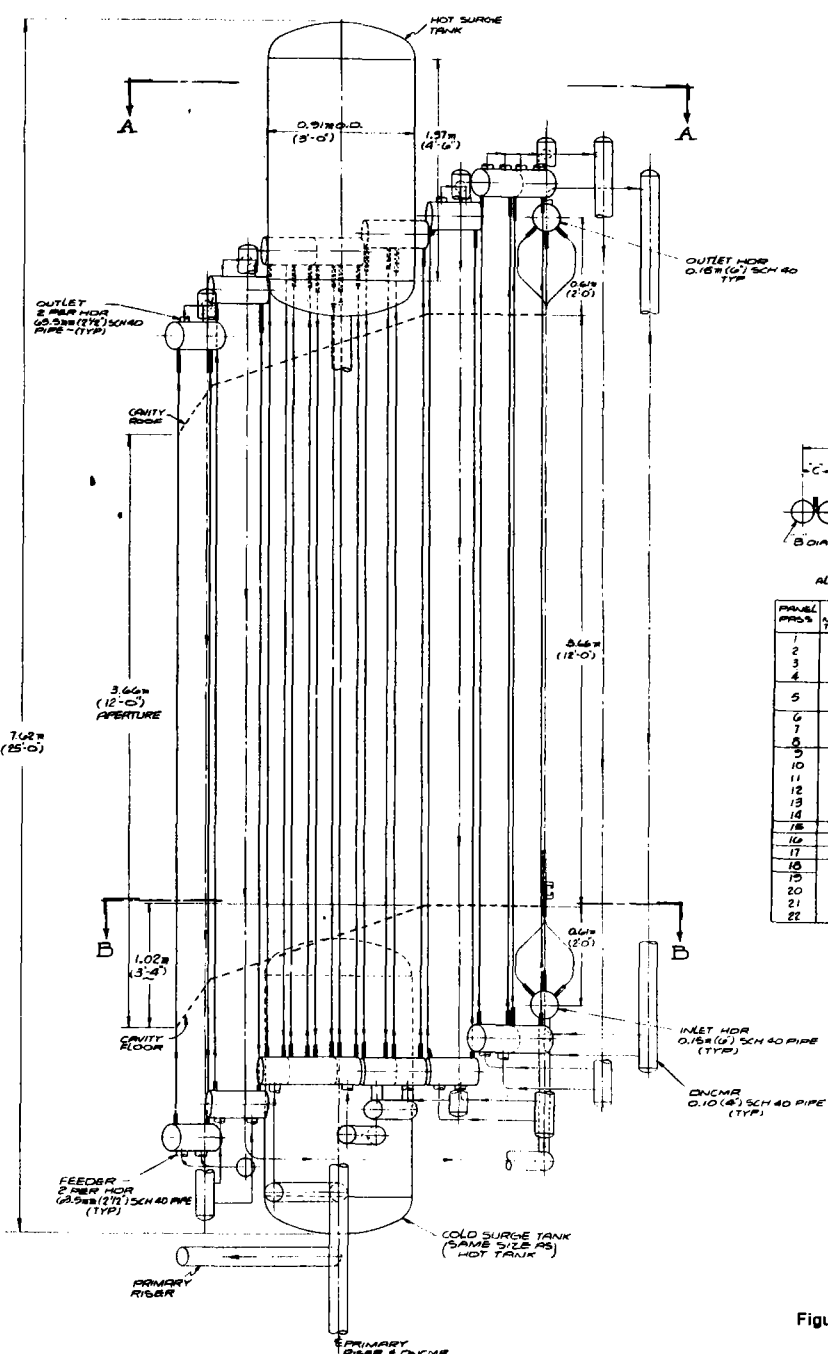
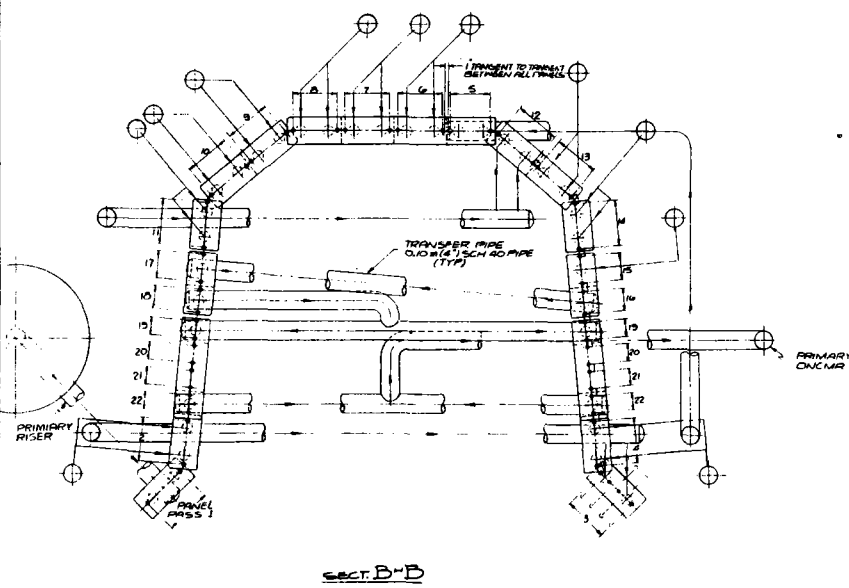
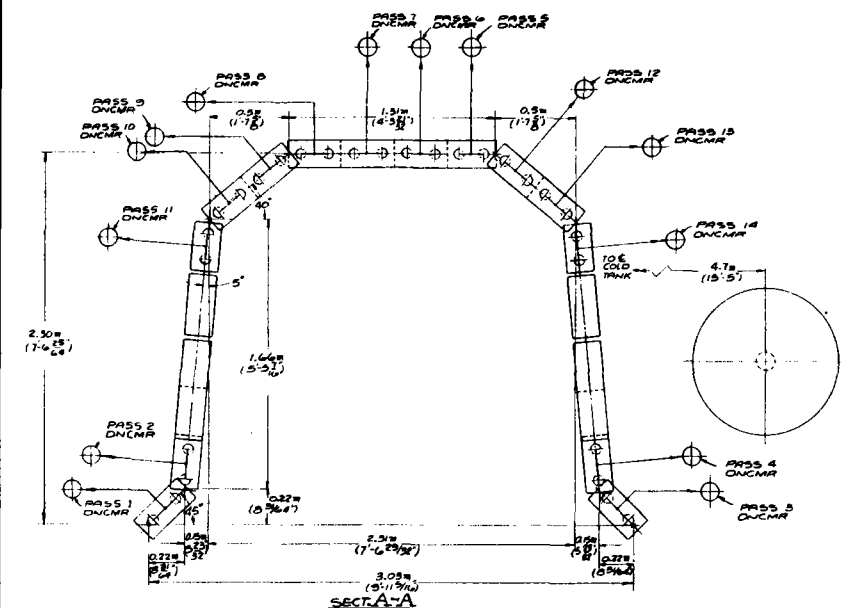
Figure 8.4 shows the modifications required for inclusion of the cavity configuration. In addition to a new receiver, modifications required include:

- Replacing receiver booster pump to increase outlet pressure from ≈2.2 to 2.9 MPa (≈315) to 415 lb/in².
- Providing level control for IST and level control valve between receiver booster pump and riser.
- Relocating OST level control valve upstream of CST receiver outlet flow diversion line and putting blocking valves in HST line and CST receiver outlet flow diversion line.

Figure 8.5 is a preliminary P&ID for the receiver panels. Not shown on this sketch is the fill/drain system.

- Test Plan. The plan for testing the receiver, which will run for 1-1/2 to 2 years, comprises three distinct phases:
 - Phase 1: Control Testing. Would investigate control using back tubewall temperature and flux data for feed-forward testing.
 - Phase 2: Cavity Performance Testing. Would follow the initial control testing and would investigate input flux, losses, overnight conditioning, and auxiliary power.

DATE: November 1982



ALL TUBES ARE 1.53 (0.046) IN

PANEL	PROG	A	B	C	D	TUBE
		NO OF	TUBE	TUBE	PANEL	MATL
		TUBES	O.D.	O.D.	WIDTH	
1	11	25.4	21.6	0.218	304	SS
2		(17)	(17)	(10 9/16)		
3						
4						
5	14	18.0	21.4	0.218	304	SS
6		(14)	(14)	(10 9/16)		
7	11	25.4	21.6	0.218	304	SS
8		(17)	(17)	(10 9/16)		
9						
10						
11	14	18.0	21.4	0.218	316	SS
12		(14)	(14)	(10 9/16)		
13						
14						
15	7	18.0	21.4	0.218	304	SS
16		(14)	(14)	(10 9/16)		
17	6	25.4	21.6	0.218	304	SS
18		(17)	(17)	(10 9/16)		
19						
20	6	18.0	21.4	0.107	1-800	
21		(14)	(14)	(4 7/8)		
22						

Figure 8.1

5 MW MOLTEN SALT
TEST CAVITY SRE

FORN NUCLEAR DEVELOPMENT CORPORATION
10000 N. 100th St., Suite 100, Minneapolis, MN 55438

RD-820-82

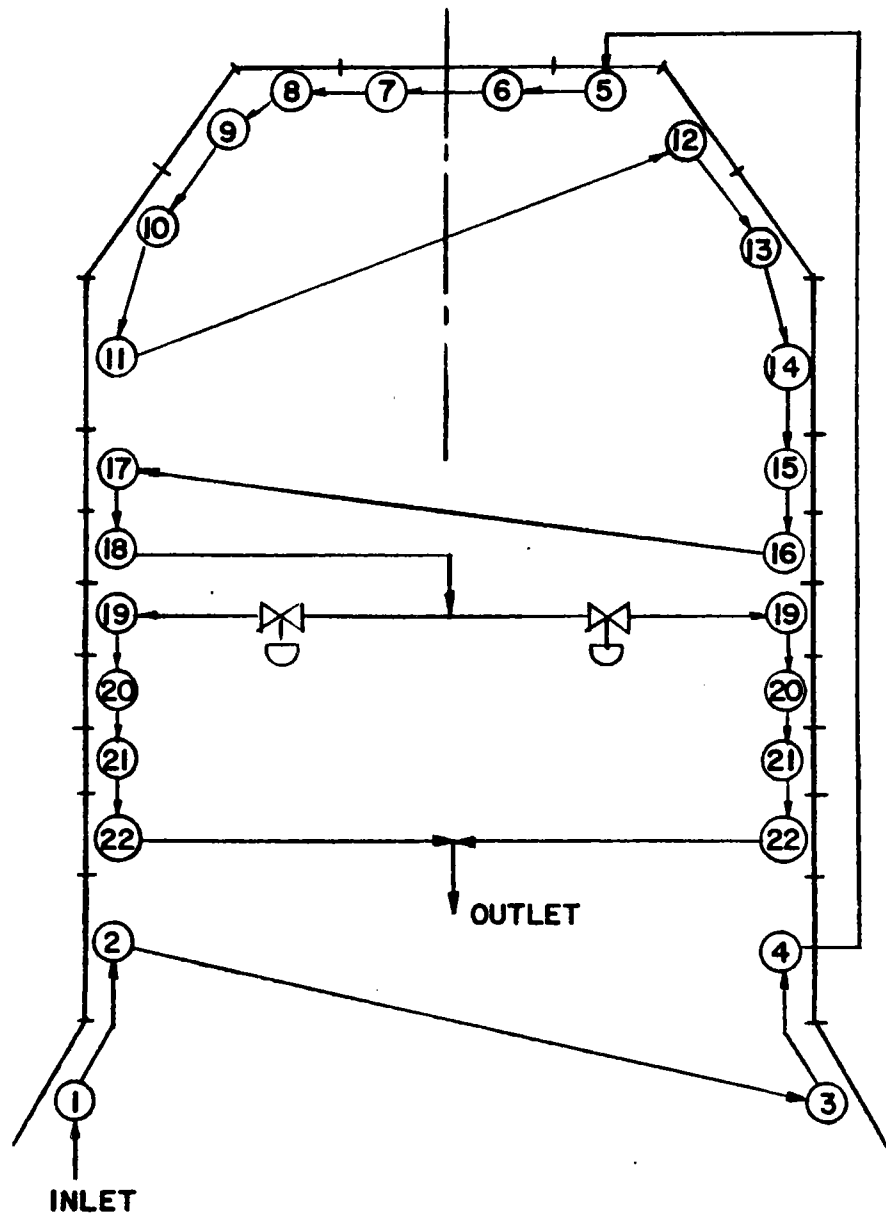
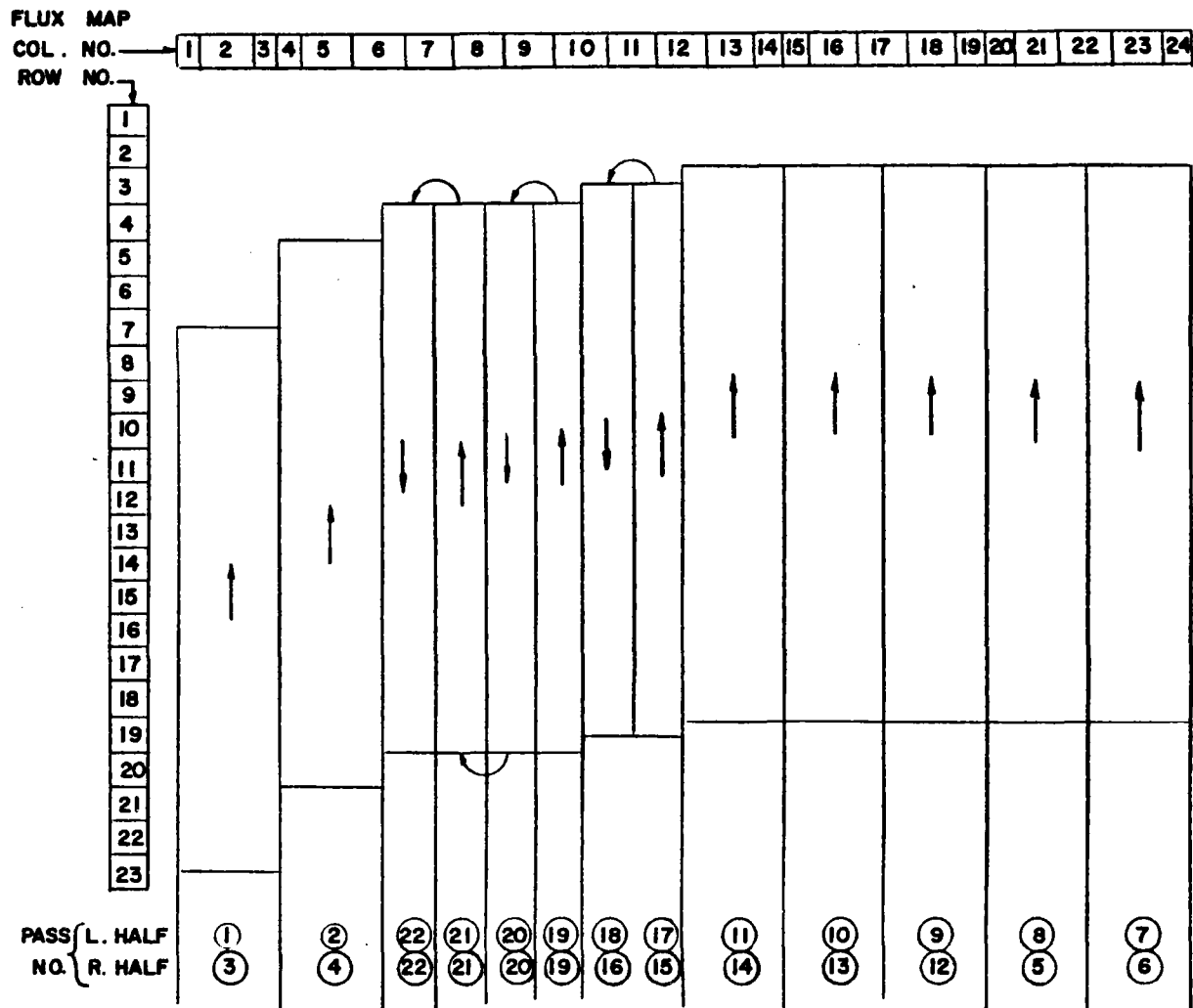


Figure 8.2 SRE Test Cavity Circuitry Schematic



8-26

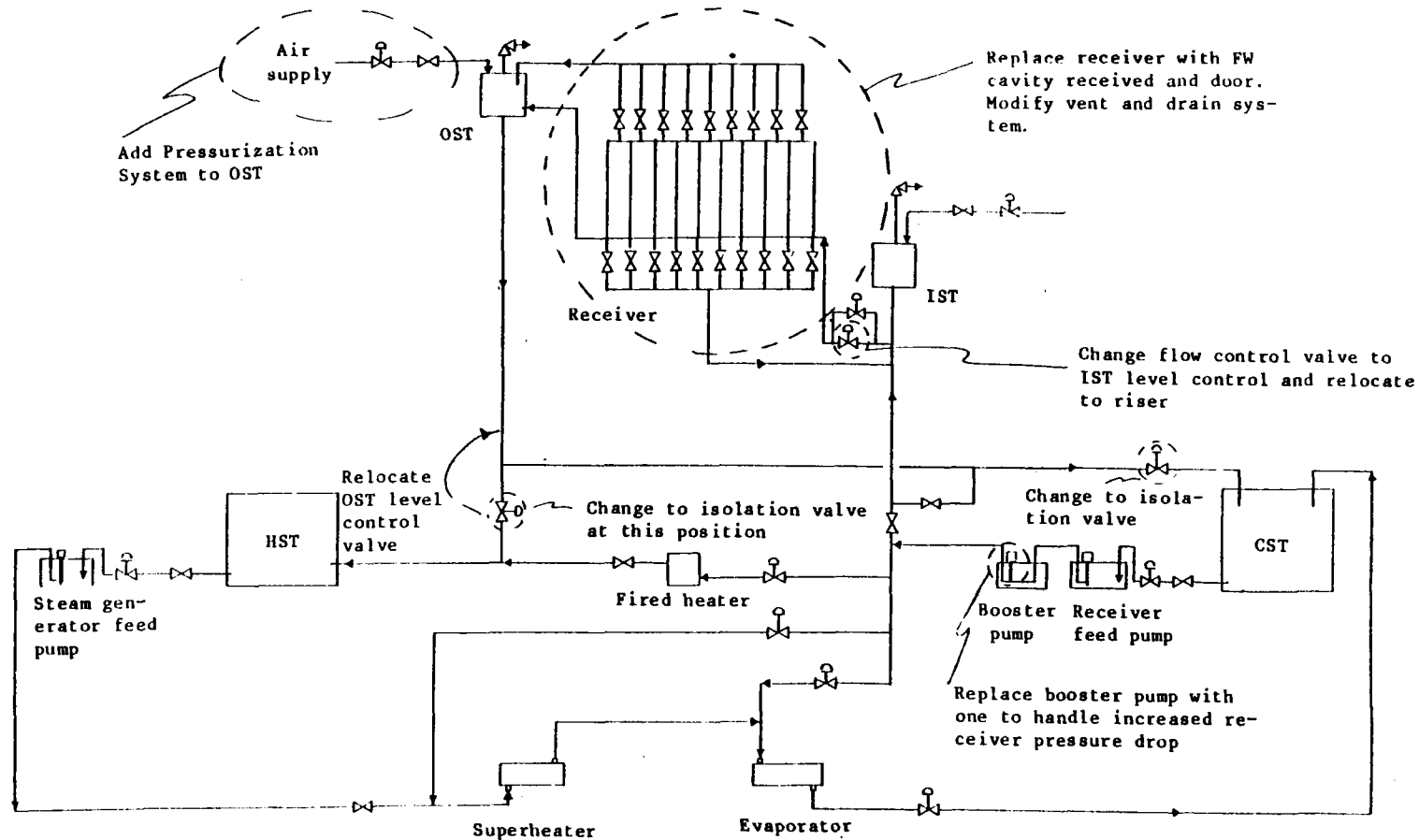


Figure 8.4 Required Modifications to MSEE P&ID for Cavity Test at CRTF

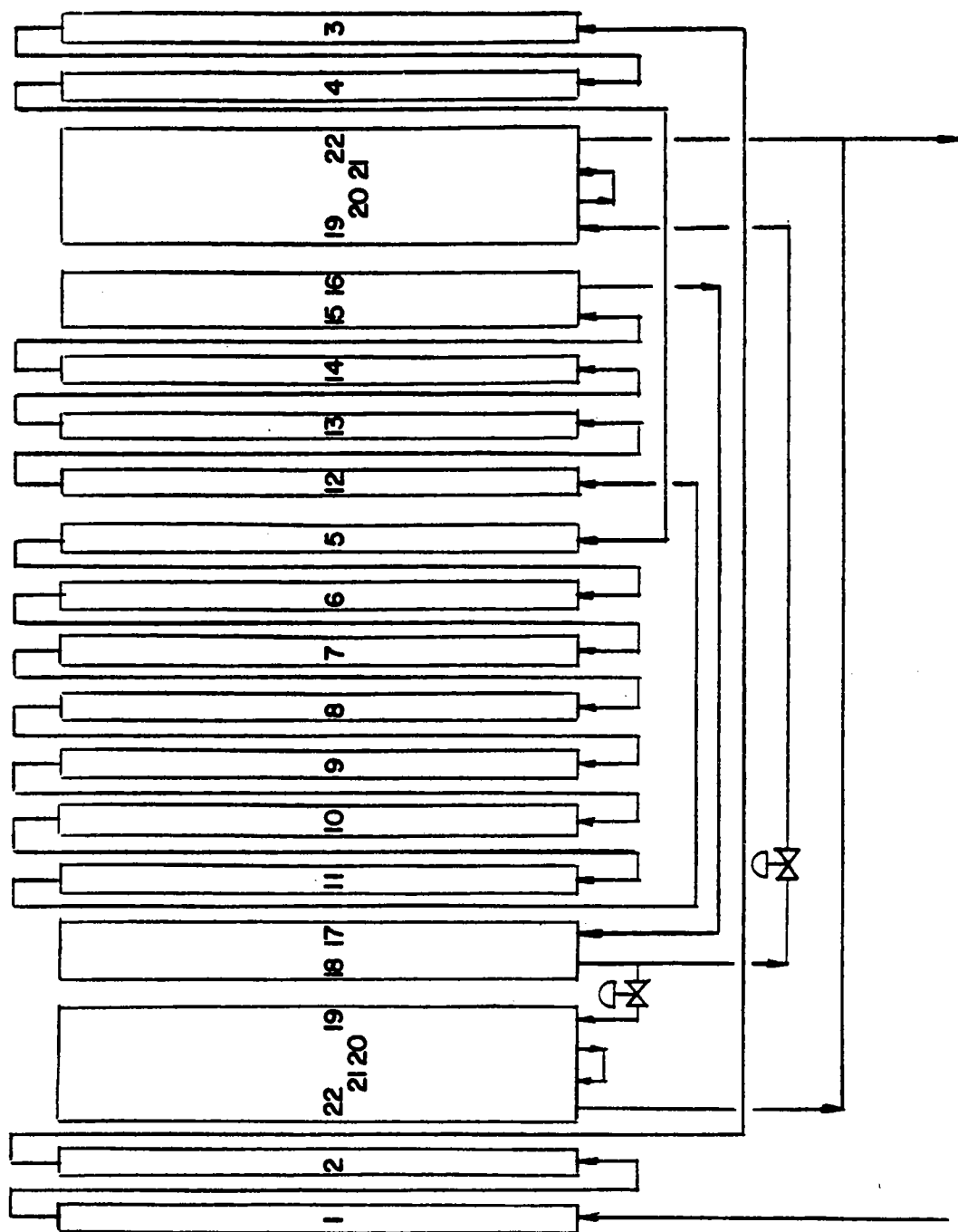


Figure 8.5 CRTF Cavity Test Preliminary P&ID

- Phase 3: Operational Testing. Would include both overnight operation with the receiver full and aperture door operation for the first 1 to 2 months of testing. The second 1 to 2 months would include overnight operation with the receiver drained and the panels preheated by the heliostats before filling. At the conclusion of these two tests, a third longer test of 6 months to 1 year would be devoted to normal daily operation using the overnight operating mode selected from the results of the earlier tests.
- o Test Conditions. Typical flux profiles for the proposed test cavity are given in Appendix K. These were calculated, for a receiver mounted atop the tower, by CONCEN using an approximate model of the CRTF heliostat field. Table 8.1 summarizes design and performance data for the proposed cavity test.

8.5.2 CRTF Panel Test Program

- Test Objectives.

- Demonstrate panel integrity and operability over panel operating envelope.
- Demonstrate panel structural support system.
- Investigate high salt bulk temperature/local flux performance, especially with respect to salt stability.

- Test Requirements.

- Simulate full-scale panel fluxes, including peak values [$\approx 0.63 \text{ MW/m}^2$ ($200,000 \text{ Btu/h}\cdot\text{ft}^2$)] and flux distributions with both longitudinal and lateral flux gradients
- Simulate full-scale panel design (i.e., tubing, fabrication, and support) and flow velocities
- Simulate panel inlet temperatures [288 to 538°C (550 to 1000°F)] and outlet temperatures [300 to 566°C (570 to 1050°F)]
- Provide instrumentation to assess panel front and back tubewall temperatures and panel deflections, also instrumentation to measure panel pressure drop.

- Test Hardware. The receiver panel would be mounted in place of the existing MSEE panel. Increased salt flow is required as a result of the lower salt ΔT associated with an individual panel test. This increase in flow rate necessitates modifications in the piping, pumps, and valves in the receiver flow loop. Also, either flow routing through the existing fired heater or an additional tower-mounted 5-MW ($17 \times 10^6 \text{ Btu/h}$) fired heater is required to provide appropriate inlet temperatures. Because the test is aimed purely at panel-related issues and not at panel control or performance, no modification to the control system is required.

Table 8.1 Commercial and SRE Comparison Summary

Description	Commercial	SRE
Nominal absorbed power, MW (Btu/h)	320.0 (1092.0 x 10 ⁶)	5.33 (18.2 x 10 ⁶)
Design maximum insolation, W/m ² (Btu/h·ft ²)	1000 (317)	1000 (317)
Salt flow rate, kg/s (lb/h)	760 (6.018 x 10 ⁶)	12.0 (95,300)
Salt inlet/outlet temperature, °C (°F)	288/566 (550/1050)	288/566 (550/1050)
Overnight salt temperature, °C (°F)	288 (550)	288 (550)
Cavity (width x depth), m (ft)	19.8 x 17.4 (65 x 57)	3.0 x 2.3 (9.9 x 7.5)
Aperture (width x height), m (ft)	19.8 x 25.8 (65 x 84.5)	3.0 x 3.7 (9.9 x 12)
Tube material	304SS/316SS/Incoloy 800	304SS/316SS/Incoloy 800
Number of panels/passages	20/5	18/22
Number of tubes per panel	88	11/12/14/48
Panel exposed (active) length, m (ft)	25.8 (84.5)	3.7 (12)
Tube O.D. x wall thickness, mm (in.)	25.4 x 1.65 (1.0 x 0.065)	25.4 x 1.65/19.1 x 1.65 (1 x 0.065/0.75 x 0.065)
Design pressure, kPa gage (lb/in ² g)	3463 (350)	2968 (300)
Peak incident heat flux, MW/m ² (Btu/h·ft ²)	0.67 (213,000)	0.67 (213,00)
Peak tubewall (O.D.) temperature, °C (°F)	633 (1171)	646 (1195)
Peak salt film (I.D.) temperature, °C (°F)	601 (1114)	604 (1120)
Peak front-to-back tube ΔT, °C (°F)	153 (275)	150 (270)

- Test Plan. The test plan would encompass a series of three to five different temperature ranges to simulate panel operation in different receiver passes. For each temperature range, operations would include both flux gradient variations and cyclic testing. The cyclic testing would involve numerous cycles per day of panel heat-up and cooldown to simulate overnight shutdown periods. In the last stages of the test at high temperatures, panel cycling could include several fill and drain cycles each day. At the end of the test, limited testing of panel operation with high fluxes and bulk temperatures would be conducted to evaluate salt film (I.D.) temperature design criteria.

8.5.3 Irradiated Panel Test Program

In conjunction with other CRTF system test operations, bleed flows from the existing hot and cold salt pump outlets may possibly be used to provide hot salt to several panel test sections to be irradiated by radiant heaters. These panel test sections [about 5 to 10 tubes wide and 1.5 to 3 m (5 to 10 ft) long] would be used exclusively to investigate salt stability and corrosion at high bulk temperature [$>510^{\circ}\text{C}$ ($>950^{\circ}\text{F}$)] and flux levels, providing film temperatures from 565 to 621°C (1050 to 1150°F).

8.5.4 Aperture Door Test Program

A receiver aperture door test should consist of steps to investigate the ability of the door, trolley, and seals to operate reliably under continual thermal cycling. Such a test would require radiant heaters to simulate the thermal loads on the door and should include some travel of the door section to verify that the trolley system will work effectively under such conditions. It should also test the seals under conditions of repeated thermal cycling.

Section 9

REFERENCES

1. L. N. Tallerics, "A Description and Assessment of Large Solar Power Systems Technology," Sandia Laboratories, Albuquerque and Livermore, Report No. SAND-79-8015, August 1979.
2. K. W. Beltham, et al., "1980 Solar Central Receiver Technology Evaluation," Sandia Laboratories, Albuquerque and Livermore, Report No. SAND-80-8235, October 1980.
3. T. R. Tracey, Martin Marietta Corporation, "Conceptual Design of Advanced Central Receiver Power System, Phase 1," Final Report DOE/ET/20314, September 1978.
4. Martin Marietta Corporation, "Solar Central Receiver Hybrid Power System, Phase 1 Final Technical Report," DOE/ET/21038, September 1979.
5. E. R. Weber, Arizona Public Service Company, "Saguaro Power Plant Solar Repowering Project," Final Technical Report DOE/SF/10739, July 1980.
6. C. R. Easton and D. L. Endicott, McDonnell Douglas Astronautics Corporation, "Sierra Pacific Utility Repowering," Final Technical Report DOE/SF/10609, July 1980.
7. A. J. Slemmons, "Line-Focus Solar Central Power System - Phase 1," SRI International, Final Report DOE/ET/20550 by SRI Project 7896, April 1980.
8. R. W. Carling, et al., "Molten Nitrate Salt Technology Development Status Report," Report No. SAND80-8052, Sandia National Laboratories, Livermore, California, March 1981.
9. R. W. Mar, et al., "Progress Report: Molten Nitrate Salt Technology Development," Report No. SAND82-8220, April 1982.
10. Martin Marietta Corporation, "Alternate Central Receiver Power System - Phase II," Final Report, Vol. II-Receiver, MCR81-1707, May 1981.
11. Southern California Edison, "Solar Energy Measurements at Selected Sites Throughout the Southwest During 1977," R. J. Yinger, prepared for The West Associates Solar Resource Evaluation Project, June 1978.
Southern California Edison, "Solar Energy Measurements at Selected Sites Throughout the Southwest During 1978," R. J. Yinger, prepared for The West Associates Solar Resource Evaluation Project, September 1979.

Southern California Edison, "Solar Energy Measurements at Selected Sites Throughout the Southwest During 1979," R. J. Yinger, prepared for The West Associates Solar Resource Evaluation Project, October 1980.

Southern California Edison, "Solar Energy Measurements at Selected Sites Throughout the Southwest During 1980," R. J. Yinger, prepared for The West Associates Solar Resource Evaluation Project, January 1982.

12. W. S. Winters, R. W. Bradshaw, and F. W. Hart, "Design and Operation of Thermal Convection Loops for Corrosion Testing in Molten NaNO_3 - KNO_3 ," Sandia National Laboratories, Report No. SAND80-8212, 1980.
13. R. W. Bradshaw, "Corrosion of 304SS by Molten NaNO_3 - KNO_3 in a Thermal Convection Loop," Sandia National Laboratories, Report No. SAND80-8856, 1980.
14. R. W. Bradshaw, "Thermal Convection Loop Corrosion Tests of 316SS and 1800 in Molten Nitrate Salts, Sandia National Laboratories, Report No. SAND81-8210, February 1982.
15. S. H. Goods, "Creep and Corrosion Characteristics of Incoloy Alloy 800 in Molten Nitrate Salts," Sandia National Laboratories, Report No. SAND81-8665, 1981.
16. McDonnell Douglas Corporation, "Molten Salt Technology," unpublished confidential draft report distributed to FWSDC, Southern California Edison, Bechtel Corporation, July 1981.
17. Criteria for Design of Elevated Temperature Class 1 Components in Section III-Division 1, of the ASME Boiler and Pressure Vessel Code, The American Society of Mechanical Engineers, New York, May 1976.
18. D. R. Diercks, "A Compilation of Elevated-Temperature, Strain-Controlled Fatigue Data on Type 316 Stainless Steel," Argonne National Laboratory, prepared for the U.S. Energy Research and Development Administration, ANL/MSD-77-8, August 1977.
19. S. Majumdar, "Compilation of Fatigue Data for Incoloy 800 Alloys," Argonne National Laboratory, prepared for the U.S. Department of Energy, ANL/MSD-78-3, March 1978.
20. S. Majumdar, "Biaxial Creep-Fatigue Behavior of Materials for Solar Thermal Systems," Argonne National Laboratory ANL-80-34, May 1980.
21. M. S. M. Rao, "An Interim Structural Design Standard for Solar Energy Applications (Evaluation of ANL Tests)," FWDC No. 9-41-441110, May 1980.
22. D. Dawson, Second Project Review Meeting, held at FWSDC, Livingston, New Jersey, May 25, 1982.

23. K. M. Gregory, Olin Corporation, Letter to G. Carli, Foster Wheeler Development Corporation, March 9, 1982.
24. D. Dawson, Sandia National Laboratories, Interoffice Correspondence, "Revised Physical Property Values for Molten Nitrate Salts," April 26, 1982.
25. E. N. Sieder and G. E. Tate, "Heat Transfer and Pressure Drop of Liquids in Tubes," Ind. Eng. Chem., Vol. 28, p. 1429, 1936.
26. H. Hausen, "Darstellung des Wärmeüberganges in Rohren durch verallgemeinerte Potenzbeziehungen," VDI Zeit, No. 4, p. 91, 1943.
27. F. W. Dittus and L. M. K. Boelter, University of California (Berkeley), Pub. Engineering, Vol. 2, p. 443, 1930.
28. K. M. Gregory, Olin Corporation, Letter Correspondence to G. Carli, June 21, 1982.
29. K. M. Gregory, Olin Corporation, Letter Correspondence to G. Carli, October 4, 1982.
30. Standards of Tubular Exchanger Manufacturers Association, Sixth Edition, E. W. Flaxbart, Ed., White Plains, New York, 1978.
31. R. V. Giles, FLUID MECHANICS AND HYDRAULICS, Second Ed., Schaum Publishing Company, New York, 1962.
32. M. Abrams and R. Grief, "Theory for Predicting the Natural Convection Energy Loss from Side-facing Solar Cavity Recivers," SAND 81-8201, January 1981.
33. J. Kraabel, Private communication of unpublished data and data correlations, J. Kraabel, Sandia Laboratories, Livermore, unpublished data.
34. E. Achenbach, "Heat Transfer from Smooth and Rough Surfaced Circular Cylinders in a Cross Flow," Kernforschungsanlage Julich GmbH, Germany.
35. M. Jakob, Heat Transfer, John Wiley and Sons, Inc., New York, New York, 1949.
36. C. M. Landell, et al., "Barstow Insolation and Meteorological Data Base," Report No. ATR-78 (7695-05), Aerospace Corporation, March 1978.
37. ASME Boiler and Pressure Vessel Code, Section III-Division 1, Code Case N-47, 1980.
38. I. Berman, et al., "An Interim Structural Design Standard for Solar Energy Applications," Report No. SAND79-8183, Sandia Laboratories, Livermore, April 1979.

39. M. S. M. Rao, et al., "Inelastic Analysis of Nonaxisymmetrically Heated Thick Cylindrical Shells," Transactions of ASME, Journal of Pressure Vessel Technology, Vol. 101, August 1979, pp. 235-241.
40. M. S. M. Rao, "NONAX - A Computer Program for Thermoelastic-Plastic-Creep Analysis of Thick-Walled Cylinders Under General Nonaxisymmetric Loading," Foster Wheeler Development Corporation, Report No. EST-78-5, 1979.
41. Nuclear Systems Materials Handbook, Hanford Engineering Development Laboratory, TID26666, February 1975.
42. J. W. Liebenberg, Sandia Laboratories, Interoffice Correspondence to J. J. Bartel, "Tower Costs for Solar Central Receivers," January 7, 1980.
43. "Tower Cost Data for Solar Central Receiver Studies," Stearns Roger Engineering Company, SAND78-8185, June 1979.
44. Foster Wheeler Solar Development Corporation, "Volume 1--Technical Proposal, Molten Salt Solar Receiver Subsystem Research Experiment," prepared for Sandia Laboratories, May 15, 1981.

INITIAL DISTRIBUTION
UNLIMITED RELEASE

Department 8450 Files (2)
Publications Division 8265, for TIC (27)
Publications Division 8265/Technical Library Processes Division, 3141
Technical Library Processes Division, 3141 (3)
M. A. Pound, 8024, for Central Technical Files (3)